

Proceedings of the International Conference on
Advanced Manufacturing Engineering and Technologies
NEWTECH 2013
Stockholm, Sweden
27-30 October 2013



Volume 1

Edited by:
Dr. Andreas Archenti & Dr. Antonio Maffei



KTH Royal Institute of Technology, Stockholm, Sweden

ISBN 978-91-7501-892-8

Copyright © 2013

All rights reserved. This publication or part thereof may not be reproduced without the written representation of the editors

Printed by Universitetservice US AB

Conference Chair

Prof. Cornel Mihai Nicolescu (KTH Royal Institute of Technology, Stockholm)

Co-Chairs

Prof. Viorel Paunoiu (University of Galati, Romania)

Prof. Miroslav Piska (Brno University, Czech Republic)

Prof. Mauro Onori (KTH Royal Institute of Technology, Stockholm)

Scientific Committee

Prof. Bengt Lindberg (KTH Royal Institute of Technology, Sweden)

Prof. Lars Mattsson (KTH Royal Institute of Technology, Sweden)

Prof. Torsten Kjellberg (KTH Royal Institute of Technology, Sweden)

Prof. Lihui Wang (KTH Royal Institute of Technology, Sweden)

Prof. Jan Wikander (KTH Royal Institute of Technology, Sweden)

Prof. Marco Santochi (University of Pisa, Italy)

Prof. Reijo Tuokko (Tampere University of Technology, Finland)

Prof. Philippe Lutz (University of Franche-Comté, France)

Prof. Fabrizio Quadrini (University of Rome Tor Vergata, Italy)

Prof. Paul Shore (Cranfield University, UK)

Prof. Laszlo Monostori (Budapest University of Technology and Economics, Hungary)

Prof. Lars Nyborg (Chalmers University of Technology, Sweden)

Prof. S.Jack Hu (University of Michigan, USA)

Prof. José Barata (New University of Lisbon, Portugal)

Prof. Patrick Martin (ENSAM, France)

Prof. Takayuki Hama (Kyoto University, Japan)

Prof. Trevor Dean (The University of Birmingham, UK)

Prof. Gino Dini (University of Pisa, Italy)

Prof. Luis Norberto Lopez De La Calle (Technical School of Engineering of Bilbao, Spain)

Prof. Satyandra K. Gupta (University of Maryland, USA)

Prof. Krzysztof Jemielniak (Warsaw University of Technology, Poland)

Prof. Johan Stahre (Chalmers University of Technology, Sweden)

Prof. Jerzy Jedrzejewski (Wroclaw University of Technology, Poland)

Prof. Paulo E. Miyagi (University of São Paulo, Brasil)

Prof. Niels Bay (Technical University of Denmark, Denmark)

Prof. Adinel Gavrus (National Institute of Applied Sciences, France)

Prof. Antonio Gonçalves Coelho (New University of Lisbon, Portugal)

Prof. Kamal Youcef-Toumi (Massachusetts Institute of Technology, USA)

Prof. Wit Grzesik (Opole University of Technology, Poland)

Prof. Patricio Franco (Technical University of Cartagena, Spain)

Prof. Terje Lien (Norwegian University of Science and Technology, Norway)

Prof. Vytautas Ostasevicius (Kaunas University of Technology, Lithuania)

Prof. P.G. Maropoulos (University of Bath, UK)

Prof. Francisco Restivo (University of Porto, Portugal)

Prof. George Chrysoulouris (University of Patras, Greece)

Prof. Shiv G. Kapoor (University of Illinois at Urbana-Champaign, USA)

Prof. Dimitris Mourtzis (University of Patras, Greece)

Prof. João Paulo Davim (University of Aveiro, Portugal)

Prof. Hong Hocheng (National Tsing Hua University, Taiwan)

Prof. Loredana Santo (University of Rome, Tor Vergata, Italy)

Prof. Luis Gomes (New University of Lisbon, Portugal)

Organizing committee at KTH Royal Institute of Technology

Dr. Andreas Archenti (Editor)

Dr. Antonio Maffei (Editor)

Tech Lic. Hakan Akillioglu

Dr. Danfang Chen

Dr. Lorenzo Daghini

Tech Lic. Joao Ferreira

Mr. Costantinos Frangoudis

Tech Lic. Pedro Neves

Mr. Johan Pettersson

Ass. Prof. Amir Rashid

Tech Lic. Tomas Österlind

Preface

Welcome to Stockholm and to NEWTECH 2013.

This autumn, in a Stockholm setting of stunning multi-coloured reflections, NEWTECH conference opens its gates to warmly welcome our distinguished guests from 20 countries with over 100 participants worldwide, researchers, and industry representatives.

Though we cannot, wish though we may, promise dazzling sunshine, we can guarantee an ardent dialog with the Advanced Manufacture at the centre of debates. Engagement in this timely discourse, both as an industry and as individuals, will help bring to light the issues of the present and the innovative solutions of tomorrow.

NEWTECH is at the dawn of creating a new tradition. After Galati 2009 and Brno 2011, Stockholm is prepared to bring together Academy and Industry in the essential debate on the role of Manufacturing in the Environmental and Societal agenda, where care of Nature should pave the way for the next generation processes and systems.

I hope that you will have lots of exciting and interesting discussions, as well as encounters with people from many different research centres and industries. I also hope that you will have the opportunity to explore Stockholm and discover the best of what this beautiful city has to offer.

Finally, may I thank the organisers personally for their hard work, the conference sponsors, and all participants that have made this event possible, and also extend my best wishes to all delegates for what will surely be an inspiring experience in Stockholm.

Prof. Cornel Mihai Nicolescu
Chairman of NEWTECH 2013

NEWTECH's legacy

The first edition of the International Conference NEWTECH was organized and hosted by the Department of Manufacturing Engineering of Dunarea de Jos University of Galati, Romania, in 23-25 September 2009.

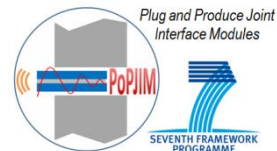
80 specialists from 10 countries took part to the Conference. Four plenary lectures and 50 papers were presented. The following topics were addressed by the participants: Reconfigurable manufacturing, Modelling and numerical simulation in metal forming and cutting processes, Technologies for composites and nanostructures materials, High speed machining, Nonconventional technologies including those for plastic deformation, Concurrent engineering, Manufacturing process optimization, Quality management.

The second edition of the International Conference NEWTECH was organized and hosted by the Institute of manufacturing technology, Brno University of Technology, Czech Republic, in 13-15 September 2011.

112 participants from 12 countries took part in the conference. The conference covered eight scientific topics, from advanced material processing to virtual manufacturing and simulation. A special focus was given to Ecodesign of machine tools and green energy management.

Conference Partners

The organizing committee would like to express their deep gratitude to all the partners for their active support and contribution, without which this event would not have been possible



Preface to the themes treated in this volume

The theme of the conference is “Advanced Manufacturing Engineering and Technologies”, and the aim of this initiative is providing a forum for researchers and practitioners working on the diverse issues of such a broad topic. In particular, authors, both from academia and industry have been invited to submit papers for all aspects of theories, methodologies, applications, and case studies related to their work in this context.

This volume collects the papers treating the following three themes: Metal Cutting, Cutting Stability and Machine Tool Design. These three themes are intrinsically related to each other and knowledge in this joint field represents the fundament of modern manufacturing technology.

The increasing importance of productivity and quality improvement in the fabrication of complex shape components with tighter tolerances and high surface accuracy have led to the introduction of new trends in machining system design, optimization and operational usage. Traditionally, the cutting process and the machine tool in a machining system were designed and optimized to machine, with rather low cutting feeds and cutting speeds, components made of conventional materials with relatively simple shapes. The geometrical and dimensional accuracy of the components, as well as the surface finish, were often in a feasible range without compromising productivity or product quality. On the other hand, products are becoming more and more complex, both in terms of geometry, surface integrity and material properties. This leads to more demanding processes for the machine system in terms of static, dynamic and thermal stability as well as energy and natural resource consumption.

The three themes treated in this volume lay the basis for industrial enterprises to develop or improve their production processes in order to continue profiting in a sustainable manner.

The Editors
Dr. Andreas Archenti & Dr. Antonio Maffei

Table of contents

Theme 1: Metal Cutting

9

Determination of characteristic values for milling operations using an automated test and evaluation system.....	11
Performance Evaluation of Different Cooling Strategies when Machining Ti6Al4V	21
3D FEM Simulation of Titanium Machining.....	31
Multi-performance Optimization in Turning of Stainless Steels using Taguchi-VIKOR-Metaheuristic Concept.....(only available in digital form)	
Machining of Stainless Steels: A Comparative Study.....(only available in digital form)	
The profiling of rack-gear tool for the generation of the helical surfaces.....	63
Investigation of side milling operations for machining carbon fibre reinforced thermoplastic composite	73
An intelligent and modular adaptive control scheme for automating the milling process.....	83
A methodology to evaluate the machinability of Alloy 718 by means of FE simulation.....	95
Short-term machinability testing of difficult to machine materials	107

Theme 2: Cutting Stability

115

In-process Control for Adaptive Spindle Speed Variation and Selection	117
Dynamics of Modified Tool Structures for Effective Cutting.....	127
Stability in turning of superalloys using two numerical methods.....	137
On the effective milling of large workpieces.....	149
New method of dynamic cutting force coefficients determination	159
Model-Based Identification of Chatter Marks during Cylindrical Grinding.....	167
Machining improvement on flexible fixture through viscoelastic damping layer	179
Analytical Stability Prediction in Five Axis Ball-End Milling.....	189
Numerical simulation of self-excited vibrations - review of methods, potential advantages and pitfalls.....	199
Non-Regenerative Dynamic Instability in Surface Grinding.....	209

Theme 3: Machine Tool Design

221

Robust Thermal Error Compensation Model of Portal Milling Centre Based on Superposition of Participating Thermal Sources.....	223
Complex Verification of Thermal Error Compensation Model of a Portal Milling Centre.....	233
Intelligent Control Using Neural Network Regarding Thermal Errors with Non-linear Behaviour of a Machine Tool	243
Application of GNNMCI(1, N) to environmental thermal error modelling of CNC machine tools.....	253
Development of modular machine tool structural monitoring system.....	263
Towards Knowledge Framework for Life-Cycle-Long Gathering of Maintenance Information for Decision Support in Machine Tool Design	273
Improved automatic experimental modal analysis of machine tool spindles.....	283
Experimental analysis of the CNx nano-damping material's effect on the dynamic performance of a milling process.....	293
Using design of experiments approach to determine the essential designing parameters for an anti-vibration turning tool with finite element analysis.....	303
Effect of thin viscoelastic material treatments of the clamping region on dynamic stiffness of the cantilever beams	313

Theme 1

Metal Cutting

- Determination of characteristic values for milling operations using an automated test and evaluation system
Thomas Auerbach, Simon Rekers, Dražen Veselovac, Fritz Klocke
RWTH Aachen University, Aachen, Germany
- Performance Evaluation of Different Cooling Strategies when Machining Ti6Al4V
Salman Pervaiz^{1,2}, Ibrahim Deiab², Amir Rashid¹, Mihai Nicolescu¹, Hossam Kishawy³
¹KTH Royal Institute of Technology, Stockholm, Sweden
²Department of Mechanical Engineering, American University of Sharjah, Sharjah, UAE
³Faculty of Engineering and Applied Sciences, University of Ontario Institute of Technology, Oshawa, Ontario, CANADA
- 3D FEM Simulation of Titanium Machining
P. Nieslony¹, W. Grzesik¹, R. Chudy¹, P. Laskowski², W. Habrat³
¹Opole University of Technology, Opole, Poland
²WSK PZL, Rzeszów, Poland
³Rzeszów University of Technology, Poland
- Multi-performance Optimization in Turning of Stainless Steels using Taguchi-VIKOR-Meta-heuristic Concept
Rastee D. Koyee^a, Siegfried Schmauder^b, R. Eisseler^a
^aIfW, University of Stuttgart, Germany.
^bIMWF, University of Stuttgart, Germany.
- Machining of Stainless Steels: A Comparative Study
Rastee D. Koyee^a, Siegfried Schmauder^b, R. Eisseler^a
^aIfW, University of Stuttgart, Germany.
^bIMWF, University of Stuttgart, Germany.
- The profiling of rack-gear tool for the generation of the helical surfaces
Virgil Teodor¹, Viorel Paunoiu¹, Silviu Berbinschi², Nicolae Oancea¹
¹"Dunărea de Jos" University of Galați, Faculty of Mechanical Engineering, Department of Manufacturing Engineering,
²"Dunărea de Jos" University of Galați, Faculty of Mechanical Engineering, Department of Mechanical Design and Graphics
- Investigation of side milling operations for machining carbon fibre reinforced thermoplastic composite
Petr Masek, Petr Kolar, Pavel Zeman
Czech Technical University in Prague, Research Center of Manufacturing Technology, Prague, Czech Republic
- An intelligent and modular adaptive control scheme for automating the milling process
Luis Rubio, Andrew Longstaff, Simon Fletcher and Alan Myers
Centre for Precision Technologies, University of Huddersfield, UK
- A methodology to evaluate the machinability of Alloy 718 by means of FE simulation
Amir Malakizadi, Stefan Cedergren, Kumar Babu Surreddi, Lars Nyborg
Chalmers University of Technology, Gothenburg, Sweden
- Short-term machinability testing of difficult to machine Materials
Joanna Kossakowska, Krzysztof Jemielniak
Warsaw University of Technology, Poland

Determination of characteristic values for milling operations using an automated test and evaluation system

Thomas Auerbach, Simon Rekers, Dražen Veselovac, Fritz Klocke

RWTH Aachen University, Aachen, Germany
T.Auerbach@wzl.rwth-aachen.de

ABSTRACT

Although the amount of composite materials in aerospace industry increases, metallic alloys remain indispensable for a variety of applications. Because of their thermal and mechanical strength, Ni-based and titanium alloys are commonly used in the compressor and turbine section of a jet engine, Aluminium alloys are widely used for structural components of aircrafts. When machining integral parts from these alloys, up to 90 % material is removed in order to obtain the parts final shape. From an economic point of view, stable machining processes with highest material removal rates at low resource consumption are of crucial interest. Optimal process parameters have to be chosen for a certain tool-work piece-engagement situation.

In this article an automated test bench is presented which offers the capability of characterizing machining processes for a given tool-work piece-engagement situation within a short period of time. Multiple cutting tests with a predefined parameter set are performed by the system automatically. The required NC code is generated by the system as well. Furthermore, a data acquisition interface, which communicates with the NC control of the machine tool, enables to trace various sensor signals, which are subsequently evaluated in terms of characteristic values. This data basis provides a foundation to choose cost and resource efficient process parameters for a certain tool-work piece-engagement situation.

KEYWORDS: milling, aerospace, automation, material, characterization

1. INTRODUCTION

A decisive indicator of a company's competitiveness is in-house knowledge and its application. This fact has been illustrated by North via a systematic approach, the so-called "stairs of knowledge" [1]. North illustrates a general way to create knowledge and to transfer this knowledge into competitive applications. Fig.1 introduces this approach and shows the respective relationships.

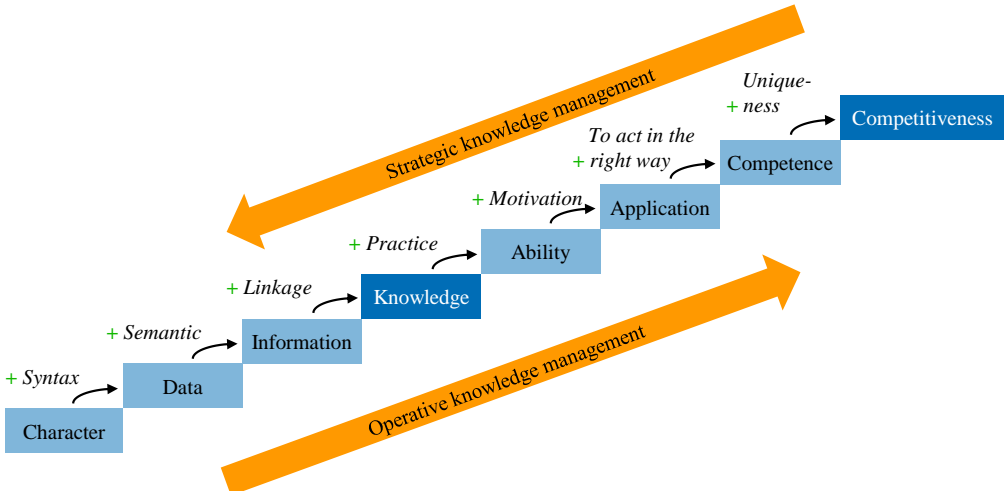


Fig.1: Stairs of knowledge in accordance to North [1].

A knowledge-based approach to enhance the controllability of milling processes is currently researched in the Cluster of Excellence “Integrative Production Technology for High-Wage Countries” [2]. The research focuses on the development of a model-based self-optimization (MBSO). The MBSO enables a milling system to realize autonomously a pre-defined machining task taking qualitative and economic objectives into account. Therefore, monitoring, control and optimization strategies will be connected at the systemic level and will be integrated into the milling machine. A detailed description of self-optimization in general or information on the model-based self-optimization approach can be found in the corresponding literature [3, 4, 5].

The implementation of the MBSO requires appropriate models of the milling process which represent the expert knowledge. In order to obtain those models a generic methodology has been developed which contains the main steps of the modelling procedure [6]. With regard to the methodology, a reliable database is the prerequisite for an appropriate model. The database includes relevant characteristics of the manufacturing process which can be derived from experiments or simulation. Thus, the reliability of the database is directly dependent on the procedure which is applied to determine the process characteristics. Regarding the stairs of knowledge the MBSO performs the step from information to knowledge. The preliminary step, from data to information, is mandatory for the MBSO. Motivated by these facts a standardized and automated approach for performing milling experiments has been developed to determine a great number of process characteristics for a broad database. According to North’s illustration, this addresses the steps of data generation and their transfer into process relevant information. The advantages of this approach are:

- **Enhanced reproducibility:** Due to the standardization each experiment is executed in the same way. Thus, the results obtained from the experiments can be compared to each other.
- **Reduction of errors:** Standardization and automation of the experimental investigation reduce the occurrence of random errors caused by the operator during the experimental tests.
- **Reduction of time exposure:** Time-consuming, manually performed steps are almost completely eliminated during the experiments. The processing time for an experiment depends only on the cutting parameters.

In this paper the developed approach is introduced based on milling operations which are of interest for aerospace industry. For High-Wage Countries such as Germany this is an important industry as it currently faces a growing market which is the result of a steadily increasing demand on mobility. According to a forecast, the number of new airplanes will grow by more than 27.000 until 2025 compared to 2005 [7]. Thus, the components to be machined will also increase significantly. Another trend is that the aerospace industry is facing challenges regarding fuel efficiency and emission efficiency. In 2001 the council for aviation research and innovation in Europe (ACARE) formulated multiple objectives until 2020 [8]. For each passenger-km the fuel consumption and the CO₂ emission should be reduced by 50%. An enabler of these objectives is lightweight construction. Important materials are aluminium alloys, titanium alloys and nickel-based alloys. In addition to these general facts, the requirements of the machining processes are different. Due to this high diversity of milling operations and the described trends the aerospace industry are particularly interested in an efficient approach to determine process relevant characteristic values for evaluation of milling parameters in manufacturing.

The paper is organized as follows. In section 2 the flow chart model of a standard milling experiment is presented. Based on this model the automated test and evaluation system are introduced in section 3 and 4. In section 5 the complete system is applied to investigate the process behavior of a five axes milling operation using different sensors integrated in the experimental setup. The paper closes with a conclusion of the presented work.

2. FLOW CHART MODEL OF A STANDARD MILLING EXPERIMENT

Initial point for the development of the automated test and evaluation system is the analysis of a milling experiment. The single steps which are performed by the operator need to be identified and transferred into a comprehensible flow chart model. Based on observations in the test field, own experiences and literature a first flow chart model of a standard milling experiment was derived. This model is introduced in Fig. 2. The model illustrates the three phases of an experiment: the preparation, implementation and evaluation phase. Each of these phases includes several sub-processes which are also illustrated.

In the preparation phase the operator defines the experimental design and setup. Based on this information a NC program is generated in advance which is used to carry out the milling tests on a machining center. In most cases operators use parameterised programs with standard routines where only cutting specific parameters are adapted during the implementation phase. Since nowadays many experimental investigations include the acquisition of process measurements it is often necessary to initialize the measurement systems before performing a milling test. After this, the actual milling test and the data acquisition are realized. Before the evaluation of the performed milling tests can be implemented some of the acquired signals must be pre-processed. Standard methods are offset correction or the transfer of a voltage signal in the respective physical unit. The last important step within the implementation phase is the adaptation of the parametric NC program in order to enable the next milling test. In the evaluation phase the relevant information are extracted from the acquired data. Therefore, signal analysis algorithms in the time and frequency domain can be applied to the acquired and pre-processed sensor signals. Afterwards, typical characteristic values can be determined such as minimum, maximum or average values. The evaluation phase closes with the storage of the extracted characteristic value in a database.

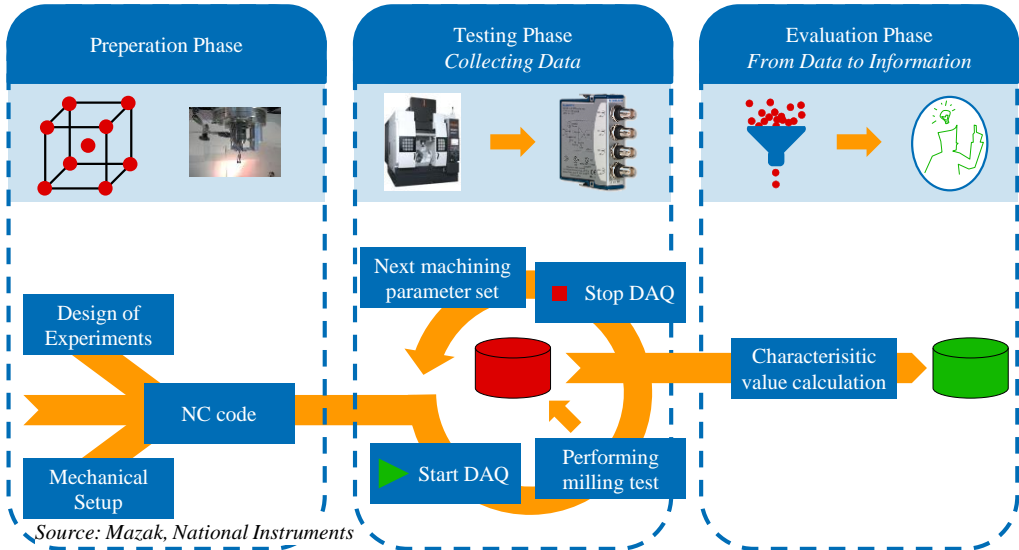


Fig.2. Flow chart model of a standard milling experiment.

Based on the presented flow chart model the steps were identified that can be automated. Only two steps are not included in the automated test and evaluation system. These are the experimental design and setup.

3. AUTOMATED TEST SYSTEM – COLLECTING DATA

Main objective of the automated test system is to collect data of the milling process during a short time. In this context it is important that different milling parameters can be applied and that the data acquisition is guaranteed during each milling test. For the implementation of the automated test several development steps were necessary.

In a first step, a standardized test procedure had to be clearly defined and described. This procedure is applied to each milling test. In this context the primary aim was to design the test procedure as simple as possible in order to limit the complexity for the automated test system. Because of that, a conventional line milling process is chosen to implement the automated milling tests, Fig. 3. It consists of a simple tool path which is clearly described by a starting and end points. This enables the use of a NC program in parametric form. By doing so, the milling parameters can be changed at each line. This applies not only to parameters such as cutting speed or feed but also enables down and up milling operations. Furthermore, the conventional line milling process can be also applied to investigate five axis milling conditions. An approach angle or tilt angle will not change the tool path and therewith it will not change the automated test procedure. Both angles only need to be considered in the parametric NC program.

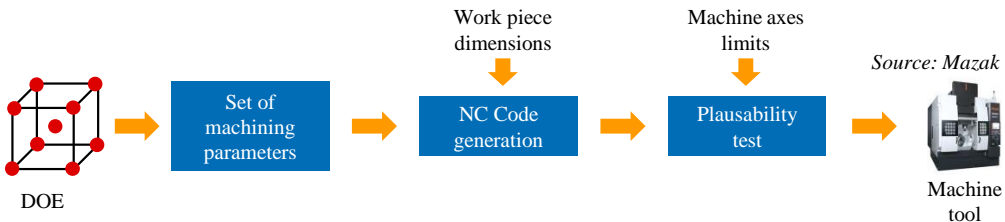


Fig.3. Standardized test procedure.

In the second development step the described test procedure was transferred into a control software. This software organizes the overall process and executes the required sub-processes automatically in a pre-defined order. The control software was programmed in the development environment LabVIEW which is provided by National Instruments. A detailed description of the software architecture and programming is not given in this paper.

The third development step to realize the automated test system is focussed on the installation of a communication infrastructure. As the operator is no longer involved in the execution of the milling tests, a communication between the machine centre, the data acquisition system and the control software is required. This communication is primarily used to trigger necessary activities at the beginning and at the end of each milling experiment, e.g. before the cutter engages the work piece the measurement systems has to be switched in the operate mode and the data acquisition has to be started. Similar to this, after the cutter leaves the work piece the data acquisition has to be stopped in order to enable the storage of the measurement file. For that purpose, so-called “M”-commands are added to the NC program which is later used for the automated milling tests. The “M”-command switches a relay which immediately provides a direct current voltage signal. This signal can be processed by the control software as well as the measurement systems in order to trigger the respective activities. As long as the “M”-command is active the machining centre will not move. In order to release the machine the control software has to provide a feedback signal. For example, this aspect prevents that the machining centre performs the milling tests, while the data acquisition is not yet started. Through this, a controlled process of the automated test system is ensured.

As the final development step, the control software was extended by a user interface. Before the automated test system can be used the operator has to parameterize the system. Via this interface the operator defines a fixed number of milling tests based on a pre-defined experimental design. Furthermore, the operator must define the work piece, the technical boundary conditions of the machine tool as well as the data acquisition system which is used during the milling experiments. By integrating this information into the control software two working steps are executed. First, an integrated plausibility test will check the operator’s input, e.g. if a defined spindle speed will exceed the performance of the spindle, the control software detects this as an error and displays it immediately to the operator. Secondly, the control software generates the complete NC program that is used for the automated milling tests. Here, the defined parameters of each milling test as well as the trigger commands will be transferred into a pre-defined parametric NC program representing the conventional line milling process. At this point, the parameterized automated test system is ready to perform the defined milling tests. Therefore, the generated NC program must be started on the numerical control of the machining centre. While running the NC program, the software controls the start and stop of each milling test as well as the acquisition of the measurement data. After each milling test the software stores the acquired data together with the respective milling parameters in a database.

4. THE EVALUATION SYSTEM - FROM DATA TO INFORMATION

The data provided by the automated test system is in the form of discrete time domain signals stored in a database. A signal processing system enables the extraction of characteristic values. The processing procedure can be divided into two sub procedures: pre-processing and characteristic value extraction. Each procedure is processed in a sequential manner.

As seen in Fig. 4 the objective of pre-processing is to obtain a data set. Depending on the number of signals in database, their duration, sample rate and resolution the amount of data

varies in size. Although computational performance was increased dramatically in the past and numerical signal processing algorithms have been optimized towards efficiency, processing of large data sets may take long time. In order to reduce the data to be processed, the signals of interest are selected from database by executing user defined queries on the database to obtain a data subset of interest.

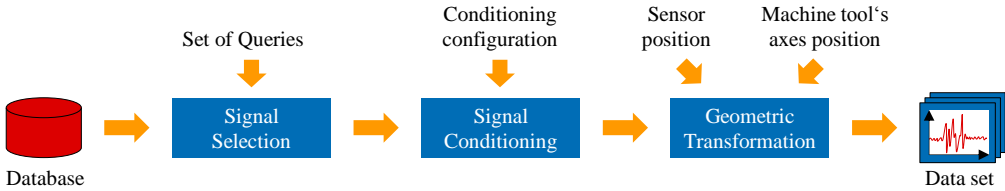


Fig.4. Flowchart of the pre-processing in evaluation phase.

To achieve the requirements of further signal processing steps each signal can be conditioned depending on a user defined configuration. Common techniques for signal conditioning are windowing, filtering, offset correction, detrending or scaling. Depending on a sensor's position as well as machine tool's axes position, the measuring direction of the sensor may differ from a coordinate system which is used for the evaluation. To keep the evaluation consistent, the signals can be transformed geometrically such that the selected signals are projected on a global coordinate system. Finally, the transformed signals are stored temporary as data set.

In the next step the characteristic values are extracted and stored in a repository. The flowchart of the evaluation phase is depicted in Fig. 5.

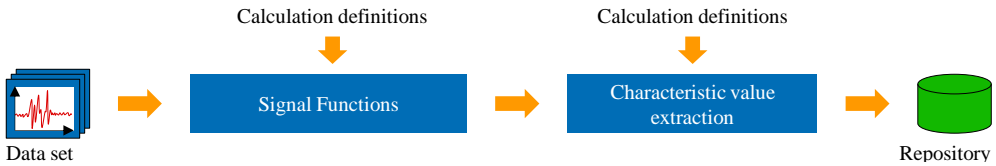


Fig.5. Flowchart of the characteristic value extraction in evaluation phase

To achieve characteristic values, the signals from the temporary dataset are processed sequential. In a first step signal functions can be applied. A list of potential signal functions is depicted in Table 1. After applying signal functions, the characteristic values are extracted from the signals.

Table 1. Signal Functions

Domain	Example
Time	Auto correlation
	Envelope
	Smoothing
Frequency	Power Spectral Density
	Fourier Transform
Time & Frequency	Wavelet Transform
	Short Time Fourier Transf.

Table 2. Characteristic values

Type	Example
Statistical	Minimum
	Maximum
	Root Mean Square
	Variance
Curve Fitting	Fitting Coefficients
User defined	Cutting Force Coefficients

Finally, the characteristic values are stored together with the related process parameters. This repository serves as basis for closing the gap between information and knowledge in the stairs of knowledge, see Fig. 1.

5. EXAMPLE

Efficient forming by milling requires well-chosen process parameters. In this example, the investigation of a finish milling process of Ti6Al4V and AlZnMgCu1.5 using a ball end mill is demonstrated. Both materials are common in aerospace technology.

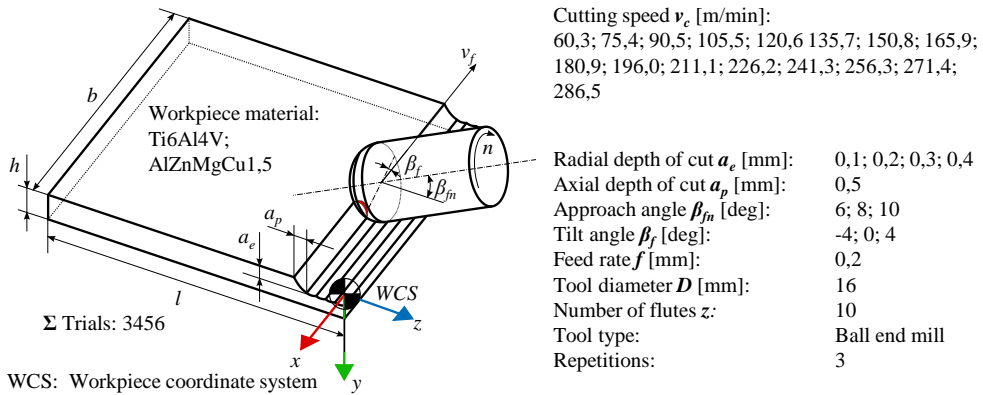


Fig.6. Preparation phase – design of experiments.

In order to obtain the processes characteristic values, the preparation phase has to be passed at first. Therefore the mechanical setup and the design of experiments have to be performed by the user. According to Fig. 6, 3456 tests in two different work piece materials are performed in a full-factorial manner. Multiple sets of machining parameters are tested by line milling. Each set of technological parameters is repeated three times to increase statistic accuracy. During the process cutting forces and tool displacement are recorded. Varying parameters are the cutting speed, radial depth of cut, approach angle, tilt angle and work piece material. Constant parameters are axial depth of cut, feed rate and all tool related parameters such as number of flutes or tool diameter.

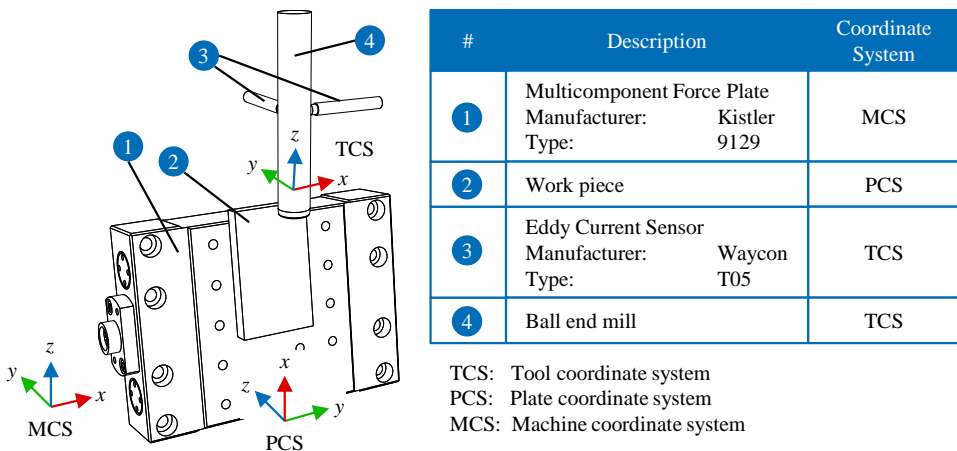


Fig.7. Preparation phase – mechanical setup.

The locations of the sensors relative to the work piece are depicted in Fig. 7. For the force measurement a piezoelectric force plate from Kistler is used. The tool deflection during milling is measured by two eddy current sensors from Waycon which are concentrated perpendicular to each other on the tool shaft. Each sensor, the work piece and the machine tool has its own coordinate system. In awareness of the work piece dimensions and origin in the machine coordinate system (MCS) as well as the experimental design, a NC code is generated automatically for the test execution. Afterwards the generated NC code is checked regarding plausibility to ensure feasibility of the tests.

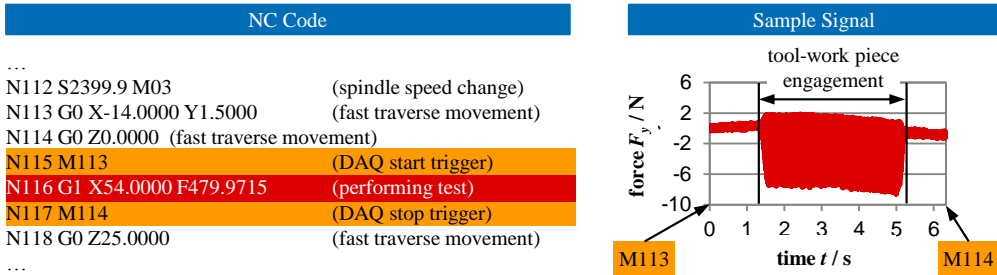


Fig.8. Testing phase – data acquisition (DAQ) procedure.

In the testing phase the data for each milling test is recorded. To reduce the amount of generated data, the data acquisition system is activated and stopped using a machine specific trigger in the NC code. Fig. 8 shows a section of the NC Code. In the diagram on the right a sample signal is shown. The start and stop trigger are marked with “M113” and “M114”. In this case the data acquisition captures a timeframe in which the tool engages with the work piece and an offset before and after machining. All sensor signals are stored in a database together with their related process parameters. Since 3456 tests are performed and 5 sensor signals per test are recorded, 17280 signals are stored in database. This database is used for the subsequent evaluation phase.

In the evaluation phase the data of interest is analysed. In this example milling forces and tool deflection is investigated for variable tilt angle and cutting speed. According to Fig. 4, the data of interest from database is selected by user defined queries. In this case a query with the following configuration is executed:

- $a_p = 0.5$ mm (Axial depth of cut)
- $a_e = 0.2$ mm (Radial depth of cut)
- $f = 0.2$ mm (Feed rate)
- $\beta_{in} = 8^\circ$ (Approach angle)
- Material: AlZnMgCu1.5

On the returned signals conditioning algorithms are applied. All force signals are conditioned by applying detrending and offset correction algorithms. The eddy current signals are not conditioned. Since the coordinate system of the force plate (PCS) and the coordinate system of the tool (TCS) are not congruent it may be necessary to transform the sensor signals geometrically in one coordinate system. The required input for the transformation is the machine tools axis position and the sensors location. For this example no geometric transformation is performed. At this point the pre-processing part of the evaluation phase is completed and the characteristic value extraction starts. As characteristic values for the cutting

forces the amplitudes and the RMS (root means square) values are calculated from the absolute value of the measured cutting force components, Eq. 1, 2, 3. The characteristic value for the tool deflection is the amplitude of the voltage, Eq. 4.

$$F_{abs}(t_i) = \sqrt{F_x^2(t_i) + F_y^2(t_i) + F_z^2(t_i)} \quad (1)$$

$$F_{amp} = \max\{F_{abs}(t_i)\} - \min\{F_{abs}(t_i)\} \quad (2)$$

$$F_{rms} = \sqrt{\frac{1}{n} \sum_{i=1}^n F_{abs}^2(t_i)} \quad (3)$$

$$U_{ec} = \max\{U(t_i)\} - \min\{U(t_i)\} \quad (4)$$

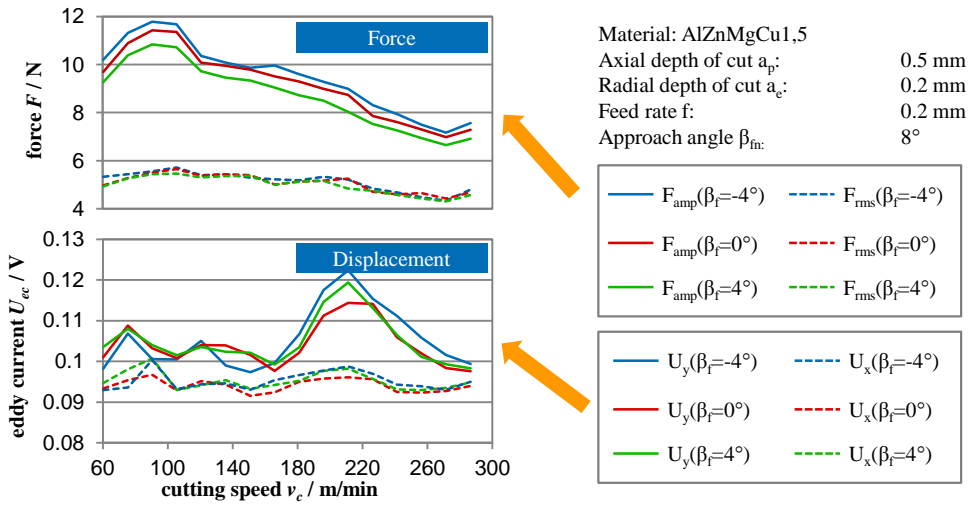


Fig.9. Characteristic values of force and displacement signals.

The results are depicted in Fig. 9. The upper diagram shows the amplitude and the RMS-values of the measured cutting forces. It can be seen that the cutting forces decrease with increasing cutting speed. An increasing tilt angle causes a cutting force reduction as well. These effects were also observed by Ozturk and Klocke [9, 10]. In the lower diagram of Fig. 9 the amplitude of the measured tool deflection is depicted. The deflection normal to the feed direction (Y-Direction in TCS) is higher than feed direction (X-Direction in TCS). In the cutting speed region $v_c = 180$ m/min to $v_c = 240$ m/min increasing deflections in normal to the feed direction is observed. This effect could be a consequence of the compliance of the spindle, tool holder and tool.

6. CONCLUSION

Optimised machining parameters are a key factor for cost and resource efficient manufacturing. In this paper a highly automated system for the generation of information about milling processes in terms of characteristic values was presented. The development of this system was driven by the demands of aerospace industry. The actions performed by the system are divided in phases: preparation, testing and evaluation. In the preparation phase the

machining parameters for machining tests are defined by using DOE methods. A set of sensors is selected for the generation of characteristic values. In the testing phase the machining tests are performed. Based on triggers, which are released by the NC code, a data acquisition system is started and stopped. Each recorded signal is stored together with their corresponding process parameters. In the evaluation phase the characteristic values are determined based on user defined calculation specifications. With this system extensive information about milling processes can be collected in a short period of time.

7. ACKNOWLEDGEMENTS

The authors would like to thank the German Research Foundation DFG for the support of the depicted research within the Cluster of Excellence "Integrative Production Technology for High-Wage Countries.

8. REFERENCES

- [1] K. North, *Wissensorientierte Unternehmensführung – Wertschöpfung durch Wissen*, Wiesbaden: Gabler, 1998.
- [2] Brecher et al., *Integrative production technology for high-wage countries*, Springer Berlin Heidelberg, 2012.
- [3] J. Gausemeier, U. Frank, H. Giese, F. Klein, A. Schmidt, D. Steffen, M. Tichy, "A design methodology for self-optimizing systems," in *Automation, Assistance and Embedded Real Time Platforms for Transportation (AAET2005)*, February 16-17, 2005.
- [4] S. Pook, J. Gausemeier, R. Dorociak, "Securing the reliability of tomorrow's systems with Self-Optimization," in *The Annual Reliability and Maintainability Symposium (RAMS 2012)*, Reno, Nevada, USA, January 23-26, 2012.
- [5] U. Thombansen et al., "Model-based self-optimization for manufacturing processes," in *Proceedings of the 17th International Conference on Concurrent Enterprising (ICE 2011)*, 2011, pp.1-9.
- [6] Auerbach et al., "Meta-modelled for manufacturing processes," in *Intelligent Robotics and Applications, Lecture Notes in Computer Science*, vol. 7102, 2011, pp 199-209.
- [7] R. K. Agarwal, "Sustainable (Green) Aviation: Challenges and Opportunities," *SAE Int. J. Aerospace*, Vol. 2, pp. 1-20, 2009.
- [8] Advisory Council for Aviation Research and Innovation in Europe: European Aeronautics, "A Vision for 2020 - Meeting society's needs and winning global leadership," Luxembourg, 2001.
- [9] E. Ozturk, L. Taner, E. Budak, "Investigation of lead and tilt angle effects in 5-axis ball-end milling processes", in *International Journal of Machine Tools & Manufacture*, vol. 49, no. 14, pp.1053-1062, 2009
- [10] F. Klocke, "Manufacturing Processes 1, Cutting" Springer Berlin Heidelberg, 2011

Performance Evaluation of Different Cooling Strategies when Machining Ti6Al4V

Salman Pervaiz^{1,2}, Ibrahim Deiab², Amir Rashid¹, Mihai Nicolescu¹ and Hossam Kishawy³

¹ Department of Production Engineering, KTH Royal Institute of Technology, Stockholm, Sweden

² Department of Mechanical Engineering, American University of Sharjah, Sharjah, UAE

³ Faculty of Engineering and Applied Sciences, University of Ontario Institute of Technology, Oshawa, Ontario, CANADA
salmanp@kth.se

ABSTRACT

Titanium alloys have replaced heavier, weaker and less serviceable engineering materials from demanding industries like aerospace, automotive, biomedical, petrochemical and power generation. High strength-to-weight ratio, high operating temperature and excellent corrosion resistance makes them suitable for challenging tasks. However their low thermal conductivity, high chemical reactivity and high strength at elevated temperature account for their poor machinability rating and short tool life. To overcome issues with poor heat dissipation generous amount of coolant is required in machining titanium alloys. Utilization of these coolants is being questioned because of their environmental and health issues. The paper presents performance evaluation of different cooling strategies when machining Ti6Al4V. The study was conducted using dry, conventional flood and a mixture of low temperature air with vegetable oil based mist cooling strategies. Each cooling strategy was examined in reference with tool life, cutting temperature and surface roughness. The study explored a combination of sub-zero temperature air and vegetable oil based mist as possible environmentally benign alternative to conventional cooling methods.

KEYWORDS: Titanium alloys, Cooling strategies, Vegetable oil mist

1. INTRODUCTION

Titanium alloys offer wide range of applications in aerospace, automotive, marine, petrochemical and biomedical sectors. Their high strength to weight ratio, extraordinary corrosion resistance and ability to operate at elevated temperatures makes them suitable for demanding engineering industries. Machinability of an engineering material is assessed by measuring tool life, material removal rate, cutting forces, power consumption, and surface roughness [1]. Titanium alloys exhibit poor machinability rating due their low thermal conductivity, high chemical reactivity at elevated temperatures and ability to maintain high hardness at elevated temperatures [2].

Metal working fluids are employed in the machining operation to enhance tool life, improve surface finish and chip removal from the cutting zone. These days metal working fluids are being questioned extensively for their economics and environmental related issues. These lubricants and coolants impose danger to environment due to their toxicity and non-biodegradability. In order to make machining process sustainable in nature, toxicity has to be reduced whereas biodegradability has to be enhanced. Near dry machining and minimum quantity lubrication (MQL) techniques are employed to encourage sustainability in machining. These techniques utilise very small amount of lubricant to reduce friction in the cutting zone. Rahim and Sasahara [3] conducted an experimental comparative study using palm oil based and synthetic ester based MQL systems. The study was performed to investigate the effectiveness of palm oil as lubricant in MQL system. The study revealed that palm oil based MQL arrangement outperformed synthetic ester based MQL system. Zeilmann and Weingaertner [4] performed drilling experiments on Ti6Al4V using uncoated and coated drills (TiAlN, CrCN and TiCN) under MQL environment. The study measured cutting temperature during drilling operation to evaluate the performance of MQL technique. The study revealed that internal MQL arrangement performed better than external MQL arrangement.

Wang et al. [5] executed orthogonal turning experiments on Ti6Al4V using dry, flood and MQL cutting environments. The study was conducted under continuous and interrupted cutting cases. The study pointed out that MQL performed better than flood cooling at higher cutting speeds due to better lubrication capacity. The study also revealed that MQL was more effective in interrupted cutting scenario. Cia et al. [6] performed end milling experiments to investigate the controlling parameters for MQL system. The study used oil flow rates of 2 ml/h – 14 ml/h for optimized value. The study revealed that diffusion wear rate was present for low oil supply rates 2ml/h – 10ml/h, however at 14ml/h no diffusion wear rate was found. Klocke et al. [7] performed machining experiments on Titanium alloys to investigate the effect of high pressurized coolant supply. The study analysed cutting tool temperature, tool wear, chip formation and cutting forces. The study pressurized the lubricant up to 300 bars (55l/min) and compared the effects with conventional flood cooling. The study revealed that 25% cutting tool temperature reduction and 50% tool wear improvement, in best case, were achieved using high pressure coolant.

Yasir et al. [8] utilized physical vapour deposition (PVD) coated cemented carbide tools to machine Ti6Al4V using MQL system. The study utilized coolant flow rates of 50 – 100 ml/h at three cutting speed levels of 120, 135 and 150 m/ min. The study revealed that mist outperformed others at the cutting speed of 135 m/min. Improved tool life was observed at 135 m/min with high flow rates. Mist was found more effective for worn tool. Su et al. [9] performed end milling machining experiments on titanium alloys to evaluate the performance of different cooling strategies by analysing the rate of tool wear. The study used dry, conventional flood, nitrogen-oil mist, compressed cold nitrogen gas (CCNG) at 0, and -10 °C, and compressed cold nitrogen gas and oil mist (CCNGOM) as the cooling strategies. The study revealed that compressed cold nitrogen gas and oil mist (CCNGOM) cooling strategy outperformed other strategies by resulting longer tool life. Yildiz et al. [10] reviewed the application methods of cryogenic coolants. The study revealed that cryogenic coolants effectively controlled the cutting temperature at cutting zone, and provided good tool life with reasonable surface finish. Sun et al. [11] evaluated the machining performance of titanium alloys by utilizing cryogenic compressed air. The study showed great potential of cryogenic compressed air cooling strategy as it reduced tool wear significantly. Bermingham et al. [12] performed machining experiments using cryogenic cooling technique. Cutting speed and material removal rate were kept constant during the study, however feed rate and depth of cut were varied to analyse cutting force. The study revealed that less heat was generated for low feed rate and high depth of cut.

In this presented study turning experiments were performed on Ti6Al4V using coated carbide tools. All of the experiments were performed using constant depth of cut under three levels of cutting speeds, feed rate and cutting environments. The study aimed to evaluate the performance of each cooling strategy by analysing surface finish, cutting temperature and tool wear.

2. EXPERIMENTAL SETUP

2.1. Workpiece Material

The workpiece material used in the turning test was $\alpha - \beta$ titanium alloy Ti-6Al-4V. Stock of Ti6Al4V material was available under ASTM B381 standard specifications, in the form of cylindrical rod. The chemical composition (wt. %) and mechanical properties of Ti6Al4V are mentioned in Table 1 and Table 2 respectively.

Table 1. Nominal chemical composition of Ti6Al4V

Element	Wt. %	Element	Wt. %
H	0.005	V	4.40
N	0.01	Al	6.15
C	0.05	Ti	Balance
Fe	0.09		

Table 2. Mechanical properties of Ti-6Al-4V at room temperature

Properties	Values	Properties	Values
Tensile strength	993 MPa	Poisson ratio	0.342
Yield strength	830 MPa	Modulus of elasticity	114 GPa
Elongation	14	Hardness (HRC)	36

2.2. Cutting Tool Material

Physical vapour deposition (PVD) coated cermet turning inserts were utilized in the experimentation work for the presented study. The specified cutting insert came with two cutting edges. Each cutting edge was used for single experimental run. Data for the cutting insert has been shown in Table 3.

Table 3. Cutting tool specifications

Sandvik Cutting Insert		ISO Code: CCMT 12 04 04 MM 1105	
Material	Cermet inserts	Nose radius	0.0157"
Rake	Positive	Coating	PVD
Relief angle	7 Degrees	Cutting direction	Neutral
Inscribed circle	1/2"	Mounting hole dia.	0.203" Screw clamp
Insert thickness	0.1875"		

2.3. Cutting Environment

The study utilized three different types of cooling strategies in order to investigate the machinability of Ti6Al4V. These cooling strategies are named as dry, conventional emulsion based flood and mixture of low temperature air with internal vegetable oil based mist (MQL+CA). Vegetable oil in MQL was operation at the flow rate of 4.6 ml/ min. The vegetable oil (ECULUBRIC E200L) was provided by ACCU-Svenska AB. The flow rate of mist was controlled by regulating the low temperature air and oil supply. The information about the vegetable oil is shown in Table 4.

Table 4. Properties of vegetable oil used in mist (ECULUBRIC E200L) [13]

Properties	Description
Chemical description	A fraction of natural triglycerides, easily biodegradable substances
Health hazard	Not hazard to human health
Flash point	325 C ⁰
Ignition point	365 C ⁰
Density (at 20 C ⁰)	0.92 g/ cm ³
Viscosity (at 20 C ⁰)	70cP
Partition coefficient	< 3%

2.4. Machining Tests and Cutting Conditions

All of the turning experiments were conducted on a CNC turning center. A Mitutoyo roughness tester SJ 201P was used for the measurement of surface finish of the generated surface. In order to add repetition in the study each machining experiments was repeated for two times. Infrared camera, UFPA – T170, was utilized to measure the temperature in cutting zone under different cooling strategies. The study was conducted using three different levels of cutting speed and feed rate as shown in Table 5. Fig. 1 shows schematic illustration of experimental set up.

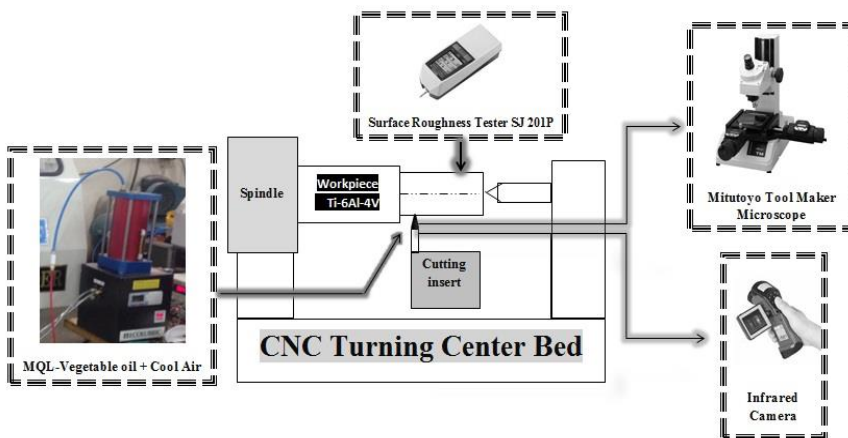


Fig.1. Schematic illustration of experimental setup

Table 5. Cutting conditions

Machining Parameters	Levels
Cutting Speed	90 – 120 – 150 m/ min
Feed rate	0.15 – 0.2 – 0.25 mm/ rev
Depth of cut	Constant 0.8 mm
Cooling strategy	Dry, Flood (flow rate@ 2 litre/ min) and Low temperature air (Sub-zero, 0 to - 4 C°) + Vegetable oil based mist (Internal) <i>MQL+CA</i> , 4 ml/ min

3. RESULTS AND DISCUSSION

3.1. Surface Roughness Analysis

Surface roughness was measured for all of the machining tests. Surface roughness defines the integrity of surface generated after machining. Surface roughness is more critical for the components manufactured from titanium alloys, because these alloys are termed as difficult to cut materials. Elevated temperatures in cutting zone, high chemical reactivity and high hardness at elevated temperatures are the main causes for low machinability rating of titanium alloys.

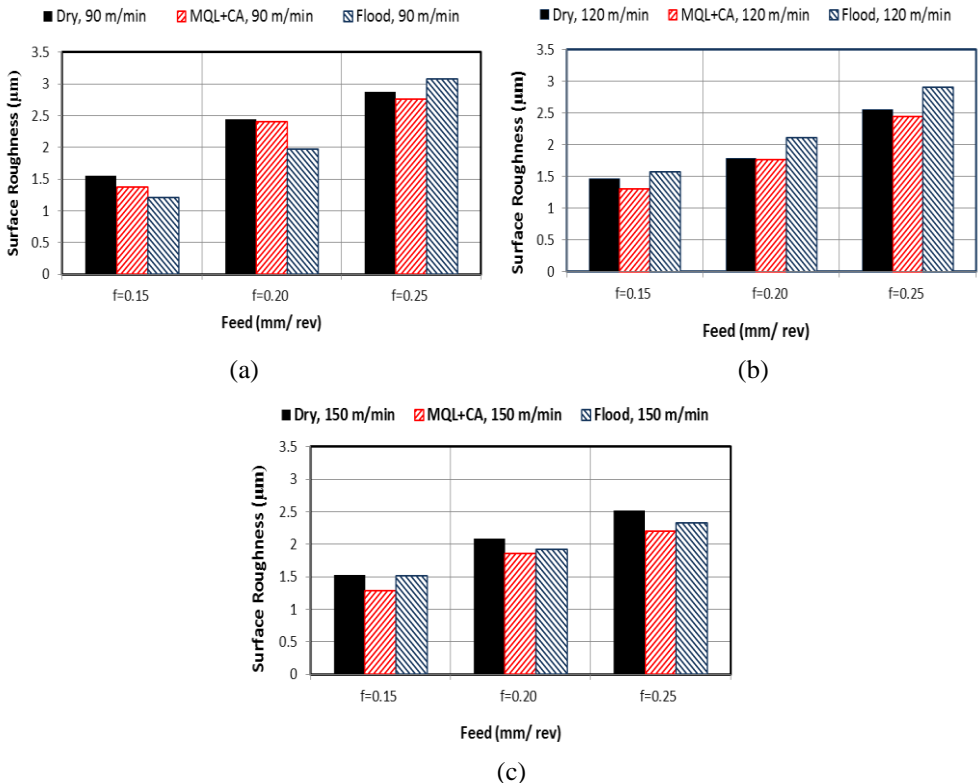


Fig.2. Surface roughness trends with respect to dry, MQL+CA, and flood cooling strategies, (a) $V_c = 90$ m/min, (b) $V_c = 120$ m/min and (c) $V_c = 150$ m/min

Fig. 2 (a) represents the surface roughness obtained for different cooling strategies at the cutting speed of 90m/ min. The dry cutting condition provided higher surface roughness at feed levels of 0.15 and 0.20 mm/ rev. At higher feed of 0.25 mm/ rev flood environment provided higher roughness. The MQL+CA based cooling strategy performed better than dry conditions at 0.15 and 0.20 mm/ rev and outclassed other strategies at higher feed of 0.25 mm/ rev. With increase of feed level surface roughness increases for all cooling strategies. Fig. 2(b) represents surface roughness trends for different cooling strategies at cutting speed of 60 m/ min. It has been observed that MQL+CA cooling strategy outperformed other cooling strategies at all three levels of feed. It was also observed that cutting speed of 60 m/ min flood environment provided the highest surface roughness at all feed levels. Seah et al. [14] also performed machining tests on steel specimen using flood cooling techniques. The study revealed that wear rate was higher for flood environment due to the shifting of crater wear near the cutting edge. This can be a possible reason for higher surface roughness in flood environment.

Fig. 2 (c) represents the plots for surface roughness for all cooling strategies at cutting speed of 150 m/ min. Fig. 2(c) also showed higher surface roughness under dry cooling strategy at all feed levels. MQL+CA strategy provided comparatively better surface roughness at all feed levels. As a general trend MQL+CA performed comparatively better at higher cutting speeds.

3.2. Tool Wear Measurement

During machining operation, cutting tool experiences loss of tool material and deformation. With the passage of time this wear increases at different locations of the cutting tool. Under the normal cutting parameters flank wear grows on the flank face and crater wear grows on the rake face. Flank tool wear is of great importance as it directly influences dimensional accuracy, topographic information and surface integrity of the generated surface. Flank tool wear evaluation is the most commonly used tool life criteria used in the metal cutting sector. In accordance with the standard ISO 3685: 1993 (E) [15], average flank wear of 0.3 mm was used in all cutting tests as tool life criteria.

Figure 3 shows the tool life observed at cutting speed of 90 m/ min for three levels of feed (0.15-0.20-0.25 mm/ rev). It was observed that MQL+CA lubrication technique out-performed dry and flood cooling at low feed of 0.15 mm/ rev as shown in Fig. 3a. However at higher feed levels MQL+CA resulted in low tool life like dry environment as shown in Figs. 3b and 3c. Figs. 3b and 3c also shows that flood cooling gave comparatively better tool life. The general trend observed in Fig. 3 shows that increase in the feed level results in less tool life. A possible explanation of this phenomenon is the low fracture toughness of cermet tools as found in agreement with literature [16]. Rapid crack formation and propagation was the reason of failure at higher feed levels. The reason of poor performance of MQL+CA at high feed rates can be the insufficient time provided to lubrication. MQL+CA cooling technique provided encouraging result at low feed rate only. At higher feed level of 0.25 mm/ rev even flood environment showed poor tool life.

Figure 4 shows the tool life observed at cutting speed of 120 m/ min for three levels of feed (0.15-0.20-0.25 mm/ rev). It has been observed that MQL+CA technique out-performed dry and flood environment at low feed level of 0.15 mm/ rev as shown in Fig. 4a. At feed level of 0.2 mm/ rev MQL+CA tool life was found little better than dry environment. Unexpectedly at higher feed level of 0.25 mm/ rev flood environment performed worst among other cooling techniques. Seah et al. [14] has also observed the negative effect of cutting fluids when machining steels. His work reveals that cutting fluid can enhance crater wear rate at the rake face. High crater wear rate weakens the cutting edge by excessive chipping. A possible explanation of low tool life under flood environment can be attributed by the presence of rapid crater wear rate and chipping at cutting edge. Performance of MQL+CA cooling technique was

reasonable. When MQL system is used alone without cool air, the oil film evaporates rapidly because of the presence of high temperature in the cutting zone. The concept of cool air was used to reduce the cutting temperature in cutting zone. The main cause of reasonable performance of MQL+CA technique is that it takes the benefit of both cool air and MQL which makes it compatible for machining Titanium alloys.

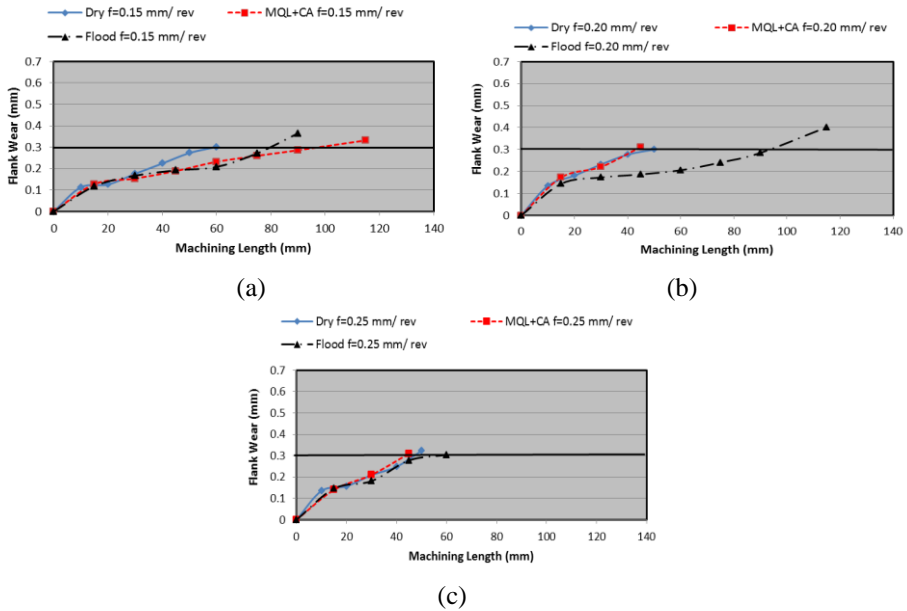


Fig.3. Flank wear for flood, dry and MQL+CA at cutting speed of 90 m/ min, (a) feed = 0.15 mm/ rev, (b) feed = 0.20 mm/ rev and (c) feed = 0.25 mm/ rev

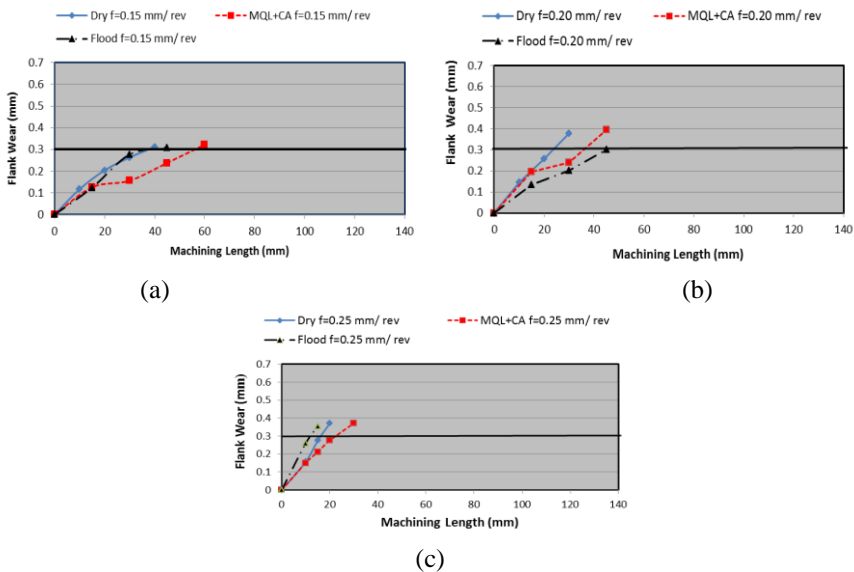


Fig.4. Flank wear for flood, dry and MQL+CA at cutting speed of 120 m/ min, (a) feed = 0.15 mm/ rev, (b) feed = 0.20 mm/ rev and (c) feed = 0.25 mm/ rev

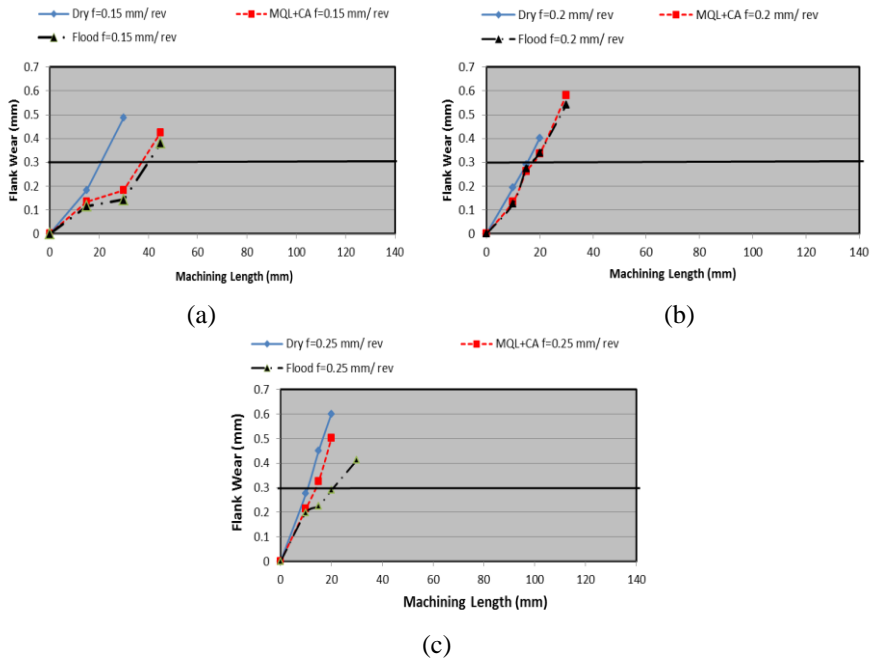


Fig.5. Flank wear for flood, dry and MQL+CA at cutting speed of 150 m/ min, (a) feed = 0.15 mm/ rev, (b) feed = 0.20 mm/ rev and (c) feed = 0.25 mm/ rev

Fig. 5 shows the tool life observed at cutting speed of 150 m/ min for three levels of feed (0.15-0.20-0.25 mm/ rev). At low feed level of 0.15 mm/ rev, MQL+CA cooling technique performed as good as flood cooling environment. At feed levels of 0.20 mm/ rev all of the cutting environments performed almost in a similar way resulting very short tool life. A general trend was observed that higher feed rate and cutting speed resulted in shorter tool life.

3.3. Cutting Temperature Analysis

Cutting temperature is an important and decisive factor towards machinability evaluation. It is a good measure to evaluate the effectiveness of a cooling strategy. Fig. 6 shows sample calculation of cutting temperature using infrared camera.

Figures 7a,7b and 7c represent plots for average values of cutting temperatures recorded under dry, MQL+CA and flood environment. It has been observed that at all levels of cutting speeds MQL+CA strategy has reduced cutting temperature. Flood cooling was found the most efficient way of heat dissipation. It was observed that MQL+CA strategy decreased average temperature by 26.6 % than the temperature obtained in dry environment at cutting speed of 90 m/ min. Similarly 17.9 % and 17.5% reduction was observed in MQL+CA strategy for cutting speeds of 120 and 150 m/ min.

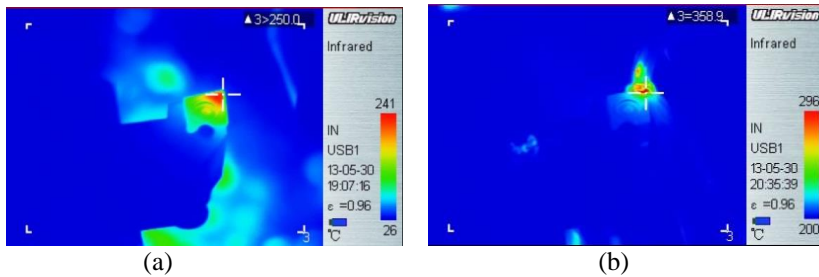


Fig.6. Sample measurements of cutting temperature under dry environment at cutting speed of 150 m/ min, (a) feed = 0.15 mm/ rev (b) feed = 0.25 mm/ rev

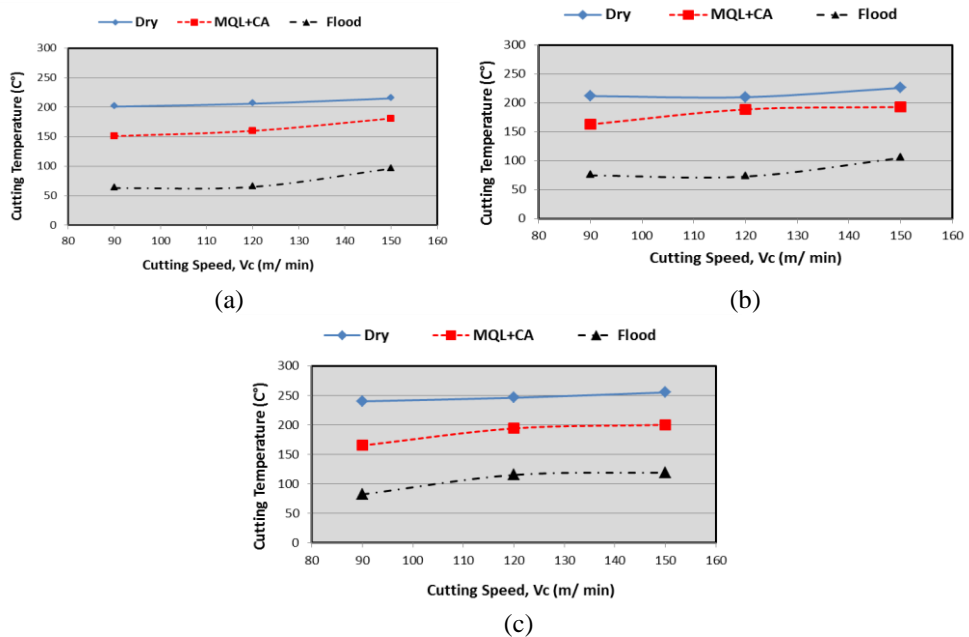


Fig.7. Cutting temperature under dry, MQL+CA and flood environment

4. CONLUCIONS

1. The conclusions drawn from the machining of Titanium alloy Ti6Al4V using coated cermet inserts are as follows; It was observed that coated cermet inserts poorly performed when machining Titanium alloy Ti6Al4V.
2. It was observed that MQL+CA cooling technique performed better than dry in almost all cases and in some conditions out performed flood environment as well. In general high temperature is present in the cutting zone during the machining of Ti6Al4V. Due to high cutting temperature, oil in MQL strategy evaporates easily without providing proper lubrication. Mixing of MQL (vegetable oil based) with cool air provides better result at cool air try to reduce temperature facilitating MQL to lubricate properly. This clearly shows potential of MQL+CA strategy as a possible replacement of flood cooling.
3. Surface roughness analysis shows that MQL+CA out-performed dry cutting in almost all cases. However, MQL+CA provided better finish than the flood environment at higher cutting speed level of 150 m/ min.

4. It has been found that MQL+CA strategy decreased average cutting temperature by 26.6%, 17.9% and 17.5% than the temperature obtained in dry environment at cutting speed levels of 90, 120 and 150 m/ min respectively.

ACKNOWLEDGMENTS

The Authors acknowledge the financial support of Emirates foundation; National Research Foundation (NRF) and Natural Sciences and Engineering Research Council (NSERC). The authors would like to thank Accu-Svenska AB for supporting the research work by providing MQL booster system.

REFERENCES

- [1] E. M. Trent and P. K. Wright, "Metal Cutting," 3rd Edition, Butterworth Heinemann, Boston, 2000.
- [2] A. R. Machado and J. Wallbank, "Machining of Titanium and Its Alloys: A Review," Proceedings of the Institution of Mechanical Engineers Part B: Management and Engineering Manufacture, vol. 204, no. 11, pp. 53-60, 2005.
- [3] E.A. Rahim and H. Sasahara, "A study of the effect of palm oil as MQL lubricant on high speed drilling of titanium alloys," Tribology International 44, pp. 309–317, 2011.
- [4] R. P. Zeilmann, W. L. Weingaertner, "Analysis of temperature during drilling of Ti6Al4V with minimal quantity of lubrication," Journal of Material Processing Technology, Vol. 179, pp. 124–7, 2006.
- [5] Z. G. Wang, M. Rahman, Y. S. Wong, K. S. Neo, J. Sun, C. H. Tan, H. Onozuka, "Study on orthogonal turning of titanium alloys with different coolant supply strategies," International Journal of Advanced Manufacturing Technology, Vol. 42, pp.621–632, 2009.
- [6] X. J. Cai, Z. Q. Liu, M. Chen and Q. L. An, "An experimental investigation on effects of minimum quantity lubrication oil supply rate in high-speed," Proceedings of the Institution of Mechanical Engineers, Part B: Journal of Engineering Manufacture, Vol. 226(11), pp. 1784–1792, 2012.
- [7] F. Klocke, H. Sangermann, A. Kramer, and D. Lung, "Influence of a High-Pressure Lubricoolant Supply on Thermo-Mechanical Tool Load and Tool Wear Behaviour in the Turning of Aerospace Materials," Proceedings of the Institution of Mechanical Engineers, Part B: Journal of Engineering Manufacture, Vol. 225, 52, 2011.
- [8] M.S.A. Yasir, C.H. Che Hassan, A.G. Jaharah, H.E. Nagi, B. Yanuar, A.I. Ghusri, "Machinability of Ti6Al4V under dry and near dry condition using carbide tools," The Open Industrial and Manufacturing Engineering Journal, Vol. 2, pp.1-9, 2009.
- [9] Y. Su, N. He, L. Li, X. L. Li, "An experimental investigation of effects of cooling/lubrication conditions on tool wear in high-speed end milling of Ti-6Al-4V," Wear , Vol. 261, pp. 760-766, 2006.
- [10] Y. Yildiz, M. Nalbant, "A review of cryogenic cooling in machining processes," International Journal of Machine Tools & Manufacture, Vol. 48, pp. 947–964, 2008.
- [11] S. Sun, M. Brandt, M.S. Dargusch, "Machining Ti–6Al–4V alloy with cryogenic compressed air cooling," International Journal of Machine Tools & Manufacture, Vol. 50, pp. 933–942, 2010.
- [12] M.J. Bermingham, J. Kirsch, S. Sun, S. Palanisamy, M. S. Dargusch, "New observations on tool life, cutting forces and chip morphology in cryogenic machining Ti-6Al-4V," International Journal of Machine Tools & Manufacture, Vol. 51, pp. 500–511, 2011.
- [13] ECULUBRIC E200L , Material Safety Data Sheet, Retrived on 25 June 2013 from the source <http://www.accu-svenska.se/wp-content/uploads/2012/04/ECULUBRIC-E200L-CAS-8002-13-9-eng.pdf>
- [14] K.H.W. Seah, X. Li, and K.S. Lee, "The effect of applying coolant on tool wear in metal machining," Journal of Material Processing and Technology, Vol 48, pp. 495 -501, 1995.
- [15] ISO 3685, Tool life testing with single-point turning tools, ISO Standard, 3685 (1993) (E).
- [16] A. A. Khan and S. S. Hajjaj , "Capabilities of Cermets Tools for High Speed Machining of Austenitic Stainless Steel," Journal of Applied Sciences, Vol. 6, pp.779-784, 2006.

3D FEM Simulation of Titanium Machining

P. Nieslony¹, W. Grzesik¹, R. Chudy¹, P. Laskowski², W. Habrat³

¹ Opole University of Technology, 76 Proszkowska str., 45-758 Opole, Poland,

² WSK PZL Rzeszów, 120 Hetmańska str., 35-078 Rzeszów, Poland,

³ Rzeszów University of Technology, 12 Powstańców Warszawy str., 35-959 Rzeszów, Poland

p.nieslony@po.opole.pl

ABSTRACT

The simulations/predictions include cutting forces, cutting temperature, plastic deformation in the cutting zone and chip formation. The CAD model of cutting inserts and measured values of the mechanical properties of a α - β titanium alloy were used in order to improve the prediction accuracy. The results obtained by means of 2D and 3D FEM modeling are compared and discussed.

KEYWORDS: FEM modelling, Titanium alloy, Constitutive material models

1. CONSTITUTIVE MATERIAL MODELS IN FEM SIMULATION

Modelling of the machining process in terms of multi-criteria optimization is currently developed in order to support the implementation of new technological chains into the production. At present, the FEM based simulation is a basic engineering tool to solve successfully this problem. However, a universal FEM model which will cover a wide spectrum of both the workpiece and cutting tool materials should be developed [1-3]. In particular, more accurate and complete constitutive material models which consider the appropriate mechanical thermophysical properties of both the workpiece and tool materials are needed [1-5].

The success in developing the constitutive models depends on solving the following important problems:

- Definition of mechanical properties of the workpiece material under real cutting conditions,
- Specification of the thermophysical properties of the workpiece and cutting tool materials also with deposited thin layered coatings [3,6,7],
- Quantification of friction in the cutting zone [8,9],
- Chip segmentation in machining [1,10].

The determination of the appropriate parameters of the constitutive material model requires numerous experimental tests and analyses. Recently, reverse solutions have also been proposed [2]. Moreover, the FEM constitutive model should meet the High Speed Cutting (HSC) and High Performance Cutting (HPC) demands which requires the implementation of high strain rate tests. In addition, it should cover a wide spectrum of cutting tool materials including multilayer coated and composite tools.

Taking into consideration all these facts, the paper is, in general, focused on the influence of the constitutive models of the workpiece material on the results and simulation accuracy when performing 2D orthogonal and 3D turning operations using TiAlN coated carbide tools with plane and grooved rake faces to machine a Ti-6Al-4V alloy.

2. METHODOLOGY OF INVESTIGATIONS

In these investigations FEM simulations were performed for two fundamental constitutive models including Power Law and J-C models.

Standard Power Law (PL) constitutive model, is mathematically expressed by the power equation, as follows

$$\sigma_f(\varepsilon_p) = \sigma_o \Theta(T) \left(1 + \frac{\varepsilon_p}{\varepsilon_p^0} \right)^{1/n} \quad (1)$$

where σ_o is the initial yield stress, ε_p is the plastic strain, ε_p^0 is the reference plastic strain, $1/n$ is the strain hardening exponent and $\Theta(T)$ is thermal softening index defined as a function of temperature according to (2). In equation (2) the c_0 through c_5 are coefficients for the polynomial fit, T is the temperature, T_{cut} is the linear cut off temperature, and T_{melt} is the melting temperature. The equation (2a) is defined for $T < T_{cut}$, where equation (2b) for $T \geq T_{cut}$.

$$\Theta(T) = c_0 + c_1 T + c_2 T^2 + c_3 T^3 + c_4 T^4 + c_5 T^5 \quad (2a)$$

$$\Theta(T) = \Theta(T_{cut}) \left(1 - \frac{T - T_{cut}}{T_{melt} - T_{cut}} \right) \quad (2b)$$

The Johnson-Cook (J-C) is defined by means of Eqn. (3):

$$\sigma_{eq} = \left(A + B \varepsilon_p^n \right) \left(1 + C \ln \left(\frac{\varepsilon_p}{\varepsilon_p^0} \right) \right) \left(1 - \left(\frac{T - T_o}{T_m - T_o} \right)^m \right) \quad (3)$$

In the Johnson-Cook constitutive model as given in Eq. (3), the model describes the flow stress as the product of strain, strain rate and temperature effects; i.e. work hardening, strain-rate hardening, and thermal softening. In Eq. (3) the parameter A is the initial yield strength of the material at room temperature. The equivalent plastic strain rate $\dot{\varepsilon}_p$ is normalized with a reference strain rate $\dot{\varepsilon}_p^0$. T_o is room temperature, and T_m is the melting temperature of the

material, and they are constants. While the parameter n takes into account the strain hardening effect, the parameter m models the thermal softening effect, and C represents strain rate sensitivity. The Johnson-Cook model is a well-accepted and numerically robust constitutive material model and highly utilized in modeling and simulation studies. The Johnson-Cook (J-C) model assumes that the slope of the flow stress curve is independently affected by strain hardening, strain rate sensitivity and thermal softening behaviors. Each of these sets is represented by the brackets in the constitutive equation [9].

Relevant parameters in the PL model were selected from the material data base of AdvantEdge FEM package for a Ti-6Al-4V alloy and the substrate (ISO P20) and TiAlN coating.

In the second step the J-C model was defined only for a titanium alloy. It should be noted that a range of models with different parameters can be found for a Ti-6Al-4V in the literature. For instance, in Table 1 a set of model parameters is specified after Calamaz et al. [11], which was coded by J-C1.

Table 1. Johnson–Cook material model parameters for Ti-6Al-4V [11].

Code	A, MPa	B, MPa	n	C	m
J-C1	968	380	0.421	0.0197	0.577

Melting temperature for the Ti-6Al-4V titanium alloy is present in the literature in the range of 1660 °C [9] to 1655 °C [12]. The Young modulus was fixed at 110 GPa, the Poisson ratio at 0.3, and the density at 4430 kg m⁻³.

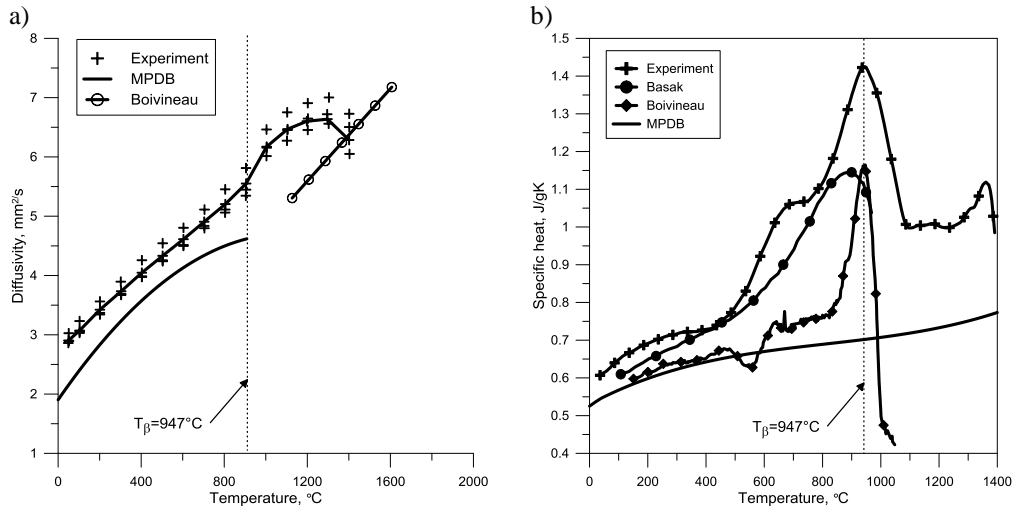


Fig.1. Thermal diffusivity (a) and specific heat (b) of Ti-6Al-4V versus temperature created for experimental and literature data [12, 13].

Moreover, own input data available in MPDB data base were implemented into the J-C model. They concern the measured values of the thermophysical properties of the titanium alloy machined, and particularly the diffusivity (Fig. 1a) and specific heat (Fig. 1b) [13]. In contrast, this part of simulations was coded by J-C2.

It can be noted in Figs. 1a and 1b that that differences between literature and experimental data are not distinct for the temperature lower then 700° . Moreover, the trend is similar for data provided by other authors [12]. However, substantial differences begin when temperature exceeds the α - β phase transformation. It is evident that for this temperature range the constitutive models should be modified, in general, in terms of changes of the specific heat as shown in Fig. 1b. The simulation conditions are specified in Table 2.

Table 2. Configurations of numerical simulations.

Cutting condition		Tool				
$v_c=80$ m/min, $a_p=0.125$ and 2 mm, $f=0.125$ and 0.1 mm/rev		Flat and grooved tool (KM) Sintered carbide insert H10 coated with TiAlN (0.003 mm) Cutting edge radius: flat rake face $r_n=20$ μ m, grooved $r_n=50$ μ m Stereometry: Orthogonal (2D) tool angle – rake -5° , relief 5° 3D tool angle – back rake -4.55° , side rake -5.41° , lead -5.0°				
Constitutive material models	AdvantEdge basic model (PL)	J-C model (J-C1)		J-C model with defined thermophysical workpiece material properties (J-C2)		
Simulation	2D	3D	2D	3D	2D	3D
Flat insert	X	-	X	-	X	-
KM insert	-	X	X	X	X	X

As mentioned above, the FEM simulations were performed for both flat and grooved rake faces. In the second case CNMG 120412-UP cutting tool inserts produced by Kennametal were used [14].

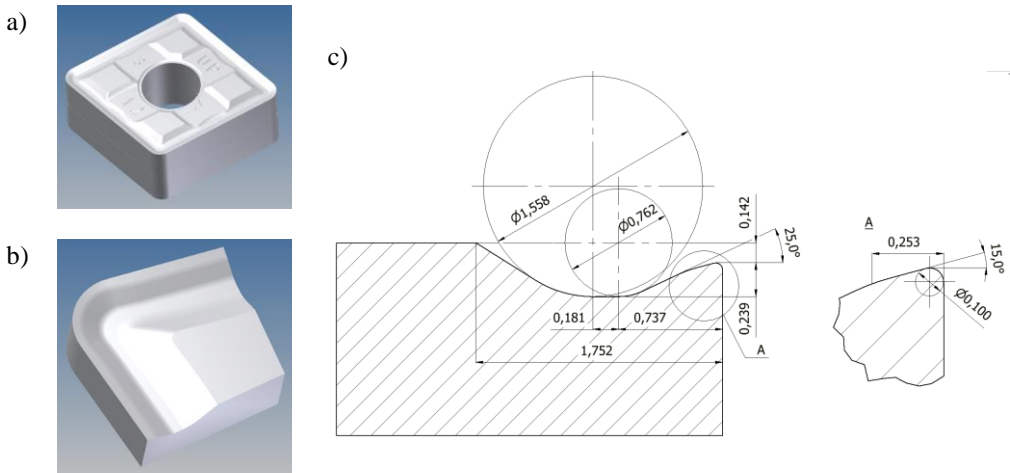


Fig.2. CAD model of Kennametal cutting insert type CNMG 120412-UP (a), the model of tool edge used in FEM simulation (b) and dimensioned cross-section of the tool model (c).

3D simulations were performed using only grooved cutting tool inserts denoted by symbol KM. The measured value of the cutting edge radius for CNMG 120412-UP insert coated by TiAlN monolayer was equal to $r_n=50$ μ m. On the other hand, for inserts with flat

rake face $r_n=20\text{ }\mu\text{m}$. 3D CAD model of the grooved cutting insert (a) and magnified corner area (b) along with dimensioned groove and cutting edge are presented In Fig. 2.

3. SIMULATION RESULTS

The simulated results of the average cutting temperature for the constitutive models considered and the wedge shapes used are presented in Fig. 3. It is evident in Fig. 3 that for both 2D and 3D cases the highest temperature of 854°C was determined for the PL AdvantEdge model denoted as the PL bar. The difference between 2D and 3D predictions was equal to 30°C and 80°C for the depth of cut of $a_p=2\text{mm}$ and $a_p=0.125\text{mm}$ respectively. This fact was not revealed for other simulations performed. On the other hand, another trend indicates substantial differences in the cutting temperature resulting from 2D and 3D predictions but for higher depths of cut. For example, for the KM J-C1 variant this difference was about 100°C when for $a_p=0.125\text{mm}$ the temperatures were comparable.

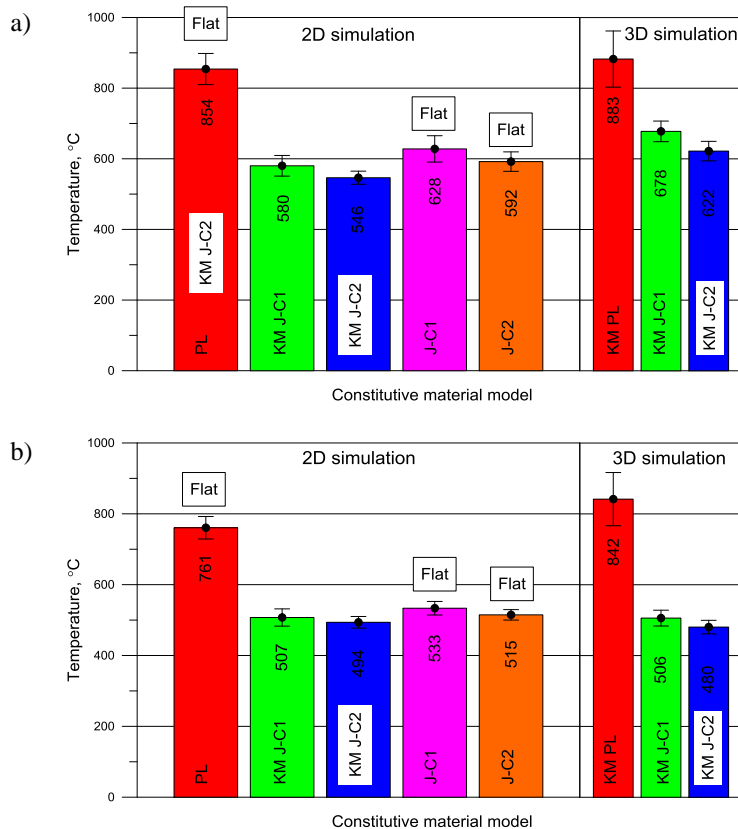


Fig.3. Comparison of mean cutting temperature for different constitutive model parameters for (a) $v_c=80\text{ m/min}$, $a_p=2\text{ mm}$, $f=0.1\text{ mm/rev}$ and (b) $v_c=80\text{ m/min}$, $a_p=0.125\text{ mm}$, $f=0.05\text{ mm/rev}$.

In general, the obtained values of the cutting temperature do not exceed the temperature of α - β phase transformation equal to 947°C . However, lower cutting temperatures were predicted by the J-C model. It is worth noticing that the temperature changes resulting from

the implementation of measured thermal properties of the machined titanium alloy are not distinct. Exemplarily, for 3D simulations with $a_p=2\text{ mm}$ and $f=0.1\text{ mm/rev}$ it is about 55°C .

The influence of cutting wedge configuration on the cutting temperature was evaluated based on 2D simulation. This comparison indicates that the higher temperature was generated when machining with flat rake face but the difference is not higher than 50°C . It can be mentioned that the dominant factor which controls the material deformation and heat generation in the cutting zone is the effective rake angle. For the grooved cutting inserts the tool-chip contact is concentrated in the vicinity of the cutting edge and in relation to its length the effective rake angle is equal to 10° or 20° . This indicates that the positive rake geometry will facilitate the deformation and decohesion processes and, as a result, will reduce the heat amount.

The mechanical aspects of cutting a 6-4 titanium alloy with TiAlN coated cutting tool inserts were characterized by the components of resultant cutting force as shown in Fig. 4. In this case study, both flat and grooved inserts were considered in 2D and 3D FEM simulations.

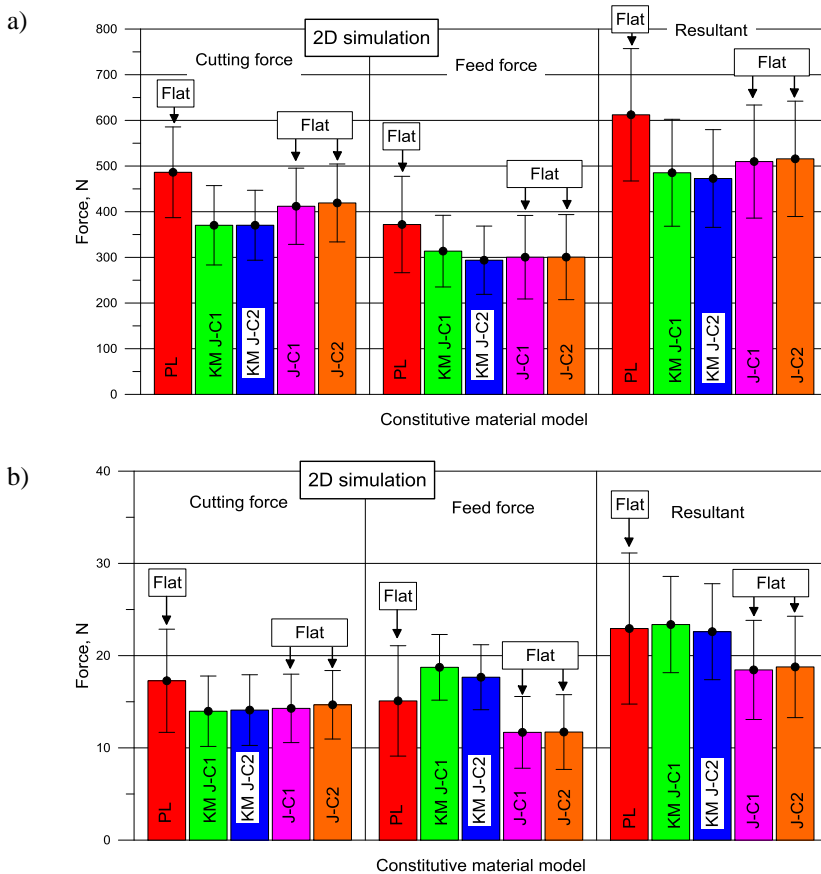


Fig.4. Comparison of force mean components for 2D simulation and different constitutive model parameters for (a) $v_c=80\text{ m/min}$, $a_p=2\text{ mm}$, $f=0.1\text{ mm/rev}$ and (b) $v_c=80\text{ m/min}$, $a_p=0.125\text{ mm}$, $f=0.05\text{ mm/rev}$.

The main focus was on the influence of the constitutive model type and model parameters on the values of the cutting and feed forces. As previously, for 2D simulations the effects of flat and grooved tools were determined.

Fig. 4 presents the values of the cutting F_c and feed F_f forces as well as the resultant cutting force obtained by 2D FEM simulation. It is evident that the force resolution depends on the constitutive model applied. In general, higher forces were predicted for the PL model. It can be noted that the same simulation conditions were kept for flat cutting inserts (cases J-C1 and J-C2).

When using grooved cutting inserts with the shape defined in Fig. 2c, the force resolution is distinctly different especially for $a_p=0.125\text{mm}$ and $f=0.05\text{ mm/rev}$. This fact can be related to the changes of wedge geometry close to the cutting edge. In particular, for small depths of cut the effective rake angle severely influences the value of feed force. It is interesting to note that the comparable value of the resultant cutting force were obtained for the PL and both KM-J-C1 and KM J-C2 models (see Fig.4b). In addition, it was observed that the modification of thermophysical properties of Ti-6Al-4V (KM J-C2 and J-C2 models) did not influence the cutting forces. On the other hand, the force signals were recorded with relatively broad scatters, which were about $\pm 30\%$ independently of the constitutive model use.

Figs. 5 and 6 present the 3D image of cutting simulations using grooved cutting tool inserts. It can be seen there that higher values of the reduced stress σ_H were recorded for the PL material model (Figs.5a and 6a). They approach 1100 MPa and are localized along the active part of the cutting edge. For J-C1 and J-C2 models the maximum values of σ_H stress were not higher than 850 MPa, as shown in Figs.5 and 6 – b and c.

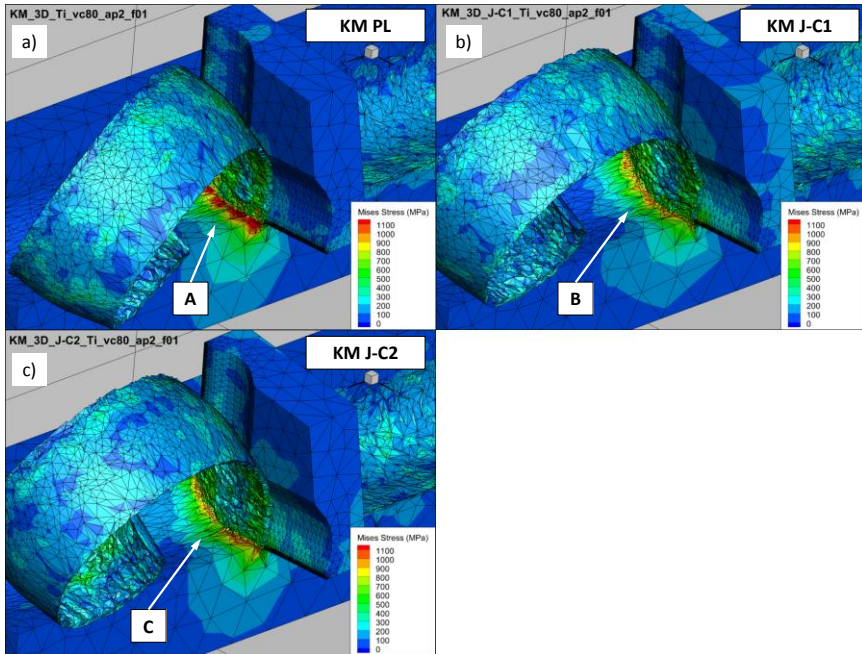


Fig.5. Mises stress 3D maps for different constitutive model parameters and $v_c=80\text{ m/min}$, $a_p=2\text{ mm}$, $f=0.1\text{ mm/rev}$

The third observation was that the constitutive model influence the chip formation and chip type produced. When machining with the minimum depth of cut, the ribbon chip was formed when the PL model was used (Fig. 6a), whereas the helical (tangle) chip was produced when the J-C was implemented into FEM package (Fig. 6b and c). In fact, helical, especially washer and snarled helical chips are typically produced in titanium machining.

Helical washer chips were observed for small depth of cut and small feed rate. On the other hand, the ribbon snarled chips are predominantly occurred for higher values of cutting conditions.

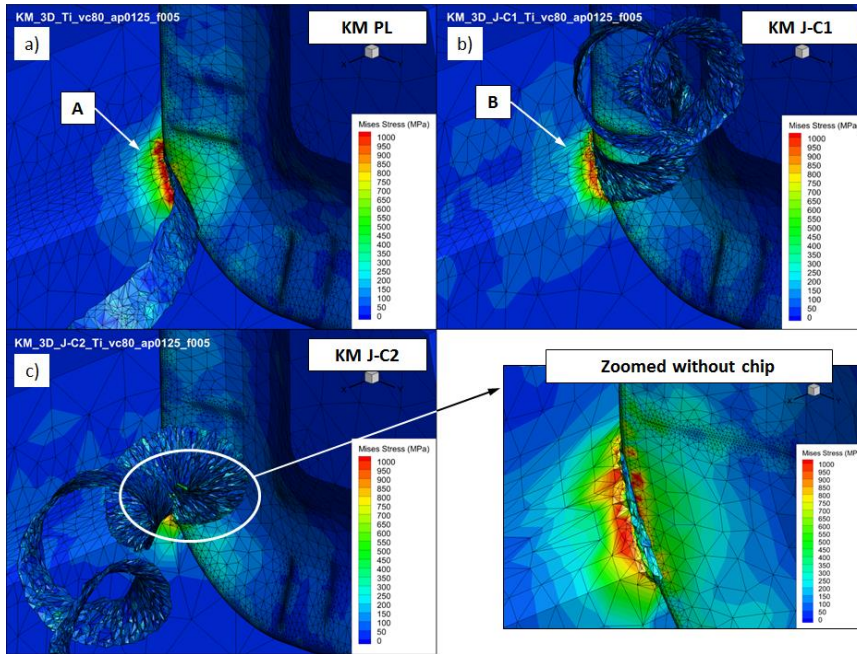


Fig.6. Mises stress 3D maps for different constitutive model parameters and $v_c=80$ m/min, $a_p=0.125$ mm, $f=0.05$ mm/rev

The analysis of the distribution of strain rate $\dot{\epsilon}$ was done for 3D simulation using a slice technique as show in Figs. 7 and 8. The cross-sectional plane was parallel to the cutting velocity vector and perpendicular to the XZ plane (the front of the workpiece bullet) on the depth equal to half depth of cut.

It was revealed that the highest strain rates correspond to finish machining operations with $a_p=0.125$ mm and $f=0.05$ mm/rev. In such cases, severe plastic deformations are most probable. Moreover, the implementation of measured thermophysical properties (c_p , λ) results in visual intensification of plastic deformation and expansion of areas with maximum strain rates $\dot{\epsilon}$ as shown in Figs. 7c and 8c.

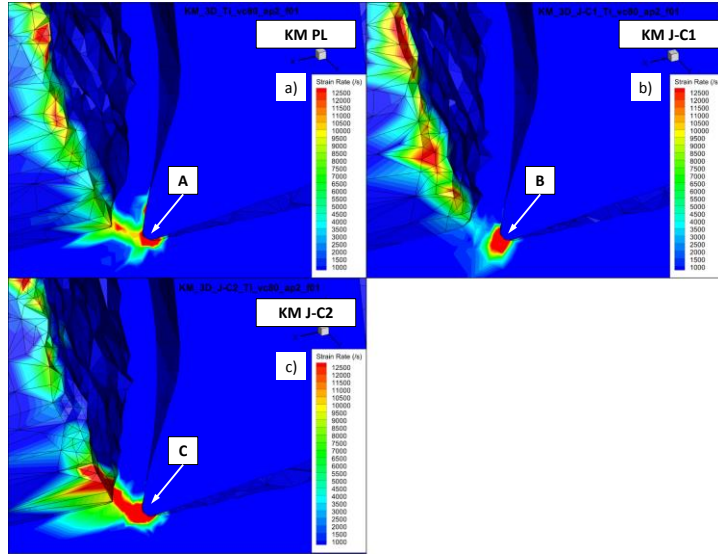


Fig.7. Slices of strain rate 3D maps for different constitutive model parameters and $v_c=80$ m/min, $a_p=2$ mm, $f=0.1$ mm/rev

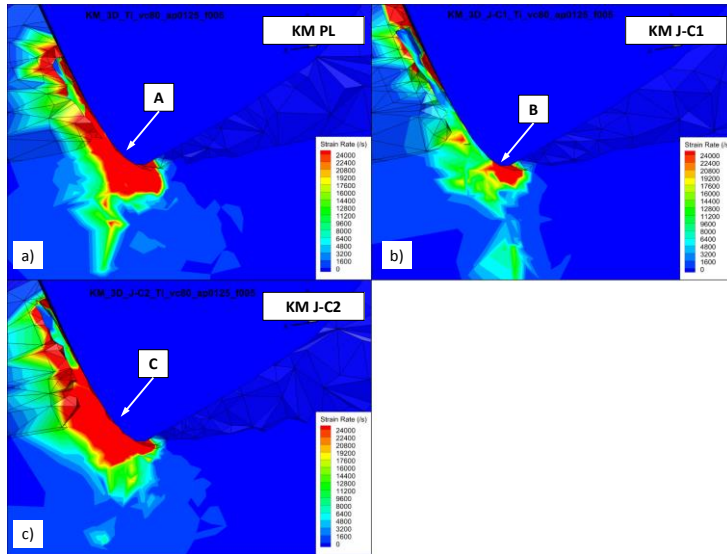


Fig.8. Slices of strain rate 3D maps for different constitutive model parameters and $v_c=80$ m/min, $a_p=0.125$ mm, $f=0.05$ mm/rev

4. CONCLUSION

Based on the experimental results and FEM predictions the conclusions are as follows:

- The power model results in the prediction of higher cutting temperature, forces and stresses in relation to the classical J-C model.

- The implementation of the temperature-dependent thermophysical properties of the workpiece material in the J-C2 model causes that the predicted cutting temperature changes. Its value decreases in comparison to the basic J-C1 model.
- The cutting forces do not change when considering models with constant and temperature-dependent thermophysical properties of a Ti-6Al-4V alloy.
- The constitutive model influenced the chip formation and chip type when 3D simulation was run.
- The maximum strain rate was determined for small depths of cut which can be related to the intensification of plastic deformation and its concentration in the smallest area. This fact correlates with the phenomenon of size effect [15].

ACKNOWLEDGEMENTS

The authors would like to acknowledge, that this research has been carried out as part of a project funded by the Polish National Center for research and Development. Project No. PBS1-178595.

REFERENCES

- [1] F. Ducobu, E. Rivière-Lorphèvre, E. Filippi, "Influence of the Material Behavior Law and Damage Value on the Results of an Orthogonal Cutting Finite Element Model of Ti6Al4V," *Procedia CIRP*, pp. 378 – 383, 2013.
- [2] F. Klocke, D. Lung, S. Buchkremer, "Inverse Identification of the Constitutive Equation of Inconel 718 and AISI 1045 from FE Machining Simulations," *Procedia CIRP*, pp. 211 – 216, 2013.
- [3] P. Nieslony, W. Grzesik, P. Laskowski, W. Habrat, "FEM-Based Modelling of the Influence of Thermophysical Properties of Work and Cutting Tool Materials on the Process Performance," *Procedia CIRP*, pp. 3-8, 2013.
- [4] Y. Chen, C. Bunget, L. Mears, T. R. Kurfess, "An Improved Empirical Constitutive Model for γ -Strengthened Nickel-Based Superalloys," *Proceedings of NAMRI/SME*, vol. 41, 2013.
- [5] P. Nieslony, W. Grzesik, "Sensitivity Analysis of the Constitutive Models in FEM-Based Simulation of the Cutting Process," *J. Machine Engineering*, vol. 13, np. 1, pp. 106-116, 2013.
- [6] T.H.C. Childs, "Numerical Experiments on the Influence of Material and Other Variables on Plane Strain Continuous Chip Formation in Metal Machining," *Int. J Mechanical Sciences*, vol. 48, pp. 307–322, 2006.
- [7] P. Nieslony, "FEM Modelling of Thermal Influences in Turning for Defined Thermophysical Properties of Cutting Tool Materials (in Polish)," in *School of Metal Cutting SOS5*, Opole, Poland, 2011, pp. 210-217.
- [8] C. Courbon, T. Mabrouki, J. Rech, et al, , "New Thermal Issues on the Modelling of Tool-Workpiece Interaction: Application to Dry Cutting of AISI 1045 steel," *Advanced Materials Research*, vol. 223, pp. 286-295, 2011.
- [9] T. Özel, Y. Karpat, "Identification of Constitutive Material Model Parameters for High-Strain Rate Metal Cutting Conditions Using Evolutionary Computational Algorithms," *Materials and Manufacturing Processes*, vol. 22, no. 5, pp. 659-667, 2007.
- [10] A. Chandra, P. Karra, J. Wang, G.Y. Kim, "Chip Segmentation in Machining: A Study of Deformation Localization Characteristics in Ti6Al4V," in *Proceedings of the ASME MSEC 2013*.
- [11] M. Calamaz, D. Coupard, F. Girod, "A new material model for 2D numerical simulation of serrated chip formation when machining titanium alloy Ti–6Al–4V," *Int. J. Machine Tools & Manufacture*, vol. 48, pp. 275–288, 2008.
- [12] M Boivineau et al, "Thermophysical properties of solid and liquid Ti-6Al-4V (TA6V) alloy," *Int. J. Thermophys*, vol. 27, pp. 507–529, 2006.
- [13] *Material Properties Database*, MPDB v. 7.51, JAHM Software, Inc. 2013.
- [14] *Kennametal* (2013, May 15), Available: <http://www.kennametal.com>.
- [15] M. C. Shaw, "Shear stress in cutting" in *Fundamentals of Metal Cutting*, Oxford: Oxford University Press, 1989, pp. 183-201.

Multi-performance Optimization in Turning of Stainless Steels using Taguchi-VIKOR-Meta-heuristic Concept

Rastee D. Koyee^a, Siegfried Schmauder^b, R. Eisseler^a

^aIfW, University of Stuttgart, Holzgartenstr.17, D-70174 Stuttgart, Germany.

^bIMWF, University of Stuttgart, Pfaffenwaldring 32, D-70569 Stuttgart, Germany.

email: rastee.ali@ifw.uni-stuttgart.de

ABSTRACT

This study experimentally addresses the multi-performance optimization of turning super duplex EN 1.4410, standard duplex EN 1.4462 and austenitic EN 1.4404 stainless steels utilizing coupled Taguchi-based designs, multiple attribute decision making (MADM) and meta-heuristic algorithms. Surface roughness, specific cutting energy, cutting power and resultant cutting forces are optimized per each material under Taguchi optimization procedure and combined as a single, cutting parameter dependent multi-performance characteristics index (MPCI) using VIKOR method. Analysis of means (ANOM) and Analysis of variance (ANOVA) are employed to designate the optimum level of cutting parameters and to investigate the influence of cutting parameters and their interactions on the computed index respectively. Finally, nature-inspired meta-heuristic algorithms like; Firefly Algorithm (FA), Accelerated Particle Swarm Optimization (APSO) and Cuckoo Search (CS) are used to constrainedly optimize the developed MPCI and find the exact setting of optimum cutting parameter.

KEYWORDS: Austenite and duplex stainless steel; Taguchi method; VIKOR method; Meta-heuristic algorithms

1. INTRODUCTION

Machining is a general term describing a group of processes that consist of the removal of material and modification of the surfaces of a workpiece after it has been produced by various methods. The term machinability is often used to describe the easiness of which the work material machined under a specific set of cutting conditions. The ease of machining of different materials can be compared in terms of the value of tool life, cutting forces or surface finish under similar cutting conditions. Other criteria, example: ease of chip disposal, cutting temperature, operator safety, etc., can also be employed [1]. Stainless steels are considered to be difficult to machine due to their high tensile strength, high ductility, high work hardening rate, low thermal conductivity and abrasive character. Ferritic steels are generally more machinable and their machinability decrease with increasing chromium content. The machinability of martensitic stainless steels is influenced by carbon content, nickel content and metallurgical structure in such away higher contents of carbon and nickel reduce machinability. Austenitic stainless steels are typically more difficult to machine than ferritic and martensitic stainless steels. Duplex alloys have chemistry similar to austenitic steels but are generally harder to machine due higher yield strength, stronger and more abrasive produced chips to tooling and lower sulfur content [2].

According to the International Stainless Steel Forum (ISSF), the production of stainless steels has obtained a huge momentum since 2000, due to the enormous growth potential of emerging countries, unmatched sustainability of stainless steels compared to other materials and overcapacity catching up and restructuring measures of industries nowadays [3]. As the production and application of stainless steels expands the opportunity of machining is expected to rise. Over the last several years, the machining of stainless steels has been analyzed by researchers; Liew et. al reported the wear of various grades of polycrystalline cubic boron nitride (PCBN) tool in ultra-precision machining of STAVAX (modified AISI 420 stainless steel) at low speeds [4]. Chien et. al developed a predictive model for the prediction of tool flank wear and an optimization model for the determination of optimum cutting conditions in machining 17-4PH stainless steel [5]. Korkut et. al determined the optimum cutting speed when turning an AISI 304 austenitic stainless steel using cemented carbide cutting tools [6]. Kumara et. al conducted machining studies on hardened martensitic stainless steel (HRC 60) to analyze the effect of tool wear on tool life of alumina ceramic cutting tools [7]. Gaitonda et. al presented the application of Taguchi based membership functions for simultaneous minimization of burr height and burr thickness when drilling austenitic stainless steel of grade AISI 316L [8]. Kaladhar et. al optimized the machining parameters in turning AISI 202 austenitic stainless steel using CVD coated cemented carbide tools [9]. Ahmadi et. al concentrated on the machining of PH-hardened duplex stainless steel to analyze the effect of tool wear on the tool life of the ceramic cutting tool with alumina base [10]. Saravanan et. al carried out experimental investigation to identify the optimal machining parameters for micromachining of super duplex stainless steel using electrochemical machining [11].

A search with the keywords ‘stainless steel’ in popular database such as Science Citation Index-Expand or Scopus would reveal thousands of recent publications. This is a vivid testimony to the potential interest on stainless steels as a key research topic by various researchers in the world [12]. However, one can hardly find a scientific article which addresses a comparative machining optimization that employs different grades of stainless steels, considers different performance characteristics and uses different meta-heuristic optimization techniques. Therefore, the objective of this research is to examine the machinability of different grades of stainless steels in seeking simultaneous improvement in performance characteristics using different statistical and mathematical tools. The flow chart of the methodology presented in this paper is shown in Fig. 1.

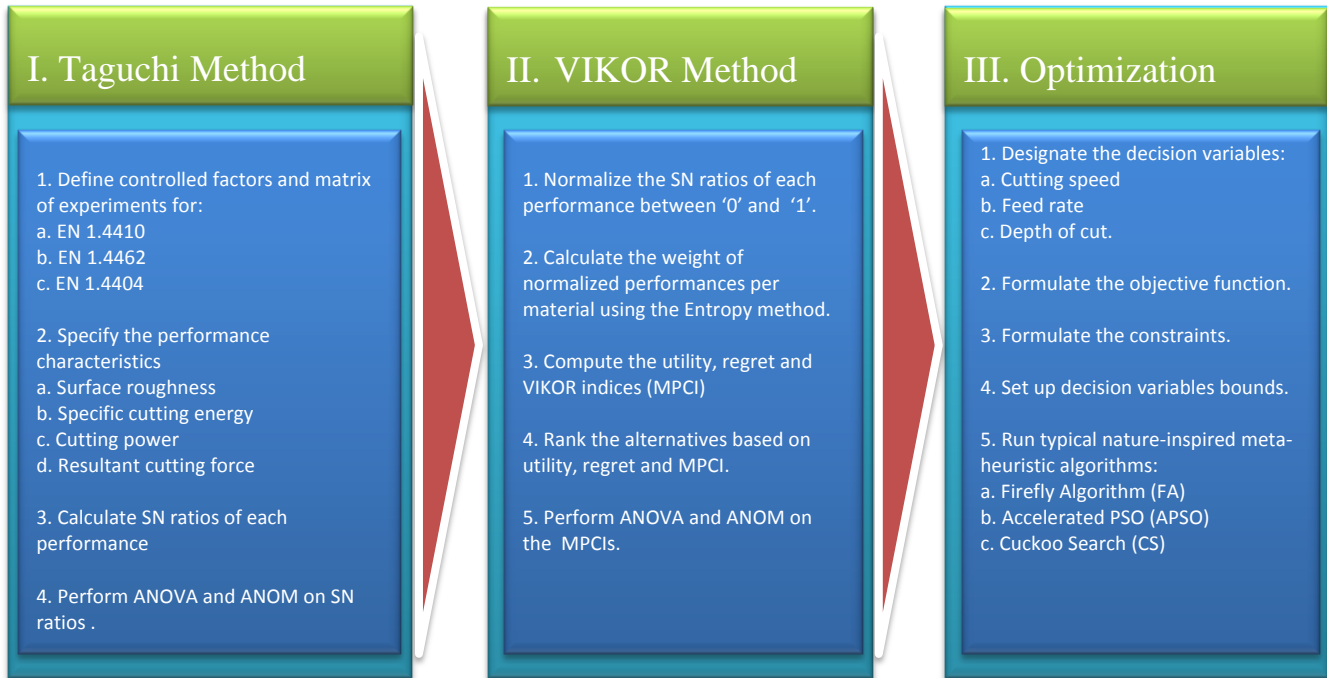


Fig. 1. The flow chart of the methodology

The signal to noise (SN) ratios of performance characteristics are normalized and unified into a single characteristic index using VIKOR method. Analysis of means ANOM and Analysis of variance ANOVA are employed to designate the optimum level of cutting parameters and to investigate the influence of each of cutting parameters on the computed SN ratios and VIKOR indices. Finally, in order to select a meta-heuristics algorithm which could fit the problem the best, constrained meta-heuristic algorithms like Firefly Algorithm (FA), Accelerated Particle Swarm Optimization (APSO) and Cuckoo Search (CS) are simultaneously adopted to find the exact optimum machining condition.

2. MATERIALS AND METHODS

In order to systematically approach the variance in controllable input factors and to observe the effect of these factors and their interactions on the output performance parameters, an $L_{25}(5^3)$ orthogonal array proposed by Taguchi is used in the present experimental procedure per each workpiece material. The control factors are the three known cutting parameters which are cutting speed (v_c), feed rate (f) and depth of cut (a_p). Factors and their levels are shown in Table 1.

Table 1. Cutting parameters and their levels.

Cutting parameters	Symbol	Unit	Cutting parameter levels (L)				
			L ₁	L ₂	L ₃	L ₄	L ₅
Cutting speed	v_c	m/min	40	80	120	160	200
Feed rate	f	mm/rev	0.1	0.175	0.25	0.325	0.4
Depth of cut	a_p	mm	0.5	1	1.5	2	2.5

Under a full factorial run and in the case of three factors with five levels, $5^3=125$ experiments should be conducted. In accordance with Taguchi's method the standard orthogonal array L_{25} with only 25 experiments could be used. However, the selection of L_{25} orthogonal array, that can have six control factors for a saturated design of three factors leaves unassigned column in the matrix which can be used to investigate first order interactions among the cutting parameters. Therefore, the first, the second and the fourth columns of the matrix represent different levels of the cutting parameters and the third column is employed for studying the interaction between the first two (i.e. cutting speed and feed rate interaction). Negative 80° rhombic-shape coated carbide inserts with ISO code of CNMG 120408-MM 2025 are used throughout the investigation. The inserts were mounted on a right hand style PCLNL-2525M-12 ISO type tool holder. Although there are

many varieties of stainless steels being cut in industry, the current research selected three common types of these materials for machining investigation. Details of the workpiece materials are shown in Table 2.

Table 2 Workpiece materials

Material	Chemical composition (% Weight)											Tensile test (MPa)	
	C	Si	Mn	P	S	Cr	Ni	Mo	N	Cu	V	Yield	Tensile
EN 1.4410	0.015	0.25	0.75	0.021	0.0007	24.92	6.91	4.06	0.3	0.1	-	579	826
EN 1.4462	0.018	0.37	0.84	0.025	0.003	22.42	5.44	3.12	0.18	-	-	514	737
EN 1.4404	0.008	0.25	1.75	0.032	0.025	16.74	10.2	2.02	0.035	-	0.057	264	576

CNC lathe CTX 420 Linear V5 with maximum drive power 25kW and a speed range of 35-7000 is used to perform the experiments. Constant cutting speed face turning experiments are performed on cylindrical bars with diameter of 55 and 20mm overhang distance. The cutting area was flooded by a synthetic soluble cutting fluid, with a cutting fluid-water ratio of 1:20. During the turning tests, the cutting force (F_c), axial force (F_a), and radial force (F_r), were measured using Kistler type 9129A three component piezo-electric dynamometer, which was connected to a charged Kistler type 5070A amplifier and personal computer through an analog to digital converter card. The surface roughness values were measured immediately after the face turning process at three different locations on workpiece using Talysurf Series 2 surface roughness tester. Equivalent specific (volumetric) cutting energy and its components are calculated as defined by Eq. (1).

$$U = \frac{F_c v_c}{f a_p v_c} \quad (1)$$

where U is the energy required to perform primary motion in (J/mm^3). Cutting power (P_c) and resultant cutting forces (R_c) are calculated using formulas:

$$P_c = F_c v_c \quad (2)$$

$$R_c = \sqrt{F_c^2 + F_a^2 + F_r^2} \quad (3)$$

Finally, the average of three consecutive readings of each measured and calculated performance characteristics are recorded and used for upcoming analyses. Table 3 lists the computed performance characteristics.

Table 3. Performance characteristics

No.	Cutting parameter levels				EN 1.4410				EN 1.4462				EN 1.4404			
	v_c	f	v_f	a_p	R_a (μm)	U (J/mm^3)	P_c (W)	R_c (N)	R_a (μm)	U (J/mm^3)	P_c (W)	R_c (N)	R_a (μm)	U (J/mm^3)	P_c (W)	R_c (N)
1	1	1	1	1	0.87	8.01	267.14	481.79	0.85	7.34	244.7	447.6	0.78	7.48	249.2	452
2	1	2	2	2	1.86	5.58	650.51	1210.31	1.76	5.12	597.3	1127	1.68	4.85	565.9	1049
3	1	3	3	3	3.19	4.13	1032.0	1968.55	3.06	4.22	1056	2003	3.53	3.79	946.3	1736
4	1	4	4	4	4.93	4.24	1837.1	3579.49	4.62	4.06	1758	3408	4.57	3.57	1546	2928
5	1	5	5	5	5.56	3.69	2460.4	4436.53	5.53	3.61	2408	4314	5.69	2.91	1938	3459
6	2	1	2	3	0.74	6.64	1328.1	1158.09	0.70	6.54	1308	1062	0.73	6.16	1233	995
7	2	2	3	4	2.16	3.52	1641.1	1491.89	2.08	3.45	1610	1537	1.90	2.88	1343	1189
8	2	3	4	5	3.50	2.79	2325.5	1931.50	3.61	2.55	2122	1771	3.46	2.57	2141	1858
9	2	4	5	1	3.56	7.39	1601.3	1314.81	3.17	6.43	1392	1173	3.34	5.65	1223	1058
10	2	5	1	2	4.47	4.19	2232.3	1959.85	4.28	4.18	2228	1919	4.25	3.95	2106	1782
11	3	1	3	5	0.80	3.73	1862.9	1163.19	0.73	3.53	1767	1117	0.73	3.21	1607	1017
12	3	2	4	1	1.97	5.91	1034.8	594.290	1.90	5.53	968	559.7	1.57	5.45	954.2	561
13	3	3	5	2	2.76	3.81	1906.4	1103.88	2.50	3.65	1823	1040	2.52	3.70	1848	1042
14	3	4	1	3	3.56	3.47	3384.4	1979.20	3.37	3.24	3157	1850	3.57	2.96	2888	1623
15	3	5	2	4	5.05	3.79	6060.6	3648.71	4.93	3.22	5151	3166	5.33	2.92	4671	2741
16	4	1	4	2	0.60	5.53	1475.9	685.510	0.54	4.88	1301	598.1	0.48	4.34	1158	540
17	4	2	5	3	1.96	3.24	2267.1	1018.18	1.47	3.05	2136	955.1	1.43	2.85	1996	878
18	4	3	1	4	3.26	3.22	4294.5	1956.39	3.39	3.25	4328	1979	3.11	2.82	3754	1595
19	4	4	2	5	4.38	2.55	5514.9	2407.30	4.53	2.89	6264	2819	4.38	2.41	5212	2220
20	4	5	3	1	4.28	6.26	3336.1	1515.13	4.36	5.66	3020	1321	4.69	5.40	2881	1248
21	5	1	5	4	0.66	3.82	2548.3	1051.95	0.57	3.71	2476	1040	0.55	3.24	2163	816
22	5	2	1	5	2.37	4.19	6115.5	2529.33	1.69	3.90	5690	2377	1.87	3.35	4893	2004
23	5	3	2	1	3.04	6.07	2527.4	940.680	2.37	5.53	2302	866.6	2.35	5.23	2178	806
24	5	4	3	2	4.02	4.06	4399.8	1561.99	3.28	3.90	4223	1508	3.53	3.84	4164	1448
25	5	5	4	3	4.88	3.64	7274.4	2772.15	4.73	3.68	7353	2802	4.18	2.92	5841	1933
Average					2.98	4.54	2775	1778.4	2.81	4.28	2667	1710	2.81	3.94	2380	1479

3. VIKOR-TAGUCHI ANALYSIS

The Taguchi robust design principle is based on matrix experiments. The classical experimental design methods are too complex and are not easy to use. If there are more parameters, a large number of experiments have to be carried out. This problem is overcome in the Taguchi method, which uses a special design of orthogonal arrays (OA) to study the entire major parameter space with only a small number of experiments. In order to minimize the variations in the quality characteristic or response, Taguchi introduced a method to transform the repetition data to another value, which is a measure of variation present in the scattered response data. This transformation consists of the computation of signal-to-noise (SN) ratio (η) that consolidates several repetitions into one performance measure which reflects the amount of variation present. The maximization of the SN ratio simultaneously optimizes the response and minimizes the effect of noise factors. For each entry 'i' in the OA, if the response (Ob) is repeated [13]:

$$\eta_i = -10 \log_{10} \left\{ \frac{1}{n} \sum_{i=1}^n Ob_i^2 \right\} \quad (4)$$

The optimum level for a factor is the level that gives the highest value of SN ratio (see Fig. 2). The optimum factor^(level) combinations while turning EN 1.4410 were: $v_c^4 f^1 a_p^2 f v_c^5$ for surface roughness, $v_c^4 f^3 a_p^5 f v_c^5$ for specific cutting energy, $v_c^1 f^1 a_p^1 f v_c^5$ for cutting power and $v_c^4 f^1 a_p^1 f v_c^5$ for resultant cutting forces. In turning EN 1.4462 the following factor^(level) combinations were optimum; $v_c^5 f^1 a_p^2 f v_c^5$ for surface roughness, $v_c^3 f^3 a_p^5 f v_c^5$ for specific cutting energy, $v_c^1 f^1 a_p^1 f v_c^5$ for cutting power and $v_c^3 f^1 a_p^1 f v_c^5$ for resultant cutting forces. Finally, in turning EN 1.4404; $v_c^5 f^1 a_p^2 f v_c^5$ for surface roughness, $v_c^4 f^5 a_p^5 f v_c^5$ for specific cutting energy, $v_c^1 f^1 a_p^1 f v_c^5$ for cutting power and $v_c^4 f^1 a_p^1 f v_c^5$ for resultant cutting forces were the optimums.

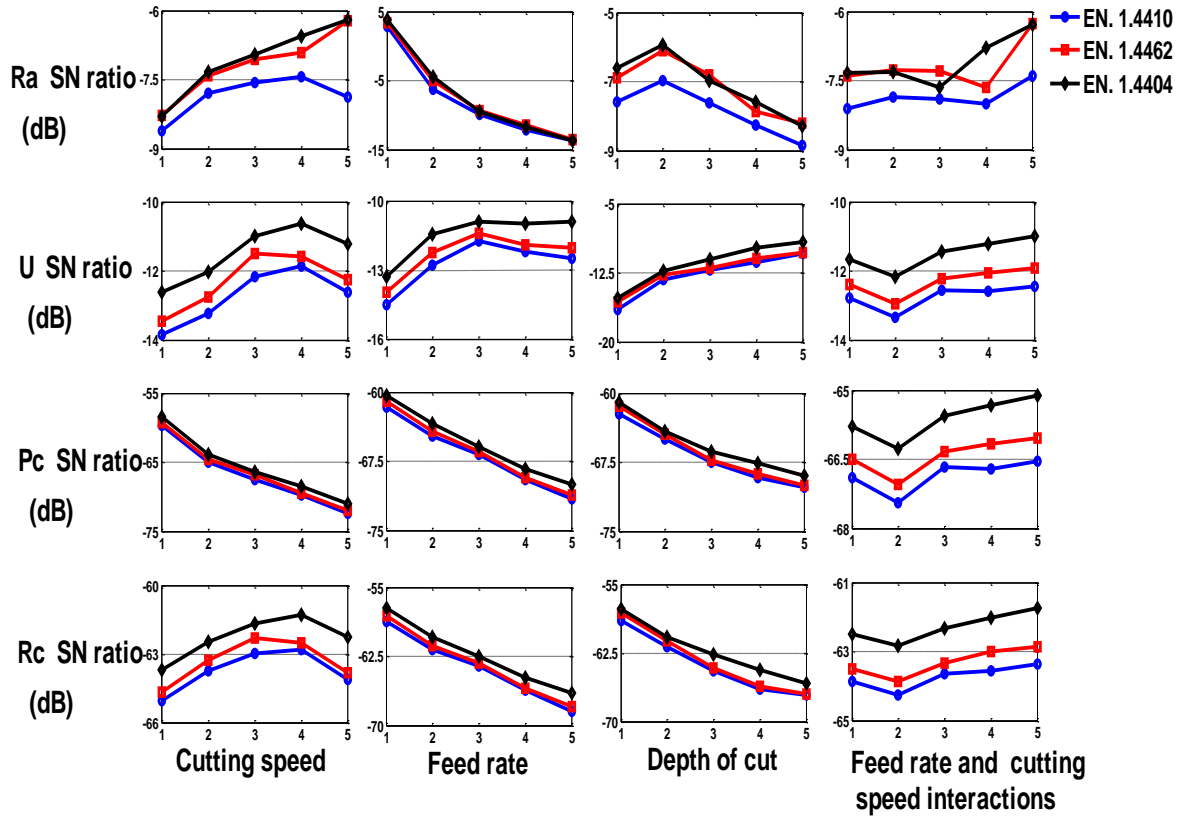


Fig. 2. Main effect plot of SN ratio in machining stainless steels.

After determining the optimal levels of control factors, ANOVA of SN ratio of all performance characteristics are performed to estimate the relative significance of each factor. Table 4 shows the result of ANOVA on SN ratios for 95% level of confidence. The P -values of cutting speed, feed rate and depth of cut smaller than 0.05 are marked in bold which indicate the statistical and physical impact on the corresponding response factor. The $F_{stat.}$ of regression for all developed models at 95% level of confidence are greater than $F_{table(4,16,0.05)} = 3.0069$ (not shown for space reasons), proving the adequacy of derived models. However, the F_{ratio} of all $v_c f$ interaction terms and of certain cutting parameter per performance are less than F_{table} which show the need of pooling. The last three column of the table shows the percent contribution (% Contribution) of each factor. Taguchi method is suitable only for single objective optimization, to perform multi-objective (multi-performance) optimization of the problem, a multi-attribute decision making (MADM) technique called VIKOR method is utilized. The VIKOR method was introduced as one applicable technique to be implemented within MCDM problem and it was developed as a multi attribute decision making method to solve a discrete decision making problem with non-commensurable (different units) and conflicting criteria. It is based on an aggregation function

representing closeness to the ideal, which originated in the compromise programming method. The proposed Taguchi-
VIKOR algorithm has the following steps:

Table 4. ANOVA of SN ratios

Factors	Degree of freedom	Sum of squares			F _{ratio}			P-Value			% Contribution		
		EN	EN	EN	EN	EN	EN	EN	EN	EN	EN	EN	EN
		1.4410	1.4462	1.4404	1.4410	1.4462	1.4404	1.4410	1.4462	1.4404	1.4410	1.4462	1.4404
Surface roughness (R _a)													
<i>v_c</i>	4	4.152	11.541	13.137	1.63	2.91	5.51	0.257	0.093	0.020	0.469	1.219	1.291
<i>f</i>	4	862.71	907.32	977.45	339.6	228.77	410.09	0.000	0.000	0.000	97.636	95.848	96.052
<i>v_cf</i>	4	1.535	5.506	5.739	0.6	1.39	2.41	0.671	0.32	0.135	0.173	0.581	0.564
<i>a_p</i>	4	10.121	14.317	16.528	3.98	3.61	6.82	0.046	0.058	0.011	1.145	1.512	1.624
Error	8	5.080	7.932	4.767							0.577	0.84	0.469
Total	24	883.59	946.61	1017.6							100	100	100
Specific cutting energy (U)													
<i>v_c</i>	4	12.805	13.674	13.088	1.32	1.78	1.97	0.341	0.226	0.192	7.734	9.875	7.749
<i>f</i>	4	22.133	18.915	20.908	2.28	2.46	3.15	0.149	0.129	0.079	13.369	13.661	12.382
<i>v_cf</i>	4	2.559	3.176	4.044	0.26	0.41	0.61	0.893	0.795	0.668	1.545	2.293	2.394
<i>a_p</i>	4	108.64	87.326	117.55	11.19	11.36	17.69	0.002	0.002	0.000	65.622	63.069	69.604
Error	8	19.415	15.368	13.293							11.73	11.102	7.871
Total	24	165.55	138.45	168.88							100	100	100
Cutting power (P _c)													
<i>v_c</i>	4	473.38	475.88	463.21	48.77	61.93	69.69	0.000	0.000	0.000	46.669	45.121	47.795
<i>f</i>	4	311.21	320.75	295.87	32.06	41.74	44.52	0.000	0.000	0.000	30.681	30.412	30.528
<i>v_cf</i>	4	2.559	3.176	4.044	0.26	0.41	0.61	0.893	0.795	0.668	0.252	0.301	0.417
<i>a_p</i>	4	207.75	239.51	192.73	21.4	31.17	29.00	0.000	0.000	0.000	20.481	22.709	19.886
Error	8	19.415	15.36	13.293							1.917	1.456	1.374
Total	24	1014.3	1054.6	969.14							100	100	100
Resultant cutting force (R _c)													
<i>v_c</i>	4	16.814	19.011	16.729	1.4	2.31	2.11	0.317	0.146	0.171	2.978	3.541	3.313
<i>f</i>	4	290.56	229.26	266.14	24.19	36.35	33.56	0.000	0.000	0.000	51.468	42.7	52.71
<i>v_cf</i>	4	2.349	3.126	3.557	0.2	0.38	0.45	0.934	0.817	0.771	0.416	0.582	0.704
<i>a_p</i>	4	230.80	269.05	202.63	19.21	32.68	25.55	0.000	0.000	0.000	40.88	50.11	40.132
Error	8	24.024	16.465	15.861							4.255	3.066	3.141
Total	24	564.54	536.91	504.91							100	100	100

Step 1. Normalize the SN ratios of the performances between ‘0’ and ‘1’ using the relation:

$$f_i(j) = \begin{cases} 0, & X_i^0(j) > \max X_i^0(j) \\ \left(\frac{\max X_i^0(j) - X_i^0(j)}{\max X_i^0(j) - \min X_i^0(j)} \right), & \min X_i^0(j) \leq X_i^0(j) \leq \max X_i^0(j) \\ 1, & X_i^0(j) < \min X_i^0(j) \end{cases} \quad (5)$$

where $X_i^0(j)$ the sequence is after the data pre-processing for i th alternative, $\max X_i^0(j)$ is the largest value, $\min X_i^0(j)$ is the smallest value, $\text{nom } X_i^0(j)$ is the nominal value of $X_i^0(j)$ and $X^0(j)$ is the desired value to be normalized of j th attribute.

Step 2. Representation of decision matrix

$$D = [f_{ij}]_{m \times n} \quad (6)$$

where $i=1,2, \dots, m$ and f_{ij} is performance of alternative A_i with respect to the j th criterion.

Step 3. Determination of the best A^* and the worst A^- values of all criterion functions. If the i_{th} function represents the benefit, then

$$A^* = \{(\max f_{ij} | j \in J) \text{ or } (\min f_{ij} | j \in J')\} \quad (7)$$

$$A^- = \{(\min f_{ij} | j \in J) \text{ or } (\max f_{ij} | j \in J')\} \quad (8)$$

where

$$J = \{j = 1, 2, \dots, n | f_{ij}, \text{ if desired response is large}\} \quad (9)$$

$$J' = \{j = 1, 2, \dots, n | f_{ij}, \text{ if desired response is small}\} \quad (10)$$

Step 4. Compute the values of utility measure S_j and regret measure R_j by respective relations:

$$S_j = \sum_{i=1}^n w_j \frac{(f_j^* - f_{ij})}{(f_j^* - f_j^-)} \quad (11)$$

$$R_j = \max_j \left[\frac{w_i(f_j^* - f_{ij})}{(f_j^* - f_j^-)} \right] \quad (12)$$

where w_j are the weights of j th criteria. The Entropy method used to estimate the weights of the various criteria from the given payoff matrix and is independent of the views of the decision maker. The process of calculation of Entropy weights can be divided into the following steps:

1. For a given normalized payoff matrix, f_{ij} , entropy E_j of the set of alternatives for criterion j is

$$E_{ij} = -\frac{1}{\ln(m)} \sum_{i=1}^m f_{ij} \ln(f_{ij}) \quad (13)$$

for $j=1,2, \dots, n$. and $i=1,2,\dots,m$. Where m is the number of alternatives and n is the number of criterion.

2. Degree of diversification of the information provided by the outcomes of criterion j is

$$D_j = 1 - E_j \quad (14)$$

3. Normalized weights of the criterion are

$$w_j = \frac{D_j}{\sum_{j=1}^n D_j} \quad (15)$$

This method is advantageous as it reduces the burden of the decision maker for large sized problem [14]. Table 5 lists the computed entropy weight for each performance per material.

Table 5. Entropy weights

Response factor	Entropy weight (w_j)		
	EN 1.4410	EN 1.4462	EN 1.4404
Surface roughness	0.275	0.265	0.269
Specific cutting energy	0.214	0.215	0.205
Cutting power	0.286	0.279	0.284
Resultant cutting force	0.225	0.241	0.242

Step 5. Compute the VIKOR indices $MPCI_j, j=1,2,\dots,J$, by the relation

$$MPCI_j = \frac{\vartheta(S_j - S^*)}{(S^- - S^*)} + \frac{(1 - \vartheta)(R_j - R^*)}{(R^- - R^*)} \quad (16)$$

where

$$\begin{aligned} S^* &= \min_j S_j, & S^- &= \max_j S_j \\ R^* &= \min_j R_j, & R^- &= \max_j R_j \end{aligned}$$

ϑ is introduced as weight of the strategy for maximum group utility, usually $\vartheta = 0.5$.

Table 6. VIKOR indices (MPCI) and alternatives rankings

Alternative	EN 1.4410		EN 1.4462		EN 1.4404	
	MPCI	Rank	MPCI	Rank	MPCI	Rank
1	0.24	5	0.27	5	0.23	5
2	0.18	3	0.19	3	0.17	2
3	0.48	11	0.51	12	0.58	12
4	0.83	21	0.8	21	0.8	18
5	0.91	23	0.92	24	0.91	23
6	0.27	7	0.37	10	0.3	8
7	0.25	6	0.28	6	0.24	6
8	0.53	13	0.54	13	0.59	13
9	0.64	15	0.57	14	0.59	14
10	0.73	18	0.73	18	0.75	17
11	0.17	2	0.18	2	0.21	4
12	0.2	4	0.23	4	0.2	3
13	0.38	10	0.35	9	0.42	10
14	0.61	14	0.59	15	0.64	15
15	0.94	24	0.87	22	0.93	24
16	0.07	1	0.03	1	0.02	1
17	0.31	9	0.28	8	0.33	9
18	0.68	16	0.71	17	0.72	16
19	0.79	20	0.89	23	0.9	22
20	0.78	19	0.78	19	0.84	21
21	0.27	8	0.28	7	0.27	7
22	0.85	22	0.79	20	0.83	20
23	0.52	12	0.46	11	0.51	11
24	0.73	17	0.71	16	0.82	19
25	0.98	25	1	25	0.95	25

Step 6. For given attribute weights, propose a compromise solution, alternative A_{b_1} , which is the best ranked by MPCI, if the following two conditions are satisfied:

Condition 1: ‘Acceptable advantage’ ($MPCI(A_{b_2}) - MPCI(A_{b_1}) \geq (\frac{1}{n-1})$) where A_{b_2} is the second-best alternative in the ranking by MPCI.

Condition 2: ‘Acceptable stability in decision making’ alternative A_{b_1} must also be the best ranked by S and/or R . This compromise solution is stable within a decision-making process, which could be: ‘voting by majority rule’ (when $\vartheta > 0.5$ is needed) or ‘by consensus’ (when $\vartheta \approx 0.5$) or ‘with veto’ (when $\vartheta > 0.5$). If one of the conditions is not satisfied, then a set of compromise solutions is proposed, which consists of:

- Alternatives A_{b_1} and A_{b_2} if only condition 2 is not satisfied
- Alternatives $A_{b_1}, A_{b_2}, \dots, A_{b_i}$ if condition 1 is not satisfied; A_p is determined by the relation $MPCI(A_{b_2}) - MPCI(A_{b_1}) \approx (\frac{1}{n-1})$, [15].

Table 6 shows the computed MPCIs. The values of first rank alternative are in acceptable advantage range (i.e. $MPCI(A_{b_2}) - MPCI(A_{b_1})$ is always greater than $(\frac{1}{25-1})$). For example, the $MPCI(A_{b_1})$ and $MPCI(A_{b_2})$ of EN 1.4410 are 0.07 and 0.17 respectively, which satisfies condition 1, i.e. $0.17 - 0.07 = 0.1$ is greater than $(\frac{1}{25-1}) = 0.04167$. Both regret and utility measure values by consensus prove the stability in decision making. Therefore, the values of MPCI are directly used in the next analyses.

Step 7. Perform ANOM and ANOVA on the computed MPCI.

To indicate the sensitivity of calculated MPCIs presented in

Table 6 to changing cutting parameters, contour plots for newly computed MPCIs are mapped as shown in Fig. 3. The optimum and near optimum regions are filled with dark blue and light blue colors. This argument initially suggests that the optimum point should locate somewhere within shown dark blue regions. The optimum level for a factor is the level that gives the minimum value of MPCI value.

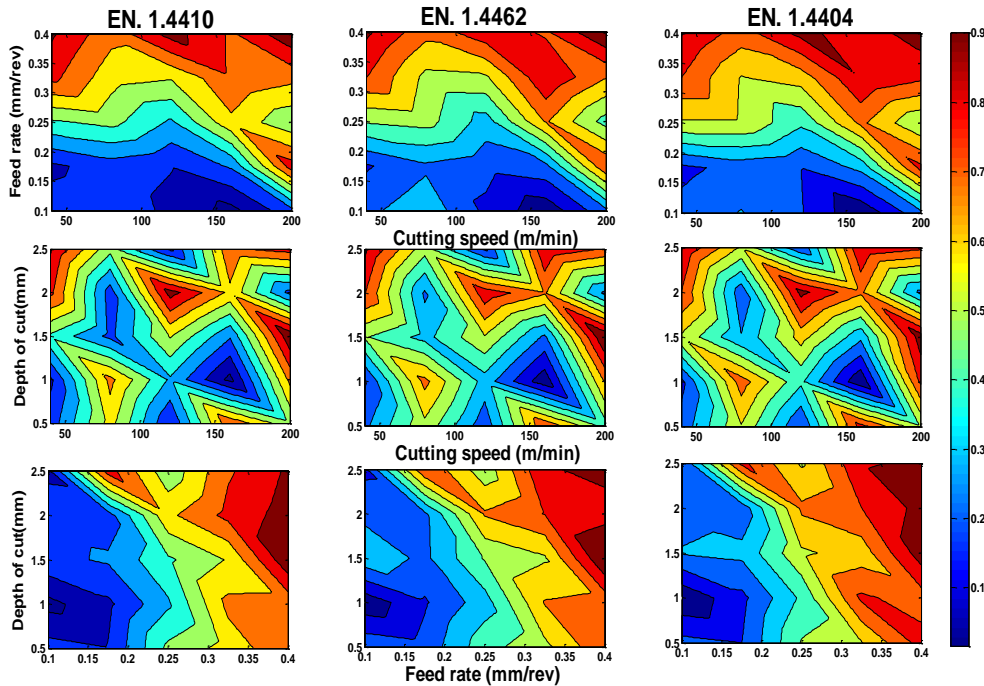


Fig. 3. Topography of computed MPCI.

The calculation of the mean MPCI at first level which determines the impact of cutting speed, feed rate and depth of cut when machining EN 1.4410 can be easily performed through computing the mean of MPCI values given in

Table 6 as follow:

$$\begin{aligned}
 MPCI_{m_{vc1}} &= (0.24 + 0.18 + 0.48 + 0.83 + 0.91)/5 = 0.528 \\
 MPCI_{m_{f1}} &= (0.24 + 0.27 + 0.17 + 0.07 + 0.27)/5 = 0.204 \\
 MPCI_{m_{ap1}} &= (0.24 + 0.64 + 0.2 + 0.78 + 0.52)/5 = 0.476 \\
 MPCI_{m_{fv1}} &= (0.24 + 0.73 + 0.61 + 0.68 + 0.85)/5 = 0.622
 \end{aligned}$$

Similar procedure is repeated to calculate the main effects of cutting parameters on MPCI values for the reminder levels. Fig. 4 presents the main effect plot of cutting parameters on the computed MPCIs. The optimum level for a factor is the level that gives the lowest value of MPCI. The overall optimum factor^(level) combinations while turning EN 1.4410 and EN 1.4462 were: $v_c^3 f^1 a_p^2 f v_c^3$, and $v_c^4 f^1 a_p^2 f v_c^5$ in turning EN 1.4404.

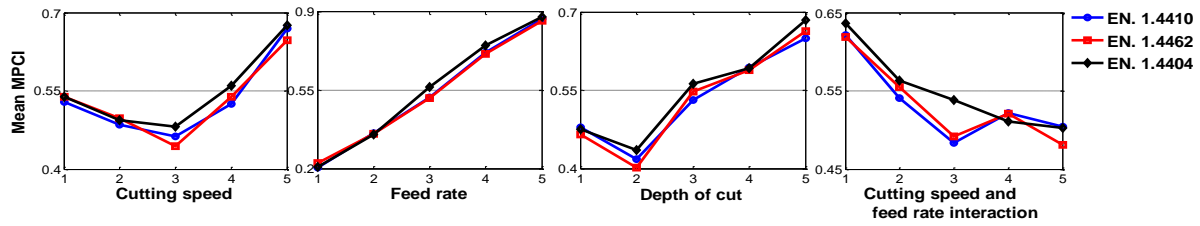


Fig. 4. Main effect plot of MPCI values in machining stainless steels.

The relative magnitude of the effect of different factors can be obtained by decomposition of variance, called ANOVA (see Table 7). The F_{ratio} , P-values and contribution percentages show the major impact of feed rate on computed MPCI. Because some of F_{ratio} values in Table 7 are smaller than the $F_{table(4,16,0.05)} = 3.0069$, the condition of 95% of confidence that all cutting parameters have effects on computed MPCIs will no longer be accurate. Therefore, a new table without those factors is required and the sums of squares of the pooled factors have to be added to the error term.

Table 7. ANOVA of computed MPCIs.

Factor	Degree of freedom	Sum of squares			F_{ratio}			P-value			% Contribution		
		EN 1.4410	EN 1.4462	EN 1.4404	EN 1.4410	EN 1.4462	EN 1.4404	EN 1.4410	EN 1.4462	EN 1.4404	EN 1.4410	EN 1.4462	EN 1.4404
v_c	4	0.1285	0.1105	0.1197	2.33	1.94	2.05	0.143	0.198	0.179	6.783	6.031	5.969
f	4	1.4317	1.3357	1.5186	25.97	23.42	26.05	0.000	0.000	0.000	75.58	72.90	75.729
$v_c f$	4	0.0561	0.0621	0.0569	1.02	1.09	0.98	0.453	0.424	0.471	2.961	3.389	2.837
a_p	4	0.1677	0.2098	0.1936	3.04	3.68	3.32	0.085	0.055	0.070	8.853	11.45	9.654
Error	8	0.1102	0.1141	0.1165							5.823	6.229	5.811
Total	24	1.8942	1.8322	2.0053							100	100	100

4. OPTIMIZATION PROCEDURE

In previous sections the conflicting responses are converted into one single dimensionless index called MPCI (VIKOR Index). However, one cannot exactly specify at which exact value of cutting parameters the performance characteristics are minimum and the first rank alternatives led to relatively high specific cutting energy. Therefore, the need for minimization of these indices arise so that a more convenient result is achieved on all aspects of the study. In this research the adopted optimization procedure could be summarized into following steps:

Step 1. Designation of decision variables: The adopted decision variables in present work are cutting speed ' v_c ' in (m/min), feed rate ' f ' in (mm/rev) and depth of cut ' a_p ' in (mm).

Step 2. Formulation of objective functions: Formulation of optimization model is one of the most important tasks in optimization process. The type of optimization modeling techniques used to express the objective function determines its accuracy and the possibility of reaching a global optimum solution. Therefore, a great attention is made to find a model expressing the case with simplest form and highest possible precision. Thousands of linear and nonlinear models are examined using NonLinearModel.fit function in Matlab. Finally, the most realistic, reliable, and easier to solve (from optimization point of view) model selected is in the format of:

$$MPCI_i = b_1 + b_2 v_c + b_3 f + b_4 a_p + b_5 v_c^2 + b_6 f^2 + b_7 a_p^2 + b_8 v_c f + b_9 v_c a_p \quad (17)$$

where $MPCI_i$ is the predicted VIKOR index per material and the b_{1-9} constants are coefficients of the model. The models adequacies are proved using ANOVA and are shown in Table 8.

Table 8. Multiple regression and ANOVA of developed objective function models.

	Estimate			Sum of Errors			t- Statistics			P-value		
	EN 1.4410	EN 1.4462	EN 1.4404	EN 1.4410	EN 1.4462	EN 1.4404	EN 1.4410	EN 1.4462	EN 1.4404	EN 1.4410	EN 1.4462	EN 1.4404
b_1	0.233	0.365	0.177	0.204	0.204	0.202	1.142	1.791	0.879	0.270	0.092	0.391
b_2	-0.005	-0.007	-0.006	0.002	0.002	0.002	-2.89	-3.34	-2.93	0.011	0.004	0.009
b_3	2.197	1.427	2.566	1.142	1.143	1.132	1.923	1.248	2.265	0.072	0.229	0.037
b_4	-0.181	-0.158	-0.149	0.154	0.155	0.153	-1.17	-1.02	-0.97	0.258	0.321	0.345
b_5	20e-6	19e-6	18e-6	72e-7	72e-7	71e-7	2.844	2.750	2.582	0.011	0.014	0.020
b_6	0.163	0.685	-1.076	2.059	2.061	2.042	0.079	0.332	-0.52	0.937	0.743	0.605

b_7	0.053	0.053	0.051	0.046	0.046	0.045	1.15	1.136	1.101	0.267	0.272	0.287
b_8	98e-5	0.004	0.003	0.003	0.003	0.003	0.28	1.307	1.021	0.783	0.209	0.322
b_9	0.001	0.001	0.001	52e-4	53e-4	52e-4	2.032	2.070	1.969	0.059	0.055	0.066
Summary of EN 1.4410 model: $RMS = 0.0967$, $R_{sq.} = 0.921$, $R_{sq.-adj.} = 0.881$, $F_{stat.} = 23.3 > F_{table(8,16,0.05)} = 2.59$												
Summary of EN 1.4462 model: $RMS = 0.0968$, $R_{sq.} = 0.918$, $R_{sq.-adj.} = 0.877$, $F_{stat.} = 22.5 > F_{table(8,16,0.05)} = 2.59$												
Summary of EN 1.4404 model: $RMS = 0.0959$, $R_{sq.} = 0.927$, $R_{sq.-adj.} = 0.89$, $F_{stat.} = 25.3 > F_{table(8,16,0.05)} = 2.59$												

The R-squared ($R_{sq.}$) and the adjusted R-square ($R_{sq.-adj.}$) values indicate that the models fit the data well. P-values of terms which are less than 0.050 are again designated as significant terms. Terms with high deviation of t-Statistic from 1 represent the significant impact on the model.

Step 3. Formulation of constraints: For the process of effective optimization, nonlinear constraint models need to be derived and incorporated in optimization model. The mathematical model for the prediction of constraint variables in terms of the decision variables can be expressed as:

$$\ln|C_{ij}| = \ln \kappa_{ij} + \alpha_{ij} \ln v_c + \beta_{ij} \ln f + \gamma_{ij} \ln a_p \quad (18)$$

Where C_{ij} is the predicted constraint for i th number of performances and j th material. κ_{ij} , α_{ij} , β_{ij} , and γ_{ij} are the model constant parameters. Exponentiate both sides of Eq. (18) using e , transform it into a power regression Eq.:

$$F_j = \kappa_{ij} * v_c^{\alpha_{ij}} * f^{\beta_{ij}} * a_p^{\gamma_{ij}} \quad (19)$$

In other words, minimization of each VIKOR index model is imposed by different nonlinear constraints namely:

Surface roughness constraint

$$R_{aj}^{min.} \leq \kappa_{1j} * v_c^{\alpha_{1j}} * f^{\beta_{1j}} * a_p^{\gamma_{1j}} \leq R_{aj}^{avg.}$$

Specific cutting energy constraint

$$U_j^{min.} \leq \kappa_{2j} * v_c^{\alpha_{2j}} * f^{\beta_{2j}} * a_p^{\gamma_{2j}} \leq U_j^{avg.}$$

Cutting power constraint

$$P_{cj}^{min.} \leq \kappa_{3j} * v_c^{\alpha_{3j}} * f^{\beta_{3j}} * a_p^{\gamma_{3j}} \leq P_{cj}^{avg.}$$

and Resultant cutting forces constraint.

$$R_{cj}^{min.} \leq \kappa_{4j} * v_c^{\alpha_{4j}} * f^{\beta_{4j}} * a_p^{\gamma_{4j}} \leq R_{cj}^{avg.}$$

Table 9 presents the estimates and ANOVA of developed constraint models and the corresponding bounds. Recommended by [1], the minimum specific cutting energy ($U_j^{min.}$) are put equal to 2 J/mm³.

Table 9. Constraint models.

EN 1.4410							
Model	Performance as a constraint	κ_{i1}	α_{i1}	β_{i1}	γ_{i1}	Min	Average
1	Roughness, $R_{a1}(\mu m)$	16.432	-0.0429	1.12	0.131	0.25	2.977
2	Specific cutting energy, $U_1 (J/mm^3)$	6.5016	-0.114	-0.1644	-0.4167	2	4.538
3	Cutting power, $P_{c1} (W)$	85.078	0.9305	0.8226	0.590	200	2775.13
4	Resultant cutting force, $R_{c1} (N)$	9597.9	-0.1498	0.8711	0.609	200	1778.42
Roughness model:		$R_{sq.} = 0.965$,	$R_{sq.-adj.} = 0.960$,	$F_{ratio} = 191$,	RMSE = 0.308		
Specific cutting energy model:		$R_{sq.} = 0.810$,	$R_{sq.-adj.} = 0.783$,	$F_{ratio} = 29.8$,	RMSE = 0.680		
Cutting power model:		$R_{sq.} = 0.938$,	$R_{sq.-adj.} = 0.929$,	$F_{ratio} = 105$,	RMSE = 494		
Resultant cutting force model:		$R_{sq.} = 0.897$,	$R_{sq.-adj.} = 0.882$,	$F_{ratio} = 60.6$,	RMSE = 344		
EN 1.4462							
Model	Performances as constraints	κ_{i2}	α_{i2}	β_{i2}	γ_{i2}	Min	Average
1	Roughness, $R_{a1}(\mu m)$	18.166	-0.0582	1.202	0.1746	0.25	2.801
2	Specific cutting energy, $U_1 (J/mm^3)$	6.262	-0.119	-0.163	-0.369	2	4.284
3	Cutting power, $P_{c1} (W)$	59.564	0.9995	0.8645	0.662	200	2667.39
4	Resultant cutting force, $R_{c1} (N)$	8076	-0.127	0.8671	0.665	200	1710.35
Roughness model:		$R_{sq.} = 0.962$,	$R_{sq.-adj.} = 0.957$,	$F_{ratio} = 177$,	RMSE = 0.320		
Specific cutting energy model:		$R_{sq.} = 0.792$,	$R_{sq.-adj.} = 0.762$,	$F_{ratio} = 26.6$,	RMSE = 0.614		
Cutting power model:		$R_{sq.} = 0.967$,	$R_{sq.-adj.} = 0.962$,	$F_{ratio} = 206$,	RMSE = 356		
Resultant cutting force model:		$R_{sq.} = 0.920$,	$R_{sq.-adj.} = 0.908$,	$F_{ratio} = 80.3$,	RMSE =295		
EN 1.4404							
Model	Performance as a constraint	κ_{i3}	α_{i3}	β_{i3}	γ_{i3}	Min	Average
1	Roughness, $R_{a1}(\mu m)$	22.405	-0.091	1.241	0.1444	0.25	2.808
2	Specific cutting energy, $U_1 (J/mm^3)$	5.7772	-0.1302	-0.198	-0.4273	2	3.938
3	Cutting power, $P_{c1} (W)$	73.51	0.9254	0.802	0.5655	200	2379.93
4	Resultant cutting force, $R_{c1} (N)$	7660.2	-0.163	0.777	0.5761	200	1479.08
Roughness model:		$R_{sq.} = 0.963$,	$R_{sq.-adj.} = 0.958$,	$F_{ratio} = 185$,	RMSE = 0.323		
Specific cutting energy model:		$R_{sq.} = 0.858$,	$R_{sq.-adj.} = 0.838$,	$F_{ratio} = 42.4$,	RMSE = 0.838		
Cutting power model:		$R_{sq.} = 0.971$,	$R_{sq.-adj.} = 0.967$,	$F_{ratio} = 236$,	RMSE = 278		

Resultant cutting force model: $R_{sq.} = 0.937$, $R_{sq.-adj.} = 0.928$, $F_{ratio} = 105$, $RMSE = 205$

Step 4. Setting up decision variable bounds:

The bounds of decision variables were selected based on their maximum and minimum values in Table 1, i.e.:

$$\begin{aligned} 40 &\leq v_c \leq 200 \text{ (m/min)}; \\ 0.1 &\leq f \leq 0.4 \text{ (mm/rev)}; \\ 0.5 &\leq a_p \leq 2.5 \text{ (mm)}. \end{aligned}$$

Step 5. Running typical nature-inspired meta-heuristic algorithms: Nature inspired meta-heuristic algorithms are among the most powerful algorithms for optimizations nowadays. Out of many meta-heuristic optimization algorithms, this paper compares three different algorithms namely:

1. Firefly Algorithm (FA)
2. Accelerated Particle Swarm Optimization (APSO)
3. Cuckoo Search (CS)

The algorithms are recently developed and simultaneously employed for comparison purposes. Table 10 summarizes the typical initializing optimization parameters for each algorithm. For more details about the used algorithms, the reader is recommended to refer to ref. no. [16].

Table 10. Initializing parameters.

Firefly Algorithm	Accelerated PSO	Cuckoo Search
Population size=20	Randomness amplitude (α)= 0.2	Number of nests=20
Number of iterations=250	Speed of convergence (β)= 0.5	Probability (P_a)=0.25
Randomization (α)=0.5	Number of particles=25	Number of iterations=250
Attractiveness (β_0)= 0.2	Number of iterations=250	
Attractiveness variation (γ)=1	Randomness (α_0)= 0.95	

The obtained optimization results showed that all three methods, i.e. Firefly Algorithm, Accelerated PSO and Cuckoo Search are highly reliable and converge consistently to the optimum solution. Table 11 presents the result of optimization for each material case. Results have showed that higher values of depth of cuts were necessary to get the optimum point when machining austenitic stainless steel in comparison to super and standard duplex stainless steel and higher values of feed rate and depth of cut with slightly lower values of cutting speed were necessary to get the optimum point when machining standard duplex stainless steel in comparison to super duplex stainless steel. The present optimum solutions are specific to the values of constants used in optimization and constraint models. Different results are expected when different objective and constraint models and different performance weighting methods are adopted.

The efficiency of each algorithm could be measured in terms of the average time consumed per each algorithm to reach the global optimum or in terms of degree of minimization. Based on this statement and running optimization algorithms on an Intel® Xeon® CPU 3.47 GHz and 24GB RAM computer, CS was seen the most efficient followed by APSO and the least efficient FA.

Table 11. Summary of optimization.

	Firefly Algorithm (FA)			Accelerated PSO (APSO)			Cuckoo Search (CS)		
Parameter	EN	EN	EN	EN	EN	EN	EN	EN	EN
	1.4410	1.4462	1.4404	1.4410	1.4462	1.4404	1.4410	1.4462	1.4404
v_c (m/min)	109.645	130.049	120.9048	111.631	133.6274	123.781	112.445	133.909	123.918
f (mm/rev)	0.10	0.1	0.1	0.1	0.1	0.1	0.1	0.1	0.1
a_p (mm)	1.626	1.60469	1.65433	1.61821	1.59066	1.64258	1.61491	1.58958	1.64196
$Q_{opt.}$	0.09249	0.12007	0.0.1064	0.092403	0.11981	0.10633	0.0923	0.11979	0.10629
time (sec)	1.9515	1.978	2.0691	1.1048	1.1859	1.2347	0.515	0.555	0.545

5. CONCLUSIONS

Taguchi method applied on an $L_{25}(5^3)$ orthogonal array. As a result, 25 experiments were conducted instead of the full factorial 125 experiments. SN ratios of performance characteristics like: surface roughness (R_a), specific cutting energy (U), cutting power (P_c) and resultant cutting force (R_c) were analyzed using ‘the smaller the better’ criteria. The mean values of specific cutting energy, consumed cutting power and resultant cutting forces during turning super duplex stainless steel EN 1.4410 were found to be higher than of standard duplex stainless steel EN 1.4462 and austenitic stainless steel EN 1.4404.

Through ANOVA, the percentage of contributions indicated that feed rate on surface roughness, depth of cut on specific cutting energy and cutting speed on cutting power have the greatest impact. For each performance and material, the optimum cutting parameter level which corresponds to the level of maximum SN ratio is determined. The optimum factor^(level) combinations while turning EN 1.4410 were: $v_c^4 f^1 a_p^2 f v_c^5$ for surface roughness, $v_c^4 f^3 a_p^5 f v_c^5$ for specific cutting

energy, $v_c^1 f^1 a_p^1 f v_c^5$ for cutting power and $v_c^4 f^1 a_p^1 f v_c^5$ for resultant cutting forces. In turning EN 1.4462 the following factor^(level) combinations were optimum; $v_c^5 f^1 a_p^2 f v_c^5$ for surface roughness, $v_c^3 f^3 a_p^5 f v_c^5$ for specific cutting energy, $v_c^1 f^1 a_p^1 f v_c^5$ for cutting power and $v_c^3 f^1 a_p^1 f v_c^5$ for resultant cutting forces. Finally, in turning EN 1.4404; factor^(level) combinations of $v_c^5 f^1 a_p^2 f v_c^5$ for surface roughness, $v_c^4 f^5 a_p^5 f v_c^5$ for specific cutting energy, $v_c^1 f^1 a_p^1 f v_c^5$ for cutting power and $v_c^4 f^1 a_p^1 f v_c^5$ for resultant cutting forces were the optimums. The exact optimum condition is highly dependent on the degree of priorities given to each performance. In this study the entropy weight method is utilized to give each performance its priority and MPCIs are derived using VIKOR method to convert the problem from a multi-performance one into a single performance for each material case. The overall optimum factor^(level) combinations while turning EN 1.4410 and EN 1.4462 were: $v_c^3 f^1 a_p^2 f v_c^3$, and $v_c^4 f^1 a_p^2 f v_c^5$ in turning EN 1.4404.

Meta-heuristic algorithms like APSO, FA and CS are coupled with hybrid Taguchi-VIKOR approach. The obtained optimization results showed that all three methods, i.e. Firefly Algorithm, Accelerated PSO and Cuckoo Search are highly reliable and converge consistently to the optimum solution. However, when it comes to comparisons based on computation time and computation results, Taguchi-VIKOR-CS outperforms Taguchi-VIKOR-APSO and Taguchi-VIKOR-FA, in converging quickly and consistently into global minima.

ACKNOWLEDGEMENT

The authors would like to thank Geschäftsbereich Sandvik Coromant for providing cutting tools and materials for this research and gratefully acknowledge the efforts of Dr. Stefan Scherbarth at Sandvik Tooling Deutschland GmbH for sharing his experience with us during the course of this research.

6. References

- [1] S. Kalpakjian & S. R. Schmid, Manufacturing processes for engineering materials, Nazanm: Pearson Hall, 2008, p. 416.
- [2] W. Grzesik, Advanced machining processes of metallic materials: theory, modelling and applications, Oxford UK: Elsevier, 2008, p. 190.
- [3] ISSF, „ISSF annual review,“ International Stainless Steel Forum (www.worldstainless.org), Brussels, 2012.
- [4] W. Liew, B. Ngoi & Y. Lu, „Wear characteristics of PCBN tools in the ultra-precision machining of stainless steel at low speeds,“ *Wear*, Vol. 254, No. 3-4, pp. 265-277, 2003.
- [5] W.-T. Chien & C.-S. Tsai, „The investigation on the prediction of tool wear and the determination of optimum cutting conditions in machining 17-4PH stainless steel,“ *Journal of Materials Processing Technology*, Vol. 140, No. 1, pp. 340-345, 2003.
- [6] I. Korkut, M. Kasap, I. Ciftci & U. Seker, „Determination of optimum cutting parameters during machining of AISI 304 austenitic stainless steel,“ *Materials and Design*, Vol. 25, pp. 303-305, 2004.
- [7] A. S. Kumara, A. R. Durai & T. Sornakumar, „The effect of tool wear on tool life of alumina-based ceramic cutting tools while machining hardened martensitic stainless steel,“ *Journal of Materials Processing Technology*, Vol. 173, No. 2, pp. 151-156, 2006.
- [8] V. Gaitonde, S. Karnik, B. Achyutha & B. Siddeswarappa, „Taguchi optimization in drilling of AISI 316L stainless steel to minimize burr size using multi-performance objective based on membership function,“ *Journal of materials processing technology*, Vol. 202, pp. 374-379, 2008.
- [9] M. Kaladhar, K. V. Subbaiah, C. S. Rao & K. N. Rao, „Optimization of process parameters inturning of AISI202 austenitic stainless steel,“ *ARP Journal of Engineering and Applied Sciences*, Vol. 5, No. 9, pp. 79-87, 2010.
- [10] E. Ahmadi, R. M. Homami & S. Rahmati, „Experimental investigation and mathematical modeling of composite ceramic cutting tools with alumina base in the machining process of PH-hardened (duplex) stainless steel,“ *Int. J. Advanced Design and Manufacturing Technology*, Vol. 5, No. 2, pp. 17-25, 2012.
- [11] D. Saravanan, M. Arularasu & K. Ganesan, „A Study on electrochemical micromachining of super duplex stainless steel for biomedical filters,“ *ARP Journal of Engineering and Applied Sciences*, Vol. 7, No. 5, pp. 517-523, 2012.
- [12] J. . K. L. Lai, C. . H. Shek & K. H. Lo, Stainless steels: an introduction and their recent developments, Vol. 1, e-book: Bentham Science Publishers, 2012.
- [13] T. Özel & P. Davim, Intelligent Machining, London: John Wiley & Sons, 2009, pp. 231-241.
- [14] S. Raju & N. Kumar, Multicriterion analysis in engineering and management, New Delhi: PHI Learning Private Limited, 2010.
- [15] R. V. Rao, Decision making in manufacturing environment using graph theory and fuzzy multiple attribute decision making methods, London: Springer-Verlag, 2007.
- [16] X.-S. Yang, Nature-inspired metaheuristic algorithms, UK: Luniver Press, 2010, pp. 65-83.

Machining of Stainless Steels: A Comparative Study

Rastee D. Koyee^a, Siegfried Schmauder^b, R. Eisseler^a

^aIfW, University of Stuttgart, Holzgartenstr.17, D-70174 Stuttgart, Germany.

^bIMWF, University of Stuttgart, Pfaffenwaldring 32, D-70569 Stuttgart, Germany.

e-mail: rastee.ali@ifw.uni-stuttgart.de

ABSTRACT

This paper investigates the machining of super duplex EN 1.4410, standard duplex EN 1.4462 and austenitic EN 1.4404 stainless steels through a two-phase experimental study. In the first phase, a new methodology based on Mamdani fuzzy interference of classified chip shapes in chip breaking charts to predict the chip volume ratio is presented. Chip volume ratios, specific cutting pressures, cutting powers and resultant cutting forces are considered as performance characteristics and converted into single indices using Technique for Order Preference by Similarity to Ideal Solution (TOPSIS), Grey Relational Analysis (GRA), VIKOR method and Utility Analysis (UA). An expert system based on fuzzy rule modeling approach is then adopted to combine the computed indices into a single Universal Characteristics Index (UCI). Results showed that converting the output of different Multiple Attribute Decision Making (MADM) methods into a single UCI index is a simple and efficient technique in determining an optimal combination of the cutting parameters. Constrained simulated annealing optimization procedure is then employed to evaluate the optimal process parameters thereby satisfying conflicting requirements of each of performance factors. First ranking UCI values are analyzed and compared with the output of multi-objective optimization techniques (MOO) using Weighted Sum Method. A remarkable improve in reduction of cutting power consumption, specific cutting pressure, resultant cutting forces are reported when first rank UCI value is directly reported as optimum point instead of performing conventional optimization. In the second phase, resultant cutting force and machine current consumption signals are adopted as indirect cutting tool wear monitoring techniques to graph the tool wear progression. Results showed that resultant cutting force and machine current consumption signals are highly sensitive to catastrophic tool failures and cutting tool performance is more stable when the machining of austenitic stainless steel is considered.

KEYWORDS: Chip volume ratio, Face turning, Universal Characteristics Index, Metaheuristic optimization

1. INTRODUCTION

The machinability of stainless steels is very difficult to characterize in definitive terms because of the broad nature of these materials. A ferretic stainless steel, such as type 430, will machine very differently from martensitic. In some sense, this is like comparing brass to carbon steel [1]. Generally, austenitic (300 series) steels are difficult to machine. Chatter can be a problem, necessitating machine tools with high stiffness. Ferritic stainless steels (also 300 series) have good machinability. Martensitic (400 series) steels are abrasive, tend to form a built-up edge, and require tool materials with high hot hardness and crater-wear resistance. Precipitation-hardening stainless steels are strong and abrasive, thus requiring hard and abrasion-resistant tool materials [2]. Duplex steels are somewhat more difficult to machine than the conventional austenitic grades, such as type 316. However, the lean duplex grade S32101 shows excellent machinability [3].

Many investigations have been carried out on machining characteristics of stainless steels [4-9]. The chip morphology has an important effect on several cutting parameters such as tool wear, chip flow, vibration etc. With the aid of chip breaking charts, visual information on the effective chip breakability is provided. Researchers have used fuzzy logic techniques to quantify the information presented visually to classify and predict chip breakability [10]. Logical fuzzy reasoning (often coupled with Taguchi method) has been also successfully applied to multiple output optimization of machining processes [11-13]. Evolutionary techniques, like simulated annealing, were effectively examined on optimization of machining processes. Yusup et. al presented an overview and the comparison of the latest five year researches from 2007 to 2011 that used evolutionary optimization techniques to optimize machining process parameter of both traditional and modern machining [14]. Researchers were considered the machining of metals with multiple performance characteristics and application of one or more MADM techniques to optimize the process parameters [15-21]. Applying cutting forces and cutting power consumptions for indirect tool wear monitoring has been reported by ref. [22-25].

A foresaid literature reveals that limited works in comparative format have been published regarding the investigation of machining of EN 1.4410, EN 1.4462 and EN 1.4404 stainless steels in terms of criterion like the required cutting forces, consumed cutting power, level of difficulty in chip control and tool wear rate. The basic elements of the first phase of present study are briefly presented in Fig. 1. Attributes like; chip volume ratios, specific cutting pressures, cutting powers

and resultant cutting forces are converted into single indices using different MADM methods. Fuzzy Logic Unit (FLU) is next employed to transform the output of MADA methods to a single response called Universal Characteristics Index (UCI). The single-response optimization process was then conducted using simulated annealing (SA). The second phase covers the investigation of tool wear progression using indirect cutting tool wear monitoring techniques like wear monitoring through studying the cutting forces and machine current signals.

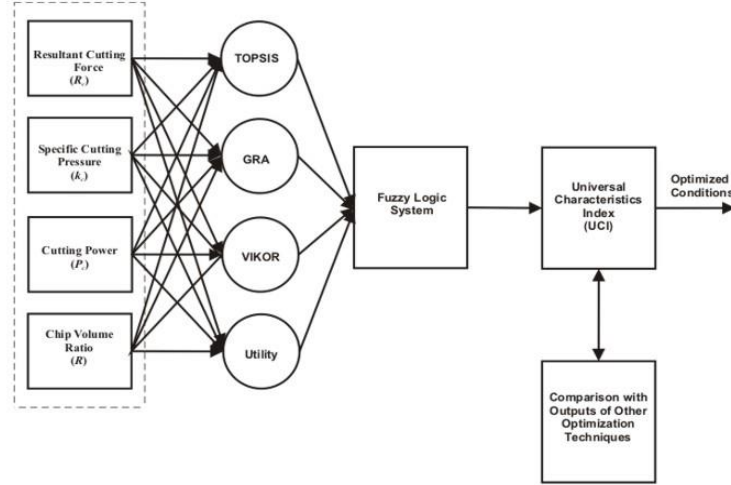


Fig. 1. Flow chart of the first phase of the study.

2. CHIP VOLUME RATIO

With regard to the metal removal rate, one has to distinguish between the volume of the removed material Q_w and the space needed for the randomly arranged metal chips Q_{sp} . The volume of the removed material identifies the volume occupied by a chip with cross sectional area A_c

$$Q_w = v_c \cdot A_c = v_c \cdot f \cdot a_p \quad (1)$$

Here, the cross-sectional area of uncut chip A_c is equal to the product of feed rate f and depth of cut a_p . The volume of the randomly arranged metal chips removed Q_{sp} is greater than the real volume of the same amount of removed material Q_w , since in a reservoir, the chips are not located on next to one another without gaps. Chip volume ratio R defines by what factor the volume of randomly arranged chips Q_{sp} is greater than the volume of the removed material Q_w .

$$Q_{sp} = R \cdot Q_w \quad (2)$$

Consequently, chip volume ratio R results from the ratio:

$$R = \frac{\text{Volume needed for randomly arranged metal chips}}{\text{Material volume of the same amount of metal removal}} \quad (3)$$

The amount of the chip volume ratio R depends on the chip shape. Fig. 2 shows the most common chip shapes, their related chip volume ratio and ratings. Each chip form is assigned to a chip volume ratio (R), which defines by what factor the transport volume needed for the specific chip form exceeds the intrinsic material volume of the chip [26].



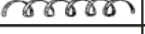





Chip Type		Chip Volume Ratio
Ribbon Chips		≥ 90
Snarled Chips		≥ 90
Flat Helical Chips		≥ 50
Cylindrical Helical Chips		≥ 50
Helical Chip Segments		≥ 25
Spiral Chips		≥ 8
Spiral Chip Segments		≥ 8
Discontinuous Chips		≥ 3

Fig. 2. Chip shapes, their related chip volume ratio and rating

3. MADM METHODS

Making decisions is a part of our daily lives. The major concern is that almost all decision problems have multiple, usually conflicting, criteria. Researches on how to solve such problems has been enormous. Methodologies, as well their applications, appear in professional journals of different disciplines. Diversifies as such problems may be, they are broadly classified into two categories: (1) Multiple Attribute Decision Making (MADM) and (2) Multiple Objective Decision Making (MODM). From a practical viewpoint, MADM is associated with problems whose number of alternatives has been predetermined. The Decision Maker (DM) is to select/prioritize/rank a finite number of courses of action. On the other hand, MODM is not associated with problems in which the alternatives have been predetermined. The DM's primary concern is to design a "most" promising alternative with respect to limited resources [27].

Despite the development of a large number of refined MADA methods, none can be considered as the 'super method' appropriate to all decision making situations. This implies that it is critical to select the most appropriate method to solve the problem under consideration, since the use of unsuitable method always leads to misleading decisions. Therefore, to avoid sticking to the use of one method or another, four of the most repeated MADM methods in literature are selected in this respect:

1. Technique for Order Preference by Similarity to Ideal Solution (TOPSIS)
2. Grey Relational Analysis (GRA)
3. The VIKOR method
4. Utility Analysis (UA).

4. MATERIALS AND METHODS

A full factorial design was selected in the first stage of experimentation, so that all interactions between the independent variables could be well investigated. The independent variables are the feed rate and depth of cut, whereas the cutting speed is fixed at 100m/min. The levels of independent variables are shown in Table 1. Face turning tests at constant cutting speed were performed on EN 1.4410, EN 1.4462 and EN 1.4404 stainless steel bars. The bars had a diameter of 55mm and length of 500mm. Negative 80° rhombic-shape coated carbide inserts (ISO code of CNMG 120408-MM 2025) with depth of cut range of (0.5-5.7mm) and feed rate range of (0.1-0.45 mm/rev) are used throughout the investigation. The inserts were mounted on a right hand style PCLNL-2525M-12 ISO type tool holder.

Table 1 Cutting parameters and their levels.

Cutting parameters	Symbol	Unit	Cutting parameter levels (L)						
			L ₁	L ₂	L ₃	L ₄	L ₅	L ₆	L ₇
Feed rate	f	mm/rev	0.1	0.175	0.25	0.325	0.4	-	-
Depth of cut	a_p	mm	0.5	1	1.5	2	2.5	3	3.5

During the turning tests, the cutting force (F_c), axial force (F_a), and radial force (F_r), were measured using Kistler type 9129A three component piezo-electric dynamometer, which was connected to a charged Kistler type 5070A amplifier and personal computer through an analog to digital converter card. The dependent variables are resultant cutting force (R_c), cutting power (P_c), specific cutting pressure (k_c) and chip volume ratio (R). The resultant cutting force (R_c) is computed using the following equation:

$$R_c = \sqrt{F_c^2 + F_a^2 + F_r^2} \quad (4)$$

The specific cutting pressure k_c was calculated from the acquired data on main cutting force F_c , using the equation:

$$k_c = F_c / (f \cdot a_p) \quad (5)$$

The electrical power signals were measured from the CNC machine controller directly and fed softly to the same personal computer. The procedure to evaluate the power consumed involved first taking measurement of instantaneous power consumed:

1. Before machining condition, which included the measurement of the idle and machine module power. The spindle is running, the machine tool box house is moving without real contact between the cutting tool and the workpiece. The power measure is designated as an idle or initial power (P_i). The net measured idle power of the machine in present study was 2507.558W
2. During machining condition, the total power consumed by the machine tool system during machining operation. The power measure in this stage is designated as total or final power (P_f).

The difference between the above two measured powers determines the actual power consumed by machining process (P_c).

$$P_c = P_f - P_i \quad (6)$$

A very useful tool for investigating the machinability of materials is a chip chart, which maps the sizes and shapes of chip forms across a depth of cut in (mm) and feed in (mm/rev) matrix, as shown in Fig. 3.

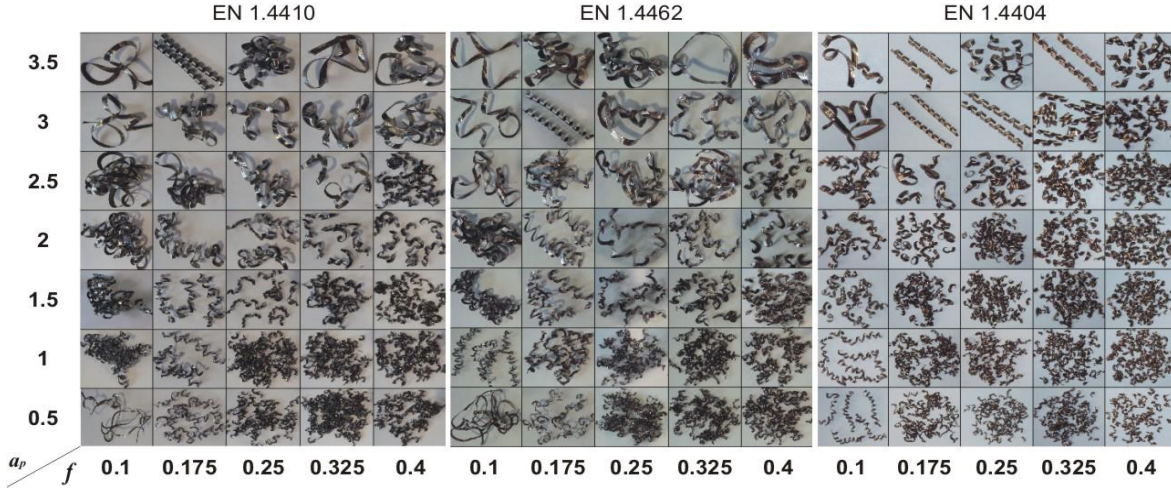


Fig. 3. Chip breaking chart at 100 m/min cutting speed.

It is well established in conventional machining, in comparison to the depth of cut and feed rate, cutting speed is a dominant parameter on tool wear. Hence, in studying wear progression, the cutting speed was varied between 50 and 300 m/min while feed rate and depth of cut were kept constant at 0.1mm/rev and 0.5 mm respectively. In the second stage of experimentation, a total of (1914) cutting trials were carried out. During which, measured cutting forces and electrical current signals were used to monitor tool wear.

5. ESTIMATION OF CHIP VOLUME RATIO

Chips produced when machining austenitic stainless steel are generally friendlier to the machine tool. Detailed observations of the chip chart provide important visual information on the effective chip breakability of workpieces. Chip morphology strongly influenced by workpiece material, feed rate and depth of cut. The harder the material the curlier the chips form. Chips produced during turning austenitic stainless steel were mainly in the form helical and spiral chips at higher feed ranges and less ribbon and snarled chip proportions at lower feed rates when compared with duplex grades. When machining super duplex EN 1.4410 and standard duplex EN 1.4462 stainless steel, snarled and ribbon chips were produced at low feed ranges and nearly all higher depth of cut ranges. At intermediate feed ranges, the produced chips were rather of flat-helical and cylindrical-helical forms. Helical and less spiral were the predominant form of chips when higher feed rates are used. Generally, the increase in depth of cut increased the curliness of chips.

In an attempt to quantify the information presented visually, fuzzy logic techniques were used to predict chip volume ratio. A new chip classification system in conjunction with forms of chip and their loose chip volume ratio (as shown in Fig. 3) is proposed in this study. The triangular membership function is applied for both input and output variables. Each level of input parameter was assigned with a corresponding fuzzy set. Thus, feed rate is classified into five fuzzy sets: Very Low (VL), Low (L), Fair (F), High (H) and Very High (VH), and depth of cut into seven fuzzy sets: Very Low (VL), Low (L), Moderately Low (ML), Moderate (M), Moderately High (MH), High (H) and Very High (VH). In order to increase the accuracy of prediction, chip forms are further divided into shorter and longer subcategories. The R output is divided into the following nine fuzzy sets: Discontinuous chips (DC), Short Spiral Chips (SSC), Long Spiral Chips (LSC), Short Helical Chip Segments (SHCS), Long Helical Chip Segments (LHCS), Short Cylindrical and Flat helical Chips (SCFC), Long Cylindrical and Flat helical Chips (LCFC), Short Ribbon and Snarled Chips (SRSC) and Long Ribbon and Snarled Chips (LRSC). Fig. 4 shows the suggested fuzzy employed to predict chip volume ratio (R).

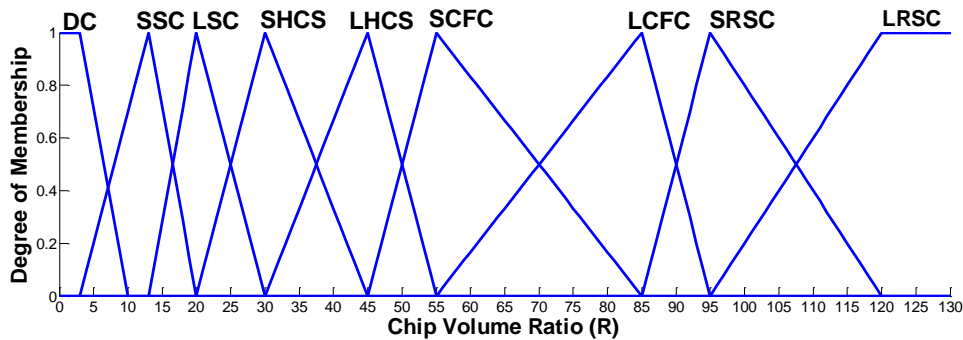


Fig. 4. Chip volume ratio membership functions.

A set of 35 rules is written per material case for activating the fuzzy inference system (FIS). For a fuzzy system involving two input parameters to yield an output, rules can be described in a matrix form. Table 2 presents the rules

between feed rate and depth of cut and the corresponding chip volume ratio in matrix format. Finally, the center-of-gravity defuzzification was applied to give crisp value of chip volume ratio.

Table 2. Chip classification fuzzy-based rules.

	EN 1.4410					EN 1.4462					EN 1.4404				
Depth of cut	Feed rate					Feed rate					Feed rate				
of cut	VL	L	F	H	VH	VL	L	F	H	VH	VL	L	F	H	VH
VL	SRSC	SCFC	SHCS	SHCS	SHCS	SRSC	SCFC	SHCS	LHCS	SHCS	LHCS	SHCS	SHCS	SSC	SSC
L	URSC	SCFC	LHCS	LHCS	SHCS	SCFC	SCFC	LHCS	LHCS	SSC	LHCS	LSC	SHCS	SSC	SSC
ML	URSC	LCFC	SCFC	LHCS	LSC	LRSC	LCFC	SCFC	SCFC	LSC	SHCS	LSC	LSC	LSC	SSC
M	URSC	LCFC	SRSC	LCFC	LHCS	LRSC	LCFC	LCFC	LHCS	LHCS	SCFC	LSC	LSC	LSC	SSC
MH	URSC	LRSC	LRSC	LRSC	LHCS	LRSC	LRSC	LRSC	LRSC	LHCS	LRSC	LHCS	LHCS	LHCS	LSC
H	URSC	LRSC	LRSC	LRSC	LRSC	LRSC	LCFC	LRSC	LRSC	LRSC	LRSC	LCFC	LCFC	LHCS	SHCS
VH	URSC	LCFC	LRSC	LRSC	LRSC	LRSC	LRSC	LRSC	LRSC	LRSC	LRSC	LCFC	LCFC	LCFC	LHCS

Table 3 shows the computed performance characteristics and contour plots for these characteristics are mapped and shown in Fig. 5. The optimum and near optimum regions are filled with dark blue and light blue colors. This argument initially suggests that the optimum point should locate somewhere within shown dark blue regions.

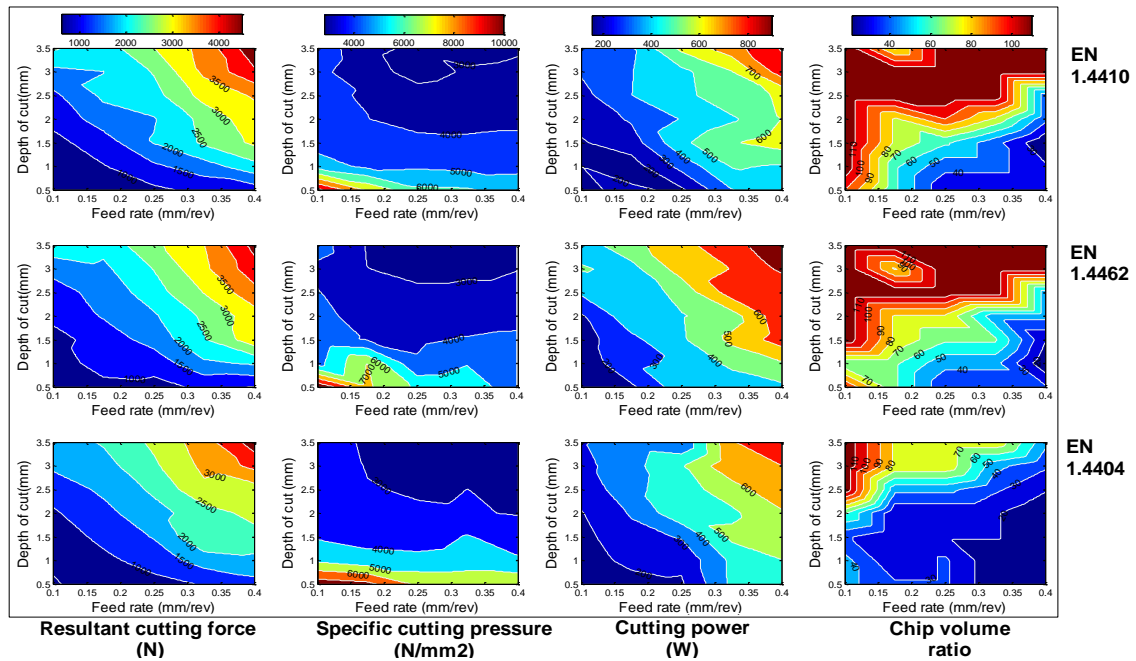


Fig. 5. Contour maps of performance characteristics

6. UNIVERSAL CHARACTERISTICS INDEX

The output of MADM methods showed different ranking results, which will cause uncertainty related to the selection of the best scenario (alternative). Therefore, to obtain a more general solution, fuzzy logic system is employed to combine the individual MPCIs into a single characteristics index called Universal Characteristics Index (UCI). Matlab software was used to construct the inference model of the UCI. The MPCIs values were first adjusted to a notionally common scale between null and one, using simple normalization methods. So that the digit 'one' represents the most desirable and 'null' is the least desirable alternative (see Table 3). The four input variables are assigned with the following fuzzy sets: Small (S), Medium (M) and Large (Lg). The output variable has the following nine levels: Extremely Low (EL), Very Low (VL), Low (L), Lower Medium (LM), Medium (M), Upper Medium (UM), High (H), Very High (VH) and Extremely High (EH). Mamdani implication method is again employed for the fuzzy inference reasoning. The relationship between system input and output is expressed by an "If-Then" type. Totally 81 fuzzy rules per material were formulated. A sample of the formulated fuzzy rules is listed below.

Rule 1:	If GRG is (S) and VIKOR is (S) and TOPSIS is (S) and UA is (S) Then UCI_i is (EL)
Rule 2:	If GRG is (S) and VIKOR is (S) and TOPSIS is (S) and UA is (M) Then UCI_i is (VL)
Rule 3:	If GRG is (S) and VIKOR is (S) and TOPSIS is (S) and UA is (Lg) Then UCI_i is (L)
.	.
.	.
Rule 80:	If GRG is (Lg) and VIKOR is (Lg) and TOPSIS is (Lg) and UA is (M) Then UCI_i is (VH)
Rule 81:	If GRG is (Lg) and VIKOR is (Lg) and TOPSIS is (Lg) and UA is (Lg) Then UCI_i is (EH)

Table 3. Performance characteristics and predicted UCI values

NO.	f (mm/rev)	a_p (mm)	EN 1.4410						EN 1.4462						EN 1.4404					
			R_c (N)	k_c (N/mm ²)	P_c (W)	R	UCI _i	Rank	R_c (N)	k_c (N/mm ²)	P_c (W)	R	UCI _i	Rank	R_c (N)	k_c (N/mm ²)	P_c (W)	R	UCI _i	Rank
1	0.1	0.5	620	10249	187	100	0.449	22	590	9962	108	100	0.604	10	451	7574	166	43	0.578	17
2	0.1	1.0	680	5551	200	118	0.619	13	560	4614	131	62	0.887	1	576	4794	142	43	0.779	5
3	0.1	1.5	859	4564	192	118	0.642	9	799	4258	157	118	0.627	8	718	3906	172	32	0.959	1
4	0.1	2.0	1132	4514	226	118	0.581	14	1131	4327	188	118	0.553	11	935	3787	195	62	0.695	8
5	0.1	2.5	1384	4206	266	118	0.518	17	1336	4075	316	118	0.393	22	1207	3766	229	118	0.312	28
6	0.1	3.0	1870	4328	310	118	0.393	25	1615	3740	412	118	0.329	24	1594	3810	268	118	0.266	30
7	0.1	3.5	2549	4798	349	118	0.294	29	2413	4513	349	118	0.271	30	1710	3564	291	118	0.260	31
8	0.175	0.5	800	7852	216	62	0.663	7	740	7178	182	62	0.735	3	739	7252	152	32	0.617	14
9	0.175	1.0	973	4737	154	62	0.846	2	1364	7012	284	62	0.542	12	877	4332	234	21	0.801	3
10	0.175	1.5	1254	4010	251	78	0.727	4	1244	3949	274	78	0.627	8	1129	3650	264	21	0.848	2
11	0.175	2.0	1754	4024	314	78	0.648	8	1540	3572	365	78	0.508	15	1361	3297	311	21	0.794	4
12	0.175	2.5	2099	3906	399	118	0.343	27	1646	3164	328	118	0.420	20	1592	3070	372	43	0.620	13
13	0.175	3.0	1992	3192	397	118	0.417	24	1893	3011	365	78	0.505	16	1814	2920	366	78	0.362	24
14	0.175	3.5	2248	3080	391	78	0.625	11	2165	2937	470	118	0.316	26	2054	2828	345	78	0.357	26
15	0.25	0.5	897	6208	183	32	0.886	1	843	5823	359	32	0.719	4	825	5803	186	32	0.683	9
16	0.25	1.0	1408	4835	335	43	0.784	3	1205	4128	313	43	0.708	5	1225	4274	226	32	0.722	7
17	0.25	1.5	2027	4429	478	62	0.545	15	1685	3802	386	62	0.518	13	1534	3533	309	21	0.752	6
18	0.25	2.0	1965	3419	405	100	0.475	19	1930	3301	393	78	0.446	19	1812	3135	474	21	0.640	11
19	0.25	2.5	2320	3185	463	118	0.342	28	2282	3123	435	118	0.310	28	2091	2888	460	43	0.478	21
20	0.25	3.0	2536	2811	472	118	0.353	26	2516	2809	546	118	0.282	29	2407	2734	492	78	0.275	29
21	0.25	3.5	2989	2942	628	118	0.284	30	2880	2840	569	118	0.261	31	2603	2549	310	78	0.359	25
22	0.325	0.5	1135	6109	396	32	0.718	5	1096	5917	333	32	0.702	6	1038	5721	418	12	0.625	12
23	0.325	1.0	1776	4716	507	43	0.623	12	1908	4902	425	43	0.517	14	1724	4438	421	12	0.651	10
24	0.325	1.5	2587	4286	593	43	0.480	18	2459	4102	525	62	0.399	21	2472	4070	523	21	0.386	23
25	0.325	2.0	2652	3497	483	78	0.469	20	2595	3352	453	43	0.454	17	2276	3069	481	21	0.587	16
26	0.325	2.5	3191	3291	584	118	0.266	31	3020	3121	649	118	0.454	17	2899	3004	549	32	0.346	27
27	0.325	3.0	3603	3059	594	118	0.266	31	3387	2894	602	118	0.241	32	3116	2723	679	43	0.260	31
28	0.325	3.5	3680	2813	759	118	0.250	33	3484	2688	669	118	0.235	33	3263	2521	690	78	0.091	35
29	0.4	0.5	1248	5492	466	32	0.711	6	983	4127	379	32	0.741	2	1335	5749	418	12	0.574	18
30	0.4	1.0	2331	4768	493	32	0.638	10	2068	4275	488	12	0.669	7	1868	4142	497	12	0.603	15
31	0.4	1.5	3102	4480	647	21	0.541	16	3313	4352	645	21	0.358	23	2329	3450	578	12	0.538	20
32	0.4	2.0	3311	3562	602	43	0.438	23	3262	3416	673	43	0.318	25	2651	2948	583	12	0.561	19
33	0.4	2.5	3551	3078	605	43	0.458	21	3836	3108	608	43	0.316	26	2759	2444	689	21	0.405	22
34	0.4	3.0	4414	3116	854	118	0.099	34	4294	2990	720	118	0.091	34	3637	2574	698	32	0.207	33
35	0.4	3.5	4860	2933	910	118	0.039	35	4670	2814	770	118	0.041	35	4255	2614	806	43	0.099	34

Spearman's rank-order correlation is used to evaluate the strength of the statistical relationship between the computed MPCIs and UCI values, see Table 4. The near to one values of UCI coefficients are good indications of strong statistical relationship with other MPCIs.

Table 4. Spearman's rank correlation coefficients

	EN 1.4410					EN 1.4462					EN 1.4404				
	TOPSIS	GRG	VIKOR	UA	UCI	TOPSIS	GRG	VIKOR	UA	UCI	TOPSIS	GRG	VIKOR	UA	UCI
TOPSIS	1.000	0.825	0.815	0.872	0.918	1.000	0.895	0.819	0.918	0.906	1.000	0.9	0.925	0.936	0.986
GRG	0.825	1.000	0.735	0.98	0.914	0.895	1.000	0.78	0.996	0.911	0.90	1.000	0.738	0.983	0.929
VIKOR	0.815	0.735	1.000	0.824	0.922	0.819	0.78	1.000	0.798	0.877	0.925	0.738	1.000	0.808	0.914
UA	0.872	0.98	0.824	1.000	0.963	0.918	0.996	0.798	1.000	0.924	0.936	0.983	0.808	1.000	0.963
UCI	0.918	0.914	0.922	0.963	1.000	0.906	0.911	0.877	0.924	1.000	0.986	0.929	0.914	0.963	1.000

It was found that the Spearman's rank correlation coefficients between the rankings as acceptable, and the coefficient between UCI and MPCIs are generally above 0.9, which demonstrates the viability of estimated UCI values. The ranks of estimated UCI values along with the ranks of the four MADM methods are shown in Fig. 6.

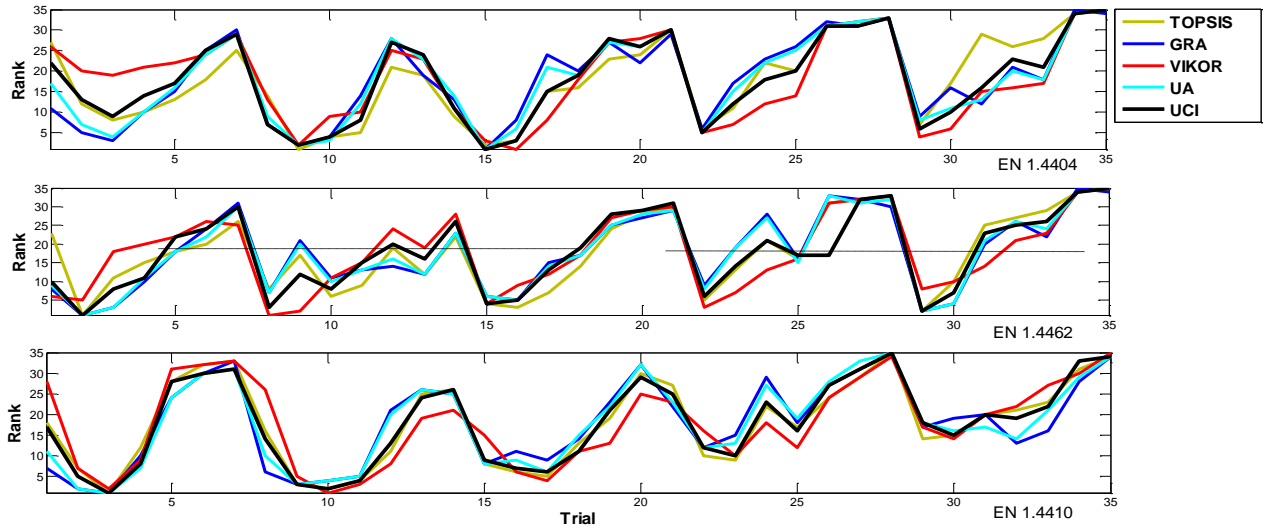


Fig. 6. Ranking the output of MADA methods and UCI

7. OPTIMIZATION

After combining the MPCIs values into one index, the next step is to find the optimal settings of the process parameters (feed rate and depth of cut) for UCI using simulated annealing algorithm. The decision variables used in this study are feed rate and depth of cut. The following objective function is developed for Multi-Objective Optimization (MOO) of the performance characteristics based on Weighted Sum Method:

$$Z = \frac{w_1}{\text{Max}(P_c)} Y(P_c) + \frac{w_2}{\text{Max}(k_c)} Y(k_c) + \frac{w_3}{\text{Max}(R_c)} Y(R_c) + \frac{w_4}{\text{Max}(R)} Y(R) \quad (7)$$

where w_1, w_2, w_3 and w_4 are the weight values assigned to P_c , k_c , R_c and R respectively. The weight values can be anything provided that $w_1 + w_2 + w_3 + w_4 = 1$. Here, equal weights for all responses are considered, i.e. $w_1 = w_2 = w_3 = w_4 = 0.25$. Using multiple regressions, a second model based on computed UCI values has been developed. Because the possibility of determining a global optimum solution and its accuracy depends on the type of optimization modeling used to express the objective function, hence, a great attention has been paid to select an accurate and reliable model. Thus, the objective function employed for predicting UCI values is:

$$\begin{aligned} UCI_i = & b_1 + b_2 f + b_3 a_p + b_4 f^2 + b_5 f \cdot a_p + b_6 a_p^2 + b_7 f^3 + b_8 f^2 \cdot a_p + b_9 f \cdot a_p^2 \\ & + b_{10} a_p^3 + b_{11} f^3 \cdot a_p + b_{12} f^2 \cdot a_p^2 + b_{13} f \cdot a_p^3 + b_{14} a_p^4 \end{aligned} \quad (8)$$

Performance characteristics are formulated using multiple nonlinear regression analysis, and applied as constraints on both objective functions separately. Simplest forms of constraints are suggested and tabulated in Table 5. The correlation factor R-squared (not shown for clear space reasons) and the $R_{adj.}$ values indicate that the models relatively fit the data well for the first three constraint models. The bound values, which correspond to the maximum performance values, are directly extracted from Table 3. The bounds of decision variables were selected based on their maximum and minimum values in Table 1, i.e.:

$$\begin{aligned} 0.1 & \leq f \leq 0.4 \text{ (mm/rev)}; \\ 0.5 & \leq a_p \leq 3.5 \text{ (mm)}. \end{aligned}$$

Table 5. Performance characteristic models as constraints with 95% confidence interval

Constraint	EN 1.4410	EN 1.4462	EN 1.4404
P_c	$1071f^{0.797}a_p^{0.375} \leq P_{cmax}$	$915.4f^{0.694}a_p^{0.367} \leq P_{cmax}$	$1094.f^{0.867}a_p^{0.346} \leq P_{cmax}$
k_c	$3412f^{-0.278}a_p^{-0.435} \leq k_{cmax}$	$3163f^{-0.291}a_p^{-0.429} \leq k_{cmax}$	$3474.f^{-0.185}a_p^{-0.445} \leq k_{cmax}$
R_c	$4196f^{0.746}a_p^{0.614} \leq R_{cmax}$	$4368f^{0.808}a_p^{0.615} \leq R_{cmax}$	$3641.f^{0.752}a_p^{0.606} \leq R_{cmax}$
R	$39.74f^{-0.318}a_p^{0.445} \leq R_{max}$	$37f^{-0.29}a_p^{0.549} \leq R_{max}$	$5.776f^{-0.767}a_p^{1.077} \leq R_{max}$
P_c model: EN 1.4410: $R_{adj}=0.891$, $RMSE=63.1$, EN 1.4462: $R_{adj}=0.913$, $RMSE=52.59$, EN 1.4404: $R_{adj}=0.902$, $RMSE=57.02$ k_c model: EN 1.4410: $R_{adj}=0.883$, $RMSE=520.2$, EN 1.4462: $R_{adj}=0.791$, $RMSE=691.3$, EN 1.4404: $R_{adj}=0.943$, $RMSE=305.3$ R_c model: EN 1.4410: $R_{adj}=0.941$, $RMSE=329.1$, EN 1.4462: $R_{adj}=0.939$, $RMSE=275.36$, EN 1.4404: $R_{adj}=0.961$, $RMSE=182.37$ R model: EN 1.4410: $R_{adj}=0.600$, $RMSE=23.54$, EN 1.4462: $R_{adj}=0.6$, $RMSE=23.08$, EN 1.4404: $R_{adj}=0.6$, $RMSE=14.622$ ¹			

The initializing optimization parameters for simulated annealing algorithms were: initial temperature=1.0, final stopping temperature= 1×10^{-10} , maximum number of rejection=2500, maximum number of runs=500, maximum number of accept=250, Boltzmann constant=1 and energy norm= 1×10^{-5} . The obtained optimization results showed that simulated annealing is highly reliable and converges consistently to the optimum solution. Table 6 presents the results of optimization, UCI and performance values at optimal level.

Table 6. Process optimization results

Factors	Objective function						Per-Table 3. first rank UCI, Average Improve cutting parameters and performance values			Average Improve	
	Model I			Model II						Model 1 (%)	Model 2 (%)
	EN 1.4410	EN 1.4462	EN 1.4404	EN 1.4410	EN 1.4462	EN 1.4404	EN 1.4410	EN 1.4462	EN 1.4404		
P_c	228.77	293.6	157.81	262.82	181.77	146.51	182.53	130.95	172.28	22.147	13.639
k_c	7227.3	6174.6	5891.4	6885.2	6315.6	4401.5	6207	4614.4	3905.4	24.364	16.019
R_c	824.08	1021.21	617.54	938.37	660.13	959.8	896.7	560.38	717.66	6.700	14.926
R	48.69	36.55	20.8	46	70.3	37.9	31.7	61.7	31.7	-28.77	19.89
f (mm/rev)	0.20	0.28	0.121	0.238	0.1	0.132	0.25	0.1	0.1		
a_p (mm)	0.50	0.50	0.732	0.5	0.959	1.365	0.5	1	1.5		
Obj.	0.384	0.329	0.323	0.828	0.743	0.898	0.886	0.887	0.959		

It should be noted here that ranking the alternatives according to UCI values offers many advantages like, simplicity, accuracy, generally lower non-beneficial performance values and the reducing the necessity of performing optimization process. At optimum UCI values, when simple ranking UCI results is used and compared to the optimum results obtained in model 1, the average improvement in cutting power consumption is 22.147%, specific cutting pressure is 24.364% and resultant cutting force is 6.7%. In contrast, optimization with model 1 could reach lower chip volume ratio with an average rate of deterioration of -28.77%. This relative large percentage is attributed to the inaccurate models used to predict chip volume ratio with margins of errors to up to 23.54, 23.08 and 14.622 for EN 1.4410, EN 1.4462 and EN 1.4404 respectively. To compensate for this inconvenience, all root mean square of errors are added to the models and optimization process ran again. Results has shown that the average improve in cutting power consumption would raise to a new level of 41.433%, specific cutting pressure of 30.961%, resultant cutting forces to 30.081% and the chip volume ratio could raise to 14.675%. This confirms the viability of derived UCI values when compared with conventional multi-objective optimization algorithms when accurate models are utilized. Although an accurate and relatively complex objective function which could best model UCI is used as a model for a second optimization process and optimization ran under the same set of constraints, using this methodology no traces of improvement is reported.

8. INDIRECT TOOL WEAR MONITORING

As a tool wear monitoring technique, using measured signals of cutting forces offers many advantages like easy to measure and having a clear phenomenological relationship with tool wear. The more the tool wears, the more the signals of worn tool differs from signals of sharp tool, in terms of both magnitude and shape. As there is no agreement in which component of cutting force has a more closed relationship with tool wear, in this study, the resultant of cutting forces was used as a useful signal. On the other hand, monitoring spindle or feed motor current signals has the advantage of simplicity in hardware implementation that does not interfere with the process and does not require high cost devices.

To accomplish measurements in phase 2, a total of (1914) cutting runs were carried out. During which, cutting forces and electrical current consumption were used to predict the tool wear. Tool life has been estimated based on 0.4mm flank wear criteria. The shape of the curve about the evolution of wear according to the cutting length or cutting time or cutting passes is similar to the typical wear curve of the tools. The tool wear curves for cutting speed of 300m/min are shown in Fig. 7. It should be noted that the resultant cutting forces slope is very steep when EN 1.4410 is cut. On the other hand, cutting EN 1.4462 and EN 1.4404 are seen more stable based on the delay of abrupt increase in resultant cutting force signals to cutting passes 26 and 36 respectively. Lowering cutting speed by six folds had remarkably increased the number of passes that utterly shows a small increase or decrease in electrical current consumption, which means more stable cutting

¹ RMSE: Root Mean Square of Errors

process and lower tool wear rates (see Fig. 8). The sensitivity of cutting force signals toward catastrophic tool failures, as it were noticed during the course of 300m/min experiments when EN 1.4410 is machined, was high. Resultant cutting forces has increased to up to three folds of the initial values. The difference in stable numbers of cutting passes of material cases was attributed to the difference in tensile strength, material hardness, thermal conductivity, chemical composition and chip breaking tendency.

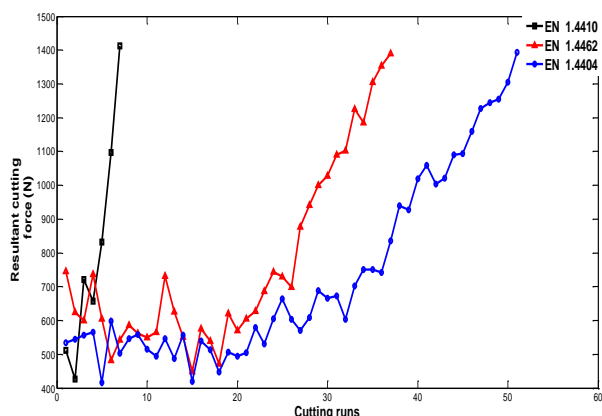


Fig. 7. Progressive increase in resultant cutting force during face turning of stainless steels at 300m/min.

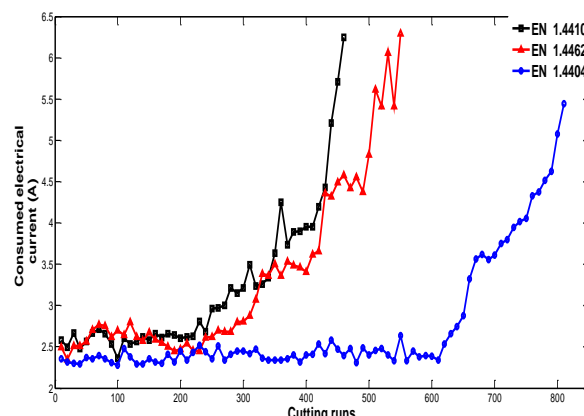


Fig. 8. Progressive increase in electrical current consumption during face turning of stainless steels at 50m/min.

9. CONCLUSION

For the range of process parameters, the resulting chip form was strongly influenced by the workpiece material and cutting conditions. When machining super duplex EN 1.4410 and standard duplex EN 1.4462 stainless steels, snarled and ribbon chips were the dominant at lower feed ranges and nearly all higher depth of cut ranges. Meanwhile, flat helical and cylindrical helical chips at medium feed ranges and helical and less spiral chips at higher feed ranges were the dominant. Chips obtained when machining austenitic EN 1.4404 stainless steel are friendlier to the machine and generally produce lower ribbon, snarled and flat helical chips. Fuzzy logic principles were applied to quantify the information presented in chip breaking chart and could successfully predicts the chip volume ratio.

In this study, the performance characteristics were chip volume ratio, specific cutting pressures, cutting powers and resultant cutting forces. Because the values of above non-beneficial performance characteristics when machining austenitic EN 1.4404 are lower than standard duplex EN 1.4462 and super duplex EN 1.4410 grades, therefore, the machinability of EN 1.4404 is better than EN 1.4462 and EN 1.4410. The multiple performance characteristics were successfully converted into single MPCII indices using GRA, TOPSIS, VIKOR method and Utility Analysis (UA). Due to the different MPCII outputs and rankings, the absence of a reference defining a 'super method' and in order to combine the output of different MADA methods, a single universal characteristics index (UCI) based on fuzzy rule modeling approach was proposed. Spearman's rank correlation coefficients have confirmed that the proposed index had a very good correlation with the output of other MPCII methods. The present optimum solutions are specific to the values of constants used in optimization and constraint models. Different results are expected when different objective and constraint models and different performance weighting methods are adopted. Predicted UCI values have been analyzed and compared with output of other optimization techniques. A remarkable improve in reduction of cutting power consumption, specific cutting pressure, resultant cutting forces has been reported when direct ranking system of predicted UCI indices are set optimum. Indirect cutting tool wear monitoring through measuring signals of cutting forces and machine electrical current showed that the tool life is highly sensitive to the catastrophic cutting tool failure. Cutting tool lasted longest when machining EN 1.4404 and shortest when machining EN 1.4410. At cutting speed of 300m/min, the cutting process was very unstable; the tool wear curve had steeper slopes and cutting tools had very shorter tool life compared to the remarkably better performances at cutting speed of 50m/min.

ACKNOWLEDGEMENT

The authors would like to thank Geschäftsbereich Sandvik Coromant for providing cutting tools and materials for this research and gratefully acknowledge the efforts of Dr. Stefan Scherbarth at Sandvik Tooling Deutschland GmbH for sharing his experience with us during the course of this research.

10. REFERENCES

- [1] M. F. McGuire, Stainless steels for design engineers, USA: ASM International, 2008, p. 182.
- [2] S. Kalpakjian and S. R. Schmid, Manufacturing engineering and technology, Singapore: Prentice Hall, 2009, p. 585.
- [3] R. W. Revie, Uhlig's corrosion handbook, Newjersy USA: John Wiley & Sons. Inc., 2011, p. 703.
- [4] W.-T. Chien and C.-S. Tsai, "The investigation on the prediction of tool wear and the determination of optimum cutting conditions in machining

- 17-4PH stainless steel", *Journal of Materials Processing Technology*, pp. 340-345, 2003.
- [5] I. Korkut, M. Kasap, I. Ciftci and U. Seker, "Determination of optimum cutting parameters during machining of AISI 304 austenitic stainless steel", *Materials and Design*, Vol. 25, pp. 303-305, 2004.
- [6] J. Endrino, G. R. Fox and C. Gey, "Hard AlTiN, AlCrN PVD coatings for machining of austenitic stainless steel", *Surface & Coatings Technology*, Vol. 200, pp. 6840-6845, 2006.
- [7] C. Maranhao and J. P. Davim, "Finite element modelling of machining of AISI 316 steel: Numerical simulation and experimental validation", *Simulation Modelling Practice and Theory*, Vol. 18, pp. 139-156, 2010.
- [8] A. K. Sahoo (a) and B. Sahoo (b), "Experimental investigations on machinability aspects in finish hard turning of AISI 4340 steel using uncoated and multilayer coated carbide inserts", *Measurement*, Vol. 45, pp. 2153-2165, 2012.
- [9] E. Ahmadi and R. M. Homami, "Experimental investigation and mathematical modeling of composite ceramic cutting tools with alumina base in the machining process of PH hardened austenitic-ferritic (duplex) stainless steel", *Int. J. Advanced Design and Manufacturing Technology*, Vol. 5, No.2, pp. 17-25, 2012.
- [10] A. Balaji, R. Ghosh, X. Fang, R. Stevenson and I. Jawahir, "Performance-based predictive models and optimization methods for turning operations and applications: Part 2-assessment of chip forms/chip breakability", *Journal of Manufacturing Processes*, Vol. Vol. 8, No. 2, pp. 144-158, 2006.
- [11] Y.-F. Tzeng and F.-c. Chen, "Multi-objective optimisation of high-speed electrical discharge machining process using a Taguchi fuzzy-based approach", *Materials and Design*, Vol. 28, pp. 1159-1168, 2007.
- [12] A. Gupta, H. Singh and A. Aggarwal, "Taguchi-fuzzy multi output optimization (MOO) in high speed CNC turning of AISI P-20 tool steel", *Expert Systems with Applications*, Vol. 38, pp. 6822-6828, 2011.
- [13] Y.-S. Yang and W. Huang, "A grey-fuzzy Taguchi approach for optimizing multi-objective properties of zirconium-containing diamond-like carbon coatings", *Expert Systems with Applications*, Vol. 39, pp. 743-750, 2012.
- [14] N. Yusup, A. . M. Zain and S. Z. . M. Hashim, "Evolutionary techniques in optimizing machining parameters: Review and", *Expert Systems with Applications*, Vol. 39, p. 9909-9927, 2012.
- [15] P. Kao and H. Hocheng, "Optimization of electrochemical polishing of stainless steel by grey relational analysis", *Journal of Materials Processing Technology*, Vol. 140, pp. 255-259, 2003.
- [16] R. WALIA, H. Shan and P. Kumar, "Multi-response optimization of CFAAFM process through Taguchi method and utility concept", *Materials and Manufacturing Processes*, Vol. 21, pp. 907-914, 2006.
- [17] C.-K. Chang and H. S. Lu, "Design optimization of cutting parameters for side milling operations with multiple performance characteristics", *Int. J. Adv. Manuf. Technol.*, Vol. 207, pp. 18-26, 2007.
- [18] V. Gaitonde^(a), S. Karnik, B. Achyutha and B. Siddeswarappa, "Taguchi optimization in drilling of AISI 316L stainless steel to minimize burr size using multi-performance objective based on membership function", *journal of materials processing technology*, Vol. 202, pp. 374-379, 2008.
- [19] V. Gaitonde^(b), S. Karnik and J. P. Davim, "Multiperformance optimization in turning of free-machining steel using taguchi method and utility concept", *JMEPEG*, Vol. 18, pp. 2351-2360, 2009.
- [20] A. Singh, S. Datta and S. S. Mahapatra, "Application of TOPSIS in the Taguchi method for optimal machining parameter selection", *J. Manuf. Sci. Prod.*, Vol. 11, pp. 49-60, 2011.
- [21] M. Kaladhar, K. V. Subbaiah, C. S. Rao and K. N. Rao, "Application of taguchi approach and utility concept in solving the multi-objective problem when turning AISI 202 austenitic stainless steel", *Journal of Engineering Science and Technology Review*, Vol. 4(1), pp. 55-61, 2011.
- [22] F. A. Al-Sulaiman, A. K. Sheikh and M. Abdul Baseer, "Use of electrical power for online monitoring of tool condition", *Journal of Materials Processing Technology*, Vol. 166, p. 364-371, 2005.
- [23] S. N. Huang, K. K. Tan, Y. S. Wong, C. W. de Silva, H. Goh and W. Tan, "Tool wear detection and fault diagnosis based on cutting force monitoring", *International Journal of Machine Tools & Manufacture*, Vol. 47, p. 444-451, 2007.
- [24] K.-J. Lee, T.-M. Lee and M.-Y. Yang, "Tool wear monitoring system for CNC end milling using a hybrid approach to cutting force regulation", *Int. J. Adv. Manuf. Technol.*, Vol. 32, pp. 8-17, 2007.
- [25] J. Ghani, M. Rizal, M. Nuawi, M. Ghazali and C. Haron, "Monitoring online cutting tool wear using low-cost technique and user-friendly GUI", *Wear*, Vol. 271, p. 2619- 2624, 2011.
- [26] H. Tschätsch , *Applied machining technology*, Dordrecht: Springer, 2009, p. 39.
- [27] Y.-J. Lai and C.-L. Hwang , *Fuzzy multiple objective decision making methods and applications*, Berlin: Springer-Verlag, 1994, pp. 1-19.

The profiling of rack-gear tool for the generation of the helical surfaces

Virgil TEODOR¹, Viorel PĂUNOIU¹, Silviu BERBINSCHI², Nicolae OANCEA¹

¹”Dunărea de Jos” University of Galați, Faculty of Mechanical Engineering, Department of Manufacturing Engineering,

²”Dunărea de Jos” University of Galați, Faculty of Mechanical Engineering, Department of Mechanical Design and Graphics

virgil.teodor@ugal.ro

ABSTRACT

The generation of the ordered whirls of profiles with the rack-gear tool is based on the principles of the generation by rolling.

The method for determination of the rack-gear tool's profile is based on the 1st Olivier theorem as so as, on complementary methods for enveloping study.

Usually, the issue of generation using the rack-gear refers to the surfaces whirls which are helical surfaces, as: helical toothed wheels; the worms of the helical pumps or the rotors of the helical compressors.

In this paper is presented a method for profiling the rack-gear tool which generated an ordered helical cylindrical surfaces whirl, associated with an axode. The proposed method is based on the principle of helical surface generation using the side mill. There are compared, by numerical examples, the end mill tool's profile, obtained by the proposed method, and the rack-gear tool's profile determined by classical method of the enveloping surfaces associated with rolling axodes.

KEYWORDS: rack-gear tool, Olivier theorem, ordered whirls of profiles

1. INTRODUCTION

The issue of surfaces generation by enveloping using the profiles ordered whirls by rolling method is very various. This issue may refers to the generation of helical surfaces using tools bounded by revolution surfaces (side mill or cylindrical tool) or surfaces generation with one-point contact (the generation with hob mill) based on the Olivier fundamental laws. In the same time, were stated theorems derived from the fundamental Olivier theorems [1], as: Gohman theorem [6], or, for the contact case between a helical surface and a revolution surface, the Nikolaev theorem [2]. They were developed complementary methods for the study of reciprocally enveloping surfaces: the “minimum distance” method, dedicated for the case of enveloping surfaces associated with a pair of

rolling centrodes [7]; the method of “substituting circles” [7], developed for the case of generating with rack-gear or gear shaped tools; the method of “in-plane generating trajectories” [8] with specific statement of the enveloping condition, characterised by the simplicity of this condition and with applications in the profiles ordered whirls associated with a pair of rolling centrodes generating process using side mill or cylindrical tool [1, 2].

Likewise, starting from the capabilities of CATIA design environment, were developed graphical methods for profiling tools which generate by enveloping using the rolling method (gear shaped and rotary cutter tool) [3].

All these methods are based on the kinematics of generation by enveloping for surfaces associated with a pair of rolling centrodes. Applying these methods need to define the relative motion of the conjugate centrodes, to determine the generated surfaces family and to determine the enveloping of this family. This enveloping is usually the primary peripheral surface of tool generating tool, namely the rack-gear tool.

In this paper is presented a method for determining the rack-gear tool reciprocally enveloping with helical cylindrical surface.

The method is based on the principles of helical surface generation using a cylindrical tool. There are presented numerical examples determined by two methods: the Gohman method, applied for enveloping surfaces associated with a rolling centrodes pair and the method proposed in this paper. The numerical results prove the identity of crossing profiles of tools determined by the two methods.

2. PROFILING OF RACK-GEAR FOR GENERATING HELICAL SURFACES ORDERED WHIRL

In Fig. 1, is presented the helical surfaces ordered whirl. These surfaces are cylindrical, with constant pitch and are associated with a revolution cylindrical axode. In the same figure, are presented the reference systems regarding which are defined the whirl of surfaces to be generated and the generating rack-gear surface. These reference systems are:

XYZ is the relative reference system associated with the surfaces whirl to be generated;

$\xi\eta\zeta$ - a relative reference system associated with the rack-gear rolling plane;

xyz – global reference system.

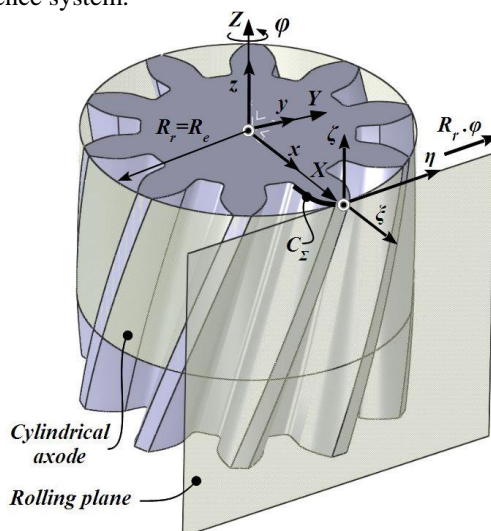


Fig. 1. Axode associated with the helical surfaces whirl; the rack-gear's rolling plane.

In the XYZ reference system, are defined the parametrical equations of the helical surface's frontal profile:

$$X = X(u); Y = Y(u); Z = 0, \quad (1)$$

with u variable parameter.

The global movement of the reference systems associated with the Σ surface and with rack-gear tool are, [1]:

$$x = \omega_3^T(\varphi) \cdot X, \quad (2)$$

$$x = \xi + a, \quad (3)$$

$$a = (Rr \quad Rr \cdot \varphi \quad 0)^T, \quad (4)$$

with φ angular parameter in the rotation motion around the Z axis.

In this way, are defined the relative motions:

$$\xi = \omega_3^T(\varphi) \cdot X - a. \quad (5)$$

The equation (5) represents the movement of the surfaces whirl regarding the rack-gear. The inverse of this motion is:

$$X = \omega_3(\varphi) [\xi + a]. \quad (6)$$

The generating rack-gear results as enveloping of the frontal profiles family, C_Σ :

$$(C_\Sigma): \xi = X(u) \cos \varphi - Y(u) \sin \varphi; \eta = X(u) \sin \varphi + Y(u) \cos \varphi, \quad (7)$$

in the relative motion regarding the rack-gear's reference system.

The specific enveloping condition is:

$$\vec{N}_{C_\Sigma} \cdot \vec{R}_\varphi = 0, \quad (8)$$

namely Gohman condition, where \vec{N}_{C_Σ} is the normal to the C_Σ profile, in principle:

$$\vec{N}_{C_\Sigma} = N_X \cdot \vec{i} + N_Y \cdot \vec{j} + N_Z \cdot \vec{k}, \quad (9)$$

and $\vec{R}_\varphi = dX/d\varphi$, from equation (6), the velocity in relative motion of the rack-gear regarding the reference system associated with the profiles whirl.

In this way:

$$\vec{R}_\varphi = (Y(u, \varphi) + R_e \sin \varphi \quad -X(u, \varphi) + R_e \cos \varphi \quad 0), \quad (10)$$

or, in vector form,

$$\vec{R}_\varphi = [Y(u) + R_e \sin \varphi] \cdot \vec{i} + [-X(u) + R_e \cos \varphi] \cdot \vec{j}. \quad (11)$$

The enveloping condition (8) may be re-written in form, see also (10) and (11),

$$[Y(u) + R_e \cdot \sin \varphi] \cdot N_X + [-X(u) + R_e \cdot \cos \varphi] \cdot N_Y = 0, \quad (12)$$

representing the enveloping condition between the frontal profile and the flank of the rack-gear tool, S , in the relative motion between the two axodes associated whit these: the revolution cylinder with radius R_e and the rack-gear rolling plane [1, 5].

The enveloping condition (12) represents a link between the u variable parameter and the φ movement parameter, on type:

$$u = u(\varphi). \quad (13)$$

The (13) equation determines a geometric locus which represents the crossing profile S of the rack-gear tool:

$$S: \xi = \xi(u, \varphi); \eta = \eta(u, \varphi); u = u(\varphi). \quad (14)$$

3. THE PROFILING OF THE CYLINDRICAL SURFACE (PLANNING TOOL)

The generating of the helical surface using planning tools which execute a straight lined movement following a direction tangent to the helical line of the surface to be generated is based on the geometric contact between a helical cylindrical surface with constant pitch and a cylindrical surface. The generatrix of the cylindrical surfaces is parallel to the tangents to the helical lines which, usually belongs to the external cylinder of the surface to be generated, see Fig. 2 and Fig. 6.

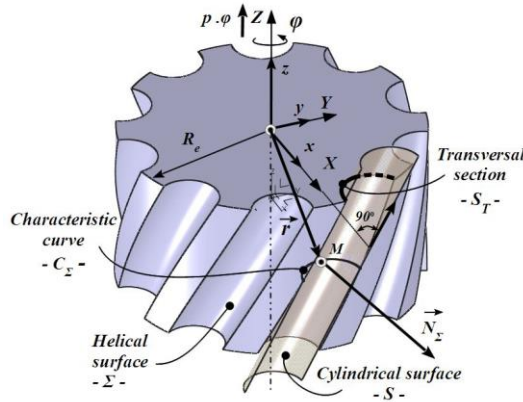


Fig. 2. Cylindrical and helical surfaces reciprocally enveloping; characteristic curve.

In the XYZ reference system are known the parametrical equations of the helical surface, in form:

$$\Sigma : X = X(u, \varphi); Y = Y(u, \varphi); Z = Z(u, \varphi), \quad (15)$$

with u and φ independents variable parameters.

If we denote with \vec{i} the versor of tangent to the helical line corresponding with the R_e radius, the external radius of the helical surface:

$$\vec{i} = \sin \beta \cdot \vec{j} + \cos \beta \cdot \vec{k}, \quad (16)$$

and with \vec{N}_Σ normal in the current point of the Σ surface:

$$\vec{N}_\Sigma = N_x \cdot \vec{i} + N_y \cdot \vec{j} + N_z \cdot \vec{k}, \quad (17)$$

then, the condition for the determination of the characteristic curve between the helical surface Σ , and the cylindrical one, with the generatrix oriented in the \vec{i} direction, (16), is:

$$\vec{N}_\Sigma \cdot \vec{i} = 0 \quad [2]. \quad (18)$$

The (18) condition, regarding (16) and (17), represent an algebraic link between the φ and u parameters, which determines on the Σ surface a geometric locus, the characteristic curve C_Σ :

$$\Sigma : X = X(u, \varphi); Y = Y(u, \varphi); Z = Z(u, \varphi); u = u(\varphi), \quad (19)$$

or,

$$C_\Sigma : X = X(\varphi); Y = Y(\varphi); Z = Z(\varphi). \quad (20)$$

In the translation motion along the \vec{i} generatrix, the characteristic curve (20) generates the cylindrical surface reciprocally enveloping with the helical surface,

$$\vec{r}_s = \vec{r}_{C_S} + \lambda \cdot \vec{t} \, , \quad (21)$$

with λ variable parameter.

By developing,

$$\begin{pmatrix} X \\ Y \\ Z \end{pmatrix} = \begin{pmatrix} X(\varphi) \\ Y(\varphi) \\ Z(\varphi) \end{pmatrix} + \lambda \begin{pmatrix} 0 \\ \sin \beta \\ \cos \beta \end{pmatrix} \quad (22)$$

so, the cylindrical surface have the parametrical equations:

$$S : X = X(\varphi); Y = Y(\varphi) + \lambda \sin \beta; Z = Z(\varphi) + \lambda \cos \beta. \quad (23)$$

The crossing section of the S surface, result from the intersection of the equations (23) with the plane

$$Z=0 \Rightarrow Z(\varphi) + \lambda \cos \beta = 0, \quad (24)$$

or, in principle, $\varphi = \varphi(\lambda)$, so, the crossing section S_T , of the S cylindrical surface have equations on form:

$$S_T : X = X(\lambda); Y = Y(\lambda). \quad (25)$$

4. NUMERICAL APPLICATIONS

In the following, they are proposed numerical applications of the presented method for various types of helical surfaces cylindrical with constant pitch, in order to show an example for the characteristic curves for the two expression form.

4.1. Helical surface with circular frontal profile

a). Generating by rolling method

In Fig. 3, it is presented the crossing profile of the helical surface, being a characteristic curve in the construction of the rotors for helical compressors.

It is defined the frontal section of the helical surface, regarding the XYZ reference system.

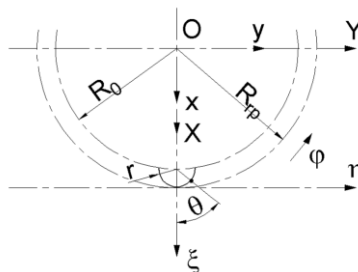


Fig. 3. Frontal section of the helical surface.

For the circular profile, the M point's coordinates, arbitrary choose on the profile, are:

$$X = R_0 + r \cos \theta; Y = r \sin \theta; Z = 0, \quad (26)$$

with θ variable parameter. The equations of the helical surface Σ with \vec{V} axis and p helical parameter are:

$$\Sigma: X = R_0 \cos \varphi + r \cos(\varphi + \theta); Y = R_0 \sin \varphi + r \sin(\varphi + \theta); Z = p\varphi, \quad (27)$$

the R_0 , r and p are constructive values, φ and θ being variables parameters.

The condition for characteristic curve determination, see (13) is give by:

$$[r \sin \theta + R_e \sin \varphi] \cos \theta + [-R_0 - r \cos \theta + R_e \cos \varphi] \sin \theta = 0, \quad (28)$$

or,

$$\sin(\varphi + \theta) = \frac{R_0}{R_e} \sin \theta, \quad (29)$$

the assembly of (27) and (29) determining the surface of the reciprocally enveloping rack-gear.

The characteristic curve at the contact between the rack-gear flank and the helical surface is give by the equations assembly:

$$\begin{cases} X = R_e \cos \varphi + r \sin(\theta + \varphi); Y = R_e \sin \varphi + r \cos(\theta + \varphi); Z = p\varphi; \\ \varphi = \arcsin \left[\frac{R_0}{R_e} \sin \theta \right] - \theta, \end{cases} \quad (30)$$

for $\varphi = \text{constant}$.

In the Fig. 4 and table 1, they are presented the form and coordinates of the rack-gear's crossing section flank, reciprocally enveloping with the helical surface.

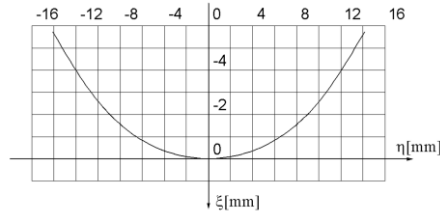


Fig. 4. Rack-gear's crossing section.

Table 1. Rack-gear's crossing section coordinates

Nr. crt.	ξ [mm]	η [mm]	Nr. crt.	ξ [mm]	η [mm]
1	-11.450	-14.125	7	-0.385	2.960
2	-6.224	-10.819	8	-1.522	5.765
3	-3.396	-8.335	9	-3.396	8.335
4	-1.522	-5.765	10	-6.224	10.819
5	-0.385	-2.960	11	-11.450	14.125
6	0.000	0.000			

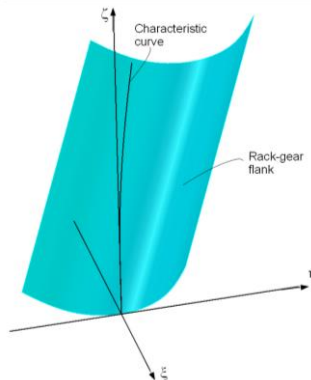


Fig. 5. Rack-gear flank, 3D model.

In Fig. 5, it is presented the 3D form of the conjugated rack-gear for the Σ surface, for the characteristic: $R_e=75$ mm; $r=10$ mm; $p=279.9$ mm; $R_0=65$ mm.

b). Generating by contact curve method (Nikolaev method)

For the same helical surface (27) it is determined the cylindrical surface, reciprocally enveloping, based on the Nikolaev theorem [2],

$$\vec{N}_\Sigma \cdot \vec{t} = 0. \quad (31)$$

In the Fig. 7, with \vec{t} was denoted the versor of tangent to the helix corresponding with the cylinder with R_e radius:

$$\vec{t} = \cos \omega \cdot \vec{j} + \sin \omega \cdot \vec{k}, \quad (32)$$

and,

$$\tan \omega = \frac{p}{R_e}, \quad \omega = \frac{\pi}{2} - \beta, \quad (33)$$

where p is helical parameter.

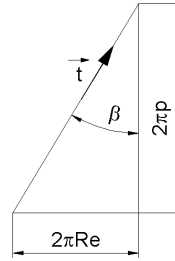


Fig. 6. Helix unwrap line.

The normal to the Σ helical surface, in the current point:

$$\vec{N}_\Sigma = \begin{vmatrix} \vec{i} & \vec{j} & \vec{k} \\ -R_0 \sin \varphi - r \sin(\varphi + \theta) & R_0 \cos \varphi + r \cos(\varphi + \theta) & p \\ -r \sin(\varphi + \theta) & r \cos(\varphi + \theta) & 0 \end{vmatrix}, \quad (34)$$

whence result the directrix parameters:

$$N_X = -p \cdot r \cos(\varphi + \theta); N_Y = -p \cdot r \sin(\varphi + \theta); N_Z = -R_e \sin \theta. \quad (35)$$

In table 2 and Fig. 7, are presented the coordinates and form of the crossing section of the cylindrical surface reciprocally enveloping with the helical one, for the same characteristic values: $r=10$ mm; $p=279.9$ mm; $R_0=65$ mm; $R_e=75$ mm.

Table 2. Rack-gear's crossing section coordinates

Nr. crt.	ξ [mm]	η [mm]	Nr. crt.	ξ [mm]	η [mm]
1	-11.450	-14.125	7	-0.385	2.960
2	-6.224	-10.819	8	-1.522	5.765
3	-3.396	-8.335	9	-3.396	8.335
4	-1.522	-5.765	10	-6.224	10.819
5	-0.385	-2.960	11	-11.450	14.125
6	0.000	0.000			

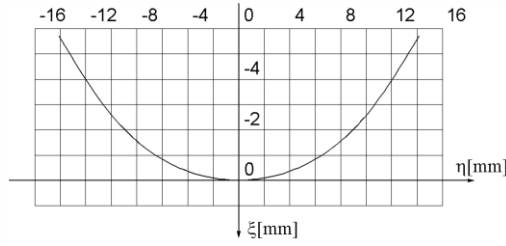


Fig. 7. Axial section of the cylindrical surface (using Nikolaev method).

The identity of the two profiles, see Fig. 4 and fig. 7, as so as table 1 and table 2, prove that the rack-gear tool's profiling method (Olivier [1]) and the proposed method leads to identical results.

5. PROOF OF METHOD EQUIVALENCE

It is possible to give an analytical demonstration of the identity between the two surfaces representing: the flank of rack-gear reciprocally enveloping with an ordered whirl of helical surfaces, cylindrical with constant pitch and the cylindrical surface reciprocally enveloping with a cylindrical helical surface (planning tool).

It is defined the cylindrical helical surface with constant pitch starting from its crossing section:

$$S_T : X = X(u); Y = Y(u), \quad (36)$$

which, in the helical motion:

$$X = \omega_3^T(\varphi) \begin{pmatrix} X(u) \\ Y(u) \\ 0 \end{pmatrix} + \begin{pmatrix} 0 \\ 0 \\ p\varphi \end{pmatrix} \quad (37)$$

describe the helical surface:

$$\Sigma : X = X(u)\cos\varphi - Y(u)\sin\varphi; Y = X(u)\sin\varphi + Y(u)\cos\varphi; Z = p\varphi, \quad (38)$$

with u and φ variable parameters and p helical parameter.

5.1. Cylindrical tool

The profiling of the cylindrical tool reciprocally enveloping with surface Σ assume the association between equations (38) and the Nikolae condition:

$$\vec{N}_\Sigma \cdot \vec{t} = 0, \quad (39)$$

where: \vec{N}_Σ is the normal to the Σ helical surface and \vec{t} is the versor of direction for the cylindrical generatrix, see figure 2.

It is calculated the normal to the Σ surface, from (38):

$$\vec{N}_\Sigma = \begin{vmatrix} \vec{i} & \vec{j} & \vec{k} \\ \dot{X}_u \cos\varphi - \dot{Y}_u \sin\varphi & \dot{X}_u \sin\varphi + \dot{Y}_u \cos\varphi & 0 \\ -X(u)\sin\varphi - Y(u)\cos\varphi & X(u)\cos\varphi - Y(u)\sin\varphi & p \end{vmatrix} \quad (40)$$

whence result:

$$N_X = p[\dot{X}_u \sin\varphi + \dot{Y}_u \cos\varphi]; N_Y = -p[\dot{X}_u \cos\varphi - \dot{Y}_u \sin\varphi]; N_Z = \dot{X}_u \cdot X(u) + \dot{Y}_u \cdot Y(u). \quad (41)$$

The \vec{i} versor, see figure 2, have the directrix parameters:

$$\vec{i} = \cos \omega \cdot \vec{i} + \sin \omega \cdot \vec{j}. \quad (42)$$

In this way, the condition (39) becomes:

$$-p \left[\dot{X}_u \cos \varphi - \dot{Y}_u \sin \varphi \right] \cos \omega + \left[X(u) \cdot \dot{X}_u + Y(u) \cdot \dot{Y}_u \right] \sin \omega = 0. \quad (43)$$

Considering the definition:

$$\tan \omega = \frac{P}{R_e} \quad (44)$$

the condition for the determination of the characteristic curve at contact with the helical surface with cylindrical tool becomes:

$$-\left[\dot{X}_u \cos \varphi - \dot{Y}_u \sin \varphi \right] + \left[X(u) \dot{X}_u + Y(u) \dot{Y}_u \right] \frac{1}{R_e} = 0. \quad (45)$$

5.2. Rack-gear tool

Starting from the S_T profile it is profiled the generating rack-gear tool for this profile.

Are defined, see Fig. 3, xyz is the global reference system; XYZ — mobile reference system joined with S_T profile; $\xi\eta\zeta$ — mobile reference system joined with rack-gear tool.

In the movement:

$$\xi = \omega_3^T(\varphi) X - \begin{pmatrix} -R_e \\ R_e \varphi \end{pmatrix} \quad (46)$$

it is defined the S_T profiles family, in form:

$$S_T : \xi = X(u) \cos \varphi - Y(u) \sin \varphi - R_e; \eta = X(u) \sin \varphi + Y(u) \cos \varphi - R_e \varphi. \quad (47)$$

The specific enveloping condition is:

$$\vec{N}_{S_T} \cdot \vec{R}_\varphi = 0, \quad (48)$$

where: \vec{R}_φ is the velocity vector in the relative motion between the XYZ and $\xi\eta\zeta$ spaces,

$$\vec{R}_\varphi = \frac{dX}{d\varphi}; \quad (49)$$

\vec{N}_{S_T} is the normal to the S_T profile, in the XYZ space,

$$\vec{N}_{S_T} = \dot{Y}_u \cdot \vec{i} - \dot{X}_u \cdot \vec{j}. \quad (50)$$

From (46), results:

$$X = \omega_3(\varphi) \left[\xi + \begin{pmatrix} R_e \\ R_e \cdot \varphi \end{pmatrix} \right], \quad (51)$$

and, hence, the R_φ vector, in form:

$$R_\varphi = \dot{\omega}_3(\varphi) \cdot \left[\xi + \begin{pmatrix} R_e \\ R_e \cdot \varphi \end{pmatrix} \right] + \omega_3(\varphi) \cdot \begin{pmatrix} 0 \\ R_e \end{pmatrix}. \quad (52)$$

After developments it is calculated the enveloping condition (48):

$$\vec{N}_{S_T} \cdot \vec{R}_\varphi = \left[Y(u) + R_e \sin \varphi \right] \dot{Y}_u - \left[-X(u) + R_e \cos \varphi \right] \dot{X}_u = 0, \quad (53)$$

or, finally,

$$\frac{X(u)\dot{X}_u + Y(u)\dot{Y}_u}{R_e} = -\dot{Y}_u \sin \varphi + \dot{X}_u \cos \varphi. \quad (54)$$

Obviously, the (45) and (53) conditions are identically as following, the profiles in the frontal plane of the rack-gear and cylindrical surface will be identically.

6. CONCLUSIONS

In this paper we prove that the rack-gear tool's profile for generation of helical teeth is identically with the profile of the cylindrical tool for generation of the same helical surface with constant pitch.

The profiling of rack-gear tool which generate an ordered whirl of helical surfaces is based on the method of reciprocally enveloping surfaces associated with a rolling centrode pair, see Fig. 1. The method is applied for profiling tools with helical teeth, rotors of helical compressors, worms of helical pumps, teeth with non-involute profile, see Fig. 8.

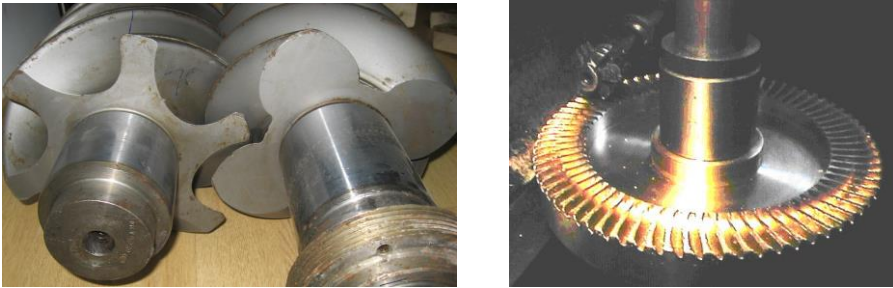


Fig. 8. Types of generated helical surface.

The proposed method, profiling of rack-gear tool using Nikolaev principle, may substitute the classical Gohman method for profiling this type of tool.

The identity between the two method was demonstrates in an analytical way and by numerical examples.

The proposed method may be applied in all situations when the helical flanks of the tooth can be analytical express.

REFERENCES

- [1] Litvin, F.L., Theory of gearing, Reference Publication 1212, NASA, *Scientific and Technical Information Division*, Washington D.C., 1984;
- [2] Liukshin V.S., Theory of screw surfaces in cutting tool design, *Machinostroyenie*, Moscow, 1968;
- [3] Berbinschi S., Teodor V., Oancea N., 3D graphical method for profiling tools that generate helical surfaces, *The International Journal of Advanced Manufacturing Technology*, Vol. 60, pag. 505-512, 2012;
- [4] Nankov, G., Ivanov, V., CAD Oriented Mathematical Model for Profiling of Tools For Machining of Helical Surfaces, *International Science Conf. AMTECH'95, Conf. Proceedings*, Ruse, Bulgaria, section 4, pag. 79-93, 1995;
- [5] Radzevich, S.P., Kinematics Geometry of Surface Machining, CRC Press, London, ISBN 978-1-4200-6340-0, 2008;
- [6] Oancea, N., Generarea suprafețelor prin înfășurare (Surface Generation Through Winding), Vol. I, "Dunărea de Jos" Publishing House, ISBN 973-627-106-4, ISBN 973-627-107-2 vol. I, 2004;
- [7] Oancea, N., Generarea suprafețelor prin înfășurare (Surface Generation Through Winding), Vol. II, "Dunărea de Jos" Publishing House, ISBN 973-627-106-4, ISBN 973-627-107-6 vol. II, 2004;
- [8] Teodor, V., Contributions to the Elaboration of a Method for Profiling Tools, Lambert Academic Publishing, ISBN 978-3-8433-8261-8, 2010.

Investigation of side milling operations for machining carbon fibre reinforced thermoplastic composite

Petr Masek, Petr Kolar, Pavel Zeman

Czech Technical University in Prague, Research Center of Manufacturing
Technology, Prague, Czech Republic
P.Kolar@rcmt.cvut.cz

ABSTRACT

This paper focuses on machining of thermoplastic composite PPS (polyphenol sulfide) with woven carbon fibers. PPS/C is a commonly used material in the aerospace and aircraft industry for internal panel design as well as structural parts. Side milling is a possible technology for finishing of the workpiece after prefabrication. In this paper two cutting tools are compared based on the criteria of the final quality of the machined surface edge and cutting forces. The Taguchi method design of experiment (DOE) was used. The main criterion was cutting forces evaluated by S/N ratio. The significance of factors and optimal adjustment of control factors was determined by this method. Secondary criteria were surface roughness and size of burr area.

KEYWORDS: Side milling, thermoplastic composite, PCD cutting tools

1. INTRODUCTION

Most of the already published papers have been focusing mainly on machining of composite materials with thermoset resin [1, 2, 3]. However, various modern composite parts are very often made of composites with a thermoplastic matrix today. Machinability of thermoplastic composites and possibilities of increasing the productivity of these materials have not been studied sufficiently yet. Hence, this paper focuses on machining of thermoplastic matrix PPS (polyphenol sulphide) with woven carbon fibres. PPS/C is commonly used in the aerospace and aircraft industry for internal panel design etc. Attention will be paid to side milling, which is used for cutting off workpiece edges after prefabrication. In this paper two cutting tools are compared based on the criteria of the final quality of the machined surface edge and cutting forces.

An earlier published paper written by König et al. [4] described the benefits of up-milling. The authors recommended using the up-milling process for any cutting conditions and any types of cutting tools. The average surface roughness R_a was found higher for any experiment for graphite epoxy laminate if down-milling was used. Then Colligan and Ramulu

[5] tested the same material and they studied delamination during up- and down-milling for various surface ply orientations. They found out that down-milling is the best solution for the minimisation of the delamination but the difference between up and down-milling was only 2%. On the grounds of the two contradictory effects of the milling strategy on the machined surface, which were observed by König and Colligan, the milling strategy was used as one of the factors in DOE. Thermoplastic composites do not have a tendency to delamination, but it was predicted as possible at the beginning of the experiment.

The influence of surface ply orientation on the delamination was identified by Colligan and Ramulu. The orientation of the surface ply could have an influence on the creation of burr as well. PW and PX orientations were chosen as levels of the ply orientation factor.

Another significant factor was chosen on the grounds of Davim's paper [6]. He and his colleagues used orthogonal arrays and the ANOVA test to choose the most significant factors for GFRP materials with different thermoset resin. They discovered that feed rate and cutting speed are statistically significant, and that feed rate has a higher influence on surface roughness than cutting speed. Davim also presented results for cutting forces. Feed rate and cutting speed was chosen as the third and the fourth factor in the experiment. It was predicted that for thermoplastic matrix the feed rate will also be more important than cutting speed in the case of surface roughness.

Puw and Hocheng [7] predicted cutting force for machining unidirectional PEEK/C. They noted that the cutting force consists of specific cutting force, thickness of chip, which is equal to feed per tooth, and depth of cut. The equations that they designed agree with experimental results for ABS/C and PEEK/C. In addition, it was presented by Sheikh-Ahmad [8] that depth of cut should have an influence on surface roughness either alone or in an interaction with feed rate. It is possible that PPS/C will behave differently. The radial depth of cut was taken into account as the fifth control factor in the experiment.

This paper deals with experimental research into the influence of the cutting conditions during side milling on the quality of the machined surface of the PPS/C material. The cutting tools with various geometries were used for the tests. The main results are values of surface roughness, size of burr area and resultant force for two PCD cutting tools. The control factors feed rate per tooth, cutting speed, radial depth of cut, strategy and surface ply orientation were selected on the basis of the literature review. The influence of control factors on the values of the main results are expressed in the experiment as values of the S/N ratio. The S/N ratio compares the magnitude of the desired signal to undesired signal, in other words called noise [9]. The experiment for this paper was designed according to the Taguchi method. It is an efficient way how to reduce the number of experiments to a minimum. Taguchi uses orthogonal arrays for this purpose. The arrays are compiled for a given number of tested parameters and levels of these parameters.

Two PCD cutting tools were used in the experiment. The main task was to compare the effect of different cutting geometries on cutting forces and surface quality of a specimen. One of the tools had a modified face of cutting edge. A chip breaker was made by laser into a hard and solid PCD tip. This modification increased the positivity of the rake angle. The more positive rake angle should improve the quality of the machined surface and decrease cutting forces. The optimal cutting conditions were determined for both tools and a direct comparison between these two tools was made. The outputs of the experiment and criteria of comparison for the tested PCD tools were the size of burr, surface roughness and cutting forces.

2. SET-UP OF THE EXPERIMENT

The effect of the two cutting tools on the surface quality and cutting forces was compared. These cutting tools were almost the same, but the second one had a small modification of the rake angle made by laser. The diameter of the cutting tools was 8 mm. The milling cutters can be seen in Fig. 1. Both cutters are commercial cutting tools which were designed for machining polymer composites with fibres.

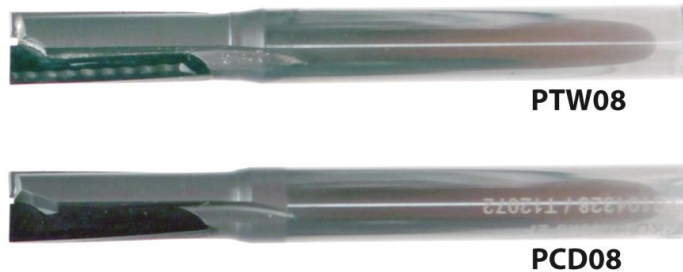


Fig. 1. PCD cutters (above with a chip breaker).

The geometry of the PCD cutters is shown in Table 1. It can be seen that the angles of the cutting edge are the same. Only the rake angle is different for both tools due to the chip breaker on the PTW08 tool. The rake angle was varying from the face of the cutting tool to the end of PCD cutting tip in regard to flatness of the PCD cutting tip. A significant rake angle, that has an influence on the cutting forces and surface quality, is the rake angle in the area of contact between cutting tool and machined material. These cutting angles were measured and they are shown in Table 1.

Table 1. Measured cutting edge angles on the tested cutters.

	PCD08	PTW08
Rake angle*	0°	20°
Rake angle	-15,58°	5,06°
Clearance angle	17,84°	17,16°
Helix angle	-5,13°	-5,09°

*Nominal value of the rake angle near the cutting tool face

The tested material was PPS/C. This is a high performance carbon fiber composite with a thermoplastic matrix. It had a woven structure of fibers. This material is used for internal panels of planes. The panels are usually produced by near-net-shape technology, but in order to achieve dimensions with specific tolerances it is necessary to use side milling operations.

Small specimens of PPS/C with dimensions 53 x 53 mm were prepared and two different orientations were machined in this experiment. The orientation PW and PX (Fig. 2) could have a significant influence on the magnitude of the response. The orientation of plies was one of the control factors which were included in the experiment.

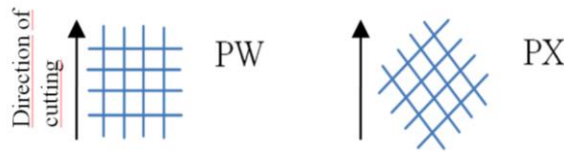


Fig. 2. The schematic illustration of PW and PX orientation of composite.

Five control factors were chosen. These five factors have the main influence on the quality of the machined surface and cutting forces. The optimal adjustment of these factors for the tested cutting tools is unknown for now. The chosen factors were feed per tooth f_t , cutting speed v_c , radial depth of cut a_e , ply orientation in composite and strategy of milling. Two levels were chosen for each factor (Table).

The Taguchi design of experiment (DOE) was proposed (Table). This design of experiment is one of the partial designs which are based on the orthogonal arrays designed by Genichi Taguchi [10]. The Taguchi DOE unites interactions with factors, but it is possible to use it for cases where the factors are independent. Its advantage consists in the shortening of the experiment and saving costs. The Taguchi DOE is mostly evaluated by S/N ratio, which is a powerful instrument for identifying the most significant control factors and an optimal adjustment of the control factors.

Table 2. Control factors and their levels.

Parameters / Factors	Unit	Symbol	Levels	
			Level 1	Level 2
feed rate per tooth	mm	f_t	0.05	0.1
cutting speed	m/min	v_c	150	300
depth of cut	mm	a_e	1	3
strategy	-	-	Up-milling	Down-milling
ply orientation	-	-	PW	PX

Table 3. Design of experiment.

Run ID	A (f_t)	B (v_c)	AB	C (a_e)	AC	D (strat.)	E (ply orient.)
1	1	1	1	1	1	1	1
2	1	1	1	2	2	2	2
3	1	2	2	1	1	2	2
4	1	2	2	2	2	1	1
5	2	1	2	1	2	1	2
6	2	1	2	2	1	2	1
7	2	2	1	1	2	2	1
8	2	2	1	2	1	1	2

Interactions AB and AC were included in DOE. Interaction AB was chosen on the basis of the preliminary tests, in which the ANOVA was used for identifying probably significant interactions. Interaction AC was chosen on the basis of heredity. Factor A had a high significance and factor C was also very significant. With regard to the high significance of these two factors, there was a possibility of interaction AC being significant.

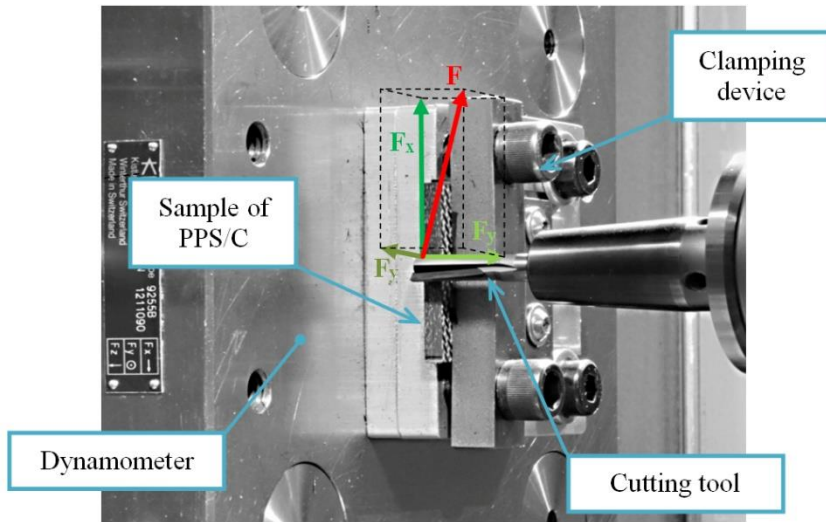


Fig. 3. Experimental setup.

A clamping device, which provided stiff clamping of the specimen without the possibility of specimen vibration, was designed for this experiment (Fig. 3). Eliminating vibration is necessary for correct measuring of the cutting forces. The clamping device was bolted directly to the dynamometer. The machine tool was a horizontal CNC milling machine tool with a wide range of revolutions and possibility of dust exhaustion.

3. EVALUATION PARAMETERS

The cutting forces were measured by a Kistler 9255B dynamometer. Three components of the cutting force were measured: F_x , F_y and F_z . The active cutting force was calculated according to equation (1). Next, the resultant cutting force was calculated according to equation (2). The resultant cutting force was a response of the experiment. It was calculated as the average of the maximal resultant cutting force from 200 engagements. Next, the average resultant force was calculated.

$$Fa = \sqrt{Fx^2 + Fy^2} \quad (1)$$

$$F = \sqrt{Fa^2 + Fz^2} \quad (2)$$

The surface roughness was measured by Surtronic 3+ from Tylor Hobson. This measuring device is a contact device. The surface roughness is picked up by a solid stylus tip. The R_z parameter was measured. This parameter gives a more real view of the surface condition than e.g. the R_a parameter. The nine values of R_z parameter were picked up for each run of the experiment (specimen) and the average was calculated.

The last measuring response was the size of burr which was measured along the whole length of the specimen. A photograph was taken of the top and bottom side of the specimen and this photograph was modified by a special program which was created in the Matlab software. The contrast of the photograph was increased and then the machined edge of the composite was identified automatically by an image processing tool in Matlab. The straight

line was interleaved across the edge of the machined composite picture on the basis of the linear regression calculation. The rest of the picture was cut off from the burrs along this straight line. Only the black pixels of burrs remain in the picture. Next, the area of the burr was calculated in square millimetres on the basis of knowledge of the one pixel size in millimetres. The procedure of the burr calculation is shown in Fig. 4.

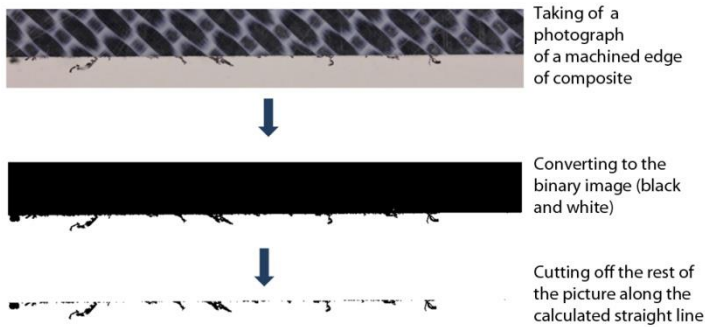


Fig. 4. Procedure of burr measuring from photograph.

4. RESULTS AND DISCUSSION

The evaluation of the resultant force was made by S/N ratio. The S/N ratio is a ratio between signal factors which are desirable and noise factors which are undesirable. It is possible to identify weak and strong factors from this statistical approach. The weak factors are those which have a small influence on the response. Optimal values of the machining setup can be achieved using this method.

The smaller-the-better (STB) (4) method was used for calculating S/N ratio. The reason for this was that the optimal adjustment of the control factors is for minimal resultant cutting forces.

$$STB = -10 \log_{10} \sum_{i=1}^n \frac{y_i^2}{2} \quad (4)$$

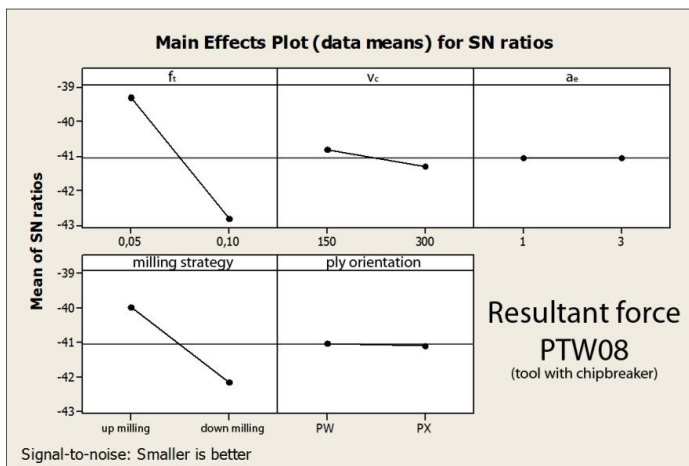


Fig. 5. Main effects plot for SN ratios of PTW08 tool (with a chip breaker).

Table 4. Response Table for Signal to Noise Ratios - Smaller is better – PTW08.

Level	f_t	v_c	a_e	Milling strategy	Ply orientation
1	-39.30	-40.82	-41.06	-39.97	-41.01
2	-42.83	-41.31	-41.07	-42.16	-41.11
Delta	3.54	0.50	0.01	2.18	0.10
Rank	1	3	4	2	5

If the PTW08 cutting tool with chip breaker was used, the most significant factor was the feed per tooth as can be seen in Table 1. It means that the resultant cutting force is influenced the most by this factor. The second one is the milling strategy. There were only two possibilities for the choice of milling strategy: up-milling and down-milling. Up-milling was better than down-milling according to Fig. 5. The engagement of tooth with the material is smoother than for down-milling because the tooth goes from minimal to maximum chip. It is necessary to choose small feed per tooth in order to decrease the resultant cutting forces (0.05 mm for the case of this experiment). It makes sense because the cutting force is usually mainly dependent on the chip cross-section which is a multiple of the feed per tooth and radial depth of cut. The third most significant factor was cutting speed. However, its significance is much smaller than f_t and milling strategy. The radial depth of cut and the ply orientation were almost insignificant.

For comparison, the same analysis was performed for cutting tool PCD08 without a chip breaker. The results were almost the same but the ply orientation was less significant than radial depth of cut this time (Table 5. Response Table for Signal to Noise Ratios - Smaller is better – PCD08. Table and Fig. 6). The significance of both these factors was very small as in the case of PTW08. The results showed that cutting speed was slightly more significant. It is probably caused by a higher difference between the results of all runs. The surface ply orientation was slightly more significant for cutting tool PCD08 than for PTW08. The measured forces were much higher for PCD08 and the differences between runs were also higher. The evaluation method was able to find higher differences between levels and control factors. The same situation can be observed for radial depth of cut.

The tests of S/N ratio found out an agreement of the control factor ranks (see Table 4 and 5). They confirmed that the most significant factor is feed per tooth and next the strategy of milling and cutting speed in the case of the cutting forces magnitude. The radial depth of cut and surface ply orientation did not have a significant influence on the forces. The surface ply orientation did not have a significant influence either because PW and PX plies alternate regularly along the whole composite specimen.

Table 5. Response Table for Signal to Noise Ratios - Smaller is better – PCD08.

Level	f_t	v_c	a_e	Milling strategy	Ply orientation
1	-44.23	-45.30	-45.97	-45.13	-45.61
2	-47.31	-46.24	-45.56	-46.41	-45.92
Delta	3.08	0.94	0.41	1.28	0.31
Rank	1	3	4	2	5

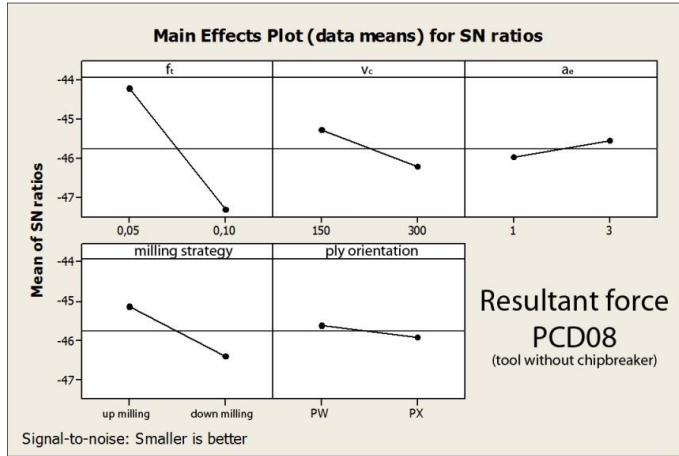


Fig. 6 Main effects plot for SN ratios of PCD08 tool (without a chip breaker).

The direct comparison showed that resultant cutting forces were by approximately 30% to 40% lower if the PTW08 was used (Fig. 1). The higher positivity of the rake angle on the cutting edge had a beneficial influence on decreasing the cutting forces. The maximal resultant cutting force is plotted in Fig. 7 for each run of the experiment.

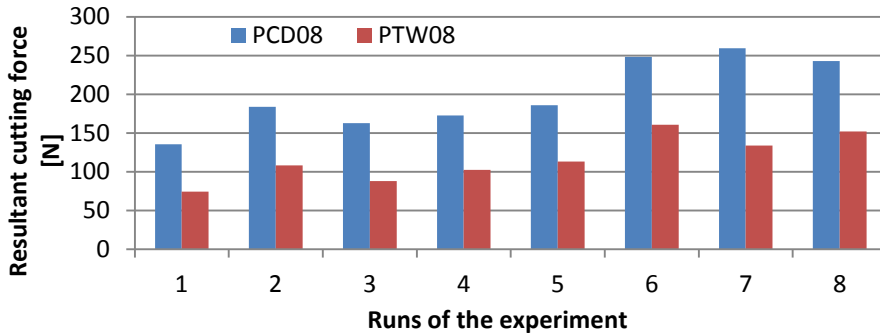


Fig. 7. Direct comparison of resultant cutting force results.

The statistical evaluation of surface roughness was made for both tools. The differences between results in runs were too small and this was the reason why the S/N ratio failed (see Fig. 8). We were not able to decide which factor was more significant than others. It was also impossible to decide how beneficial the chip breaker was in the case of surface roughness. The differences between cutting tools were smaller than differences between runs and both were smaller than the measuring device uncertainty of measurement. The STB method does not give meaningful results if the variance is not high between measurements. The average surface roughness was only slightly smaller for cutting tool PTW08. The average surface roughness for PTW08 was 4.84 μm and for PCD08 5.27 μm .

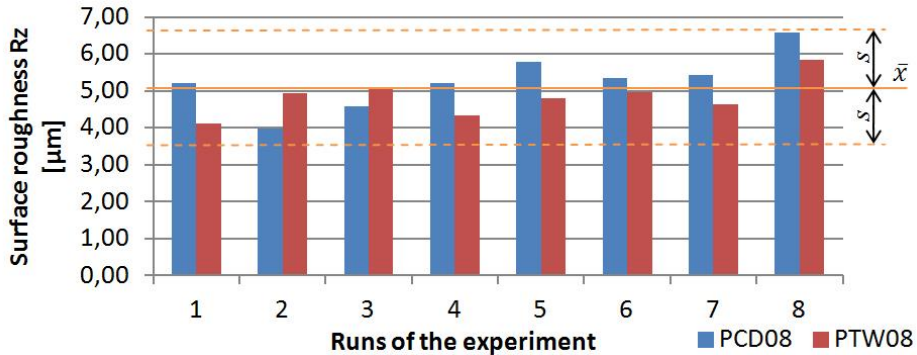


Fig. 8. Direct comparison of surface roughness.

The statistical comparison fails for measuring of the burrs as well. The method of measuring used is considerably influenced by the place of cutting on the specimen and the definition of the photograph. The resolution ability of this method is decreased by this. It was not possible to apply the S/N ratio method due to small differences between results in the experiment runs for PTW08 and PCD08. However, there was an obvious difference between the results for both tools (Fig. 9). The tool with the chip breaker created hardly any burrs as can be seen in **Fel! Hittar inte referensskälla..** The higher positivity of the rake angle caused elimination of the burr creation.

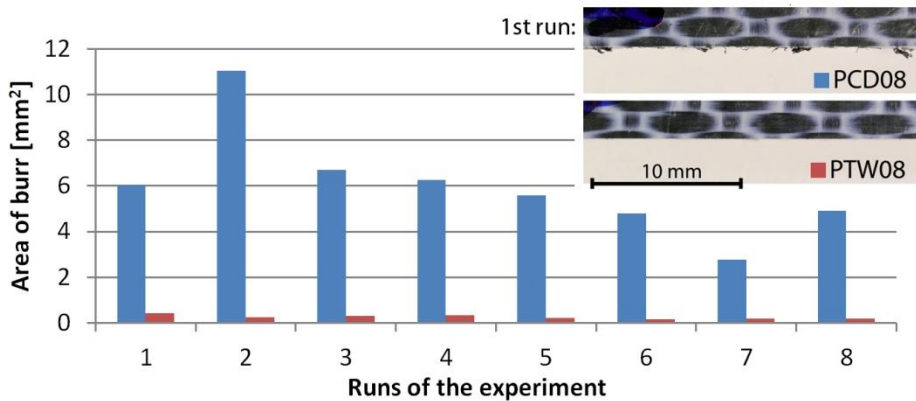


Fig. 9. Direct comparison of burr area.

5. CONCLUSION

The main goal of this paper was a comparison of the PCD tools with and without a chip breaker. The near-net-shape composite parts with thermoplastic resin have to be machined in order to obtain the right dimensions in specific tolerances and a neat composite part edge without burrs. The right choice of the cutting tool and cutting conditions is paramount. The cutting tool has to withstand the high abrasion of the carbon fibres as well as create surfaces without burrs. The PCD tools usually produced without a chip breaker create a large amount of burrs due to the zero or negative rake angle. The positive rake angle can be produced on the face of the cutting edge by laser. Subsequently, the cutting process creates smaller cutting forces and burr-free surface. The disadvantage of the tool with a lasered chip breaker lies in the fact that it is almost twice as expensive. Carbide tools are an alternative solution to

obtaining a machined shape without burrs due to easier production of the high positivity of cutting edge. However, the life time of uncoated carbide tools is up to 10 times shorter [11]. It can be the reason why the machining cost will be higher if a carbide tool is used instead of the PCD tool with a chip breaker.

The optimal adjustment of cutting conditions was determined in order to minimize the resultant cutting force. This adjustment is independent on the cutting tool geometry. The feed per tooth was the most significant control factor and its more profitable value was 0.05 mm in this study. The second one was the milling strategy. It is much better to use down-milling for machining of PPS/C composite than up-milling. The third most significant factor was cutting speed, whose cutting force was smaller for value 300 m/min in this case. Other factors were insignificant for PTW08. Some significance of other control factors was only identified for cutting tool PCD08. The results showed that the fourth most important factor was radial depth of cut with a value of 1 mm for minimizing of cutting force. The least significant factor was orientation of plies where the better position was PX.

ACKNOWLEDGMENTS

The authors would like to thank the European Community for funding the large-scale EU project „FibreChain – Integrated Process Chain for Automated and Flexible Production of Fibre-Reinforced Plastic Products“ as part of the European Community’s Seventh Framework Programme under grant agreement no. 263385.

REFERENCES

- [1] P. Sreejith, R. Krishnamurthy, S. Malhotra and K. Narayanasamy, “Evaluation of PCD tool performance during machining of carbon/phenolic ablative composites,” *Journal of Materials Processing Technology*, vol. 104, pp. 53-58, 2000.
- [2] J. Davim and P. Reis, “Damage and dimensional precision on milling carbon fiber-reinforced plastics using design experiment,” *Journal of Materials Processing Technology*, vol. 160, pp. 160-167, 2005.
- [3] K. Palanikumar, L. Karunamoorthy and R. Karthikeyan, “Optimizing the machining parameters for minimum surface roughness in turning of GFRP composites using design of experiments,” *J. Mater. Sci. Technol.*, vol. 4, no. 20, pp. 373-379, 2004.
- [4] W. König, P. Wulf, P. Graß and H. Willerscheid, Machining of fibre reinforced plastics, *Annals of the CIRP* 34, 1985, pp. 537-548.
- [5] K. Colligan and M. Ramulu, Delamination in surface plies of graphite/epoxy caused by the edge trimming process, Washington: PED-CPû.49/MD-Vol.27, *Processing and manufacturing of composite materials - ASME*, 1991.
- [6] P. J. Davim, P. Reis and C. C. Antonio, A study on milling of glass fiber reinforced plastics manufactured by hand-lay up using statistical analysis (ANOVA), Porto, Portugal: *Elsevier - Composite structures* 64, 2004, p. 493500.
- [7] H. Y. Puw and H. Hocheng, Machinability test of carbon fiber-reinforced plastics in milling, Hsinchu, Taiwan: Materials and manufacturing processes, 8(6), 1993, pp. 717-729.
- [8] J. Y. Sheikh-Ahmad, Machining of polymer composites, New York: *Springer Science + Business Media*, 2009, p. 320.
- [9] S. Maghsoodloo, G. Ozdemir, V. Jorda and a. al, “Strenghts and limitations of Taguchi's contributions to quality,” *Journal of Manufacturing Systems*, vol. 23, no. 1, pp. 73 - 126, 2005.
- [10] G. Taguchi and S. Konichi, “Taguchi methods, Orthogonal arrays and linear graphs, tools quality engineering,” *MI: ASI Press*, 1987.
- [11] R. Teti, Machining of composite materials, Elsevier : *CIRP Annals - Manufacturing Technology*, 2002, pp. 611-634.

An intelligent and modular adaptive control scheme for automating the milling process

Luis Rubio*, Andrew Longstaff, Simon Fletcher and Alan Myers

Centre for Precision Technologies, University of Huddersfield, UK

*L.R.Rodriguez@hud.ac.uk

ABSTRACT

This research work describes an intelligent and modular architecture for controlling the milling process. For this purpose, it is taking into account the admissible input cutting parameters given by the stability lobes and restrictions of the system, calculating the quasi-optimal cutting parameters. The quasi-optimal cutting parameters are obtained considering a cost function with multi-objective purpose. Furthermore, parallel multi-estimation adaptive control architecture is proposed in order to allow adaptation of the system when the cutting parameters are changed, for example, due to production requirements. It incorporates an intelligent supervisory system to address the problem of choosing the most adequate control signal at each required time. The fundamental idea of the control system is to work automatically, with a simple interface with the operator, based around the admissible cutting parameter space given by the well-known stability lobes.

KEYWORDS: Milling, Adaptive Control, Optimization

1. INTRODUCTION

Dynamic complexity of milling processes combined with their exigent performance requirements requires sophisticated and complex control systems. The selection of adequate cutting parameters for multi-objective optimization in milling processes has been the subject of extensive research in manufacturing literature [1-3], where computer aided programming planning, decision support systems and bio-inspired systems have been used to cope with the problem of multi-objective optimization. Moreover, the control of milling forces has been applied successfully in a broad range of milling applications [4-6].

This paper presents an intelligent and modular architecture for controlling the milling process. It is intelligent because finds out parameters of the system. Moreover, it has the ability to learn from previous experience. Its modularity is based on the idea that the control represents one external module which can be implemented in the system. It is based on models of the milling process. The dynamic equation leads to the time-domain and the well-known stability plots and the linearization around the equilibrium points is represented by transfer functions.

Then, taking into account the admissible input cutting parameters given by the stability lobes and restrictions of the system, the quasi-optimal cutting parameters are calculated. The quasi-optimal cutting parameters are obtained while taking into account a cost function with a multi-objective purpose. In this way, the quasi-optimal cutting parameters can be found automatically based on the multi-criteria of maximising material remove rate and tool life while minimising the surface roughness and maintaining a robust, stable working point. This first toolbox of the modular architecture is designed so the operator can interact with it in a simple and efficient manner, leading to schedule programmed cutting parameters in production.

Furthermore, parallel multi-estimation adaptive control architecture is proposed in order to allow adaptation of the system when the cutting parameters are changed, for example, due to variability in production requirements. It deals with non-linearity, cutting parameter and material dependent milling process factors. Each estimator of the parallel scheme incorporates a recursive least square estimator and produces a control law at the same sampling instant.

The parameters of each transfer function, such as the dynamics and the parameters of the cutting process can vary at each working point and in the transitions between working points. To address this problem, an intelligent supervisory system is presented which selects adequate trajectories in the state space according to design requirements. Furthermore, it is able to learn trajectories and compare them based on a cost function from previous states to generate a knowledge based. This supervisory system closes the control loop. A simulation example is provided to explain how the system acts giving an intuitive understanding of the problem.

2. SYSTEM DESCRIPTION

Milling processes are well characterized as mechanical systems that are particularly sensitive to acquiring vibrations. In this section, the milling process is modelled as a second order differential equation, which is excited by forces whose inherent terms describe excitation of the modal parameters of the system. This fact results in the conversion of resultant energy into vibrations of the system. Those vibrations are generated under certain cutting conditions depending on the process being carried out, clamping of the workpiece, tool and workpiece materials, etc.

2.1. Self-excited vibrations

The standard milling system can be described as a second order differential equation excited by the cutting forces,

$$M \cdot \ddot{r}(t) + B \cdot \dot{r}(t) + C \cdot r(t) = F(t) \quad (1)$$

where $r(t) = \{x(t), y(t)\}^T$ are the relative displacements between the tool and the workpiece in the $X-Y$ plane, $F(t) = \{F_x(t), F_y(t)\}^T$, and M, B and C are the modal mass, damping and stiffness matrices respectively, all of them represented in two dimensions. The milling cutting force is represented by a tangential force proportional to the instantaneous chip thickness, and a radial force which is expressed in terms of the tangential force [6],

$$F_t(t) = K_t \cdot a_{dc} \cdot t_c(t) \text{ and } F_r(t) = K_r \cdot F_t(t) \quad (2)$$

where K_t and K_r , the tangential and radial specific cutting constants which are dependent on the tool material for any specific geometry, a_{dc} , the axial depth of cut and, $t_c(t)$

, the chip thickness, obtaining the cutting forces in Cartesian coordinates. The most critical variable in the equation of motion, the chip thickness, $t_c(t)$, consists of a static part and a dynamic one. The static part is proportional to the feed rate and it is attributed to the rigid body motion of the cutter. The dynamic part models two subsequent passes of the tool through the same part of the work-piece. The phase shift between two consecutive passes of a tool tooth on the work-piece is widely modelled and represented [6] by,

$$t_c(t) = f_r \cdot \sin \phi_j + [x(t-\tau) - x(t)] \cdot \sin \phi_j + [y(t-\tau) - y(t)] \cdot \cos \phi_j \quad (3)$$

where f_r is the feedrate, ϕ_j the immersion angle and τ is a delayed term defined as

$$\tau = \frac{60}{N_t S_s} \quad , \quad N_t \text{ is the number of teeth and } S_s \text{ the spindle speed in } rpm .$$

Figure 1 pictures this mathematical representation in a drawing.

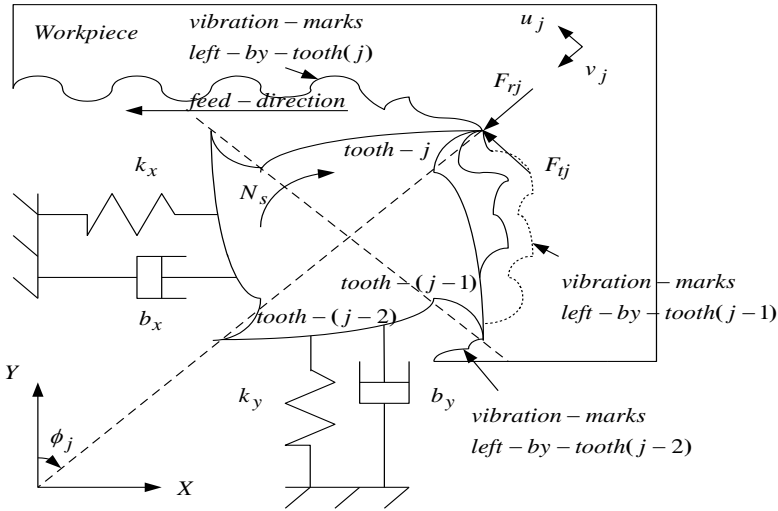


Figure 1: Cross-sectional view of a milling tool [4].

2.2. Machine tool transfer function

The transfer function of the system, in chatter and resonant free zones, can be separated as a series decomposition of the transfer function that relates the actual feed delivered by the drive motor and the resultant force due to the deflection of the tool and, the transfer function that represents the computerized numerical control (CNC). Then, a continuous transfer function which relates both signals, measured resultant force and the actual feed delivered by the drive motor can be shown as a first order dynamic [4],

$$G_p(s) = \frac{F_p(s)}{f_a(s)} = \frac{K_c a_{dc} r(\phi_{st}, \phi_{ex}, N_t)}{N_t S_s} \frac{1}{\tau_c s + 1} \quad (4)$$

where $K_c (N/mm^2)$ is the resultant cutting pressure constant, $a_{dc} (mm)$ is the axial depth of cut, $r(\phi_{st}, \phi_{ex}, N_t)$ is a non-dimensional immersion function, which is dependent on

the immersion angle and the number of teeth in cut, N_t is the number of teeth in the milling cutter, $S_s(rpm)$ the spindle speed and $\tau_c = 1/N_t S_s$. At the same time, the relationship between the machine tool controls, the CNC and, the motor drive system can be approximated as a first order system within the range of working frequencies [4]. This transfer function relates the actual, f_a , and the command, f_c , feed velocities,

$$G_s(s) = \frac{f_a(s)}{f_c(s)} = \frac{1}{\tau_s s + 1} \quad (5)$$

where τ_s represents an average time constant.

The combined transfer function of the system is given by,

$$G_c(s) = \frac{F_p(s)}{f_c(s)} = \frac{K_p}{(\tau_c s + 1)(\tau_s s + 1)} \quad (6)$$

$$\text{with } K_p \left(\frac{kN \cdot s}{mm} \right) = K_c a_{dc} r_{dc} / N_t S_s$$

3. COST FUNCTION FOR SELECTION OF OPTIMAL CUTTING PARAMETERS

A novel cost function has been conceived to allow an inference engine to carry out the selection of suitable cutting parameters. The tool cost model for a single milling process can be calculated using the following equation,

$$J(TOL, MRR, SURF; R, c_{i(i=1, \dots, 3)}) = c_1 \cdot NF_1 \cdot TOL + c_2 \cdot NF_2 \cdot MRR + c_3 \cdot NF_3 / SURF \quad (7)$$

The cost function has three terms. Each term is composed of a weighting factor (c_i), a normalisation factor (NF_i) and the function that defines the process efficiency. These functions are: the life of the tool, TOL ; the material remove rate, MRR ; and the desired surface finish, $SURF$. The tool cost function is designed to be directly proportional to the life of the tool and material remove rate and inversely proportional to surface roughness. Hence, optimal solutions will maximise TOL and MRR while minimising $SURF$. These parameters play an important role when selecting cutting parameters since they are usually used as benchmark indices in industries to measure the performance of the system.

The authors describe in [7] the definition of the parameters and the algorithm that automatically manages the selection of adequate cutting parameters. Nine parameters that compose the cost function and two algorithmic methodologies to manage the weighting factors of the cost function are required, depending on production requirements. The paper also discusses restrictions which limit the milling process and some expert skills are included in order to solve the optimization process, giving a complete procedure to obtain quasi-optimal cutting parameters. These definitions are applied in the example application described in section 4 in this paper.

The cost function calculates cutting parameters depending on process requirements. The below explained model reference adaptive control scheme is able to keep the forces below a prescribed upper bound in spite of sudden changes on cutting parameters, spindle speed and depth of cuts, pre-programmed by the optimization algorithm.

4. MODEL REFERENCE ADAPTIVE CONTROL SCHEME

The objective of this section is to provide a control scheme which improves the transitory behaviour of the system and the transitions in between optimal working points through an intelligent plan. For this purpose, the trajectory between optimal cutting parameters in the state space parameter is selected.

4.1. State space trajectories generation

Consider $q_a = (S_{s,a}, a_{dc,a}, f_{c,a})$ and $q_b = (S_{s,b}, a_{dc,b}, f_{c,b})$ the points which optimise J (equation 7) and it is required transition between. Consider the transfer functions $G_a = \frac{N_a}{D_a}$ and $G_b = \frac{N_b}{D_b}$ which describe the behaviour of the system in those points. The transfer function which describes the system at equilibrium points between q_a and q_b can be described as:

$$G_\alpha(s) = \frac{N_\alpha(s)}{D_\alpha(s)} = \frac{\alpha N_a(s) + (1-\alpha)N_b(s)}{\alpha D_a(s) + (1-\alpha)D_b(s)} \quad (8)$$

for any $\alpha \in [0,1]$ which is dependent on the equilibrium point. This parameterization allows moving around the state space; just adjusting the parameter α , provides the system with the capacity to improve transitory states and enhance transitions in between optimal working points travelling through different states in the state space.

The transfer function around each equilibrium point can be defined by an α -value in equation 8. The trajectory of the system passes through the different operational points when the system changes from one to other optimal cutting parameters due to process requirements. Then, the linear model with the best approximation to the behaviour of the system at each instant will vary during the switching process. This motivates the idea of considering different linear models of the system, each one associated with one different possible working point in between two optimal cutting parameters of the system to be switched, i.e., with a different value of α in equation 8. Furthermore, the objective of the discrete controller is to follow the prefixed dynamics of a reference model. For this reason, it is considered as a discretization for each linear model to design the controller. In this sense, it is defined a set of possible values of α as $S_\alpha = \{\alpha^{(1)}, \alpha^{(2)}, \dots, \alpha^{(n_\alpha)}\}$, with $\alpha^{(i)} \in [0,1]$ for $1 \leq i \leq n_\alpha$. Then, the multi-model scheme is composed from different discretization for each working point. The set of discrete transfer functions can be written as.

$$H_{\alpha^{(i)}}(z) = H^{(i)}(z) = Z[h(s) \cdot G_{\alpha^{(i)}}(s)] = \frac{B_\alpha(z)}{A_\alpha(z)} = \frac{k_\alpha \cdot B'_\alpha(z)}{A_\alpha(z)} \quad (9)$$

for $1 \leq i \leq n_\alpha$. The different models are used to parameterize the set of controllers which generate the possible control signals. Each discrete control signal is reconstructed through a zero order hold (ZOH). Then, the effect of the continuous system over the milling system is simulated, obtaining a set of outputs defined as $F_p^{(i)}(t)$ for $1 \leq i \leq n_\alpha$. Those signals are

compared with the reference continuous output, $F_{pm}(t)$, to obtain a following error, $e^{(i)}(t)$, associated with each discrete linear model. Figure 2 shows the control scheme for the full set of α -values. In this figure, there are n_α blocks, each one consists of basic controllers explained below.

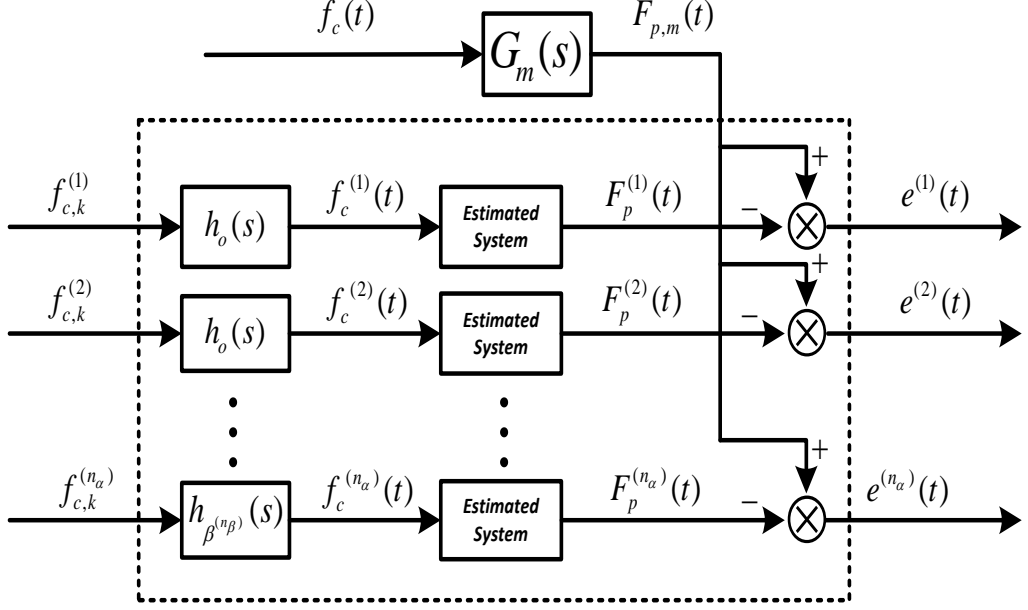


Figure 2: Proposed control scheme.

4.2. Performance index

The supervisory controller evaluates a performance index based on the following error associated to each possible discrete time model. The used index has the following form:

$$J_k^{(i,j)} = \gamma \sum_{l=k-M}^k \lambda^{k-l} \int_{(l-1)T_s}^{lT_s} (F_{pm}(\tau) - F_p^{(i,j)}(\tau)) d\tau + (1-\gamma) \sum_{l=k+1}^{k+M} \lambda^{l-k} \int_{(l-1)T_s}^{lT_s} (F_{pm}(\tau) - F_p^{(i,j)}(\tau)) d\tau \quad (10)$$

for $1 \leq i \leq n_\alpha$, where $\lambda \in (0,1]$ and $M > 0$ are real parameters of the design. λ is a “forgetting factor” that gives more importance to the last sampling instants. $F_{pm}(t)$ denotes the reference continuous output to be followed and $F_p^{(i)}(t)$ is the output obtained from simulating the effect of the controller associated with the non-linear milling system.

4.3. On-line updating of the α gain

When the supervision system chooses switching from the active controller, which is associated to the gain of the linear model α_{old} , to another controller associated to the gain of

the linear model α_{new} , this switching does not carry out instantaneously. The transition from one α -value to another is implemented over a predetermined number of samples. At the same time, the controller is selected associated to the gain of the linear model α_k^{act} , with $\alpha_k^{act} \in [\alpha_{old}, \alpha_{new}]$ if $\alpha_{old} < \alpha_{new}$ or $\alpha_k^{act} \in [\alpha_{new}, \alpha_{old}]$ if $\alpha_{old} > \alpha_{new}$, at each sampling time $t_k = kT_s$ in the switching process. For this reason, α_k^{act} could not be one of the possible values of S_α and they can take any value in the interval $[0, 1]$.

The following algorithm describes the switching mechanism and, in particular, the method of updating the value of the gain α_k^{act} which determines the value, α , of the active discrete model used to parameterize the applied controller.

if $k = jN_r$, **then**

$$\alpha_{new} = \alpha^{(i_{\min})} \text{ with } i_{\min} = \arg \left(i : J_k^i = \min_{1 \leq i \leq n_\alpha} (J_k^i) \right)$$

$$\alpha_{old} = \alpha_k^{act}$$

end if

$$\alpha_{k+1}^{act} = \begin{cases} \min \left(\alpha_k^{act} + (\alpha_{new} - \alpha_{old}) / N_\alpha, \alpha_{new} \right) & \text{if } \alpha_{new} \geq \alpha_{old} \\ \max \left(\alpha_k^{act} + (\alpha_{new} - \alpha_{old}) / N_\alpha, \alpha_{new} \right) & \text{if } \alpha_{new} \leq \alpha_{old} \end{cases}$$

where N_α is the number of samples over which the scheme updates the value of α_k^{act} from α_{old} to α_{new} .

4.4. Basic controller

Finally, it is necessary to calculate as many control laws as there are linear discrete models. Moreover, since the active value of α_k^{act} in the active discrete model can be different to the included in S_α , it is necessary to calculate $n_\alpha + 1$ control signals. However, only the control signal associated to α_k^{act} will be used to generate the actual control signal.

In the control scheme, the reference discrete transfer function is calculated as follows:

$$H_m(z) = \frac{B_m(z)A_o(z)}{A_m(z)A_o(z)} = Z[h_o(s) \cdot G_m(s)] \quad (11)$$

where $A_o(z)$ is cancelled in order to design a causal controller. Now, define $B_m(z) = B'_m(z)k^{(i)}$, where $k^{(i)} = k_{\alpha^{(i)}}$ is the gain in equation 11. Then, the polynomials of the controller are $T(z) = B'_m(z)A_o(z)$, and $R^i(z)$ (monic) and $S^i(z)$ which are unique solutions of the Diophantine equation

$$A^{(i)}(z)R_1^{(i)}(z) + k^{(i)}S^{(i)}(z) = A_m(z)A_o(z) \quad (12)$$

fulfilling the following conditions on the polynomial grades:

$$gr(S^{(i)}) = 2n - 1; gr(A_o) = 2n - gr(A_m) - gr(B^{(i)}) - 1$$

$$gr(R^{(i)}) = gr(A_o) + gr(A_m) + gr(B^{(i)}) - n$$

for $1 \leq i \leq n_\alpha$ with $R^i(z) = B^i(z)R_1^i(z)$ at each sampling time. Leading to the

$$\text{following control law, } f_{c,k}^{(i)} = \frac{\hat{T}(q^{-1})}{\hat{R}_k^{(i)}(q^{-1})} f_{c,k} - \frac{\hat{S}_k^{(i)}(q^{-1})}{\hat{R}_k^{(i)}(q^{-1})} F_{p,k}^{(i)}$$

$$(13) \text{ for } 1 \leq i \leq n_\alpha.$$

with $\hat{\theta}_{k+1}^{(l)} = \hat{\theta}_k^{(l)} + \frac{P_k^{(l)} \phi_k^{(l)} e_k^{(l)}}{1 + \phi_k^{(l)} P_k^{(l)} \phi_k^{(l)}}$; $\hat{\theta}_o^{(l)}$ arbitrary, provided that $\text{tr} \begin{pmatrix} \hat{A}_o & \hat{B}_o \end{pmatrix}$ is a co-prime pair,

$$P_{k+1}^{(l)} = P_k^{(l)} - \frac{P_k^{(l)} \phi_k^{(l)} \phi_k^{(l)\top} P_k^{(l)}}{1 + \phi_k^{(l)} P_k^{(l)} \phi_k^{(l)}}; P_o^{(l)} = P_o^{(l)\top} > 0 \text{ where } e_k^{(l)} = F_{p,k} - \hat{F}_{p,k}^{(l)} \text{ is the identification error}$$

for the k^{th} sample $\forall l \in N_\alpha = \{1, 2, \dots, n_\alpha\}$.

An example of implementing the proposed control scheme is described in the next section.

5. EXAMPLE APPLICATION

A practical 3-tooth, 30 mm diameter end mill with the modal characteristics in the X and Y directions corresponding to table 1 is chosen for this example. The work-piece is a rigid aluminium block whose specific cutting energy is $k_t = 600 \text{ kN} \cdot \text{mm}^{-1}$ and the proportional factor is taken to be $k_r = 0.07$.

Table 1 Modal parameters of the tool.

	$\omega_n (\text{rad} \cdot \text{s}^{-1})$	$\xi (\%)$	$k (\text{KNmm}^{-1})$
X	603	3.9	5.590
Y	666	3.5	5.715

For the model reference control, the transfer function of equation 6 has a cutting pressure selected to be constant and equal to $1200 \text{ N} \cdot \text{mm}^{-2}$ in all range of cutting parameters, the CNC time constant, $\tau_m = 0.1 \text{ ms}$ and, $\tau_c = 1/N_t S_s$. The continuous model reference system of the adaptive control is chosen to be a typical continuous second order plant with $\xi = 0.75$ and $\omega_n = 2.5/(4 \cdot T)$, where T is the sampling period. Also, it is desirable for the reference force to be maintained at 1200 N .

The input space parameter where the system searches for quasi-optimal cutting parameters is given by the stability borderline (first graph of figure 3). This figure indicates that if programming cutting parameters are over the borderline then chatter vibrations will appear and the system will become unstable [4]. However, if programmed cutting parameters are below this borderline the system will work correctly without suffering chatter vibrations. Other mechanical and electrical restrictions when searching for programming adequate cutting

parameters are related to spindle power consumption and feed drive limitations. Other safety constraints can be added in order to avoid uncertainty in searching regions and avoiding impractical minima during optimisation.

For example purposes, it is supposed that the following two cutting parameters represent two Pareto optimal fronts, $S_{s1} = 2710$ and $a_{dc1} = 0.3710$, as point 1, and $S_{s1} = 3260$, $a_{dc1} = 0.4127$, as point 2. A more in-depth explanation of how to obtain Pareto optimal cutting parameters is provided by Rubio et al. [7].

Regarding the control scheme, it is taken into account that $\alpha = \{1, 0.7, 0.5, 0.3, 0\}$, being $\alpha_{\min} = 1$ and $\alpha_{\max} = 0$, corresponding with the points 1 and 2, respectively. Figure 3 depicts, from top to bottom, the stability lobes with the situation of the suggested Pareto optimal cutting parameters, the system output (resultant and reference forces) and the programmer feed rate when it is required to change the cutting parameter from point 1 to point 2 with and without applying the controller. The left hand figures show the outputs and control commands when the control scheme is applied. The right side corresponds to the case where the control scheme is not implemented. When the cutting conditions change, a peak appears in the resultant forces. This peak can lead to excessive wear and damage or even breakage of the tool or machine components. Moreover, those peaks can have a detrimental influence on the surface finish of the workpiece. In the proposed control algorithm the cutting forces are maintained constant by adjusting the feed rate according to the presented algorithm.

Then, as shown in figure 3, the Pareto optimal cutting parameters proposed by the self-optimized system are below the stability borderline in the stable zone. Furthermore, the presented controller is able to move automatically around the allowable cutting space parameter, keeping the forces below a prescribed upper limit bound while programming feasible command federate in spite of changes in cutting parameters.

Finally, the implemented controller can also be tuned in order to reduce the overshoot of the transitory state, which could also lead to damage or breakage of the tool or tool-holder and machine components and leave uneven surface finish.

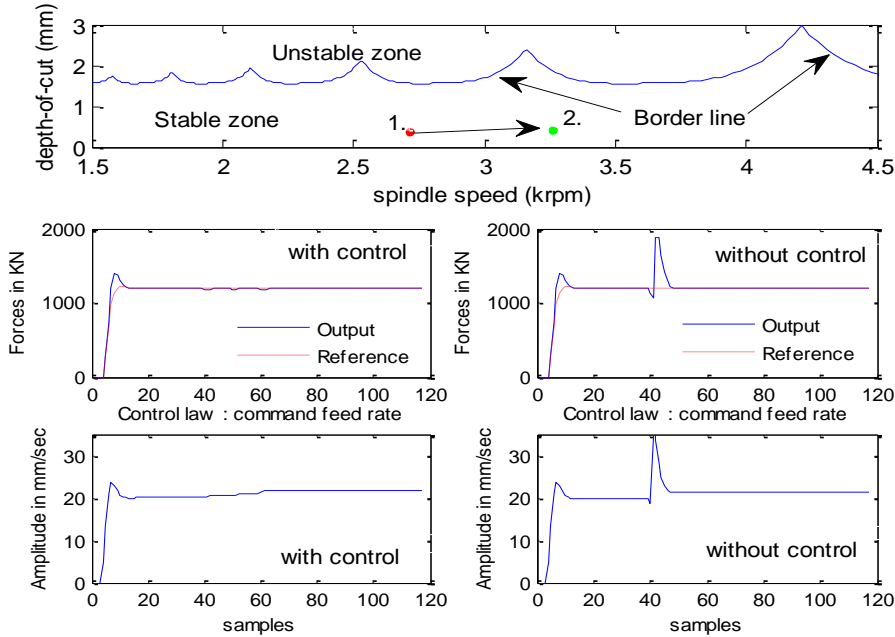


Figure 3: Situation of the programmed cutting parameters in stability lobes, output force signal and control signal with and without applying the control

6. CONCLUSIONS

This paper proposes a novel control scheme for controlling cutting parameters in milling applications. It is composed of two levels. In the first level, the self-optimised cutting parameters layer comprises life of the tool, material remove rate, surface roughness and the robustness of the system. While the second layer, the parallel multi-estimation controller, provides an environment to control the milling process automatically under changes in cutting conditions. The change of the cutting parameters is scheduled by production requirements. For this purpose, an algorithm methodology is proposed in order to automatically adjust the parameter α choosing the most suitable controller among the set designed for each programmed optimal cutting parameters. The designed controller is able to smooth the transition between discrete control models and so reduce the peaks which appear when sudden changes are made in the cutting parameters.

The fundamental idea of the control system is to work automatically, with a simple interface with the operator, based around the admissible cutting parameter space given by the well-known stability lobes. First, the optimization cost function is used to obtain the cutting parameters according to multiple objectives optimization. Secondly, the adaptive control scheme proposes different control laws working in parallel to address the non-linear and changeable milling process. Finally, the supervisory scheme manages the system so it can work automatically in between optimal working points. Simulation results support the performance of the system.

ACKNOWLEDGEMENTS

The authors gratefully acknowledge the UK's Engineering and Physical Science Research Council (EPSRC) funding of the EPSRC Centre for Innovative Manufacturing in Advance Metrology (Grant Ref: EP/I033424/1).

REFERENCES

- [1] F. Cus, and J. Balic, "Optimization of cutting process by genetic algorithm approach," *Robotics and computer integrated manufacturing*, vol. 19, pp. 113-121, 2003.
- [2] J.V. Abellan, F. Romeros, H.R. Siller, A. Estrud and C. Vila, "Adaptive control optimization of cutting parameters for high quality machining operations based on neural network," *Advance in robotics, Automation and Control*, I-tech, Vienna, Austria, 2008.
- [3] U. Zuperl, and F. Cus, "Optimization of cutting conditions during cutting using neural networks," *Robotics and computer integrated manufacturing*, vol. 19, no. 1-2, pp. 189-199, 2003.
- [4] Y. Altintas, *Manufacturing automation*, Cambridge University Press, 2012.
- [5] U. Zuperl, F. Cus and M. Milfelner, "Fuzzy control strategy for an adaptive force control of forces in milling processes," *Journal of Material Processing Technology*, pp.1472-1478,2005.
- [6] L. Rubio, M. De La Sen, and A. Bilbao-Guillermo, "Intelligent adaptive control of forces in milling processes," *Proceedings of the 2007 IEEE Mediterranean Conference on Control, and Automation*, pp. 1-6, 2007.
- [7] L.Rubio, M. De La Sen, A.P.Longstaff and S. Fletcher, "Model-based expert system to automatically adapt milling forces in Pareto optimal multi-objective working points", *Expert Systems with Applications*, 40, 2312-2322, 2013.

A methodology to evaluate the machinability of Alloy 718 by means of FE simulation

Amir Malakizadi, Stefan Cedergren, Kumar Babu Surreddi, Lars Nyborg

Chalmers University of Technology, Department of
Materials and Manufacturing Technology, SE412 96, Gothenburg, Sweden
email: amir.malakizadi@chalmers.se

ABSTRACT

In recent years, different numerical and statistical methods have been developed to evaluate machinability of difficult-to-cut materials. One way to examine potential machinability of workpiece materials is to employ statistical models provided with large amount of input data obtained either experimentally or by means of material modelling software. However, these methods lead to a qualitative ranking of workpiece materials. This study presents a methodology involving the application of 3D Finite Element (FE) modelling of metal cutting, including the initial derivation of calibrated material parameters from 2D case by means of inverse modelling of orthogonal machining, where the optimum combination of Johnson-Cook material parameters and the friction coefficients of a pressure dependent shear friction model was determined. An FE based wear model is then developed incorporating Usui's empirical wear rate equation to simulate the flank wear progression during face turning of Alloy 718 in aged condition with uncoated carbide cutting tool. Finally, the application of current methodology is discussed and guidelines for further implementations are presented.

KEYWORDS: Alloy 718, Machinability, Wear modelling, Inverse Identification

1. INTRODUCTION

Alloy 718 is a nickel based superalloy widely used in aircraft engine parts, steam turbines, pressure vessels and space applications, the reasons being its strength, thermal stability, corrosion resistance, thermal fatigue resistance and creep resistance at high temperatures [1]. However, this alloy is known to be a difficult-to-cut material owing to its combination of high strength at elevated temperatures, poor thermal conductivity, strain hardening response and presence of abrasive carbide particles [2].

The machinability is a term that refers to the ease with which a work material can be machined under a given set of cutting conditions. Shaw et al. [3] and Trent et al. [4] outlined that tool life, surface finish, cutting forces and surface integrity are the main parameters for assessing the machinability of a material. These parameters are influenced by work material, cutting tool characteristics (properties and geometry) and cutting parameters. It can be

envisaged that the material characteristics in terms of representative mechanical and thermal properties are essential. One way of structuring these properties has been proposed by Ståhl and Andersson [5]. They introduce so-called polar diagrams in which five different aspects are included; namely abrasiveness captured via the potential presence of hard particles (e.g. carbides), ductility represented by the elongation to fracture value, strain hardening depicted by the tensile stress/yield stress ratio and finally yield stress (or hardness) indicating the resistance to yielding. These characteristics can be derived from experimental data and published material data. Of prime interest is then to depict how a change in material composition within a given standard specification could impact on the potential machinability. To do so based only on experimental data would require enormous amount of experiments. Hence, since the radar approach using polar diagrams could be considered as an initial qualitative approach to assess potential machinability, virtual methods involving use of materials database software and simulation to construct polar diagram would be highly beneficial. Such approach has been developed by Olovjsö et al. [6], who derived meta-models by using the software JMatProTM [7] (Java based Material Property software) and statistical modelling. Having access to extensive tool wear and work material specification data, Avdovic et al. [8] have derived empirical relations and shown the correlation between carbon content of Alloy 718 and flank wear depicted as abrasiveness.

For detailed modelling and evaluation of machinability of Alloy 718, it is beneficial to get consistent material data which should consider all possible variations such as chemical composition, heat treatment and precipitates present. At first hand, application of material databases and materials modelling software, tend to be attractive to retrieve the necessary information. There are several material databases available such as online material property database MatWeb [9] and Material Properties Database MPDB software from JAHM [10]. In most databases, the mechanical and thermal properties of Alloy 718 are available at either room temperature or for a single composition. Also, in order to explore thermal properties, it is necessary to take into account use of thermodynamic modelling tools such as Thermocalc, MatCalc and JMatProTM to calculate the equilibrium and phase relationships of Alloy 718 for different compositions and heat treatments. In this context, JMatPro offers the interesting solution to calculate and predict mechanical and thermo-mechanical material properties using large amount of material property database and CALPHAD method [7]. It is possible to calculate mechanical and thermo-physical properties e.g. tensile strength, hardness, flow curves and thermal conductivity. There is still one concern when using material data retrieved from JMatPro in simulation of metal cutting processes. Although being well anchored to appropriate theoretical models and experimentally verified [7], the results refer to global material behavior, whereas the metal cutting process involves highly localized thermo-mechanical response of the work material. Hence, any derivation of mechanical properties by either theoretical calculations or mechanical testing will not necessarily fully depict the behavior of the work material in metal cutting [11].

In recent years, with drastic improvement in computing power of computers and robustness of computational algorithms, finite element method (FEM) has widely been used to simulate different cutting processes [12]. FE modelling of metal cutting process can provide a possible solution to minimize experiments aimed at optimizing the machining operations and thus may play a vital role in product and process development, which will contribute to sustainable production. However, there are several challenges regarding the accurate boundary conditions, reliable material models and also well-defined material parameters, which need to be addressed first to attain reliable predictions [12]. One way of circumventing these challenges and to further judge how material property data will suffice in modelling of metal cutting is to derive empirical material models for use in FEM codes by inverse modelling of orthogonal cutting experiments. In this study, initially the parameters of the Johnson-Cook

(JC) material model together with the optimal friction coefficients are therefore determined. The turning process is then simulated in 3D to attain the contact temperatures, pressures and sliding velocities required for flank wear simulations. With this as a base, the empirical model by Usui [13], is applied to demonstrate the FE-based wear modelling in 3D and further development of the wear modelling is discussed. The approaches presented in this study are supposed to contribute to sustainable production from both economic and environmental points of view as they provide means of safe and robust product and process development.

2. EXPERIMENTS AND RESULTS

2.1. Inverse identification of flow stress properties of Alloy 718

Several experimental methods such as Split Hopkinson Pressure Bar (SHPB) test [14] have been used to determine the flow stress properties of work material in metal cutting process. However, these methods encounter several limitations including limited range for attainable strain and strain rates, often significantly lower than the values encountered in the vicinity of the cutting zone [11]. To overcome these drawbacks, inverse modelling of orthogonal cutting test have widely been used to determine the flow stress properties of the workpiece material [15-17].

In this study, an inverse methodology based on Response Surface Methodology (RSM) and FE analysis of the orthogonal cutting test was employed to identify the optimum combination of material parameters and friction coefficients [18]. Fig. 1 shows the steps of the proposed inverse methodology.

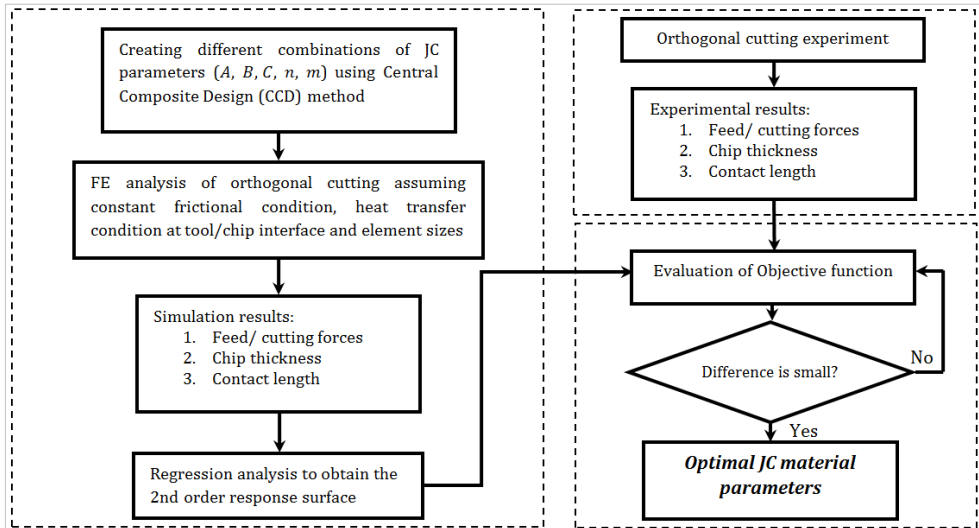


Fig.1. Flowchart showing the steps of inverse methodology to obtain the JC parameters.

In this method, Central Composite Design (CCD) is initially used to generate certain combinations of JC material parameters (see equation 1). Accordingly, an FE simulation is performed at predefined frictional condition (see equation 2) for each set of material parameters as an input. The response surfaces are then generated by regression analysis to

determine the relation between the material parameters and the outputs of FE analysis including the cutting/feed forces, chip thickness and contact length. Finally, the optimal combination of material parameters and friction coefficients are determined as the deviation between the simulation results (response surfaces) and the corresponding experimental measurements provided at similar cutting conditions is smaller than an error tolerance.

Material and experimental details

The cutting tests were carried out in a SOMAB Optimab 400 CNC lathe. Orthogonal condition was met through transverse machining of 2 mm flanges. All cuts were duplicated with a new tool edge for each test. No cutting fluid was applied. Silicon carbide whiskers reinforced alumina inserts from Greenleaf were used (WG-6218-2A grade WG300), with an entering angle of 90° and 0° rake angle. The feed rate was kept constant at 0.1 mm/rev and the cutting speed was varied in two levels, 30 and 60 m/min. Cutting forces were measured with a Kistler type 9121 three component dynamometer. The contact lengths and chip thicknesses were measured accordingly as input for the inverse methodology. Material from the same wrought bar of Alloy 718 was used during all experiments, with an outer diameter of 126.5 mm, average grain size of 16 µm and chemical composition given in Table 1. The material was heat treated using the standard ageing cycle [19], resulting in a Vickers hardness of 445, measured with 10 kg load.

Table 1. Nominal composition of Alloy 718 and the composition of the bar, wt. % [1].

Alloy	Ni	Cr	Co	Fe	C	Mo	Al	Ti	Nb	B	Mn	Si	Cu
Nominal	Bal	19	0	18.5	0.04	3.0	0.5	0.9	5.1	0.006	0.2	0.2	0
Actual bar	Bal	18.36	0.33	17.49	0.04	3.15	0.56	0.92	5.46	0.001	0.09	0.05	0.14

Derivation of material model

As shown in Fig.1, certain number of FE simulations at specific frictional and thermal boundary conditions and mesh densities were performed to obtain the relation between the JC material parameters and the simulation outputs. DEFORM 2D commercial software was used to simulate the orthogonal cutting process providing the different combinations of material parameters A , B , C , n and m for the Johnson-Cook (JC) constitutive model, expressed as;

$$\sigma = (A + B\varepsilon^n) \left(1 + C \ln \left(\frac{\dot{\varepsilon}}{\dot{\varepsilon}_0} \right) \right) \left(1 - \left(\frac{T - T_w}{T_m - T_w} \right)^m \right) \quad (1)$$

where σ is the flow stress of the workpiece material and ε , T and $\dot{\varepsilon}$ represent strain, temperature and strain rate values, respectively. $\dot{\varepsilon}_0$ is the reference strain rate here taken as $\dot{\varepsilon}_0 = 1$ and T_m and T_r are melting and room temperatures, respectively.

Only 4 mm segment was modelled to have reasonable solution time; however, care was taken to ensure that the thermo-mechanical steady state condition was reached at the end of simulation. The workpiece includes approximately 10000 elements. The cutting conditions were set similar to the orthogonal cutting tests. JMatProTM software was used to obtain temperature dependent thermal properties for Alloy 718 under investigation. In order to apply a more realistic model representing the frictional condition at tool/chip interface, a pressure dependent shear friction model was also implemented by means of a FORTRAN subroutine using the equation:

$$\tau = m_0 [1 - \exp(\alpha P)] k \quad (2)$$

where τ is the shear stress, k is the shear strength of the workpiece material, P is the pressure and α and m_0 are the model constants.

The regression analysis was performed to obtain the second order response surfaces relating the outputs of FE simulations to the JC material parameters. Then the optimum JC material parameters under a certain frictional and thermal boundary conditions and for a specific mesh density are determined by minimizing the following objective function;

$$F(X) = \sum_{m=1}^4 \left\{ w_m \left[\sum_{n=1}^N \left(\frac{Y_{mn} - Y_{mn,EXP}}{Y_{mn,EXP}} \right)^2 \right] \right\} \quad (3)$$

where X is a vector including the JC parameters, w_m is the weighting factors, Y_{mn} represents the quadratic response surfaces for cutting/feed forces, chip thickness and contact length as functions of JC material parameters and $Y_{mn,EXP}$ is the corresponding experimental measurement for each response. N is the number of cutting conditions used for inverse modelling procedure. The optimum JC parameters and corresponding friction coefficient determined using the proposed inverse methodology for Alloy 718 in aged condition is given in Table 2.

Table 2. The optimal JC parameters and friction coefficient.

Material	A(MPa)	B(MPa)	C	n	m	T_m	m_0	α
Alloy 718	1562	300	0.0164	0.25	1.7	1200	1	0.0015

2.2. 3D FE model of the real cutting process

Several studies have been conducted on 3D modelling of cutting processes [21, 22]. Simulation of cutting process in 3D results in a more realistic distribution of the temperature and stress on the tool edge that can consequently be used to optimize the tool micro geometry and cutting conditions to attain controlled tool life and/or desired surface integrity on the workpiece material. In this study, DEFORM 3D commercial FE software was used to model the face turning process. The two different cutting conditions addressed, termed A and B, are given in Table 3.

Table 3. The cutting conditions used in 3D simulation of cutting process.

	Cutting speed (m/min)	Feed rate (mm/rev)	Depth of cut (mm)
Condition A	30	0.05	1
Condition B	30	0.1	1

Since the aim of this study was to simulate the flank wear, the element size at the vicinity of the cutting edge was kept at 5 μm , to ensure more uniform distribution of the contact pressure, sliding velocities and nodal temperature on the tool edge, and later on the flank wear land when simulating wear progression. The optimum JC parameters and friction coefficients given in Table 2 were used in all FE simulations. Since all tool life experiments were performed under wet condition (see section 2.3), the heat transfer coefficient to the environment was assumed at 1500 W/(m²K) to include the cooling effects [23].

2.3. Flank wear modelling for carbide tool

Having known distribution of temperature, contact pressure and the sliding velocities on the tool edge, it is possible to model the flank wear by using an appropriate wear model. Several studies have been dedicated to the simulation of wear progression in 2D and 3D by coupling wear models and FE simulations [24-26]. Different wear models have been proposed and validated by different authors [13, 27] to assess the wear progression associated with various wear mechanisms; adhesion and abrasion wear at lower cutting speeds and diffusion and oxidation wear at higher cutting speeds.

In this study, Usui's empirical model is used to model the wear rate, and the rate equation for flank wear progression is derived based on experimental observation. Later the model is implemented and an algorithm is proposed for simulation of wear simulation in 3D.

Experimental details

Machining tests were performed on EMCO 365 CNC lathe, with mineral oil based emulsion Blaser Swisslube Blasocut BC25-MD, with a concentration of 7%. The inserts were uncoated standard cemented carbides without chip breaker (Sandvik Coromant TCMW16T304 grade H13A) with 0.4 mm nose radius, 0° rake angle, 7° clearance angle and 91° entering angle. Cutting forces were measured with a Kistler type 9275A three component dynamometer. Tool wear was evaluated in stereo optical microscope Zeiss Discovery V20 according to the ISO standard [28]. The work material was the same as in the orthogonal cutting tests, with a 126.5 mm outer diameter and a 20 mm hole drilled in the center. This resulted in a spiral cutting length of 245.1 m for cutting condition A and 122.5 m for condition B for each pass, with a time of cut of 8.17 min and 4.09 min respectively.

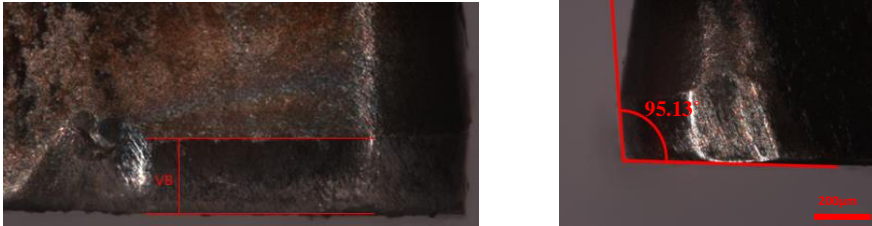


Fig.2. Experimental observations of the flank wear width.

Wear model: derivation of flank wear rate equation and implementation

The wear rate in Usui's empirical equation [13] is related to contact pressure (σ_n), sliding velocity between tool and chip/workpiece (V_c) and contact temperature in Kelvin (T) as;

$$\dot{w} = \frac{dw}{dt} = C_1 \sigma_n V_c \exp\left(-\frac{C_2}{T}\right) \quad (4)$$

where \dot{w} represents the volume loss per unit time and C_1 and C_2 are the model constants. In order to simulate the flank wear width VB the relation between the rate of volume loss and VB is to be derived. As experimentally observed during wear measurements (Fig. 2), the angle (β) between the flank wear land and the normal to the rake face was approximately 5°, and therefore it needs to be taken into account when calculating the volume loss. The total volume loss (V_{total}) along the cutting edge for an infinitesimal time increment dt is given as:

$$\dot{w} \equiv \frac{dV_{total}}{dt} = \left[VB(\tan \alpha + \tan \beta) \left(1 + \frac{\pi r_n}{2} \right) \right] \frac{dVB}{dt} \quad (5)$$

where α is the clearance angle, r_n is the nose radius and $l \approx ap - r_n$. In this study, depth of cut (ap) is 1 mm and therefore $l \approx 0.6$ mm (see Fig. 3). Using equations 4 and 5, the flank wear rate equation can then be obtained as:

$$\frac{dVB}{dt} = \left(\frac{C_1}{[VB(\tan \alpha + \tan \beta) \left(1 + \frac{\pi r_n}{2} \right)]} \right) \sigma_n V_c \exp\left(\frac{-C_2}{T}\right) \quad (6)$$

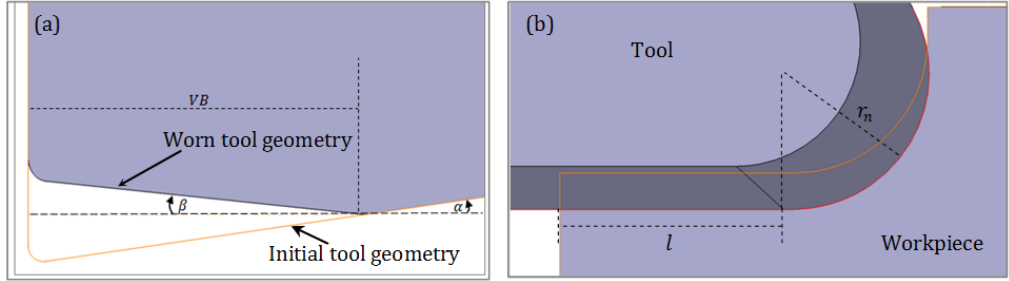


Fig.3. Tool geometry change during flank wear progression (a) and representation of cutting edge length (b)

Subsequently, the flank wear width (VB) can be calculated by solving the rate equation 6, once C_1 and C_2 are known. In order to determine the model constants, cutting condition A was simulated at different flank sizes and the average temperature, contact pressure and the sliding velocity were calculated at the end of the simulation by means of a FORTRAN subroutine. Having known these values, equation 6 was calibrated by minimizing the deviation between experimental measurements and prediction of the rate equation at corresponding cutting times, resulting in the equation with the derived constants as follows:

$$\frac{dVB}{dt} = \left(\frac{0.00325}{VB} \right) \sigma_n V_c \exp\left(\frac{-18258}{T}\right) \quad (7)$$

Figure 4 shows the steps of modelling flank wear progression. Initially, a 3D FE model was built for cutting condition B assuming the initial flank wear width of 10 μm . It was seen that after 3 mm of cut, the temperature at the tool/workpiece interface reaches steady state condition, and therefore the simulations were stopped at this length of cut. The FORTRAN subroutine was then called to calculate the average values of nodal temperature, contact pressure and sliding velocities at the end of simulation. Accordingly, equation 6 was solved using Runge Kutta 4th order method, having known flank size (VB) at the beginning of each time step and given time increment ($\Delta t \approx 245$ s). Then, the tool geometry and its position with respect to the workpiece were updated and the FE simulation of cutting process with the modified flank size model was performed. This loop has to continue until the cutting time reaches a desired value.

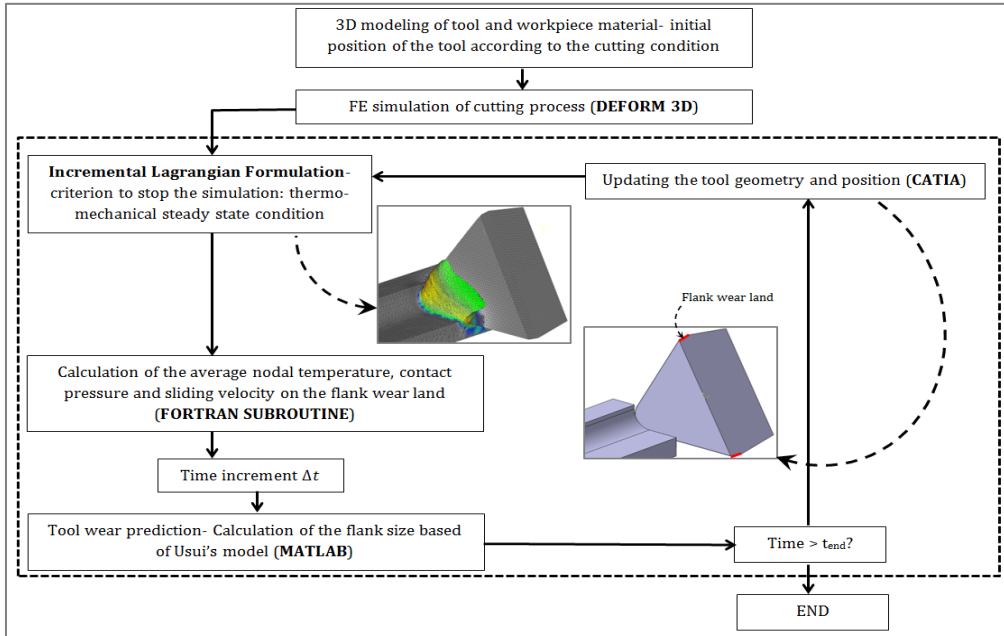


Fig.4. The flank wear modelling steps.

3. RESULTS AND DISCUSSION

It is envisaged that the establishment of a calibrated JC material model is a necessary part of the approach to achieve reliable prediction when FE modelling used to simulate metal cutting processes. Fig. 5a shows the comparison between the 2D FE simulation results incorporating the optimum JC parameters and friction coefficients given in Table. 2 and the corresponding experimental measurements at two cutting conditions described in section 2.1. Fig. 5b shows the FE simulation results at similar cutting conditions incorporating flow stress properties obtained from JMatPro commercial software. As evident from Fig. 5, the fit between experimental data and FE-simulations is better when using the optimal JC parameters compared to incorporating data from JMatPro. Accordingly, Fig. 6a shows the cutting temperatures computed by means of FE simulations at both cutting conditions and their comparison with FE simulation results incorporating optimal JC parameters given in Table.2.

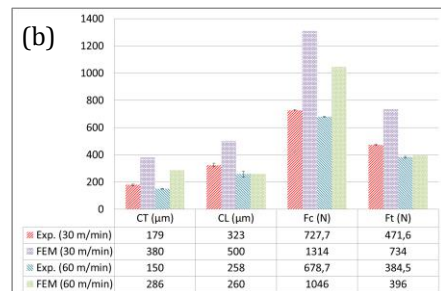
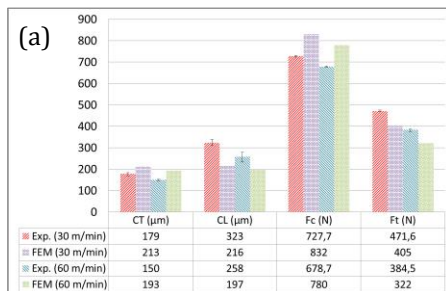


Fig.5. Comparison between experimental [20] and 2D FE simulation results at two different cutting conditions incorporating optimum JC material parameters (a) and flow stress properties obtained from JMatPro commercial software (b).

As can be seen, at both cutting conditions, the cutting temperatures using JMatPro flow stress properties are about 10% higher than those calculated incorporating the optimal JC parameters. However, it must still be emphasized that use of JMatPro data in the FE-modelling means that the trend between different machining conditions is correctly captured. The temperature distribution during chip formation at 30 m/min and 0.1 mm/rev feed rate is shown in Fig.6b.

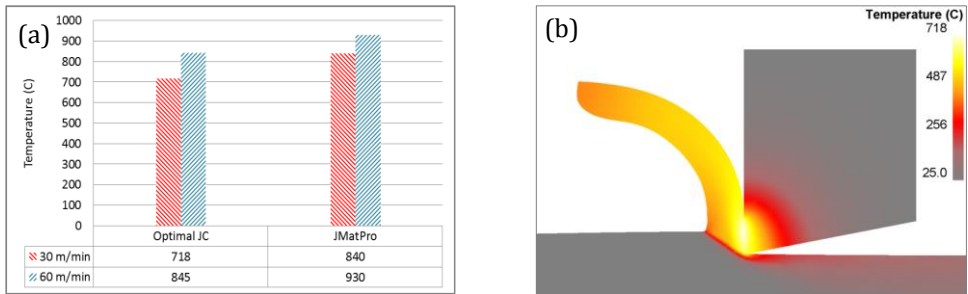


Fig.6. Comparison between maximum tool temperatures obtained from 2D FE simulations of orthogonal cutting experiments at two different cutting conditions incorporating the optimum JC parameters and flow stress curves using JMatPro (a) and temperature distribution during chip formation at 30 m/min and 0.1 mm/rev feed rate (b).

Figure 7 shows the results of the flank wear modelling at cutting condition B for different cutting times. As can be seen, the distribution and maximum temperatures at the vicinity of the cutting edge increase with increase of the flank wear land. The FE simulation results using fresh and worn inserts with different flank sizes show that the maximum temperature initially occurs on the rake face and as the flank wear progresses during the cutting process, its location moves to the flank land. This is due to the fact that with increase of the wear land, larger area of the tool is in contact with the surface of the workpiece material and therefore more is heat generated as a result of frictional contact. However, it should be noted that the difference between the maximum temperature at the rake and flank faces were less than 30 °C.

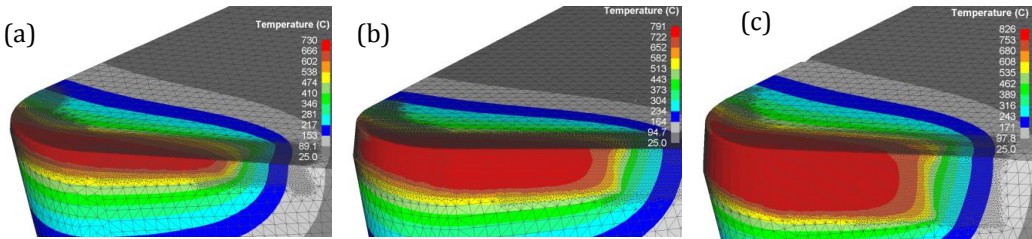


Fig.7. Flank wear progression after: $t = 245$ s (a), $t = 735$ s (b) and $t = 1225$ s (c) for cutting condition B.

Figure 8a shows the effect of flank size on the cutting, feed and passive forces measured experimentally and derived from simulation of the cutting process for condition A. As can be seen, feed force gradually increases as the flank width increases. It should also be noted that there is a good correlation between experimental measurements and predicted forces. The experimental flank size measurements at both cutting conditions and prediction results for cutting condition B are shown in Fig.8b.

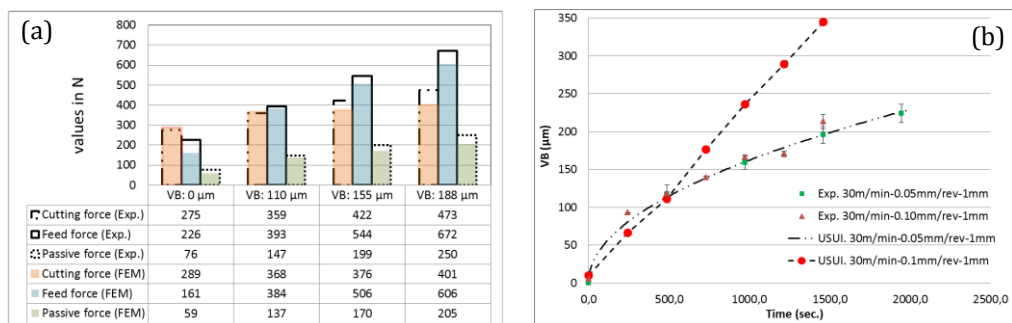


Fig.8. Comparison between the simulated force components and experimental measurements for different flank wear widths at cutting condition A (a) and experimental flank wear widths for conditions A and B as well as simulated values for condition B (b).

As can be seen, the measured flank wear width for both condition A and condition B are approximately similar, while the results of flank wear simulation for cutting condition B incorporating Usui's model deviate increasingly from the experimental measurements up to 70% at the end of the simulation. This deviation is probably due to effect of strain hardening on the hardness of the machined surface. Ståhl et al. [29] investigated the thickness of strain hardened layer on the machined surface when machining aged Alloy 718 at different cutting conditions. They reported that the thickness of the strain hardened layer at low feed rates can be in same order of magnitude as the feed rate, and consequently the tool edge will cut through the strain hardened layer with considerably higher hardness compared to the virgin material. This can explain the source of error in flank wear prediction results using Usui's model, where in this study, its corresponding parameters were determined employing only one cutting condition (condition A). Usui's wear model is exponentially temperature dependent and as the temperature increases on the flank side during its progression (see Fig. 5), the rate of wear predicted increases significantly. This temperature dependence is not consistent with experimental observations as evidenced from the results in this study. To overcome this problem, several wear tests need to be performed at different cutting conditions to identify the parameters of the wear model. In this way, it is possible to tune the wear model to capture the rates of different wear mechanisms (adhesive, abrasive and diffusive) at various regimes of cutting temperatures as well as additional effects of strain hardened layer in Alloy 718. Other way to improve the reliability of wear simulation results is to employ the modified Usui's model incorporating temperature dependent coefficients [26, 30-31]. Using this approach, the appropriate set of coefficients representing certain wear mode can be determined for a specific cutting regime and therefore, the prediction of the wear model can be improved significantly.

4. CONCLUSIONS

In this study, a methodology to simulate flank wear progression during machining of Alloy 718 using uncoated cemented carbide tool is presented. The methodology is based on the initial derivation of calibrated material models from 2D case by means of inverse modelling of orthogonal machining, followed by use of the optimum Johnson-Cook (JC) material model in 3D representation and modelling of real machining conditions, whereafter a Finite Element (FE) based wear model is applied incorporating Usui's empirical wear rate equation to simulate the flank wear progression in face turning of aged Alloy 718 with uncoated carbide tools. It was shown that the calibrated constitutive model and well-tuned wear rate equation are essential to achieve reliable predictions when FEM is being used to simulate the cutting processes. Some guideline for further improvement in wear modeling was also suggested and left for future developments.

ACKNOWLEDGEMENTS

This study was performed within the framework of Sustainable Production Initiative at Chalmers University of Technology, the support of which is gratefully acknowledged. Support via the Metal Cutting Research and Development Centre (MCR) at Chalmers University of Technology is also acknowledged.

REFERENCES

1. R. C. Reed, "The superalloys: Fundamentals and Applications," Cambridge University Press, 2006.
2. R. Arunachalam and M. Mannan, "Machinability of nickel-based high temperature alloys," *Machining Science and Technology*, vol. 4, pp. 127-168, 2000.
3. M. C. Shaw, *Metal cutting principles* vol. 2: Oxford University Press New York, 2005, pp. 20-24.
4. E. D. Trent, P. K. Wright, *Metal Cutting*, 4th edition: Butterworth-Heinemann, 2000, pp.251-252.
5. J. E. Ståhl and M. Andersson, "Polar Diagram Machinability Diagram-a Model to Predict the Machinability of a Work Material," *Swedish Production Symposium*. 2007.
6. S. Olovsjö, P. Hammersberg, P. Avdovic, J.-E. Ståhl, and L. Nyborg, "Methodology for evaluating effects of material characteristics on machinability-theory and statistics-based modelling applied on Alloy 718," *The International Journal of Advanced Manufacturing Technology*, vol. 59, pp. 55-66, 2012.
7. Z. Guo, N. Saunders, J. Schillé, and A. Miodownik, "Material properties for process simulation," *Materials Science and Engineering: A*, vol. 499, pp. 7-13, 2009.
8. P. Avdovic, X. Linhong, M. Andersson, and J.-E. Stahl, "Evaluating the Machinability of Inconel 718 Using Polar Diagrams," *Journal of engineering for gas turbines and power*, vol. 133, 2011.
9. www.matweb.com
10. http://www.jahm.com/pages/about_mpdb.html
11. J. Pujana, P. Arrazola, R. M'saoubi, and H. Chandrasekaran, "Analysis of the inverse identification of constitutive equations applied in orthogonal cutting process," *International Journal of Machine Tools and Manufacture*, vol. 47, pp. 2153-2161, 2007.
12. M. Vaz Jr, D. Owen, V. Kalhori, M. Lundblad, and L.-E. Lindgren, "Modelling and simulation of machining processes," *Archives of computational methods in engineering*, vol. 14, pp. 173-204, 2007.
13. E. Usui, T. Shirakashi, and T. Kitagawa, "Analytical prediction of cutting tool wear," *Wear*, vol. 100, pp. 129-151, 1984.
14. U. Lindholm and L. Yeakley, "High strain-rate testing: tension and compression," *Experimental Mechanics*, vol. 8, pp. 1-9, 1968.
15. A. Shroft and M. Bäker, "Inverse Identification of Johnson-Cook Material Parameters from Machining Simulations," *Advanced Materials Research*, vol. 223, pp. 277-285, 2011.
16. T. Özel and Y. Karpaz, "Identification of constitutive material model parameters for high-strain rate metal cutting conditions using evolutionary computational algorithms," *Materials and manufacturing processes*, vol. 22, pp. 659-667, 2007.
17. B. Shi, H. Attia, and N. Tounsi, "Identification of Material Constitutive Laws for Machining: Part II: Generation of the Constitutive Data and Validation of the Constitutive Law," *Journal of manufacturing science and engineering*, vol. 132, 2010.

18. A. Malakizadi, I. Sadik, and L. Nyborg, "Wear Mechanism of CBN Inserts During Machining of Bimetal Aluminum-grey Cast Iron Engine Block," *Procedia CIRP*, vol. 8, pp. 187-192, 2013.
19. S. Aerospace, "Aerospace material specification 5662 M," ed, 1965.
20. P. Malm and A. Hagberg, "Material Deformation Mechanisms during Machining of Superalloys," M.Sc.Thesis, Chalmers University of Technology, 2010.
21. G. M. Pittalà and M. Monno, "3D finite element modelling of face milling of continuous chip material," *The International Journal of Advanced Manufacturing Technology*, vol. 47, pp. 543-555, 2010.
22. X. Man, D. Ren, S. Usui, C. Johnson, and T. D. Marusich, "Validation of Finite Element Cutting Force Prediction for End Milling," *Procedia CIRP*, vol. 1, pp. 663-668, 2012.
23. B. Rao, C. R. Dandekar, and Y. C. Shin, "An experimental and numerical study on the face milling of Ti-6Al-4V alloy: tool performance and surface integrity," *Journal of Materials Processing Technology*, vol. 211, pp. 294-304, 2011.
24. B. Li, "A review of tool wear estimation using theoretical analysis and numerical simulation technologies," *International Journal of Refractory Metals and Hard Materials*, vol. 35, pp. 143-151, 2012.
25. Y.-C. Yen, J. Söhner, B. Lilly, and T. Altan, "Estimation of tool wear in orthogonal cutting using the finite element analysis," *Journal of Materials Processing Technology*, vol. 146, pp. 82-91, 2004.
26. A. Attanasio, E. Ceretti, and C. Giardini, "3D FEM Simulation of Flank Wear in Turning," in *AIP Conference Proceedings*, 2011, p. 561.
27. Y. Huang and S. Y. Liang, "Modelling of CBN tool flank wear progression in finish hard turning," *Transactions of the ASME, Journal of Manufacturing Science And Engineering*, vol. 126, pp. 98-106, 2004., Vol. 126, pp. 98-106, 2004.
28. ISO Standard 3685:1993(E), *Tool life testing with single-point turning tools*, pp.11, 1993.
29. J.-E. Ståhl, P. Avdovic, V. Bushlya, J. Zhou, "Modelling tool life in the machining of strain-hardening material - Alloy 718," *4th International Swedish Production Symposium*, pp. 151-159, 2011.
30. A. Attanasio, E. Ceretti, A. Fiorentino, C. Cappellini, and C. Giardini, "Investigation and FEM-based simulation of tool wear in turning operations with uncoated carbide tools," *Wear*, vol. 269, pp. 344-350, 2010.
31. L. Filice, F. Micari, L. Settineri, and D. Umbrello, "Wear modelling in mild steel orthogonal cutting when using uncoated carbide tools," *Wear*, vol. 262, pp. 545-554, 2007.

Short-term machinability testing of difficult to machine materials

Joanna Kossakowska, Krzysztof Jemielniak

Warsaw University of Technology, Chair of Automation, Machine Tools and Metal Cutting
j.kossakowska@zaoios.pw.edu.pl

ABSTRACT

Random changes of machinability of workpiece material from one batch to another are tedious disruption of the production process, as it can lead to premature tool wear or even catastrophic tool failure. It is especially important in the aerospace industry where difficult to machine materials are everyday practice. The paper presents a simple, fast method of testing machinability of difficult to machine materials. It is based on several short cutting tests of longitudinal turning with geometrically growing cutting speed. The last, highest speed reached before the tool failure is assumed to be an estimation of the Taylor constant C and machinability coefficient. Comparison of obtained coefficient with the reference value allows for correction of applied cutting speed for new batch of the material. Performed tests proved, that the method is fast, efficient, does not vast a lot of material, and can be applied to factory floor condition without any special equipment.

KEYWORDS: Machinability, Difficult to machine materials

1. INTRODUCTION

In the aerospace industry difficult to machine materials such as stainless steel, titanium, or Inconel are used very often. Machining of these materials is a relatively new issue therefore there is little experience in selection of the most efficient, economical cutting conditions for such materials. One of such materials is Inconel 718 which machinability is low considering both tool wear criterion and others such as the quality of the surface layer, the type of chips and cutting forces. Moreover its machinability is unrepeatable from one delivery to another. The randomness of machinability makes selection of cutting parameters even more difficult and forces to test the machinability of each batch of material, in order to make an adjustment of economic cutting speed. There are theoretical attempts to determine the machinability based on the analysis of the chemical composition or properties of the material, such as hardness or tensile strength. However, the machinability is not a specific property of a material, but a mode of behaviour of the material during cutting, therefore the machinability evaluation should, specify the general cutting conditions for which the assessment is valid [10]. The most reliable way to determine the machinability is tool life testing. Conventional tool life tests can reproduce exactly the cutting conditions applied in production. Such tests are the most

accurate, but they are time consuming, disrupt the production process and therefore usually uneconomical. The most often used is classical tool life testing based on the ISO 3685 standard [1]. The tests consist of longitudinal turning of the workpiece with several constant cutting speeds. As a result the dependence of tool life on cutting speed $T(v_c)$ is determined, in form of the Taylor's equation (1):

$$v_c T^{1/k} = C \quad (1)$$

Generally the Taylor constant C depends on the work piece material and other cutting conditions and the exponent k depends mainly on the tool material and the tool life criterion. The Taylor formula can be used for calculating the cutting speed v_{cT} corresponding to selected (e.g. economical) tool life T , e.g. v_{c15} is the cutting speed for a 15 minutes tool life:

$$v_{cT} = C T^{1/k} \quad \text{e.g.} \quad v_{c15} = C 15^{1/k} \quad (2)$$

Selection of cutting speeds for particular cutting conditions is based on this formula. On the other hand, if the v_{cT} is established for fixed, normalized other cutting conditions it can be used as the absolute machinability index. It is even more useful for machinability comparison based on relative machinability index K_v , defined as [9]:

$$K_v = \frac{v_{cTB}}{v_{cTA}} * 100\% \quad (3)$$

where v_{cTA} - cutting speed for a given tool life T for material A, (reference material), v_{cTB} - cutting speed for a given tool life T for material B (tested material).

The methods described above, however accurate, are difficult to direct use in industrial conditions as they are tedious, time-consuming, and expensive. Therefore simpler, faster methods of determining machinability index are needed, and there are many attempts to find such a method. For example, in [8] the short time method for testing the machinability of PM steels is presented. It is based face turning of the common small ring-shaped specimens as test pieces from the surface of the center hole to the circumference at constant workpiece rotational speeds, feed and depth of cut. In this test, the cutting speed increases continuously towards the outer diameter of the workpiece. The test is finished at the cutting speed at diameter at which the tool failed totally or according to another tool-life criterion. The critical number of cutting passes up to a tool flank wear of $VB = 0.3$ mm, critical time, critical volume of removed material, surface finish and morphology of the chips were the criteria for checking the technical effectivity of the method applied. In [4] relative machinability of the sintered materials was evaluated through drilling and turning tests. During drilling uncoated HSS drills were used to drill blind holes. Machinability was measured as the number of drilled holes up to drill failure. During turning uncoated and coated inserts were used. Machinability was evaluated by measuring the insert wear after cutting a certain distance or number of passes. Both the uncoated HSS drill bits and WC inserts were chosen to obtain accelerated tool wear during limited number drilling/turning operations for comparison of machinability between materials. In [3] Volvo Standard Machinability Test was applied as a standardized short-term test for ranking materials by their machinability. The result of the test is a so called B-index. The machinability is given in percent of the machinability of a free cutting steel, whose machinability has been given the index 100. The index makes it possible to rank (or compare) materials by their machinability with respect to tool wear. To determine the B-index of other materials, they have to be machined until a certain flank wear is obtained on the cutting tool. By plotting the amount of removed volume and repeating the test for several cutting speeds,

material lines can be created and compared to the referenced material. Another approach is looking for a cause–effect relationship between machinability rate and in-process variables (cutting forces, temperature, and plastic strain) through experimental study [2]. These methods have limitations that prevent their use in industrial applications. It is a special necessity of workpiece preparation or use of large quantities of material. Hence, there is still a need for a simple, cheap and reliable test of machinability, and more precisely determining the relative index of machinability.

This paper presents a new proposal for of short-term method of testing and comparing machinability and experimental verification of the method applied for evaluation of relative machinability of different batches of Inconel 718 [6].

2. SHORT-TERM MACHINABILIBLTY TESTING

The method of short-term machinability testing bases on a preliminary tool life test recommended by Annex E of ISO 3685 [1] for selecting the cutting speeds which results in a reasonable tool life. The test consists of short cuts beginning with a relatively low cutting speed. Cutting time at each cut should be short. The standard does not specify a particular value suggesting that in various cases may be different. After each cut the tool should be examined for indications of failure, and if none appears, a further cut is taken with the cutting speed increased. This procedure is repeated until the tool failure. The standard underlines that the machining time at lower speeds during the preliminary test is an insignificant part of the tool life. The last speed and cutting time can be used for calculating the cutting speed for the first tool life desired in standardized tool life testing using the formula:

$$v_{c1} = v_{ck} \left(\frac{T_1}{T_k} \right)^{1/k} \quad (4)$$

where: v_{c1} , T_1 – cutting speed and desired tool life during the first operation of the standardized test, v_{ck} , T_k – cutting speed and cutting time during the last cut of the preliminary test, k – estimated value of Taylor exponent (-7 for High Speed Steel, -4 for cemented carbides, -2 for ceramics).

In order to use the above described procedure for comparative machinability evaluation, the following assumptions were added:

- critical speed v_{ck} , at which the edge reached the tool failure, should be approximately equal to the Taylor constant C and will be considered as the absolute machinability index used in the formula (3)
- to make the last cut more dominating, and previous cuts less significant, the cutting speed should increase geometrically with ratio R , equal to $R = 1.06$ for the high-speed steel, $R = 1.12$ for cemented carbides, $R = 1.26$ for ceramics.

Basics cumulative wear determination for tool working with various cutting parameters are given in [5, 7]. The tool wear as a function of time (neglecting short period of accelerated, preliminary wear) can be generally described as:

$$w = C_w t^u \quad (5)$$

where: t – cutting time, u – exponent, C_w – constant, which is a function of the tool-life criterion and cutting conditions.

The cutting time required to reach a tool-life criterion w_k is a tool life T , thus for $t=T$, equation (5) takes the form:

$$w_k = C_w T^u \quad (6)$$

Hence:

$$C_w = \frac{w_k}{T^u} \quad (7)$$

After the first cut taken with the first set of cutting parameters over a period of time Δt_1 the tool wear reaches the value:

$$w_1 = C_{w1} \Delta t_1^u \quad (8)$$

In the second cut the tool works with the second set of cutting parameters (here the increased speed) and the tool wear changes according to the formula:

$$w = C_{w2} t'^u \quad (9)$$

If the tool were working from the beginning with the second set of parameters, it would reach the tool wear w_1 after a period of time t' :

$$w_1 = C_{w2} (t')^u \quad (10)$$

Comparing (8) and (10) the period of time t' is:

$$t' = \left(\frac{C_{w1}}{C_{w2}} \right)^{1/u} \Delta t_1 \quad (11)$$

Thus the tool wear after the second cut with the next period of time Δt will reach the value:

$$w_2 = C_{w2} (t' + \Delta t_2)^u = (C_{w1}^{1/u} \Delta t_1 + C_{w2}^{1/u} \Delta t)^u \quad (12)$$

In general, after m cuts the tool wear will come to:

$$w_m = \left[\sum_{i=1}^m (C_{wi}^{1/u} \Delta t_i) \right]^u \quad (13)$$

Substituting (7) into (13) it takes the form:

$$w_m = w_k \left(\sum_{i=1}^m \frac{\Delta t_i}{T_i} \right)^u = w_k (\sum_{i=1}^m \Delta T_i)^u \quad (14)$$

where: ΔT_i - the used part of the tool life in the i -th cut, m - the number of cuts with successive cutting speeds.

If the tool works up to the tool failure ($w_m = w_k$), that is to the end of tool life, the equation (14) simplifies to:

$$\sum_{i=1}^m \Delta T_i = 1 \quad (15)$$

which can be read as: "the sum of used-up part of tool life until tool failure is equal to 1".

Worth noticing is elimination of the exponent u from the equation. This means that commutation of used- up parts of tool live does not depend on the form of the tool wear.

In the considered case at a short-term testing of material machinability the subsequent periods of cutting time are equal and the only variable cutting parameter is the cutting speed.

Using the Taylor equation (1) ΔT_i value for the particular cutting speed can be described as follows:

$$\Delta T_i = \Delta t \left(\frac{v_{ci}}{C} \right)^{-k} \quad (16)$$

Assuming that the last, critical cutting speed v_{ck} should be equal to the Taylor constant C , and that the cutting speed increases geometrically (with a ratio R), the generalized formula for the cutting speed in the cut can be expressed as:

$$v_{ci} = \frac{C}{R^{m-i}} \quad (17)$$

By substituting (17) into (16) and (15) the following relationship can be obtained:

$$\Delta t = \left(\sum_{i=1}^m R^{k(m-i)} \right)^{-1} \quad (18)$$

The resulting values of the period of single cut Δt for the values of coefficients R and k given by the ISO standard [1] are presented in Table 1.

Table 1 Calculated period of single cut Δt for different tool materials

Tool materials	Number of cuts		
	m=4	m=5	m=6
HSS $R=1.06$ and $k = -8$	0.441	0.413	0.397
cemented carbides $R= 1.12$ and $k = -4$	0.436	0.407	0.390
Ceramics $R= 1.26$ and $k = -2$	0.439	0.411	0.395

Application of cutting time indicated in Table 1 would result in the tool failure at the end of the m -th cut. As the Taylor exponent k is an approximation the strict definition of the cutting time Δt is not possible. Thus, it was assumed that the tool failure should not necessarily occur at the end of the m -th cut, but during this cut. Therefore the cutting time in a single cut was assumed a little bit longer: $\Delta t = 0.5$ min. The theoretically calculated courses of the used part of tool life for different number of cuts were calculated according to the formula:

$$\Delta T = \Delta t \sum_{i=1}^m R^{k(m-i)} \quad (19)$$

The obtained results for $R = 1.12$ and $k = -4$ are shown in Figure 1. Each curve corresponds to a different number of cuts; each part of the course corresponds to a different cutting speed. Regardless of number of cuts m (that is, regardless of the first cutting speed), the tool fails at a speed equal C for the assumed $\Delta t = 0.5$ min.

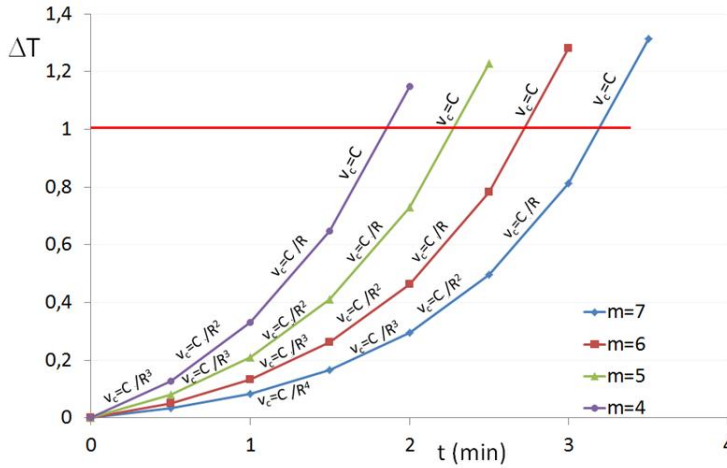


Fig.1. The used-up part of tool life ΔT in short-term machinability testing, for various number of cuts m

Sample of the actual tool wear while short-term machinability testing is shown in Figure 2. In this example, during turning with cutting speed v_{c6} , tool life criterion was achieved. Thus, in this case the $v_{c6} = v_{ck}$

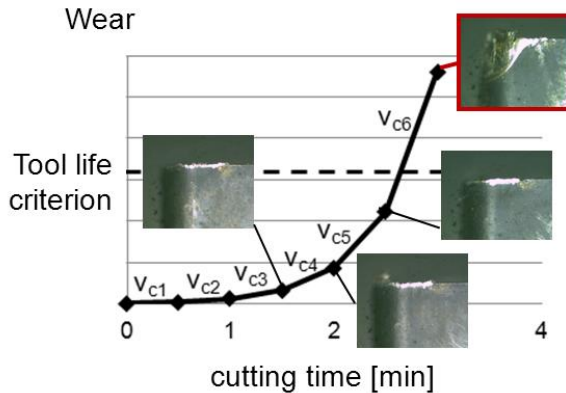


Fig.2. Sample of the actual tool wear while short-term machinability testing

3. THE TEST OF MACHINABILITY OF INCONEL 718

The proposed method of short-term machinability testing has been verified by evaluation of relative machinability of two different batches of Inconel 718 provided by the industrial partner taken from the recent production. Both materials have undergone the same heat treatment process, however, they have distinctly different hardness.

The experiments were performed on a conventional lathe TUD 50 using two different tools. The first tool was hR117.17-2525 (CTGPR) equipped with a TPGN 160304, uncoated

carbide insert (H13A) to assure fast tool wear and a small amount of machined material. The second tool was DCLNR 2020K 12 equipped with CNMG 120408-QM cermet 1105 inserts. This tool was actually used in production. For the first tools feed $f = 0.08$ mm/rev and depth of cut $a_p = 1$ mm was used. The second tool was tested with cutting parameters used in the production i.e. $f = 0.2$ mm/rev and $a_p = 1,2$ mm.

The short-term machinability testing was carried out using geometrically increasing cutting speed ($R = 1.12$), starting from $v_c = 45$ m/min. Each test was repeated twice, every time yielding the same result. The obtained critical speeds $v_{ck} = C$ for both tested materials, for both inserts: TPGN and CNMG-QM are shown in Table 2.

Table 2 Critical cutting speed $v_{ck} = C$ obtained in the short-term machinability testing of Inconel 718

Type of insert	batch A	batch B
TPGN	$v_{ck} = 63$ m/min	$v_{ck} = 80$ m/min
CNMG-QM	$v_{ck} = 63$ m/min	$v_{ck} = 80$ m/min

The values of C obtained with both tools were incidentally the same, as the tools were used with completely different cutting conditions: other insert shape, angles, feeds, etc. In all cases larger critical speed was achieved with batch B, which means that the Inconel from this delivery has better machinability. The value of the relative machinability index K_v of the batch B with respect to the batch A (3) was established at 127% for both inserts. This concurrence of obtained K_v value confirms its merit proving the consistency of the results. It means, that for fast, not expensive testing of relative machinability the weaker tools (here: uncoated carbide insert H13A) can be used, reducing the time and cost of testing without influence on the results.

As an auxiliary verification of the results tests of tool life tests were carried out using CNMG-QM inserts with cutting speed $v_c = 40$ m/min for both batches of Inconel 718. The test on batch A resulted in tool life 4.8 minutes, while for the batch B the tool life 9.2 min was achieved which is in good agreement with obtained relative machinability index.

4. SUMMARY

The presented method of short-term machinability testing allows for fast, relatively inexpensive evaluation of machinability changes from one workpiece material delivery to another. It can be carried out directly on the machine tool used in factory floor, without any special measuring equipment, assuming that tool failure is identified the same way as in standard production. It allows for application of tool materials of low cutting ability, which lowers time necessary for testing as well as the amount of workpiece material used, without affecting the obtained results.

The method was successfully applied for evaluation of machinability of Inconel 718 in the aerospace industry.

ACKNOWLEDGEMENTS

Financial support of Structural Funds in the Operational Programme - Innovative Economy (IE OP) financed from the European Regional Development Fund - Project "Modern material technologies in aerospace industry", Nr POIG.01.01.02-00-015/08-00 is gratefully acknowledged.

REFERENCES

- [1] ISO 3685, "Tool-life testing with single-point turning tools", 1993.
- [2] I. Arriola, E. Whitenton, J. Heigel, P.J. Arrazola, "Relationship between machinability index and in-process parameters during orthogonal cutting of steels", *CIRP Annals - Manufacturing Technology*, vol. 60, 2011. pp. 93–96.
- [3] K. Björkeborn, U. Klement, H. Oskarson, "Ranking of materials by their machinability applying a Short-Term Test", *2nd International Conference Innovative Cutting Processes & Smart Machining*, 2008.
- [4] B. Hu, "Performance Characteristics of a Newly Developed Machinability Additive for PM Applications", *Advances in Powder Metallurgy & Particulate Material's*, 2008.
- [5] K. Jemielniak, „Metal Cutting” (in Polish), OWPW, 1998.
- [6] K Jemielniak, J. Kossakowska, "Development of the method of short-term machinability testing of aerospace alloys", report from the project "*Modern material technology in aerospace industry*" – see acknowledgments, 2012.
- [7] K. Jemielniak, M. Szafarczyk, J. Zawistowski, "Difficulties in Tool Life Predicting when Turning with Variable Cutting Parameters", *Annals of the CIRP*, vol. 3, no. 1, 1985, pp. 113-116.
- [8] A. Salak, K. Vasilko, M. Selecka, H. Danninger, "New short time face turning method for testing the machinability of PM steels", *Journal of Materials Processing Technology*, vol. 176, 2006, pp. 62–69.
- [9] D. A. Stephenson and J. S. Agapiou, *Metal Cutting Theory and Practice*, Boca Raton, FL, USA: CRC Press, 2006.
- [10] E.M. Trent, *Metal Cutting*, Butterworths, London, 1977.

Theme 2

Cutting stability

- In-process Control for Adaptive Spindle Speed Variation and Selection
Jens Friedrich, Alexander Verl
Institute for Control Engineering of Machine Tools and Manufacturing Units,
- Dynamics of Modified Tool Structures for Effective Cutting
Vytautas Ostasevicius, Vytautas Jurenas, Arturas Juskevicius
Kaunas University of Technology, Lithuania
- Stability in turning of superalloys using two numerical methods
Gorka Urbicain Pelayo¹, Jorge Alberto Palacios Moreno², Daniel Olvera Trejo², Asier Fernández Valdivielso¹, Alex Elías-Zúñiga², Luis Norberto López de Lacalle¹
¹ University of the Basque Country UPV/EHU, ETSI, Bilbao, Spain.
² Department of Mechanical Engineering, Instituto Tecnológico y de Estudios Superiores de Monterrey, Mexico
- On the effective milling of large workpieces
Aleš Polzer, Miroslav Piška, Zdeněk Fiala
Institute of manufacturing technology, FME BUT, THE CZECH REPUBLIC
- New method of dynamic cutting force coefficients determination
Krzysztof Jemielniak, Mirosław Nejman, Dominika Śniegulska-Grądzka, Rafał Wypysiński
Warsaw University of Technology, Poland
- Model-Based Identification of Chatter Marks during Cylindrical Grinding
Paolo Parenti¹, Marco Leonesio², Alberto Cassinari², Giacomo Bianchi², Michele Monno¹
¹Department of Mechanical Engineering, Politecnico of Milan, Italy
²CNR, Institute of Industrial Technology and Automation, Milan, Italy
- Machining improvement on flexible fixture through viscoelastic damping layer
Alex Iglesias¹, Qilin Fu², Julen Landa¹, Amir Rashid²
¹Dynamics and Control, IK4-Ideko, Elgoibar, Spain
²KTH Royal Institute of Technology, Stockholm, Sweden
- Analytical Stability Prediction in Five Axis Ball-End Milling
Mahdi Eynian
University West, Sweden
- Numerical simulation of self-excited vibrations - review of methods, potential advantages and pitfalls
Krzysztof Jemielniak, Rafał Wypysinski
Warsaw University of Technology, Faculty of Production Engineering
- Non-Regenerative Dynamic Instability in Surface Grinding
Marco Leonesio¹, Paolo Parenti², Alberto Cassinari¹, Giacomo Bianchi¹
¹CNR – Institute of Industrial Technology and Automation, Milan, Italy
²Department of Mechanical Engineering, Politecnico of Milan, Italy

In-process Control for Adaptive Spindle Speed Variation and Selection

Jens Friedrich, Alexander Verl

Institute for Control Engineering of Machine Tools and Manufacturing Units,
University of Stuttgart, Seidenstr. 36, D-70174 Stuttgart, Germany
Jens.Friedrich@ISW.Uni-Stuttgart.de

ABSTRACT

The productivity of the milling process is limited by the cutting depth. The critical cutting depth varies for different spindle speeds. Unstable processes can be stabilized by varying the spindle speed. This paper presents a new approach to stabilize the process by using adaptive spindle speed variation and selection (ASSV/ASSS). Based on the current cutting conditions the parameters of the ASSV are calculated by an in-process feedback controller to stabilize the process. In parallel a new stable spindle speed for the cutting depth is derived and selected (ASSS). Even if there exists no stable spindle speed for the cutting depth, the ASSV stabilizes the process. The results are verified with simulations and with experiments on a commercial milling machine. The application of ASSV/ASSS increases the stable cutting depth and thus the productivity with constant speed by 233% and reduces the displacement of the tool tip by the factor of 10.

KEYWORDS: spindle speed variation, chatter control, milling process stability

1. INTRODUCTION

The appearance of chatter vibrations is one of the most important factors limiting the productivity of today's machining industries. The chatter vibrations in milling excited by the interaction between tool and work piece, not only cause a bad surface but can also lead to damage of the tool, the part and the machine tool. The appearance of chatter depends on the spindle speed, the material, the tool, the tool wear, the depth and width of cut [1]. Due to the various parameters influencing the stability the selection of suitable cutting parameters is difficult. The selection of the cutting parameters is mostly based on the experience of the workers. The parameters cannot be chosen to conservative, because it lowers the productivity. Thus the process can become unstable due to changing cutting conditions. Due to that fact it is very important to detect instabilities and find stable process parameters.

The chatter effect is a self-excited vibration caused by the interaction of the tool with the surface left by the last cut. Thus the effect can be described as a system with time delay [2]. The time delay is given by the rotation speed of the spindle and the number of teeth of the tool. Depending on the spindle speed, and thus the time delay, the maximum stable depth of

cut is varying. The critical depth of cut a_{crit} marks the border between stable and unstable values for the depth of cut and can be analytically calculated and graphically shown in the so called stability lobe diagram (SLD) [3]. Schmitz also developed a mathematical representation of the SLD, which can be used for optimization [4].

With a SLD of a process the maximal stable depth of cut could be selected. The SLD can be extended by the width of cut, so the pairs of width and depth of cut with maximum material removal rate can be selected [5]. In real production the combination of width and depth of cut cannot freely be chosen, because the geometry of the final part defines the cutting depth. Another method to calculate the stability of systems with time delay is the discretization [6] or the semi-discretization method [7]. The analytical estimation of the SLD needs high efforts of measurements of the process dynamics and has to be done for each tool-material-machine-combination. The SLD can also be measured experimentally. Quintana et al. presented a method based on sound measurement, but for each tool material combination 600 measurements are necessary [8]. Thus the SLD is not available for the real production process and the spindle speed with maximum depth of cut cannot be chosen. Moreover time variant conditions like wear cannot be considered.

Another approach is to avoid self-excited vibrations by having a not constant time delay. The use of cutters with variable pitch leads to a varying time delay for each tooth [9]. Modulating the spindle speed has a similar effect [10]. The modulation of the spindle speed is much more flexible than having variable pitch cutters, because the shape, the amplitude and the frequency can be influenced. Insperger investigated different methods of modulating the spindle speed [10]. These several possibilities for spindle speed variation lead to arbitrary combinations of parameters. Due to that the method is not really used in real production processes yet [11].

Tarng et al. presented a possibility for optimizing turning applications by calculating the “magic stable spindle speeds” with maximum stable depth of cut [12]. A similar approach was developed by Liao and Young, based on the process forces measured with a dynamometer the chatter frequency is derived and based on this information a stable spindle speed is calculated [13]. Both methods need additional measurement equipment and hardware because of the computational effort to estimate the frequency, which is not available on commercial control. An in-process controller calculating a new stable spindle speed by optimizing a cost function including the perturbation motion and the spindle capability was presented by Doppenberger et al. [14]. But large steps in the spindle speed are often not allowed due to the process technology. Tsai et al. presented an algorithm, which increases the spindle speed in steps, to the maximum possible spindle speed [15]. Lower spindle speeds are not taken into account and the positive effect of spindle speed variation is not used.

In this paper a new approach of spindle speed variation and selection realized as an in-process feedback controller is presented. Based on the changing process stability, measured during milling, the parameters for the adaptive spindle speed variation (ASSV) are calculated automatically and in parallel the adaptive spindle speed selection (ASSS) is performed to find a stable spindle speed for the current cutting conditions. In the following section the dynamics of milling and the simulation model for the verification is presented. In section three the concept for the new ASSV/ASSS algorithm is shown. The results of the application of the algorithm are described and verified with a simulation model and with real experiments in section four. The paper ends with the conclusion and gives an outlook on future research topics.

2. MILLING DYNAMICS AND SIMULATION MODEL

The chatter effect can be described as self-excited vibrations. Due to the flexibility of the tool and the machine tool structure the interaction of the current tooth of the tool with the surface left by the tooth of the last cut results in vibrations. The flexible structure can be modelled as two decoupled spring and damper systems one in feed direction and one normal to the feed direction [16]. The dynamics of the milling process and the process force resulting from different cutting conditions are illustrated in Fig. 1.

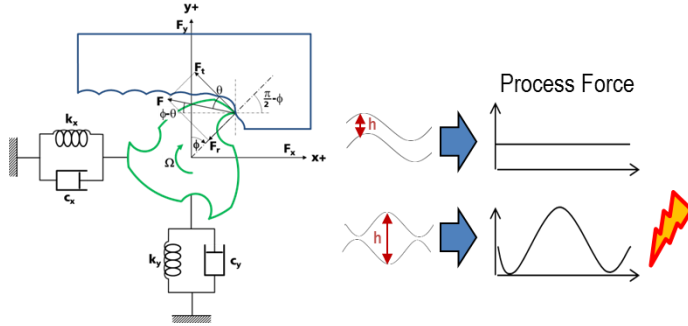


Fig. 1. Process dynamics and resulting process force

The time delayed differential equation of motion in feed and normal direction are given in equation (1) and (2). With the time delay $T = \frac{60}{zn}$, depending on the spindle speed n and the number z of teeth of the tool.

$$m_x \ddot{x} + c_x \dot{x} + k_x x = F(x(t), x(t - T)) \quad (1)$$

$$m_y \ddot{y} + c_y \dot{y} + k_y y = F(y(t), y(t - T)) \quad (2)$$

Each tooth in the material generates a cutting force. To simplify the model it is assumed that there is at maximum one tooth cutting at a time. For a tool with three cutting edges that can be guaranteed by constraining the maximum radial depth of cut to the radius of the tool. Using the radial immersion position $\Phi(t)$ of the tool, the chip thickness $h(t)$ and the axial depth of cut a , the tangential ($F_t(t)$) and the radial ($F_r(t)$) cutting forces can be calculated as described in equation (3) to (7).

$$\phi(t) = 2\pi n t \quad (3)$$

$$F_t = K_t a h(\phi) \quad (4)$$

$$F_r = K_r K_t a h(\phi) \quad (5)$$

$$F(\phi) = K_t \sqrt{1 + K_r^2} a h(\phi) \quad (6)$$

The tangential (K_t) and the radial (K_r) cutting force coefficient depend on the tool-material-combination. With the feed per tooth f_z the chip thickness $h(\Phi)$ can be calculated as given in equation (7) to (9).

$$\Delta x = x(t) - x(t - T) \quad (7)$$

$$\Delta y = y(t) - y(t - T) \quad F_r = K_r K_t a h(\phi) \quad (8)$$

$$h(\phi) = f_z \sin(\phi(t)) + \Delta x \sin(\phi(t)) + \Delta y \cos(\phi(t)) \quad (9)$$

As it can be seen in Fig. 1 the inputs of the dynamic milling model are the forces in feed (F_x) and in normal direction (F_y). These forces can be calculated as described in equation (10) to (12).

$$\theta = \tan^{-1}(K_r) \quad (10)$$

$$F_x(\phi) = -F(\phi) \cos(\phi(t) - \theta) \quad (11)$$

$$F_y(\phi) = F(\phi) \sin(\phi(t) - \theta) \quad (12)$$

The tangential (K_t) and the radial (K_r) cutting coefficients of the model were estimated by doing straight cuts in steel with constant spindle speed and depth and width of cut while the cutting force was measured with a table dynamometer. The tool was a 20 mm end mill with inserts and three teeth. Moreover a modal analysis of the tool with an impact hammer has been performed to estimate the modal mass (m_x , m_y), the stiffness (k_x , k_y) and the damping (c_x , c_y). To have a realistic behaviour the chip thickness is limited and thus also the process force and the displacement cannot go to infinity.

The FRF is similar in x and y direction, thus a 1-DOF analytical calculation of the stability is suitable to get a rough idea of the stability behaviour. The full discretization method was used [6]. The calculated stability lobe diagram is shown in Fig. 2.

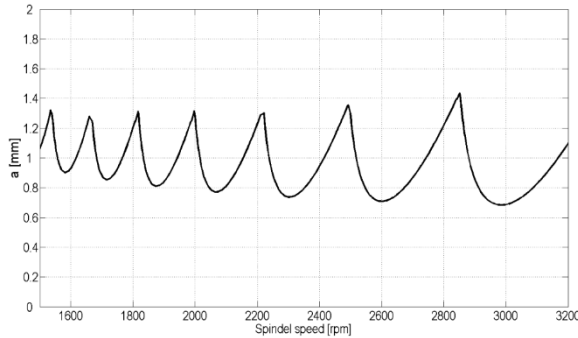


Fig. 2. SLD calculated using the full-discretization method

3. ADAPTIVE SPINDLE SPEED ADAPTION AND SELECTION

The method of spindle speed variation is suitable to increase the critical depth of cut a_{crit} and suppress chatter vibrations [10, 17]. But it is not easy to find suitable parameters for the frequency and the amplitude [11, 18]. Moreover the spindle speed variation cannot be active all the time, because if it is applied during stable process conditions it causes a bad surface [19]. Thus an in-process controller is necessary to adapt the parameters to the current process conditions. Even during unstable process conditions another spindle speed, which is stable under that certain conditions should be found instead of applying spindle speed variation for a longer time, because the application of spindle speed variation increases the tool wear [20] and the energy consumption.

The approach presented in this paper uses the advantages of spindle speed variation while a new stable spindle speed for the current cutting conditions is found. The parameters for the adaptive spindle speed variation (ASSV) are estimated automatically based on the

current stability conditions with respect to the spindle and tool capabilities. The ASSV is only applied to improve the process stability for a short time until a new stable spindle speed for the current cutting conditions is found. If no stable spindle speed can be found by the ASSS because of the limited range of allowed speeds for a tool, the ASSV will automatically stabilizes the process.

The spindle speed variation method as it is known, modulates the nominal spindle speed n_0 with a symmetric function (e.g. sinusoid, triangle, random noise) thus the mean spindle speed is not changed n_0 . The idea of the ASSV/ASSS is to apply an unsymmetrical modulation function, thus the mean spindle speed is changing and a stable spindle speed can be found. For the ASSV/ASSS a triangular modulation was chosen. To reduce the problem of having different parameters (amplitude A , frequency f) to control, the ASSV/ASSS algorithm controls the switching interval Δt_{com} of the direction s_d of the slope s_s of the triangle. The block diagram of the ASSV/ASSS and an example of the result is given in Fig. 3. The stability was judged based on the displacement of the tool tip.

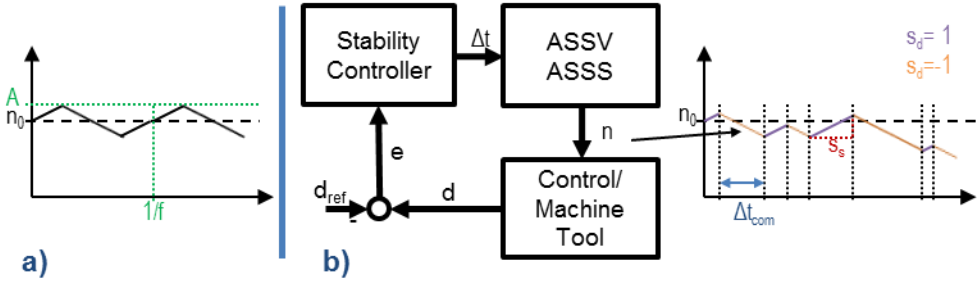


Fig. 3. a) classic triangular SSV; b) ASSV and ASSS principle

The switching interval Δt_{com} for the direction of the slope is controlled by the stability controller as it can be seen in Fig. 3. A very simple approach is using a P-controller as stability controller given in equation (13). To estimate the stability of the process the displacement d of the tool tip is compared to a reference displacement d_{ref} of the stable process. To make the signal suitable to be used for the controller it is lowpass filtered.

$$\Delta t_{com} = (d - d_{ref}) \cdot K_p \quad (13)$$

To avoid problems with negative Δt_{com} and high switching frequencies a minimum switching interval Δt_{min} is defined. If the controller output is smaller than Δt_{min} the spindle speed remains the same and the ASSV is switched off because the process is assumed to be stable. To save the tool and restrict the search to a suitable range the maximum n_{max} and minimum n_{min} spindle speed is defined. As the ASSV/ASSS is realized in a simulation model and will be integrated into a digital control it has to be discretized with the sampling time t_s . In each step the direction of the slope s_d of the triangle is calculated using the time since the last change of the direction Δt as given in equation (14).

$$sd = \begin{cases} -1 & \forall n_{last} > n_{max} \\ 1 & \forall n_{last} < n_{min} \\ -s_d & \forall \Delta t \geq \Delta t_{com} \\ s_d & \forall \Delta t < \Delta t_{com} \end{cases} \quad (14)$$

Based on the results of equation (14) in each step a new spindle speed can be calculated using the spindle speed of the step before n_{last} as described in equation (15).

$$n = \begin{cases} n_{last} & \forall \Delta t_{com} < \Delta t_{min} \\ n_{last} + t_s \cdot s_s \cdot sd & \forall \Delta t_{com} \geq \Delta t_{min} \end{cases} \quad (15)$$

The parameters to setup the ASSV/ASSS control can be easily estimated. The maximum (n_{max}) and minimum (n_{min}) spindle speed can be derived from the maximum and minimum allowed cutting speed of the tool. The maximum switching frequency of the spindle defines the minimum switching interval Δt_{min} . The minimum amplitude A_{min} of the resulting ASSV is depending on the slope s_s of the triangle and the minimum switching interval Δt_{min} . The minimum switching interval Δt_{min} also influences the static error e_s caused by the P-controller. Thus the parameters of the ASSV/ASSS can be calculated as given in equation (16) and (17).

$$s_s = \frac{2A_{min}}{\Delta t_{min}} \quad (16)$$

$$K_P = \frac{\Delta t_{min}}{e_s} \quad (17)$$

Selecting the amplification of the P-controller K_P too high causes a small static error, but this will lead to very long switching interval Δt_{com} even for very small errors and thus the effect of the SSV will be reduced.

4. VERIFICATION AND RESULTS

A simulation model of the milling model described in section 2 was developed and implemented in Matlab/Simulink®. The ASSV/ASSS algorithm was integrated into the simulation model and this model was used to check the capability and the effect of the application of the ASSV/ASSS method.

To verify the effect, the results with and without ASSV/ASSS are compared and assessed. Moreover the simulated results are compared to the analytically calculated SLD of the process shown in Fig. 2. The parameters used in the simulation are given in table 1.

Table 1. ASSV/ASSS Parameters

K_P	s_s	Δt_{min}	n_0	n_{max}	n_{min}	d_{ref}
20000	300	0.3	2300	3200	1500	0.00003

The cutting depth was increased in steps of 0.2 mm, from 0.6 mm, which is stable according to Fig. 2, to 1.6 mm, which is unstable according to Fig. 2. At the selected initial spindle speed 2300 rpm the critical depth of cut a_{crit} is at about 0.7 mm. In Fig. 4 the results of the application of the ASSV/ASSS algorithm to cuts with different depth of cuts a are shown. For the stable cutting depth 0.6 mm the spindle speed is not changed. At the initial speed the depths of cut 0.8 mm, 1.0 mm and 1.2 mm are unstable, the ASSV/ASSS selects stable spindle speeds in the stable areas next to the initial speed (refer to Fig. 2).

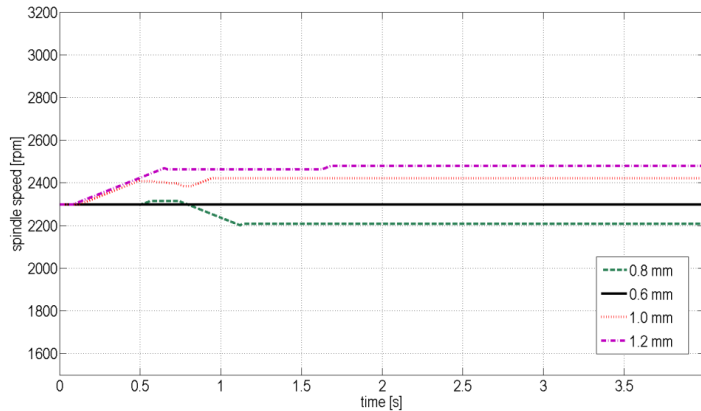


Fig. 4. Results of the application of the ASSV/ASSS at different depth of cut

Due to the change of the spindle speed the displacement of the tool tip is significantly decreased. In Fig. 5 the displacement due to the ASSV/ASSS algorithm can be seen. To show the effect of the application of ASSV/ASSS, the displacement of the cut with $a=1.2$ mm without ASSV/ASSS and the desired reference d_{ref} are also drawn as a comparison in Fig. 5.

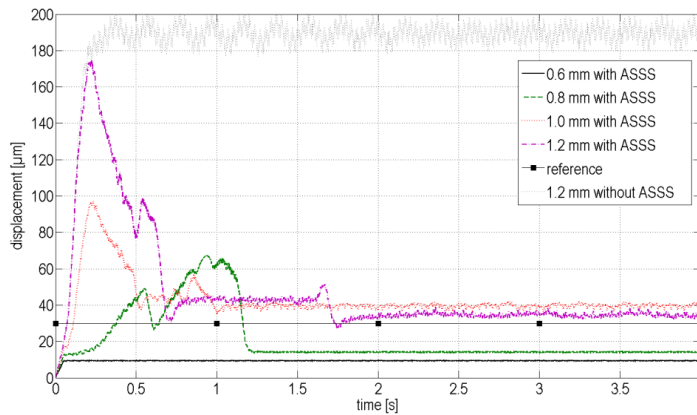


Fig. 5. Reduced displacement due to the application of ASSV/ASSS

The selection of the new spindle speed leads to a stable process without the need of any continuous spindle speed variations. The stable depth of cut and the productivity can be doubled by increasing the stable depth of cut from 0.6 mm to 1.2 mm. As it can be seen in Fig. 2 there exists only one spindle speed which is stable for 1.4 mm. Thus the selection of the spindle speed for $a=1.4$ mm takes time, but the variation of the spindle speed leads to a reduction of the displacement even if the new spindle speed is not found yet. This is the known effect of the application of spindle speed variation to unstable processes. The application of the ASSV/ASSS algorithm also leads to stabilization for unstable cuts with a depth of cut 1.6 mm, for which no stable spindle speed exist as it can be seen in Fig. 6. The displacement of the tool tip can be reduced more than ten times due to the application of the ASSV/ASSS algorithm.

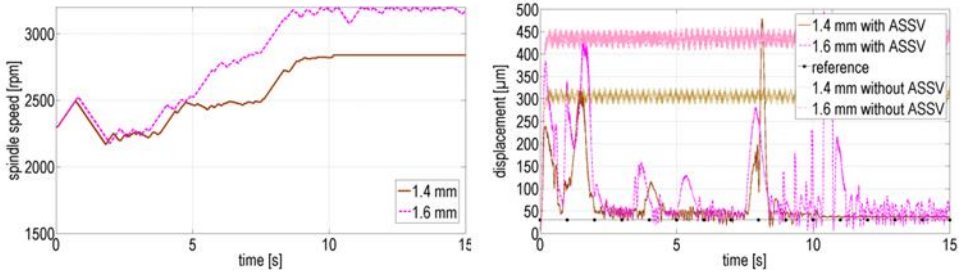


Fig. 6: Improved stability of unstable process

The proposed ASSV algorithm was also implemented in a Siemens 840D control using synchronized actions to show the capability in real production environment. The process measurement was done by a modified Omat VCM Sensor which measures the RMS value of the acceleration, the velocity and the displacement in real-time. The experiments were performed on a Hermle UWF 1202 H 5-axes milling machine. A 20 mm cutter with inserts was used to cut a block of steel with a width of cut of 5 mm and different depths of cut. To see the behaviour with changing cutting conditions the cut was interrupted (grey areas in Fig. 7) and then continued with the same depth of cut. The data was captured using Siemens Software SinucomNC. The results of the experimental verification are presented in Fig. 7.

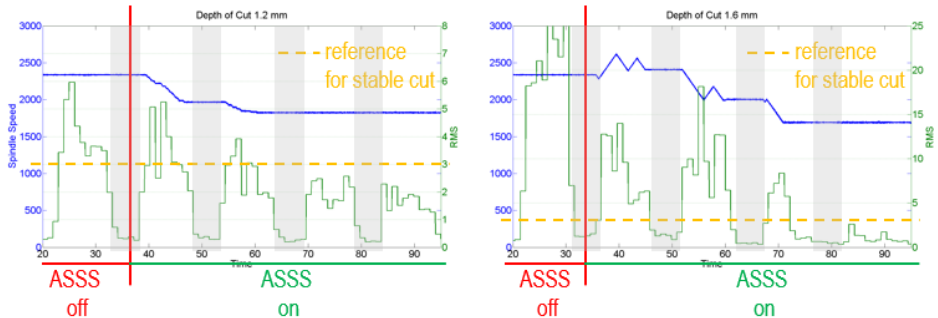


Fig. 7: Experimental results of the application of ASSV/ASSS

The left picture of Fig. 7 shows the experimental results for a cutting depth of 1.2 mm and the right for a cutting depth of 1.6 mm. For each cutting depth first part was done without ASSV/ASSS with the programmed spindle speed. As it can be clearly seen the ASSV/ASSS algorithm starts changing the spindle speed immediately when it is switched on. The change of the spindle speed has a positive effect on the stability as it can be seen in the sensor signal. If the cutting conditions change or the cutter leaves the material (grey areas in Fig. 7) the spindle speed is kept constant and it is changed again, if the sensor signal exceeds the reference value. For both depths of cut the ASSV/ASSS does not change the spindle speed as the stable spindle speed was found.

5. CONCLUSION AND OUTLOOK

In this paper a new algorithm for adaptive spindle speed variation and adaption is presented. The algorithm is an in-process controller selecting the parameters of a triangular

spindle speed variation automatically. While the ASSV is applied to the process a new stable spindle speed is found and selected, thus the variation can be stopped and a stable cut is performed using the new stable cutting conditions. The algorithm calculates the new spindle speed with respect to the spindle capability and the technological parameters of the cutting process. Even if no stable spindle speed for the cutting depth exists within the range of the spindle speeds, the spindle speed variation leads to a decrease of the tool tip displacement. The algorithm can be calculated in real-time with discrete time steps and it was implemented in a commercial numerical control.

In Fig. 8 the calculated SLD and the selected spindle speeds can be compared. It can be seen, that the ASSV/ASSS algorithm finds the stable spindle speeds for the different depths of cut. The very small band of stable spindle speeds for 1.4 mm depth of cut is found by the algorithm, though it takes some time. But the displacement is already decreasing during the search of the new spindle speed due to the ASSV.

The depth of cut with stable spindle speeds can be increased up to 233% from 0.6 mm to 1.4 mm. Due to the selection of a new stable spindle speed the displacement of the tool tip can be decreased by the factor of 10 from 300 μm (for $a = 1.4$ mm, $n = 2300$ rpm) to 30 μm (for $a = 1.4$ mm, $n = 2840$ rpm). The level of the displacement stays low, even if the ASSV is switched of at the new spindle speed and the cut is performed at the new speed with constant turning speed of the spindle.

The ASSV/ASSS algorithm also increases the stability of unstable processes if no stable spindle speeds exist. The tool tip displacement is also decreased by the factor 10 (450 μm to 45 μm) while the ASSV is applied to the process.

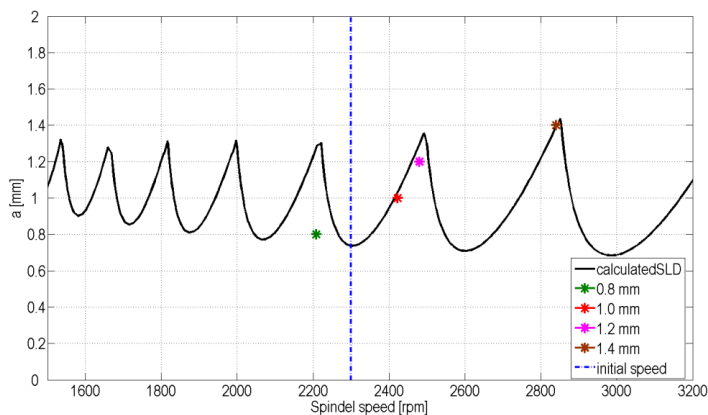


Fig. 8. Calculated SLD and selected spindle speeds of the ASSS algorithm

This positive effect of the ASSV/ASSS algorithm could also be shown in real experiments on a commercial milling machine (reduction from 25 to 2.5) as it could be seen in Fig. 7.

The proposed algorithm improves the chatter stability significantly, but the effect of the algorithm can be possibly improved in combination with higher sophisticated control strategies or other variation strategies to reduce the time to find stable spindle speeds. The effect of the algorithm should be tested under production conditions. Moreover the ASSV/ASSS can probably be used with machine internal signals (e.g. motor currents, axes velocities) or with signals derived from them, like reconstructed process forces, which can be

used to extract vibrations and the stability conditions. Thus no additional sensor would be necessary, which will increase the acceptance for a wide application in machining industry.

ACKNOWLEDGEMENTS

The research presented in this paper was done within the AIMACS project founded by the 7th framework program of the European Commission.

REFERENCES

- [1] Altintas, Yusuf. *Manufacturing automation: metal cutting mechanics, machine tool vibrations, and CNC design*. Cambridge university press, 2012.
- [2] Tobias, S. A., and W. Fishwick. "Theory of regenerative machine tool chatter." *The Engineer* 205 (1958): 199-203.
- [3] Altıntaş, Y., and E. Budak. "Analytical prediction of stability lobes in milling." *CIRP Annals-Manufacturing Technology* 44.1 (1995): 357-362.
- [4] Schmitz, Tony L. "Automatic trimming of machining stability lobes." *International Journal of Machine Tools and Manufacture* 42.13 (2002): 1479-1486.
- [5] Budak, Erhan, and A. Tekeli. "Maximizing chatter free material removal rate in milling through optimal selection of axial and radial depth of cut pairs." *CIRP Annals-Manufacturing Technology* 54.1 (2005): 353-356.
- [6] Ding, Ye, et al. "A full-discretization method for prediction of milling stability." *International Journal of Machine Tools and Manufacture* 50.5 (2010): 502-509.
- [7] Insuperger, Tamás, and Gábor Stépán. "Semi-discretization method for delayed systems." *International Journal for numerical methods in engineering* 55.5 (2002): 503-518.
- [8] Quintana, Guillem, et al. "Sound mapping for identification of stability lobe diagrams in milling processes." *International journal of machine tools and manufacture* 49.3 (2009): 203-211.
- [9] Budak, Erhan. "An analytical design method for milling cutters with nonconstant pitch to increase stability, part 1: theory." *Journal of manufacturing science and engineering* 125.1 (2003): 29-34.
- [10] Insuperger, T. "Stability analysis of periodic delay-differential equations modeling machine tool chatter." Budapest University of Technology and Economics, Budapest, Ph. D. Thesis (2002).
- [11] Brecher, C., et al. "Simulative Parameterization of Dead Time Variable Rotation Speed Behavior to Improve Process Stability in High Performance Cutting." *Procedia CIRP* 4 (2012): 2-10.
- [12] Tarn, Y. S., Y. W. Hsieh, and T. C. Li. "Automatic selection of spindle speed for suppression of regenerative chatter in turning." *The International Journal of Advanced Manufacturing Technology* 11.1 (1996): 12-17.
- [13] Liao, Y. S., and Y. C. Young. "A new on-line spindle speed regulation strategy for chatter control." *International Journal of Machine Tools and Manufacture* 36.5 (1996): 651-660.
- [14] Doppenberg, E. J. J., et al. "Active in-process chatter control." *CIRP 2nd International Conference on High Performance Cutting*, Vancouver, Canada, paper. No. 100. 2006.
- [15] Tsai, N. C., D. C. Chen, and R. M. Lee. "Chatter prevention and improved finish of workpiece for a milling process." *Proceedings of the Institution of Mechanical Engineers, Part B: Journal of Engineering Manufacture* 224.4 (2010): 579-588.
- [16] Altintas, Y., and M. Weck. "Chatter stability of metal cutting and grinding." *CIRP Annals-Manufacturing Technology* 53.2 (2004): 619-642.
- [17] Sastry, Sridhar, Shiv G. Kapoor, and Richard E. DeVor. "Floquet theory based approach for stability analysis of the variable speed face-milling process." *Journal of manufacturing science and engineering* 124.1 (2002): 10-17.
- [18] Yilmaz, Alpay, Emad Al-Regib, and Ni Jun. "Machine tool chatter suppression by multi-level random spindle speed variation." *Journal of manufacturing science and engineering* 124.2 (2002): 208-216.
- [19] Al-Regib, Emad, Jun Ni, and Soo-Hun Lee. "Programming spindle speed variation for machine tool chatter suppression." *International Journal of Machine Tools and Manufacture* 43.12 (2003): 1229-1240.
- [20] Albertelli, P., et al. "An experimental investigation of the effects of Spindle Speed Variation on tool wear in turning." *Procedia CIRP* 4 (2012): 29-34.

Dynamics of Modified Tool Structures for Effective Cutting

Vytautas Ostasevicius, Vytautas Jurenas, Arturas Juskevicius

Kaunas University of Technology, LT-44244 Kaunas, Lithuania
vytautas.ostasevicius@ktu.lt

ABSTRACT

The better surface quality of the machined workpiece could be obtained when the cutting tool is excited at vibration modes, which are characterized by higher frequencies and lower vibration amplitudes generating vibration cutting effect. Traditionally excitation of high-frequency vibrations at the tool cutting edge needs special equipment, which is not relatively simple to implement in industrial environment. More effective could be the possibility to excite higher vibration modes due to cutting tool's structural changes.

The main idea of the reported research work is based on treating cutting tool as a flexible structure characterized by several modes of natural vibrations, structural modification of which leads to the self-excitation of higher vibration modes during cutting. The intensification of the higher natural vibration modes results in higher frequencies and lower vibration amplitudes of cantilever type cutting tools generating vibration cutting effect, that gives the better quality of the treated surface. Consequently the intensification of the higher modes increases the magnitude of internal energy dissipation inside tool material and thereby makes the tool, without any passive vibration absorber, a more effective damper, which positively influences the amplitudes of workpiece or machine tool itself, providing the possibility to reduce chatter. Increase in cutting effectiveness related with the intensification possibility of cutting regimes avoiding the tool-workpiece resonance zones.

KEYWORDS: Flexible structures, vibration modes, vibro-impact motion.

1. INTRODUCTION

Initial studies, carried out by the author of this paper in the field of vibration turning [1], suggested new ideas for improving performance of vibration cutting processes and encouraged to perform a more thorough investigation of associated dynamic phenomena. A stiffer cutting tool does not improve stability significantly. It means, that better way of passive control technique is related to the effective control of higher modes of flexible tool structures. It is based on the excitation of a particular higher vibration mode of a tool, which leads to the reduction of deleterious vibrations in the machine–tool–workpiece system through intensification of internal energy dissipation in the tool material.

The passive control technique does not need complicated hardware and the end-user does not need to introduce new handling routines. Implementations of passive damping in tooling equipment are already available on the market. The location and the value of the passive vibration absorbers mostly are related to response energy in the first three modes of the structures. Sharma *et al* [2] the boring bar, simulate as a cantilever Euler-Bernoulli beam and only its first mode of vibration was considered. The stability of the two-degree-of-freedom model was analyzed constructing the stability diagram, dependent on the bar characteristics and on the absorber parameters (mass, stiffness, damping and position). Two analytical approaches for tuning the absorber parameters were compared. The selection criterion consisted on the maximization of the minimum values of the stability-lobes diagram. Subsequent analysis performed in this work, allowed formulating of new analytical expressions for the tuning frequency improving the behavior of the system against chatter. Miguelez *et al* in paper [3] deals with the application of tunable vibration absorbers for suppression of chatter vibrations in the boring manufacturing process. The boring bar is modeled as a cantilever Euler-Bernoulli beam and the tunable vibration absorber composed of mass, spring and dashpot elements. In addition, the effect of spring mass is considered in this analysis. After formulation of the problem, the optimum specifications of the absorber such as spring stiffness, absorber mass and its position are determined using an algorithm based on the mode simulation method. The analog-simulated block diagram of the system is developed and the effects of various excitations such as step, ramp, etc. on the absorbed system are simulated, chatter stability is analyzed in dominant modes of boring bar. Results show that at higher modes, larger critical widths of cut and consequently more material removal rate can be achieved.

Moradi *et al* [4] show that stability of the cutting tool can be considerably enhanced with a higher damping ratio of the cutting tool structure, which is related to the higher vibration modes, essentially when a cutting tool of low stiffness is used. According to Vela-Martinez *et al* [5], a stiffer cutting tool does not improve stability significantly. It means, that better way of passive control technique is related to the effective control of higher modes of flexible tool structures. It is based on the excitation of a particular higher vibration mode of a tool, which leads to the reduction of deleterious vibrations in the machine–tool–workpiece system through intensification of internal energy dissipation in the tool material. Paper [6] proposes to extend the stability limits of the machining system by enhancing the structure's damping capability via a unified concept based on the distribution of damping within the machining system exploiting the joints composing the machine tool structure. The design solution proposed is based on the enhancement of damping of joint through the exploitation of viscoelastic polymers' damping properties consciously designed as High Damping Interfaces.

The main idea of the reported research work is based on treating cutting tool as a flexible structure which is characterized by several modes of natural vibrations. In such machining processes as internal turning the structural configuration of the tool resembles cantilever beam. The first vibration mode of cantilever is characterized by maximum amplitudes of free end vibrations. The establishment of structural modifications of cutting tool as flexible structure is related with intensification of the higher natural vibration modes, similar to the vibration cutting conditions, results in reduction of magnitude of unwanted deleterious vibrations generated during machining. This suggests that excitation of higher natural vibration modes could be advantageous for this purpose since it is known that as the amplitude of higher modes becomes more intensive, energy dissipation inside tool material increases significantly and thereby makes the tool a more effective damper, which positively influences the amplitudes of the workpiece or machine tool itself, providing the possibility to reduce chatter.

The manuscript consists of two main parts: numerical and experimental. It is organized as follows. In chapter 2, finite element model of a boring tool is presented. Chapter 3 is

dedicated to description of qualitative and quantitative modeling results received during simulation. Chapter 4 is dedicated for practical realization of boring tool. Chapter 5 deals with experimental investigation of modified boring tools. The paper is finalized with concluding remarks.

2. ANALYSIS OF VIBRO-IMPACT CUTTING PROCESS

The tool vibration during cutting could be described as vibro-impact process. As any kind of tool has distributed mass, stiffness and other parameters it is necessary to consider the dynamics of such elastic structure that is characterized by several modes of natural vibrations. The impact interaction between elastic links is characterized by a rich spectral content of excitation impulses capable to excite a wide range of natural modes. In boring process the structural configuration of the tool resembles cantilever beam. Fig.1 presents a computational scheme of the developed finite element (FE) model of impacting boring tool on the work piece internal surface expressed by the rheological properties - stiffness and viscous friction. The model consists of $i = 1, 2, \dots, m$ finite elements.

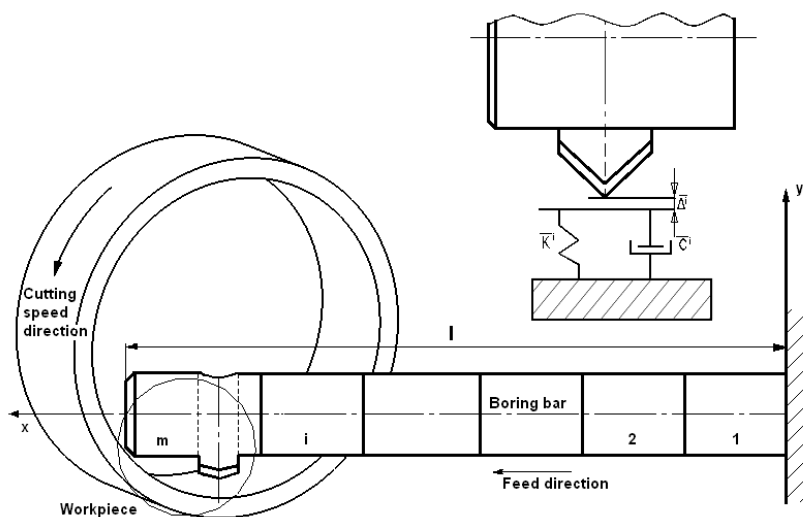


Fig.1. Model of boring tool on the work piece surface.

Impact modeling is based on contact element approach and makes use of Kelvin-Voigt (viscoelastic) rheological model, in which linear spring is connected in parallel with a damper—the former represents the impact force and the latter accounts for energy dissipation during impact.

After proper selection of generalized displacements in the inertial system of coordinates, model dynamics is described by the following equation of motion given in a general matrix form:

$$[M]\{\ddot{y}(t)\} + [C]\{\dot{y}(t)\} + [K]\{y(t)\} = \{F(y, \dot{y}, t)\} \quad (1)$$

Where $[M]$, $[C]$, $[K]$ are mass, damping and stiffness matrices respectively, $\{y(t)\}$ $\{\dot{y}(t)\}$ $\{\ddot{y}(t)\}$ — displacement, velocity and acceleration vectors respectively. $\{F(y, \dot{y}, t)\}$.

Vector of interaction forces between tool cutting edge and the workpiece, the components of which express the reaction of the tool cutting edge impacting workpiece and acquire the following form:

$$f_i(y_i, \dot{y}_i, t) = \bar{K}^i (\bar{\Delta}^i - |y_i(t)|) + \bar{C}^i \dot{y}_i(t) \quad (2)$$

where, \bar{K}^i, \bar{C}^i - stiffness and viscous friction coefficients of the work piece material, $\bar{\Delta}^i$ - distance from the cutting edge located at the i -th nodal point of the tool structure to the surface of the workpiece. In the case of considered model the assumption of proportional damping is adequate therefore internal damping is modeled by means of Rayleigh damping approach [7]:

$$[C] = \alpha_{dM} [M] + \beta_{dK} [K] \quad (3)$$

where α_{dM}, β_{dK} are mass and stiffness damping parameters respectively that are determined from the following equations using two damping ratios ξ_1 and ξ_2 that correspond to two unequal natural frequencies of vibration ω_1 and ω_2 [7]:

$$\begin{aligned} \alpha + \beta \omega_1^2 &= 2\omega_1 \xi_1 ; \\ \alpha + \beta \omega_2^2 &= 2\omega_2 \xi_2 . \end{aligned} \quad (4)$$

The presented FE model of the vibro-impact system was implemented.

3. NUMERICAL ANALYSIS OF THE TOOL VIBRATIONS

Vibro-impact process consists of free vibrations of the tool in the intervals between the impacts and its vibration during the impact interaction with workpiece. Therefore, profound investigation of free and impact vibration of elastic tool is essential. The modes of natural transverse vibrations of elastic cantilever beam-shaped tool presented in Fig.2 consist of transverse displacement Y . Of the whole range of natural vibrations, the first five modes are distinguished (I, II, III, IV, V) which in the intersection with the axis line form nodal points marked by numbers that express the ratio between the distance x from the fixing site of the cantilever beam-shaped tool and its whole length l . The letter Y_{ij} , denote the values of the maximum amplitudes (deflections) of the flexural modes. As it is known, the first vibration mode of a cantilever is characterized by maximum amplitudes of free end vibrations as the amplitudes of each higher mode gradually decrease.

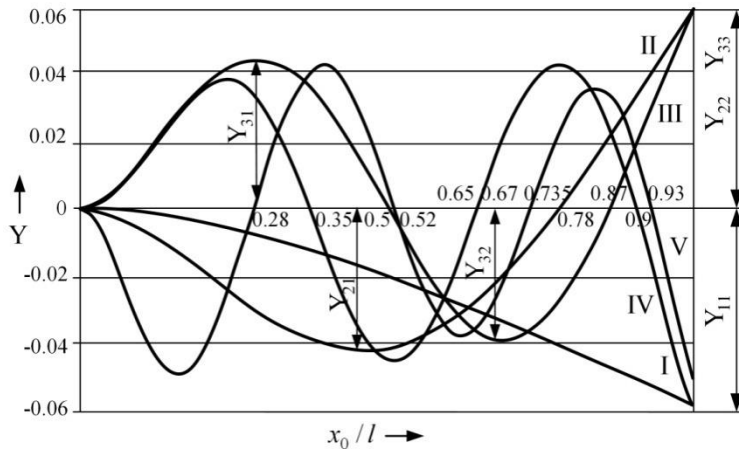


Fig.2. The modes of natural transverse flexural vibrations of tool. x_0/l denotes ratio between the distance x_0 from the anchor of the tool and its whole length l , Y_{ij} - maximum amplitudes of the flexural: index i - number of vibration mode, j - sequence number of the maximum amplitude point with respect to the anchor point.

Fig.3 represents different vibration modes of the boring tool. Natural frequencies depend from structural parameters by changing which it is possible to approach transverse and rotational frequencies by changing structural parameters of boring tool.

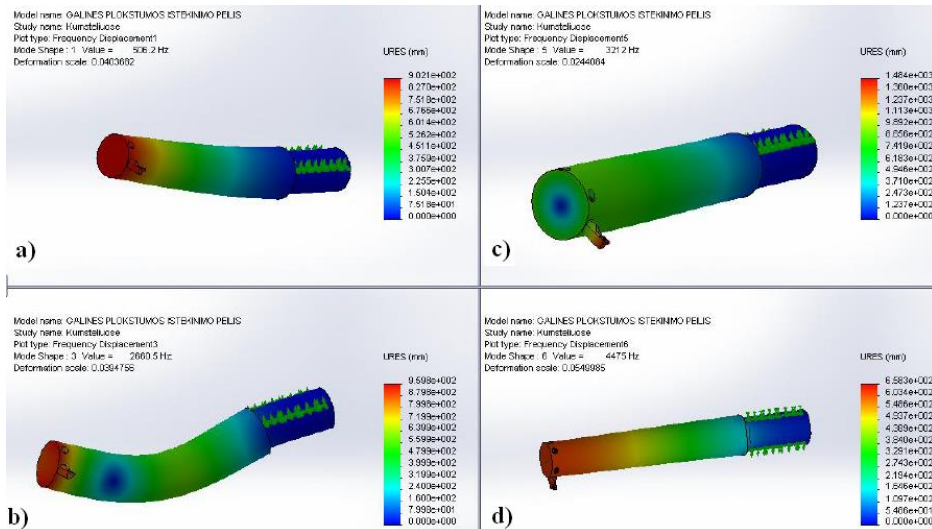


Fig.3. The modes of natural vibration of boring tool: a) the first natural transverse vibration mode, b) the second natural transverse vibration mode, c) the first natural rotational vibration mode, d) the first natural longitudinal vibration mode.

Identically to the process of free impact vibrations of cantilever released from statically deformed position bouncing the support the process of free impact vibrations of boring tool is simulated. The main purpose of such simulation is to imitate the cutting process which is

characterized by the wide frequency range of cutting forces during chip formation when the tool contacts with elastically recovered surface of the work piece. Fig.4 presents the dimensionless dependence of the maximum amplitude of the post-impact rebound $z_{\max} = y_{\max}/l$ on the position of the tool cutting edge where the smallest rebound amplitudes are obtained when the cutting edge is located at points coinciding with $x_0/l = 0.87$ or $x_0/l = 0.67$. A slight decrease in the rebound amplitude is also observed at $x_0/l = 0.78$. The lower curve in Fig. 4, that asymptotically approaches the axis line, corresponds to the deflection of the free end of the tool during the impact with the workpiece. According to Fig.2 points $x_0/l = 0.87$ and $x_0/l = 0.67$ coincide with particular points of the third mode of transverse vibrations of cantilever, when the point $x_0/l = 0.78$ with the nodal point of the second mode.

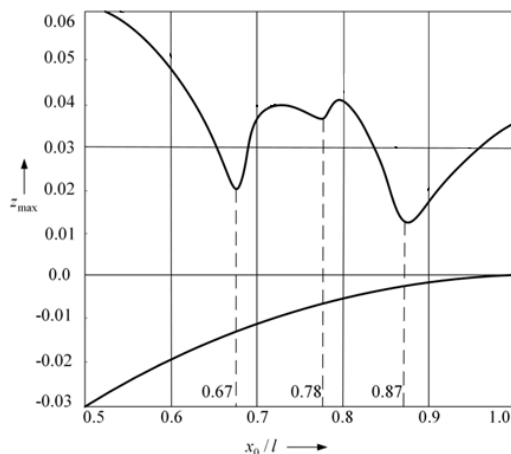


Fig.4. Dependence of dimensionless rebound amplitude of the tool $z_{\max} = y_{\max}/l$ on the position of the cutting edge expressed as a ratio between the distance x_0 from the anchor of the tool and its whole length l .

4. PRACTICAL REALIZATION OF SELF EXITING TOOL STRUCTURE

The practical issue of given simulation results could be the modified boring tool structure (Fig. 5) in which the cutting edge is located at the distance 0.87 from the anchor point of the tool [8]. The main purpose of this invention is an improvement of cutting conditions by decreasing tool vibration amplitude and consequently increasing frequency. For example, a desire of being able to perform a cutting operation into pre-drilled holes in a workpiece limits the diameter or cross-sectional size of the boring bar during boring when the vibrations are a cumbersome part of the manufacturing process [9]. Usually a boring bar is comparatively long and slender, and is thereby more sensitive to excitation forces. Vibrations usually dominate by the first resonance frequency in either of the two directions of the boring bar. This process usually is not stationary. The vibrations of the boring bar affect the result of machining and surface finish in particular. The tool life is also likely to be influenced by vibrations. The tool structure consists of the end part 1 for the fixation in machine-tool spindle and the cantilever part 2 of length l constant cross-section tool holder. At the distance 0,87 l the cutting insert 3 is fixed. When the tool is cutting the variable force excites vibro - impact motion. As cutting insert is located in the nodal point of the third mode of flexural vibrations of the cantilever shaped structure the third mode of construction vibrations is predominated.

This mode is distinguished by lower amplitudes and higher frequencies resulting in vibration cutting regime. Intensification of the vibration energy dissipation in the tool holder material decreases not only the amplitudes of tool, but also the amplitudes of workpiece and machine-tool vibrations.

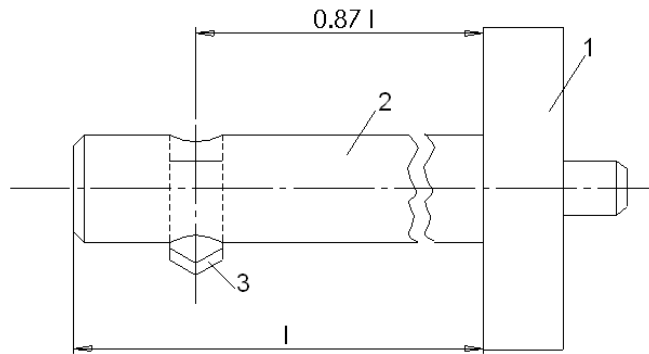


Fig.5. Modified boring tool structure with cutting edge located in the nodal point of the third natural vibration mode at the distance $0.87l$ from the anchor point.

Practical realization of the modified boring tool is presented in Fig.6. On the boring tool holder 1 the cutting insert 2 could be fixed at the distance, which coincides with the nodal points of the higher modes of flexural vibrations in radial direction. As vibrations usually dominate in either of the two directions of the boring bar two sensors- accelerometers – KD91 (RFT, Germany) 3 and 4 are placed in the two perpendicular planes. Sensor 3 is attached in the same plane as cutting part and is capable to measure vibrations in radial direction as well as sensor 4 in perpendicular direction for tangential direction to cutting surface measurements.

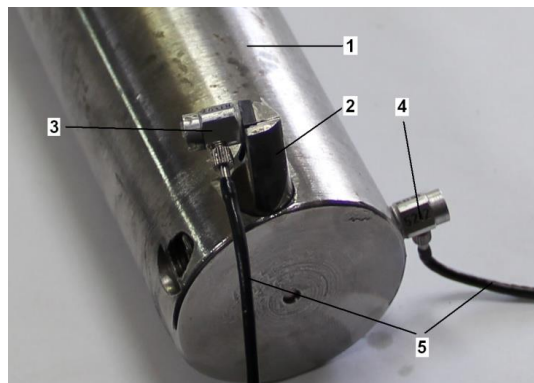


Fig.6. Practical realization of modified tool structure: 1-boring tool holder, 2-cutting insert, 3-sensor for radial and 4-for tangential vibrations measurements, 5-cables.

The experimental study was carried out with intention to demonstrate tool vibrations. Workpiece from steel 37 was machined using identical cutting parameters with conventional and modified tools: feed $f - 0.14$ mm/rev, spindle rotation $n - 310$ rpm, cutting depth $a - 0.25$ mm Fig.7. The vibrations of conventional tool, when cutting insert is located at the free end of the boring bar (in red-dashed line), are characterized by higher amplitudes and lower

frequency than the vibrations of passive tool, modified by fixing cutting insert in the place of third mode nodal point at the distance $0,87 l$ (in blue-continues line).

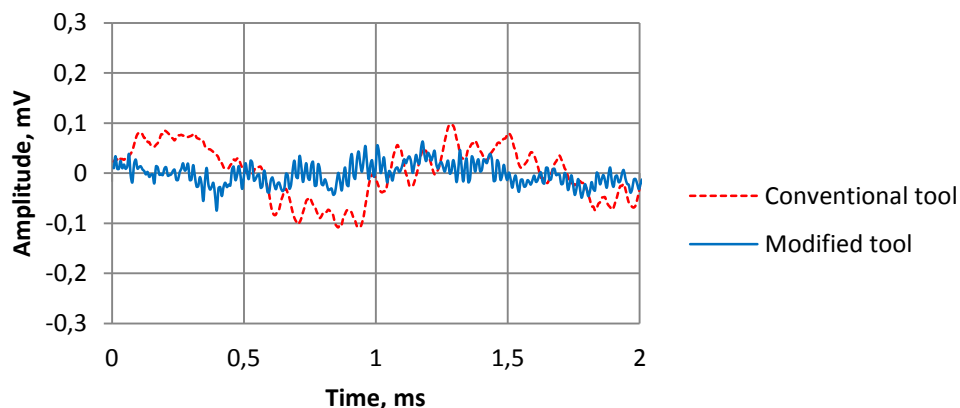


Fig.7. Boring bar vibrations in direction of radial cutting force in the case of conventional (in red) and modified (in blue) tool with cutting insert fixed in nodal point of the third mode of flexural vibrations at $0.87l$.

As is indicated in Fig.7 during boring operations with modified tools the higher modes of transverse vibrations of cutting tools are expressed by higher frequencies and by the few times reduced vibration amplitudes which generate vibration cutting effect. As cutting insert is located in the nodal point of the third mode of flexural vibrations of the cantilever shaped structure the third mode of construction vibrations is predominated, which is distinguished by lower amplitudes and higher frequencies resulting in vibration cutting regime.

5. EXPERIMENTAL RESEARCH OF BORING TOOL STRUCTURE WITH SELECTED RATIO OF TORSION AND TRANSVERSE VIBRATION FREQUENCIES

Other possibility to modification of boring tool is related to the dimensional change of the tool holder parameters coinciding the first frequency of torsion to the second one of transverse vibrations. For intensification of the second mode of flexural vibrations of boring bar the cutting insert should be placed at the distance $0.78l$, which coincides with the nodal point of the second mode of flexural vibrations in radial direction. Fig.8 illustrates distinguished increase of tangential vibrations amplitudes, when cutting insert is fixed at the point $0.78l$ (in blue-continues line) accordingly to vibration amplitudes of conventional tool (in red-dashed line). It means, that this is the rotational resonance case, which could be useful for the reduction of transverse vibrations in radial direction. The coincidence of two natural frequencies initiates the intensification of the first mode of rotational vibrations and the second mode of flexural as well as dissipation of energy in the tool holder material (in blue-continues line) decreasing consequently the transverse vibration amplitudes.

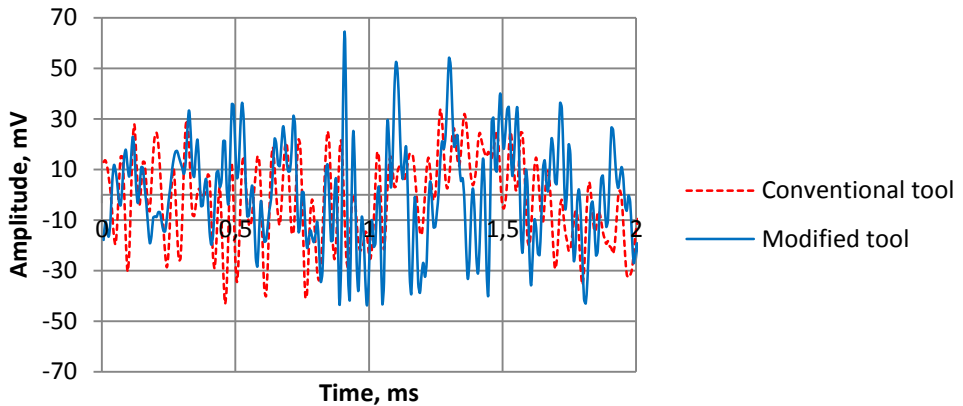


Fig.8. Boring bar vibrations in direction of tangential cutting force case of conventional (in red) and modified (in blue) tool with cutting insert fixed in nodal point of the second mode of flexural vibrations at $0.78l$.

Fig. 9 confirms this statement, because the vibration amplitudes of boring bar decrease few times (in blue-continues line) when cutting insert is located at the distance $0.78l$, in the nodal point of second mode of transverse vibrations of boring bar. The coincidence of two natural frequencies initiates the intensification of second mode of transverse vibration amplitudes and consequently dissipation of energy in the tool holder material (in blue-continues line).

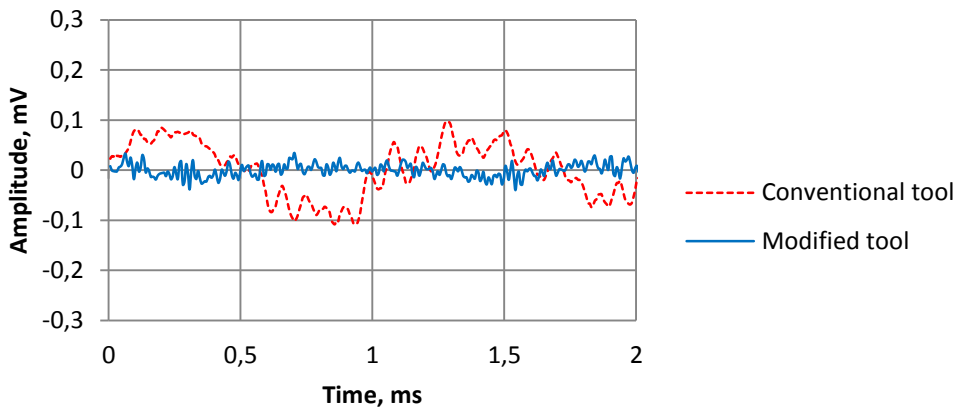


Fig.9. Boring bar vibrations in direction of radial cutting force in the case of conventional (in red) and modified (in blue) tool with cutting insert in nodal point of the second mode of flexural vibrations at $0.78l$.

6. CONCLUSIONS

Modified means related to tools structural changes are proposed for excitation of high frequency vibrations during boring. Cutting tool as a flexible structure that is characterized by several modes of natural vibrations and intensification of some of them. Intensification of the

higher vibration modes increases tool vibration frequency, which becomes similar as during vibration cutting, and decreases tools cutting part vibration amplitudes assuring improvement of surface finish. The experimental settings demonstrate better tool behavior, decrease of vibration amplitudes, justifying numerical analysis results and presumptions for controlling tool vibrations during cutting process, with modifications made for the structure of boring tool, on the basis of computational results. The structural changes of tools and possibilities to excite higher modes are related to the modification of tools structure by fixing cutting insert in the nodal point of laterally vibrating tool holder or approaching the first frequency of torsion of the tool holder to the second one of transverse vibrations. This, in turn, has important practical implications since the presented approach of modified tool mode control is relatively simple to implement in industrial application as it does not require sophisticated control devices.

ACKNOWLEDGEMENTS

This research work was funded by EU Structural Funds project "In-Smart" (Nr. VP1-3.1-ŠMM-10-V-02-012), ministry of education and science, Lithuania.

REFERENCES

- [1] V.Ostasevicius, R.Gaidys, J.Rimkevičienė, R.Dauksevicius. "An approach based on tool mode control for surface roughness reduction in high-frequency vibration cutting // Journal of Sound and Vibration. London : Elsevier Science. ISSN 0022-460X. 2010, Vol. 329, iss. 23, p. 4866-4879.
- [2] V.S.Sharma, M.Dogma, N.M.Suri, Proc.ImechE Vol. 222 Part B: J. Engineering Manufacture
- [3] M.H. Miguelez, L. Rubio, J.A. Loya, J.Fernandez-Saez, Improvement of chatter stability in boring operations with passive vibration absorbers, International Journal of Mechanical Sciences 52 (2010) 1378-1384.
- [4] H. Moradi, F. Bakhtiari-Nejad, M.R. Movahhedy, Tuneable vibration absorber design to suppress vibrations: An application in boring manufacturing process. Journal of Sound and Vibration 318 (2008) 93-108.
- [5] L.Vela-Martinez, J.C.Jauregui-Correa, E.Rubio-Cerda, G.Herrera-Ruiz, A.Lozano-Guzman, Analysis of compliance between the cutting tool and the workpiece on the stability of a turning process. International Journal of Machine Tools and Manufacture 48 (2008) 1054-1062.
- [6] L.Daghini, Improving Machining System Performance through designed-in Damping: Modelling, Analysis and Design Solutions. PhD Thesis, KTH Royal Institute of Technology, Stockholm, Sweden, ISBN 978-91-7501-328-2.
- [7] K.J. Bathe, E.L.Wilson, *Numerical Methods in Finite Element Analysis*; Prentice-Hall: Englewood Cliffs, NJ, USA, (1976).
- [8] V.Ostasevicius et al "Internal turning tool holder" SU invention Nr.1590206.
- [9] L.Petersson, Vibration analysis of a boring bar. Research report, Department of telecommunications and signal processing, Blekinge Institute of technology, Sweden, 2002.

Stability in turning of superalloys using two numerical methods

Gorka Urbicain Pelayo¹, Jorge Alberto Palacios Moreno², Daniel Olvera Trejo², Asier Fernández Valdivielso¹, Alex Elías-Zúñiga², Luis Norberto López de Lacalle¹

¹University of the Basque Country UPV/EHU, ETSI

Alda. de Urquijo s/n, 48013 Bilbao, España.

²Department of Mechanical Engineering, Instituto Tecnológico y de Estudios Superiores de Monterrey, Monterrey Campus

Av. Eugenio Garza Sada 2501 Sur, 64849, Monterrey, México.

gorka.urbikain@ehu.es

ABSTRACT

Chatter is a self-excited vibration between the work piece and the cutting tool that limits the maximum admissible depth of cut in a cutting operation. This has some important drawbacks such as poor surface quality, tool life reduction or possible damages to the spindle bearings. Mathematically, regenerative chatter phenomenon is defined by a delay differential equation leading to different solving methods. This paper presents two numerical methods to mathematically describe the stability problem in turning operations. The study presents the formulation with the Enhanced Multistage Homotopy Perturbation Method (EMHPM) and the Chebyshev Collocation Method (CCM) which have been verified against experimental tests on nickel superalloys.

KEYWORD: Chatter, stability turning, Chebyshev polynomial, Homotopy, Inconel 718.

1. INTRODUCTION

The first techniques to find stability diagrams in machining problems appeared in the 60's. However, the technology available at that time did not allow the experiments accurate results. It was not until the 90's when new methodologies began to appear and subsequently in the year 2000 the rise in the development of stability by means of different techniques was triggered. The available literature makes use of a large amount of approaches: starting from the well-known mechanistic methods to semi-discretization methods, full discretization methods, collocation methods, etc. often based on approximating the stability solution and representing the system by a characteristic or transition matrix [1-6].

On the other hand, recently the applications of the superalloys are expanding to the aeronautics industry. Common types include the commercial trademarks Inconel, Waspalloy or Rene, which are used in disks, cases, rings or shafts. Such materials are able to withstand the challenging operating conditions in the hottest parts of the gas turbine engines (see Fig. 1). These superalloys have excellent response to aggressive conditions but present, at same time, low machinability due to their abrasive carbides content, tendency to work hardening, low thermal conductivity and chemical affinity.

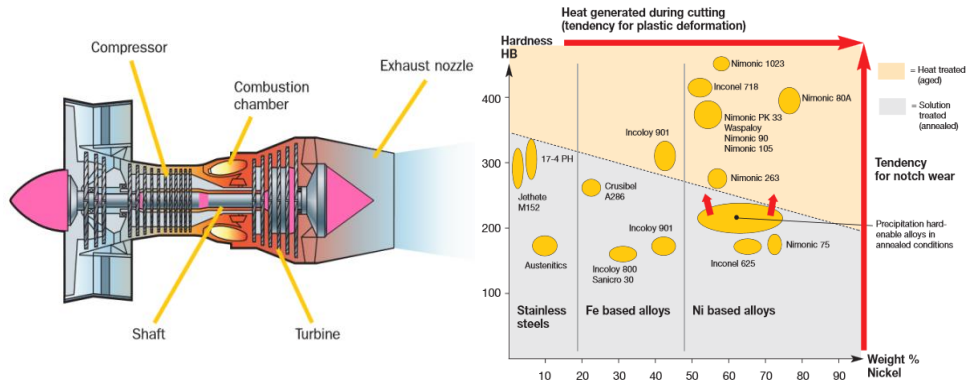


Fig.1.(a)HRSA application areas in gas turbine; (b)HRSA: alloy groups (from Sandvik©).

This paper presents two numerical approaches to analyze the stability of turning operations when the dominant mode comes from the tangential direction what can occur during the turning of large and heavy cases and rings made from nickel superalloys. The numerical approaches are the Enhanced Multistage Homotopy Perturbation Method (EMHPM) which was applied to milling in the past and has been readapted for turning operations and the Chebyshev Collocation Method (CCM) because these includes the effects of the cutting parameters to construct precise stability charts. The model has been applied to longitudinal turning of Inconel 718 using flexible tools in tangential direction to reproduce similar dynamic conditions that of real cases. For example, a multi-purpose vertical lathe used in aeronautics for manufacturing motor housings, ship propellers or electric motors. In such cases, the ram covers long distances in the longitudinal-axis, and dynamic displacements of the tool tip may result in chatter on the regenerative plane.

2. ENHANCED MULTISTAGE HOMOTOPY PERTUBATION METHOD

A wide variety of engineering problems are systems with time delay which require solving delay differential equations (DDE). The Enhanced Multistage Homotopy Perturbation Method (EMHPM) allows to obtain stability lobes based on the discretization of the time delay in subintervals of equal length. For the calculation of the stability for delay differential equations, the matrix representation is given by the following state-space form:

$$\dot{\mathbf{y}}(t) = \mathbf{A}(t)\mathbf{y}(t) + \mathbf{B}(t)\mathbf{y}(t - \tau) \quad (1)$$

where $\mathbf{y}(t) = [\mathbf{y} \quad \dot{\mathbf{y}}]$, $\mathbf{A}(t + \tau) = \mathbf{A}(t)$, $\mathbf{B}(t + \tau) = \mathbf{B}(t)$ and τ is the delay.

Subsequently, the expression in state-space is transformed to:

$$\dot{\mathbf{y}}_i(T) - \mathbf{A}_i \mathbf{y}_i(T) \approx \mathbf{B}_i \mathbf{y}_i^T(T) \quad (2)$$

where $\mathbf{y}_i(T)$ denote the order of solution m in the above equation in the i -th subinterval which must satisfy the following initial conditions $\mathbf{y}_i(0) = \mathbf{y}_{i-1}$. The delay is discretized into a total of N equally spaced points. Consequently each subinterval has a size equal to $\Delta t = \tau/(N - 1)$. It can be defined:

$$\mathbf{y}_i^T(T) \approx \mathbf{y}_{i-N} + \frac{N-1}{\tau} (\mathbf{y}_{i-N+1}T - \mathbf{y}_{i-N}T) \quad (3)$$

Consequently, the approximated system takes the form:

$$\dot{\mathbf{y}}_i(T) = \mathbf{A}_i \mathbf{y}_i(T) + \mathbf{B}_i \mathbf{y}_{i-N} + \frac{N-1}{\tau} \mathbf{B}_i \mathbf{y}_{i-N+1}T - \frac{N-1}{\tau} \mathbf{B}_i \mathbf{y}_{i-N}T \quad (4)$$

Now, building the Homotopy function of the above expression:

$$H(\mathbf{Y}, p) = L(\mathbf{Y}_i) - L(\mathbf{y}_{i0}) + pL(\mathbf{y}_{i0}) = p \left(\mathbf{A}_i \mathbf{Y}_i + \mathbf{B}_i \mathbf{y}_{i-N} + \frac{N-1}{\tau} \mathbf{B}_i \mathbf{y}_{i-N+1}T - \frac{N-1}{\tau} \mathbf{B}_i \mathbf{y}_{i-N}T \right) \quad (5)$$

In addition the expansion of \mathbf{Y}_i of order m can be written as

$$\mathbf{Y}_i(T) = \mathbf{Y}_{i0}(T) + p\mathbf{Y}_{i1}(T) + \dots + p^m \mathbf{Y}_{im}(T) \quad (6)$$

After substituting the \mathbf{Y}_i expansion with the initial condition $\mathbf{y}_{i0} = \mathbf{y}_{i-1}$ in the equation $H(\mathbf{Y}, p)$, solving the resulting first order differential equations:

$$\mathbf{Y}_{i0}(0) = \mathbf{y}_{i-1} \quad (7)$$

$$\mathbf{Y}_{i1} = \mathbf{A}_i \mathbf{y}_{i-1}T + \mathbf{B}_i \mathbf{y}_{i-N}T + \frac{1}{2} \frac{N-1}{\tau} \mathbf{B}_i \mathbf{y}_{i-N+1}T^2 - \frac{1}{2} \frac{N-1}{\tau} \mathbf{B}_i \mathbf{y}_{i-N}T^2 \quad (8)$$

$$\mathbf{Y}_{i2} = \frac{1}{2} \mathbf{A}_i^2 \mathbf{y}_{i-1}T^2 + \frac{1}{2} \mathbf{A}_i \mathbf{B}_i \mathbf{y}_{i-N}T^2 + \frac{1}{6} \frac{N-1}{\tau} \mathbf{A}_i \mathbf{B}_i \mathbf{y}_{i-N+1}T^3 - \frac{1}{6} \frac{N-1}{\tau} \mathbf{A}_i \mathbf{B}_i \mathbf{y}_{i-N}T^3 \quad (9)$$

$$\begin{aligned} \mathbf{Y}_{ik} &= \frac{1}{k!} \mathbf{A}_i^k \mathbf{y}_{i-1}T^k + \frac{1}{k!} \mathbf{A}_i^{k-1} \mathbf{B}_i \mathbf{y}_{i-N}T^k \\ &+ \frac{1}{(k+1)!} \frac{N-1}{\tau} \mathbf{A}_i^{k-1} \mathbf{B}_i \mathbf{y}_{i-N+1}T^{k+1} - \frac{1}{(k+1)!} \frac{N-1}{\tau} \mathbf{A}_i^{k-1} \mathbf{B}_i \mathbf{y}_{i-N}T^{k+1} \end{aligned} \quad (10)$$

The previous set of expressions can be written as follows:

$$\mathbf{Y}_{ik} = \mathbf{Y}_{ik}^a + \mathbf{Y}_{ik}^b, \quad k = 1, 2, 3 \dots \quad (11)$$

where:

$$\mathbf{Y}_{i0}^a = \mathbf{y}_{i-1} \quad (12)$$

$$Y_{i0}^b = 0 \quad (13)$$

$$Y_{ik}^a = \frac{T}{k} (A_i Y_{i(k-1)}^a + g(k) B_i y_{i-N}) \quad (14)$$

$$Y_{ik}^b = \frac{T}{k+1} \left(A_i Y_{i(k-1)}^b + g(k) \left[\frac{N-1}{\tau} T (-B_i y_{i-N} + B_i y_{i-N+1}) \right] \right) \quad (15)$$

The final solution of order m is obtained by the sum of all k approaches of the Y_{ik} equation. Therefore the solution can be written as:

$$y_i \approx P_i(T) y_{i-1} + Q_i(T) y_{i-N+1} + R_i(T) y_{i-N} \quad (16)$$

Where:

$$P_i(T) = \sum_{k=0}^m \frac{1}{k!} A_i^k T^k \quad (17)$$

$$Q_i(T) = \begin{cases} \sum_{k=0}^m \frac{N-1}{(k+1)!} A_i^{k-1} B_i T^{k+1} & m \geq 1 \\ 0 & m = 0 \end{cases} \quad (18)$$

$$R_i(T) = \begin{cases} \sum_{k=0}^m \frac{1}{k!} A_i^{k-1} B_i T^{k+1} - Q_i & m \geq 1 \\ 0 & m = 0 \end{cases} \quad (19)$$

Using this, it is possible to develop a mapping of the y_i solution through a matrix that allows to predict the behavior in a next time. This can occur if there is the following relationship:

$$w_i = D_i w_{i-1} \quad (20)$$

where w_i is a vector of coefficients of dimension equal to the number of discretizations. In addition, this vector contains all vectors from y_{i-1} to y_{i+1} . D_i matrix is defined by

$$D_i = \begin{bmatrix} P_i & 0 & 0 & \cdots & 0 & Q_i & R_i \\ I & 0 & 0 & \cdots & 0 & 0 & 0 \\ 0 & I & 0 & \cdots & 0 & 0 & 0 \\ \vdots & \vdots & \vdots & \ddots & \vdots & \vdots & \vdots \\ 0 & 0 & 0 & \ddots & 0 & 0 & 0 \\ 0 & 0 & 0 & \cdots & I & 0 & 0 \\ 0 & 0 & 0 & \cdots & 0 & I & 0 \end{bmatrix} \quad (21)$$

Finally, the Floquet transition matrix Φ is calculated over the period $\tau = (N-1)\Delta t$ with the product:

$$\Phi = D_{N-1} D_{N-2} \cdots D_2 D_1 \quad (22)$$

As a result the eigenvalues of the transition matrix are calculated and the desired parameters stabilities are obtained following the Floquet theory [7].

3. CHEBYSHEV COLLOCATION METHOD

The combination of Floquet's theory [7] and Chebyshev polynomials [3, 8] has been useful to solve the stability of periodic systems. Similarly to the EMHPM, the problem is initiated from Eq. (1) which solution is: $\mathbf{y}(t)=\boldsymbol{\phi}(t)$ in $-\tau \leq t \leq 0$. τ represents the delay time, t is the current time, $\dot{\mathbf{y}}(t)$ is a $nx1$ state vector in the interval $[0, \tau]$ and $\boldsymbol{\phi}(t)$ is a $nx1$ state vector in the previous interval $[-\tau, 0]$. Using N collocation points, Eq. (1) is numerically approximated as:

$$\hat{\mathbf{D}} \{v_j\} = \mathbf{M}_A\{v_j\} + \mathbf{M}_B\{\phi_j\} \quad (23)$$

where $\{v_j\}$ and $\{\phi_j\}$ are the Chebyshev polynomial discretizations of the vectors $\mathbf{y}(t)$ and $\mathbf{y}(t - \tau)$ at the collocation points ($t_j = \cos(j\pi/(N - 1))$, $j = 0, 1, \dots, N - 1$). \mathbf{M}_A and \mathbf{M}_B are the approximation matrices, extended at the same collocation points, which depend on the modal parameters and specific cutting forces and \mathbf{D}_N represents the differentiation matrix which relates the discretized vector $\mathbf{x}(t)$ and its derivative, and is built from essential differentiation matrix \mathbf{D} whose elements are described as:

$$\begin{aligned} D_{11} &= \frac{(2(N - 1)^2 + 1)}{6}, & D_{jj} &= \frac{-y_{j-1}}{2(1 - t_{j-1}^2)}, \quad j = 2, \dots, N - 1 \\ D_{mm} &= -\frac{(2(N - 1)^2 + 1)}{6}, & D_{ij} &= \frac{c_i}{c_j} \frac{-1^{i+j}}{(t_{i-1} - t_{j-1})}, \quad i \neq j, \\ c_j &= \begin{cases} 2, & i = 1, N \\ 1, & i \neq 1, N \end{cases} \end{aligned} \quad (24)$$

Finally, the stability is studied calculating the most dominant eigenvalues of the monodromy matrix \mathbf{U} built from:

$$\mathbf{U} = (\hat{\mathbf{D}}_N - \mathbf{M}_A)^{-1} \mathbf{M}_B, \quad (25)$$

If the maximum eigenvalues have modulus equal to unity, the system is critically stable.

4. DYNAMIC FORCE MODEL

For large tool overhangs, the weakest direction of the tool is the tangential direction. In this case, the variation of the chip thickness is due to a vertical movement in Y axis. This distortion is accompanied by a horizontal movement represented by $\delta x = v \cdot \delta y$, where v is the dynamic displacement coefficient.

The model is based on the following assumptions: 1) rigid work piece and compliant tool, 2) dominant mode in the tangential direction, 3) variable cutting coefficients with cutting speed and depth of cut, 4) Process damping and wear are not considered.

For a model of 1 DOF with one mode in the tangential direction the chip thickness may be obtained through:

$$h(t) = -v (y(t) - y(t - \tau)) \quad (26)$$

where v is the dynamic displacement coefficient [9] and $(y(t) - y(t - \tau))$ the current and previous displacements of the tool.

The procedure to obtain the dynamic displacement factor was derived in [10]. In chatter due to a tangential mode, the stability of the system is strongly determined by the dynamic displacement coefficient which has a decisive influence on the chip thickness. This dimensionless parameter depends on the dynamic characteristics of the systems well as on tool geometry. In fact, this parameter is built from:

$$v = \frac{k}{K_{cy}(V_c, a_p)b} \left[\left(\frac{\omega_c}{\omega_n} \right)^2 - 1 \right] \quad (27)$$

where K_{cy} are the specific cutting forces, a_p is the depth of cut, V_c is the cutting speed, k is the modal stiffness, ω_n is the natural frequency and ω_c is the vibration frequency. If $v < 0$ the cutting edge is displaced against the workpiece, the thickness of the chip is increased and the frequency of vibration is reduced. On the other hand, if $v > 0$, the cutting edge tends to move outside the workpiece.

Therefore, for a system of 1 degree of freedom, the equation of motion can be expressed as:

$$m \ddot{y}(t) + c \dot{y}(t) + k y(t) = F \quad (28)$$

where m, c and k are the modal parameters obtained by hammer impact tests and F is the dynamic force, which depends on two successive displacements:

$$F = K_{cy} a_p v [-(y(t) - y(t - \tau))] \quad (29)$$

Introducing this relation into the equation of motion and rearranging:

$$\ddot{y}(t) + 2\xi\omega_n \dot{y}(t) + \left[\omega_n^2 + \frac{K_{cy} a_p v}{m} \right] y(t) = \frac{K_{cy} a_p v}{m} y(t - \tau) \quad (30)$$

Regarding the terms and transforming the dynamic equation into state-space representation:

$$\dot{\mathbf{y}}(t) = \mathbf{A}(t)\mathbf{y}(t) + \mathbf{B}(t)\mathbf{y}(t - \tau) \quad (31)$$

where:

$$\mathbf{A}(t) = \begin{bmatrix} 0 & 1 \\ -\left[\omega_n^2 + \frac{K_{cy} a_p v}{m} \right] & -2\xi\omega_n \end{bmatrix}, \quad \mathbf{B}(t) = \begin{bmatrix} 0 & 0 \\ -\frac{K_{cy} a_p v}{m} & 0 \end{bmatrix} \quad (32)$$

5. EXPERIMENTAL METHODOLOGY

The tests were carried out in a multi-tasking centre, CMZ® model TC25BTY (Fig. 2a), with a maximum speed and power of 4000 r.p.m and 14 kW. Force measurements were carried out using a Kistler® dynamometer (9192AA) and then, the signals processing was completed with an amplifier and a multi-channel analyzer (Oros35 NV-Gate by

Oros®, Fig. 2b). Finally, the experimental forces were filtered and post-processed with Matlab® software.



Fig.2.(a) TC25BTY of CMZ®; (b) Multi-channel analyzer (Oros35 NV-Gate by Oros®).


The conditions for the characterization tests can be seen in Table 1. Before each test the edge was removed by a new cutting edge to ensure the programmed depth of cut and to avoid vibrations due to tool wear. This aspect is especially delicate when machining difficult-to-cut materials.

Table 1. Cutting conditions for characterization tests

Tool	workpiece	Cutting speed V_c (m/min)	Depth of cut a_p (mm)	Feedrate f_z (mm/rev)
SNMG 120408 PM	Inconel®718	50-125	0.2-1	0.1-0.2

Stability limit of common orthogonal turning can be calculated accurately by means of a 1D stability model. However, in some cases geometrical parameters such as lead cutting angle, rake angle or tool nose radius cannot be neglected. This is the case here where the depth of cut is comparable to tool nose radius. The reason for using such type of insert is found on its robustness due to the low lead cutting angle. More aggressive tools (such as CNMG or VBMT) give as result accelerated wear and dramatic notching when machining superalloys. Table 2 shows the basic parameters of this tool.

Table 2. Geometrical properties of SNMG tool

Tool		Nose radius r_ϵ (mm)	Lead angle κ_r (°)	Rake angle γ (°)	Inclination angle λ_s (°)
SNMG 120408 PM		0.8	45	-8	0

The corresponding specific cutting forces are calculated for different cutting depths and cutting speeds. Then these values are taken to the software Design Expert® to detect the most significant factors and dependences. After analyzing them by ANOVA (variance analysis), the polynomials on Table 3 are obtained. These surface functions are accurate approximations of the experimental forces.

Table 3. Specific cutting forces (*units in [I.S.]*)

Tool	Feed rate f_z (mm/rev)	K_{cy} (N/m ²)	R^2
SNMG 120408 PM	0.1	$5.929 \times 10^9 - 2.567 \times 10^8 V_c - 4.69 \times 10^{12} a_p$ $- 1.251 \times 10^{12} V_c a_p + 3.459 \times 10^7 V_c^2$ $+ 4.328 \times 10^{15} a_p^2$	0.998
	0.2	$4.572 \times 10^9 - 3.494 \times 10^8 V_c - 1.167 \times 10^{12} a_p$	0.997

Frequency Response Functions were obtained from hammer impact tests using an instrumented hammer (086C03, PCB Piezotronics®), an accelerometer (352C22, PCB Piezotronics®) and the same data acquisition system. Table 4 shows the modal parameters of the tool obtained by modal fitting (*peak-picking*):

Table 4. Modal parameters

Tool	f_n (Hz)	k (N/m)	ζ
SNMG 120408 PM	1650	3.09×10^7	0.0662

6. EXPERIMENTAL VALIDATION

This section shows the correlation between the analytical predictions and the experimental results. As chatter criterion, the cutting forces were recorded and transformed into the frequency range in order to display the dominant peak and its relative location with respect to the natural frequency and the cutting frequency multiples. The graphics were obtained with a mesh density of 100x100 dots and a total of 1200 collocation points following the procedure in [10]. To obtain stability graphics as a function of the cutting speed and averaged diameter of the work piece was chosen from all the cutting passes.

Figures 3a and 3b show the corresponding graphs in the case of the square insert. On one hand, similar tendencies and absolute values are found. So for this tool, increasing the feed rate does not penalize excessively the maximum allowable depth of cut. However, introducing high feed rates reduces the transition zone between stable cases and chatter and so, the depth of cut must be carefully programmed. For example, point $V_c=75$ [m/min]/ $a_p=0.80$ [mm] showed a nearly stable cutting ($f_c=1600$ [Hz]) for $f_z=0.1$ [mm/rev] while $f_z=0.2$ [mm/rev] lead to clear chatter ($f_c=1482$ [Hz]). Due to the high order of the simulated lobes the stability maps are not constituted in this case by typical smooth-rounded lobes but by an envelope curve. It is noted as well the high dependence on the cutting speed.

To determine the efficiency of the methods the convergence of each one was determined taking into account the variation with respect to a certain number of discretizations for the characteristic value of a stable point and for an unstable point, as in [11].

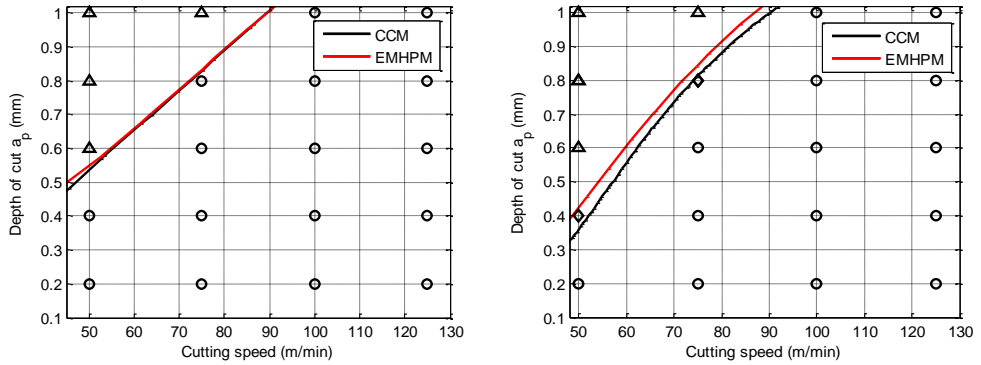


Fig.3.Computer simulations vs. experimental results.a. $f_z=0.1$ [mm/rev]; b. $f_z=0.2$ [mm/rev]
Stable - o, Chatter - diamond

Fig. 4 shows this convergence for both points, the stable point was taken at $V_c = 100$ m/min and $a_p = 0.6$ mm whereas the unstable point was $V_c = 50$ m/min and $a_p = 0.8$ mm. In the case of EMHPM, it can be said that the convergence for a stable point (reached for 600 discretizations) is faster (Fig. 4a) than the CCM convergence, with accuracy of $|\mu - \mu_0| = 0.048$ for EMHPM and $|\mu - \mu_0| = 0.093$ for CCM. On the other hand, analysing the unstable point (Fig. 4b), the EMHPM shows better results with accuracy of $|\mu - \mu_0| = 0.144$ for EMHPM and $|\mu - \mu_0| = 0.148$ for CCM but presenting both methods similar tendency. For the information with respect to the solution time, it's have that CCM counts with 24.046 seconds for each sequence, while EMHPM counts with 36.67 seconds for each sequence. So, the CCM reaches the convergence faster than the EMHPM.

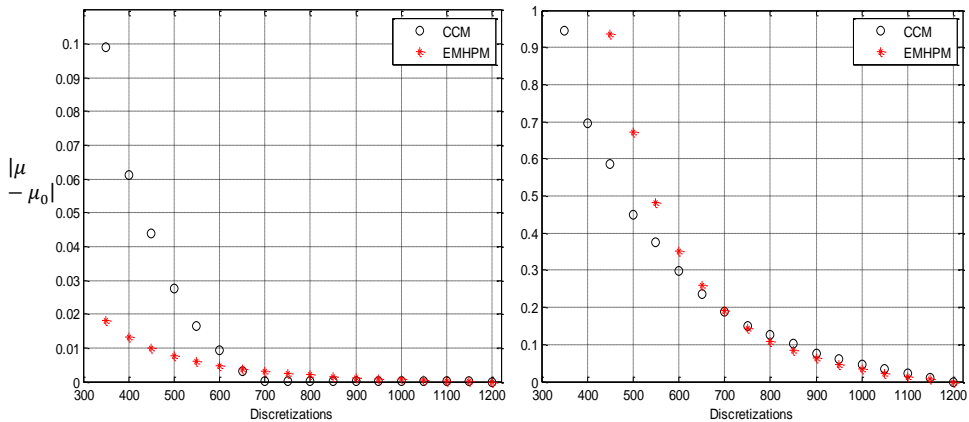


Fig 4. Convergence of the methods taking the eigenvalue ($f_z = 0.2$ mm/rev).
a. Stable ($V_c = 100$ m/min with $a_p = 0.6$ mm); b. Unstable ($V_c = 50$ m/min with $a_p = 0.8$ mm)

7. CONCLUSIONS

In this work, a new approach has been used to simulate the instability in longitudinal turning due to a non-rigid tool in the tangential direction. This type of chatter is not usually studied but may appear in external and internal turning of deep cylindrical parts. The stability boundaries using both methods profit from using variable cutting parameters with the cutting speed and depth of cut. The methods have been validated for a low machinability material but no influence of wear has been considered throughout the work. Some of the contributions are:

- Two numerical methods have been developed and used to obtain stability charts in longitudinal turning including 1-DOF dynamic modelling in tangential direction and dynamic characterization of the tool by means of the dynamic displacement factor ν .

- In chatter cases due to modes in tangential direction, the effect of cutting speed is more pronounced than in other common turning cases where the relative work-tool displacement takes place in chip thickness regenerative plane XZ. The envelope of the stability diagrams is no longer a horizontal or quasi-horizontal curve and high differences are found in terms of the maximum allowable depth of cut. However, machining at high cutting speeds is especially sensitive in terms of wear and tool breakage in difficult-to-cut alloys and a proper balance must be found for this parameter.

- Both methods presented have proved to be accurate since 90% of the tested points were in touch with reality. The accuracy has been manifested in all cases below 15-20% of the depth of cut. For equal number of discretizations, CCM is faster than EMHPM being the convergence of both methods similar.

- The main limitations are: on one hand, the simulations need information about the frequency vibrations. Due to this, dynamic tests are required not only for model validation but also to account for the vibration frequencies. On the other hand, computational times are a drawback of the methods, even more at low cutting speeds and/or high natural frequencies.

REFERENCES

- [1] T. Insperger y G. Stépán, "Semi-discretization method for delayed systems", *International Journal for Numerical Methods in Engineering*, vol. 55, p. 503–518, 2002.
- [2] T. Insperger y G. Stépán, "Updated semi-discretization method for periodic delay-differential equations with discrete delay", *International Journal for Numerical Methods in Engineering*, vol. 61, p. 117–141, 2004.
- [3] E. A. Butcher, P. Nindujarla y E. Bueler, "Stability of up- and down-milling using chebyshev collocation method", *ASME International Design Engineering Technical Conferences & Computers and Information in Engineering Conference*, pp. 1-10, 2005.
- [4] D. Olvera Trejo, A. Elías-Zúñiga, C. Rodríguez González, L. N. López de Lacalle, F. J. Campa Gómez y H. Siller Carrillo, "Estabilidad en el proceso de fresado a través del emhpm y validación experimental", *Memorias del XVII congreso internacional anual de la SOMIM 19 al 21 de septiembre*, pp. 789-796, 2012.
- [5] Y. Ding, L. Zhu, X. Zhang y H. Ding, "A full-discretization method for prediction of milling stability", *International Journal of Machine Tools & Manufacture*, vol. 50, p. 502–509, 2010.
- [6] M. Siddhpura y R. Paurbally, "A Review of Chatter Vibration Research in Turning", *International Journal of Machine Tools & Manufacture*, vol. 61, pp. 27-47, 2012.
- [7] G. Floquet, "Sur les équations différentielles linéaires à coefficients périodiques", *Annales de l'École Normale Supérieure*, vol. 12, p. 47–88, 1883.
- [8] E. A. Butcher, H. Ma, E. Bueler, V. Averina y Z. Szabo, "Stability of linear time-periodic delay-differential equations via Chebyshev polynomials", *International Journal for Numerical Methods in Engineering*, vol. 59, p. 895–922, 2004.

- [9] S. Tobias, *Machine Tool Vibration*, Nueva York: Wiley, 1965.
- [10] G. Urbikain, A. Fernández, L. López de Lacalle y M. Gutiérrez, "Stability lobes for general turning operations with slender tools", *International Journal of Machine Tools & Manufacture*, vol. 67, pp. 35-44, 2013.
- [11] T. Insperger, "Full-discretization and semi-discretization for milling stability prediction: Some comments" *International Journal of Machine Tools & Manufacture*, vol. 50, p. 658–662, 2010.

On the effective milling of large workpieces

Aleš Polzer, Miroslav Píška, Zdeněk Fiala

Institute of manufacturing technology, FME BUT, THE CZECH REPUBLIC

polzer@fme.vutbr.cz

piska@fme.vutbr.cz

fialaml@centrum.cz

ABSTRACT

Cutting tool geometry and cutting conditions have significant influence on cutting forces and loading of the machine, workpiece, tool and other clamping and supporting fixtures. Very high removal rates with productive milling heads can be reached. However, the problems arise when a structural workpiece is released and a stress relaxation follows. Some unexpected deformations out of tolerances can be found due to mechanical and thermal impacts of the machining operation. This paper deals with complex analyses of the active and passive forces acting on the workpiece, analyses of the specific cutting pressures for three different cutting heads, thermal fields measured with a thermo-camera, deflection of the workpiece material and analyses of the system vibrations during machining of two grades of steel (1.0553 and 1.1191) of large parts. The results have showed that it is very difficult to find a simple optimal solution, but an acceptable effective compromise with advanced CNC machining can be found.

KEYWORDS: Milling, stability, forces, thermal fields

1. Introduction

Machining with high speed (HSM) and feed rate (HFM) are modern technologies, which in comparison with conventional machining methods increase the machining efficiency, accuracy, quality of a workpiece and decrease of machining time [1]. However the modern methods of machining can cause vibration of a cutting tool or a low-rigidity workpiece, a workpiece structural release and a stress relaxation. The situation can be more complicated at steel blanks with some big holes that have been made e.g. by plasma cutting accompanied with non-equilibrium transformation phases at the surfaces and deformations up to several millimetres after machining can be expected.

2. Theory

A choice of the cutting tool geometry and cutting conditions is not easy because the thermal and mechanical loading of the systems when machining is changing and rigidity and a mass of the workpiece as well. Positive cutting tools tend to pull the cutting tool out of the spindle and contribute to the problems of chatter and undercutting in general [4]. In opposite, negative cutting tools can increase the material removal rate, but the passive force components initiate the workpiece vibrations significantly. Cutting tool geometry has significant influence on the direction of the cutting forces in relation to the stability of the workpiece [1-3].

Cutting forces can be measured with piezoelectric sensors today very effectively [3]. More complicated is the measurement of temperatures on the cutting tool or in the tool-workpiece interface. The surface temperature evaluation using thermal-camera (Fig. 1) can be expressed as

$$W_{tot} = \varepsilon\tau W_{obj} + (1 - \varepsilon)\tau W_{refl} + (1 - \tau)W_{atm} \quad (1)$$

where $\varepsilon\tau W_{obj}$ is received radiation from the object, $(1-\varepsilon)\tau W_{refl}$ is the reflected radiation from surrounding objects and $(1-\tau)W_{atm}$ is the radiation from the atmosphere [5,6].

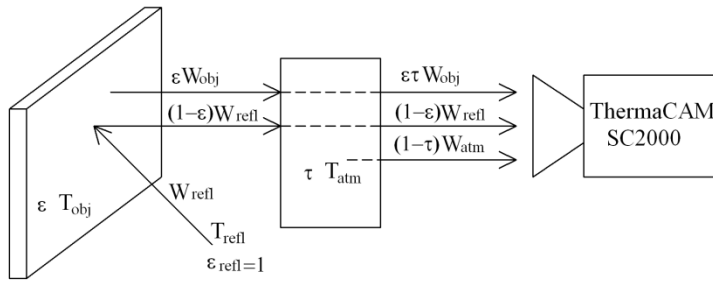


Fig.1. Scheme of the experimental measurements [5].

The first step in the tests was a measurement of the emissivity. The emissivity coefficient indicates the radiation of heat from a “grey body” according to the Stefan-Boltzmann’s Law [7], compared with the radiation of heat from the ideal “blackbody” and the emissivity coefficient $\varepsilon=1$ [6,8]:

$$\varepsilon_{\lambda} = \frac{W_{\lambda o}}{W_{\lambda b}} \quad , \quad (2)$$

where $W_{\lambda o}$ is the measured radiated power of an object and $W_{\lambda b}$ is the performance of a blackbody. However, the shiny tool surfaces could affect the results significantly.

3. Experimental works

The experimental measurements have been realized in two areas. First, cutting forces for the three milling heads (Table 2) were measured and used for stress-strain analyses. The

piezoelectric dynamometer Kistler 9275B fully controlled by a computer was used. Secondly, thermal field analyses of the milling process were recorded and analyzed - with the use of the thermal camera TermaCAM SC2000 – Fig. 2.

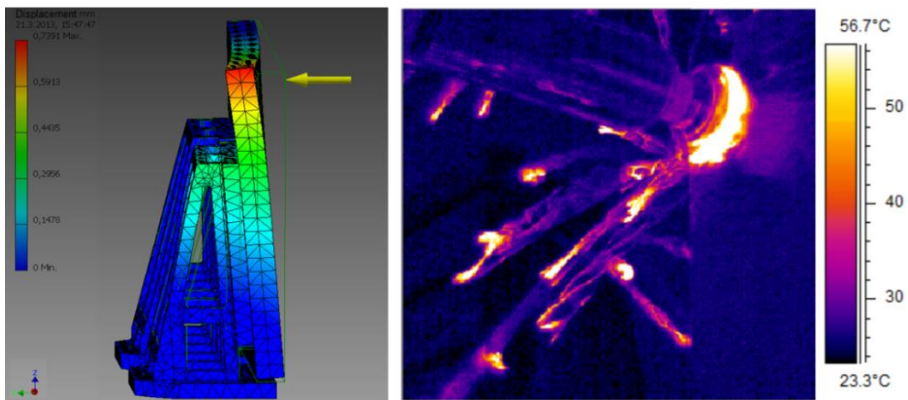


Fig.2. Deflections of the flexible workpiece and a thermal field of milling (workpiece – simple desk, fixation – the standard angle plate A1 101 B1/ZPS-Foundry, CZ).

3.1. Analysis of the cutting forces and tool wear

The main goal of the research was focused on the milling head selection and their suitability for machining of large flexible workpieces. The wear of cutting inserts and time series of cutting loading for two grades of steels have been analysed -Table 1, because the high levels of the cutting and passive forces affect the stress relaxation and vibration of flexible workpiece too. In production, those workpieces are machined by milling (roughing and finishing) of the flat surfaces and by milling and drilling of the holes and pockets (roughing and finishing).

Table 1. Machined materials – chemical compositions [wt.%] and mechanical properties.

	C	Si	Mn	Ni	P	S	Cr	Mo
DIN 1.0553	0.42 - 0.50	max. 0.4	0.5 - 0.8	max. 0.4	max. 0.03	max. 0.035	max. 0.4	max. 0.1
	C	Si	Mn	N	P	S	Cu	CEV
DIN 1.1191	0.22	max. 0.55	max.1.6	max. 0.012	max. 0.035	max. 0.035	max. 0.55	max. 0.47
	R_{p0.2} [MPa]	R_{eH} [MPa]	R_m [MPa]	HB [-]	A [%]	Z [%]	KV - transv. [J]	KV - long. [J]
DIN 1.0553	310	340	580	255	8	40	14	25-50
DIN 1.1191	300	275	600	258	10	42	15	27

Table 2. Types of milling heads and cutting conditions.

Type of milling head	Mitsubishi ASX445-125 B08R (T1)	Hitachi ASRF-4066 RM-5-27 (T2)	Kennametal 63A06RS90 ED14D (T3)
Diameter [mm]	125	66	63
Cutting insert	SEMT13TAGSN- JH VP15TF	SDMT1205 ZDTN JX1045	EDPT140412 PDERHD
Cutting speed [m/min]	176	186	140
Feed per tooth [mm]	0.36	2.00	0.30
Axial depth of cut [mm]	2.00	1.50	3.00
Radial depth of cut [mm]	80	48	48

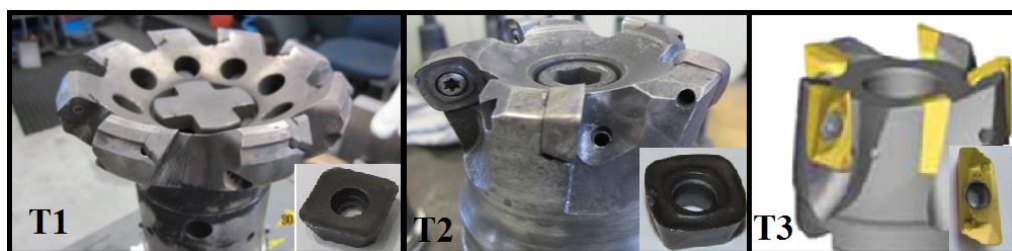


Fig. 3. Tested milling heads (an overview).

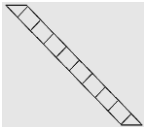
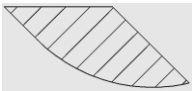
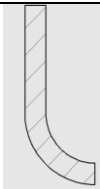
Table 3. Cutting geometry and material removal rates for the tested tools.

Tool number	Cutting tool	Rake angle $\gamma_o [^\circ]$	Flank angle $\alpha_o [^\circ]$	Main cutting angle $K_r [^\circ]$
1	Milling cutter	20	8	45
2	High-feed cutter	7	8	variable
3	End mill tool	7	8	90

Cutting tests with the tools were performed at the vertical milling machine FV 50 (TOS Kurim) – Table 2. All milling heads were fitted by one new or worn-out cutting insert. Dimensions of the workpiece were 200x90x200 mm with irregular sides - Fig. 5. According to a recommendation of the tool producer A the dry machining was set up. Geometry of milling heads and cutting inserts are shown in Fig. 3, Table 3.

However, different cutting conditions were set for all milling heads. Nevertheless, the chip cross-sections depend on the cutting conditions too, so the real values were calculated with the Autodesk software - Table 4. Due to the different cutting conditions, the cutting forces cannot be compared so the specific cutting energy was used to compare the cutting performance of the tools.

Table 4. Non-deformed chip cross sections shapes and values (simplified).

Milling head insert	T1	T2	T3
Shape of the cross section			
Chip cross-section [mm ²]	0.72	2.786	1.035
Chip thickness eq. [mm]	0.23	3.92	0.29

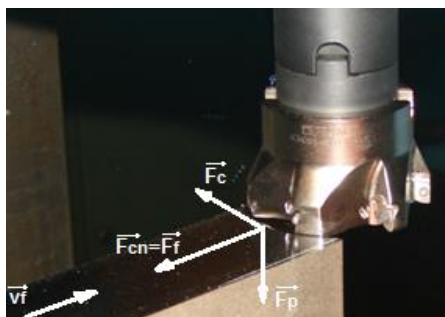


Fig. 4. Cutting forces in face milling.

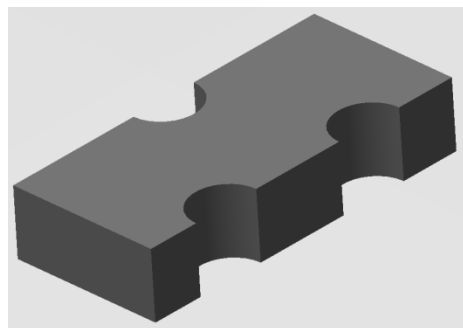


Fig. 5. The shape of the workpiece.

Results

The experimental machining was carried out in two machining strategies, both for up and down milling. The instant decreases of the cutting forces were observed because of irregular shape of the workpiece - Fig. 4,5.

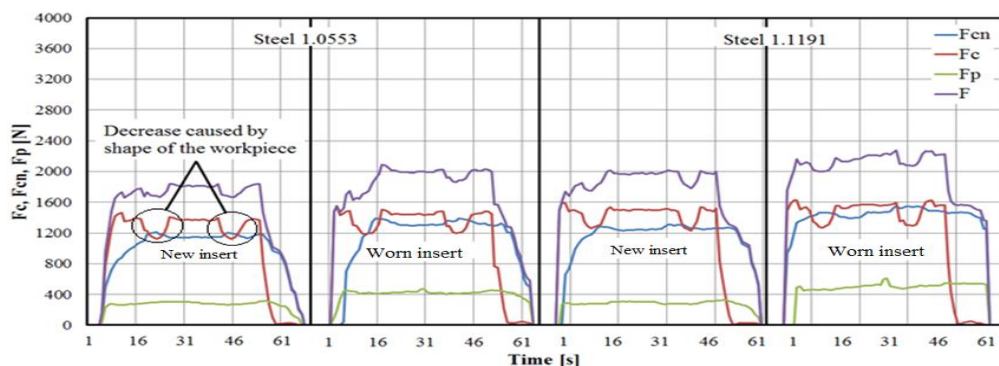


Fig. 6. Time series of the forces (down milling) for the milling head T1.

The comparison of machined materials showed minimal differences (up to 100 N only) in the cutting forces when machining by the milling head T1 with sharp and worn cutting inserts – Fig. 6,7.

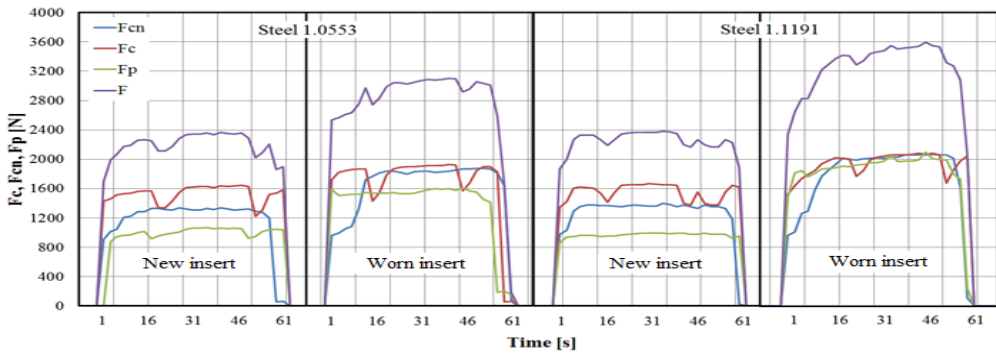


Fig.7. Time series of the forces (down milling) for the milling head T2.

Some similar differences of the cutting forces were observed at the machining by the milling heads with sharp (Fig. 7) and worn cutting inserts. The comparison of machined materials showed minimal differences (up to 320 N) in the cutting forces compare to the machining with sharp inserts. Statistically significant differences ($\alpha=0.05$) of the cutting forces were observed at machining by the milling head T2 with worn cutting tool insert. The passive force was higher about 400 N for machining with wear cutting insert of the steel 1.1191 compared to the steel 1.0553. Similar differences were found for up milling – Fig. 8.

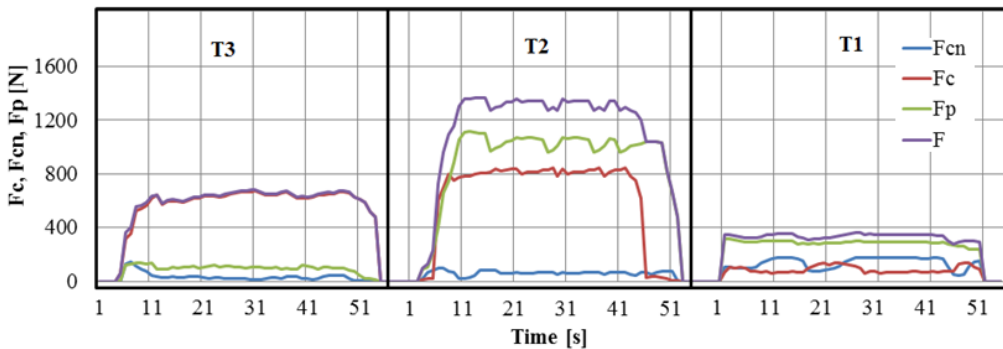


Fig. 8. Time series of the forces at machining of steel 1.0553 (up milling) for all tested milling heads.

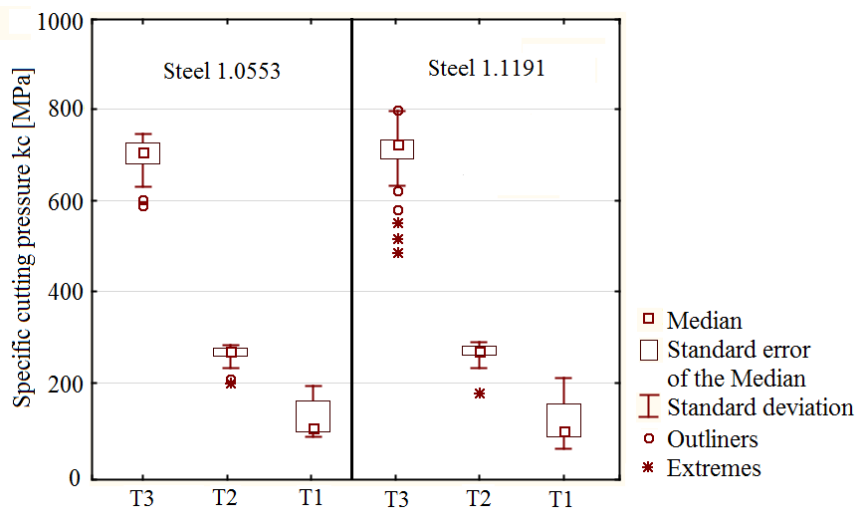


Fig. 9. Boxplots and whiskers diagrams of the specific cutting pressures.

The combination of various cutting chip cross sections and the cutting conditions result in the different force load of tested milling heads. The highest values of the cutting forces were measured for the tool T2, but the highest specific cutting force was calculated for milling head T3 – Fig. 9. A typical mechanism of wear was abrasive, with some marks of chipping due to chattering for all tested inserts.

3.2. Thermal field analysis of milling process

The second part of tests deals with complex analysis of the thermal fields measured with the thermo-camera for the three different cutting heads in the real production conditions with WRD 170 machine (TOS Varnsdorf) - Table 5. However, a big problem of the workpiece had been arising in deflections and torsions after removal of workpiece clamps after machining with the tool T2 (up to 1.5 mm).

Table 5. Cutting conditions for the cutting tools.

Tool No.	Cutting tool	MRR [cm ³ /min]	Number of inserts [-]	Cutting speed v_c [m/min]	Feed per tooth f_z [mm]	Depth of cut a_p [mm]	Width of cut a_e [mm]
1	Milling cutter Kr = 45°	180	8	196	0.3	100	1.5
2	High-feed cutter	625	5	180	2	48	1.5
3	End mill cutter Kr = 90°	122	6	80	0.42	48	2.5

Comment: All tools performed the down milling.

Material removal rate was calculated according to the equation:

$$MRR = \frac{a_p \cdot a_e \cdot v_f}{1000}, \quad (3)$$

where a_p is depth of cut, a_e is width of cut and v_f is feed rate (mm/min). The cutting conditions for face milling are listed in Table 5 (workpiece 1.0570; size 800x550x60 mm).

The next step was focused on the surface temperatures of the cutting tools in a cutting action. Optional parameters for thermo-camera TermaCAM SC2000 in the experiments were set as following:

- relative humidity 45 %,
- atmospheric temperature 24.5 °C,
- distance between camera and the object 1 m,
- temperature range from -40 to +120 °C for workpiece measuring,
- secondary option from 0 to 500 °C for cutting tool and chip measuring.

Measuring were carried out in the wavelength band $\lambda = 7.5\text{-}12.0 \mu\text{m}$.

The typical surface temperatures of the cutting inserts according to the time of machining can be seen in Fig.10. Here, the face milling operation with worn cutting tools (4 cuts are gathered in the picture) is shown.

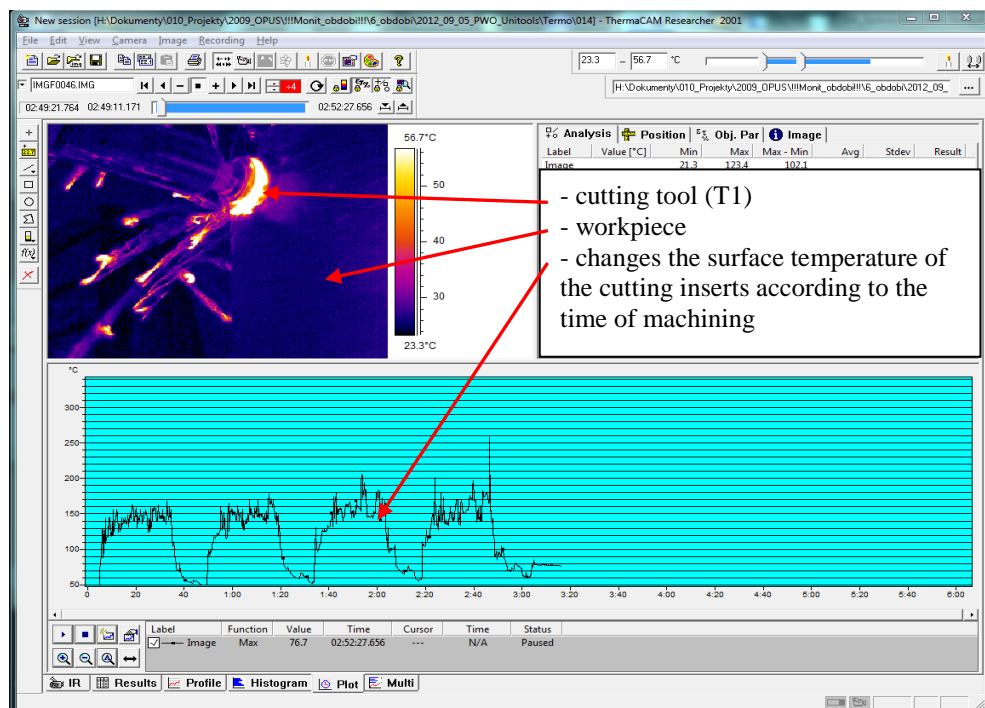


Fig. 10. An example of the temperature time series for a cutting tool.

Results

The rise of average temperatures can be seen in the Fig. 11. Statistical values of the temperatures for new and worn tools are listed in Table 6 and Table 7.

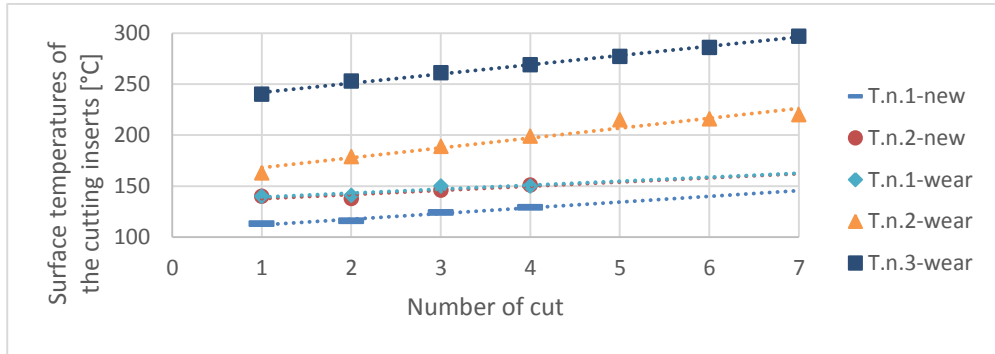


Fig. 11. Average temperatures of the cutting tools as a function of the cuts.

Table 6. Temperature statistical parameters of the new cutting tools.

Tool no.	Statistical parameter	Number of cut						
		1	2	3	4	5	6	7
1	Average	112	116	124	129	-	-	-
	Min. value	76	76	77	100	-	-	-
	Max. value	151	139	174	158	-	-	-
	Standard deviation	11	13	18	13	-	-	-
2	Average	140	138	146	151	-	-	-
	Min. value	88	106	120	122	-	-	-
	Max. value	197	180	185	192	-	-	-
	Standard deviation	19	18	19	18	-	-	-
3	Average	160	166	182	189	-	-	-
	Min. value	135	141	152	166	-	-	-
	Max. value	194	204	215	235	-	-	-
	Standard deviation	21	24	21	26	-	-	-

Table 7. Temperature statistical parameters of the worn cutting tools.

Tool No.	Statistical parameter	Number of cut						
		1	2	3	4	5	6	7
1	Average	140	141	150	150	-	-	-
	Min. value	88	90	95	89	-	-	-
	Max. value	168	179	205	258	-	-	-
	Standard deviation	14	18	21	23	-	-	-
2	Average	163	179	189	199	215	216	220
	Min. value	114	112	92	135	173	153	183
	Max. value	212	222	244	254	249	257	260
	Standard deviation	28	31	37	30	22	26	21
3	Average	240	253	261	269	277	286	297
	Min. value	135	161	198	219	240	247	228
	Max. value	294	294	302	310	309	319	336
	Standard deviation	26	24	21	16	13	12	17

4. Conclusions

It is difficult to compare so different cutting tools and conditions, however, some useful conclusions can be made:

- ***analysis of cutting forces and influence of workpiece material***

when machining with sharp cutting inserts, the different grades of the tested steels affect the average cutting forces by 2% only. The tool T2 was assessed as the most productive milling cutter ($MRR = 625 \text{ cm}^3/\text{min}$) amidst of the tested cutting tools. However, the effect of wear caused significant differences of the force loading, esp. in passive forces in milling with the head T2 and complicated residual deformations follow after releasing the workpiece from the jigs. Nevertheless, the specific cutting force was the most favourable with standard milling head T1 and relatively low deformations were observed (below 0.2–0.4 mm);

- ***temperature field analyses of the milling process***

The minimal temperatures were recorded for the cutting tool T1 and sharp cutting inserts ($140 \pm 14 \text{ }^\circ\text{C}$), the highest temperature were measured for milling head T3 and worn inserts ($269 \pm 18.2 \text{ }^\circ\text{C}$). For information, the surface temperature of the workpiece reached for all sharp cutting tools values in the range $30 \pm 5 \text{ }^\circ\text{C}$, for the worn tools $32 \pm 6 \text{ }^\circ\text{C}$.

ACKNOWLEDGEMENTS

This research work was supported by the BUT, Faculty of Mechanical Engineering, Brno, Specific research 2011, with the grants “*Research of advanced CNC methods for perspective applications*”, FSI-S-11-28, ID 1438 and the BUT Specific Research 2013, “*Analysis of specific cutting force for new materials*”, FSI-J-13-2135, ID 2135.

REFERENCES

- [1] Schulz, H., Moriawaki T. High speed machining, Annal. of the CIRP, 1992, t. 41, nr 2, s. 637 – 642.
- [2] Cus, F. The inclusion of geometrical shape of the cutter into the optimization of milling process. Int J Advance Manufacturing Tech, 16 (2000), pp. 392–403
- [3] Forejt, M. - Piska, M.: Theory of Machining, Forming and Cutting Tools, pp.226, CERM, Brno, 2006.
- [4] STAHL, Jan-Eric. SECO TOOLS AB. *Metal Cutting Theories and Models*. Lund, Sweden: Lund University, Metal Cutting Theories and Models. ISBN 978-91-637-1336-1.
- [5] User's Guide. FLIR T6xx. 2011. T559669.
- [6] YENER, Yaman. *Heat conduction*. 4th ed. New York: Taylor, 2008, xix, 434 s. ISBN 978-1-59169-046-7.
- [7] Stefan–Boltzmann law. In: *Wikipedia: the free encyclopedia* [online]. San Francisco (CA): Wikimedia Foundation, 2001- [cit. 2013-09-08]. Dostupné z: http://en.wikipedia.org/wiki/Stefan%E2%80%93Boltzmann_law
- [8] Emissivity Coefficients of some common Materials. *The Engineering ToolBox* [online]. 2013 [cit. 2013-09-08]. Dostupné z: http://www.engineeringtoolbox.com/emissivity-coefficients-d_447.html

New method of dynamic cutting force coefficients determination

Krzysztof Jemielniak, Mirosław Nejman, Dominika Śniegulska-Grądzka,
Rafał Wypysiński

Warsaw University of Technology, Poland
k.jemielniak@wip.pw.edu.pl

ABSTRACT

The paper presents the methodology and special test rig for instantaneous cutting force measurement under variable uncut chip thickness. It is based on elastically supported dynamometer vibrating with the tool. Inertial forces influencing the cutting force measurement are compensated by simultaneous measurement of vibrating dynamometer acceleration. The experiments were conducted using own, innovative and patented method and test rig.

KEYWORDS: dynamics characteristic of cutting process, cutting forces, chatter

1. INTRODUCTION

Avoiding self-excited vibrations is necessary for the proper machining process. Prediction of stability limit is based on characteristics of cutting forces and machine tool system. The latter is usually determined by applying the modal analysis. Dynamic characteristic of cutting force is the force dependence on uncut chip thickness, and tool geometry changing due to relative displacements between the workpiece and the tool. Despite, the quite complex models of that characteristic [e.g. 4, 5, 9] have been known since long time, the most popular is Altintas linear model [2]. In that model, the dynamic forces are proportional to the changes of the uncut thickness:

$$F_{jd} = k_{jd} b h_d \quad (1)$$

where, F_{jd} - dynamic component of cutting force F_t or F_r , $j = t$ or r - index of direction tangential or orthogonal to cutting speed, k_{jd} - dynamic cutting coefficient; b - width of the cut; h_d - dynamic component of uncut chip thickness.

This approach is very easy to use, however it has two main drawbacks. Firstly, the dynamic cutting coefficient is assumed to be constant only for relatively significant uncut chip thickness. When it is close to zero – what occur during milling at the entrance or exit from the material, this model is very inaccurate. Secondly, this model does not take into account damping of the cutting process. This damping – as it is assumed nowadays – has a significant impact on the stability [3,7,8,10]. The damping of the cutting process is a result of interfering

of the flank surface with the machined surface that takes place only in a limited part of the oscillation period, when the tool moves towards the workpiece. In analytical prediction of stability limit the damping component of the cutting force, is usually simplified to be proportional to the inclination of effective cutting speed which is proportional to the vibration velocity r' , which means averaging over the entire vibration period. Thus the model of dynamic cutting force becomes [4]:

$$F_{jd} = b(k_{jd}h_d - c_j r') \quad (2)$$

where r' - velocity of vibration in the uncut chip thickness direction; c_j - damping coefficient of the j -th cutting force.

Regardless, of the assumed model, dynamic cutting coefficients (k_{jd} and c_j) are generally identified from static tests (without vibrations) [2, 4, 5, 9] or using theoretical modelling of interference between flank and machined surfaces [3, 8, 10, 11]. An interesting approach was presented in the [1] where coefficients of a new dynamic cutting force model were identified from controlled oscillating tests with the aid of a special test rig equipped with a fast tool servo. The tool servo was rigidly mounted on the turret of the machine. Three-component load cell was integrated in the tool holder to measure the dynamic cutting forces, the displacement of the tool was measured with a laser sensor. The connection between the load cell and tool servo was also rigid. While the CNC lathe provided the feed motion and nominal value of uncut chip thickness h_0 , the fast tool servo generated vibrations at the desired frequency and amplitude. The inner and outer waves were synchronized to be in phase by generating an integer number of vibration cycles per spindle revolution. The tool displacement and cutting forces were measured simultaneously. The inertial forces originating from the mass between the load cell and the cutting edge, inevitably acting on the load cell were not taken into account.

The paper presents an innovative method of determination of dynamic cutting force coefficients based on direct measurements of cutting forces acting on the vibrating tool during cutting. A special test rig with elastically supported dynamometer vibrating with the tool [6] was used here. The method allows measuring instantaneous cutting forces related to the instantaneous uncut chip thickness and vibration speed responsible for cutting process damping. This creates new possibilities for measuring, modelling and verification of any dynamic cutting force coefficients.

2. THE PRINCIPLE OF DIRECT MEASUREMENTS OF CUTTING FORCES DURING VIBRATIONS

The main idea of the new method of dynamic cutting force coefficients identification is a direct measurement of the cutting forces during relative displacements between the workpiece and the tool. That means that the cutting tool has to be rigidly fixed to the dynamometer supported by flexible elements. Thus the dynamometer directly measures the cutting forces acting on the tool under vibratory changes of uncut chip thickness and the tool geometry. The idea of the test stand is presented on Fig. 1. The top and the bottom support plates are connected with flat springs that assure that the system stiffness in the uncut chip thickness direction r is much lower than in other directions. The triaxial dynamometer with accelerometer mounted on it is placed on the top plate. Furthermore, a contactless inductive displacement sensor rigidly mounted to the base is used for measuring the displacements of the dynamometer.

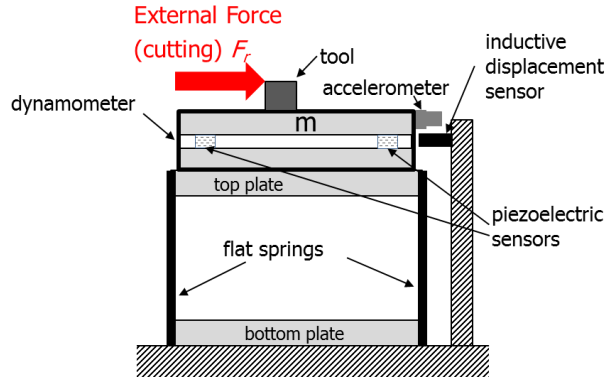


Fig.1. The concept of the test rig for measurements of the dynamic components of the cutting forces.

The dynamometer signal is proportional to the forces acting on the piezoelectric transducers. In a classic application, when the dynamometer is rigidly mounted to the base (it is not moving), the measured signal is proportional to the external force (e.g. cutting force). However, when the dynamometer vibrates, then the transducers are affected by the inertial force proportional to the mass m of the upper part of the dynamometer and elements mounted on top of it and acceleration of the oscillatory motion. In this case the dynamometer is working as an accelerometer. This inertial force adds to the real external force resulting in the changed measured force:

$$F_z = F_r + F_a = F_r + ma \quad (3)$$

where F_z - measured “force” (signal obtained from the dynamometer multiplied by the gain coefficient); F_r - real external force affecting on the dynamometer; F_a - inertial force acting on upper part of the dynamometers and items mounted on it, m - modal mass of the upper part of the dynamometers and items mounted on it; a - acceleration of the dynamometer.

In order to measure the real force acting on the dynamometer (the cutting force in this case) the mass m must be determined and the acceleration of the oscillation motion needs to be measured. Although the second task is relatively easy, the determination of the mass is more difficult.

If the unloaded device is stimulated for free vibration by a hit, the dynamometer registers the hit force first, and then the dynamometer oscillations. The vibrations of device will be closed to self-vibration frequency that is in the practical range about 270 Hz. Fig. 1a presents the exciting force F_w (signal from the modal hammer), signal F_z measured by the dynamometer and the acceleration signal a taken from the accelerometer. After removing the initial part of the measured signals containing the modal hammer impact, signals registered during the free oscillations of dynamometer are obtained. For this period there is no external force acting on the dynamometer, and the registered signal F_z is proportional to the mass m and measured acceleration a . Applying linear regression to these data and equation:

$$F_z = F_a = ma \quad (4)$$

the modal mass m can be found – see Fig.2.b. Calculated inertial force F_a is also presented in Fig.2a. Now the real external force F_r acting on the dynamometer can be calculated as:

$$F_r = F_z - F_a = F_z - ma \quad (5)$$

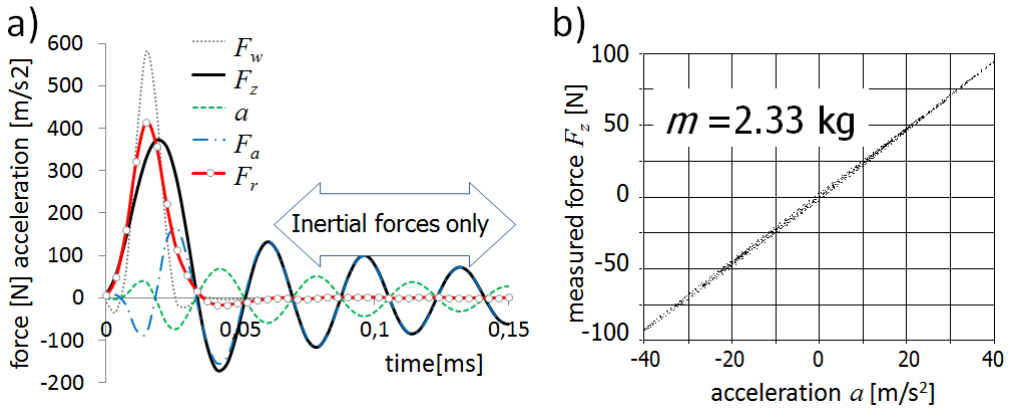


Fig. 1. Determination of the real external force impacting the dynamometer: a) measured and calculated signals b) measured inertial force vs. acceleration.

The real force F_r is presented on Fig. 1a, with the bold line with circle points. As can be seen there, the influence of the inertial force has been eliminated. The calculated real force corresponds to the force measurements taken from the hammer taking into account much larger inertia of the dynamometer than those of used hammer.

The modal mass obtained this way and the formula (5) were used also used for removing the influence of the dynamometer oscillations on the force measurements during cutting. Fig. 1 presents the results of measuring cutting forces with use of oscillating dynamometer: direct measurements F_z and the calculated real force F_r and other signals.

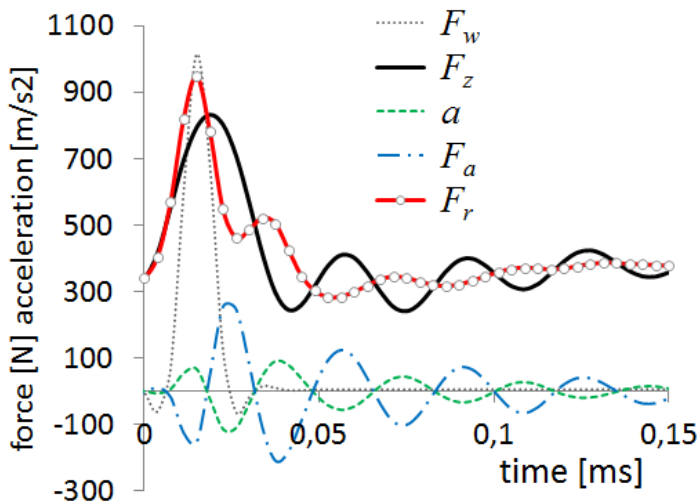


Fig. 3. Measurements of the real external force acting on the dynamometer during cutting.

3. EXPERIMENTAL VERIFICATION

3.1. Experimental setup

Fig. 4 presents the test rig for measuring cutting forces during vibrations, based on the concept presented in **Fel! Hittar inte referenskölla**. [6]. The base unit, with the dynamometer supported on flat springs, is fixed onto T-slots of slide lathe (for conventional lathes) or to the milling machine table. Furthermore, the oscillations of the dynamometer and elements mounted on it are registered by the contact-less displacements sensors and accelerometer. The complete measuring chain consists of the following sensors:

- KISTLER type 9257BA dynamometer with 5233A1 amplifier
- Brüel & Kjær 8207 modal hammer with rubber ending
- Brüel & Kjær 4514-001 single-axis accelerometer mounted on dynamometer and connected to a Brüel & Kjær NEXUS 2693 amplifier
- OT18 inductive sensors mounted housing associated with the rigid base; connected to a dedicated amplifier

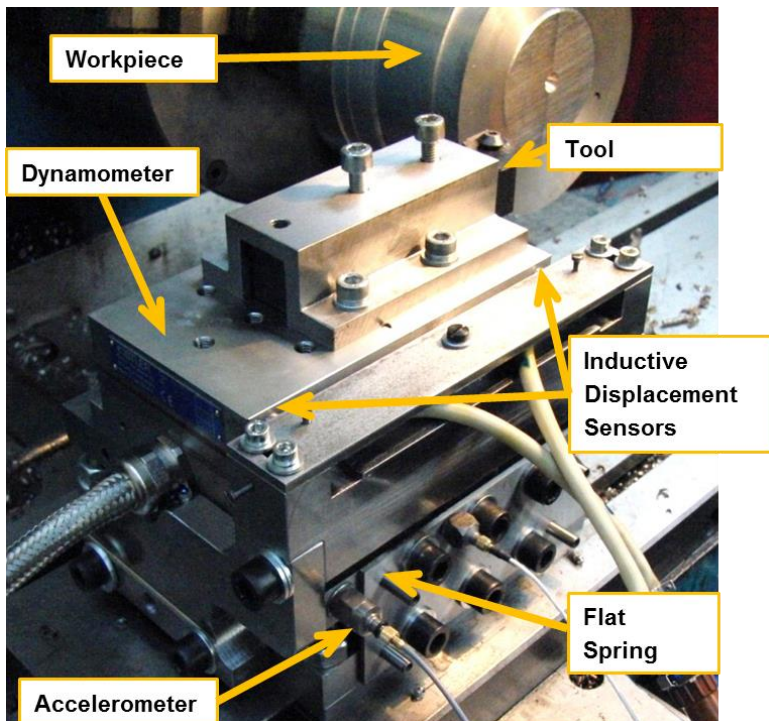


Fig. 4. Test rig mounted on the lathe.

Modal analysis of the test rig proved that this is 1DOF system and only one mode of vibrations occurs. Conventional TUD 100 lathe was used with the STGCR2525-M16 turning tool with PAFANA TCMT 16T308 inserts. Approach angle $\kappa_r = 90^\circ$ thus the feed (0.08mm/rev) was equal to nominal uncut chip thickness h_0 and the depth of cut $a_p = 2\text{mm}$ was equal to the width of cut. The cutting speed was $v_c = 60\text{m/min}$ and the workpiece material was C45 steel.

3.2. Results and discussion

Each test started from the idle feed during which series of modal hammer hits at the dynamometer in a direction of the feed force were executed. These measurements were used for automatic evaluation of the modal mass m necessary for calculation of the inertial force. Next, when the actual cutting started another sequence of hits was executed. The time between the hits was big enough to complete dumping of the free vibrations excited by the hammer hits. It was also higher than time of several workpiece revolutions, and the cutting was stable thus there was no influence of the wave left on the workpiece surface (outer modulation). Thus measured displacement of the dynamometer and the tool fixed on top of it were exactly equal to the h_d – dynamic component of uncut chip thickness. Example signals registered from the dynamometer during such experiment are shown in Fig.5.

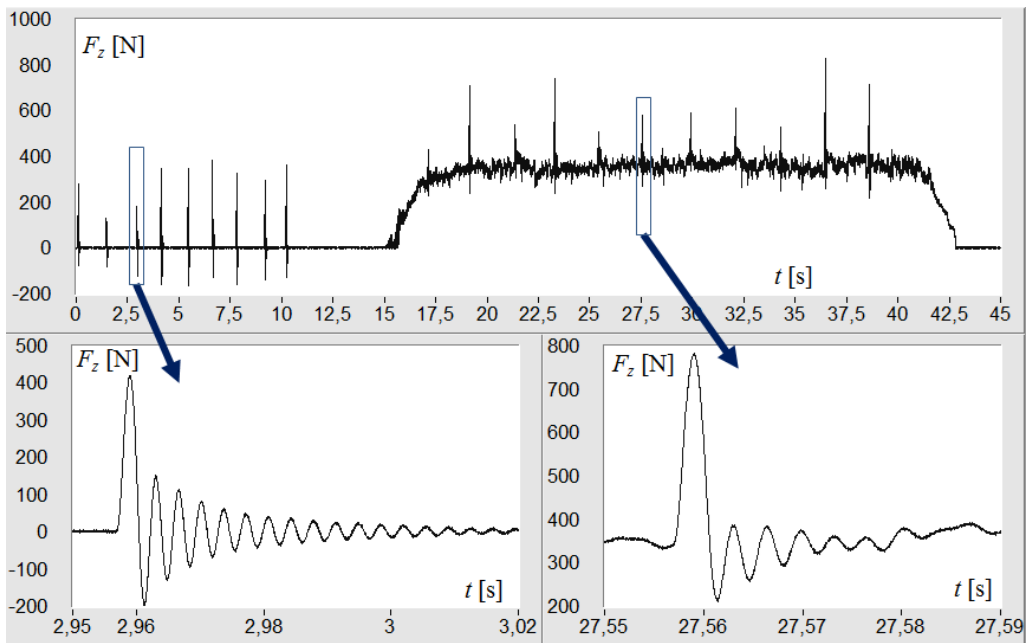


Fig.5. The measured force during idling and cutting.

The developed software automatically selects the signal segments containing hits and rejects those which are not correct (overload, too weak, double hits etc.) All other calculations are also executed automatically up to presenting real radial force acting on the tool during cutting.

The real radial force acting on the tool vibrating freely during cutting versus dynamic component of uncut chip thickness ($h_d = -r$) was presented in Fig. 6a. Ellipse formed by this plot evidently shows the damping of the cutting force. At first approximation it can be described by the formula:

$$F_{rd} = F_{r0} + b(k_{rd} h_d - c_r r') = F_{r0} - b k_{rd} r - b c_r r' \quad (6)$$

where F_{rd} - dynamic component of the feed force, r - displacement in a direction opposite to the feed direction; r' - velocity of the displacement in the r direction, F_{r0} - feed force static component.

Dynamic coefficients of cutting force k_{rd} and c_r can be obtained using this formula and linear regression. The obtained values of the coefficients were applied for modelling of the dynamic feed force:

$$F_{r_mod} = F_{rk} + F_{rc} = -bk_{rd} r - bc_r r' \quad (7)$$

Fig. 6b presents modeled stiffness F_{rk} and damping F_{rc} components of the dynamic feed force, together with their sum (model F_{r_mod}) and measured dynamic feed force F_r . Despite the formula (6) describes quite simple model, it can be taken as a starting point for the presented method validation. In the nearest future more precise model will be built based on the direct measurements of dynamic cutting forces.

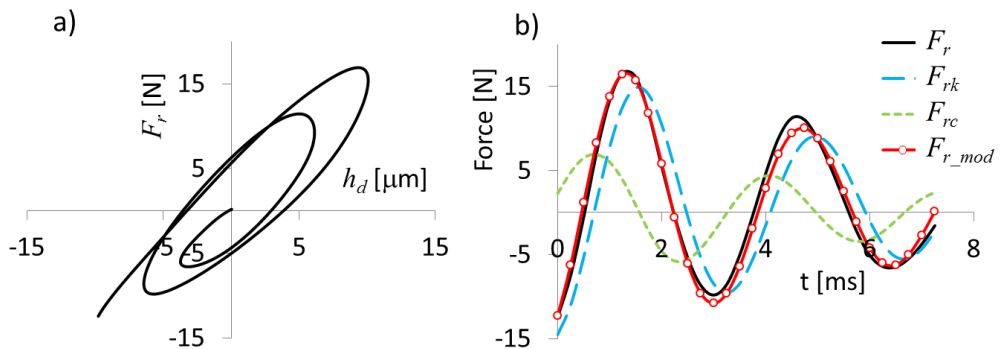


Fig.6. a) Correlation between dynamic radial force F_r and dynamic uncut chip thickness h_d ; b) measured and modelled dynamic radial force.

Table 1 presents example results of calculating dynamic cutting process coefficients for $v_c = 19\text{m/min}$, $a_p = 3\text{mm}$, $f = 0.08\text{mm/rev}$.

Table 1. Example results of calculating dynamic cutting process coefficients.

F_0 [N]	k_{rd} [N/mm ²]	c_r [Ns/mm ²]	correlation coefficient
371,7	1317,9	0,378	0,842
377,6	1597,9	0,302	0,679
371,4	1486,6	0,377	0,990

4. SUMMARY

The performed experiments proved correctness and usability of the described test rig. The developed methodology enables much more accurate determination of dynamic cutting force coefficients, analyzing their dependence on various factors neglected so far as well as any nonlinearity. The described methodology requires further improvements, especially in the area of analysis and interpretation of the collected force signals as they are naturally randomly

disturbed by the cutting process. Furthermore, as the inertial force is much higher than the dynamic component of the cutting force, special care in signal processing is needed.

The presented results are just preliminary. The experiments will be repeated for a wider range of cutting parameters, different cutting edge geometries. Registration of precise angular position of the workpiece will allow to make the direct measurement of dynamic cutting forces during the actual chatter, when both inner and outer modulation of uncut chip thickness affects the force.

ACKNOWLEDGEMENTS

Financial support of Structural Funds in the Operational Programme - Innovative Economy (IE OP) financed from the European Regional Development Fund - Project "Modern material technologies in aerospace industry", Nr POIG.01.01.02-00-015/08-00 is gratefully acknowledged.

REFERENCES

- [1] Y. Altintas, M. Eynian, H. Onozuka, "Identification of dynamic cutting force coefficients and chatter stability with process damping", *CIRP Annals - Manufacturing Technology* vol. 57, 2008, 371–374
- [2] E. Budak, Y. Altintas, E.J.A Armarego, "Prediction of Milling Force Coefficients From Orthogonal Cutting Data", *Journal of Manufacturing Science and Engineering*. 118, 1996, 216-224
- [3] E. Budak, L.T. Tunc, "Identification and Modeling of Process Damping in Turning and Milling Using a New Approach", *CIRP Annals - Manufacturing Technology*, vol. 59, 2010, 403–408
- [4] M.K. Das, S.A. Tobias, "The Relation Between the Static and the Dynamic Cutting of Metals", *International Journal of Machine Tool Design and Research* vol. 7, 1967,s. 63-89
- [5] K. Jemielniak, "Modelling of Dynamic Cutting Coefficients in Three - Dimensional Cutting", *International Journal of Machine Tools and Manufacture*, vol. 32, 1992, 509-519
- [6] K. Jemielniak, M. Nejman, D. Śniegulska-Grądzka, R. Wypysiński, „Urządzenie do pomiaru dynamicznych składowych sił skrawania” („Device for dynamic components of cutting force measurement”). Patent P-398818, April 15, 2012.
- [7] K. Jemielniak, M. Nejman, D. Śniegulska-Grądzka, "Analityczne i numeryczne wyznaczanie granicy stabilności przy toczeniu", *Inżynieria maszyn*, vol. 17, no. 1, 2012, str. 81-92
- [8] V. Sellmeier, B. Denkena, "High speed process damping in milling", *CIRP Journal of Manufacturing Science and Technology*, vol. 5, 2012, 8–19
- [9] S. A. Tobias, W. Fishwick, "Theory of Regenerative Machine Tool Chatter" *The Engineer*, vol. 205, 1958, pp. 199-203, 1958
- [10] L.T. Tunc, E. Budak, "Effect of cutting conditions and tool geometry on process damping in machining", *International Journal of Machine Tools&Manufacture*, vol. 57, 2012, 10–19
- [11] E. Turkes, et al. "A new process damping model for chatter vibration", *Measurement*, vol. 44, 2011, 1342–1348

Model-Based Identification of Chatter Marks during Cylindrical Grinding

Paolo Parenti¹, Marco Leonesio², Alberto Cassinari²,
Giacomo Bianchi², Michele Monno¹

¹ Department of Mechanical Engineering, Politecnico of Milan, via La Masa 1, Milan, Italy

² CNR, Institute of Industrial Technology and Automation, via Bassini 15, Milan, Italy
paolo.parenti@polimi.it

ABSTRACT

The following paper presents an online model-based monitoring algorithm that identifies and quantifies the level of waviness caused by grinding chatter exploiting accelerations measured on the machine. A Weighted Least Squares method has been applied in the frequency domain that leads to a clear interpretation of the forcing effect caused by the waviness at particular frequency components exciting the machine structure. A sensitivity analysis has been carried out in order to define the limits of applicability and the precision of the approach in relation to the adopted analytical models. The development has been supported by simulations produced by an integrated model implemented in Matlab/Simulink® environment. Finally, experiments on the real machine confirmed the good estimation performance of the algorithm.

KEYWORDS: surface waviness, grinding chatter, process monitoring

1. INTRODUCTION

Grinding process is considered one of the most complex chipping process to model due to the simultaneous presence of critical features like the undefined cutting edge, the wheel geometry subjected to non-uniform wear, the process nonlinearities, the thermal problems and many other aspects. Furthermore as in many other chipping process like turning and milling, process vibration play a key role and frequently represent the main limitation for reaching precise and high-productive cuttings.

Grinding process vibration can be ascribed to different origins such as unbalances, external excitations and regenerative chatter: all of these phenomena produce the same type of defect, i.e. the so-called chatter marks on the ground workpiece and under certain circumstances (i.e. wheel regenerative chatter) on the wheel surface. The possibility to determine the presence of waviness and then characterize the machining state, by means of the on-line monitoring algorithms developed in this paper represents unquestionably a key tool for optimizing the machining operations.

Many different approaches have been proposed over the years regarding the monitoring of waviness and the related grinding chatter [1]. Two basic types exist: the direct and indirect approach. Direct methods involve the direct measurement of the wheel and workpiece waviness. The measurements are normally carried out in post-process by means of different contact or contactless transducers (e.g. LVDT), high resolution cameras, scattered light sensors, pressure transducers, or specific profile and roundness measurement equipment [2, 3]. The identification of workpiece waviness in cylindrical grinding process have been accomplished, by the authors in [4] exploiting the Wavelet transform. This analysis is applied to post-process measurements of ground surface obtained by a mechanical stylus profiler. Some researchers have developed in-process direct measuring systems (either for wheel and workpiece) for real-time monitoring purposes. In [5] an optical sensor that exploits the principle of laser triangulation, is used to measure the topography of the wheel including chatter waviness during a cylindrical external grinding process. While direct probing of the wheel surface becomes impossible because of probe wear when scanning the profile approaches, the proposed optical method does not suffer of this limitation and relies on the capacity of the optical sensor to measure very little relative displacements between the sensor head and the target surface. In [7] the authors have studied how, a dynamic run-out of the wheel affects the waviness pattern of the resulting workpiece in surface grinding. They showed that an optimal phase-shift between wheel rotation and table feed exists to minimize the generation of the waviness (and then optimize the optical appearance) on the ground surface. The measurement has been made in post-process by confocal-white-light microscopy surface scans. In general the optical solutions demonstrated to be very accurate and reliable, but have a main important limitation related to the protection of the sensor heads against coolants and other process residues and with the sensors fixtures on the machines that need to be very stiff and isolated by the surrounding vibration (quite demanding in for industrial application). Their cost is also a relevant issue [8].

On the other side grinding chatter monitoring can be performed through the so-called indirect methods which relies on the analysis of machining process parameters and sensor signals. As stated by many papers, grinding force measurements can definitely lead to the determination of the chatter occurrence [1,9,10]. Since grinding force cannot always be obtained easily in industrial operations, the use of accelerometers to detect chatter have become the most used method [2,11]. Acoustic emission sensors are also suitable to detect chatter vibrations in grinding [10,12]. An effective surface quality assessment technique with regard to chatter marks, has been proposed by the author in [13] for roll grinding machines. This technique adopts a frequency normalized spectrum and rely on the accelerometer readings. Actually, it is one of the few that tries to relate quantitatively vibration measurements acquired during cutting with physical features of the resulting surface waviness.

The objective of this research is to develop a monitoring tool that can indirectly quantify the wheel and workpiece waviness in cylindrical grinding without requiring time consuming direct measuring. The developed in-process monitoring tool is oriented to the waviness which usually represents the final features of interest, rather than to the solely vibration. In section 2 the modelling technique is discussed: the waviness, the grinding process and the machine dynamic models are explained together with the identification scheme. Section 3 analyses the experimental set-up for the validation of the algorithm and the related results. Finally discussion and conclusions are presented in section 4.

2. MODEL BASED APPROACH: SYSTEM MODELLING

Regenerative Chatter conditions frequently rise during roughing operation where high material removal rates are obtained by means of high infeed and high traverse speed (i.e. with

low, at limit null wheel overlap). However, the present work is not aimed at investigating the vibration growth during unstable conditions, but it considers only the steady-state effect of the actual waviness on both wheel and cylinder side, which generates a pulsating cutting force due to the modulation of the actual infeed. As claimed in [14], the validity of the approach relies on the well-known fact that the growth and decay time for grinding vibrations is large, thus, they are essentially steady over any short period of observation. The waviness can be estimated starting from the fact that this pulsating forces induce a machine dynamic response at specific frequencies and levels depending on the rotational velocities, on the waviness severity and on the machine dynamic stiffness.

2.1. Wheel and Workpiece lobes modelling

Consider a generic case of roughing operation, with no wheel overlap, in traverse cylindrical grinding characterized by the presence of waviness. If the radial displacement (in X-direction, Fig.1) is taken into account, the instantaneous kinematic infeed $X_{kin}(t)$, producing the actual cutting force can be defined:

$$X_{kin}(t) = X_{NOMINAL} - X_{WheelWear_mean}(t) - X_{WorkpieceWear_mean}(t) + [X_{WAV_S}(\vartheta_S) + X_{WAV_W}(\vartheta_W)] \quad (1)$$

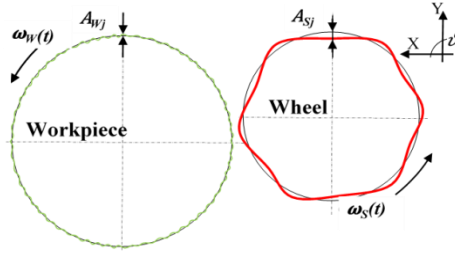


Fig. 1: Waviness representation of Workpiece and Wheel waviness waviness

where $X_{NOMINAL}$ is the commanded infeed value, $X_{WheelWear_mean}(t)$ and $X_{WorkpieceWear_mean}(t)$ are the mean radius reduction due to wear and material removal and $X_{WAV_S}(\theta_S)$ and $X_{WAV_W}(\theta_W)$ are the waviness amplitudes on the wheel and the workpiece, respectively.

It is worth to notice that the waviness is function of the angular coordinate of the system θ . In principle the Waviness can be assumed of sinusoidal shape and in a general case with multiple waviness principles (caused by different chatter frequencies, in conjunction with more rotational speeds) the following relation can be expressed:

$$\begin{aligned} X_{WAV_S}(\vartheta_S) &= \sum_{j=1}^{N_{armS}} A_{Sj} \cdot \sin(NL_{Sj} \cdot \omega_S(t) \cdot t + \varphi_{Sj}) \\ X_{WAV_W}(\vartheta_W) &= \sum_{j=1}^{N_{armW}} A_{Wj} \cdot \sin(NL_{Wj} \cdot \omega_W(t) \cdot t + \varphi_{Wj}) \end{aligned} \quad (2)$$

where N_{armS} and N_{armW} are the total considered wavelengths (i.e. waviness principles) for the wheel and the workpiece respectively, NL_{Sj} and NL_{Wj} are the number of lobes around the perimeter for each principle, $\omega_S(t)$, $\omega_W(t)$ are the actual rotational speeds, A_{Sj} , A_{Wj} are the Waviness amplitudes and φ_{Sj} , φ_{Wj} are the phase shift for each waviness principles. In presence of Wave-Filtering [1] during the generation process (i.e. under-cut) the waviness are not

expected to be of sinusoidal shape. In all the other situations with limited vibration amplitudes, low chatter frequencies and low rotational speeds the sinusoidal assumption holds.

2.2. Grinding Force model

In grinding the radial force can be assumed as a function of the kinematic infeed. One of the most complete expression for the normal grinding force in traverse grinding, [6] is as follows:

$$F_n(t) = \frac{K \cdot \varepsilon \cdot b_{cut} \cdot \mu}{V_s} \cdot \left(\frac{V_w}{V_s} X_{act}(t) \right)^{\varepsilon-1} \cdot \left(V_w X_{act}(t) + L_c(t) \dot{X}_{act}(t) \right) \quad (3)$$

where X_{act} is the actual infeed, K is the specific energy [J/mm³], ε is a non-linear constant, b_{cut} is the actual cutting width [mm], μ represents the ratio between F_n and F_t which are the normal and tangential cutting force respectively, V_s is the wheel tangential speed [m/s], V_w is the cylinder tangential speed [m/s] and L_c is the contact arc length [mm]. This latter parameter is calculated by taking into account the geometrical intersecting cords [16]:

$$L_c(t) = \sqrt{X_{act}(t) \cdot \frac{D_w \cdot D_s}{D_w + D_s}} \quad (4)$$

with D_w and D_s diameters of the workpiece and the wheel respectively. According to the model, by considering $\varepsilon=1$ (linear cutting model) and neglecting the process damping, the cutting force is proportional to the material removal rate by a constant that is the specific energy K .

Let the actual infeed be defined as:

$$X_{act}(t) = X_{kin}(t) - X_{disp}(t) \quad (5)$$

where X_{disp} is the radial system displacement caused by grinding force and by the compliance of the machine.

Let now the (3) be transformed in frequency domain and assume a linear force model as reasonable for steady-state cylindrical grinding [6]:

$$F_n(\omega) = K_g \cdot X_{act}(\omega) + K_{gd} \cdot X_{act}(\omega) \cdot i\omega \quad (6)$$

ω is the independent complex variable and the Grinding Stiffness K_g and the Grinding Damping K_{gd} constants are expressed as:

$$K_g = \left[\frac{K \cdot b \cdot \mu \cdot V_w}{V_s} \right] \quad (7)$$

$$K_{gd} = \left[\frac{K \cdot b \cdot \mu \cdot L_c}{V_s} \right]$$

The above cutting constants, need to be determined experimentally for every pair of wheel/workpiece. This can be straightforwardly done by performing some few chatter-free

cutting passes by measuring spindle current and actual infeed and feeding a regression scheme that produces an estimation of the two cutting parameters (further details can be found in [17]). It is worth to point out that, in the analysis, the contact stiffness is considered constant for all the wheel width (independently from the actual cutting width) therefore its contribute can be included in the relative machine compliance [1,6]. Additionally, in order to limit the complexity of the identification scheme, the geometric contact length L_c (4), is approximately considered time-invariant. Thus, instead of considering the whole actual infeed X_{act} (5), that in turn contains the effect of the waviness and then of the time, only its static contribute is considered. Since this latter value is purely a function of the kinematic infeed imposed to the cutting and of the static machine stiffness, it can be estimated in advance leading to the determination of the constant value L_c to use in the identification scheme. Clearly, this approximation holds only if the static contribute of the infeed is much greater than the waviness which is typically true at the vibration onset until they become extremely large. However, with such large vibration the geometry of the cutting is strongly affected (i.e. detachment of the wheel and the workpiece) and the cutting model adopted in this paper would no more be suitable to describe the cutting forces.

2.3. Open loop structural dynamic and system transmissibility

In order to take into account the behavior of the real dynamic system a simplified linear dynamic model of the structure, with few degrees of freedom, can be taken into account. Alternatively the measured relative radial compliance, obtained by impact testing technique, can be considered. It must be said that only the radial direction is taken into account here, without any contribute of the tangential cutting force on the radial compliance. The considered model is time-invariant and no changes in the dynamic behavior of the system can be modeled (e.g. due to the position of the traverse axis which is common for large machines). Additionally, in order to refer the accelerometer readings \ddot{X}_{acc} to the cutting process area (and then to the displacement imposed by the waviness) the structural dynamic transmissibility T_{acc} , is exploited. For the sake of clarity, this function is defined as sensor displacement over contact point displacement.

$$\ddot{X}_{acc}(\omega) = T_{acc}(\omega) \cdot i\omega^2 \cdot X_{disp}(\omega) \quad (8)$$

2.4. Closed loop frequency response (machine + process)

The cutting process acting on the machine structure, can be interpreted as an additional stiffness and damping (section 2.2). Therefore, to represent the overall machine compliance during the process, the overall closed loop dynamic response H_{NCL} is computed (Fig.2) which represents the coupling machine dynamics and process:

$$H_{NCL}(\omega) \stackrel{def}{=} \frac{X_{disp}(\omega)}{X_{kin}(\omega)} = \frac{H_N(\omega) \cdot (K_g + K_{gd} \cdot i\omega)}{1 + H_N(\omega) \cdot (K_g + K_{gd} \cdot i\omega)} \quad (9)$$

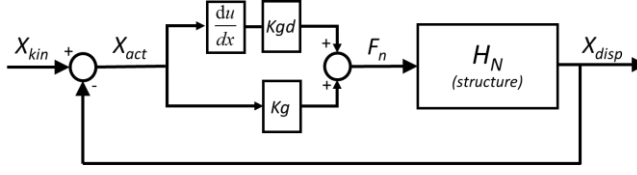


Fig. 2: Block Scheme of the system

2.5. Waviness identification scheme

By means of proper substitutions involving equations (1), (2), (5), (6), (8) and (9), the basic relation between the measured accelerations to the existing wheel waviness (X_{WAVS}) and workpiece waviness (X_{WAVW}) can be obtained:

$$\ddot{X}_{acc}(\omega) = T_{acc}(\omega) \cdot i\omega^2 \cdot H_{NCL}(\omega) \cdot \left\{ \mathfrak{I}X_{WAVS_j} \quad \mathfrak{I}X_{WAVW_j} \right\}^T \left\{ a_{Sj} \quad a_{Wj} \right\} \quad (10)$$

where a_{Sj} and a_{Wj} are the complex scale coefficients of the waviness amplitudes and phases, \mathfrak{I} denotes the Fourier transform. It is worth to note that, due to the focus on vibration, the (10) does not expressly consider the static and quasi-static contributes of (1) but consider only the dynamic related to waviness.

The use of a weighted Least Squares (LS) method in the frequency domain permits a clear interpretation of the forcing effect caused by the waviness at defined frequency components that excite the machine structure dynamic. The noise rejection by means of band-pass filters, is also simplified. The required fundamental assumption is to consider a steady-state response of the system vibration. This must be verified in particular under variable speed conditions i.e. spindle speed variation: the system can be considered in steady-state only if this transient response to a speed changes is much quicker than the imposed speed variation period. This aspect will be assessed using the integrated simulation model (section 2.6).

2.5.1. Batch identification through LS identification

Let us write the matrix equation corresponding to the (10) for an arbitrary number of sensors ($k=1,2,...N_{sensors}$) and wheel/workpiece velocities, that results in different values of excitation frequency ω_r :

$$\ddot{\underline{X}}_{acc} = \left\{ \begin{array}{c} \left\{ \ddot{X}_{acc_r}(\omega_r) \right\}_1 \\ \vdots \\ \left\{ \ddot{X}_{acc_r}(\omega_r) \right\}_k \\ \vdots \\ \left\{ \ddot{X}_{acc_r}(\omega_r) \right\}_{N_{sensors}} \end{array} \right\} = \left[\begin{array}{c} [A_{rj}(\omega_r)]_1 \\ \vdots \\ [A_{rj}(\omega_r)]_k \\ \vdots \\ [A_{rj}(\omega_r)]_{N_{sensors}} \end{array} \right] \cdot \underline{a} \quad (11)$$

with:

$$\underline{a} = \{a_{sj} \quad a_{wj}\}^T$$

$$\left[A_{rj}(\omega_r) \right]_k = T_{acc_k}(\omega_r) \cdot i\omega_r^2 \cdot H_{NCL}(\omega_r) \cdot [\Im X_{WAV_{sjr}}(\omega_r) \quad \Im X_{WAV_{wjr}}(\omega_r)]$$

The waviness amplitude and phases can be extracted from the complex elements of \underline{a} as following:

$$A_{sj} = \sqrt{\text{Re}(a_{sj})^2 + \text{Im}(a_{sj})^2}; \quad \varphi_{sj} = \text{atan}\left(\frac{\text{Im}(a_{sj})}{\text{Re}(a_{sj})}\right)$$

$$A_{wj} = \sqrt{\text{Re}(a_{wj})^2 + \text{Im}(a_{wj})^2}; \quad \varphi_{wj} = \text{atan}\left(\frac{\text{Im}(a_{wj})}{\text{Re}(a_{wj})}\right)$$
(12)

The estimation of the waviness amplitude is found by applying a Weighted Least-Squares identification:

$$\hat{\underline{a}} = \arg \left(\min_{\underline{a}} \left(\ddot{\underline{X}}_{acc} - \ddot{\underline{X}}_{acc} \right)^T \cdot \text{diag}(\underline{w}) \cdot \left(\ddot{\underline{X}}_{acc} - \ddot{\underline{X}}_{acc} \right) \right)$$
(13)

The vector \underline{w} is the weighting vector by which it is possible to maximize the fitting performance selecting those frequencies and sensors that are supposed to contain more information related to waviness.

2.5.2. Fitting Parameters and Method

The development of the presented methodology has been followed by the definition of the related technological guidelines. The monitoring algorithm requires the accelerations and the two rotational speeds to be measured with sufficient bandwidth in respect to the expected maximum chatter frequency. The batch implementation adopts a time window with a certain degree of overlap. The observation period must be shorter enough to follow the growth rate of the waviness with the proper promptness, otherwise only a mean contribute can be estimated. Afterwards, data windowing is applied to avoid leakage and Fourier transform is calculated. The inverse of the observation period, representing the spectral resolution, must be chosen according to grinding conditions. Under constant rotational speeds the waviness contributes are represented by localized spectral lines: on one side longer periods implies more defined spectra, with clearly distinguishable waviness contributes, improving the identifiability but, on the other side, the identification becomes more sensible to errors regarding the waviness frequency. Indeed the determination of the number of lobes to identify, that represents an input of the algorithm, can be deduced by the observation of the chatter frequency and the connected rotational speeds but this can be subjected to slight errors. Moreover it can be seen, from (11), that the identification matrix $A_{rj}(\omega)$ becomes ill-conditioned when the wheel and workpiece kinematic infeeds are equals for every ω_r . For this reason the algorithm requires a shift of the rotational speeds from the values that characterize the waviness formation (i.e. chatter). Another method to avoid aliasing between waviness components is to adopt continuously variable rotational speeds of the wheel and the workpiece. In this way the waviness appears in the spectrum as energy bands due to the effect of the speed (i.e. frequency) modulation. It must be said that continuous speed variation, if properly tuned, not only improves the waviness identifiability but also helps to avoid chatter onset, making it recurrently adopted in industry.

2.6. Preliminary Simulation with Integrated Simulink® module

In order to test the robustness of the approach with respect to the modeling approximation and to obtain an overall assessment on its performance, an integrated simulation model, implemented in Matlab/Simulink® environment, has been exploited. The model includes a process model as well as simple model of the machine dynamic with 2 DoF and is fed by the pulsing infeed caused by the wheel and workpiece waviness (Fig. 3).

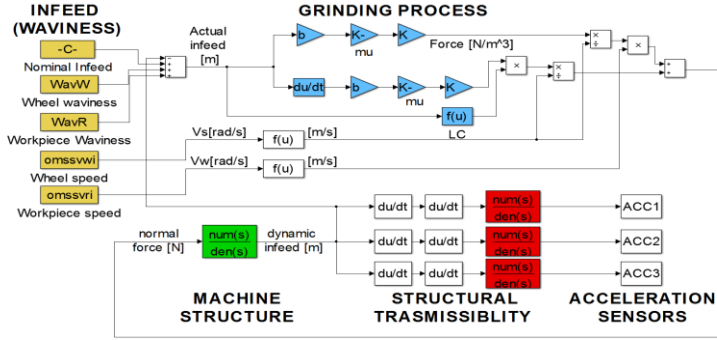


Fig. 3: Integrated dynamic model

The simulated signals contains both free and forced response (but not regenerative as addressed in [15]) and thus permit to verify the assumption regarding the steady-state of the system under speed variation condition. In addition the simulation contains an arc of contact L_c (4) calculated from the actual infeed and not from its estimation, as required by the implementation of the algorithm. There is another difference that is worth to analyze, that grows under variable speed conditions. By definition the grinding coefficients vary accordingly to the instantaneous rotational velocities (7). In the fitting model these changes have only been partly included calculating a mean value of the speed within the considered time windows. Including these amplitude modulation effects (generated by the adoption of variable grinding coefficients on the response) would rather require the use of non-linear identification approaches which are generally less easy to manage in practical situations.

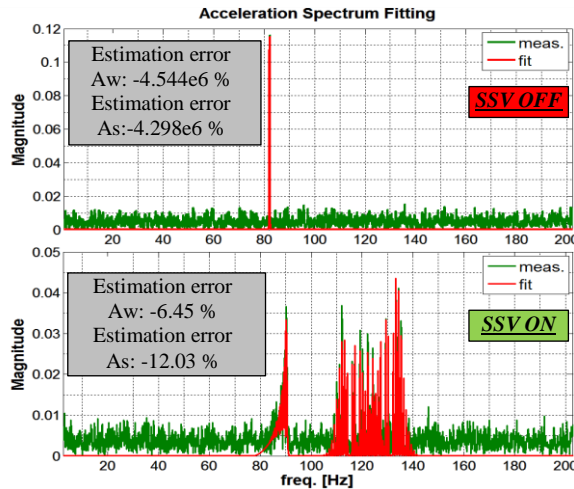


Figure 4 A-B: Simulated Signal Fitting, Magnitude of FFT

Finally, analyzing the simulations, it can be stated that none of the above issues deteriorates the fitting performance significantly for the technological cases under study. In the first example (Fig. 4-A) the algorithm is applied on a waviness generated by chatter at around 80Hz. The identification is performed neither shifting the rotational speed each other nor applying a continuous speed variation causing the identification system to be ill-conditioned. This is clear since a wheel and workpiece waviness are not observable if they introduce vibration at the same frequency. Adopting a slight speed change on one side as well as applying the Spindle speed variation (Fig. 4-B), the observability of the waviness is restored leading to a good prediction. This is true even adding a prominent fictitious noise (white noise) to represent the measurement errors.

3. EXPERIMENTAL VALIDATION CAMPAIGN

3.1. Experimental Set-Up

In order to understand the actual performance and limitations of the identification algorithm an experimental campaign on a real machine has been performed. The tests were performed on a Roll Grinding Machine equipped with piezo-accelerometers (PCB of 1V/g) connected to an external acquisition board (National Instrument CDAQ + NI9234).

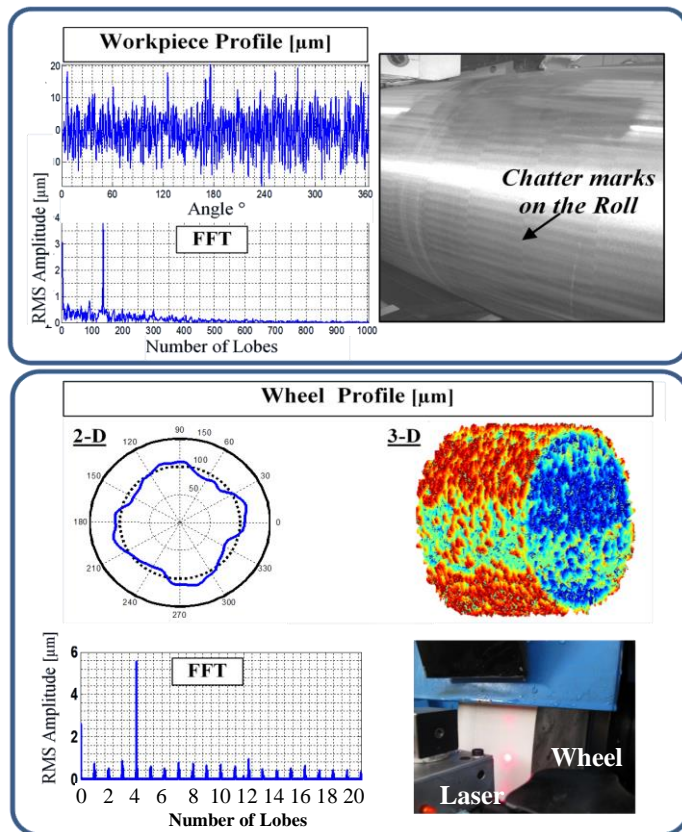


Figure 5 A-B: Direct Measurement of the waviness

The machine numerical control (Siemens 840d-sl) has been connected to the acquisition system in order to supply the actual speed signals. The machine was equipped with a mid-steel roll of diameter 507mm and with a resin bonded wheel (Tyrolit 458AG07H6B1) with a diameter of 789mm. The first sensor is installed on the wheel head with an orientation perpendicular to the machine axes. The other two sensors are installed on the neckrests.

3.2. Testing Procedure

First of all the impact test technique is applied to obtain the Frequency Response Function of the machine (FRF). Then some stable grinding passes are performed to estimate the cutting coefficients. Afterwards the "generation phase" is carried out to produce the waviness defects on the workpiece and wheel surfaces by experiencing chatter. This is achieved by performing an high-demanding grinding cycle with bad cutting parameters in respect to chatter (e.g. high infeed, high workpiece velocity etc). The process is then abruptly interrupted to keep the waviness unchanged. After that a direct "measurement phase" is carried out: a laser triangulation sensors is used to directly measure the waviness accumulated on the wheel surface, Fig.5-B. On the other side, an automated caliper (already installed on the machine) has been exploited to measure the amount of waviness on the cylinder surface, for a section in the middle of its axis, Fig.5-A. The next step has consisted in chattered "cutting test" (i.e. under the influence of the existing waviness) in which the vibration induced by the process, as well as the actual speed of the cylinder and the wheel, were measured.

The fitting algorithm has then been applied to obtain the predicted level of the waviness, for many different runs.

3.3. Tests Results: predicted and measured waviness

Several tests have been carried out following the above mentioned procedure.

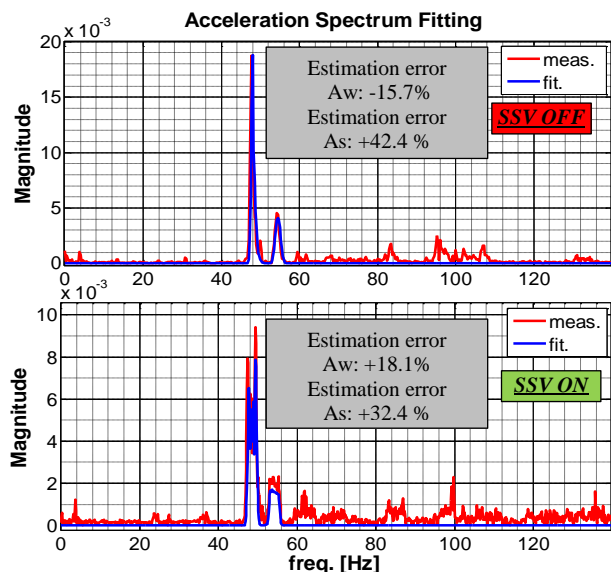


Figure 6: Experimental signals Fitting [Magnitude of FFT]

Table 1

Fitted Waviness	CASE A)	CASE B)
As (Wheel)	17.3 μ m	12.2 μ m
Aw (Workpiece)	5.4 μ m	3.8 μ m

The validation procedure was complicated by the inhomogeneity of the waviness amplitude on the workpiece perimeter and along its axis that does not agree perfectly with the adopted steady-state assumption. However, it can be stated that the fitting performance are mostly good and the average fitting errors have magnitude around $\pm 40\%$, all over the range of the possible waviness amplitudes. One example is given in Fig.6 and Table 1.

4. DISCUSSION AND CONCLUSION

In this work an on-line waviness identification algorithm for cylindrical traverse grinding has been developed. It has been shown that it is possible to identify the wheel and workpiece waviness generated by chatter, starting from acceleration measurements and exploiting a model-based approach with a Weighted Least-Squares identification. The method includes a simple model of the waviness, a linearized model of the cutting process and the machine dynamics behavior (in terms of relative radial compliance between wheel and workpiece for a specific axes position).

The experiments have shown that a sinusoidal model of the waviness is suitable as long as geometric wave filtering does not take place. The adoption of constant cutting parameters is a modelling simplification that must be evaluated in respect to the actual encountered variability. In this analysis the machine behavior (i.e. static and dynamic) is considered time-invariant. These two sets of parameters, must be identified prior to applying the algorithm by means of dedicated testing procedures (e.g. Cutting Test by measuring the absorbed cutting power and the actual infeed, Experimental Modal Analysis)

The monitoring scheme has been tested first in simulation and then on the real system, confirming that a good on-line estimation of the waviness can be achieved. To work properly on a real grinding machine equipped with industrial numerical control, the algorithm requires a strict synchronization between the accelerometers and the machine drives data (i.e. wheel and workpiece rotational speeds).

The monitoring algorithm can therefore provide a valuable feedback to grinding operators regarding the actual state of the process and additionally support the development of real-time algorithms for automatic grinding process optimization.

Further experimental activities will be addressed to validate the algorithm from a statistical point of view, in order to take into account all the sources of variability of the real application and quantify their effects on the achieved estimation performance.

Further additions to the implemented waviness monitoring modules can include the adoption of LPV modelling of the machine dynamic to take into account its variability with the axes position.

ACKNOWLEDGEMENT

This work has been supported by funding of the Italian Ministry of Economic Development under the research program Industria 2015.

REFERENCES

- [1] Inasaki I, Karpuschewski B, Lee H, "Grinding chatter origin and suppression" *CIRP Annals Manufacturing Technologies*, 50:515 – 534 (2001)
- [2] Tönshoff, H.K. et al., "Process Monitoring in Grinding" *CIRP Annals - Manufacturing Technology*, Volume 51, Issue 2, 2002, Pages 551–571
- [3] Karpuschewski B., Inasaki I., "Monitoring Systems for Grinding Processes." *Condition Monitoring and Control for Intelligent Manufacturing*. Springer London, 2006. 83-107
- [4] Gonzalez-Brambila O. et al., "Chattering detection in cylindrical grinding processes using the wavelet transform", *International Journal of Machine Tools & Manufacture* 46 (2006) 1934–1938
- [5] E. Brinksmeier, F. Werner, "Monitoring of Grinding Wheel Wear", *CIRP Annals - Manufacturing Technology*, Volume 41, Issue 1, 1992, Pages 373-376
- [6] Inasaki, I., and Yonetsu, S., "Regenerative Chatter in Grinding," *Proc. 18th Int. Machine Tool Design and Research Conf.*, pp. 423–429 (1977)
- [7] D. Biermann, M. Feldhoff, "Influence of controlled tool orientation on pattern formation and waviness in surface grinding", *Production Engineering*, February 2011, Volume 5, Issue 1, pp 31-36
- [8] Huynh V. M., Fan Y., "Surface-texture measurement and characterization with applications to machine-tool monitoring", *International Journal of Advanced Manufacturing Technology*, 04/1992; 7(1):2-10
- [9] Govekar E et al. "A new method for chatter detection in grinding". *Ann CIRP* 1:267–270. (2002)
- [10] Gradisek J. et al. "Automatic chatter detection in grinding", *International Journal of Machine Tools & Manufacture* 43 (2003) 1397–1403
- [11] Fu J. et al., "Chatter classification by entropy functions and morphological processing in cylindrical traverse grinding", *Precision Engineering* 18 (2–3) (1996) 110–117
- [12] Wakuda, M., Inasaki, I. et al., "Monitoring of the grinding process with an AE sensor integrated CBN wheel", *Journal of Advanced Automation Technology*, 5(4), pp. 179–184. (1993)
- [13] Wu, C. Y. , "Surface Quality Assessment Using Vibration Signals for Transverse Roll Grinding", *China Steel Technical Report*, 17; 37-42, (2003)
- [14] Thompson R. A., "The Character of Regenerative Chatter in Cylindrical Grinding", *J. Eng. Ind.* 95(3), 858-864 (1973)
- [15] Weck M. et al., "Dynamic Behaviour of Cylindrical Traverse Grinding Processes", *CIRP Annals - Manufacturing Technology* 2001, 50 (1), 213-216.
- [16] Rowe W.B., "Principles of modern grinding technology", Book, William Andrew, First edition 2009, ISBN: 978-0-81-552018-4
- [17] Leonesio M. et al., "A time-domain surface grinding model for dynamic simulation", *3rd CIRP Conference on Process Machine Interactions, CIRP Procedia*, Volume 4, 2012, Pages 166–171

Machining improvement on flexible fixture through viscoelastic damping layer

Alex Iglesias¹, Qilin Fu², Julen Landa¹, Amir Rashid²

¹Dynamics and Control, IK4-Ideko, Elgoibar, Spain

²KTH Royal Institute of Technology, Stockholm, Sweden

e-mail: aiglesias@ideko.es

ABSTRACT

Chatter is a critical problem in milling processes that affects surface quality and tool life. The present work analyses the effect of modifying the dynamic response of the system by introducing a viscoelastic material in one of the joints of a flexible structure. The purpose of this modification is to increase the damping and therefore improve the dynamic response of the structure. A flexible fixture with an aluminium workpiece on the top, emulating a slender part or a thin walled structure, is analysed. Different configurations are simulated and experimentally tested in order to quantify the achieved cutting capability and determine the accuracy of the simulations. Cutting performance is successfully improved through the damping layer. Both system response and stability simulations correlate accurately with experimental tests. The effectiveness of a damping layer located in a zone of the structure different from where the maximum vibration strain energy is concentrated is demonstrated.

KEYWORDS: damping, chatter, joint interface module, aluminium milling, flexible fixture.

1. INTRODUCTION

In milling processes, chatter poses a serious problem which hampers cutting process, jeopardises workpiece surface quality, reduces tool life and damages mechanical components of the machine. This self-excited vibration effect is originated by the regeneration of the chip thickness that arises between two consecutive tool cutting edge passes.

Since chatter was described more than 50 years ago [1,2], different methods to predict cutting stability limit have been developed in order to obtain higher productivity. Altintas and Budak [3] presented a semi analytical prediction of the stability diagrams. The method is based on a single frequency model which obtains a fast analytical solution. The results obtained with this modelling method are accurate when the radial immersion of the tool is high, but they lack of precision as the process becomes more interrupted. The semi discretization method [4] and the multifrequency model [5] are used to calculate accurately the stability limit of the interrupted milling processes. These methods provide an accurate solution for every milling process.

There are different techniques to increase the stability limit in machining processes. A traditional chatter mitigation strategy is to modify the cutting parameters in order to bring the process to a stable area of the stability lobe diagram, which usually brings along a dramatic decrease of productivity. It is also possible to use techniques like spindle speed variation [6] and variable pitch or helix cutters [7], which avoid the regenerative effect of the chip thickness.

Another approach seeks to increase the dynamic stiffness of the structure through passive or active damping methods. A passive mass damper or dynamic vibration absorber (DVA) is a device that introduces an inertial force through a tuned mass and transfers the kinetic vibration energy from the main structure to the tuned mass, increasing damping of the system. It has been successfully used in workholding systems in a milling machine, reducing vibration significantly [8]. Active dampers measure the vibration signal and exert a compensation force, achieving a similar effect to the passive mass damper [9,10].

It is well known that damping of multiple component systems is defined by structural joints [11]. Therefore, it is also possible to change the dynamic properties of a system by acting in its joints, changing their stiffness and damping [12]. An effective means of increasing the damping of the system in a considerable extent is to introduce a viscoelastic material (VEM) in a joint of the structure. High vibration strain energy of the dominant modes must be present at the damped joint in order to be effective. The dynamic characteristics of the system can be enhanced and their value can be tuned through a controlled joint preload [13].

Daghini et al [14] claimed the benefit of applying a high damping interface in the turret of a turning machine, and confirmed the improvement of surface finish in the machined parts. However, as they introduced VEM simultaneously in both tool and turret interfaces, the exact contribution of the damping interface in the turret was not verified. The specific effect of the high damping interface design parameters, such as thickness or material properties, was not analysed either.

The present work analyses the cutting stability increase achieved through an embedded viscoelastic material layer in the joint of a flexible fixture. This fixture is used in order to imitate the dynamic behaviour of slender parts and thin walled structures and develop the analytical and experimental tests.

The viscoelastic material shows its highest effect when placed in the highest vibration strain energy region of the structure, but this is usually not feasible in most structures. In the present case it is not possible to place the damping layer on the highest vibration strain energy location either and, therefore, the closest joint to the cutting point is chosen for the VEM layer location.

The exact contribution of the damped joint interface is quantified by comparing with a conventional set up. The effect of the normal pressure at the joint interface on the global dynamics is also analysed, with the aim of studying its tuning capability.

Different thickness VEM layers and positions are analysed in virtual simulations, and experimentally tested. Milling operations are used to characterize the improvement of machining performance when introducing the damping layers in the structure.

2. NUMERICAL SIMULATIONS

The flexible fixture used to perform this work consists of a mass supported by two flexible blades. This fixture has a dominant vibration mode due to the flexure hinges at both ends of the blades. A joint interface is created between this fixture and a base plate under it, which is used to introduce the damping material. The dynamic characteristics of the joint are tuned through bolt preload. The base plate is rigidly clamped to the work table of the milling

machine. The system imitates a slender part or thin wall system, with an aluminium workpiece placed on top of the aforementioned fixture mass.

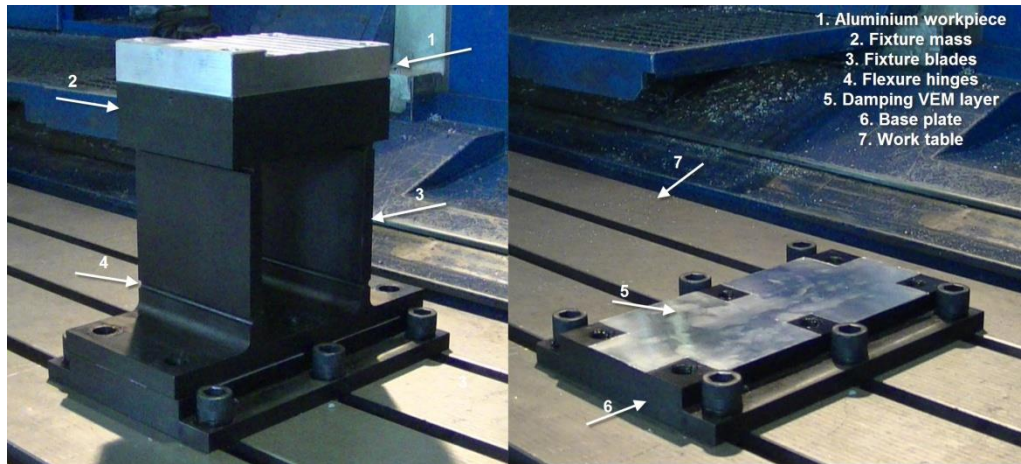


Fig.1. Parts of the flexible fixture.

The system was simulated through a finite element model (FEM) and different system configurations were calculated in order to identify the highest dynamic stiffness case. The dynamic stiffness is limited by the main flexure mode, which is shown in Fig.2.

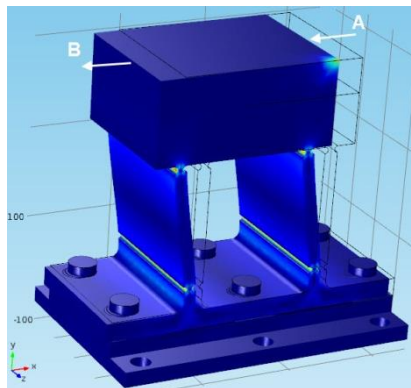


Fig.2. Main mode shape (colour scale indicates highest vibration strain energy density).

The investigated parameters are the different types, thickness and locations of the VEM layers. The specific cases calculated are described below:

- **Case I (Without VEM):** Original system, no VEM layer added.
- **Case II (1mm damping layer):** 2 viscoelastic layers with aluminium foil (3M™ 112 VEM) embedded between the base plate and the flexible fixture.
- **Case III (1mm damping layer in base and screws):** 2 viscoelastic layers with aluminium foil (3M™ 112 VEM) embedded between the base plate and the flexible fixture, and between the screws and the flexible fixture (see Fig.3).
- **Case IV (3mm damping layer):** 6 viscoelastic layers with aluminium foil (3M™ 112 VEM) embedded between the base plate and the flexible fixture.

- **Case V (6mm Sylomer):** 1 Sylomer layer (Sylomer ® SR850-6) of 6mm between the base plate and the flexible fixture.
-

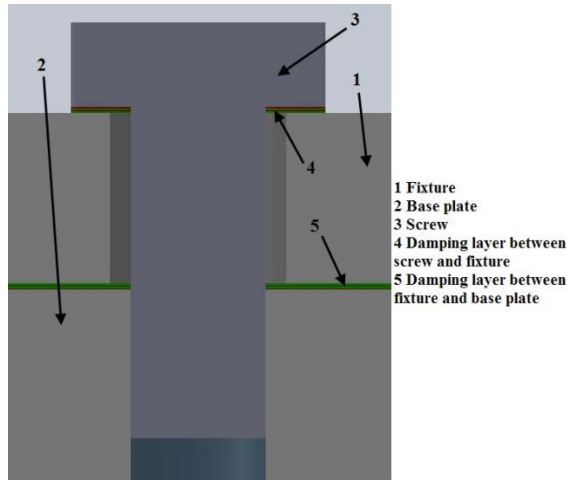


Fig.3. Detail of Case II damping layer location (screw section view).

Layer 5 covers all the interface geometry except a 50x50mm square in the screws zone (as shown in Fig.1.), whereas layer 4 surrounds the holes of the screws with a square VEM layer of 50x50mm. The characteristics of the materials used for the numerical simulations are specified in Appendix I in Table 4 and Table 5.

The simulated frequency response is obtained in the flexible direction of the structure (x), exciting at point A and measuring on point B (see Fig.2) for every configuration. The results are shown in Fig.4.

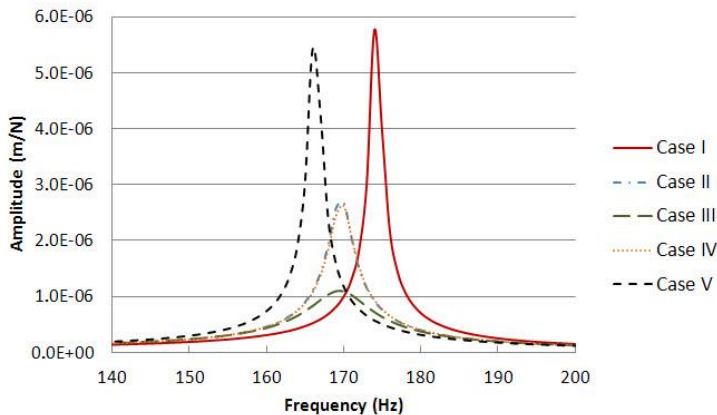


Fig.4. Simulated frequency response functions of tested configurations.

Cases II and IV improve original response to a great extent, although Case III gives the optimum response. Case V, on the other hand, increases system damping slightly but at the same time decreases its static stiffness, which results in a similar dynamic stiffness system as Case I.

3. EXPERIMENTAL TESTS

The simulations performed in chapter 2 were experimentally corroborated. Firstly, the dynamic characterization of the undamped and damped systems was carried out, comparing the obtained theoretical dynamic stiffness with the experimental one. Secondly, cutting tests over the aluminium workpiece on top of the flexible fixture were performed in order to confirm cutting capability improvement from the undamped to the damped case.

3.1. Dynamic characterization

The dynamics of the different joint configurations with embedded VEM analysed through the numerical simulations were experimentally characterized. The frequency response functions (FRF) were measured on top of the device using an impact hammer to introduce the excitation and a triaxial accelerometer to measure the response. The bolt tightening torque was 270Nm. This procedure was repeated for all the configurations analysed.

Fig.5 shows the comparison of the frequency response functions of the different cases tested and the extracted dynamic parameters are summarised in Table 1.

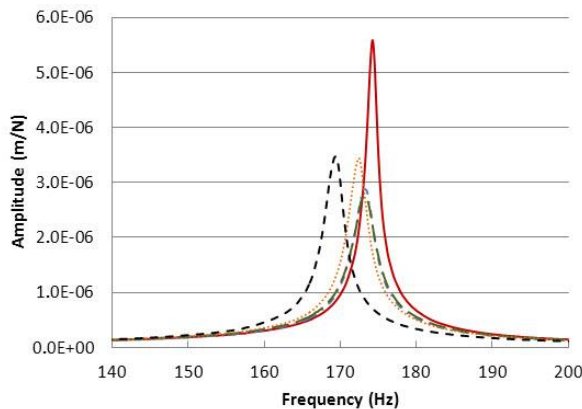


Fig.5. Comparison of the FRF of different system configurations.

Table 1. Dynamic parameters of the different configurations tested.

	Natural frequency (Hz)	Maximum dynamic flexibility ($\mu\text{m/N}$)	Damping ratio (ξ)
Case I	174.25	5.59	0.389%
Case II	173.25	3.05	0.743%
Case III	173.25	2.75	0.823%
Case IV	172.50	3.44	0.678%
Case V	169.50	3.74	0.695%

The experimental dynamic response is very similar to the virtual case, for all the cases except Case II, in which the VEM layer under the screws is overloaded because the bolt preload is excessive for the small damping layer area under the bolt head.

Any of the damped cases (Case II, III, IV and V) improves the dynamic stiffness of the original system. Case III, with a damping interface under the tightening screws of the joint,

does not show a significant variation with Case II, where only the interface between the fixture and the base plate is damped. Increasing the damping layer thickness (Case IV and V) produces a decrease in the mode stiffness and therefore results in a lower dynamic stiffness. Therefore, the different configurations of damped joints studied do not improve significantly the result obtained with 1mm damping layer (Case II).

In order to study the joint tuning capability through bolt preload, the resulting FRFs under different bolt preloads (270Nm, 203Nm and 135Nm) to fix the fixture and the base plate in Case II were obtained. Results are shown in Fig.6 and Table 2.

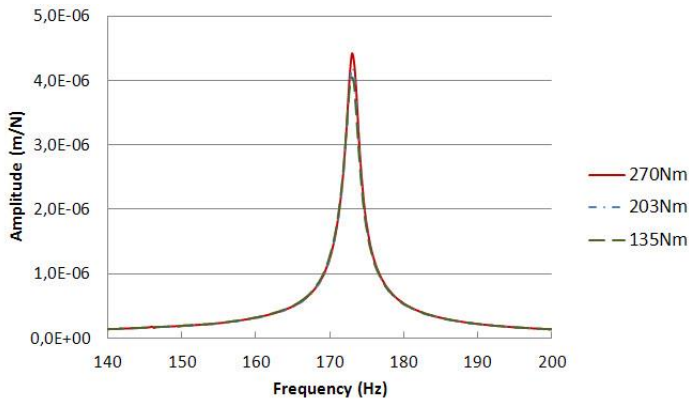


Fig.6. Comparison of the FRFs of different tightening torques.

Table 2. Mode frequency, dynamic flexibility and damping values for different tightening torques.

	Natural frequency (Hz)	Maximum dynamic flexibility ($\mu\text{m/N}$)	Damping ratio (ξ)
270Nm	173.00	4.42	0.505%
203Nm	173.00	4.28	0.523%
135Nm	173.00	4.05	0.557%

In view of Fig.6, it can be concluded that once the polymer is placed in the joint, the tightening torque of the screws does not have a significant effect on the dynamic response of the system although, as expected [12], a slight damping increase with torque reduction is noticed. The difference of damping between the maximum and minimum tightening torque is only 10%. These results confirm that the tuning capacity of this structure through bolt preload is limited due to the intrinsic low stiffness of the system stiffness, which is more important than the stiffness of the joint itself in the global flexibility. It has also been experimentally observed that joint preload does not have a significant effect on high frequencies [12].

After verifying simulation results, the 1mm layer case (Case II) was selected for machining performance validation. The system was assembled again. Fig.7 and Table 3 show the frequency response function and the extracted dynamic parameters respectively.

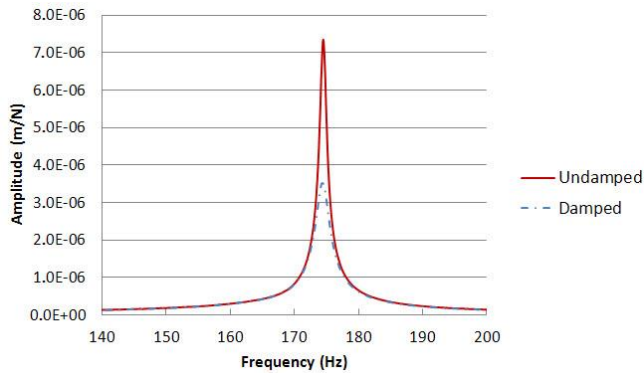


Fig.7. Comparison of FRFs between the configuration without and with 1mm VEM.

Table 3. Mode frequency, dynamic flexibility and damping values for damped and undamped cases.

	Natural frequency (Hz)	Maximum dynamic flexibility ($\mu\text{m/N}$)	Damping ratio (ξ)
Undamped	174.50	7.7	0.295%
Damped	174.50	3.7	0.604%

The use of 1mm damping foil on the base of the flexible fixture increases the original damping value by 105% and the dynamic stiffness rises from $0.130\text{N}/\mu\text{m}$ to $0.270\text{N}/\mu\text{m}$.

3.2. Cutting tests

Case II configuration was assembled and an aluminium Al 7075 T6 workpiece was machined with a 20mm and 2-fluted tool with a helix angle of 30° (HMKendu 902.60.020000.20). Down-milling cuttings with a radial immersion of 4mm and increasing cutting depth from 0.5mm to 6mm were performed. The feed direction was perpendicular to the dominant vibration mode of the flexible fixture. The spindle speeds studied were 5300rpm, 5500rpm 6000rpm, 7000rpm and 8000rpm, with a feed rate of 0.2mm/tooth.

Stability simulations were conducted using the single frequency model proposed by Altintas and Budak [3]. The results obtained for the two analysed assemblies show an important increase of the cutting stability when the VEM is introduced in the joint of the fixture. The cutting tests carried out confirm this stability increase (see Fig.8). The correlation between the analytical simulations and the milling tests is very accurate for the first three speeds studied whereas the experimental tests stability is slightly higher at spindle speeds of 7000rpm and 8000rpm.

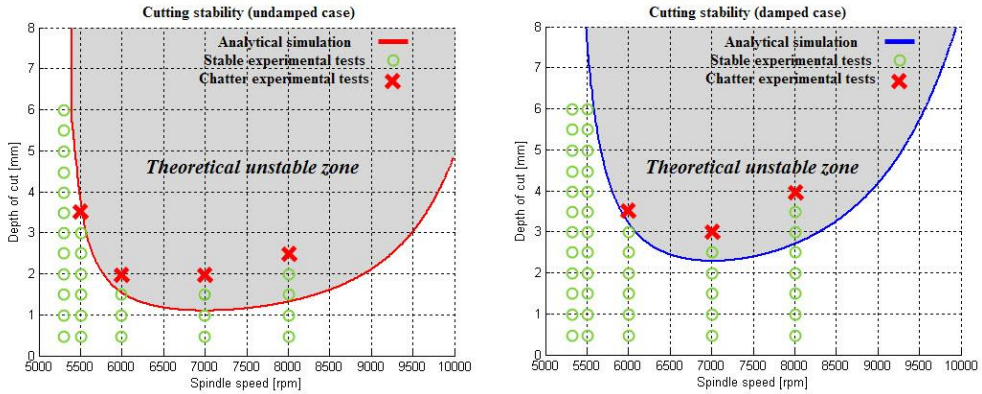


Fig.8: Predicted stability lobe and cutting tests of the undamped case, without VEM, (left) and damped case, with VEM (right).

4. CONCLUSIONS

Parts made of highly flexible structures, such as slender bars or thin walls, show a limited machinability due to vibrations during the cutting process. A procedure to improve the dynamic stiffness of a mechanical structure by modifying the joints used in assemblies has been proposed. This strategy consists of introducing a viscoelastic material in the nearest joint to the cutting point, in order to increase damping capacity. The numerical analysis shows an improvement of the dynamic response of the flexible fixture when a viscoelastic layer is embedded in the joint, even if the damping layer location does not correspond to the maximum vibration strain energy zone of the structure. The dynamic stiffness of the damped fixture can be more than 50% higher than the undamped case, which boosts cutting capability to a similar extent. The related loss of static stiffness is not significant, since intrinsic flexibility, typical of slender parts and thin walled structures, is already rather high.

Changes on the joint preload or damping layer thickness do not have a noticeable effect on the dynamic performance of the system. Therefore, in flexible structures, where joints do not hold a significant share of the global stiffness of the system, the tuning of the system through the joint preload in order to optimise the dynamic stiffness is not possible and the passive damping approach is enough for cutting performance enhancement.

The different damping configuration cases simulated have been experimentally tested with the objective of obtaining the frequency response of each system and correlate simulations with experimental results. A high correspondence between simulated and experimental results has been proved.

The theoretical stability diagrams simulated according to the experimentally measured dynamic parameters also show a very good correlation with the experimental cutting tests at the analysed spindle speeds, although the actual stability of the experimental tests performed at high speeds is slightly higher than the expected from the numerical simulations.

APPENDIX I

For the different assembly cases simulation study, the essential parameters of the materials are listed in Table 4:

Table 4. Mechanical parameters of the simulated materials.

Material	Young's Modulus (GPa)	Isotropic loss factor	Poisson's ratio	Density (Kg/m ³)
Steel	190	0.008	0.28	7850
Aluminium	69	0.008	0.35	2700
3M Viscoelastic Damping Polymer 112-130	Varies depending on frequency	Varies depending on frequency	0.49	980
Sylomer SR-850	Varies depending on frequency	Varies depending on frequency	0.45	850

The variation of the Young modulus and the loss factor of the damping materials are described in Table 5, as a function of the frequency.

Table 5. Frequency dependency of Young modulus and loss factor of the damping materials.

3M 112 VEM			Sylomer SR-850		
Frequency (Hz)	Young's Modulus (Pa)	Loss factor	Frequency (Hz)	Young's Modulus (MPa)	Loss factor
0.1	238400	0.25	0	9	-
1	536400	0.6	1	10	0.08
5	1043000	0.8	10	11	0.10
10	1490000	0.9	30	12.5	0.13
100	5960000	1	50	14	0.16
200	8940000	0.95	100	15.5	0.18
400	12218000	0.9	200	17	0.2

ACKNOWLEDGEMENTS

The research leading to these results has received funding from the Seventh Framework Programme (FP7/2007-2013) of the European Union, under grant agreement no. 260048 (PoPJIM project).

REFERENCES

- [1] J. Tlustý and M. Poláček, "Beispiele der behandlung der selbsterregten Schwingung der Werkzeugmaschinen," *FoKoMa, Hanser Verlag*, Munich, 1957.
- [2] S.A. Tobias and W. Fishwick, "Theory of regenerative machine tool chatter," *The Engineer*, pp. 205, 1958.
- [3] Y. Altintas and E. Budak, "Analytical prediction of stability lobes in milling," *CIRP Annals*, 44(1), 357-362, 1995.
- [4] T. Insperger and G. Stépán, "Semidiscretization of delayed dynamical systems," in *Proceedings of ASME Design Engineering Technical Conferences and Computers and Information in Engineering Conference*, Pittsburg, 2001.
- [5] E. Budak, "Mechanics and dynamics of milling thin walled structures," *Doctoral Thesis*, University of British Columbia, Vancouver, Canada, 1994.

- [6] Y. Altintas; S. Engin and E. Budak, "Analytical Stability Prediction and Design of Variable Pitch Cutters," *Journal of Manufacturing Science and Engineering. Transactions of the ASME*, vol. 121, pp. 173-178, 1999.
- [7] T. Hoshi, N. Sakisaka, I. Moriyama and M. Sato, "Study for Practical Application of Fluctuating Speed Cutting for Regenerative Chatter Control," *CIRP Annals*. vol. 25, pp. 175-179. 1977.
- [8] A. Rashid and C. M. Nicolescu, "Design and implementation of tuned viscoelastic dampers for vibration control in milling," *International Journal of Machine Tools and Manufacture*, vol.48, pp. 1036-1053, 2007.
- [9] A. Bilbao-Guillerna, A. Barrios, I. Mancisidor, N. Loix, J. Munoa, 2010. "Control laws for chatter suppression in milling using an inertial actuator," in *Proceedings of ISMA International Conference on Noise and Vibration Engineering*, Leuven, Belgium, 2010.
- [10] A. Harms, B. Denkena, N. Lhermet; "Tool adaptor for active vibration control in turning operations," in *9th International Conference on New Actuators, Actuator*, Bremen, Germany, 2004.
- [11] F. Koenigsberger and J. Tlustý, "Machine tool structures," *Pergamon Press*, vol.1, 1970.
- [12] C. Frangoudis, A. Rashid, C. M. Nicolescu, "Experimental analysis of a machining system with adaptive dynamic stiffness," *Journal of Machine Engineering*, vol. 13, no. 1, 2013.
- [13] Q. Fu, A. Rashid and C.M. Nicolescu, "Improving machining performance against regenerative tool chatter through adaptive normal pressure at the tool clamping interface," *Journal of Machine Engineering*, vol.13, pp. 93-105, 2013.
- [14] L. Daghini, A. Archenti and T. Österlind, "Extending stability limits by designed-in damping," *Journal of Machine Engineering*, vol. 13, pp. 45-56, 2013.

Analytical Stability Prediction in Five Axis Ball-End Milling

Mahdi Eynian

University West, Sweden
Email: mahdi.eynian@hv.se

ABSTRACT

In five axis ball-end milling, the cutting edge is a continuous curve and the engagement with workpiece changes as the cutting tool rotates. Therefore the sensitivity to vibration varies along the cutting edge and as the tool rotates. In this paper, the vibration-force relationship (VFR) is obtained for infinitesimal length of cutting edge as a function of tool's rotation angle. Numerical integration results in the VFR of the whole cutting edge and the tool. VFR of the tool is coupled to the dynamic vibration model of the tool and the workpiece to predict the possibility of vibrational instability. This algorithm is then used to predict the effects of changing the lead angle in a test setup with a flexible depth of cut direction. The analytical results, along with experiments demonstrate that the large lead angles considerably improve the stability of the process.

KEYWORDS: five-axis, ball-end milling, chatter, stability, lead angle

1. INTRODUCTION

Five-axis ball-end milling is used for machining of complex surfaces. In some of these machining operations it is possible to choose the tool orientation with respect to the workpiece and affect the quality of the machining process. Different cutting strategies in five axis machining were studied by Xu, Schueller and Tlustý among others. They investigated different tool movement strategies and recommended “step-up” geometry, which could be described as a five axis machining with a large lead angle [1].

An important concern in five-axis ball-end milling, especially in machining of thin walls and sections is machining chatter. Chatter is the self-excited vibration between the tool and the workpiece and leaves a rough machined surface. In addition it could damage the tool and the machine tool. Doi and Kato have identified the phase difference between vibration waves left from the previous tool pass and the instantaneous vibrations as the root cause of chatter [2]. Chatter prediction algorithms for turning and drilling [3, 4] and milling [5-10] investigate stability of the closed loop machining system against chatter. Prediction of unstable chatter in five axis machining is an ongoing challenge due to the complexities in tool-workpiece

engagement calculation. Unlike cylindrical tools with up-milling and down milling geometries with specific depth of cut and width of cut, the engagement region of the tool and workpiece has a complex geometry which is dependent on the width and depth of cut. Ozutrk and Budak investigated the stability and other machining characteristics in five axis milling by slicing the tool into disks along its axis [9]. They studied effects of lead and tilt angle with a flexible tool and demonstrated positive effects of lead angles of 15 or 30 degrees and positive lead angle increases the limit depth of cut. However they used an iterative approach in their stability prediction method. The numerical integration method used in present paper avoids such iteration. The experimental approach in this work is focused on investigation of 5 axis stability with flexibility in the depth of cut direction in the workpiece, rather than the tool flexibility and it also confirms the positive effects of the large lead angles.

This paper is organized as follows: in section 2 the algorithms is presented, experiments are discussed in section 3 and the results are discussed in section 4 of this paper.

2. STABILITY PREDICTION ALGORITHM

The orientation of the ball end mill with respect to the workpiece is determined by tilt and lead angles as shown in Fig. 1. The engagement of an infinitesimal length of cutting edge and the orientation of the possible cutting forces could be investigated by establishing geometrical relationships between the orientation of the cutting edge, and the cutting speed at that location with respect to a fixed coordinate system or rotating/non-rotating coordinate systems aligned with the tool's orientation.

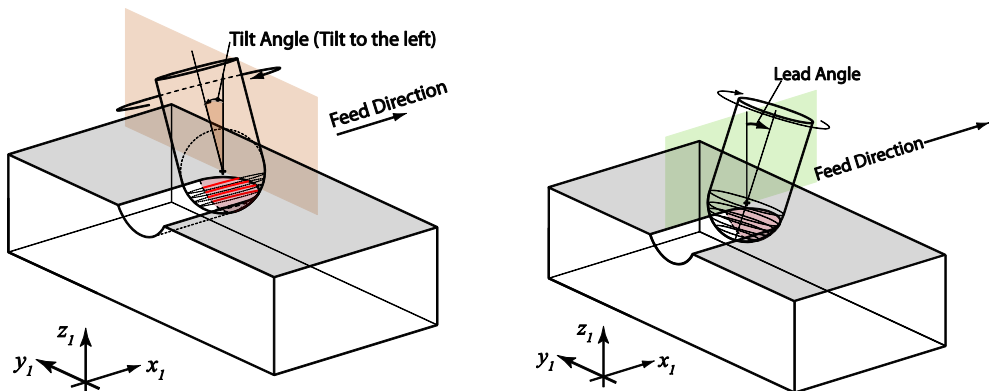


Fig. 1. Tilt and lead angles in ball end milling

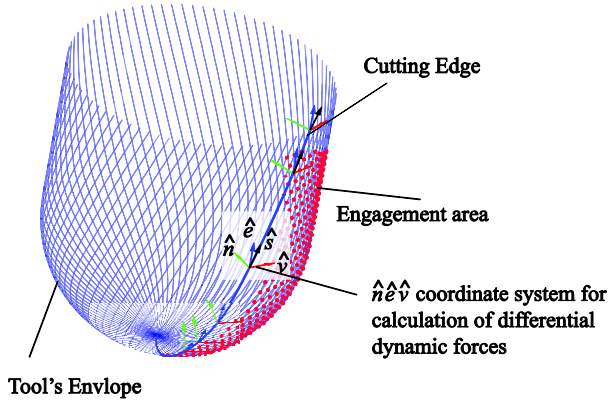


Fig. 2. Geometry of cutting edge and engagement of the tool with the workpiece. $\hat{n}\hat{e}\hat{v}$ coordinate system, tool's envelope and engagement area are also shown

The outline for stability prediction is shown in a flowchart in Fig. 3. The algorithm starts by calculation of the sensitivity of cutting forces on an incremental length of a cutting edge to the vibrations in three orthogonal degrees of freedom to obtain the Vibration-Force Relationship (VFR) at that length. Then by numerical integration along the cutting edge produces the VFR matrix along a cutting edge. This matrix will be the same for all cutting edges if they have the same geometry, but may be dependent on edge if the edge geometries differ (e.g. if each cutting flute had a different helix angle).

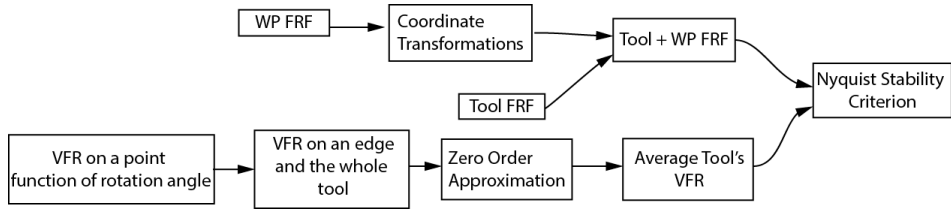


Fig. 3. Flow chart for stability prediction

To calculate the VFR at a point, the $\hat{n}\hat{e}\hat{v}$ coordinate system is constructed with \hat{v} axis along the cutting speed direction, \hat{e} axis on the plane made by the tangent to the cutting edge and the \hat{v} and normal to \hat{v} and $\hat{n} = \hat{v} \times \hat{e}$. Proper combinations of rotation matrices as described in Fig. 4 are applied to translate the movements of both the workpiece and the tool to the changes of the effective chip thickness (\hat{n} direction) along the infinitesimal cutting edge length (dS). Since the movements are assumed to be infinitesimal, the relationship between the cutting forces and the displacements will remain linear [11]. Thus matrix relationships could be employed to describe the relationship between the changes in the forces and the displacements in the present cut and the previous tool pass.

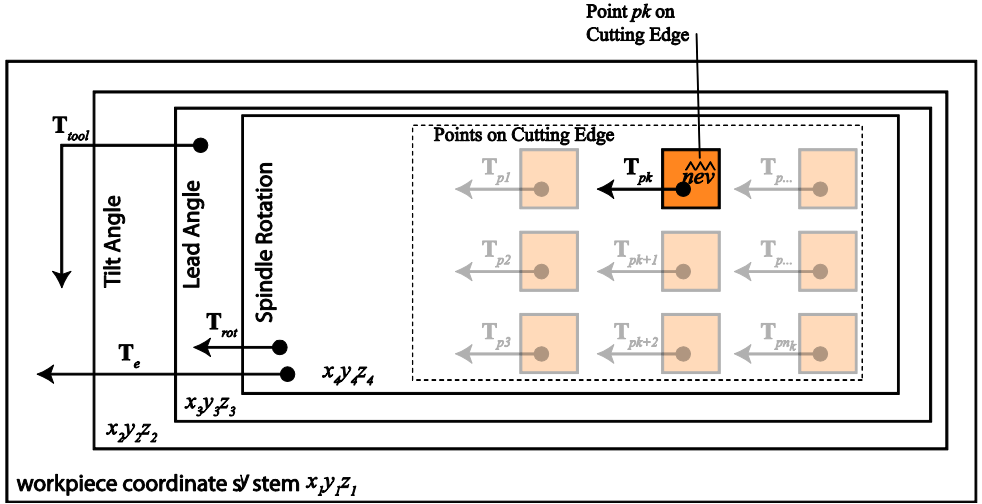


Fig. 4. Coordinate systems used in modeling of five axis milling. $\hat{n}\hat{e}\hat{v}$ coordinate system is aligned with the cutting speed and edge direction of infinitesimal length of the cutting edge, $x_4y_4z_4$ coordinate system is attached to the tool and it is rotating with it. $x_3y_3z_3$ is the non-rotating coordinate system, aligned with the tool. $x_1y_1z_1$ is the coordinate system fixed to the workpiece and oriented with the feed speed and normal to the workpiece surface. T_{pk} transformation transfers the vectors from $\hat{n}\hat{e}\hat{v}$ coordinate system to $x_4y_4z_4$ coordinate system. Other transformation matrices are also shown in the diagram.

Vibrations are not modeled in the rotating $x_4y_4z_4$ coordinate system since such modeling would need inclusion of centrifugal and Coriolis accelerations, while not causing significant change in the stability limit [12]. The dynamic chip thickness at point pk is calculated by inner product of the displacement vectors X (vibrations of the tool, described in $x_3y_3z_3$), Y (vibration of the workpiece, described in $x_1y_1z_1$) and the \hat{n} . Vibrations in the previous pass have the opposite contribution to the chip thickness and are indicated by subscript τ_j .

$$h(t) = h_0 - g \left\{ (T_e \hat{n})^T (X - X_{\tau_j}) + (T_{rot} \hat{n})^T (Y - Y_{\tau_j}) \right\} \quad (1)$$

τ_j is the time delay between passing of the flute j and previous flute from the same angular position. For equally spaced tools, this could be calculated from speed $n \left(\frac{rev}{min} \right)$ and the number of flutes (N):

$$Y_{\tau_j}(t) = Y(t - \frac{60}{n \cdot N}) \quad (2)$$

Incremental dynamic force is calculated similar to [13] (dF_{reg} : contribution of an incremental length along cutting edge) in the $x_3y_3z_3$ coordinate system:

$$dF_j(t) = -g \cdot (\hat{e} \cdot \hat{s}) dS \cdot T_{rot} \cdot \mathbf{T}_{pk} \begin{bmatrix} K_n \\ K_e \\ K_t \end{bmatrix} \left\{ (T_e \hat{n})^T (X - X_{\tau_j}) + (T_{rot} \hat{n})^T (Y - Y_{\tau_j}) \right\} \quad (3)$$

K_n is the cutting coefficient in the normal to the cut surface, K_e is the side cutting direction cutting coefficient, and K_t is the cutting coefficient in the cutting speed direction. These coefficients could be extracted from the shear stress in cutting τ_s , rake angle α , inclination angle i and friction angle β as shown by Budak et. al in [13]. These coefficients could be related to the shear stress in the cutting zone and rake angle and inclination angle (angle between edge and \hat{e}). Furthermore, it is possible to select these parameters as a function of cutting speed. This might be necessary since in ball end milling the cutting speed varies considerably from the tip of the ball to the full diameter of the tool. The middle part of the Eq. (3) could be separated as 3x3 matrices:

$$\begin{aligned} dB_j &= -g \cdot (\hat{e} \cdot \hat{s}) dS \cdot T_{rot} \cdot \mathbf{T}_{pk} \begin{bmatrix} K_n \\ K_e \\ K_t \end{bmatrix} (T_e \hat{n})^T \\ &= -g \cdot (\hat{e} \cdot \hat{s}) dS \cdot T_{rot} \cdot \mathbf{T}_{pk} \begin{bmatrix} K_n \\ K_e \\ K_t \end{bmatrix} (T_{tool} \cdot T_{rot} \hat{n})^T \\ dC_j &= -g \cdot (\hat{e} \cdot \hat{s}) dS \cdot T_{rot} \cdot \mathbf{T}_{pk} \begin{bmatrix} K_n \\ K_e \\ K_t \end{bmatrix} (T_{rot} \hat{n})^T \end{aligned} \quad (4)$$

And

$$dF_j(t) = dB_j (X - X_{\tau_j}) + dC_j (Y - Y_{\tau_j}) \quad (5)$$

Having following equation:

$$(T_e \hat{n})^T = (T_{tool} \cdot T_{rot} \hat{n})^T = (T_{rot} \hat{n})^T T_{tool}^T \quad (6)$$

Results in:

$$dB = dC \cdot T_{tool}^T \quad (7)$$

Integrating the dB and dC matrices along the cutting edge results in the instantaneous force displacement relationship for the cutting edge j from Eq. (5):

$$F_j(t) = B (X - X_{\tau_j}) + C (Y - Y_{\tau_j}) \quad (8)$$

This integration is performed using numerical integration methods (e.g. Simpson's integration method) after evaluation of dB and dC on integration points. Since elements of dB are periodic functions of rotation angle, B itself will become a periodic function of the spindle's rotation angle. The zero order chatter prediction method [7] averages process

coefficient matrices for one period (and multiplies it to the number of cutting edges) and obtains an approximate relationship between forces and vibrations as:

$$F_j(t) = \bar{B}_j (X - X_{\tau_j}) + \bar{C}_j (Y - Y_{\tau_j}) \quad (9)$$

Where

$$\bar{B}_j = \frac{1}{2\pi} \int_0^{2\pi} B_j d\phi, \quad \bar{C}_j = \frac{1}{2\pi} \int_0^{2\pi} C_j d\phi \quad (10)$$

The \bar{B}_j matrix for each cutting edge will be different if the cutting edges had different geometries that could affect the edge length and cutting coefficients. Otherwise, the \bar{B}_j and \bar{C}_j are identical for all of the cutting edges and the subscript j could be dropped. Considering (7) results in:

$$B = C.T_{tool}^T \quad \text{and} \quad \bar{B} = \bar{C}.T_{tool}^T \quad (11)$$

An alternative to the averaging is approximation of the periodic matrix B with harmonics (Fourier series) which leads to the multi-frequency solution [14]. Multi-frequency solution is more accurate when the tool-workpiece engagement is highly interrupted (e.g. during flank milling with small radial depth of cuts).

Equation (9) in Laplace domain becomes:

$$\begin{aligned} F_j(s) &= \bar{B}X(s).(1 - e^{-\tau_j s}) + \bar{C}Y(s).(1 - e^{-\tau_j s}) \\ &= [\bar{B}X(s) + \bar{C}Y(s)].(1 - e^{-\tau_j s}) \end{aligned} \quad (12)$$

Considering all of the flutes on the tool:

$$F_{reg}(s) = \sum_{j=1}^N F_j(s) = \left[\sum_{j=1}^N (1 - e^{-\tau_j s}) \right] [\bar{B}X(s) + \bar{C}Y(s)] \quad (13)$$

F_{reg} is represented in the tool coordinate system. The force on the workpiece is calculated by pre-multiplication of the T_{tool} to this vector:

$$F_{wp}(s) = T_{tool} F_{reg}(s) \quad (14)$$

With a linear structure, the relationship between forces and the displacements would be expressed with transfer function matrices in Laplace domain:

$$X(s) = \Phi_{wp}(s).F_{wp}(s) \quad (15)$$

And

$$Y(s) = \Phi_{tool}(s) \cdot F_{reg}(s) \quad (16)$$

From (14) and (15):

$$X(s) = \Phi_{wp}(s) \cdot T_{tool} F_{reg}(s) \quad (17)$$

From (13), (16) and (17):

$$F_{reg} = \left(N - \sum_{j=1}^N e^{-\tau_j s} \right) [\bar{B}X + \bar{C}Y] = [\bar{B}\Phi_{wp}(s) \cdot T_{tool} + \bar{C}\Phi_{tool}] F_{reg}(s) \quad (18)$$

and since $\bar{B} = \bar{C} \cdot T_{tool}^T$ from Eq. (11):

$$\begin{aligned} F_{reg} &= \left(N - \sum_{j=1}^N e^{-\tau_j s} \right) [\bar{C} \cdot T_{tool}^T \Phi_{wp}(s) \cdot T_{tool} + \bar{C}\Phi_{tool}] F_{reg}(s) \\ &= \left(N - \sum_{j=1}^N e^{-\tau_j s} \right) \bar{C} [T_{tool}^T \Phi_{wp}(s) \cdot T_{tool} + \Phi_{tool}] F_{reg}(s) \end{aligned} \quad (19)$$

It is possible to define an effective transfer function Φ_{eff} as:

$$\Phi_{eff} = [T_{tool}^T \Phi_{wp}(s) \cdot T_{tool} + \Phi_{tool}] \quad (20)$$

Then

$$F_{reg}(s) = \left(N - \sum_{j=1}^N e^{-\tau_j s} \right) \bar{C} \Phi_{eff}(s) F_{reg}(s) \quad (21)$$

$$\Rightarrow \left[I_{3 \times 3} - \left(N - \sum_{j=1}^N e^{-\tau_j s} \right) \bar{C} \Phi_{eff}(s) \right] F_{reg}(s) = \mathbf{0} \quad (22)$$

The characteristic equation of the closed loop machining system is obtained by equating the determinant of the matrix $[I_{3 \times 3} - (N - \sum_{j=1}^N e^{-\tau_j s}) \bar{C} \Phi_{eff}(s)]$ to zero [12]:

$$CH(s): \det \left(I_{3 \times 3} - \left(N - \sum_{j=1}^N e^{-\tau_j s} \right) \bar{C} \Phi_{eff}(s) \right) = 0 \quad (23)$$

The stability of the system is determined by checking for presence of unstable poles in this characteristic equation using Nyquist stability criterion. With the eigenvalue method and Nyquist method “s” in the Laplace domain equations is replaced by $j\omega$; however, in the eigenvalue characteristic equation is forced to become zero by solving for a depth of cut that makes the characteristic equation zero in a certain chatter frequency ω_c , but with the Nyquist stability criterion, characteristic equation doesn't have to be equal to zero, and presence of the encircling of the center of the complex plane will indicate instability for a machining system with known depth of cut, spindle speed and other cutting conditions.

3. EXPERIMENTS

Main motivation for this research was modeling of the machining on light-weight casings of jet engines. In these operations the depth of cut direction is often much more flexible and causes chatter. In order to have repeatable experiments, a simple setup is designed where it is possible to replace workpiece after each test to avoid changes in the natural frequency and stiffness of the setup (Fig. 5), notable sources of changes in dynamics of this setup will be differences in clamping forces of the experiment samples which is minimized by tightening the bolts with the same torque. The other source of change is the slight change in the vibration frequency of the structure due to the reduction of mass in form of chips. However, no significant change has been observed in stability of individual processes from the start to the end of machining in this setup during experiments.

The cutting tool is a 25 mm diameter, 70° helix angle, two flute tungsten carbide ball end mill. Cutting parameters of the steel in the experiment is calculated from milling at different feed rates with cylindrical tools using the method described in [13] as: Shear strength at cutting: $\tau_s = 554 \text{ MPa}$, friction angle: $\beta = 24^\circ$ and shear angle: $\phi_s = 29^\circ$. The two first mode shapes of the setup are calculated using finite element modal analysis of Ansys WB software, and presented in Fig. 6. The solution was linear and contacts between the assembly elements were assumed to be ideal.

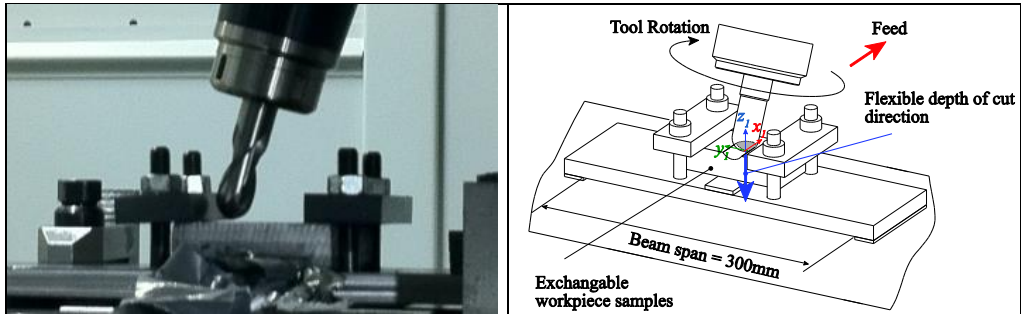


Fig. 5. system with flexibility in the depth of cut direction

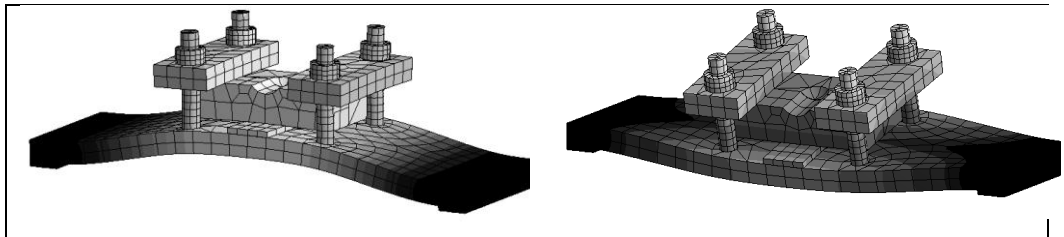


Fig. 6. First and second mode shapes of the experiment setup (Mode shapes are calculated by Ansys WB, v. 13). The beam material is hot rolled AISI 1045 steel, its thickness and width are 15 and 100mm respectively. The average beam mesh is about $7\text{mm} \times 7\text{mm} \times 7\text{mm}$. The first mode is about 510Hz and tooth passing frequency is 133Hz.

Modal stiffness of the second mode is considerably higher than the first mode; therefore the dynamic receptance in the depth of cut direction (z_1z_1 , dominated by the first mode) is 100 times larger than the dynamic receptance in the feed direction (x_1x_1 , dominated by the second mode). Receptance in the depth of cut direction is measured by impact tests and the result is presented in Fig. 7. Slotting operation with three different lead angles of 0° , 15° , and 25° are tested, with a zero tilt angle. Acceleration during machining is measured using a small accelerometer attached to the setup under the machining zone. The amplitude of vibration (x) at the dominant frequency (ω) is estimated by converting acceleration a to displacement in a harmonic movement ($a = -\omega^2x$) which shows a very large vibration at zero lead milling. The effect of these vibrations is also printed on the workpiece surface as shown in Fig. 8. The analytically predicted boundary has a jagged shape due to the approximation of the continuous rotation and engagement with a set of discrete integration points.

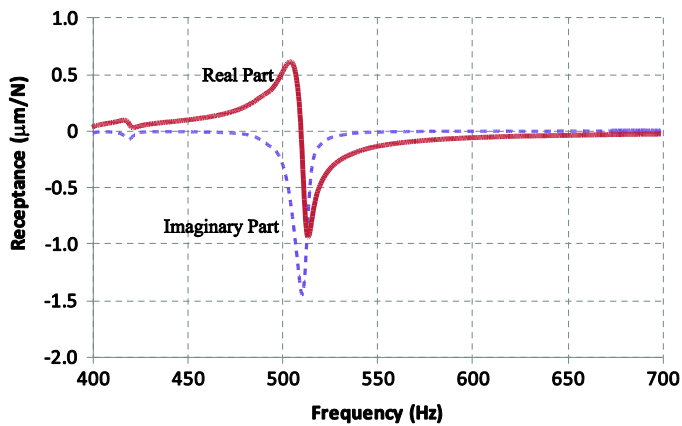
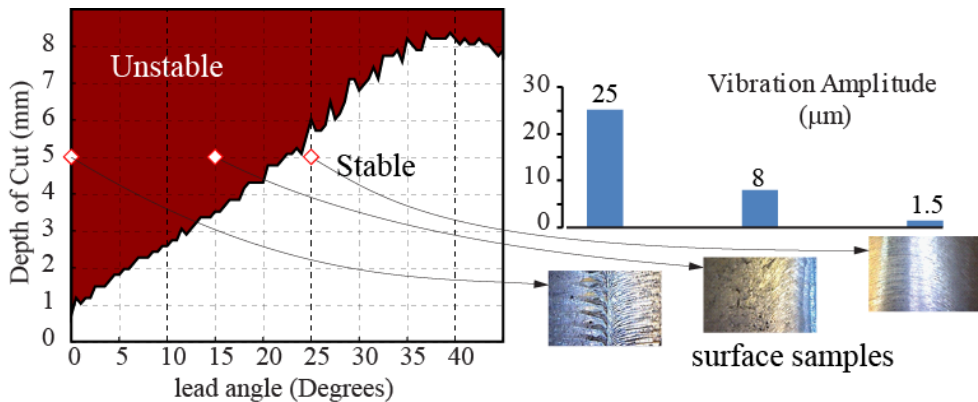


Fig. 7. FRF of the workpiece in depth of cut direction



Slotting, spindle speed = 4000rev/min, tilt angle = 0°

Fig. 8. Experiment results compared to the theoretical predictions. The spindle speed was 4000rev/min.

4. CONCLUSION

Analytical stability prediction method for five axis milling is presented based on application of coordinate transformations between various coordinate systems, discretization of cutting edge, numerical integration and Nyquist stability criterion. Experiments with variable lead angle shows agreement between the theoretical predictions and the experiment results. However, the limit predicted by the method may suffer from discontinuities introduced by finite number of integration points in derivation of numerical integrations. The numerical integration method is powerful since it could be used in stability prediction for complex geometries of the tool-workpiece engagement area, therefore it is suitable in stability prediction in a virtual machining packages where the tool-workpiece intersection is not simply describable with depth of cut and width of cut, but by boundaries of the tool-workpiece engagement area.

ACKNOWLEDGEMENT

This work is performed to support the research project "Vibrations during Milling of Thin walled Aerospace Components" and supported by a grant from the Vinnova FFI program. This support is highly appreciated.

REFERENCES

- [1] L. Xu, J. K. Schueller, and J. Tlustý, "A Simplified Solution for the Depth of Cut in Multi-Path Ball End Milling," *Machining Science and Technology*, vol. 2, pp. 57-75, 1998.
- [2] S. Doi and S. Kato, "Chatter vibration of lathe tools," *Transactions of the American Society of Mechanical Engineers*, vol. 78, pp. 1127-1134, 1956.
- [3] J. Tlustý and M. Polacek, "The stability of machine tool against self excited vibrations in machining," *International research in production engineering, ASME*, , pp. 465-474, 1963.
- [4] S. A. Tobias and W. Fishwick, "A theory of self-excited chatter," *The engineer*, 1958.
- [5] R. Sridhar, R. E. Hohn, and G. W. Long, "A Stability Algorithm for the General Milling Process - Contribution to machine tool chatter research-7," *ASME Journal of Engineering for Industry*, pp. 330-334, 1968.
- [6] "<MachinigSuggestions.pdf>."
- [7] Y. Altintas and E. Budak, "Analytical Prediction of Stability Lobes in Milling," *CIRP Annals - Manufacturing Technology*, vol. 44, pp. 357-362, 1995.
- [8] E. Budak and Y. Altintas, "Analytical Prediction of Chatter Stability in Milling - Part1," vol. 120, pp. 22-30, 1998.
- [9] E. Ozturk and E. Budak, "Dynamics and Stability of Five-Axis Ball-End Milling," *Journal of Manufacturing Science and Engineering*, vol. 132, p. 021003, 2010.
- [10] Y. Altintas, S. Engin, and E. Budak, "Analytical Stability Prediction and Design of Variable Pitch Cutters," *Journal of Manufacturing Science and Engineering*, vol. 121, pp. 173-178, 1999. [11] M. Eynian, "Chatter stability of turning and milling with process damping," University of British Columbia, 2010.
- [12] M. Eynian and Y. Altintas, "Analytical Chatter Stability of Milling With Rotating Cutter Dynamics at Process Damping Speeds," *Journal of Manufacturing Science and Engineering*, vol. 132, p. 021012, 2010.
- [13] E. Budak, Y. Altintas, and E. J. A. Armarego, "Prediction of Milling Force Coefficients From Orthogonal Cutting Data," *Journal of Manufacturing Science and Engineering*, vol. 118, pp. 216-224, 1996.
- [14] E. Budak and Y. Altintas, "Analytical Prediction of Chatter Stability in Milling - Part1," vol. 120, pp. 22-30, 1998.

Numerical simulation of self-excited vibrations - review of methods, potential advantages and pitfalls

Krzysztof Jemielniak, Rafal Wypysinski

Warsaw University of Technology, Faculty of Production Engineering
k.jemielniak@wip.pw.edu.pl

ABSTRACT

Machining stability is one of the most important factors influencing the geometrical and dimensional accuracy of the machined parts. Regenerative chatter is a major limitation to the productivity and quality of machining operations due to poor surface finish and faster tool wear. In general there are two methods of stability analysis: solution of differential equations of the system motion in frequency domain and numerical simulation in time domain. Fast and easy calculations in the frequency domain are possible using a simplified linear model of cutting process. Important limitations of these methods are difficult or impossible consideration of changes dynamic cutting force coefficients and dynamic characteristic of a process. Numerical simulation has not these limitations and regards many specific phenomena of the cutting process, therefore it is often used in the stability analysis. The paper presents main advantages of numerical simulation, which differentiates it from the analytical solutions, as well as some inevitable difficulties and limitations.

KEYWORDS: numerical simulation, nonlinear chatters, cutting dynamic

1. INTRODUCTION

Self-excited vibrations occurring in the cutting process are a major limitation for the achievable performance, machining quality, tools life and durability of machine tools. Hence there is a need of stability limit prediction allowing for selection of chatter-free cutting parameters. Despite the real machine-tool-workpiece system has a very complex structure with many degrees of freedom, for most applications, such as turning and milling, it can be reduced to a multimodal system with two degrees of freedom [7, 27] (Fig. 1). It still allows for consideration of two main causes of self-excited vibrations in machining, which are mode coupling and regenerative effect.

The variable cutting force components F_r and F_t depend on dynamic changes of the uncut chip thickness caused by relative displacement between the workpiece and the tool in radial direction (inner modulation of the uncut chip thickness r_i) and the machined surface waviness left during the previous pass (outer modulation r_T) and the velocity of these displacements (r_i'). Influence of vibration in tangential direction t is generally ignored. Forces

F_r and F_t projected to the x, y directions cause vibration of the machine-tool system. Stability analysis is usually based on analytical or numerical [16] solution of differential equations of the system motion in the frequency domain. Despite the convenience of stability limit calculation the main disadvantage of these methods is the inability (or very high difficulty) to consider machine-tool system characteristic changes in a space and time, especially in case of complex non-linear characteristics of the cutting process. These limitations stimulate attempts of stability analysis based on time domain numerical simulation by many research centers.

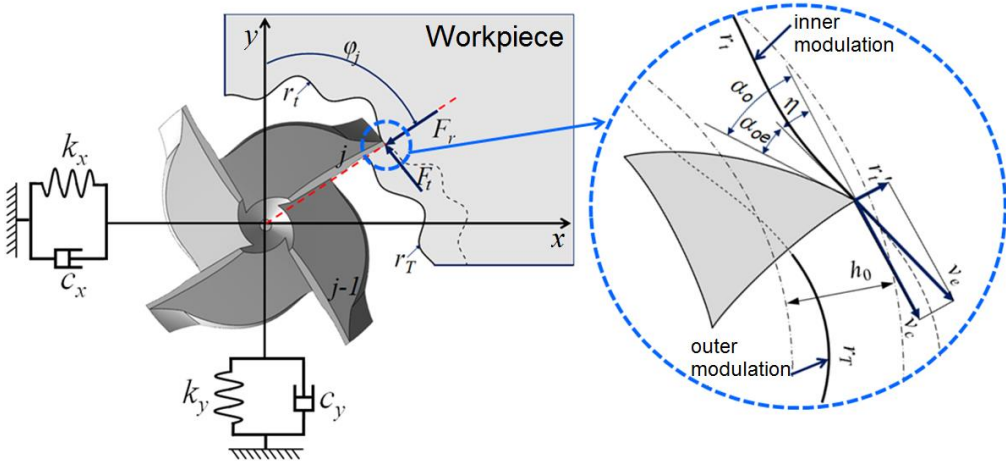


Fig.1. Dynamic system in milling.

In a single iteration of a typical algorithm of numerical simulation (Fig. 2) the following steps can be identified:

- 1) calculation of the current displacement (x_i, y_i) and velocity (x_i', y_i') for the each vibration mode i separately, and subsequently summed up,
- 2) projection of displacements and velocities of the system (x, y) to the r direction, individually for each segment of the cutting edge, and storing the displacements r as an outer modulation r_T used in the next tool pass,
- 3) determination of the variable force components F_r and F_t in the cutting process coordinates based on the selected model dependences of these forces on r_t, r_t' and r_T ,
- 4) projection of the F_r and F_t forces to the F_x and F_y forces and summing them up along the cutting edge.

The first step contains the main difference between stability analysis in frequency domain and numerical simulation in the time domain prediction of the vibration progress. In fact, it contains the basic algorithm of the simulation. Each step presented above and in Fig. 2 presents many possibilities, which differentiates numerical simulation from the analytical solutions, as well as some difficulties and limitations which are discussed in the following paper sections.

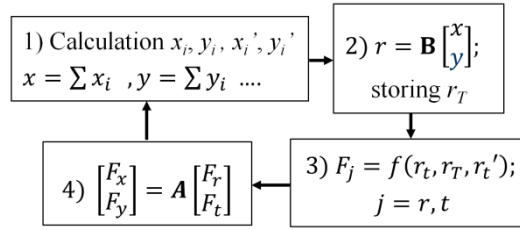


Fig.2. A single iteration algorithm of numerical simulation of self-excited vibrations.

2. DETERMINATION OF THE SYSTEM DISPLACEMENTS

There are two main approaches to the problem of numerical simulation in the time domain. The first one, the most commonly used, is based on Runge-Kutta (first or fourth order) numerical integration methods [34]. The second one, also often used, is the algorithm resented in [37]. According to this algorithm each of the vibration modes of the multimodal system is analyzed separately, and then the displacements are summed up. The index „i” indicating the vibration mode was omitted here to simplify the notation. The calculations start with the determination of accelerations, velocities and displacements in the current iteration:

$$p'' = (F_{pB} - c_p p_B' - k_p p_B) / m_p \quad (1)$$

$$p' = p_B' + p'' dt; p = p_B + p' dt \quad (2)$$

where $p = x$ or y , index B – forces, displacement and velocities in the previous iteration, m_p, c_p, k_p – mass, damping and stiffness of machine-tool system.

Then the displacements and velocities are summed up for all vibration modes of the multimodal system in both directions.

3. DETERMINATION OF DYNAMIC CUTTING FORCES COMPONENTS

3.1. Dependence of the uncut chip thickness and effective clearance angle

The source of the cutting force variation are changes of the uncut chip thickness (h) and effective clearance angle α_{oe} determined by the inclination of effective cutting speed η (see Fig. 1):

$$h = h_0 - r_t + r_T = h_0 + h_d; h_d = -(r_t - r_T) \quad (3)$$

$$\eta \approx \tan \eta = r_t' / v_c \quad (4)$$

where h – uncut chip thickness, h_d – dynamic component of h , h_0 – nominal h , η – inclination angle of the tool path. When analyzing the complex cutting edge, forces acting on the small individual segment are considered separately and then there are summed up. Transition from machine-tool system x - y to the cutting process system r - t (step 2 in Fig. 2) is a simple

transformation (rotation) of the coordinate systems. It should be noted however, that while x and y displacement are related to the whole machine-tool system, during milling with helical flute cutter, displacements are projected on r and t directions for each individual part of cutting edge separately, as the angular position φ_{ij} of the segment depends on the angle of cutter rotation and the angle of twist of considered segment. Fig. 3 shows the scheme of angle φ_{ij} determination. Full consideration for any complex shape of the cutter can be found in [10], however the principles stay the same. The displacement of the cutting edge segment in perpendicular direction to the corresponding workpiece surface and the speed of this displacement can be described as (Fig. 3):

$$r_{tij} = x_i \sin \varphi_{ij} + y_i \cos \varphi_{ij}; \quad r'_{tij} = x'_i \sin \varphi_{ij} + y'_i \cos \varphi_{ij} \quad (5)$$

$$\varphi_{ij} = \varphi_{ni} + \varphi_{zj}; \quad \varphi_{zj} = \frac{2z_j}{D \cot \lambda_s} \quad (6)$$

where i – iteration (time) index, j – index of considered segment distance from the cutter face, φ_{ni} – rotation angle of considered flute on the cutter face, φ_{ij} – rotation angle of considered segment, z_j – distance of the segment from cutter face, λ_s – inclination angle of the cutting edge, D – cutter diameter.

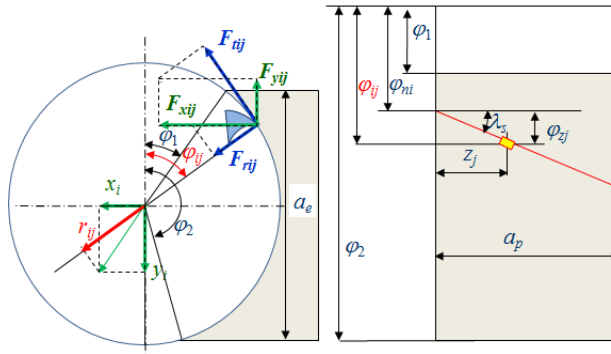


Fig.3. Discretization of the cutting edge and the distribution of cutting forces for helical flute cutter.

Instantaneous uncut chip thickness for the considered segment of the cutting edge can be described as follows:

$$h_{ij} = f_z \sin \varphi_{ij} - r_{ij} + r_{Tij} \quad (7)$$

where f_z – feed per tooth. Obviously, equation (7) remains valid only for angles φ_{ij} between entry angle φ_1 and exit angle φ_2 (Fig. 3) [3, 18]. However, backside cutting can occur at a tooth rotation angle φ_{ij} located outside (φ_1, φ_2) region [21].

The cutting edge segmentation should depend on the tool shape and include the distribution of cutting forces on the cutting edge. Therefore, for milling tools with round corner (radial or ball end-mills) radial segmentation is preferred [41]. However (especially in the analytical method or numerical integration) division into equal segments is often used [13, 21]. In the case of end-mills the distribution along the axis of the elementary parts with the same shape and the same height is justified [25].

Numerical simulation also enables to consider the effect of the tool run out on the uncut chip thickness. It can be achieved by the assumption of circular (movement in one direction) or trochoidal tool trajectory [11]. In both cases, the geometric parameters of the process are constant along the tool path, but run out of the cutter is introduced to the each single point of cutting edge [9]. The most complex case specifies different trochoidal paths for each tooth, which means different active diameter for each tooth. Then the uncut chip thickness for the current tooth is the difference between the current and the previous tool path along the line segment connecting the center of the tool with the current cutting edge. This approach is used instead of the low computational cost approximation, proposed by Martellotti [28]: $f_z \sin(\varphi)$. Trochoidal tool path improves simulation effect of entry ($\varphi_1=0^\circ$) and exit ($\varphi_2=180^\circ$) tool zone, where uncut chip thickness is not equal 0 and it can achieve significant values when run out is considered. When taking into account the lateral and torsional tool vibration, the angular positions of the current (φ_j) and previous (φ_{j-1}) cutting edge can be determinate as follows [22]:

$$\varphi_j = \tan \frac{x_t(j)-x_c(j-1)}{y_t(j)-y_c(j-1)}, \varphi_{j-1} = i_{prev} \varphi_P \varphi_c(j-1) \quad (8)$$

where index c means variables related to the center of the tool, $j-1$ is a previous edge distant by pitch P , t – current position, φ_P – angle of tool pitch. This complex vibration case makes a difference (φ_v) between two angular positions of the cutter (φ_j, φ_{j-1}):

$$\varphi_v = \varphi_j - \varphi_{j-1} = \tan \frac{x_t(j)-x_c(j-1)}{y_t(j)-y_c(j-1)} - \varphi_{j-1} \quad (9)$$

When φ_v reaches zero, then two angles φ_j, φ_{j-1} and two positions on the cutting edge ($x_t(j), y_t(j)$ and ($x_c(j-1), y_c(j-1)$) coincide with the considered cutting edge segment. If φ_v is not equal zero, then φ_m (previous initial rotation angle of the cutter center) is changing until φ_v reach 0 value. Dynamic cutting thickness is calculated using the current and previous position of the cutting edge when φ_v reach 0.

3.2. Storage of the surface created in previous cut

Considering the outer modulation of the uncut chip thickness requires storage in a computer memory the relative tool-workpiece displacements in radial direction r_t and introducing it to the calculation of instantaneous uncut chip thickness during the next cutting edge pass as r_T (Fig. 1, eq. 3 and 7). While it is quite simple for turning, it is much more complicated for milling. It can be realized by storage of all positions of the tool (and the workpiece if necessary) or storage of the generated surface (generating surface profile). Outer modulation can be reconstructed from the instantaneous position of the cutting edge segment, calculated for the j -th tooth, the k -th level along the tool axis and the i -th iteration step the tool having vibration and run out as [25]:

$$x(i, j, k) = [R + \Delta R(j, k)] \sin \varphi(i, j, k) + x_t(i, k) - x_{tw}(i, k) + i \frac{N_f f_t}{N} \quad (10)$$

$$y(i, j, k) = [R + \Delta R(j, k)] [1 - \cos \varphi(i, j, k)] + y_t(i, k) - y_{tw}(i, k) \quad (11)$$

where N – number of iterations per revolution, R – cutter radius, $\Delta R(j, k)$ – cutter run out for j -th cutting edge and k -th level along the tool axis, N_f – number of teeth, φ – angular position, f_t – feed per tooth, x_t, y_t, x_{tw}, y_{tw} – displacements of tool and workpiece in x and y directions.

Another solution is based on storage of milling tool centers and cutting edge positions used for the generated surface calculation. The positions can be stored in the array as a function of rotation angle with the j index or simulation time intervals. Simulation of the milling process necessitates tree-dimensional surface determination, which requires registration of three coordinate position of cutting edge (x, y, z), three coordinates of the cutter center (x_c, y_c, z_c) and angular position of the cutting edge (φ) [6].

Storage of the tool positions history is not very memory consuming, but requires determination of outer modulation r_T for each iteration and for all segments of the cutting edge (eq. 5). The alternative is storage of the tool-workpiece displacements in radial direction r_i and use them in the next passes as r_T , which admittedly requires more computer memory but reduces the calculation cost.

The main non-linearity of the cutting process is exiting the tool from the workpiece, resulting in vanishing of cutting forces. It can be taken into account by more precise definition of the r_T value (outer modulation): it must be determined as a trace left on the surface generated in the previous or earlier passes [17, 18, 24, 37]:

$$r_T = \text{minimum} \{ r(t-T), h_0 + r(t-2T), 2h_0 + r(t-3T) \dots \} \quad (12)$$

3.3. Dynamic force dependence on the uncut chip thickness changes

Fundamental importance for the stability analysis results has assumed model of the cutting process – the dependence of dynamic cutting forces on uncut chip thickness changes (F_{rk}, F_{tk}) and velocity of vibrations in r direction (F_{rc}, F_{tc}). These dependencies refer to the elementary segment of the cutting edge (for example 1mm), as shown in section 3.1, Fig. 3. Experimentally determined the dependence of static (without vibration) forces on the static uncut chip thickness h_0 can be expressed as (Fig. 4a) [31]:

$$F_{j0} = C_j b h_0^a \text{ for } j=r, t, a \approx 0,7 \quad (13)$$

For the analytical stability limit determination these relationships can be linearized at the operating point (Fig. 4b [14, 17, 30]). Thus components dependent on uncut chip thickness are:

$$F_{jk} = b h_d \frac{dF_{j0}}{dh} \Big|_{h=h_0} = b C_j a h_0^{a-1} h_d = b k_{jd} h_d \quad (14)$$

This solution is sufficiently accurate for turning, when the nominal uncut chip thickness h_0 is constant. However, in milling uncut chip thickness is inherently variable, sometimes from zero to the maximum. Thus, the most common is Altintas model [5], which is a simplified linear dependence $F_j(h_d)$ (Fig. 4c). As can be seen in Fig. 4c, this assumption is very inaccurate at low uncut chip thickness. Therefore sometimes set of local models are used [12, 32], covering the different cutting conditions, e.g. within a certain range of the uncut chip thickness (Fig. 4d). It should be strongly emphasized here that numerical simulation allows for application of any characteristics of the dynamic cutting forces even in the form (13) or in tabular form based on experimental data, and accurately calculate its value at each iteration for each point of the cutting edge and corresponding actual uncut chip thickness. It is worth noting that there were many efforts devoted to the modeling of the actual cutting forces dependence on uncut chip thickness and these results can be easily used for numerical simulation of self-excited vibration [19, 26, 40].

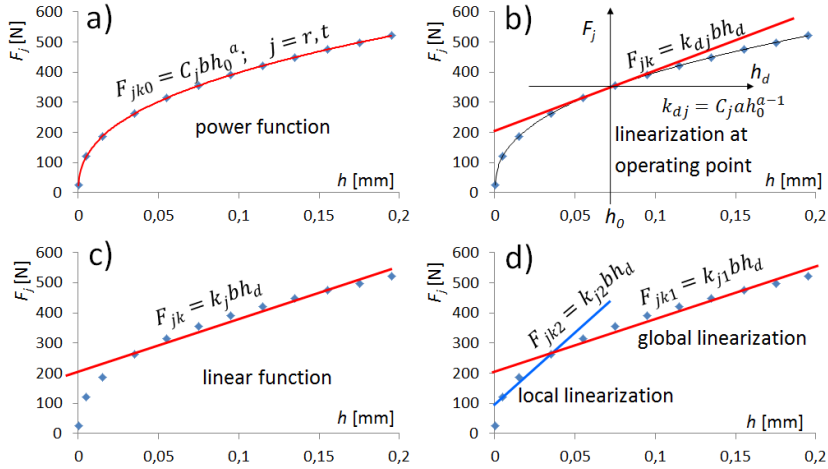


Fig.4. Dependence of cutting force on the uncut chip thickness: a) power function, b) linearization at the operating point, c) linear function, d) local and global linearization.

3.4. Damping of the cutting process

Since the earliest works the influence of the effective clearance angle on the stability limit was noticed [20, 38, 39]. Damping component of the cutting force, usually is assumed to be proportional to the inclination of effective cutting speed η which is proportional to the vibration velocity r_t' , (Fig. 1, eq. 4) [1, 15, 35, 36]:

$$F_{jc} = \frac{c_j r_t'}{v_c} b \quad (15)$$

where c_j – process damping coefficient. The value of the c_j is constant, averaged for the entire oscillation period, often determined by comparing the experimentally and analytically obtained stability limit [8, 29]. However well-known low speed stability effect is caused by interference between the flank face of the cutting surface [20], resulting from the declining effective clearance angle (α_{oe} Fig. 1), which occurs only for negative values of vibration velocity r_t' . Recently many attempts to model this phenomenon were undertaken by modeling of contact pressure and the volume of the deformed material under flank face [7, 33, 35]. However, even after such complex evaluation, the final results are simplified to one linear factor as in equation (15).

Again, using numerical simulation any nonlinearities of the process, including its damping can be easily taken into account. The damping force can be calculated for each iteration step separately, considering any complex dependencies of this force on instantaneous conditions. In [17] it was assumed, that angle α_{oe} cannot be negative thus its approach to zero results in an increase of the damping cutting force to infinity. This effect was achieved by using dependence describing the damping force in the form:

$$F_{jc} = \begin{cases} -c_j b r_t' & \text{dla } r_t' \geq 0 \\ -c_j b r_t' + LSS \frac{r_t'/v_0}{\alpha_0 + r_t'/v_0} & \text{dla } r_t' < 0 \end{cases} \quad \text{dla } j = r, t \quad (16)$$

where LSS – low speed stability coefficient determined experimentally.

Obviously this dependence can be replaced by any other, resulting from modeling or experimental results. Sometimes the influence of tool wear on process damping is considered [1, 2]. In [4] the influence of the flank-wave contact was modeled by considering both slope (r_t'/v_c) and curvature (r_t''/v_c^2) of the waves.

3.5. Determination of resultant cutting forces

The resultant cutting force is the sum of the forces acting on each small segment of cutting edge engaged in cutting process due to the regeneration and tool rotation (Fig. 3), for all flutes. Each elementary force is calculated on the base of the assumed cutting force model (see above) as a sum of all components of cutting force. In a specific angular position of the cutter φ_{ij} cutting force distribution changes along the cutting edge. Projection of forces acting on the edge segments in the process system (F_{ij} , F_{rij}) to the machine system (F_{xij} , F_{yij}) also changes along the edge with the angle φ_{ij} :

$$F_j = \sum_{k=1}^{z_n} \sum_{i=\varphi_1}^{\varphi_2} \sum_{j=1}^{a_p} (F_{jk} + F_{jc}) \text{ for } j = r, t \quad (17)$$

where i subsequent angular cutter position φ , k – index of the tooth, z_n – the teeth number, j – segment number along the axis.

4. COMPUTING COST OF SIMULATION

Simulation accuracy depends strongly on the number of cutting edge segments inversely proportional to the segment size, especially when the number is small. The same is with the iteration time (step dt eq.3 and 4). – the shorter the better. Of course, computation time is proportional to number of cutting edge segments and number of iteration steps per second. However after crossing some number of segments and iteration steps the accuracy effectiveness becomes less and less eminent still causes the rise of computational costs [18]. Also shape of a round cutting edge segments has a strong influence on simulation accuracy and computational cost. For this reason division of the ball end-mill to equal segments along the tool axis seems to be not justified [21]. A significant computing cost reduction (simulation time), especially for the stability lobes determination, can be achieved by separation of triangular and quadrilateral segments [23, 35] or matching discretization steps according to the distance from the stability limit, determined by successive approximations [18]. Therefore it is recommended to take relatively large steps in the beginning (far from the designated stability limit), while decreasing near to the final solution. Final validation should be done by real cutting.

5. SUMMARY AND CONCLUSIONS

Analytical prediction of the stability limit in time domain provides fast and easy obtainable results. However they are based on radically simplified, linear models of the cutting process and machine tool characteristics. It is impossible or very difficult to take into account these nonlinearities and – which is even more harmful – to consider continuous changes of these characteristics due to e.g. change of the workpiece shape. Numerical simulation of self-excited vibrations has not these limitations. Any characteristic of the cutting force or the machine tool system can be easily implemented, even in the form of direct experimental results, tables. The main limitation and drawback of the numerical simulation is a high computational cost (time

of calculations). Therefore the algorithms and data structures in simulation program are very important and should be carefully prepared. On the other side, increasing computing power allows for prediction of greater use of numerical simulation especially for virtual machining. Nowadays however there are only few practical systems and equipment available on the market for chatter detection and control. Even those installed in factory floor are not frequently used, presumably because they are too difficult to understand, not user friendly enough. This aspect should be carefully taken into account in future developments.

ACKNOWLEDGEMENTS

Financial support of Structural Funds in the Operational Program - Innovative Economy (IE OP) financed from the European Regional Development Fund - Project "Modern material technologies in aerospace industry", Nr POIG.01.01.02-00-015/08-00 is gratefully acknowledged.

REFERENCES

- [1] K. Ahmadi, S. Ismail, "Analytical stability lobes including nonlinear process damping effect on machining chatter," *International Journal of Machine Tools and Manufacture*, vol. 51, 2011, pp. 296–308.
- [2] K. Ahmadi, S. Ismail, "Experimental investigation of process damping nonlinearity in machining chatter," *International Journal of Machine Tools and Manufacture*, vol. 50, 2010, pp. 1006–1014.
- [2] Y. Altintas, "Modeling approaches and software for predicting the performance of milling operations at MAL-UBC," *Machining Science and Technology: An International Journal*, vol. 4, 2000, pp. 445–478.
- [4] Y. Altintas, M. Eynian, H. Onozuka, "Identification of dynamic cutting force coefficients and chatter stability with process damping," *CIRP Annals*, vol. 57, 2008, pp. 371–374.
- [5] Y. Altintas, P. Lee, "Mechanics and Dynamics of Ball End Milling," *J. Manuf. Sci. Eng.*, vol. 120, no. 4, 1998, pp. 684–692.
- [6] L. Arnaud, O. Gonzalo, S. Seguy, "Simulation of low rigidity part machining applied to thin-walled structures," *International Journal of Advanced Manufacturing Technology*, vol. 54, 2011, pp. 479–488.
- [7] E. Budak, L.T. Tunc, "Identification and modeling of process damping in turning and milling using a new approach," *CIRP Annals*, vol. 59, 2010, pp. 403–408.
- [8] A. Damir, E-G. Ng, M. Elbastawi, "Force prediction and stability analysis of plunge milling of systems with rigid and flexible workpiece," *International Journal of Advanced Manufacturing Technology*, vol. 54, 2011, pp. 853–877.
- [9] K. Desai, A.P.K. Garwal, P.V.M. Rao, "Process geometry modeling with cutter runout for milling of curved surfaces," *International Journal of Machine Tools and Manufacture*, vol. 49, 2009, pp. 1015–1028.
- [10] S. Engin, Y. Altintas, "Mechanics and dynamics of general milling cutters. Part I: helical end mills," *International Journal of Machine Tools and Manufacture*, vol. 41, 2001, pp. 2195–2212.
- [11] H. Faasen, "An Improved Tool Path Model Including Periodic Delay for Chatter Prediction in Milling," *Journal of Computational and Nonlinear Dynamics*, vol. 2, 2007, pp. 167–179.
- [12] O. Gonzalo, J. Bernstein, "Time Domain Identification of the Milling Specific Force Coefficients with Cutter Run-out," *Proceedings of 4th CIRP Int. Conf. HPC*, 2010, paper A10.
- [13] B.M. Imani, M.H. Sadeghi, M.A. Elbastawi, "An improved process simulation system for ball-end milling of sculptured surfaces," *International Journal of Machine Tools and Manufacture*, vol. 38, 1998, pp. 1089–1107.
- [14] T. Insuperger, G. Stepan, "Increased Stability of Low-Speed Turning Through a Distributed Force and Continuous Delay Model," *Journal of Computational and Nonlinear Dynamics*, vol. 4, 2009, pp. 403–408.
- [15] K. Jemielniak, "Modelling of dynamic cutting coefficients in three-dimensional cutting," *International Journal of Machine Tools and Manufacture*, vol. 32, no. 4, 1992, pp. 509–519.
- [16] K. Jemielniak, M. Nejman, D. Sniegulska-Gradzka, "Analytical and numerical determination of stability limit in turning," *Inzynieria maszyn*, vol. 17, no. 1, 2012, pp. 81–92.

- [17] K. Jemielniak, A. Widota, "Numerical simulation of non-linear chatter vibration in turning," *International Journal of Machine Tools and Manufacture*, vol. 29, 1989, pp. 239-247.
- [18] K. Jemielniak, R. Wypysinski, "Determination of stability limit in turning by numerical simulation," *Inzynieria maszyn*, vol. 17, no. 1, 2012, pp. 93-104.
- [19] M. Kaymakci, Z.M. Kilic, Y. Altintas, "Unified cutting force model for turning, boring, drilling and milling operations," *International Journal of Machine Tools and Manufacture*, vol. 54-55, 2012, pp. 34-45.
- [20] R.L. Kegg, "Chatter Behaviour at Low Cutting Speeds," *CIRP Annals*, vol. 17, 1969, pp. 97-106.
- [21] J.H. Ko, "3D Ball-End Milling Force Model Using Instantaneous Cutting Force Coefficients," *Journal of Manufacturing Science and Engineering*, vol. 127, 2005, pp. 1-12.
- [22] J.H. Ko, Y. Altintas, "Time domain model of plunge milling operation," *International Journal of Machine Tools and Manufacture*, vol. 47, 2007, pp. 1351-1361.
- [23] B. Y. Lee, Y. S. Tarn, S.C. Ma, "Modeling of the process damping force in chatter vibration," *International Journal of Machine Tools and Manufacture*, vol. 35, 1995, pp. 951-962.
- [24] H. Li, X.P. Li, X.Q. Chen, "A novel chatter stability criterion for the modelling and simulation of the dynamic milling process in the time domain," *International Journal of Advanced Manufacturing Technology*, vol. 22, 2003, 619-625.
- [25] H. Li, Y.C. Shin, "A Comprehensive Dynamic End Milling Simulation Model," *Journal of Manufacturing Science and Engineering*, vol. 128, 2006, pp. 86-95.
- [26] S-Y Lin, C-K Chen, "Construction of a dynamic cutting force model for oblique cutting," *Proc. IMechE 224 Part B: J. Engineering Manufacture*, vol. 224, no. 3, 2010, pp. 361-372.
- [27] E. Mahdi, "Chatter stability of turning and milling with process damping," *PhD thesis, The University of British Columbia*, Vancouver, 2010.
- [28] M.E. Martellotti, "An analysis of the milling process," *Trans. of the ASME*, vol. 63, 1941, pp. 677-700.
- [29] I.M. Mehrabadi et al., "Investigating chatter vibration in deep drilling, including process damping and the gyroscopic effect," *International Journal of Machine Tools and Manufacture*, vol. 49, 2009, pp. 939-946.
- [30] F. C. Moon, T. Kalmar-Nagy, "Nonlinear models for complex dynamics in cutting materials," *Phil. Trans. R. Soc. Lond. A*, vol. 359, 2001, pp. 695-711.
- [31] D. Otkar, M. Polacek, L. Spacek, J. Tlustý, "Selbsterregte Schwingungen an Werkzeugmaschinen," *Veb Verlag Technik*, 1962.
- [32] H. Paris, D. Brissaud, A. Gousskov, "A More Realistic Cutting Force Model at Uncut Chip Thickness Close to Zero," *CIRP Annals*, vol. 56, 2007, pp. 415-418.
- [33] R. Rahnama, M. Sasjjadi, S.S. Park, "Chatter Suppression in Micro End Milling with Process Damping," *Journal of Materials Processing Technology*, vol. 209, 2009, pp. 5766-5776.
- [34] J. Roukema, Y. Altintas, "Generalized modeling of drilling vibrations. Part I - Time domain model of drilling kinematics, dynamics and hole formation," *International Journal of Machine Tools and Manufacture*, vol. 47, 2007, pp. 1455-1473.
- [35] V. Sellmeier, B. Denkena, "High speed process damping in milling," *CIRP Journal of Manufacturing Science and Technology*, vol. 5, 2012, 8-19.
- [36] V. Sellmeier, F. Hackeloer, B. Denkena, "Process Damping in Milling – Measurement of Process Damping Forces for Chamfered Tools by Means of an Electromagnetically Guided Spindle," *12th CIRP Conf. on Modelling of Machining Operations*, 2009.
- [37] J. Tlustý, F. Ismail, "Basic Non-linearity in Machining Chatter," *CIRP Annals*, vol. 30, 1981, pp. 21-25.
- [38] J. Tlustý, F. Ismail, "Special aspects of chatter in milling," *ASME J. of Eng. for Industry*, vol. 105, 1983, pp. 24-32.
- [39] A. Tobias, W. Fishwick, "Chatter of lathe tools under orthogonal cutting conditions," *Trans of ASME:B*, 1958, pp. 1079-1088.
- [40] M. Wan, W-H. Zhang, J-W. Dang, Y. Yang, "A novel cutting force modelling method for cylindrical end mill," *Applied Mathematical Modelling*, vol. 34, 2010, pp. 823-836.
- [41] M. Wan, W-H. Zhang, G. Tan, H. Qing., "An in-depth analysis of the synchronization between the measured and predicted cutting forces for developing instantaneous milling force model," *International Journal of Machine Tools & Manufacture*, vol. 47, 2007, pp. 2018-2030.

Non-Regenerative Dynamic Instability in Surface Grinding

Marco Leonesio¹, Paolo Parenti², Alberto Cassinari¹, Giacomo Bianchi¹

¹CNR – Institute of Industrial Technology and Automation, via Bassini 15, Milan, Italy

²Department of Mechanical Engineering, Politecnico of Milan, via La Masa 1, Milan, Italy
marco.leonesio@itia.cnr.it

ABSTRACT

In this paper a particular type of non-regenerative instability in surface grinding is studied: it can be traced back to the properties of the process force field that excites the dynamical system constituted by machine and workpiece. Clear evidences have been collected suggesting that vibrations can occur suddenly even during the first wheel pass and just after wheel dressing, circumstances that exclude workpiece and wheel surface regeneration as instability origin, whereas both surfaces have to be considered ideal. Therefore, the stability of the dynamic system constituted by an oscillating ideal wheel immersed in a positional and velocity-dependent process force field has been studied, demonstrating that in some circumstances the force field itself exhibits an unstable behaviour. The instability occurrence is strictly related to the oscillation direction of the wheel centre according to the mode shape associated to the dominant resonance, with respect to the direction of the grinding force (identified by the ratio between tangential and normal components). Then, the analysis leads to the identification of a simple necessary condition for instability occurrence. The analytical results are confirmed by proper time domain grinding simulations and compared with experimental evidences.

KEYWORDS: surface grinding, chatter, machine dynamics

1. INTRODUCTION

Surface grinding is one of the oldest and most widely used grinding processes: to date there are still few alternatives available for producing perfectly smooth surfaces which are acceptable both technically and from a cost point of view. On the other side, the quality of a workpiece resulting from a grinding process is strongly influenced by the static and dynamic behaviour of the mechanical system, composed by machine tool, wheel, fixture and workpiece; in particular, the dynamic compliance may cause vibrations leading to poor surface quality. For these reason, the comprehension and modelling of grinding process dynamics assume a paramount importance both for end-users and grinder manufacturers.

The dynamics of the process of surface grinding – as well as plunge and roll grinding – has been conventionally analysed with respect to regenerative chatter theory (e.g.,[1][2]). The wheel-workpiece relative dynamics is usually reduced to the sole normal direction and the

Differential Delayed Equation (DDE) governing the dynamic equilibrium is studied for a simple 1DoF system, taking into account wheel and workpiece waviness regeneration, grinding forces non-linearities and wave filtering effect. In [3] an improved model of chatter in grinding is presented, including the effect of torsional dynamics and displacements along normal and tangential directions: stability boundaries are identified and verified with time domain simulations, but the relationship between these boundaries and system dynamic parameters is not pointed out. In order to avoid complex analytical treatments, other approaches to vibration analysis exploit rich time-domain numerical models that enable the simulation of grinding force evolution including dynamic instability occurrence [4][5]; however, these approaches do not provide a deep insight into the involved physical phenomena: in particular, these models have never been exploited to verify the possibility to experience the onset of a some kind of chatter that cannot be ascribed to wheel and/or workpiece regeneration mechanism.

If the broader literature concerned with other material removal processes is considered, there exists a plenty of research dealing with non-regenerative instability occurrence, basically focused on turning and milling. In this case, it is demonstrated that dynamic instability might be traced back to frictional chatter [6], mode coupling [7], termomechanical instability [8] and other complex effects due to system non-linearities [9]. In grinding an attempt in this direction is represented by [10], where a non-linear model force without regeneration phenomenon is proved to exhibit unstable and chaotic evolutions.

In this paper a particular type of non-regenerative instability in surface grinding is studied. Clear evidences have been collected suggesting that vibrations can occur suddenly even during the first wheel pass and just after wheel dressing, circumstances that exclude workpiece and wheel surface regeneration as instability origin, whereas both surfaces have to be considered ideal. The stability analysis is traced back to the properties of the positional and velocity-dependent grinding force field – originated by ideal wheel and workpiece surfaces – that interacts with machine dynamics. The stability condition is identified for a simplified 1DoF system, whose displacement is inclined with respect to the feed direction: this situation approximates the case of a grinder whose wheel head exhibits a dynamic compliance characterized by a dominant resonance.

In section 2, the force model is introduced. Section 3 analyses the equations of dynamic equilibrium and the computation of stability limit in terms of dynamic and process parameters. In section 4, the stability condition is identified for a real industrial case; then, stability limit is verified by means of time-domain simulations and compared with the experimental results of a preliminary testing campaign. Discussion and conclusions are developed in section 5.

2. FORCE MODEL

In most of the available literature, the grinding power exerted by wheel spindle is regarded as a monotonic function of the Material Removal Rate (MRR) [11]; considering a reference frame located at the ideal contact point between the wheel and the workpiece, the tangential grinding force associated to that power can be obtained knowing the wheel velocity, while the normal component is considered proportional to the tangential one. In the case of surface grinding, the tangential component is directed like workpiece feed velocity V_w , while the normal direction is orthogonal to the workpiece plane (see Fig.1).

Based on these assumptions, the following force model is considered, which can be generalized for any kind of wheel-workpiece engagement (see [5]):

$$\begin{Bmatrix} F_x \\ F_z \end{Bmatrix} = b \cdot K_t \begin{Bmatrix} \text{sgn } \Omega \\ \mu \end{Bmatrix} \cdot \left(\frac{MRR}{V_s} \right) \quad (1)$$

where:

- b : grinding width;
- K_t : specific energy associated to the tangential component;
- μ : ratio between normal and tangential component;
- V_s : grinding velocity that is basically the wheel peripheral velocity;
- “ $\text{sgn } \Omega$ ”: sign of wheel velocity (according to the convention depicted in Fig.1);
- x and z : feed and normal axes.

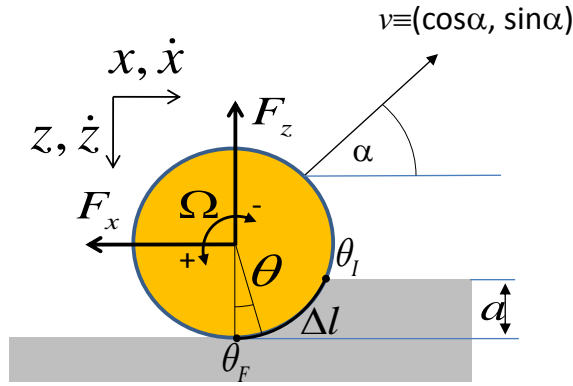


Fig. 1. Surface grinding schema

In the static nominal case, the MRR is given by the following expression:

$$MRR = b \cdot a \cdot V_w \quad (2)$$

where a is the nominal infeed and V_w the workpiece velocity. A general expression for the MRR - taking into account also the dynamic components - can be obtained linearizing the expression of the material flow through the contact length Δl associated to the contact arc $\Delta\theta = [\theta_I; \theta_F]$, when the wheel centre is subject to a position and velocity perturbation $\delta x, \delta \dot{x}, \delta z, \delta \dot{z}$. For small perturbations, it yields:

$$MRR = b \left((V_w + \delta \dot{x}) (a + \delta z) + \delta \dot{z} \sqrt{a D_w} \right) = MRR_0 + b \left(a \delta \dot{x} + V_w \delta z + \delta \dot{z} \sqrt{a D_w} \right) \quad (3)$$

where MRR_0 is the material removal rate in the static case given by (2).

Finally, the (3) can be substituted into the (1) to write the expression of the force perturbation around the equilibrium, that is:

$$\begin{aligned} \begin{Bmatrix} \delta F_x \\ \delta F_z \end{Bmatrix} &= bk_t \begin{Bmatrix} \operatorname{sgn} \Omega \\ \mu \end{Bmatrix} \cdot \left(\frac{a\delta\dot{x} + V_w\delta z + \delta\dot{z}\sqrt{aD_w}}{V_s} \right) = \\ &= \frac{bk_t}{V_s} \begin{bmatrix} a\operatorname{sgn} \Omega & \sqrt{aD_w} \operatorname{sgn} \Omega \\ \mu a\operatorname{sgn} \Omega & \mu\sqrt{aD_w} \operatorname{sgn} \Omega \end{bmatrix} \begin{Bmatrix} \delta\dot{x} \\ \delta\dot{z} \end{Bmatrix} + \begin{bmatrix} 0 & V_w \operatorname{sgn} \Omega \\ 0 & \mu V_w \operatorname{sgn} \Omega \end{bmatrix} \begin{Bmatrix} \delta x \\ \delta z \end{Bmatrix} \end{aligned} \quad (4)$$

3. DYNAMIC EQUILIBRIUM AND STABILITY ANALYSIS

In order to point out a possible mechanism provoking a non-regenerative dynamic instability, let a simple 1DoF dynamical system be excited by the dynamic grinding force (perturbation) expressed by (4). The dynamical system is constituted by a single point (wheel centre) vibrating along a given direction belonging to XZ plane, according to a dominant eigenmode. Let v be the eigenvector associated to the dominant eigenmode, oriented by an angle α with respect to the x axis (see Fig. 1); grinding force equation can be reduced to v by the following constraint equations:

$$\begin{Bmatrix} \delta x \\ \delta z \end{Bmatrix} = \begin{Bmatrix} \cos \alpha \\ -\sin \alpha \end{Bmatrix} d; \quad \delta F_d = \begin{Bmatrix} \cos \alpha \\ -\sin \alpha \end{Bmatrix}^T \begin{Bmatrix} \delta F_x \\ \delta F_z \end{Bmatrix}; \quad (5)$$

where d is the modal coordinate.

Then, the resulting equilibrium equation can be written:

$$\begin{aligned} m\ddot{d} + \left(c + \frac{bk_t}{V_s} \begin{Bmatrix} \cos \alpha \\ -\sin \alpha \end{Bmatrix}^T \begin{bmatrix} a \cdot \operatorname{sgn}(\Omega) & \sqrt{aD_w} \cdot \operatorname{sgn}(\Omega) \\ a\mu & \sqrt{aD_w}\mu \end{bmatrix} \begin{Bmatrix} \cos \alpha \\ -\sin \alpha \end{Bmatrix} \right) \dot{d} + \\ + \left(k + \frac{bk_t V_w}{V_s} \begin{Bmatrix} \cos \alpha \\ -\sin \alpha \end{Bmatrix}^T \begin{bmatrix} 0 & \operatorname{sgn}(\Omega) \\ 0 & \mu \end{bmatrix} \begin{Bmatrix} \cos \alpha \\ -\sin \alpha \end{Bmatrix} \right) d = 0 \end{aligned} \quad (6)$$

where m , c , k are the modal mass, damping and stiffness respectively. For ease of notation, let the following quantities be defined:

$$\begin{aligned} \Delta \hat{c} &= \begin{Bmatrix} \cos \alpha \\ -\sin \alpha \end{Bmatrix}^T \begin{bmatrix} a \operatorname{sgn} \Omega & \sqrt{aD_w} \operatorname{sgn} \Omega \\ a\mu & \mu\sqrt{aD_w} \end{bmatrix} \begin{Bmatrix} \cos \alpha \\ -\sin \alpha \end{Bmatrix} = \\ &= \left(\operatorname{sgn} \Omega a \cos^2 \alpha - \operatorname{sgn} \Omega \sqrt{aD_w} \sin \alpha \cos \alpha - a\mu \cos \alpha \sin \alpha + \mu\sqrt{aD_w} \sin^2 \alpha \right); \end{aligned} \quad (7)$$

$$\begin{aligned} \Delta \hat{k} &= \begin{Bmatrix} \cos \alpha \\ -\sin \alpha \end{Bmatrix}^T \begin{bmatrix} 0 & \operatorname{sgn} \Omega \\ 0 & \mu \end{bmatrix} \begin{Bmatrix} \cos \alpha \\ -\sin \alpha \end{Bmatrix} = \\ &= \left(\mu \sin^2 \alpha - \operatorname{sgn} \Omega \cdot \sin \alpha \cos \alpha \right) \end{aligned} \quad (8)$$

Now, the terms $(bk_t/V_s)\Delta\hat{c}$ and $(bk_tV_w/V_s)\Delta\hat{k}$ can be interpreted as additional damping and stiffness introduced in the system by the grinding process. Then, the (6) can be rewritten as it follows:

$$m\ddot{d} + \left(c + \frac{bk_t}{V_s} \Delta\hat{c} \right) \dot{d} + \left(k + \frac{bk_tV_w}{V_s} \Delta\hat{k} \right) d = 0 \quad (9)$$

The (9) is the equation of a free harmonic oscillator, whose global damping and stiffness are influenced by process parameters. It is straightforward that the (9) yields unstable solutions if at least one of following conditions are satisfied:

$$\bullet \quad \left(c + \frac{bk_t}{V_s} \Delta\hat{c} \right) < 0 \quad (\text{dynamic instability}) \quad (10)$$

$$\bullet \quad \left(k + \frac{bk_tV_w}{V_s} \Delta\hat{k} \right) < 0 \quad (\text{static instability}) \quad (11)$$

3.1. Dynamic instability

Since the structural damping c is always positive, a necessary condition for dynamic instability is $\Delta\hat{c} < 0$. Based on the reasonable assumption that:

$$\frac{D_w}{a} \gg 1 \quad (12)$$

it can be demonstrated that $\Delta\hat{c} < 0$ if

$$\begin{cases} \alpha \in \left[0, \tan^{-1} \frac{1}{\mu} \right] & \text{for } \text{sign}(\Omega)=1; \\ \alpha \in \left[-\tan^{-1} \frac{1}{\mu}, 0 \right] & \text{for } \text{sign}(\Omega)=-1; \end{cases} \quad (13)$$

The condition (13) represents a relationship between geometrical properties of a machine mode shape and grinding force and constitutes the key point for an integrated optimization of the grinding process. Once the condition (13) is verified, the system may be led to instability by acting on the following term that can be interpreted like a gain on the negative component of the equivalent damping of the dynamical system:

$$\psi \stackrel{\text{def}}{=} \frac{bk_t}{V_s} \quad (14)$$

When ψ is large enough, $(c + \psi\Delta\hat{c}) < 0$ and the system becomes unstable (dynamic instability). In order to ease the intuition, let the term $\Delta\hat{c}$ be depicted by considering $\sqrt{aD_w} = 0.2$ and $\mu = 2$.

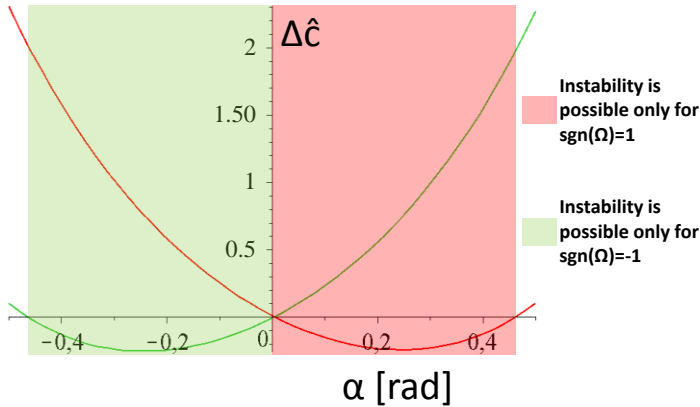


Fig. 2. Necessary condition for dynamic instability

Finally, it is worth to be noted that the infeed parameter a appearing in the equations refers to the actual value, which is always lower than the nominal one, due to the overall system compliance, including the wheel deformation. According to the most of literature (for instance [12]), considering an approximated linear compliance, the actual infeed can be derived as it follows:

$$a = \frac{a_{nom}}{1 + \frac{K_G}{k_z}} \quad (15)$$

where k_z is the static stiffness of the machine in z direction and K_G is the so-called “grinding stiffness”, that defines the linear relationship between actual infeed and the normal grinding force. Considering the (1) and the (2), it can be shown that $K_G = b\mu k_t V_w / V_s$.

3.2. Static instability

Another form of instability occurs when $\Delta\hat{k} < 0$: in this case, the static component of grinding force diverges exponentially (static instability). It can be demonstrated that the necessary condition for static instability is still the (13), namely the same of that for dynamic instability. Once this condition is verified, the system may be led to static instability by acting on the following term, that can be interpreted like a gain on the negative component of the equivalent stiffness of the dynamical system:

$$\rho = \frac{k_t V_w b}{V_s} \quad (16)$$

When ρ is large enough, $(k + \rho\Delta\hat{k}) < 0$ and the system becomes unstable (static instability). Now, it is worth to analyse which kind of instability (i.e. dynamic or static) has more chance to occur, considering an average sample situation for machine dynamics and process parameters. On this purpose, let the following indicator be defined:

$$R = \frac{\kappa \Delta \hat{c}}{\rho \Delta \hat{k}} \frac{k}{c} : \quad (17)$$

it compares a relative change in equivalent damping due to grinding force field with the corresponding change in equivalent stiffness. If R is largely greater than 1, dynamic instability is more likely, as it means that the relative variation of equivalent damping due to process is more important than stiffness variation. Dually, lower values of R indicates that static instability is more prone to rise. Let the R value be computed for a realistic surface grinding operation (whose parameters are reported in Table 1), with a plausible eigenmode (whose parameters are reported in Table 2) and considering a wheel displacement direction corresponding to the worst situation (minimum value for both $\Delta \hat{c}$ and $\Delta \hat{k}$, that can be demonstrated to be $\alpha = 1/2 \tan^{-1}(1/\mu)$).

Table 1. Grinding parameters

D_w [mm]	b [mm]	k_t [J/mm ³]	μ	Ω [rpm]	V_w [m/min]	a_{nom} [mm]
600	100	30	1.5	+1000	32	0.03

 Table 2. Modal parameters and overall stiffness in z direction

m [Kg]	k [N/m]	Freq. [Hz]	c [Ns/m]	k_z [N/m]
3000	1.13e8	31	3.49e+003	5.10e7

It yields:

$$R = \frac{\frac{bk_t}{V_s} \sqrt{aD_w}}{\frac{V_w bk_t}{V_s}} \frac{k}{c} = \frac{\sqrt{aD_w}}{V_w} \frac{k}{c} = 595 \quad (18)$$

Therefore, dynamic instability seems to be definitely more critical than static instability.

4. NUMERICAL AND EXPERIMENTAL VERIFICATIONS

According to the presented approach, the stability limit has been studied for a large surface grinding machine with a gantry architecture (see Fig. 3). A preliminary grinding test campaign has been carried out in order to calibrate the grinding parameter k_t and μ for the considered nominal infeed of 0.03mm. The normal and tangential forces grinding were measured by means of a Kistler™ piezo dynamometer 9255B connected to a National Instrument™ DAQ (NI9215). The workpiece was constituted by a block of low-carbon steel (Fe510 - EN10027) of dimension 260x210x40mm. The machine was equipped with an Aluminum Oxide wheel, resin bonded, by Rappold™ (dimension: 610x100x127, code: 7A36I9V15), characterized by a quite large grit size and a soft grade. The obtained parameters values are those previously presented in Table 1.

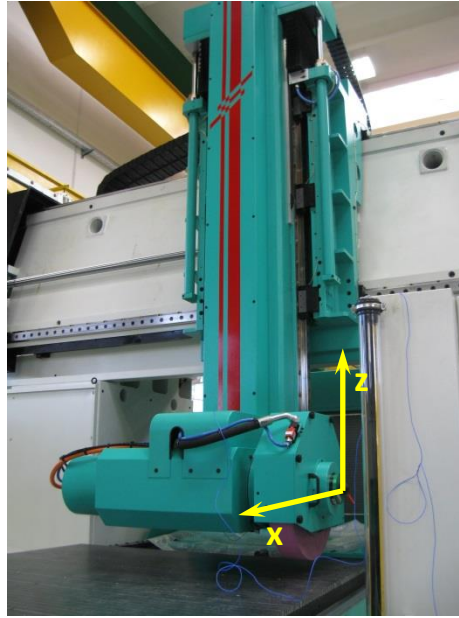


Fig. 3. The tested grinding machine

The co-located dynamic compliance at wheel surface in x direction (feed) and z direction (normal) has been measured via impulsive excitation (hammer test), measuring the acceleration with proper piezo-accelerometers. A modal identification has been performed by means of *SDTool* Matlab™ toolbox, imposing the modes to be real: the most relevant resonances have been identified, along with the corresponding modal mass, stiffness and relative damping (from which the absolute damping can be easily derived). The direct responses in x and z are shown in Fig. 4 along with the corresponding modal identification.

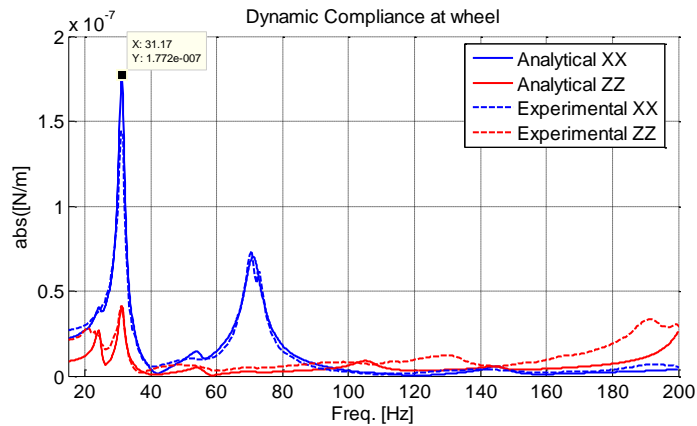


Fig. 4. Measured and Identified machine Dynamic compliance at wheel

A paramount resonance can be noticed at about 31Hz: the modal parameters associated to this resonance are those already reported in Table 2. By plotting the absolute value of the displacement along z on the displacement along x direction, the eigenmode inclination angle can be identified (Fig. 5): it is equal to 0.454rad (26deg).

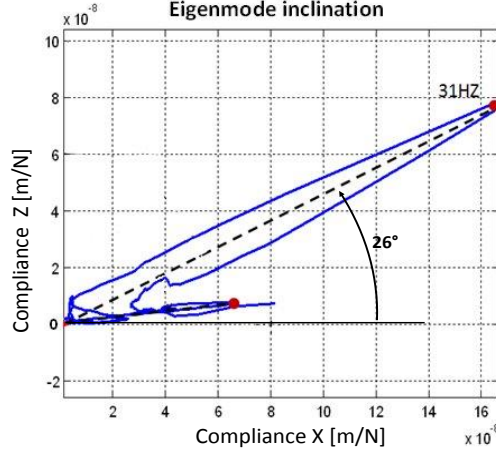


Fig. 5. Inclination of the dominant eigenmode

Considering the process parameters of Table 1, the necessary condition for instability yields $\alpha \in [0, 0.588rad]$; it can be observed that the eigenmode at 31Hz satisfies this condition. Then, $\kappa\Delta\hat{c}$ can be computed for the considered process parameters and eigenmode:

$$\kappa\Delta\hat{c} = -2.7e+4 \frac{Ns}{m} \quad (19)$$

Given the structural damping of the considered eigenmode (Table 2), it follows that $c + \Delta\hat{c} = -2.4e4$, therefore the system is unstable.

A time-domain simulation (example 1) has been performed exploiting the model described in [5] – that does not model wheel wear (thus avoiding possible wheel regenerative chatter) – starting from an ideal workpiece and considering the above mentioned dominant eigenmode in terms of modal parameters and inclination angle. The results, in terms of normal cutting force (time and frequency domain) are depicted in Fig. 6.

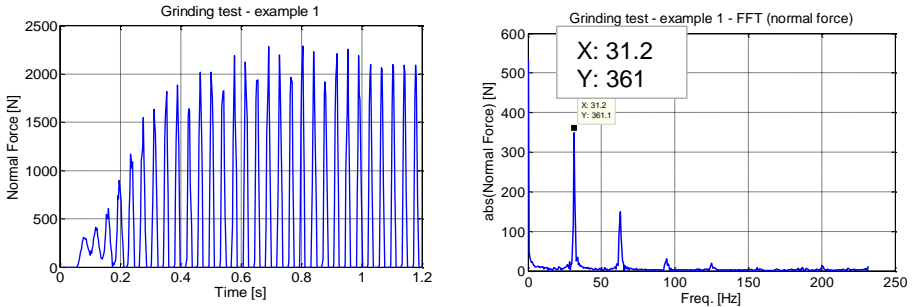


Fig. 6. Simulated normal force for example 1 ($\alpha=0.454rad$): time and frequency domain (Magnitude of FFT)

The dynamic component due to chatter occurrence is clearly visible at about 31.2Hz. The subsequent harmonics are due to the discontinuities associated to the detachment of the wheel from the workpiece when the vibration amplitude becomes greater than the actual infeed. Now, let a different inclination angle be introduced in the simulation model, in particular $\alpha=0.580\text{rad}$. This value still belongs to the instability region, but yields $c + \Delta\hat{c} = 6e2$ and the system is stable. The simulation results (example 2), in terms of cutting normal cutting force (time and frequency domain) is depicted in Fig. 7.

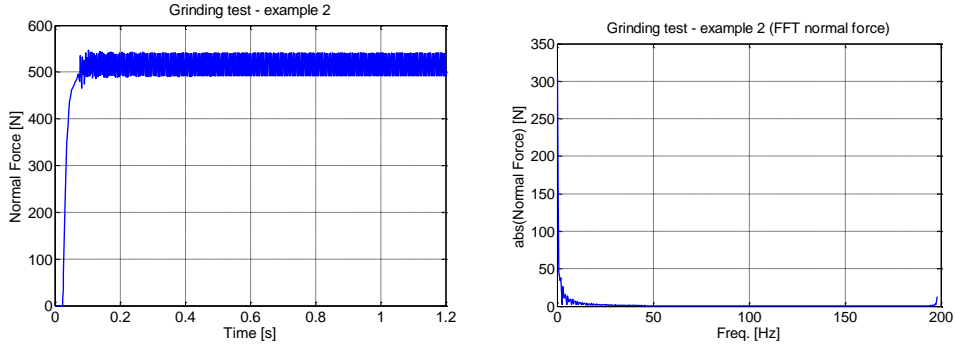


Fig. 7. Simulated normal force for example 2 ($\alpha=0.580\text{rad}$): time and frequency domain (Magnitude of FFT)

Coherently with the prediction, in this case the grinding process is stable and the normal force dynamic components are substantially absent (neglecting small perturbations due to the discretization numerical noise).

A grinding test corresponding to the same parameters of Table 1 has been performed by the grinder under examination, while measuring the grinding forces in x and z direction. The normal force measurement (time and frequency domain) is depicted in Fig. 8, while an image of the resulting surface is given in Fig. 9.

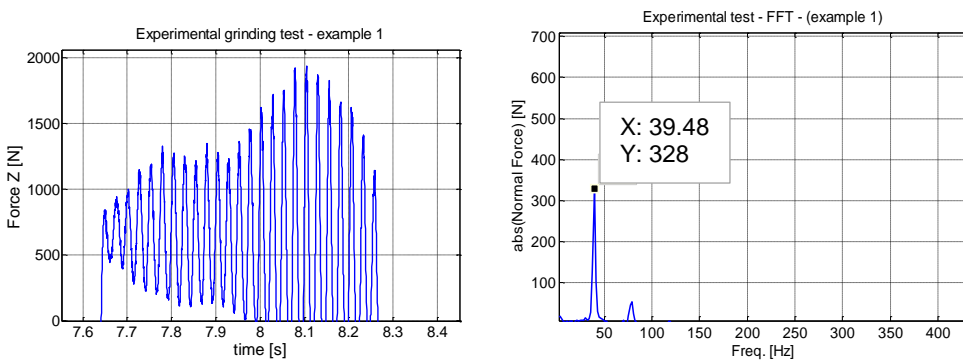


Fig. 8. Measured normal force for example 1: time and frequency domain (Magnitude of FFT)

Chatter occurrence is clearly recognizable, while the dynamic component associated to instability is located at about 39.5Hz, a frequency that is higher than the main resonance appearing in dynamic compliance. This frequency shift could be due to a variation of machine dynamic response while loaded by grinding force during the process, but further investigations are necessary on this topic.

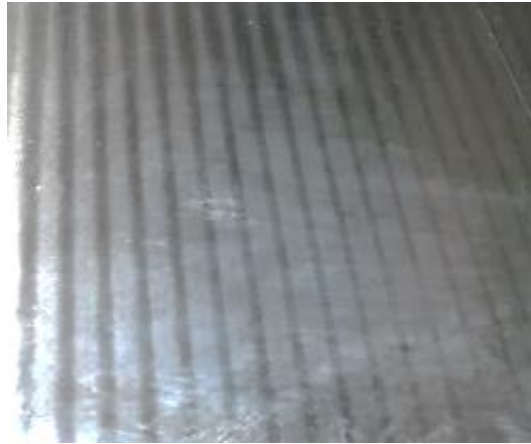


Fig. 9. Resulting surface for unstable grinding

5. DISCUSSION AND CONCLUSIONS

A particular kind of chatter in surface grinding has been studied: it has been traced back to a relationship between grinding force field and wheel-workpiece relative dynamics. A necessary condition has been established, stating that instability can occur only if the vibration direction is comprised between the feed direction and a particular angle depending on grinding force direction: the sufficient condition is a sub-interval whose extent depends on the system damping and grinding severity (nominal force level). The aforementioned instability condition represents the key for a joint design of machine and process, suggesting optimal geometrical properties for the structural mode shapes that move the wheel: in few words, the wheel displacement associated to the dominant mode shapes should be as aligned as possible to feed or normal direction.

Time-domain grinding simulations based on workpiece numerical discretization have confirmed the theoretical predictions. Furthermore, a preliminary experimental campaign showed the compatibility of the predicted stability limit with some grinding force measurements during unstable grinding passes.

Future experimental activities are needed to fully validate the prediction of stability limit. Moreover, a more complete analytical model taking into account also workpiece and wheel regeneration should be addressed to get by a single theoretical framework a deep insight to the major possible sources of grinding instability.

ACKNOWLEDGEMENT

Thanks are extended to the Italian Ministry of Economic Development for the MICHELANGELO project (Industria 2015) grant support and to the ROSA Ermando SpA that provided the availability of the machine.

REFERENCES

- [1] Thompson, R. A., "The Dynamic Behavior of Surface Grinding Part 1 – A mathematical treatment of surface grinding", *Journal Of Engineering For Industry*, (70), 492–497, 1971
- [2] Thompson, R. A., "The Dynamic Behaviour of Surface Grinding Part 2 – Some surface grinding tests", *Journal Of Engineering For Industry*, (70), 492–497, 1971
- [3] Hesterman, D., Stone, B., "Improved model of chatter in grinding, including torsional effects", *Proceedings of the Institution of Mechanical Engineers, Part K: Journal of Multi-body Dynamics*, 216(2), 169–180, 2002, (doi:10.1243/14644190260070402.)
- [4] Hongqi Li, Yung C. Shin, "A Time-Domain Dynamic Model for Chatter Prediction of Cylindrical Plunge Grinding", *Journal of Manufacturing Science and Engineering*, Vol. 128, 2006, ASME.
- [5] Marco Leonesio, Paolo Parenti, Alberto Cassinari, Giacomo Bianchi, Michele Monno, "A time-domain surface grinding model for dynamic simulation", *3rd CIRP Conference on Process Machine Interactions (3rd PMI)*, Nagoya, Japan, 29-30 October 2012.
- [6] Wiercigroch, M. and Krivtsov, A.M., "Frictional chatter in orthogonal metal cutting", *Philosophical Transactions of the Royal Society of London: Part A*, Vol. 359, 713-738, 2001
- [7] Wu, D. W., and Liu, C. R., "An Analytical Model of Cutting Tool Dynamics - Part 1:Model building, - Part 2: Verication", *Trans. ASME, J. Engng. Ind.*, Vol. 107, 107-118, 1985.
- [8] M. A. Davies, and T. J. Burns, "Thermomechanical Oscillations in Material Flow During High-Speed Machining", *Philosophical Transactions of the Royal Society*, 359, 821–846, 2001
- [9] Gradisek, J., "Chatter Onset in Non-Regenerative Cutting: a Numerical Study", *Journal of Sound and Vibration*, 242(5), 829–838, 2001 (doi:10.1006/jsvi.2000.3388).
- [10] Stanescu, N.D., "Chaos in grinding process", *WSEAS TRANSACTIONS on APPLIED and THEORETICAL MECHANICS*, n.4, Vol.4, 2009
- [11] Marinescu I.D., Hitchiner M., Uhlmann E., Rowe B.W., Inasaki I., *Handbook of machining with grinding wheels*, 2007, CRC Press.
- [12] Inasaki, I., Tonou, K., Yonetsu, Y., Regenerative Chatter in Cylindrical Plunge Grinding, *Bulletin of the JSME*, Vol. 20, n. 50, December 1977.

Theme 3

Machine Tool Design

- Robust Thermal Error Compensation Model of Portal Milling Centre Based on Superposition of Participating Thermal Sources In-process Control for Adaptive Spindle Speed Variation and Selection
Martin Mareš, Otakar Horejš, Jan Hornych
Research Center of Manufacturing Technology of the Czech Technical University in Prague, Czech Republic.
- Complex Verification of Thermal Error Compensation Model of a Portal Milling Centre
Otakar Horejš, Martin Mareš, Jan Hornych
Research Center of Manufacturing Technology of the Czech Technical University in Prague, Czech Republic.
- Intelligent Control Using Neural Network Regarding Thermal Errors with Non-linear Behaviour of a Machine Tool
Ikuo Tanabe
Nagaoka University of Technology
- Application of GNNMCI(1, N) to environmental thermal error modelling of CNC machine tools
Ali M Abdulshahed, Andrew P Longstaff, Simon Fletcher, Alan Myers
Centre for Precision Technologies, University of Huddersfield, UK
- Development of modular machine tool structural monitoring
Akshay Potdar, Andrew Longstaff, Simon Fletcher, Ali Abudulshahed
Centre for precision Technology, University of Huddersfield, UK
- Towards Knowledge Framework for Life-Cycle-Long Gathering of Maintenance Information for Decision Support in Machine Tool Design
P. Ferreira, M. Sayed, S. Osei, N. Lohse
The University of Nottingham, Manufacturing Division
- Improved automatic experimental modal analysis of machine tool spindles
Piotr Andrzej Bąk, Krzysztof Jemielniak
Warsaw University of Technology, Poland
- Experimental analysis of the CNx nano-damping material's effect on the dynamic performance of a milling process
Constantinos Frangoudis, Qilin Fu, Md.Masud-Ur-Rashid, Cornel-Mihai Nicolescu, Amir Rashid
KTH Royal Institute of Technology, Stockholm, Sweden
- Using design of experiments approach to determine the essential designing parameters for an anti-vibration turning tool with finite element analysis
Qilin Fu, Amir Rashid, Cornel-Mihai Nicolescu
KTH Royal Institute of Technology, Stockholm, Sweden
- Effect of thin viscoelastic material treatments of the clamping region on dynamic stiffness of the cantilever beams
Mahdi Eynian
University West, Sweden

Robust Thermal Error Compensation Model of Portal Milling Centre Based on Superposition of Participating Thermal Sources

Martin Mareš, Otakar Horejš, Jan Hornych

Research Center of Manufacturing Technology of the Czech Technical University in Prague,
Horská 3, 12800, Prague 2, Czech Republic.
M.Mares@rcmt.cvut.cz

ABSTRACT

This paper is a continuation of scientific work on the modeling of highly nonlinear machine tool (MT) thermal errors using thermal transfer functions (TTF). The method is dynamic (uses machine tool thermal history) and its modeling and calculation speed is suitable for real-time applications. The method does not require interventions into the MT structure and uses minimum of additional gauges (just temperature probes placed close to main heat sources).

The model solves separately each elements participating on thermal error such as spindle rotation, forced convection, cooling system and environmental temperature influences or impact of machine axes movement which are superposed into resulting description of thermally induced deformations. The paper discusses the development of the robust thermal model of real machine tool (portal milling centre) in detail. Moreover, the model was verified within an action of all above-mentioned influences.

KEYWORDS: machine tool, thermal error, transfer function, electrospindle, feed drives

1. INTRODUCTION

The constant increase in spindle speeds and feed motions of machine tool assemblies entails higher and dynamically changing power losses. As a result, the precision of machine tools and their operations is affected by the generated heat and its accumulation in the machine tool structure (and its environment) and by the heat transmission.

Moreover, machine tools placed in ordinary shop floors (without additional air conditioning) are exposed to thermally varying surrounding environment. The continuously changing operating conditions of a machine and thermally varying surrounding environment have a nonlinear and dynamically changing relation with the thermal errors at the tool center point (TCP).

Generally, there are three influences on the working accuracy of a machine tool: static, dynamic and thermo-dependent behavior. Due to scientific achievements in the static and dynamic field of research, the thermal influence on machine tool behavior increases [1].

Thermal effects caused by internal (motors, drives, bearings, ball screws and their nuts, gear box etc.) and external heat sources (effect of the environment, machine operator, radiation etc.) can contribute more than 50% to the overall error [2, 3]. Furthermore, there are continuously increasing demands for machining accuracy in recent years. Therefore this topic is the focus of significant recent research activities [4, 5].

The interest of the manufacturing industry in this topic can also be seen in the latest international standards. In the last two decades a number of international standards [6-8] with measurement standards and performance parameters to assess the thermal behavior of machine tools under no load and finishing conditions have been developed.

2. STATE OF ART

Different approaches exist to minimize thermal errors. In general, it is possible to divide the thermal error issue into three basic groups [3], [9]:

- **Design of the machine tool system to reduce sensitivity to heat flow** (e.g. thermally symmetrical machine tool structure, high-cost materials with low values of thermal expansion coefficient [10], thermal insulation [11] etc.).
- **Temperature control of machine tool and its environment** (e.g. control of machine tool cooling system [12], electric heater [13], thermal actuator [14], air conditions [15] etc.).
- **Compensation of the thermal errors** - generally, two alternatives for the compensation of thermo-dependent TCP displacement can be classified: **direct compensation** (the resulting displacements are intermittently measured and superposed to the desired position value of the particular axis, the disadvantage of the direct approach is the required interruption of the process in order to measure the displacement) or **indirect compensation** methods (readjustment of the axes positioning by the machine tool's control based on mathematical models).

Thermal deformation of machine tool structure cannot be sufficiently eliminated at the design stage and/or using temperature control without high additional cost. On the contrary, indirect thermal error compensation is becoming a cost-effective way to improve accuracy of machine tools.

A lot of mathematical models to compensate the thermal errors are developed. The most common model for prediction of thermally induced displacements of machine tools is obtained by multiple linear regressions (MLR) [16]. These models, which are established in the form of an empirically calibrated polynomial expression, are overly restrictive since their coefficients are assumed to be constant for all operating conditions. While the processing time is small, the accuracy and reliability of the estimated thermal deflection are generally poor, because there is information missing from the unmeasured points on the structure [17, 18].

Furthermore, the displacement of the TCP can be calculated by an artificial neural network (ANN) [19], a fuzzy logic [20] or a transfer function model (TF) [21].

The input of the estimated TF can be NC-data like spindle speed, effective power, electric current, torque or feed rate [22, 23] or the temperatures of the machine structure can also be used as an input (thermal transfer function denominated as TTF) [24]. TF contains the nature of the heat transfer principles. Thus the calibration of the empirical parameters is simple and the model is in addition more reliable with untested inputs and it can even be used

reliably to extrapolate data, since it forces the data to conform to the same mathematical form as the real process.

The modeling of thermally induced displacements of mechanical systems by using TTF requires only few temperature probes in comparison with e.g. ANN, and provides quality comparable to time-consuming methods such as finite element analysis (FEM) [25].

Works treating advanced thermally induced displacements modeling based on TTF, which combines different inputs such as temperature sensors placed on milling machine tool structures and rotational spindle speed and proves model portability among machines of the same type set, are presented in [18], [26]. This study primarily concentrates on extending of heretofore described nonlinearities in the MT thermal behaviour and modelling approach using TTF in detail. The model was applied on a portal milling centre and verified within an electrospindle speed spectrum combined with movement in machine axes. The principle of the discussed indirect compensation method is shown in Fig. 1.

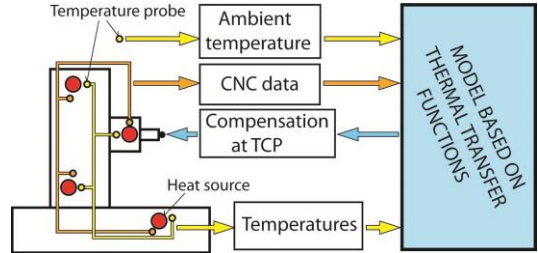


Fig.1. Scheme of the indirect compensation method based on TTF.

3. MATHEMATICAL APPROACH

All data processing and TTF identification, as well as MT thermal behaviour modelling and verification, were performed in *Matlab* and *Matlab Simulink*.

The main advantage of the TTF model lies in its decomposition into individual elements and blocks describing the above-mentioned nonlinear behavior of MT (the TTFs themselves are estimated via linear parametric models ARX and OE [27]). All of these elements are solved independently, and it is possible to extend them as necessary in response to the requirements of individual applications.

The discussed TTF model consists of a variety of TFs controlled by CNC data (electrospindle revolution n in this example).

A discrete 2nd order TF was used to describe the link between the excitation and its response. The differential form of the TF in the time domain is introduced in (1):

$$y(k) = \frac{u(k-1)a_1 + u(k)a_0 - y(k-2)b_2 - y(k-1)b_1}{b_0} \quad (1)$$

where $u(k)$ is the TTF input vector in time domain, $y(k)$ the output vector in time domain, a_i are weight factors of TTF input, b_i are weight factors of TTF output and $k-n$ means the n -multiple delay. Linear parametric models of ARX (autoregressive with external input) or OE (output error) identifying structures were used [27]. The quality of each TTF was examined through linear time invariant (LTI) step response [28].

The excitation in TTF case generally means temperature measured close to a heat source and the response stands for caused deflection on TCP.

The error of approximation is expressed as shown in (2). It also represents the fictitious deformation obtained after implementing the model in the control system.

$$residue = Y - Y_{HAT} \quad (2)$$

The approximation quality of the simulated behavior is expressed by the *fit* (%) value (3). This value expresses the percentage of the output variations that is reproduced by the model [28].

$$fit = \left(\frac{\|Y - Y_{HAT}\|}{\|Y - \bar{Y}\|} \right) \cdot 100 \quad (3)$$

The Y value in (2) and (3) means the measured output (thermal deformation), Y_{HAT} is the simulated/predicted model output and \bar{Y} in (3) expresses the arithmetic mean of the measured output.

4. EXPERIMENT

Data recording, along with the implementation of thermo-elastic models as a control system, were performed with the National Instruments diagnostic devices and LabVIEW.

Compensations of thermal errors at TCP have been developed and experimentally verified on a portal milling center (Fig. 2). The maximum revolutions of the electro-spindle were 12000 rpm and axes speeds were up to 15 m/min in both further discussed directions. A procedure for obtaining a compensation algorithm based on TTF combines mathematical modeling with empirical calibration.

4.1. Experimental setup

The machine tool was equipped with 70 thermal probes (RTD) for calibration measurements. The number of thermal probes was reduced from the original 70 to 6 probes (one for each main heat source / sink [24]):

T_{30} , T_{58} , T_{61} , T_{62} , T_{63} and T_{68} (T_{30} taking electro-spindle temperature, T_{58} taking ambient temperature, T_{61} taking x direction feed drive temperature, T_{62} and T_{63} taking coolant temperatures at the inlet and outlet of the electro-spindle cooling circuit and T_{68} taking z direction feed drive temperature) for the prediction of thermal displacement in direction x , y and z based on the TTF compensation algorithm (an additional input of the TTF model is electro-spindle rotational speed).

Capacitive sensors were employed for noncontact sensing of displacements at the TCP (in directions x , y and z according to Fig. 2) in nanometre resolution. Thermal displacements in the x and y axes were measured in 2 points to observe also angular displacement (the distance between sensors was 100 mm).

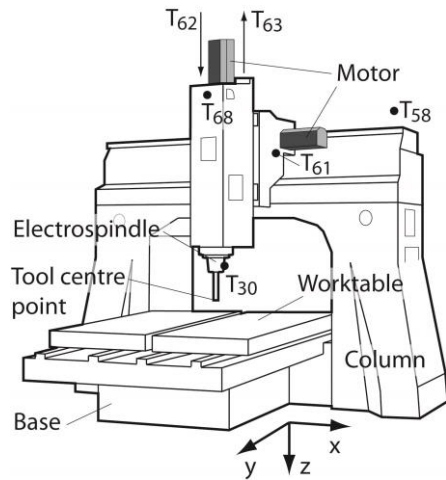


Fig.2. Resistance thermometers on a portal milling centre.

4.2. Calibration measurements

Generally, 5 calibration measurements were carried out to obtain 12 TTFs describing the machine tool thermal behaviour with the help of a TTF model. The total time of the calibration measurements was up to 84 hours of deflection description in all three directions. It was necessary to realize 2 calibration measurements (heating phase at 6000 rpm and cooling phase at 6000 rpm) for describing the thermal behaviour of the electro-spindle due to its rotation (16 hours) [18]. The ETVE (environmental temperature variation error according to [8]) test was used for the calibration measurement of ambient temperature influence (48 hours). Appreciable influence and necessity of this time-consuming calibration was shown in [18]. However, the influence of the ambient temperature doesn't have to be significant in the following tests. The last set of experiments was carried out for obtaining description of machine axes influence in x and z directions (heating phases; 20 hours in total).

The result of identification of spindle influence during 6000 rpm is depicted in Fig.3.

Behaviors of important temperatures (Fig.2) are shown in the figure besides measured and simulated deformations. The growth of the temperature measured close to the active heat source (electro-spindle bearings) T_{30} is a crucial factor. Temperatures measured close to the rest of heat sources (which are non-active during the test) follow the gradient of ambient temperature T_{58} .

The similar behavior is possible to observe during calibration of the rest of the thermal sources as well. Fig.4 (in left) presents the result of identification of moving machine axis impact in x direction (slide) and Fig.4 (in right) shows impact of moving machine axis in z direction (headstock). In this case deformations in x direction are not negligible.

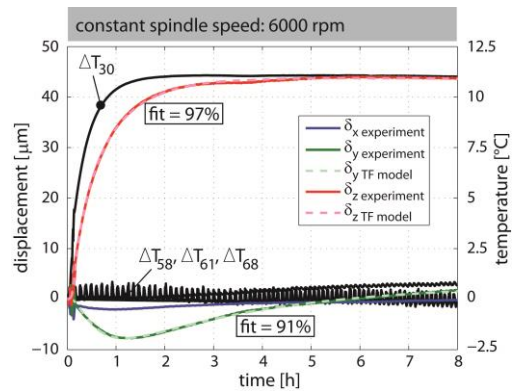


Fig.3. Calibration of TTFs describing thermal errors caused by electro-spindle rotation in z and y direction.

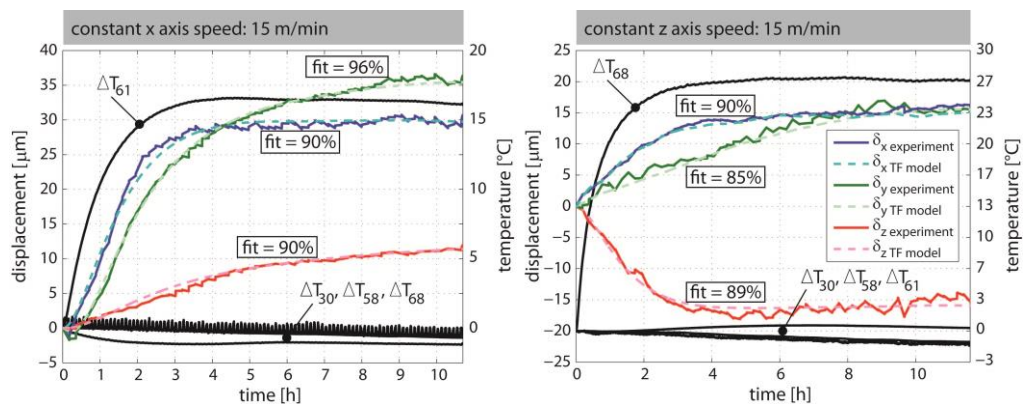


Fig.4. Calibration of TTFs describing thermal errors caused by movement in x (left) and z (right) machine axes.

Behavior of temperatures measured close to the active heat sources (T_{61} in left and T_{68} in right graph of Fig.4) demonstrates transient characteristic between two thermodynamic states of equilibrium according to T_{30} in Fig.3. The rest of temperatures follow the gradient of ambient temperature.

5. MODEL BASED ON THERMAL TRANSFER FUNCTIONS

Regarding of possibility to describe a laboratory model of the most complicated structure of MT (from the thermal symmetry point of view) by one TTF [29] the idea of the thermal-transfer model lies in partial linearization of the problem. It means to isolate particular thermal elements, solve them separately and build up a complex approximation thermo-elastic model with their subsequent superposition (4) and (5).

$$\delta = \delta_{AT} + \delta_{sp} + \delta_{drive x} + \delta_{drive z} \quad (4)$$

$$\delta = \Delta T_{58} \cdot \varepsilon_{AT} + \Delta T_{30} \cdot \varepsilon_{sp} + \Delta T_{68} \cdot \varepsilon_{drive x} + \Delta T_{61} \cdot \varepsilon_{drive z} \quad (5)$$

where δ is the resultant approximation in one direction, δ_{AT} the deformation element caused by ambient temperature impact, δ_{sp} the deformation element caused by electro-spindle rotation (reconstruction of this nonlinear deformation element is described in detail in [18]), $\delta_{drive x}$ the deformation element caused by x feed drive heat source impact, $\delta_{drive z}$ the deformation element caused by z feed drive heat source impact, Δ is nomenclature of a zeroed temperature excitation (temperature difference) and ε is nomenclature of relevant thermal transfer function in time domain.

The model built up in *Matlab Simulink* is shown in following picture.

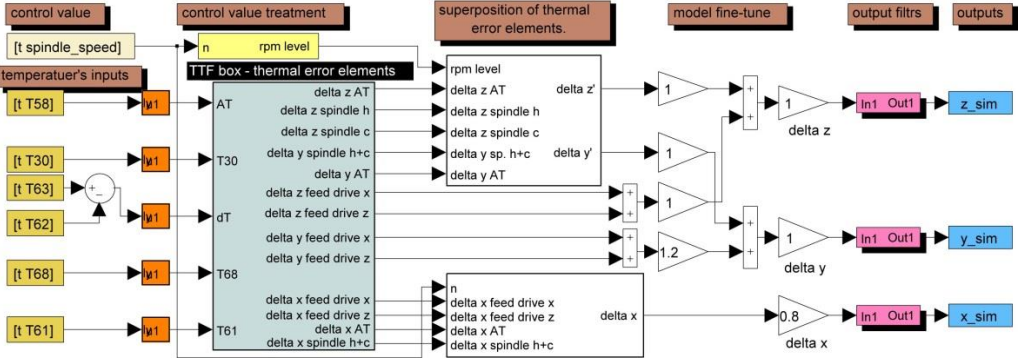


Fig.5. Robust machine tool thermal model in Matlab Simulink.

Construction of a thermo-elastic model of horizontal milling machine is discussed in [13]. This-article-focused-model of portal milling centre demonstrates few divergences in comparison with the former.

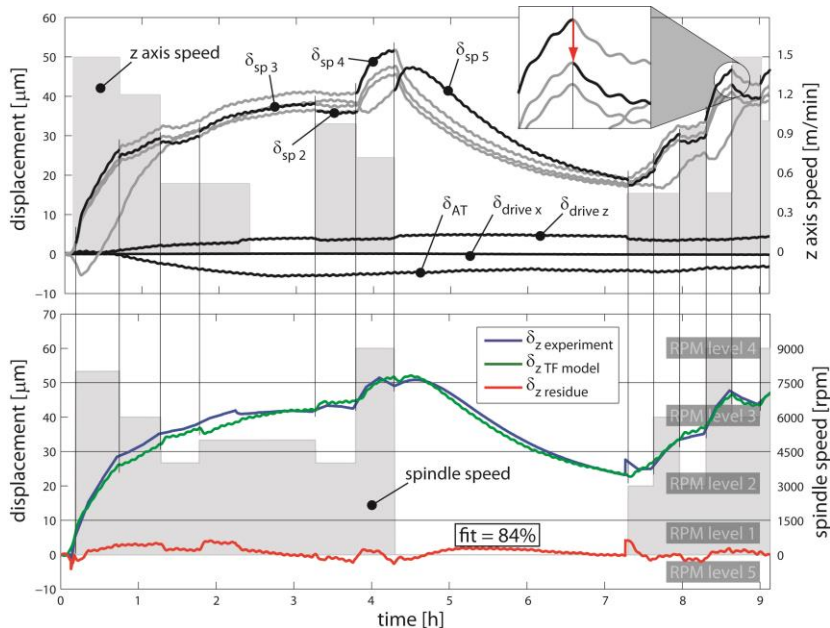
Electro-spindle rotations are used as an only control input value into the TTF model (Fig.5) and similarly to [13] is model divided into six rpm levels (possible situations which can occurred in case of a real working cycle). These are assembled in following table.

Table 1. Levels of electro-spindle speed.

Electro-spindle speed [1/min]		Rpm level number
from	to	
1	1500	1
1500	4500	2
4500	7500	3
7500	Max. (12000)	4
Cooling phase	0	5
ETVE state		6

Rpm level numbers 1 to 4 pertain to the heating phase. Allocation of the heating phase into 4 levels permits fine tune of nonlinear convection component [18] across the whole electro-spindle revolution spectrum. Rpm level number 5 is dedicated to a general cooling phase. The return of MT into the thermodynamic equilibrium (MT thermo-elastic equalization with a surrounding) is described by rpm level number 6. The time constant of switch this level on is approximately 12 hours in which MT is remaining in cooling phase. In the case of rpm level number 6 the thermo-elastic description is depending only on TTFs calibrated during ETVE (environmental temperature variation error [8, 18]) test. The rest of the MT thermal history is possible to clear (refresh of the temperature inputs in Fig.5).

The TTFs are fed by continuous flow of input data. Selection of the appropriate TTF is then based on the control value (rpm level numbers) with no needs for zeroing inputs during the process or follow-up tying of deformation elements of individual rpm levels [13]. The main advantage of this attitude rests on easier embodiment of other influences (feed drives in this case) into model structure. Model operation is indicated in the following picture. Fig.6 describes thermal deformation approximation in z direction caused by interaction of three thermal sources (electro-spindle bearings, feed drive in z direction and surrounding).

Fig.6. Principle of composition of resultant thermal error approximation in z direction.

In upper graph of Fig.6 is recorded output from 8 TTFs describing MT thermal behavior during the impact of above mentioned thermal sources (the deformational element numerical subscripts correspond to rpm level number in Tab.1). Description of thermal deformation at TCP is result of superposition of highlighted sections of approximation curves. A discontinuity emerged during change in rpm levels is smoothed out by the output filters (detail in the same picture). This description along with measured data of thermally induced deflection in z direction and their residuum is depicted in lower part of Fig.6. The same picture indicates principle of dividing electro-spindle speed interval into rpm levels. The resultant suppression of thermal deformation is equal to 85% in observed direction.

6. COMPENSATION RESULTS

A scheme of incremental coaction of calibrated thermal sources (electro-spindle bearings, feed drives and ambient temperature) was designed for clear verification of compensation algorithm (upper graphs in Fig.7). Electro-spindle revolutions are active in the whole first part of the spectrum and are in cooperation with movement in x and then z direction (without decay phase). The axes speed is equal to 10 m/min. The eight-hours-long cooling phase follows. Cooperation of all calibrated heat sources together is carried out in the very last part of the schema. The result of the approximation is shown in lower part of Fig.7 for all compensated directions x , y and z .

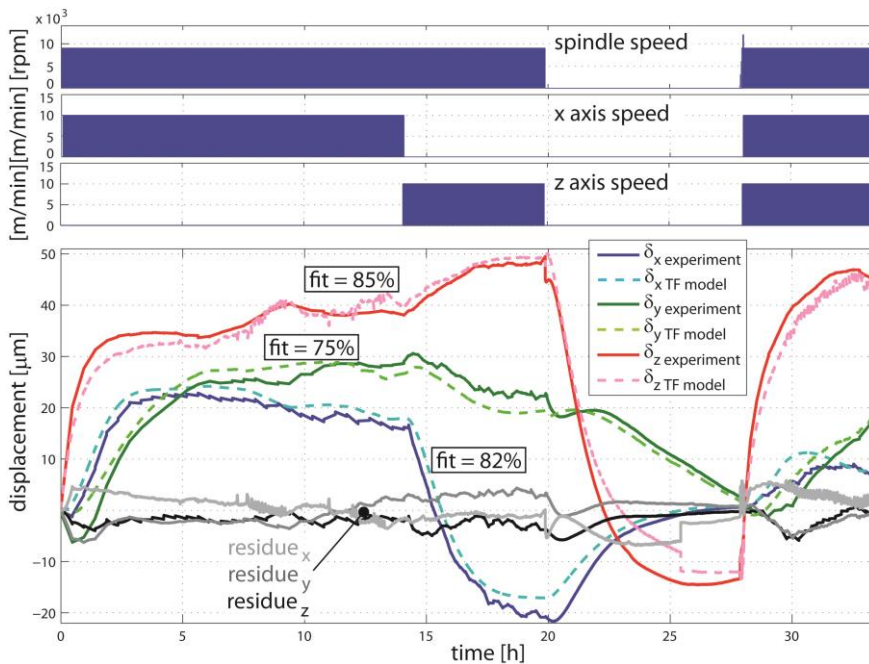


Fig.7. Compensation result of TTF model during cooperation of all identified heat sources.

The *fit* value of thermal deformations simulated by the described TTF model (Fig. 5) is equal to 82% for x , 75% for y and 85% for z direction. In other words reduction from a former 72 μm to 13 μm was achieved in all direction altogether.

7. CONCLUSIONS

Models based on TTFs present a robust approach to modelling of MT thermal behaviour, use a minimum of additional gauges (One temperature sensor employment for each active thermal source description is fully sufficient in comparison with the commonly used method of MLR analysis [16]) and solve each influence participating in thermal error separately with subsequent superposition.

The modelling approach was applied on the portal milling centre (Fig.2). This article enlarges the acknowledgement obtained in [18] by include other heat sources (machine drive axes influences) into the model validity and provides detail look into TTF model construction. Thermo-mechanical Impacts of those heat sources on MT structure are visible in Fig.4 and it is possible to compare them with thermal deformations caused by spindle rotation recorded in Fig.3. Thermal errors in x direction are above all done by x (up to 30 μm) and z (around 15 μm) axis speed. An Influence of spindle rotation in x direction is equal to influence of surrounding and is neglected for this purpose. This is not possible in y direction case where all above mentioned influences have significant impact (35 μm for x axis speed, 15 μm for z axis speed and 10 μm for spindle speed was reached during calibration tests). Spindle speed impact remains substantial in z direction (up to 45 μm). Impacts of speed in machine axes on z direction were recorded less than half of that excited by the spindle. The most important part of the calibration experiments was observation of thermal independence of each active thermal source (temperature behaviours in Fig.3 and Fig.4.). Model improvement is average 82% during a two-days-long verification working cycle (Fig.7) in comparison with the uncompensated state in all directions. These kind of models are open to extension of other thermal error elements such as heat sources generated during cutting process, coolant impact etc.

An advantage of the milling machine thermal description is a law mutual impact of the thermal sources between each other (Fig.3 and Fig.4). Admittedly, this advantage needs not to be a rule.

8. ACKNOWLEDGEMENTS

The results have been obtained as part of the TE01020075 Competence Center – Manufacturing Technology project supported by the Technology Agency of the Czech Republic.

REFERENCES

- [1] C. Brecher et al., “Messtechnische Untersuchung von Prozess und Maschine, Beurteilung und Abnahme von Werkzeugmaschinen (ab 1960),” In *Weck M (ed) 100 Jahre Produktionstechnik*, Springer, Berlin, pp. 437-448, 2006.
- [2] J. Bryan, “International Status of Thermal Error Research,” *Annals of the CIRP*, vol. 39, no. 2, pp. 645-656, 1990.
- [3] M. Weck, P. McKeown, R. Bosner, U. Herbst, “Reduction and compensation of thermal errors in machine tools,” *Annals of the CIRP*, vol.44, no. 2, pp. 589-598, 1995.
- [4] J. Jedrzejewski et al., 2008, “Precise Model of HSC Machining Centre for Aerospace Parts Milling,” *Journal of Machine Engineering*, vol. 8, no. 3, pp. 29-41, 2008.
- [5] J. Mayer, et al., 2012, “Thermal issues in machine tools,” *Annals of the CIRP*, vol. 61, no. 2, 2012.
- [6] ISO 10791-10, “Test Conditions for Machining Centres – Part 10: Evaluation of Thermal Distortion,” Genf, Switzerland, 2007.

- [7] ISO 13041-8, "Test Conditions for Numerically Controlled Turning Machines and Turning Centres – Part 8: Evaluation of Thermal Distortions," Genf, Switzerland, 2004
- [8] ISO 230-3, "Test Code for Machine Tools – Part 3: Determination of Thermal Effects," Genf, Switzerland, 2007.
- [9] R. Ramesh, M. A. Mannan, A. N. Poo, "Error compensation in machine tools - a review, Part II: thermal errors," in *International Journal of Machine Tools & Manufacturing*, 40, pp. 1257 -1284, 2000.
- [10] E. Uhlmann et al., "Compensation of Thermal Deformations at Machine Tools using Adaptronic CRP-Structures," in: *Proceedings of 41st CIRP Conference on Manufacturing Systems: Manufacturing Systems and Techniques for the New Front*, pp. 183-186, 2008.
- [11] J. Jedrzejewski, "Effect of Thermal Contact Resistance on Thermal Behaviour of the Spindle," *Int. J. Mach. Tools Manufacturing*, vol. 28, no. 4, pp. 409-416, 1998.
- [12] P. Bárta et al., "Thermal transfer function based control of a machine tool cooling system," in: *Proceedings of the topical meeting: Thermal Effects in Precision System*, Maastricht, Netherlands, pp. 18-19, 2007.
- [13] M. Mareš et al., "Control and Detailed Modeling of Machine Tool Highly Nonlinear Thermal Behavior Based on Thermal Transfer Functions." *World Academy of Science, Engineering and Technology*, vol. 59, 2735-2740, ISSN 2010-376X, 2011.
- [14] M. Mitsuishi et al., "Development of an Intelligent High-Speed Machining Centre," *Annals of the CIRP*, vol. 50, no. 1, pp. 275-280, 2001.
- [15] Y. Zhao et al., "Optimization and Temperature Mapping of an Ultra-High Thermal Stability Environmental Enclosure," *Precision Engineering*, vol. 34, pp. 164-170, 2010.
- [16] Z. C. Du et al., "Modelling approach of regression orthogonal experiment design for the thermal error compensation of a CNC turning center," *J. Mater. Process Technol.*, vol. 129, pp. 619-623, 2002.
- [17] S. Fraser et al., "Modelling, Identification and Control of Thermal Deformation of Machine Tool Structures: Part 4-A Multi-Variable Closed-Loop Control System." *Trans. ASME, Manufacturing Science and Engineering*, vol. 120, pp. 509-516, 1999.
- [18] M. Mareš et al., "Robustness and Portability of Machine Tool Thermal Error Compensation Model Based on Control of Participating Thermal Sources," *Journal of Machine Engineering*, vol. 13, no. 1, pp. 24-36, 2013.
- [19] C. D. Mize et al., "Neural network thermal error compensation of a machining center," in: *Precision Engineering*, vol. 24, pp. 338-344, ISSN 01416359, 2000.
- [20] J. H. Lee et al., "Thermal error modeling of a horizontal machining center using fuzzy logic strategy," *J Manuf. Process*, vol. 3, pp. 120-127, 2001.
- [21] S. Fraser, M.H. Attia, M.O.M. Osman, "Control-Oriented Modeling of Thermal Deformation of Machine Tools Based on Inverse Solution of Time-Variant Thermal Loads with Delayed Response," *Trans. ASME, J. of Manufacturing Science and Engineering*, pp. 286-296, 2004.
- [22] T. Moriwaki et al., "Analysis of Thermal Deformation of an Ultra Precision Air Spindle System," in: *CIRP Annals*, vol. 47, pp. 283-286, ISSN 00078506, 1998.
- [23] C. Brecher et al., "Compensation of Thermo-elastic Machine Tool Deformation Based on Control internal Data," in: *CIRP Annals*, vol. 53, pp. 299-304. ISSN 00078506, 2004.
- [24] M.H. Attia, S. Fraser, "A Generalized Modeling Methodology for Optimized Real-Time Compensation of Thermal Deformation of Machine Tool and CMM Structures," *Int. J. Machine Tools and Manuf. Design, Research and Applications*, vol. 39, pp. 1001-1016, 1999.
- [25] M. Mareš, O. Horejš, P. Kohút, J. Hornych, P. Bárta, "Application of mechatronic approach to modelling, identification and control of machine tool thermal errors," in: *Proceedings of the 29th IASTED International Conference: Modelling, Identification and Control (MIC 2010)*, Innsbruck, Austria, pp. 284-290, 2010.
- [26] O. Horejš et al., "Advanced compensation of thermally induced displacement of machine tools based on transfer functions," *MM Science Journal, Special Issue / MATAR 2012*, ISSN 1803-1269 (print), ISSN 1805-0476 (online), 2012.
- [27] L. Ljung, "System identification toolbox 7 User's guide," www.mathworks.com (The MathWorks), 2009
- World Commission on Environment and Development, "Our common future," Oxford Univ. Press, Oxford, 1987.
- [28] M. Mareš, P. Bárta, "Mechatronic approach in modelling, identification and control of thermal deformation of quill," *MM Science Journal*, 10, pp. 25–29, 2008.
- [29] M. Mareš et al., "Compensation of Machine Tool Angular Thermal Errors using Controlled Internal Heat Sources," *Journal of Machine Engineering*, vol. 11, no. 4, pp. 78-90, 2011.

Complex Verification of Thermal Error Compensation Model of a Portal Milling Centre

Otakar Horejš, Martin Mareš, Jan Hornych

Research Center of Manufacturing Technology, Horská 3, 128 00 Prague, Czech Republic
O.Horejš@rcmt.cvut.cz

ABSTRACT

Thermal errors at the tool centre point (TCP) of machine tools are dominant sources of inaccuracy and are often the most difficult to reduce nowadays. This paper is a continuation of the previous work on modelling of thermally induced displacements based on thermal transfer functions (TTF). It concerns with complex verification of the thermal (software) compensation based on TTF extended on impact of machine axes movement in x and z direction and implementation of the compensation algorithm into a standard CNC controller. Thermal compensations have been experimentally verified on a portal milling centre on varied working cycle over 5 days. Moreover, the results of the TTF model were compared with two models obtained via multiple linear regressions (MLR) as a case study. It was shown much better accuracy and reliability of the TTF model, particularly under highly varied operating conditions.

KEYWORDS: thermal error, compensation, transfer function, precision machining, machine tool

1. INTRODUCTION

Achieving high workpiece accuracy is the long-term trend of machine tool designers as well as the requirement of customers. Because machine inaccuracy is a major source of workpiece errors, control of machine error sources is critically important [1].

There are three major influences on machine inaccuracy: static, dynamic and thermo-dependent behavior (thermal errors). However, it is well known that thermal errors are usually the most critical errors in machining [2] and it is difficult to deal with [3]. It is primarily caused by a large number of internal and external heat sources (or heat sinks) affect the temperature distribution of the structural loop. Typical examples are the heat generated by friction in joints, gearboxes and spindle bearings, or the machine's environment (environmental temperature in a shop floor, ventilation, solar radiation etc.). Thus the temperature field of a machine tool changes constantly according to the instantaneous working cycle (time-varying strength of inner heat sources) and various environmental conditions. The resulting time-varying thermal distortions of the various components produce thermal errors at the tool center point (TCP) that dominate the achievable accuracy.

Many solutions exist for the machine tool builder to reduce thermal errors that can be applied at the design stage including symmetric machine tool structures, liquid circulation cooling systems, low thermal expansion coefficient materials, thermal insulation or thermal actuator, electric heaters etc. Nevertheless a design effort together with cooling systems cannot absolutely eliminate thermal errors but only help to reduce them.

Therefore in today's high precision machines, advanced techniques are applied for a real-time software compensation of errors caused by varying machine temperature field (also called indirect compensation [4] or thermal compensation). The principle of the thermal compensation is that the estimation of the relative thermal displacements between the tool and the workpiece (thermal errors) can be computed with various numerical algorithms, e.g. multiple linear regressions (MLR) [5-7], artificial neural network [8, 9], fuzzy logic [10, 11], a transfer function model (TF) [12, 13] etc. Thereafter predicted thermal errors are used as a feedback control signal to activate a controller, thus bringing the tool and workpiece to their correct relative position [14]. Herein, the use of a feedback control system to affect the desired compensation emerges as a logical and practical solution [14].

Generally, software compensation of thermal errors is one of the widely employed techniques to reduce the thermal errors due to its cost-effectiveness and ease of implementation [15]. Indirect (thermal) compensation strategies are usually based on measured auxiliary variables [4]. Here in most cases temperature values of representative points of the machine structure are used for calculation of the resulting displacements by an empirically determined mathematical model obtained by MLR. The major obstacle for implementing MLR models into machine tool control system is the low robustness of these thermal error models which can suit a variety of machine conditions.

This paper is a continuation of the previous work [16-20] on advanced modelling of thermally induced displacements based on thermal transfer functions (TTF). The applicability and robustness of the TTF models have been already verified on the different machine tool structures (vertical milling center built on the supporting frame in the C form [16], horizontal milling centers [17-20]). The main spindle of a machine tool is, without any doubt, the major heat source within the machine structure. It practically means also the main source of thermal errors at the TCP. Therefore a previously published scientific work on robust modelling of thermally induced displacements based on TTF [16-20] was predominantly focused on models describing only spindle as the cause of the overall thermal errors at the TCP together with environmental temperature influences on resulting time-varying thermally induced displacements. The remaining inner heat sources were neglected in previous compensation algorithms [16-20]. At present, however, this is the state of the art (majority developed thermal compensation algorithms of machine tool consider the main spindle as the sole source of thermally induced errors). The paper concerns with complex verification of the indirect thermal compensation based on TTF extended on impact of machine axes movement in x and z direction and implementation of the indirect compensation algorithm into a standard CNC controller. Indirect compensations of thermal errors at TCP have been experimentally verified on a portal milling centre on varied working cycle over 5 days. Moreover, the results of the TTF model are compared with models obtained via MLR as a case study. It was shown much better accuracy and reliability of the TTF model, particularly under highly varied operating conditions (combination of various spindle speeds and movements in x and z direction).

2. COMPENSATION OF A PORTAL MILLING CENTRE

Compensations of thermal errors at TCP have been developed and experimentally verified on a portal milling centre shown in Fig. 1.

2.1. Experiment

Experimental set-up

The machine tool was equipped with 70 resistance temperature detectors (RTD) for estimation of TTF (calibration measurements). The number of thermal probes was reduced from the original 70 to 6 probes: T_{30} , T_{58} , T_{61} , T_{62} , T_{63} and T_{68} (T_{30} represents the spindle temperature, T_{58} represents the ambient temperature, T_{61} represents the x direction feed drive temperature, T_{62} and T_{63} are coolant temperatures at the inlet and outlet of the electrospindle cooling circuit and T_{68} represents z direction feed drive temperature) for the prediction of thermal displacement in direction x , y and z based on the TTF compensation algorithm see Fig.1). Utilizing a coverage factor $k=2$, the expanded uncertainty of temperature measurements is ± 0.31 °C.

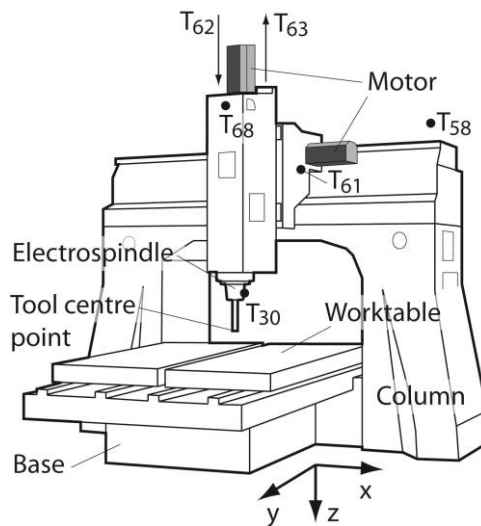


Fig.1. Scheme of the experimental set-up.

An additional input of the TTF model is spindle rotational speed. Eddy current sensors PR 6423 [24] were employed for noncontact sensing of relative displacements between the tool and the workpiece (the displacements sensors are placed on worktable) in directions x , y and z according to Fig. 1. The expanded uncertainty of displacements measurements is ± 1.7 μm (coverage factor $k=2$).

In order to estimate TTFs parameters (in detail see e.g. [18]) calibration experiments were performed on portal milling centre according to ISO230-3 [22]. Namely three group of tests for the determination of thermal effects on machine tools: an environmental temperature variation error (ETVE) test, a test for thermal distortion caused by rotating spindles (constant spindle speed to steady state and cooling phase, tests with variable spindle speed), and a test for thermal distortion caused by moving linear axes in x and z directions. The tests were each carried out once.

The total time of the calibration measurements was up to 84 hours. All data acquisition was carried out with National Instruments programmable automation controller (PAC) cRIO 9014 and software LabVIEW.

2.2. Compensation algorithm based on TTF and its implementation

Data processing and TTFs identification, as well as machine tool thermal behavior modeling, were performed in software Matlab/Simulink® [23].

The merit of the compensation algorithms based on TTF is that it enable to solve each influence (heat source or heat sink) participating in resultant thermally induced errors separately [24, 25]. Herein the predicted thermal errors (in x , y and z directions according to Fig. 1) is result of superposition of each component (causes of thermal errors at the TCP which are described by 8 estimated TTFs). Superposition principle of TTFs was already applied in previously published papers [24, 25].

The apparatus cRIO 9014 (previously applied for data acquisition) was employed for implementation of compensation algorithm into a CNC controller in order to compensate for thermal errors in real-time. Three analog output voltage signals from cRIO 9014 to machine tool controller are used for transfer of corrections (predicted relative thermal displacements between the tool and the table) in x , y and z directions. Predicted displacements in x , y and z direction are superposed as an offset to the desired position values in x , y and z machine axis. In order to perform it, the developed thermal compensation Simulink® model based on TTF was converted in Labview code. However, different technique of implementation in a portal milling centre controller environment from software Simulink® can be applied, e.g. Simulink PLC Coder™ [23] generates hardware-independent Structured text from Simulink® models for programmable logic controllers (PLC) according to international standard IEC 61131-3 [26]. As a result, compensation algorithm based on TTF can be compiled and deployed to numerous PLC and PAC devices or directly into a CNC controller of examined portal milling centre using additional effort.

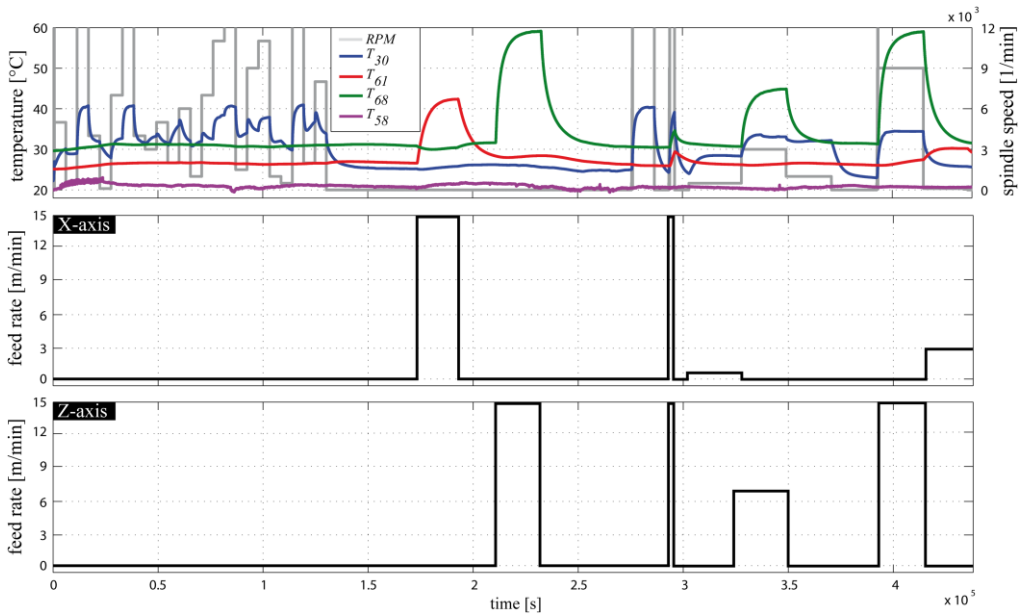


Fig.2. Temperature time behavior (inputs of the estimated TTF) and varied working cycle over 5 days (spindle speed spectrum, feed rates in x and z machine axis).

3. VERIFICATION OF COMPENSATION ALGORITHM

The developed thermal compensation algorithm based on TTF have been experimentally verified on a portal milling centre on varied working cycle over 5 days (120 hours), see Fig. 2.

The verification experiment includes spindle speed spectrum (grey curve in upper graph in Fig. 2, the maximum revolutions of the spindle were 12000 rpm) combined with various feed rates in x and z machine axis (maximum feed rates were 15 m/min during the verification experiment) as shown in bottom graphs shown in Fig. 2 (black curves). The working cycle was chosen to cover wide range of operating conditions of the machine tool. Figure 2 also depicts temperatures time behavior T_{30} , T_{58} , T_{61} and T_{68} which are used as inputs of the estimated TTFs.

A residual error (the difference between the simulated thermal displacement and the measured thermal displacement without application of compensation algorithm) in z direction after implementation of indirect compensation algorithm into a CNC controller based on TTF compared with uncompensated state (measured thermal displacement at the TCP without application of the compensation algorithm) is shown in Fig. 3.

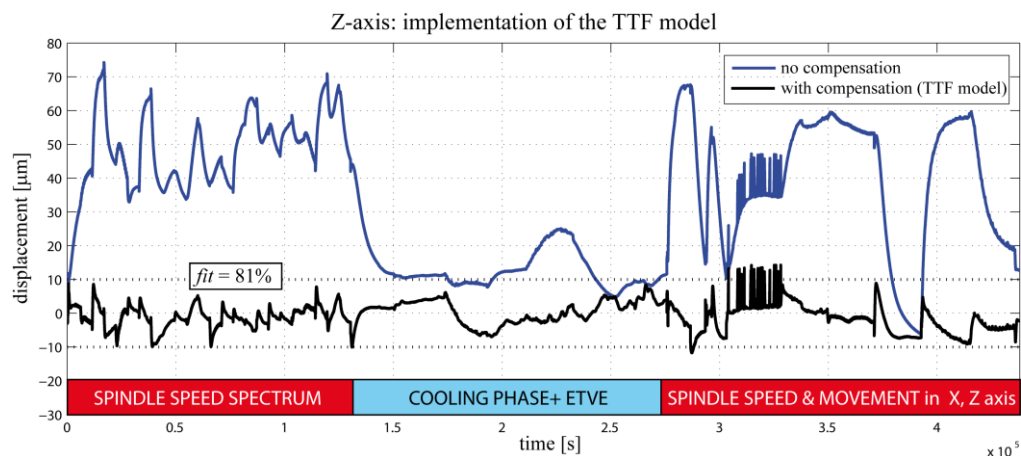


Fig.3. Comparison of thermally induced displacements at the TCP in z direction without and with implemented indirect thermal compensation algorithm based on TTF model.

Black curve in Fig. 3 represents residual error in z direction and blue curve in Fig. 3 denotes uncompensated state.

Further, a residual error in x direction after implementation of indirect compensation algorithm based on TTF (black curve) compared with uncompensated state (blue curve) is shown in Fig. 4.

And finally, a residual error in y direction after implementation of indirect compensation algorithm based on TTF (black curve) compared with uncompensated state (blue curve) is shown in Fig. 5.

The results of the thermal displacements prediction by TTF model in z directions will be discussed hereafter. Since the compensation results in x and y direction attain similar approximation quality and likewise the thermally induced displacement at the TCP in z

direction is the most critical issue (the portal milling centre has the worst thermal behavior in z direction).

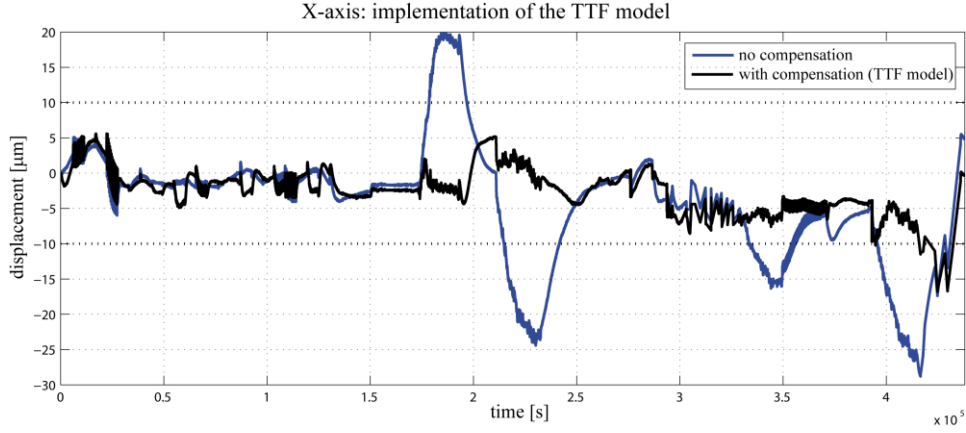


Fig.4. Comparison of thermally induced displacements at the TCP in x direction without and with implemented indirect thermal compensation algorithm based on TTF model.

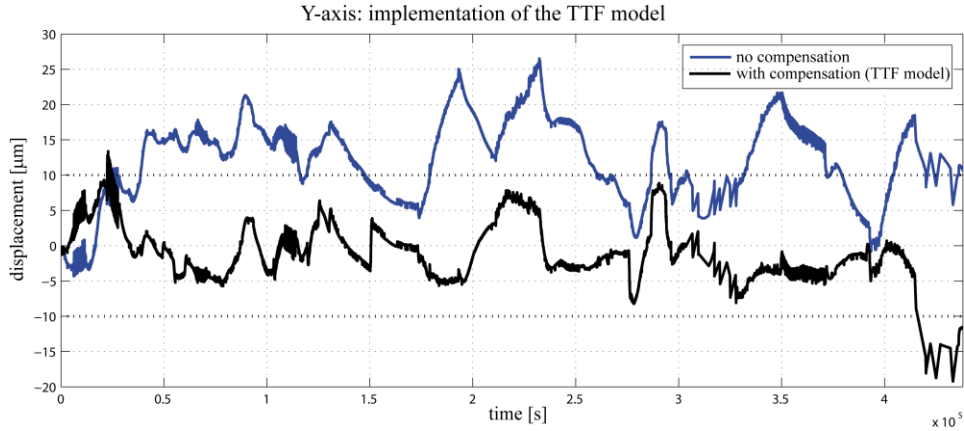


Fig.5. Comparison of thermally induced displacements at the TCP in y direction without and with implemented indirect thermal compensation algorithm based on TTF model.

The approximation quality of the simulated displacement behavior in z direction is expressed by the *fit* (%) value (1) in Fig. 3 (fit value of 81 %). This value expresses the percentage of the output variations that is reproduced by the model [27]:

$$fit = \left(\frac{Y - Y_{HAT}}{Y - \bar{Y}} \right) \cdot 100 \quad (1)$$

The Y value in (1) means the measured output (thermal displacement), Y_{HAT} is the simulated/predicted model thermal displacement (by TTF model) and \bar{Y} in (1) expresses the arithmetic mean of the measured output.

The results of the compensation algorithm are in good agreement with measured displacements. In case of the verification spectrum (Fig.2), the uncompensated displacement at the TCP in z direction is located between $0\ \mu\text{m}$ and $74\ \mu\text{m}$. The compensation based on TTF reduces it to a range between $-12\ \mu\text{m}$ and $+14\ \mu\text{m}$. There are only a few regions where the simulated displacement is noticeable different from the measured displacement.

A similar result has been achieved in x and y direction (Fig. 4 and Fig. 5). Especially, the implementation of the compensation algorithm based on TTFs into a CNC controller reduces significantly the thermal displacements at the TCP during the machine axes movement. It is transparently depicted in Fig. 4 (in the middle of the verification experiment) in case of the thermal displacement in x axis.

4. COMPARISON WITH MLR MODELS – CASE STUDY

In this chapter the compensation results obtained by the TTF model are compared with two models obtained via MLR as a case study.

Several MLR models were tested for a comparison with results of the TTF model. Finally, 2 MLR models were chosen for comparison with the TTF model presented in this paper. Both MLR models using the same type and number of temperatures inputs as the TTF model (6 probes: T_{30} , T_{58} , T_{61} , T_{62} , T_{63} and T_{68} , see Fig. 1) to transparently compare results of both types of software thermal compensation (TTF model in comparison with widely employed static MLR model). MLR models differ from the length of the measurements (also type of the tests) which were employed for calibration of the mathematical models.

A first MLR model (denoted as MLR model 1) is based on 10 hours of the calibration test with constant spindle speed revolution 9000 rpm (including cooling phase without rotation of the main spindle). The length of the test was chosen to characterize typical calibration scheme of a MLR models commonly used in the industry by machine tool builders.

In contrast to MLR model 1, a second MLR model (denoted as MLR model 2) is based on 138 hours of the tests on the portal milling centre including all tests applied for calibration of the TTF models. It includes tests for thermal distortion caused by rotating spindles (constant spindle speed to steady state and cooling phase, tests with variable spindle speed), a tests for thermal distortion caused by moving linear axes in x and z direction and ETVE test.

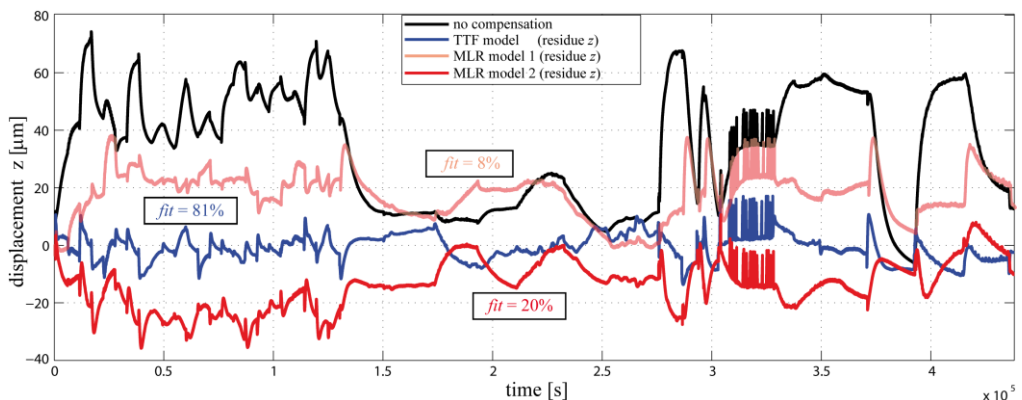


Fig.6. Residual errors in z directions obtained by the two MLR models and TTF model, thermally induced displacements in z direction without any compensation (black curve).

Since the thermally induced displacement at the TCP in z direction is the most critical issue of the portal milling centre, the comparison of the TTF model with MLR models is carried out only for thermally induced displacements at the TCP in z directions.

Comparison of compensation results obtained by the TTF model with two MLR models is carried out for five-days-long working cycle (verification experiment, see Fig.2).

A comparison of the TTF model and two MLR models is shown in Fig. 6. The graph in Fig. 6 depicts the residual errors in z directions obtained by the MLR model 1 (light red curve), MLR model 2 (red curve), TTF model (blue curve) and thermally induced displacements in z direction without any compensation (black curve). In other words, the black curve in Fig. 6 represents the measured thermal displacement at the TCP in z direction without application of any thermal compensation algorithm.

The approximation quality of the simulated displacement behavior in z direction in Fig. 6 is expressed by the *fit* (%) value according to (1) for each mathematical model of software thermal compensation. The *fit* value of thermal displacements simulated by the described TTF model (Fig. 6) is equal to 81%, only 8% by MLR model 1 and 20% by more robust MLR model 2.

The accuracy and reliability of the estimated thermally induced displacements at the TCP in z direction using MLR models are poor, as was expected. Conclusions from previous research were repeatedly verified. It is caused by a low robustness of the MLR models in general. MLR models are unsuitable for accurate prediction of thermally induced displacement at the TCP caused by the wide range of operating conditions (better results can be obtained for working cycles which are similar to one applied for calibration of the MLR model).

The accuracy of the MLR model increases with a length of the tests used for calibration of the model. Nevertheless, even the accuracy of the MLR model 2 which utilizes more tests for its calibration is incomparable with the compensation results of the TTF model. In case of the verification spectrum (Fig.2), the compensation based on MLR model 2 reduces thermally induced displacement at the TCP in z direction to a range only between $-37\text{ }\mu\text{m}$ and $+12\text{ }\mu\text{m}$ compared to range between $-12\text{ }\mu\text{m}$ and $+14\text{ }\mu\text{m}$ obtained via TTF model.

5. SUMMARY AND CONCLUSION

The applicability and robustness of the TTF models have been already verified on the different machine tool structures (vertical milling center built on the supporting frame in the C form [16] or horizontal milling centers [17-20]). The important advantage of the TTF models is that the thermal error model is in addition more reliable with untested inputs.

Thermally induced displacements modeling based on TTF can combine different inputs of TF such as temperature of machine tool structures (or ambient temperature) and CNC data (e.g. rotational spindle speed, feed rate, motor current, power etc.), the portability among machines of the same type set were also proved and previously presented, e.g. in [17, 25].

Previously published papers on fast and robust modelling of thermally induced displacements based on TTF were predominantly focused on models describing spindle as the sole cause of the overall thermally induced displacement at the TCP together with environmental temperature influences. However, another merit of the compensation algorithm based on TTF is that it enable to solve each influence (heat source or heat sink) participating in resultant thermally induced errors at the TCP separately [24, 25]. Thus compensation model of machine tool thermally induced displacement at the TCP can be extended using the superposition principle.

This paper concerns with the complex verification of the software thermal compensation based on TTF extended on impact of machine axes movement in x and z direction and

implementation of the algorithm into a standard CNC controller. Thermal compensations have been experimentally verified on the portal milling centre (Fig. 1) on varied working cycle over 5 days (Fig. 2). The *fit* value describing the approximation quality of the TTF model is equal to 81%. The compensation results (Fig. 3, Fig.4 and Fig.5) confirmed suitability of the applied superposition principle of TTF.

Moreover, the results of the TTF model were compared with two models obtained via MLR (widely employed techniques to reduce the thermal errors at the TCP) as a case study. It was shown much better accuracy and reliability of the TTF model, particularly under highly varied operating conditions. The case study confirmed that results and conclusions of thermally induced displacements modeling based on TTF can be generalized for other types of machine tool configurations.

In the future it is the aim to include heat sources produced by cutting process, coolant impact etc. into the TTF model using superposition principle analogously as was shown in this paper.

ACKNOWLEDGEMENTS

The results have been obtained as part of the TE01020075 Competence Center – Manufacturing Technology project supported by the Technology Agency of the Czech Republic.

REFERENCES

- [1] J. Yuan and J. Ni, "The real-time error compensation technique for CNC machining systems," *Mechatronics*, vol. 8, pp. 359-380, 1998.
- [2] J. Mayr, J. Jedrzejewski, E. Uhlmann, M. Alkan Donmez, W. Knapp, F. Härtig, K. Wendt, T. Moriwaki, P. Shore, R. Schmitt, C. Brecher, T. Würz and K. Wegener, "Thermal issues in machine tools," *CIRP Ann.Manuf.Technol.*, vol. 61, no. 2, 2012.
- [3] J. Yang, J. Yuan and J. Ni, "Thermal error mode analysis and robust modeling for error compensation on a CNC turning center," *Int.J.Mach.Tools Manuf.*, vol. 39, no. 9, pp. 1367-1381, 1999.
- [4] C. Brecher, P. Hirsch and M. Weck, "Compensation of thermo-elastic machine tool deformation based on control internal data," *CIRP Ann.Manuf.Technol.*, vol. 53, no. 1, pp. 299-304, 2004.
- [5] D. Lee, J. Choi and D. Choi, "ICA based thermal source extraction and thermal distortion compensation method for a machine tool," *International Journal of Machine Tools and Manufacture*, vol. 43, no. 6, pp. 589-597, 2003.
- [6] S. Postlethwaite, J. Allen and D. Ford, "The use of thermal imaging, temperature and distortion models for machine tool thermal error reduction," *Proc.Inst.Mech.Eng.Pt.B: J.Eng.Manuf.*, vol. 212, no. 8, pp. 671-679, 1998.
- [7] Z. Du, J. Yang, Z. Yao and B. Xue, "Modeling approach of regression orthogonal experiment design for the thermal error compensation of a CNC turning center," *J.Mater.Process.Technol.*, vol. 129, no. 1, pp. 619-623, 2002.
- [8] Y. Kang, C. W. Chang, Y. Huang, C. L. Hsu and I. F. Nieh, "Modification of a neural network utilizing hybrid filters for the compensation of thermal deformation in machine tools," *Int.J.Mach.Tools Manuf.*, vol. 47, no. 2, pp. 376-387, 2007.
- [9] C. Mize and J. Ziegert, "Neural network thermal error compensation of a machining center," *Precision Engineering*, vol. 24, no. 4, pp. 338-346, 2000.
- [10] J. Lee, J. Lee and S. Yang, "Thermal error modeling of a horizontal machining center using fuzzy logic strategy," *Journal of manufacturing processes*, vol. 3, no. 2, pp. 120-127, 2001.
- [11] K. C. Wang, "Thermal error modeling of a machining center using grey system theory and adaptive network-based fuzzy inference system," in *Cybernetics and Intelligent Systems, 2006 IEEE Conference on*, 2006.
- [12] T. Moriwaki and E. Shamoto, "Analysis of thermal deformation of an ultraprecision air spindle system," *CIRP Ann.Manuf.Technol.*, vol. 47, no. 1, pp. 315-319, 1998.
- [13] C. Brecher, A. Wissmann and W. Klein, "Influence of ambient temperature versus influence of spindle load:

- Thermally conditioned deformation behavior of milling machines," *VDI-Z Integr.Prod.*, vol. 152, no. 9, pp. 78-81, 2010.
- [14] S. A. M. O. M. Fraser, "Modelling, identification and control of thermal deformation of machine tool structures, Part 1: Concept of generalized modelling," *J.Manuf.Sci.Eng.Trans.ASME*, vol. 120, no. 3, pp. 623-631, 1998.
 - [15] J. Zhu, "Robust thermal error modelling and compensation for CNC machine tools," PhD. thesis, The University of Michigan, Michigan, 2008.
 - [16] P. Bárta, J. Hornych and O. Horejš, "Active control of a machine tool cooling system," in *Proceedings of the 10th anniversary international conference of the EUSPEN*, Zürich, 2008.
 - [17] O. Horejš, M. Mareš and P. Kohút, "Advanced Compensation of Thermally Induced Displacements of Machine Tools based on Transfer Functions," *MM Science Journal, Special Issue, MATAR 2012 - 9th International Conference on Machine Tools, Automation, Technology and Robotics*, ISSN 1803-1269 (print), ISSN 1805-0476 (on-line), 2012.
 - [18] O. Horejš, M. Mareš and L. Novotný, "Advanced Modelling of Thermally Induced Displacements and Its Implementation into Standard CNC Controller of Horizontal Milling Center," *Procedia CIRP*, vol. 4, pp. 67-72, 2012.
 - [19] O. Horejš, M. Mareš, P. Kohút, P. Bárta and J. Hornych, "Compensation of machine tool thermal errors based on transfer functions," *MM Science Journal*, no. March, 2010, pp. 162-165, 2010.
 - [20] O. Horejš, M. Mareš, P. Kohút, P. Bárta and J. Hornych, "A Compensation Technique of Machine Tool Thermal Errors Built on Thermal Transfer Functions," *Proceedings of 5th International Conference on Leading Edge Manufacturing in 21st Cent*, pp. 197-202, 2009.
 - [21] PROFESS, "PR 6423 series Eddy current displacement sensor," 2013. [Online]. Available: http://www.profess.cz/dynamic/produkty/dokument/PR6423_DL_EN.pdf.
 - [22] ISO 230-3, 2007. Test Code for Machine Tools – Part 3: Determination of Thermal Effects, Genf, Switzerland.
 - [23] Matlab/Simulink, <http://www.mathworks.com/>.
 - [24] Mareš, M., Horejš, O., Bárta, P., Hornych, J., & Kohút, P. (2011). Control and Detailed Modeling of Machine Tool Highly Nonlinear Thermal Behavior Based on Thermal Transfer Functions. *World Academy of Science, Engineering and Technology*, 59, pp. 2735-2740.
 - [25] M. Mareš et al., "Robustness and Portability of Machine Tool Thermal Error Compensation Model Based on Control of Participating Thermal Sources," *Journal of Machine Engineering*, vol. 13, no. 1, pp. 24-36, 2013.
 - [26] International Electrotechnical Commission, *IEC 61131-3 2nd Edition*, IEC publications, 2003.
 - [27] L. Ljung, "System identification toolbox 7 User's guide," www.mathworks.com (The MathWorks), 2009.

Intelligent Control Using Neural Network Regarding Thermal Errors with Non-linear Behaviour of a Machine Tool

Ikuo TANABE¹

¹Nagaoka University of Technology
tanabe@mech.nagaokaut.ac.jp

ABSTRACT

In this paper, intelligent control of thermal errors with non-linear behaviour using neural network was developed and evaluated for a lathe with high precision. At first, in the experiment, thermal behaviour of a lathe was measured for a few basic study data of the neural network. Next, the neural network was used to learn the relationship between the measured temperatures and the thermal errors on the lathe. Then the neural network was rewritten for some algebraic equations, and the algebraic equations were carried in the lathe with PC. At last, thermal errors was controlled in the NC program by using both the algebraic equations and temperature distribution of the lathe. It is concluded from the results that (1) Proposed method was effective in order to reduce thermal errors. (2) Device for the proposed method was only measuring device of temperature, and a forced cooling device or a linear scale were not necessary.

KEYWORDS: Thermal Errors, Non-Linear Behaviour, Neural Network, Control, Lathe, Intelligent Control

1. INTRODUCTION

As higher precision machining is required, reducing thermal errors of a machine tool becomes more important [1], [2]. Recently, research for thermal deformation in machine tool have systematically investigated and collected[3]. And more complex countermeasures were also adopted for high accuracy [4]. The thermal errors have strongly non-linear behavior, therefore the control is very difficult. In the previous report [5], a new method for estimating optimum temperature of cooling oil on a spindle was established. Inverse analysis using neural network was used for calculating optimum oil temperature, because neural network is suitable for controlling non-linear phenomenon.

In this paper, intelligent control of thermal errors with non-linear behavior using neural network was developed and evaluated for a lathe with high precision. Thermal behavior with non-linear behaviour of a lathe was firstly measured for a few teaching data of the neural network. Next, the neural network was used to learn the relationship between the structural temperatures of the lathe and the thermal errors with non-linear behavior on the lathe. Then

the neural network was rewritten for an equation, and the algebraic equation was carried in the lathe with PC. The thermal errors X and Z were lastly revised by the function of tool wear correction using macro program. The function of tool wear correction is the existing function in ordinary NC machine tool. Therefore this control become easy, cheapness and correct behavior. Thermal errors on the lathe with or without the controls using the system were investigated for evaluation in several experiments.

2. EXPLANATION OF SIMPLE INTELLIGENT CONTROL USING NEURAL NETWORK

Simple and intelligent control system using neural network was shown in Fig. 1. This system can use for the machine tool with open NC or the NC machine tool with macro-program. Here the explanation is performed regarding the case of the machine tool with open NC. Relationship between the structural temperatures of the machine tool and the thermal errors with non-linear behaviour for several working conditions was firstly measured in the experiments. Then the neural network was made by the measured data; input data is the structural temperatures of the machine tool and output data (=teaching data) is the thermal errors with non-linear behaviour. Relationship between the temperatures and the thermal errors is rewritten to an algebraic equation using the neural network, and the algebraic equation was carried in the lathe with personal computer. Next the structural temperatures on the lathe are measured, the data send to the PC in the lathe, and the thermal errors with non-linear behaviour are calculated at real time by the PC with the algebraic equation. Then the thermal errors X and Z were lastly revised by the function of tool wear correction using macro program and the results of calculation using the algebraic equation. The good points of the system will be that very simple algebraic equation can estimate the very complex thermal errors with non-linear and the lathe becomes highly intellectual machine by small improvement.

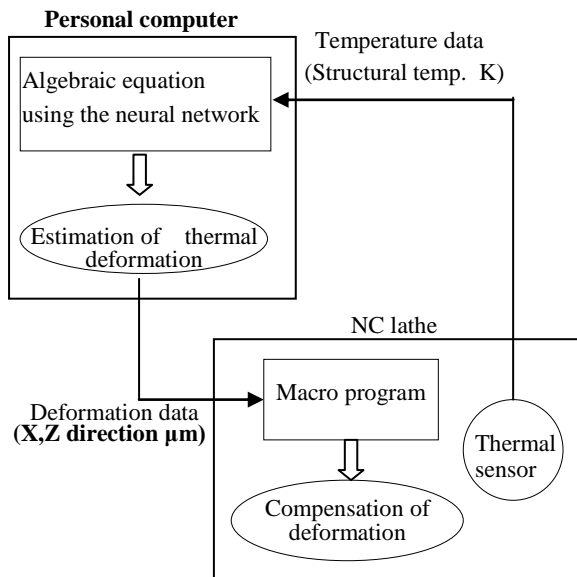


Fig. 1. Flow chart about development of a lathe with a intelligent control of thermal errors using neural network

3. CONSTRUCTION OF NEURAL NETWORK AND ITS ALGEBRAIC EQUATION

Schematic view of the NC lathe used in the experiment is shown in Fig. 2. And specification of the machine is also shown in Table 1. This machine is the lathe with open NC. There are front and rear bearings, main motor, oil unit, chucking cylinder, servo motors and drivers of X and Z directions for inner heat sources. Thermal errors of X, Y, Z directions were measured by three inductive gauging sensors with accuracy $\pm 0.1\mu\text{m}$ on the tool post. 20 thermo-couples with type T were set for measuring the structural temperatures of the lathe (marks ○ and ● in Fig. 2). 3 thermo-couples with type T were used for measuring the room temperatures.

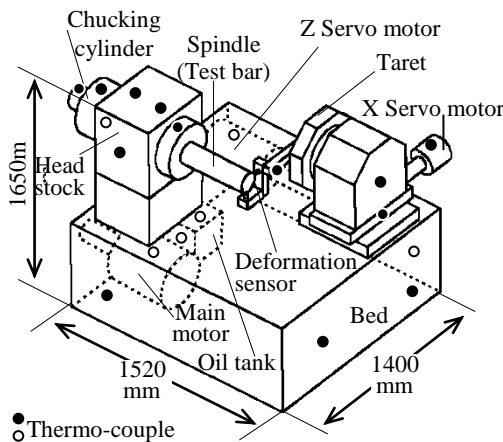


Fig. 2. Schematic view of the NC lathe used

Table 1. Specifications of the NC lathe used

Spindle	Nose shape	JIS A2-5
	Bearing inside diameter	$\phi 75\text{mm}$
	Spindle speed	Max. 3500min^{-1}
Tool post	Max. stroke	X:90mm Z:230mm
Motor	Spindle motor	AC 3.7/5.5kW
	Feed motor	X:0.9kW Z:1.4kW
	Oil-hydraulic motor	0.75kW
	Cutting fluid motor	0.25kW
Size	Height of spindle center	950mm
	Length×Width×Height	1520×1400×1650
	Mass	2250kg

Experimental parameters for teaching data of the neural network are shown in Table 2. The experiment was performed in a general factory. There are spindle speed 1800min^{-1} (constant), spindle speed 3600min^{-1} and NC program for automobile parts in the parameters. And several intermissions which are 15 or 60 minutes are also included in the working.

For example, temperature changes and thermal errors of the NC lathe are shown in Fig. 3. This experiment is performed from at 9:00 to at 17:00, spindle speed is 3600min^{-1} (constant), carriage is moving and rest times are from at 10:00 to at 10:15, from at 12:00 to at 13:00 and from at 15:00 to at 15:15. The 30 teaching data (—○—) can gather every 15 minutes from the results of the experiment. Similar teaching data can gather from each experiment.

The neural network using the teaching data is shown in Fig. 4. This neural network has structure with three layer. Numbers of data in input layer are 13; working time t , 6 structural temperatures at time t , 6 structural temperature changes from $(t-30)$ minutes to t . Numbers of middle layer are 32. Numbers of data in output layer are 2; the thermal errors regarding X and Z directions. Sigmoid function was used in the middle layer, and a linear function was used in output layer respectively. Only 6 structural temperatures in Fig. 3 were selected from the 23 measured temperatures, were used for the neural network. In study of the neural network, weight W_{ji} , V_{jk} and offset β_j , γ_k were decided by steepest descent method (Back

Table 2. Working cinditions for teaching data

Spindle speed	Tool post move	Rest time
1800 min ⁻¹	×	×
3500 min ⁻¹	×	×
Random change	×	×
1800 min ⁻¹	Simple cycle	×
3500 min ⁻¹	Simple cycle	×
Random change	Simple cycle	×
Cutting program I		×
Cutting program II		×
Cutting program I		12:00~13:00
Cutting program II		12:00~13:00
3500 min ⁻¹	×	12:00~13:00 10:00~10:15, 15:00~15:15

Spindle speed on each experiments

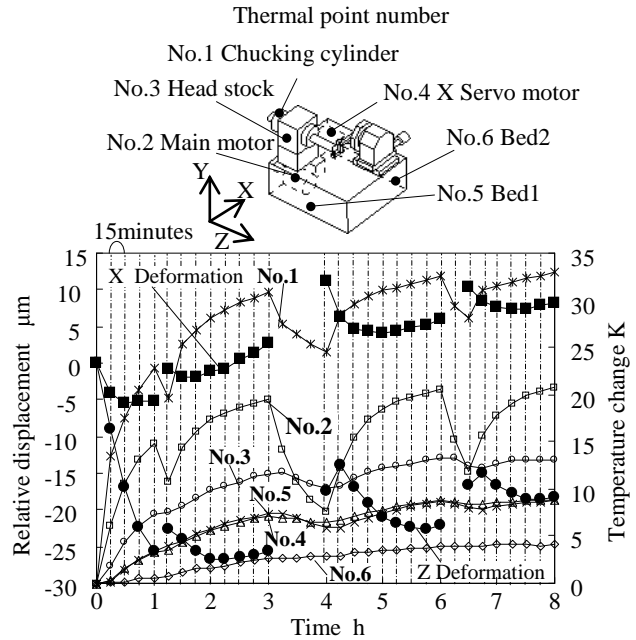


Fig. 3. Thermal and deformation behavior of the NC lathe

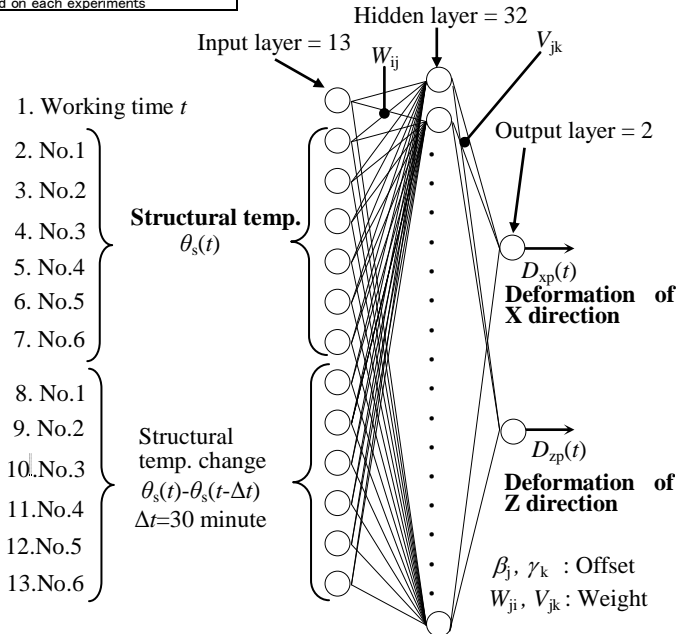


Fig. 4. Neural network between the structural temp. of the lathe and the thermal errors with non-linear behaviour

propagation) for the condition which total (such as equation (1)) of square of difference between the teaching data and the output value becomes most small value. Here W_{ji} is weight between the input and middle layers, V_{jk} is weight between the middle and output layers, β_j is offset for middle layer, γ_k is offset for output layer. Error function E_p of study pattern p is shown in equation (1).

$$E_p = \frac{1}{2} \sum_k (T_{kp} - D_{kp})^2 \quad (1)$$

Where T_{kp} is teaching data for unit k of study pattern p , and D_{kp} is output value for unit k of study pattern p . Here study pattern p is the measured temperatures every 15 minutes. When the neural network was used 11 data set and 30 times every data sets, Error function E_p becomes to 1.7×10^{-5} for 1000 times of study and can converge.

Then the neural network was rewritten for an algebraic equation. Relationship between the structural temperatures $\theta_s(t)$ of the lathe and the thermal errors $D_{kp}(t)$ was shown by using weight W_{ji} , V_{jk} and offset β_j , γ_k such as equation (2).

$$D_{kp} = f\{W_{ji}, V_{kj}, \beta_j, \gamma_k, \theta_s(t), \theta_s(t-0.5), t\}$$

$$= \sum_{p=1}^{\text{Hidden layer number}} \frac{V_{kp}}{1 + \exp\left(-\sum_{q=1}^{\text{Input layer number}} (W_{pq} \cdot I_q + \beta_p)\right)} + \gamma_k \quad (2)$$

Where I is such as equation (3).

$$I = \begin{bmatrix} I_1 \\ I_2 \\ I_3 \\ \vdots \\ I_{\text{Input layer no.}} \end{bmatrix} = \begin{bmatrix} t \\ \theta_s(t) \\ \theta_s(t) - \theta_s(t-0.5) \end{bmatrix} \quad (3)$$

Where the structural temperatures $\theta_s(t)$ are still unknown. The algebraic equation was carried in the NC lathe with PC. If the structural temperatures $\theta_s(t)$ and $\theta_s(t-0.5)$ are measured at time t and those values are substituted to the equation (2), thermal errors $D_{kp}(t)$ for X and Z direction will calculate very easy.

4. SIMPLE AND INTELLIGENT CONTROL REGARDING THERMAL DFFORMATION WITH NON-LINEAR AND ITS APPLICATION

4.1. Remodelling of NC lathe and utilization of NC program

Explanation regarding remodelling of the NC lathe was shown in Fig. 5. This lathe has open NC. Procedure of intelligent control is as following; Structural temperatures in the NC lathe are firstly measured by several thermo-couples. The data sends to the PC in the NC lathe, then the thermal errors were calculated by using equation (2), and the thermal errors X and Z

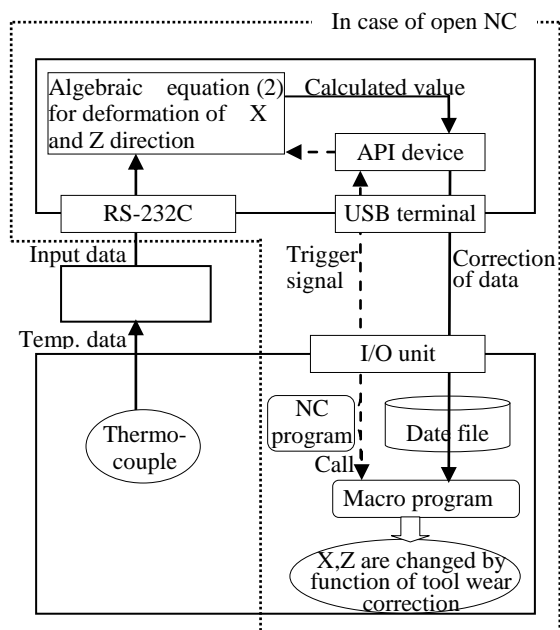


Fig. 5. Schematic view of control system using neural network for compensation of thermal errors with non-linear behavior of the NC lathe

were lastly revised by the function of tool wear correction using macro program. This working is perfectly and automatically performed. Therefore the NC lathe can perfectly and automatically revise the thermal errors by oneself. The NC lathe lastly has simple and intelligent control system regarding thermal errors. Here remodelling of hardware was only for setting several thermo-couples on the NC lathe and the data logger. Those are very easy and low cost.

Next, flow of macro program on this system is shown in Fig. 6. Working of cutting was firstly performed in main NC program, the macro program for revision of thermal errors was periodically called by “function M” and performed in main NC program, and measurement of temperature, calculation of thermal errors using the algebraic equation (2) and revision of the thermal errors using the function of tool wear correction were also performed by “function M”.

4.2. Evaluation for new system

Experimental conditions for evaluation of the new system are shown in Table 3. Teaching data was gathered from 26th September 2012 to 20th October 2012, and this evaluation for new system was gathered from 23rd October 2012 to 28th October 2012. Season was autumn. Both room temperature changes were from 18.0 °C to 25.0 °C. Therefore all experiments for evaluation were performed in the similar condition at teaching data regarding the room temperature. The NC lathe is controlled using the condition of Table 3, the thermal errors with non-linear behaviour was revised every 15 minutes by using macro program, thermal errors of X, Z directions were measured by two inductive gauging sensors with accuracy $\pm 0.1\mu\text{m}$ on the tool post at the same time.

Results of experiments for evaluation are shown in from Fig. 7 to Fig. 12. In case of (a) temperature change in each figure, the structural temperatures were rising for the working condition of the NC lathe. In case of (b) thermal displacement in each figure, there are two

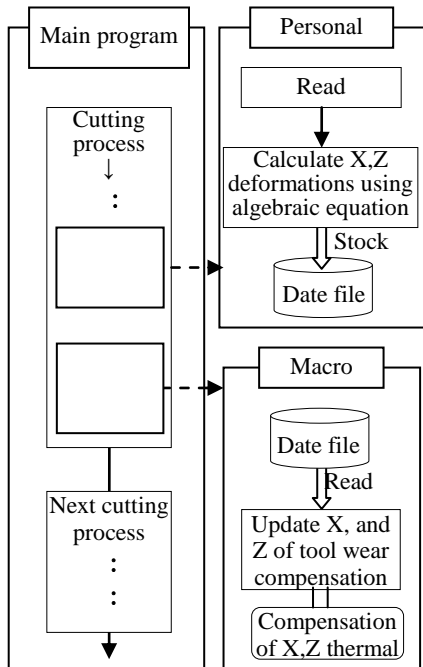
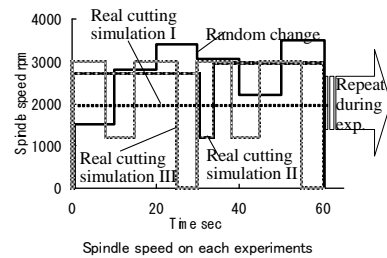


Fig. 6. Macro program for controlling thermal errors of the NC lathe (Time in sec)

Table 3. Experimental condition for evaluation

No.	Spindle speed	Tool post move	Rest time	Results
I	3500 min ⁻¹	×	×	Fig.7
II	3500 min ⁻¹	×	12:00~13:00 10:00~10:15 15:00~15:15	Fig.8
III	2400 min ⁻¹	×	12:00~13:00 10:00~10:15 15:00~15:15	Fig.9
IV	Cutting program I		12:00~13:00 10:00~10:15 15:00~15:15	Fig.10
V	Cutting program II		×	Fig.11
VI	Cutting program III		×	Fig.12



results for the NC lathe with and without new system on the figures. Revision of the thermal errors with non-linear behaviour was performed under excellent condition in spite of no forced cooling. Particularly the conventional NC lathe had large thermal errors at lunch time from at 12:00 to at 13:00, however the NC lathe with new system can perfectly settle the problem. When the temperatures of the machine tool were in the teaching data of the neural network, thermal errors were restrained in $\pm 10\mu\text{m}$ and the proposed system could use for several and practical conditions

Results of similar experiments at 7th and 8th January 2013 (winter season) were shown in Fig. 13. Previous teaching data for the neural network is for autumn season, and isn't for winter season. This experiment was performed for check of behaviour regarding new system except range of the study using the teaching data in the neural network. (a) is thermal errors with No.1 in Table 3, when the room temperature change from 12.0 °C to 16.0 °C. Revision of the thermal errors with non-linear behaviour was performed under excellent condition, because this structural temperatures and the room temperature at 7th January 2013 were similar to the teaching data at autumn. (b) is thermal error with "Random change" with tool post moving and rest time (from at 10:00 to at 10:15, from at 12:00 to at 13:00 and from at 15:00 to at 15:15.) in Table 3, when the room temperature change from 8.0 °C to 18.0 °C. Revision of the thermal errors with non-linear behaviour was unsuccessful, because this structural temperatures and the room temperature at 8th January 2013 weren't similar to the teaching data at autumn. Such as results at 8th January 2013, the neural network using the teaching data of autumn season doesn't use to revision of the thermal errors. If the neural network using the teaching data of both autumn and winter was remade, revision of the thermal errors at 8th

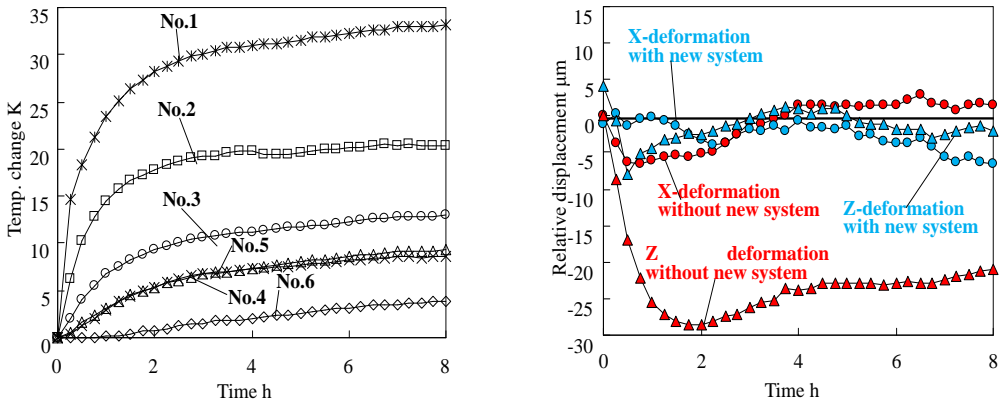


Fig. 7. Experimental results I for evaluation (Experimental No. I in Table 3.)

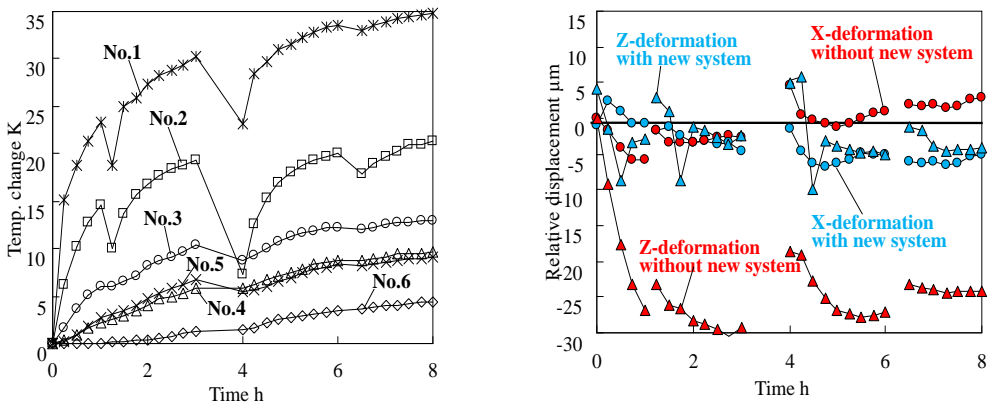


Fig. 8. Experimental results II for evaluation (Experimental No. II in Table 3.)

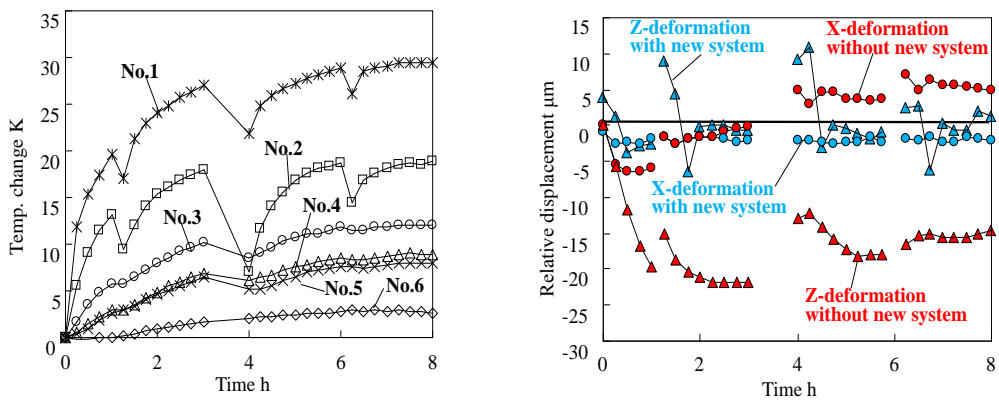


Fig. 9. Experimental results III for evaluation (Experimental No. III in Table 3.)

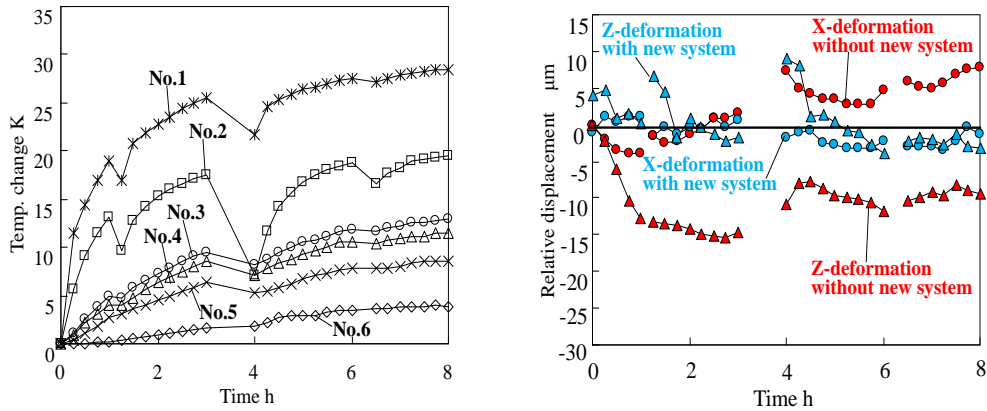


Fig. 10. Experimental results IV for evaluation (Experimental No. IV in Table 3.)

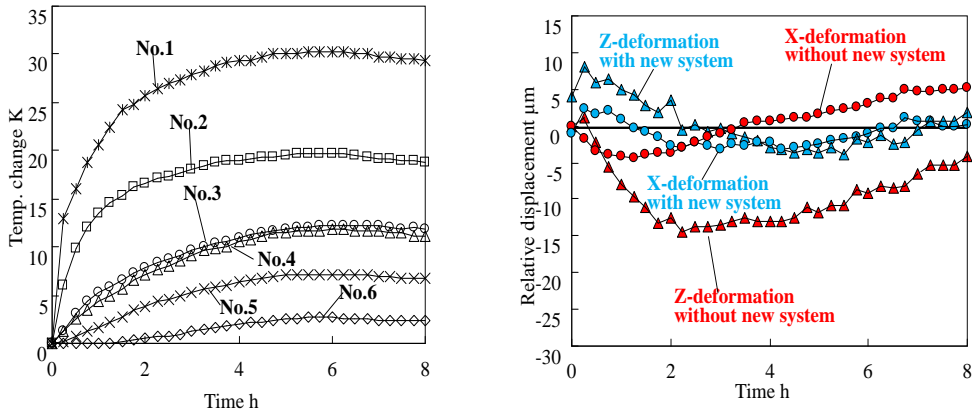


Fig. 11. Experimental results V for evaluation (Experimental No. V in Table 3.)

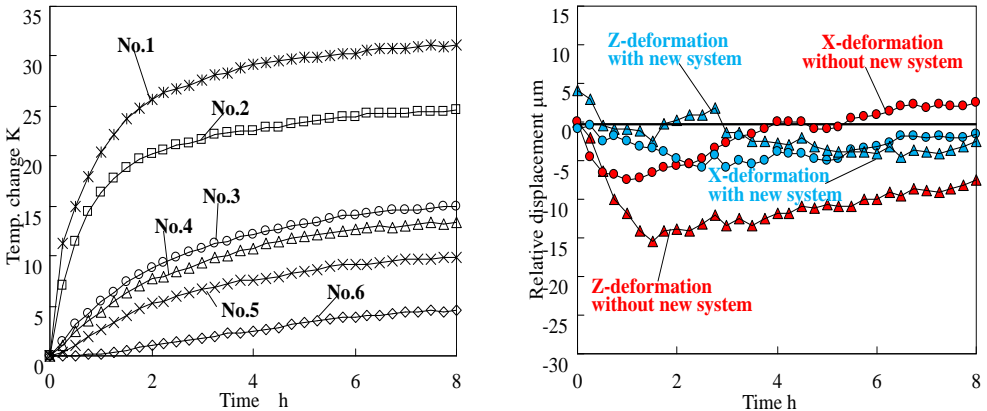
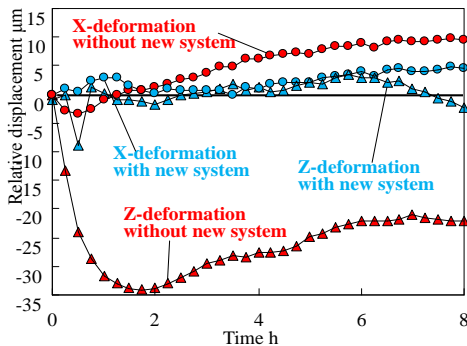
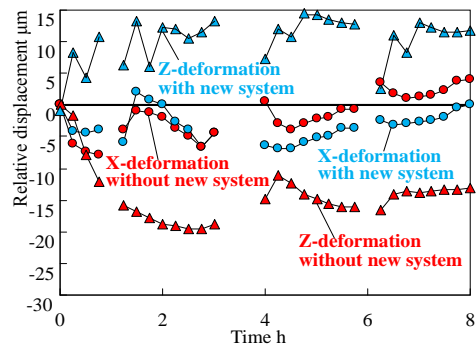


Fig. 12. Experimental results VI for evaluation (Experimental No. VI in Table 3.)



(a) Thermal displacement of Experimental No. I in Table 3 (at 7th January 2013)



(b) Thermal displacement of Random change in Table 2 with the tool post moving and rest time (at 8th January 2013)

Fig.13 Experimental results of thermal displacement for evaluation (In Winter)

January 2013 will be performed under excellent condition [6].

In this research, only thermal errors in machine tool were investigated. However, the temperatures of work piece, the vibration of machine and the deformation of both machine and tool for cutting force are also influence to accuracy of the work piece. After this research, I would like to investigate for that.

5. CONCLUSION

It is concluded from the results that;

- (1) Proposed method was effective in order to reduce thermal errors.
- (2) Necessary device for the proposed method was only measuring device of temperature, and a forced cooling device or a linear scale were not necessary.
- (3) Revision of the thermal errors with non-linear behaviour was performed under excellent condition inside the range of study for the neural network, however revision of the thermal errors was unsuccessful outside the range of study for the neural network.

REFERENCES

- [1] I. TANABE, K. YANAGI, S. NAKAMURA and K. URANO. Adaptation of Dual Cooling Jacket to Machine Tool Spindle and Feed Forward Control of Its Temperature and Thermal Deformation (in Japanese). Transaction of the Japan Society of Mechanical Engineers, Series C, Vol. 60, No. 576, pp.2860-2866, 1994.
- [2] Y. KANEKO, I. TANABE, M. ISOBE and M. MAEDA. Development of a High Precision Lathe with Countermeasure of Environmental Preservation for Thermal Deformation (in Japanese). Transaction of the Japan Society of Mechanical Engineers, Series C, Vol. 70, No. 700, pp.3611-3616, 2004.
- [3] Y. Ito. THERMAL DEFORMATION in Machine Tools, McGraw-Hill companies, pp1-201, 2010
- [4] Y. ONDA, M. MIZUTANI, M. MORI, Machine Tool Main Spindle Bearings with "Air Cooling Spacer", NTN TECHNICAL REVIEW No.80, pp38-41, 2012
- [5] I. TANABE, S. IKEDA and K. URANO. Estimation of Optimum Temperature for Cooling Oil on a Spindle Using Inverse Analysis of Neural Network (Effect of Relearning) (in Japanese). Transaction of the Japan Society of Mechanical Engineers, Series C, Vol. 69, No. 679, pp.819-824, 2003.
- [6] I. TANABE, T. IKARIYAMA, A. NISHIYAMA and K. URANO. Estimation of the Most Suitable Temperature for Cooling Oil on a Spindle Using Inverse Analysis of Neural Network (in Japanese). Transaction of the Japan Society of Mechanical Engineers, Series C, Vol. 66, No. 647, pp.2443-2448, 2000.

Application of GNNMCI(1, N) to environmental thermal error modelling of CNC machine tools

Ali M Abdulshahed, Andrew P Longstaff, Simon Fletcher, Alan Myers

Centre for Precision Technologies, University of Huddersfield, UK, HD1 3DH

Email: Ali.Abdulshahed@hud.ac.uk

ABSTRACT

Thermal errors are often quoted as being the largest contributor to inaccuracy of CNC machine tools, but they can be effectively reduced using error compensation. Success in obtaining a reliable and robust model depends heavily on the choice of system variables involved as well as the available input-output data pairs and the domain used for training purposes. In this paper, a new prediction model “Grey Neural Network model with Convolution Integral (GNNMCI(1, N))” is proposed, which makes full use of the similarities and complementarity between Grey system models and Artificial Neural Networks (ANNs) to overcome the disadvantage of applying a Grey model and an artificial neural network individually. A Particle Swarm Optimization (PSO) algorithm is also employed to optimize the Grey neural network. The proposed model is able to extract realistic governing laws of the system using only limited data pairs, in order to design the thermal compensation model, thereby reducing the complexity and duration of the testing regime. This makes the proposed method more practical, cost-effective and so more attractive to CNC machine tool manufacturers and especially end-users.

KEYWORDS: Machine tool, Thermal error, Modelling, Grey neural network.

1. INTRODUCTION

Thermal errors of machine tools, caused by external and internal heat sources, are one of the main factors affecting CNC machine tool accuracy. A significant amount of research work has been devoted to the effects of internally generated heat from, for example, spindle motors, friction in bearings, etc. [1]. External heat sources are attributed to the environment in which the machine is located, such as neighbouring machines, opening/closing of machine shop doors, variation of the environmental temperature during the day and night cycle and differing behaviour between seasons. The complex thermal behaviour of a machine is created by interaction between these different heat sources. Ambient effects are arguably one of the most important, but most neglected in thermal error compensation systems [2]. An integrated model can be used in machine tool error compensation, taking into account the different heat sources [1]. An example of such a model for a CNC machine tool is given by White *et al.* [3].

Longstaff *et al.* [2] presented several Environmental Temperature Variation Error (ETVE) tests conducted on a wide range of machine tools and discussed the implications for produced parts. The authors also described a number of interesting phenomena when the machines were subjected to a wide variety of environmental conditions. Attention was also drawn to the prohibitive downtime required to conduct the ETVE test. Modification of the machine shop conditions is possible and can effectively reduce thermal errors on a number of machines at once, but may be difficult and costly to achieve. Fletcher *et al.* [4] provided useful information about daily cyclic environmental temperature fluctuations and associated drifts. Experimental results indicated, through error compensation, a reduction of the environmental errors by more than 50% to just $\pm 7\mu\text{m}$ over a 65 hour test, but also drew attention to the detrimental amount of machine downtime for the thermal characterisation tests. Rakuff and Beaudet [5] measured and modelled the ETVE of a machine tool over 23 h with no traffic in the workshop. They show how certain process variables, such as opening and closing of doors around the machine, affect the ETVE. Mian *et al.* [6] proposed a novel offline environmental thermal error modelling approach based on a finite element analysis (FEA) model that reduces the machine downtime usually needed for the ETVE test from a fortnight to 12.5 hours. Their modelling approach was tested and validated on a production machine tool over a one-year period and found to be very robust. However, building a numerical model can be a great challenge due to problems of establishing the boundary conditions and accurately obtaining the characteristic of heat transfer.

Research on thermal error compensation for machine tools by both academic institutions and industry has been rapidly accelerated recently in response to the growing demand of product quality. Effective compensation depends on the accuracy of the prediction model. Thermal error modelling and compensation techniques introduced to date have been found to suffer from a number of drawbacks that make their application in practical machining environments time consuming. Different structures of empirical models have been used to predict thermal errors in machine tools such as multiple regression analysis [7], artificial neural networks [7], adaptive neuro-fuzzy inference system [8, 9], Grey system theory [10] and a combination of several different modelling methods [11].

Whilst empirical models can be good at predicting thermal errors, they require a large amount of data with different working conditions to determine the governing laws of the original data. However, a realistic governing law may not exist even when a large amount of data has been measured. Furthermore, the process of obtaining such data can take several hours for internal heating tests and several days or more for the environmental test.

This paper aims to develop an effective and simple method to predict the Environmental Temperature Variation Error (ETVE) of machine tools. The work proposes a novel Grey Neural Network model with Convolution Integral GNNMCI(1,N), combining the Grey prediction model with convolution integral GMC(1,N) and PSO neural network model, and also adopting the GMC(1,N) model when selecting the inputs. The proposed model is a type of dynamic model described by a PSO neural network to extract realistic governing laws of the system using only a limited number of data pairs. The dynamic characteristic of the GNNMCI(1,N) model results from introducing the Grey accumulated generating operation (AGO) into the neural network. The benefits and novelty of this work are that a thermal model can be efficiently built with the minimum amount of temperature data in a very short time scale.

2. MODELLING THE THERMAL ERROR USING A GREY NEURAL NETWORK

The Grey systems theory, established by Deng in 1982 [12], is a methodology that focuses on solving problems involving incomplete information or small samples. The technique works on uncertain systems with partially known information by generating, mining, and extracting useful information from available data. So, system behaviours and their hidden laws of evolution can be accurately described. GM(1, N) is the most widely used implementation in literature [13], which can establish a first-order differential equation featured by comprehensive and dynamic analysis of the relationship between system parameters. The accumulated generating operation (AGO) is the most important characteristic of the Grey system theory, and its benefit is to increase the linear characters and reduce the randomness of the samples. Based on the existing GM(1,N) model, Tzu-Li Ties [14] proposed a GMC(1,N) model, which is an improved grey prediction model. The modelling values by GM(1,n) are corrected by including a convolution integral. However, Grey models lack the ability to self-learn, self-adapt or otherwise considering a feedback value.

Compared with other empirical models, artificial neural networks (ANNs) have a strong capacity for processing information, parallel processing, and self-learning. However, they have some disadvantages such as the need for a large number of learning samples, thus needing a long training computation time, and the non-interpretable problem of such “black box” systems. In addition, the working conditions of machine tools are in general complex and susceptible to unexpected noises. Therefore, ANN models in isolation have significant drawbacks as a modelling approach for thermal error compensation [3].

Because the way of presenting information for neural network and Grey models have some commonality in format, the two methods can be fused. Two levels can be added; an initial Grey level will process the input information and a whitening level after to process the output information to obtain good results [15]. Therefore, the Grey meaning is contained in the neural network. The advantages of both can be used to build a high-performance neural network model with a minimum amount of training data.

2.1. GNNMCI(1, N) Prediction Model

The fusion model of Grey system and neural network is employed in the modelling of the ETVE of machine tools. The model can reveal the long-term trend of data and, by driving the model by the AGO, rather than raw data, can minimize the effect of some of the random occurrences. Therefore, the first step for building GNNMCI(1,N) is to carry out 1-AGO (first-order Accumulated Generating Operation) to the data, so as to increase the linear characteristics and reduce the randomness from the measuring samples. Then the GNNMCI(1,N) model is trained with a PSO algorithm to generate the desired GNNMCI(1,N) model. Finally an IAGO (inverse Accumulated Generating Operation) is performed to predict the ETVE and generate the final compensation values. The model fully takes the advantages of neural networks and Grey models, and overcomes the disadvantages of them, achieving the goal of effective, efficient and accurate modelling. The modelling details are described as follows:

The Grey prediction model with convolution integral GMC(1, n) [14] is:

$$\frac{dX_1^{(1)}}{dt} + b_1 X_1^{(1)} = b_2 X_2^{(1)} + b_3 X_3^{(1)} + \dots + b_N X_N^{(1)} + u \quad (1)$$

where b_1 is the development coefficient, $b_i (i = 2, 3, \dots, N)$ the driving coefficient, and u is the Grey control parameter. Therefore, time response sequences can be obtained.

$$\hat{x}_1^{(1)}(k+1) = x_1^{(1)}(1)e^{-b_1k} + u(t-1) \times \sum_{\tau=1}^k \left\{ e^{-b_1(k-\tau+\frac{1}{2})} \cdot \frac{1}{2} [f(\tau) + f(\tau-1)] \right\} \quad (2)$$

Where $u(t-1)$ is the unit step function [14]; $f(\tau) = \sum_{j=2}^N b_j X_j^{(1)}(\tau) + u$ $k=1,2,\dots,n$.

To calculate the coefficients b_j and u , the neural network method can be used to map equation (2) to a forward neural network. Then, the neural network model is trained until the performance is satisfactory. Finally, the optimal corresponding weights are used as the Grey neural network weights to predict ETVE.

We can process equation (2) more. Let

$$G = u(t-1) \times \sum_{\tau=1}^k \left\{ e^{-b_1(k-\tau+\frac{1}{2})} \cdot \frac{1}{2} [f(\tau) + f(\tau-1)] \right\} \quad (3)$$

We can rewrite equation (2) as:

$$\hat{x}_1^{(1)}(k+1) = \left(x_1^{(1)}(1) \right) e^{-b_1k} + G \quad (4)$$

Then equation (4) can be converted into equation (5) as follows:

$$\begin{aligned} \hat{x}_1^{(1)}(k+1) &= \left[x_1^{(1)}(1) \frac{e^{-b_1k}}{1+e^{-b_1k}} + G \frac{1}{1+e^{-b_1k}} \right] (1+e^{-b_1k}) \\ \hat{x}_1^{(1)}(k+1) &= \left[x_1^{(1)}(1) \left(1 - \frac{1}{1+e^{-b_1k}} \right) + G \frac{1}{1+e^{-b_1k}} \right] (1+e^{-b_1k}) \\ &= \left[x_1^{(1)}(1) - x_1^{(1)}(1) \frac{1}{1+e^{-b_1k}} + G \frac{1}{1+e^{-b_1k}} \right] (1+e^{-b_1k}) \end{aligned} \quad (5)$$

Map equation (5) into a neural network, and the mapping structure is shown in Fig. 1.

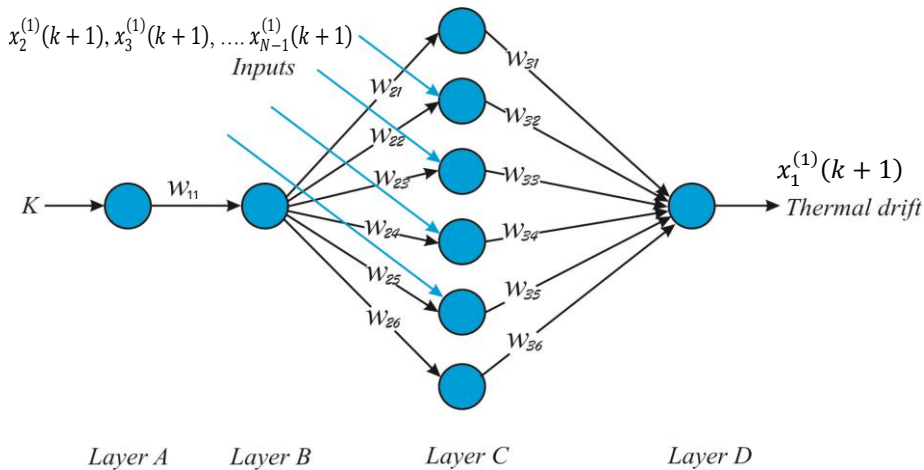


Fig. 1. The mapping structure of GNNMCI(1, N).

Where k is the serial number of input parameters;

In this study, $x_1^{(1)}(k+1)$ is chosen as the thermal displacement data series (network output) and $x_2^{(1)}(k+1), x_3^{(1)}(k+1), \dots, x_{N-1}^{(1)}(k+1)$, as a data series of temperature sensors (N is the number of network inputs);

$w_{11}, w_{21}, w_{22}, \dots, w_{2n}, w_{31}, w_{32}, \dots, w_{3n}$ are the weights of the network;

Layer A, layer B, layer C, and layer D are the four layers of the network, respectively.

Where, the corresponding neural network weights can be assigned as follows:

Let us assume that $d_1 = f(b_2), d_2 = f(b_2), \dots, d_{N-2} = f(b_{2-N}), d_{N-1} = f(u)$

$w_{11} = b_1, w_{21} = -x_1^{(1)}(1), w_{22} = d_1, w_{23} = d_2, \dots, w_{2N-1} = d_{N-2}, w_{2N} = d_{N-1}$

$w_{31} = w_{32} = w_{33} = \dots = w_{3N} = 1 + e^{-b_1 k}$

The bias Θ value of $x_1^{(1)}(k+1)$ is:

$$\Theta = \left(-x_1^{(1)}(k+1)\right)(1 + e^{-b_1 k}) \quad (6)$$

The transfer function of Layer B is a sigmoid function $f(x) = \frac{1}{1+e^{-x}}$, the transfer functions of other layer's neuron are adopted as a linear function $f(x) = x$.

2.2. GNNMCI(1, N) learning algorithm

The learning algorithm of GNNMCI(1, N) can be summarised as follows:

Step 1: For each input series, $(k, X_j^{(1)}(k))$, $(k = 2, 3, \dots, N)$, the output of each layer is calculated.

Layer A: $a = w_{11}k$;

Layer B: $b = f(w_{11}t) = \frac{1}{1+e^{-w_{11}k}}$;

Layer C: $c_1 = bw_{21}, c_2 = x_2(k)bw_{22}, c_3 = x_3(k)bw_{23}, \dots, c_{n-1} = x_n(k)bw_{2n-1}, c_n = bw_{2n}$;

Layer D: $d = w_{31}c_1 + w_{32}c_2 + \dots + w_{3n-1}c_{n-1} + w_{3n}c_n - \Theta$

Step 2: A PSO algorithm [16] is adopted to train the GNNMCI(1, N) model. Each weight of model is encoded to each component of particle position, which means that each particle represents a specific group of weights. In the course of training, the model is repeatedly presented with training pairs. The model parameters are then adjusted until the errors between the predicted output and real output meet a tolerance criterion, or a pre-determined number of epochs has passed (in this work, ten training epochs are determined as the stopping criteria).

Step 3: export the optimal solution. $(w_{11}, w_{21}, w_{22}, w_{2N}, \dots, w_{31}, w_{32}, \dots, w_{3N})$.

3. EXPERIMENTS

In this study, an ETVE test was performed on a small vertical milling centre (VMC). This test was conducted to reveal the effects of ambient temperature changes on the machine and to predict the thermal displacement during other performance measurements [2]. In order to obtain the temperature data of the machine tool, a total of 27 temperature sensors were placed on the machine. Thirteen temperature sensors were attached on the spindle carrier, six on the column, and one on each axis ballscrew nut. Another six temperature sensors were

placed around the machine to detect the ambient temperature. Four non-contact displacement transducers (NCDTs) were used to measure the displacement of a test bar (used to represent the tool) while the spindle remained stationary. Three were used to measure displacement of the test bar in each axis direction. A fourth directly monitored displacement of the casting next to the spindle in the Z-axis direction to differentiate expansion of the tool from the machine. A general overview of the experimental setup is shown in Fig. 2.

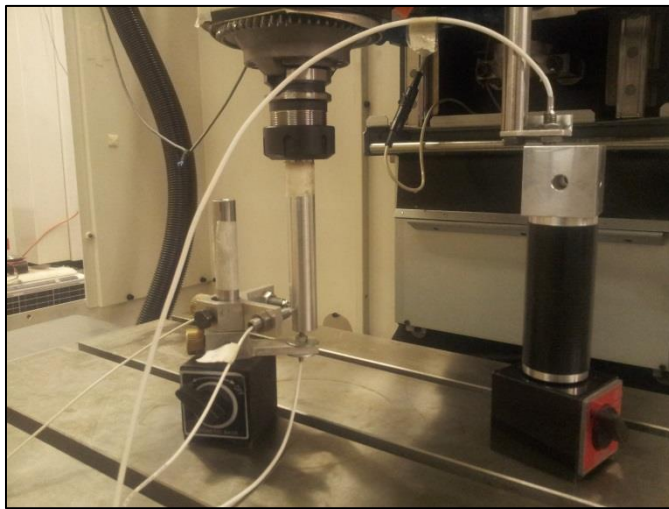


Fig. 2. A general overview of the experimental setup.

Results of an ETVE test are shown in Fig. 3. This test was carried out over a five-day period during spring bank holiday, with no significant activity in the workshop, followed by approximately three normal working days (160 hours). This data was sampled once every minute. The environmental temperature conditions for machine shop change due to the day /night cycle, where the temperature fluctuates by about 5 °C throughout the day, with lower temperatures in the morning and higher temperatures in the late afternoon and evening. The strongest response to the ambient change from the machine is in the Z-axis direction. There is a clear relation between the fluctuation in the environmental temperature and the resulting displacement. For example, the anomaly at the beginning of the test can be attributed to a short period (30 minutes) of the workshop door being opened. Externally, the conditions were snowy, which caused a drop in workshop temperature to below 11°C. The overall movement caused by this phenomenon is 35 µm in the Z-axis and 25 µm in the Y- axis for an overall temperature swing of approximately 9 °C over the 30 minutes. Two similar events can be seen between 120 and 140 minutes. The magnitude of the environmental error can be compared to that from two hours spindle-heating test conducted according to ISO-230:3 which only produced 30µm of error in the Z-axis.

To demonstrate the modelling of ETVE using the Grey neural network approach, four temperature sensors were selected based on our work in [9]. Temperature sensors T1, T2, T5, and T9, which are located on the carrier, column, ambient near spindle, and ambient near the column, were selected according to their influence coefficient value using the GMC(1, N) model. They were used as the input variables for the GNNMCI(1, 5) model and the thermal drift in Z direction was used as a target variable.

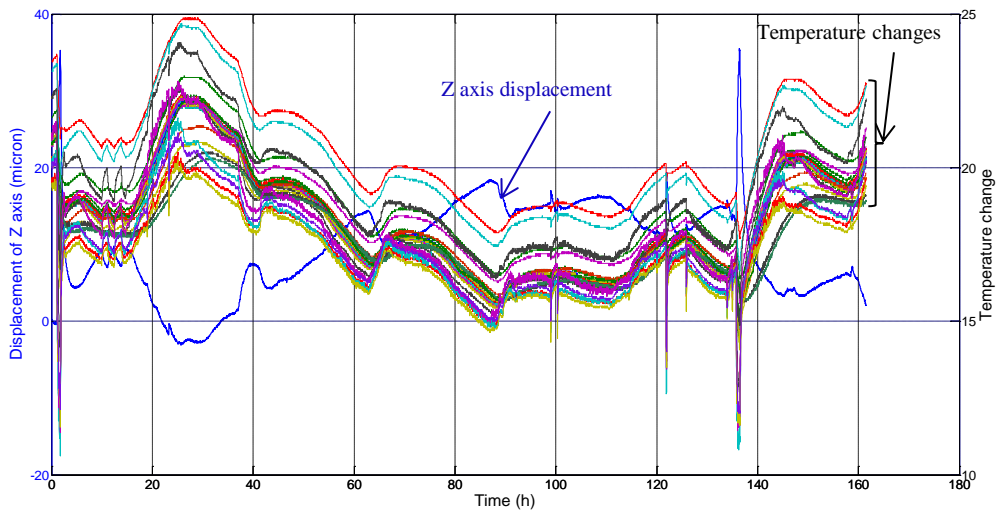


Fig. 3. Temperature measurements and machine movement due to environment.

For this study, a GNNMCI(1, 5) with a structure of 1-1-6-1 was chosen. The details are: layer A has one node, the input time series k ; layer B has one node; layer C has six nodes, the input variables nodes are from two to five, respectively; T_1 , T_2 , T_5 , and T_9 are the input variable data. Layer D has an output variable node, which is the thermal displacement in Z-axis direction. The GNNMCI(1, 5) structure is shown in Fig. 1. The MATLAB software was used to realize the model.

Two compensation methods can be used to predict ETVE. The first is an off-line, pre-calibrated method. This means to obtain the GNNMCI(1, 5) model according to the thermal displacement and the temperature change during a short test, and then to use this model to predict the thermal displacement of other processes. The second method is to obtain the GNNMCI(1, N) model at the first stage of the manufacturing process, and then to use this model to predict the machine movement during the rest of the process. This uses additional measurement effort before the process begins.

To apply the first method, another test was carried out for 80 minutes on the same machine during a normal working day. During the experiment, the thermal errors were measured by the NCDTs and the temperature data was measured using the same selected sensors, sampling every ten seconds. The training samples were obtained from the first 5 readings (less than one minute) after the test had been started. All raw data was converted to AGO series, as discussed in section 2.1. Ten training epochs are adapted as the stopping criteria. In the PSO neural network, the number of population was set to be 90 whilst the maximum and minimum velocity values were 1.5 and -1.5, respectively. These values were obtained by optimization.

After finishing the training of the model, there were two ways to obtain the prediction values: directly obtaining the prediction values from the trained model; or taking out the Grey differential equation parameters from the trained model to equation (2) and then solving the equation to obtain the prediction values. Although both methods are similar theoretically, a large number of experiments have found that the first method needs less computation. Fig. 4 shows simulation results for 80 minutes.

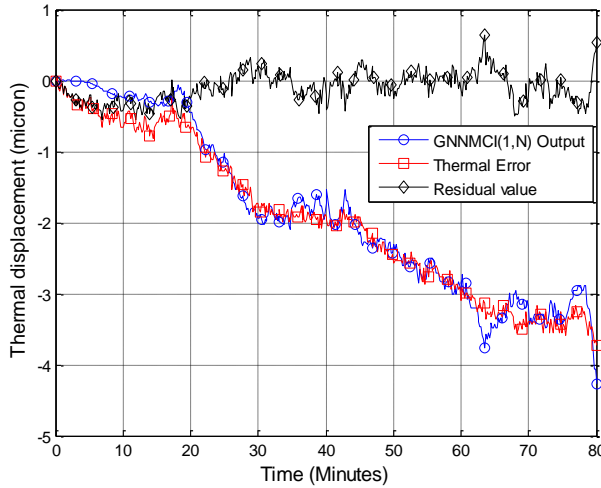


Fig. 4: Simulation results for 80 minutes.

The process was repeated to create a GNNMCI (1, 5) model for the Y-axis direction. To validate the robustness of these proposed models on non-training data, a normal environmental simulation was run using the temperature data presented in Fig. 3. The measured and simulated profile results were plotted for the Z-axis and Y-axis. Compared to the measured results, the correlations were 97% for the Z displacement profiles Fig. 5, and 98% for the Y displacement profiles Fig. 6. The residual errors were less than $\pm 10 \mu\text{m}$ for the Z axis and less than $\pm 6 \mu\text{m}$ for the Y axis even when considering the rapid changes due to the opened workshop door. Under more predictable conditions, which could be achieved by better management of the environment, $\pm 3\mu\text{m}$ would be achieved in each axis. Thus, the proposed GNNMCI (1, 5) model can predict the normal daily cyclic error accurately and also can track sudden changes of thermal error from a relatively small training sample.

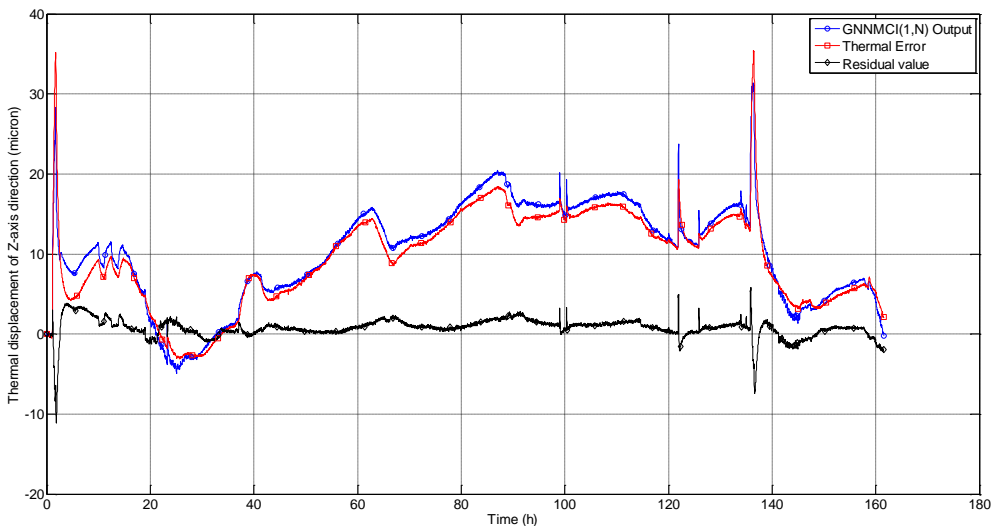


Fig. 5. Correlation between the measured and simulated Z-axis displacement.

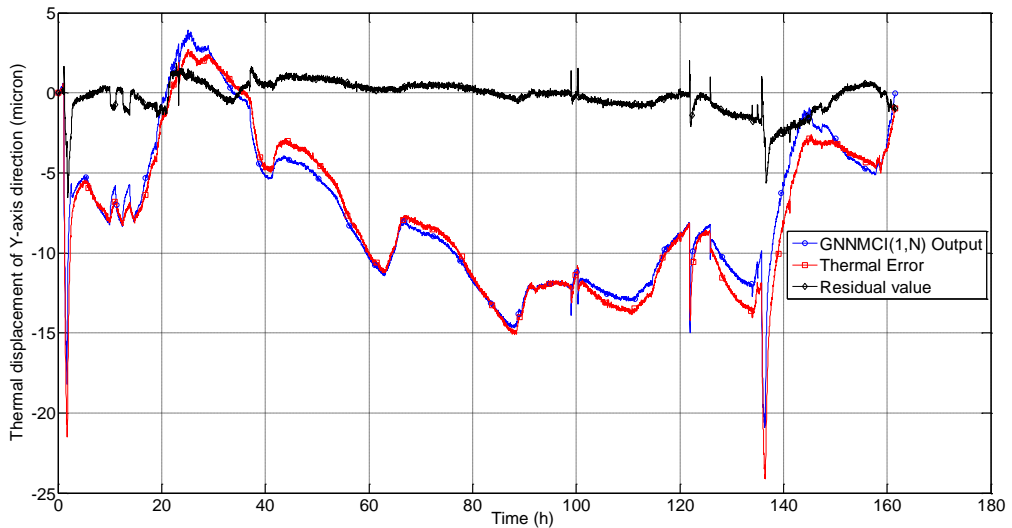


Fig. 6. Correlation between the measured and simulated Y-axis displacement.

4. CONCLUSIONS

Temperature-induced effects on machine tools are a significant part of the error budget. Changes in ambient conditions are an often overlooked effect that can be difficult to model, especially in unpredictable environments.

In this paper, a novel thermal error modelling method based on Grey system theory and neural networks was developed to predict the environmental temperature variation error (ETVE) of a machine tool. The proposed model has been found to be flexible, simple to design and rapid to train.

The model is trained using data obtained from a short test of less than ninety minutes, which is desirable for minimising machine downtime. The accuracy of the model has not been compromised by restricting the training data. ETVE results in the Z-axis direction over a 160 hour test showed a reduction in error from over $20\mu\text{m}$ to better than $\pm 3\mu\text{m}$ considering the normal daily cycles. When also considering unexpected phenomena, such as the rapid change in temperature when a workshop door was opened, the model still performs well, with an improvement from $40\mu\text{m}$ to less than $\pm 10\mu\text{m}$.

Similar results were achieved in the Y-axis direction, with this study not considering the X-axis direction due to symmetry of the machine.

It is anticipated that further improvement in correlation could be achieved by including rapid changes as part of the training data. However, this would compromise the aim of this work which is to train the model with “normal” data, but validate across a range of conditions.

The proposed method is a significant advantage over other models based on a single technique that have been used by many previous scholars where the data used to build the models is obtained from very long tests. The proposed model has significantly reduced the machine downtime required for a typical environmental testing from hours to only few minutes. According to experimental work, little machine downtime is needed to apply this modelling approach except to re-establish the model if needed.

The thermal error compensation model using GNNMCI(1, N) introduced in this study can be applied to any CNC machine tool because the model does not rely on a parametric

model of the thermal error behaviour. In addition, this method is open to extension of other different physical inputs meaning that alternative sensors can be deployed with minimal retraining required.

ACKNOWLEDGEMENTS

The work carried out in this paper is partially funded by the EU Project (NMP2-SL-2010-260051) "HARCO" (Hierarchical and Adaptive smaRt COmponents for precision production systems application). The authors do wish to thank all the partners of the consortium.

The authors also gratefully acknowledge the UK's Engineering and Physical Sciences Research Council (EPSRC) funding of the EPSRC Centre for Innovative Manufacturing in Advanced Metrology (Grant Ref: EP/I033424/1).

REFERENCES

- [1] J. Mayr, *et al.*, "Thermal issues in machine tools," *CIRP Annals - Manufacturing Technology*, vol. 61, pp. 771-791, 2012.
- [2] A. P. Longstaff, *et al.*, "Practical experience of thermal testing with reference to ISO 230 Part 3," in *Laser metrology and machine performance VI*, Southampton, 2003, pp. 473-483.
- [3] A. White, *et al.*, "A general purpose thermal error compensation system for CNC machine tools," in *Laser Metrology and Machine Performance V*, Southampton, 2001, pp. 3-13.
- [4] S. Fletcher, *et al.*, "Flexible modelling and compensation of machine tool thermal errors," in *20th Annual Meeting of American Society for Precision Engineering*, Norfolk, VA, 2005.
- [5] S. Rakuff and P. Beaudet, "Thermally induced errors in diamond turning of optical structured surfaces," *Optical Engineering*, vol. 46, pp. 103401-103409, 2007.
- [6] N. S. Mian, *et al.*, "Efficient estimation by FEA of machine tool distortion due to environmental temperature perturbations," *Precision engineering*, vol. 37, pp. 372-379, 2013.
- [7] J. Chen, *et al.*, "Thermal error modelling for real-time error compensation," *The International Journal of Advanced Manufacturing Technology*, vol. 12, pp. 266-275, 1996.
- [8] K. C. Wang, "Thermal error modeling of a machining center using grey system theory and adaptive network-based fuzzy inference system," in *Cybernetics and Intelligent Systems*, Bangkok, 2006, pp. 1-6.
- [9] A. Abdulshahed, *et al.*, "Comparative study of ANN and ANFIS prediction models for thermal error compensation on CNC machine tools," in *Laser Metrology and Machine Performance X*, Buckinghamshire, 2013, pp. 79-88.
- [10] Y. Wang, *et al.*, "Compensation for the thermal error of a multi-axis machining center," *Journal of materials processing technology*, vol. 75, pp. 45-53, 1998.
- [11] K. C. Wang, "Thermal error modeling of a machining center using grey system theory and HGA-trained neural network," in *Cybernetics and Intelligent Systems*, Bangkok, 2006, pp. 1-7.
- [12] D. Ju-Long, "Control problems of grey systems," *Systems & Control Letters*, vol. 1, pp. 288-294, 1982.
- [13] L. Sifeng, *et al.*, "A brief introduction to grey systems theory," in *Proceeding of IEEE International Conference on Grey Systems and Intelligent Services 2011*, Nanjing, 2011, pp. 1-9.
- [14] T.-L. Tien, "A research on the grey prediction model GM (1, n)," *Applied Mathematics and Computation*, vol. 218, pp. 4903-4916, 2012.
- [15] J. Yuan, *et al.*, "Modeling of Grey Neural Network and Its Applications," in *Advances in Computation and Intelligence*. vol. 5370, L. Kang, *et al.*, Eds., ed: Springer Berlin Heidelberg, 2008, pp. 297-305.
- [16] V. G. Gudise and G. K. Venayagamoorthy, "Comparison of particle swarm optimization and backpropagation as training algorithms for neural networks," in *Swarm Intelligence Symposium, 2003. SIS'03. Proceedings of the 2003 IEEE*, 2003, pp. 110-117.

Development of modular machine tool structural monitoring system

Akshay Potdar*, Andrew Longstaff, Simon Fletcher, Ali Abudulshahed

Centre for precision Technology, University of Huddersfield, Queensgate, HD1 3DH, UK

*Akshay.potdar@hud.ac.uk

ABSTRACT

Although designed to be structurally stiff, machine tool deformation takes place due to the various sources of errors such as shifting mass, component weight, temperature etc. In order to facilitate research activities and acquire further scientific insight on the deformation process, a computer-based on-line monitoring system has been developed. A variety of sensors can be used to capture data for numerous parameters like temperature, displacement, strain etc.

This paper presents the design and implementation of a LabVIEW based multi-sensor data acquisition program. It was designed in a three layer modular structure. In addition to data acquisition, the program is also capable of data processing, logging and implementing various error reduction techniques using online communication between LabVIEW and the MATLAB run-time engine for computation purpose. These calculated compensation values are then transferred to the machine controller via Ethernet. This paper also describes an example of application of such a system for a 5-axis CNC machine tool.

KEYWORDS: Machine tool structural monitoring system, Multi-sensor data acquisition system, Modular structure, LabVIEW

1. INTRODUCTION

The primary goal of the machine tool is to automate the cutting process to achieve higher accuracy to meet the greater quality requirements. Several factors play a crucial role such as machining conditions, cutting tool, type of workpiece etc. Various sources of error like shifting mass, component weight, temperature etc., hinder the possibility of achieving strict accuracy demands for the manufacturing process. Errors arise during building of the machine or occur over the time [1, 2]. Error reduction requires greater understanding of the machine tool capabilities and error sources. This results in the need for a machine tool structural monitoring system. Studies have been carried out on monitoring techniques that are based on the application of single or multiple sensors [3, 4]. Application of different sensors provides the ability to detect a wide range of system parameters like temperature, displacement, strain etc.

Sensor fusion culminates in a more holistic view of the process and in turn the state of the machine[4]. For example by observing the change in the strain of the structure with respect to variation in temperature provides the response of the system, which would be difficult to obtain by simply monitoring either strain or temperature; change in strain can derive from several causes while explicit prediction of distribution from temperature is a major challenge. Synergetic combination of data available from multiple sensors is called sensor fusion [5]. It can provide more reliable and accurate information. Varieties of techniques are used for sensor fusion such as Kalman filter, algebraic functions, weighted average, Bayesian estimation etc. [5, 6]. For high performance operational systems neural network [7, 8] and fuzzy logic [9, 10] techniques are applied for fusion purposes.

Developing data acquisition software (DAQ) for machine tool monitoring sensor fusion is a major challenge. At the moment, any commercial sensor in the market has either some application provided by manufacturer or open source software for capturing and/or analysing data. There is no general DAQ software available for this purpose. Software provided by manufacturers has restricted usage for research application. They often lack the flexibility and extensibility required for research.

The motivation for this work came from a practical application for a modular machine tool structural monitoring and compensation system requiring the development of a multi-sensor data capture system. This DAQ system can capture data from several sensors like digital temperature sensor, laser position sensor and Fibre Bragg Grating (FBG) sensor for measuring temperature, displacement and strain respectively. Data can be logged in a format that can be used off-line by third party applications such as MATLAB or Microsoft Excel. Apart from these tasks, this application is programmed to implement compensation techniques during the process using parametric models and artificial intelligence techniques such as Artificial Neural Network (ANN) and Adaptive Neuro Fuzzy Inference System (ANFIS). Obtained compensation values are then transferred to the machine controller using Ethernet.

The Objectives of this paper are to design a simple, reliable and flexible DAQ system, to implement this program to integrate different sensors and test the application on a real machine application.

2. SYSTEM OVERVIEW

In this paper a computer based on-line monitoring system has been developed. A block diagram of this system is as shown in fig. 1. The system hardware consists of a number of sensors and a computer. The system communicates with a CNC machine tool Siemens 840D interface. The Sensors used are:

The digital temperature sensors used are 1-wire protocol and have programmable resolution of 12 bit (0.0625°C) with response time of 750ms. They have a temperature range of -55°C to $+125^{\circ}\text{C}$. To communicate with a computer, it additionally requires an adapter either USB or serial port.

The laser position sensors used are Riftek RF603. They are used for measuring displacement. They work on the principle of laser triangulation and have a base distance of 10mm with measurement range of 2 mm. Resolution of this sensor is 0.01% of its measurement range. This sensor uses a serial port interface to communicate with the computer, which in some cases requires a RS232-USB converter.

The Fibre Bragg Grating (FBG) sensors are used for strain measurement purpose[11]. They are supplied by SMARTTEC. They use Fabry-Perot Tuneable filter technology. Multiple FBG sensors are used in the wavelength range of 1510 to 1570 nm. FBG sensors have their own reading unit by Micron Optics, which can read at 2 Hz and has 4 optical channels

expandable up to 16 channels. The reading unit communicates with the computer using the Ethernet protocol.

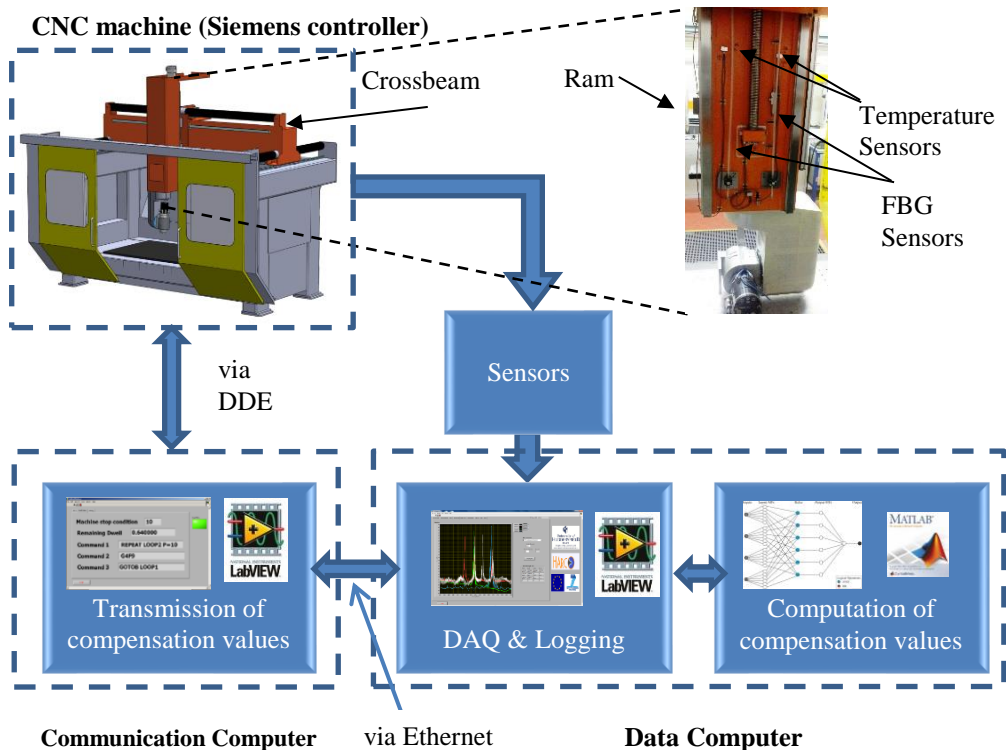


Fig. 1. System Overview

FBG sensors and temperature sensors can be used for structural monitoring of the machine tool for off-line and on-line research purposes. Strain values obtained from FBG and temperature values from temperature sensors can be captured and recorded over the desired time period. Logged data can be used for further off-line analysis purpose.

The software installed on the Data Computer (DC) performs all the major tasks like data acquisition, logging and processing. To make advanced on-line analysis and computation more efficient, the software includes a live interface with the MATLAB run time engine. This program computes the compensation values which are transferred to another LabVIEW program on the Communication Computer (CC). This communication is realized through the Ethernet protocol.

The Program on the CC uses a Dynamic Data Exchange (DDE) link to communicate with the machine controller via Ethernet. Finally compensation values are applied to the machining process by updating values in the part program. This rudimentary method of compensation is suitable for research purpose, but would be replaced by more robust methods in a commercial implementation.

3. SOFTWARE DESIGN

This section discusses the different criteria that were kept in the mind while designing the software. It also talks about the software architecture.

3.1. Design Criteria

The software was designed to provide a simple machine tool structural monitoring system for researchers using LabVIEW based multi sensor data acquisition program. Several aspects that were considered are mentioned as follows:

Usability: All the functions of the program can be performed under the required conditions reliably. Flexibility: It should be flexible enough to modify various parameters and configurations for different sensors. Reusability: Modules designed in this program should be able to be used by other programs without any modification or with trivial changes. Extensibility: Additional features can be easily incorporated without any substantial alterations to the program structure. Cost-efficiency: Cost involved in the development and maintenance of the program should not be high.

Numerous factors need to be considered while selecting the programming language, such as programming skills of the developer, availability of the drivers for various sensors, time required for the development of the program, parallel programming capability, ease of debugging etc., [12, 13] Considering the above mentioned factors and due to the several other advantages of LabVIEW over other text based languages, it was selected for developing a data acquisition program [14, 15].

3.2. Software structure

For any software, well designed architecture is crucial for its success. This program was designed in a modular fashion to offer independent as well as interconnected control of various signals and the three tier structure was implemented for the development.

The top layer consists of graphical user interface developed using a LabVIEW user interface control. The low level tier is designed for the communication by means of hardware drivers and LabVIEW I/O commands to send and receive data from sensors and hardware devices. The middle tier connects top and bottom layer and provides platform for the development. It performs many tasks and is made up of some of the core modules: FBG Module, Temperature sensor module, laser position sensor module, Controller communication, LabVIEW and MATLAB online communication, data logging and error handling module. Each of these key modules are discussed in detail in later sections. All the principle modules are programmed in independent loops to improve the reusability of the program. The three tier structure is as shown in the fig.2.

A modular structure in the software allows integration of new types of sensors or additional sensors without making considerable modifications to the system architecture to easily achieve the desired extensibility. Apart from sensors, extensibility permits the addition of new features in the software as per the requirement in the later stages of research.

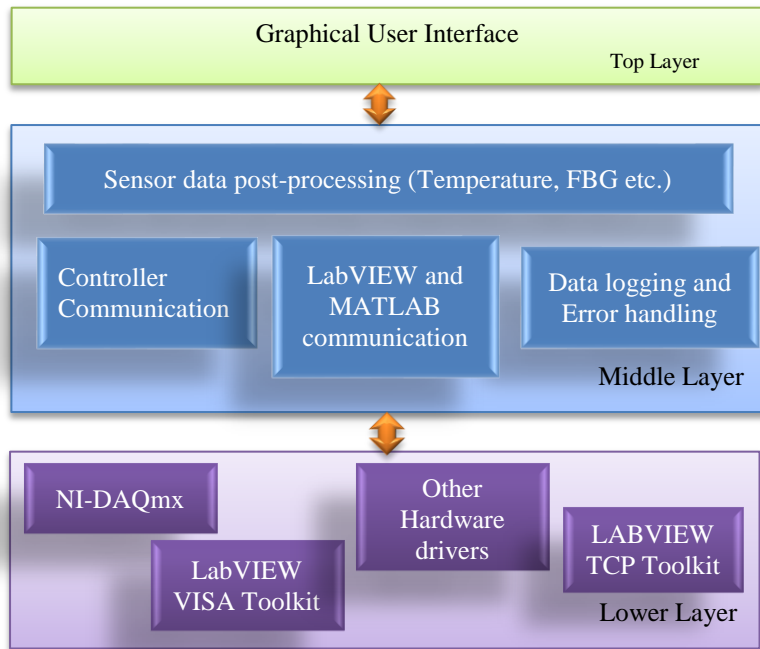


Fig. 2. Three tier structure of the program

3.3. Data acquisition process.

A typical data acquisition process is as illustrated in Fig. 3. The system is first initialised to establish a communication between computer and different sensors. In the second step, depending on the type of the sensor, the program either reads the raw data or sends configuration command. For example, in case of laser position sensor, it reads the raw data; for temperature sensor, a convert command is sent for temperature conversion and for FBG sensors, channels are configured. Subsequent steps in the flowchart are based on the parameters set by the user. Data acquisition process is started from capturing the data form the sensors. Sampling rate of each type of sensor can be controlled individually. Raw data is processed to obtain engineering values before displaying it and saving it to a file if required. After data is read from all the configured sensors, program completes the acquisition operation.

4. IMPLEMENTATION OF MAIN MODULES

4.1. Sensor data acquisition Module

Different modules are created for different sensors to maintain the modularity of the structure. Software Development kit (SDK) for programming these sensors is provided by their manufacturers. These SDK's contain sample LabVIEW sub-VIs (Virtual Instrument) and driver files necessary to perform fundamental operations.

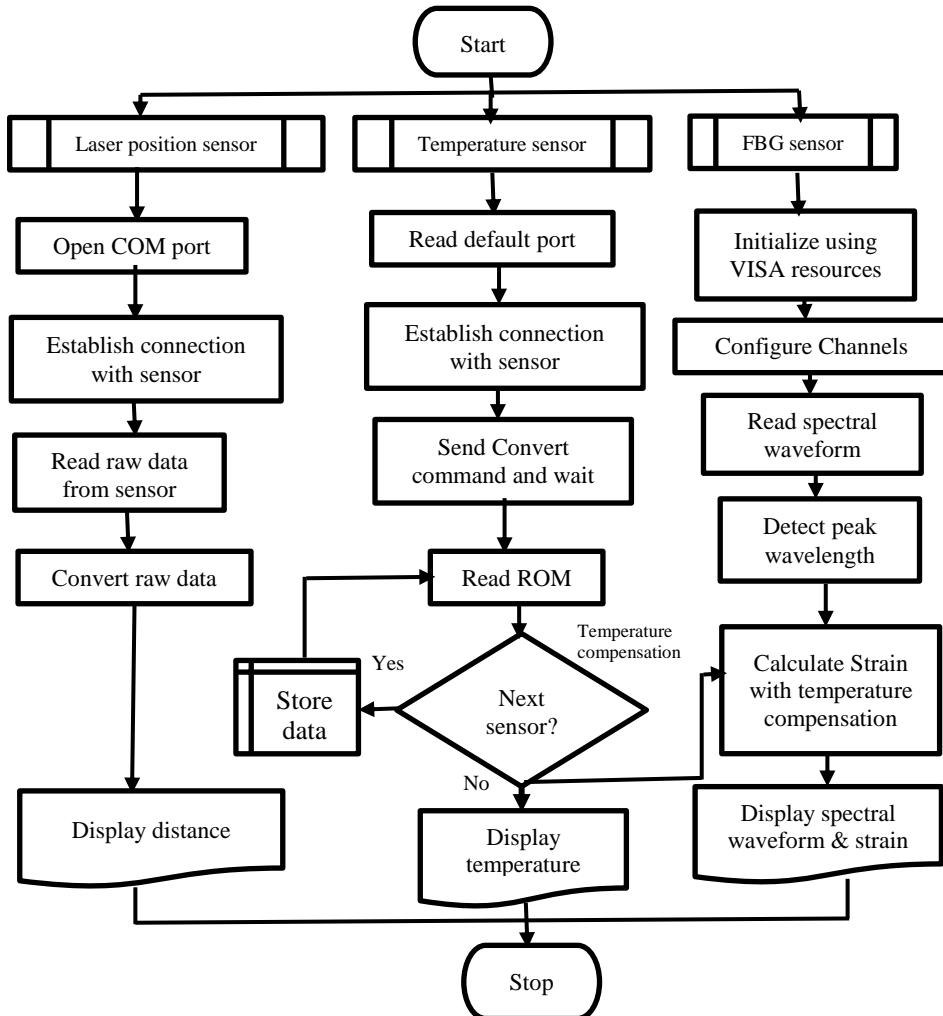


Fig. 3. Flowchart for data acquisition system

4.2. LabVIEW and MATLAB interface module

This LabVIEW DAQ program is designed to implement various machine tool error compensation algorithms based on ANFIS, ANN and physical models. Modelling, training and analysis of these compensation techniques was carried out in MATLAB. Due to this many complex inherent functions of the MATLAB were utilized during the design phase. It was observed that direct conversion of MATLAB code into the LabVIEW was time consuming and prone to error during translation which potentially could generate different output for the same input. Thus an interface between LabVIEW and MATLAB was used to simplify the adoption of off-line optimised model with reduced uncertainties that would be involved in the code conversion.

This interface was achieved using LabVIEW's MATLAB Script module. It uses Microsoft ActiveX technology for communication. Thus .m file generated by MATLAB can be directly imported into the LabVIEW eliminating the need for code conversion. Some of the

off-line models such as ANFIS generate files in “.fis” format. Such a files can be called in the LabVIEW code without any recompilation.

Data captured from various sensors by LabVIEW is passed in the MATLAB Script code containing compensation model, which in turn generates the corresponding output. This output is returned backed to LabVIEW which is passed to the machine controller.

4.3. Controller communication module

The purpose of this module is to establish a bi-directional communication between the machine tool controller and the CC. This communication link is established in two steps. In the first step calculated compensation value is transferred from the DC to CC using Ethernet. Standard TCP (Transmission Control Protocol) toolkit is used for this purpose. In the second step the DDE link using Ethernet is used to communicate with the controller. These compensation values are then used to modify the parameters in the controller which are subsequently used by the CNC code to modify the values of Machine Co-ordinate System (MCS) during the machining process. MCS values can be transferred from the controller back to the LabVIEW program for analysis.

4.4. Data logging module

Data captured from all the sensors as well as MCS values with absolute time can be logged using this module. This is achieved with the help of LabVIEW file I/O functions. Data is saved in “.CSV” (comma separated values) format. This format was chosen because it can be easily imported in other applications for further analysis purpose. Data logging time is programmable.

5. DEMONSTRATION OF THE SOFTWARE

5.1. Program overview

In this section a brief introduction to the developed LabVIEW program is provided. Screenshot of the front panel of the software is illustrated in Fig. 5. For each individual module such as for different sensors, compensation, communication and data logging separate tab is created. This way modularity of the structure is maintained in the front panel as well.

The front user interface contains 7 key segments: FBG spectrum, strain, temperature, laser sensor, compensation, communication and data log. Various configuration settings and sampling time for each type of sensor is programmable. Data for each sensor can be plotted live. Different compensation models can be configured as per the required parameters and their output can be plotted and observed in continuous manner.

5.2. Example of the software application

In this section three brief examples of the software application are mentioned. In the first two examples tests were performed on a 5-axis Geiss machine tool. Third example discusses about the performance evaluation test of the laser tracker (LT).

Test 1 was performed for the period of 14 days and machine was not in operation during this period. The purpose of this test was to monitor the thermal response of the crossbeam structure of the machine tool with change in environmental temperature. FBG sensors were mounted on the crossbeam structure (refer fig 1) with digital temperature sensor to observe the

thermal response. Data for all the sensors was logged every minute. All the measured data was used for the post analysis purpose. Test result is shown in fig. 4.

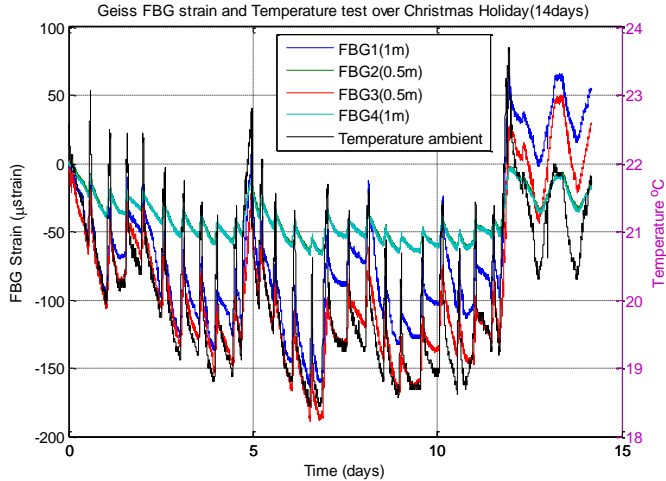


Fig. 4 Test results for environmental thermal response of crossbeam

The primary motive of the 2nd test was to observe the deformation taking place in the ram of the machine along the Z-axis direction due to the heating of the C-axis motor during prolonged operation and to compensate it during the running process itself.

FBG sensors were mounted on each side of the ram structure (refer fig 1). Output of the FBG sensors was used by the ANFIS compensation model. Calculated compensation values were used to modify the CNC code to maintain the position of the ram. Laser position sensors were used for the validation purpose. Data for all the sensors was logged at every 1 second. On-line screenshot of the output of the compensation model and laser sensor is shown in fig 5 and test results are shown in fig 6. Residual error in the range of 10 μm was observed during the test.

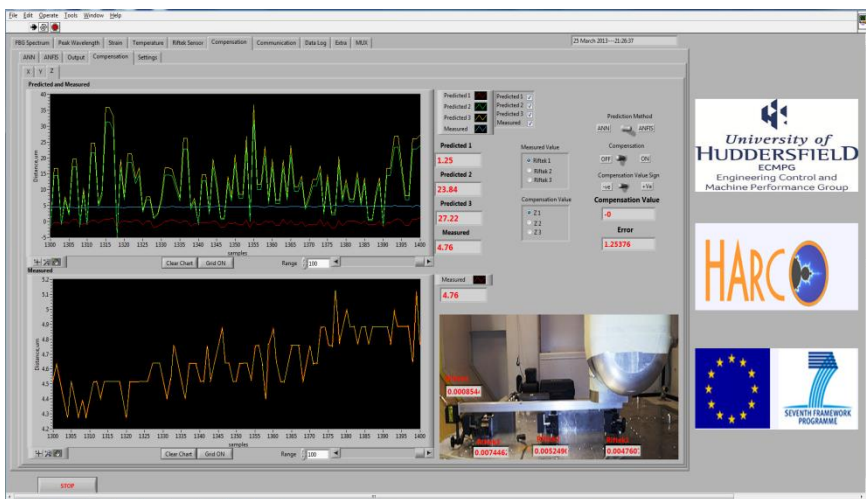


Fig. 5 Compensation model output during the operation

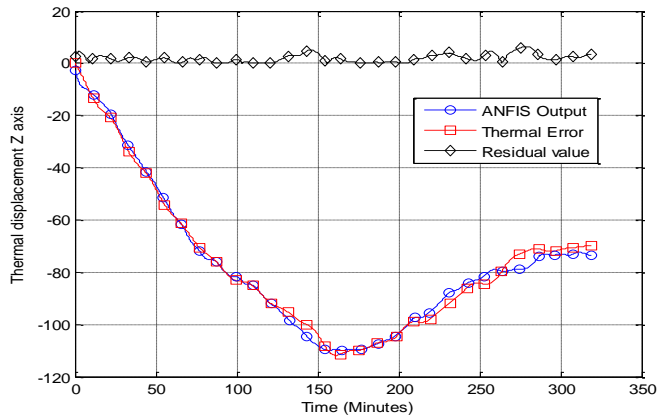


Fig. 6. Test Results for thermal displacement of Z-axis

In the third example only temperature measurement module of the software was used for performance evolution of the laser tracker. This test was carried out for the period of 14 hours and data was logged at every 25 sec. Data acquisition for temperature and LT was carried out using different software applications. Fig 7 illustrates test results showing effect of temperature variation on reparability of LT.

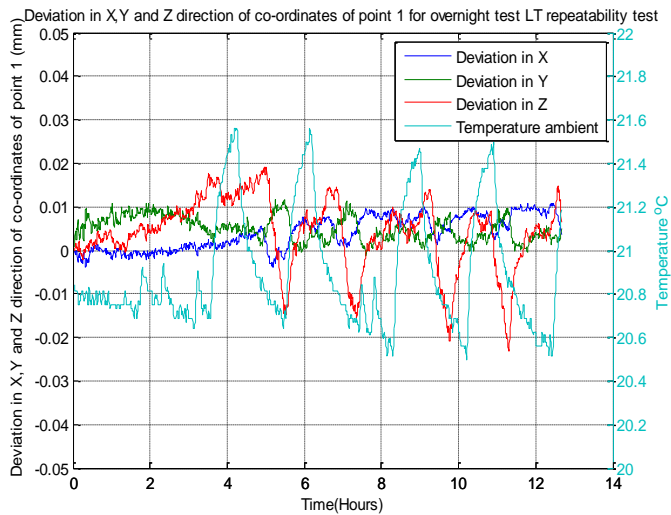


Fig. 7. Test results for thermal response of laser tracker

In addition this software was used for several other similar tests for structural monitoring of the Geiss machine tool. As this program can be used for data acquisition from various types of sensors, it has wide range of applications.

6. CONCLUSION

Using the LabVIEW environment a machine tool structural monitoring application was developed, offering researchers the prospect of using computer based data processing to

expedite the development path. This program was created in the modular structure to provide user friendly software and to allow desired flexibility and extensibility. Various modules prepared in this program can be easily used for other applications with minimal or no alterations. Software testing is in validation and verification phase.

This paper also describes an example of application of such a system for data monitoring, logging, control model calculation and communication for compensation values for a 5-axis CNC machine tool. The system is now being used to facilitate data fusion and assist with improving performance of the machining. The extensibility of the design is of paramount importance to efficient development.

ACKNOWLEDGEMENTS

The authors gratefully acknowledge the UK's Engineering and Physical Sciences Research Council (EPSRC) funding of the EPSRC Centre for Innovative Manufacturing in Advanced Metrology (Grant Ref: EP/I033424/1).

The work carried out in this paper is partially funded by the EU Project (NMP2-SL-2010-260051) "HARCO" (Hierarchical and Adaptive smaRt COmponents for precision production systems application). The authors do wish to thank all the partners of the consortium.

REFERENCES

- [1] Ramesh, R., M.A. Mannan, and A.N. Poo, *Error compensation in machine tools — a review: Part I: geometric, cutting-force induced and fixture-dependent errors*. International Journal of Machine Tools and Manufacture, 2000. **40**(9): p. 1235-1256.
- [2] Ramesh, R., M.A. Mannan, and A.N. Poo, *Error compensation in machine tools — a review: Part II: thermal errors*. International Journal of Machine Tools and Manufacture, 2000. **40**(9): p. 1257-1284.
- [3] Möhring, H.C., K.M. Litwinski, and O. Gümmer, *Process monitoring with sensory machine tool components*. CIRP Annals - Manufacturing Technology, 2010. **59**(1): p. 383-386.
- [4] Denkena, B., H.-C. Möhring, and K. Litwinski, *Design of dynamic multi sensor systems*. Production Engineering, 2008. **2**(3): p. 327-331.
- [5] Luo, R.C., Y. Chih-Chen, and S. Kuo Lan, *Multisensor fusion and integration: approaches, applications, and future research directions*. IEEE Sensors Journal, 2002. **2**(2): p. 107-119.
- [6] Banerjee, T.P. and S. Das, *Multi-sensor data fusion using support vector machine for motor fault detection*. Information Sciences, 2012: p. 96-107.
- [7] Fekih, A., H. Xu, and F.N. Chowdhury, *Neural networks based system identification techniques for model based fault detection of nonlinear systems*. International Journal of Innovative Computing, Information and Control, 2007. **3**(5): p. 1073-1085.
- [8] Ghosh, N., et al., *Estimation of tool wear during CNC milling using neural network-based sensor fusion*. Mechanical Systems and Signal Processing, 2007. **21**(1): p. 466-479.
- [9] Mahajan, A., K. Wang, and P.K. Ray, *Multisensor integration and fusion model that uses a fuzzy inference system*. Mechatronics, IEEE/ASME Transactions on, 2001. **6**(2): p. 188-196.
- [10] Aliustaoglu, C., H.M. Ertunc, and H. Ocak, *Tool wear condition monitoring using a sensor fusion model based on fuzzy inference system*. Mechanical Systems and Signal Processing, 2009. **23**(2): p. 539-546.
- [11] Panopoulou, A., et al., *Dynamic fiber Bragg gratings based health monitoring system of composite aerospace structures*. Acta Astronautica, 2011. **69**(7-8): p. 445-457.
- [12] Flandorfer, H., F. Gehringer, and E. Hayer, *Individual solutions for control and data acquisition with the PC*. Thermochimica Acta, 2002. **382**(1-2): p. 77-87.
- [13] Anjos, J.M.S., G.K. Coracini, and E. Villani, *A proposal and verification of a software architecture based on LabVIEW for a multifunctional robotic end-effector*. Advances in Engineering Software, 2013. **55**: p. 32-44.
- [14] Whitley, K.N., L.R. Novick, and D. Fisher, *Evidence in favor of visual representation for the dataflow paradigm: An experiment testing LabVIEW's comprehensibility*. International Journal of Human-Computer Studies, 2006. **64**(4): p. 281-303.
- [15] Wang, L., et al., *The Application of LabVIEW in Data Acquisition System of Solar Absorption Refrigerator*. Energy Procedia, 2012. **16**: p. 1496-1502.

Towards Knowledge Framework for Life-Cycle-Long Gathering of Maintenance Information for Decision Support in Machine Tool Design

P. Ferreira, M. Sayed, S. Osei, N. Lohse

The University of Nottingham, Manufacturing Division
p.ferreira@nottingham.ac.uk

ABSTRACT

The design process of machine tools is a costly and complex one. During the design phase often decisions are made based on the estimated reliability and expected performance characteristics of the various components that go into the design. Therefore, it is very essential to estimate these performance characteristics as accurately as possible. Traditionally these estimates used to be calculated from theoretical and physical models. However, these theoretical models have often been found to be inaccurate and dependent on various difficult-to-predict operational conditions. Conversely, maintenance information is becoming increasingly available in the form of maintenance records. These maintenance records hold valuable information about the real performance characteristics of the various machine tool designs and components. Such information represents a valuable source of knowledge for supporting design decisions if properly captured, abstracted and fed-back to the machine tool designers.

In this paper we propose the establishment of a knowledge framework for life-cycle-long gathering of maintenance-related knowledge in the machine-tools industry.

KEYWORDS: Machine tools, Maintenance, Knowledge-gathering, Decision Support

1. INTRODUCTION

The design of machine tools is a process that is heavily dependent on the expertise and experience of the designer. This is mainly due to the complexity of the process and the high level of machines variants. The decisions of the designer are based on estimated reliability and expected performance characteristics of the various components of the machine. However, machine designers rely mainly on their past experience, since the existing support tools are quite complex and not integrated with a design environment [1]. In fact the existing solutions are based in theoretical models which have often been found to be inaccurate and highly dependent on various difficult-to-predict operational conditions.

The advances in information technology have provided the means to facilitate the capture of maintenance information in a more accessible manor. However, this advances just provide access since there is no standard format for maintenance reporting. In fact, one of the main challenges of using the available data is the lack of mechanisms to merge information. Nevertheless, the availability of such information could prove critical for the improvement of machine tool design process.

In this paper we propose the establishment of a knowledge framework for life-cycle-long gathering of maintenance-related knowledge in the machine-tools industry. The framework would aim to systematically formalize the maintenance data capturing process during various maintenance activities. This should be done in a way that facilitates knowledge reuse for design decision support through different abstraction levels. The main aim is to enable the transformation of data captured in maintenance records from various machines and clients into meaningful knowledge in the form of key maintenance-related indicators, both for components and machine designs.

2. LITERATURE REVIEW

In order to timely respond to the dynamic nature of the market trends, availability, reliability and continues production have become key indicators to run reliable and efficient machines. According to [2] the need to attain near-Zero downtime while maintaining reliability and efficiency in machine tools design is fast becoming an unavoidable necessity [3]. Designing machines tools to meet such expectations will require the use of every available effective and efficient knowledge framework to support such design decisions. Machine maintenance, both proactive and reactive over the years have been the means to keep machines running in order to attain the expected level of quality, availability and productivity. Preventive maintenance: is planned maintenance activity aimed at the avoidance of machine breakdowns or component failure. The main aim is to eliminate machine breakdowns if possible thereby reducing downtime and also to enhance machine reliability [4]. On the other hand proactive maintenance: is in response to component failure or machine breakdown. This usually results in long machine downtime especially when the failure mode requires component replacement which also depends on availability [2].

These activities often result in significant loss of productivity either because a machine will have to be shut down during production or a machine will be forced to operate at an unacceptable level [2]. In such a high competitive market like the manufacturing industry, the design of reliable, efficient and easily maintained machine tool is paramount. To maintain productivity, machines are regularly maintained either as a reactive or proactive measure to keep them running [5]. Consequently in the area of diagnosis and machine maintenance management, many papers and reports have been published. However as machine maintenance management and diagnosis is not the objective of this paper, we have summarised work in this domain in order to appreciate how machine maintenance information can be captured, processed, stored and reused for design decisions. Maintenance are carried out in different forms, reactive maintenance which is in respond to a component failure, this has proven to be very effective, however this increases production cost, machine down time and diagnostic time cause by the frequent breakdown. Alternatively scheduled maintenance is intended to improve upon the rate of breakdown thereby reducing the downtime [6]. This approach also leads to unnecessary maintenance activity which negatively affects production time [2]. In fact, machines are either over maintained or under maintained which leads to waste of limited maintenance resources or increased maintenance cost due to regular break downs of under maintained machines [7]. This highlights the need to more accurately predict

machines breaking downs and use this information to prevent it from happening [8]. In line with this need [2] proposed a shift from the reactive maintenance approach to a proactive maintenance approach, which can assess and monitor machine performance and predict component failure even before they occur. This new paradigm targeted a collaborative product Life-Cycle Management (CPLM) which would enable products (Machines) to be assessed, monitored and improved through the life cycle. The assessment of machine performance degradation was achieved by various modules, from sensory data capturing, storage, processing (extraction of features relevant to the description of product performance) and performance assessment based on time-series analysis [2]. [9] state that this type of information will be critical for improving the product design decision making process.

Nevertheless the solution is limited in terms of the generation of knowledge to make recommendations to the design of equipment, herein referred to as design for service. [7] also reported a maintenance management system developed along these same principles. The aim of the system is to help an advance manufacturing company to reduce the maintenance cost to the lowest level and also improve overall system effectiveness. With the help of some mathematical methods [10] like weibull distribution, using captured data like mean time to failure (MTTF), a preventive maintenance scheduler which incorporated mean time between failures was developed. This included an online feedback method to the maintenance management system which allow the assistance of the decision making process of rescheduling maintenance activities. Even though the company undoubtedly reduced equipment failure rate, the principles and methodology developed did not cater for the capture of information important for the purposes of machine design.

The concept of life-cycle long knowledge gathering was also explored in the area of robotics. This reports an expert decision support system (ROBODOC) to help maintenance staff diagnose and maintain robots. The solution is based on the sensory data captured and previous maintenance data which are used to infer knowledge [9]. The result of this work as proposed could contribute to the design and development of expert systems, by proposing design recommendations based on the past experience, however this is quite specific to the robotics domain. The sector of manufacturing facility management also provides insight into the life-cycle knowledge gathering in this case for the effective management of manufacturing facilities [11], [12] proposed a maintenance data management framework which allows the collection and processing of maintenance data, making it reusable for operation, planning and facility design purposes. The framework is comprised of two modules: the data management system which allows the generation of feedback and collection of malfunction cases at any phase of the facility; and the feedback data generation system, which allows the abstraction and inference of these malfunctioning cases for both maintenance and facility design. Prior to this [11] had applied a similar framework to predict and manage deterioration in order to control manufacturing facility degradation. This framework only allowed the reuse of the maintenance data which further assisted in the designing of reliable and maintainable facilities.

More recently the need for the life-cycle knowledge gathering for machine tool design was identified [1]. It stated that despite the extensive research on the topic from other domains, there is no solution for the integration of life-cycle knowledge gathering of maintenance information to facilitate reuse for machine tool design. The aim of this paper is to provide an operational framework which will systematically formalize the maintenance data capturing from multiple sources during various maintenance activities, allow the aggregation of the captured data in more structured manner and then also allow the generation of meaningful knowledge in the form of key maintenance-related indicators both for components and machine designs.

3. PROBLEM DEFINITION

The machine tool design process is quite complex, requiring extensive knowledge not only of existing machine tool designs but also the individual components within the machine. Information on machine components is normally generic and provided by the suppliers. However, this information is a rough estimate of the component behaviour. In fact components tend to behave differently when placed into different machine tool designs. This means that the information on how components behave in certain machine tool conditions is lost. In order to improve the design of machine tools it is critical to feedback this information in order to support the decision making process for the selection of components.

The need for the selection of components is not the only thing one needs to consider in the machine tool design process. The machine structure and configuration is another critical aspect. This process normally follows existing templates, but depending on the requirements can produce completely new machine tool designs. However, even if new designs prove to have better reliability, there is currently no means to feedback this information. Critically, designers tend to go back to their traditional machine tool designs disregarding for lack of knowledge the potential gains of new designs.

The main problem with all this process is the lack of information at the design stage of the machine tool life cycle. However, information does exist for other aspects across the machine life-cycle. So the question is can this information be used at a design stage, and more critically can this information be structure into knowledge in order not to overwhelm the designer with unnecessary context-specific information. The idea here is not to make information available, but rather to provide the right information at the right time for supporting the designer's decisions.

The first step for making this possible is to identify the sources of information that are provided across the machine life-cycle. The main source of information that can be identified across all machine tools is maintenance information. In some specific cases there are machines that include embedded intelligence that enables the provision of other operational data. However, this data would always be included in maintenance reporting. Therefore, it would be redundant to create mechanisms to extract this information automatically. This means that the information can always be obtained from maintenance activities which are common practice for machine tools. The question that is raised is how to unify the process of gathering information from various maintenance activities.

Currently maintenance activities can be classified into either preventive or reactive maintenance. It is important to distinguish between these activities in order to establish which type of information can be acquired from each activity. Also it is important to create a knowledge capturing mechanism that does not overwhelm the maintenance engineers, but rather encourages them to provide the necessary information by supporting in their activities when possible (for example troubleshooting support and maintenance recommendation). The idea is that maintenance engineers will be more willing to use new solutions if they see a direct gain on their main activities. Therefore, the aim will be to provide a framework that supports the maintenance engineers in their typical activities while encouraging them to capture maintenance reports. These reports will contain structured information that is relevant for the machine tool design, and can be used to generate knowledge that will help the machine tool designer.

4. KNOWLEDGE FRAMEWORK FOR LIFE-CYCLE-LONG GATHERING OF MAINTENANCE INFORMATION FOR DECISION SUPPORT IN MACHINE TOOL DESIGN

In order to establish a knowledge framework for the life-cycle-long gathering of maintenance information for decision support in machine tool design, one needs to analyse the machine tool life-cycle. Machine tools are typically designed to meet very specific requirements. The design process has to provide not only the machine structure but also the components that will be used to build the machine, since this choice has an impact on the design itself. Information at this stage of the machine life-cycle is quite dependent on the designer's knowledge and the component information provided by suppliers. There are some decision support tools which provide estimates calculated from theoretical and physical models. However, these have often been found to be inaccurate and dependent on various difficult-to-predict operational conditions. Currently there is no direct or indirect mechanism for designers to access the information on the performance of past machine designs. Moreover, currently there is also no mechanism for designers to propagate their knowledge to other stages of the machine tool lifecycle.

Knowledge in the machine tool domain is not propagated across the machine life-cycle. To do so, one requires the creation of a semantic model that is common across all stages of the machine tool life-cycle [1]. A model is currently being developed within the TRANSPARENCY project which provides the basis for the description of machine tools and machine tools designs[1]. The model provides the means to formalize machine tool design procedure and annotate information accordingly. This means information can be aggregated across each machine life-cycle, but most importantly this means that one can use this to generate knowledge about the performance of machine designs. The concept is simple if information is properly structured and annotated one can generate knowledge by cross checking between the different machine/component performances.

The machine tool performance information needs to be defined and properly structured within the semantic model for the purposes of the design process. Performance is traditionally restricted to the machine operation, however, from a machine design perspective there is information related with the servicing of the machine which is critical. The component accessibility sometimes might take the majority of the service effort, particularly for unexpected failures. Designers due to the high reliability of certain components sometimes consider that access is not that important. While in some cases this might be true, in others it will not be, thus it is important to be able to capture frequency of failures along with actual component access time information, and relay it back to the designer. It is important to note that information in its raw form would not help the designer, what is intended is to provide useful knowledge for each stage of the design.

Fig.1 provides an overview of the proposed knowledge framework which was designed for a major European machine tool builder. It clearly establishes the semantic model as the backbone of the whole machine tool life-cycle, while only providing information about the machine tool design and machine tool maintenance. It also provides the important distinction between data and knowledge. Data can be collected while knowledge needs to be inferred from data. It is proposed that a dedicated mobile software application should be designed and used to enable user-friendly maintenance data capturing.

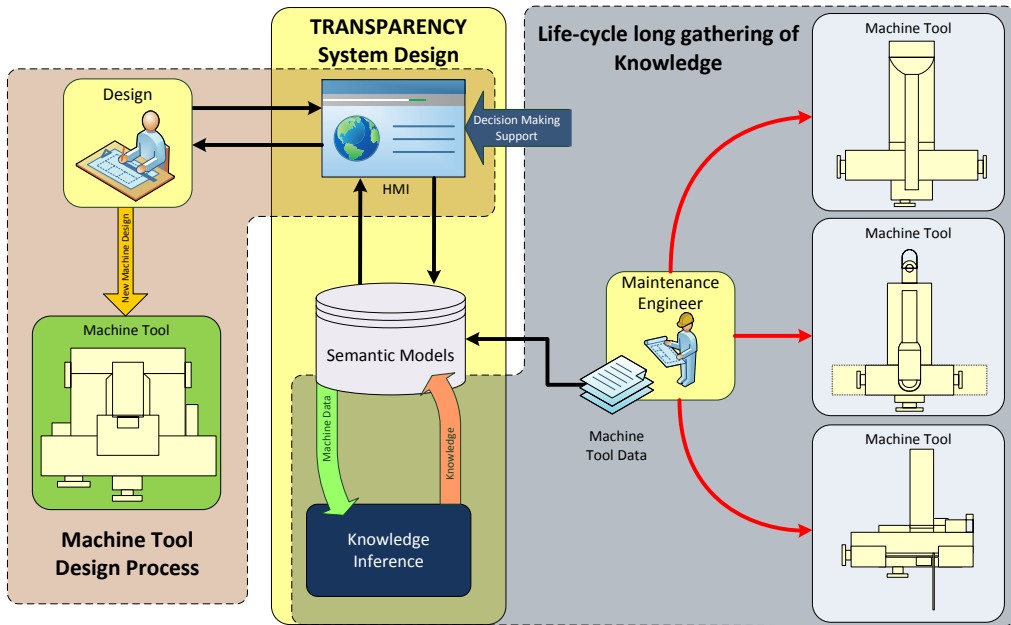


Fig.1. Life-cycle long gathering of knowledge Framework Overview.

The success of this framework is highly reliant on the ability to generate knowledge from the captured data. Thus it is critical to define the process of attaining knowledge. Knowledge can be inferred based on information or directly provided by designers. During the design of a machine the designer can introduce specific knowledge related to a machine, such as relating certain breakdowns to specific components of the machine. This mechanism enables the knowledge sharing between different designers, but also provides critical information for the maintenance engineers which can result in time saving. Moreover, this is viewed as it is a part of the plan to get the maintenance engineers buy-in to the new maintenance approach. The buy-in plan will rely on the engineer's access to information that will facilitate their work, in conjunction with easy to use software interface that generates automatically maintenance reports, thus reducing effort.

The collected information needs to be processed before knowledge can be inferred from the maintenance reports over time. It is important to state knowledge can either be created or updated. The idea is that sometimes there is some base knowledge provided by the machine designer, which over time will be perfected based on the information coming from the system. If no knowledge exists it should be created. Either way knowledge needs to be annotated in some form in order to be used. Fig.2 provides an overview of the necessary steps to establish knowledge, and semantically annotate it so it can be useful in future machine designs.

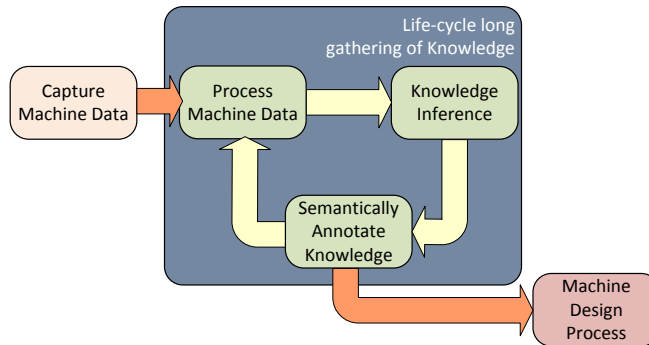


Fig.2. Cycle for life-cycle long gathering of knowledge.

It is important to distinguish between the two distinct types of maintenance activities in order to enable the knowledge generation. The source of the information is sometimes as important as the information itself. In this particular case there are two sources of information from preventive maintenance and reactive maintenance. Preventive maintenance is carried out according to predefined plans that specify how frequent the activity needs to take place according to the machine/component supplier's specifications. Reactive maintenance activities are typically carried in response to a specific disturbing event such as break down or a component failure. The two maintenance types differ only by the fact that reactive maintenance activities will typically be preceded by a diagnosis phase. In this phase the root cause of the failure needs to be identified in order to decide what maintenance or corrective action(s) need to be completed in response. This information is of great interest for component suppliers and machine designers to understand how difficult is the diagnostic task associated with certain failures to assist with design alternatives during the design phase. Preventive maintenance one mainly focuses on the corrective actions performed and analysing their usefulness.

Gathering information from the traditional maintenance reports would be a time consuming process. The main issue is that reports are designed for human readers, thus the information is quite unstructured and cannot be easily extracted. For this reason the development of a mechanism that can help in capturing this information in a meaningful and structured manner is proposed.

Maintenance reports are based on activities performed in the client site. Therefore, the developed mechanism to acquire data targets a mobile device with the aim of making it more user-friendly. The "main" screen is intended to be the starting point where the activities can be started. Once in that screen one can either create new maintenance reports, breakdown or scheduled, check past reports or select tasks to perform maintenance. The data for this is set by the requirements and each field has a direct relation with the semantic model. The tool is designed to facilitate where possible the process of logging a breakdown. To the end, all information that exists in the environment is preloaded. Similarly, the logging of a scheduled maintenance task will be treated as a new maintenance task. Again, this is driven by the semantic model and all data that is required should be preloaded. These two functionalities are considered for the back office, meaning they are not required for creating maintenance tasks. These tasks can be generated in the design environment and loaded for maintenance execution.

The main functionality of this mechanism is the ability to choose from a list of maintenance activities, both scheduled and breakdown. The selection requires the choice of a

client, which leads to a list of machines for that client. Then a selection of a machine can be performed, which will lead to the list of tasks for the given machine. The task selection can lead to two different screens depending on the type of maintenance activity, breakdown or scheduled. The main difference between these two types is that the breakdown maintenance activity will have a diagnostics screen before going into to the actual maintenance activity. In both cases the maintenance engineer will be able to store information about the tasks performed, including time-related information which will be in the form of various durations that different parts of the maintenance activity have taken to complete. The only difference is that during diagnosis information on those activities is also captured. Fig.3 provides an overview of the maintenance information gathering mechanism.

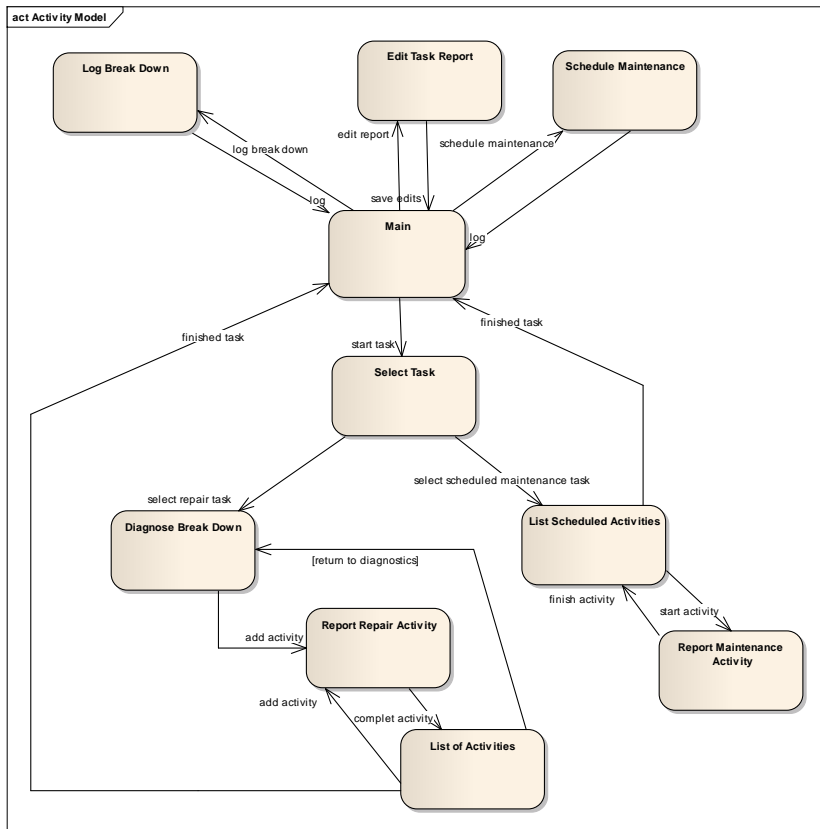


Fig.3. Maintenance information gathering mechanism overview.

5. ILLUSTRATIVE EXAMPLE

The concept of the knowledge feedback framework can be better demonstrated with the aid of an illustrative example. Considering a machine tool while in operation, it requires some preventive maintenance activities that are planned according to specifications from the machine tool designer. One example of that could be bearings “x” that need to be cleaned and inspected for remanufacture after 600 hours of operation. Other maintenance activities would

also occur due to some reactive unscheduled activities in repose to unplanned failures. Unscheduled maintenance activities could include things such as the failure of component “y”.

In this scenario it would be important that the performed maintenance activities use the proposed maintenance information gathering mechanism in order to obtain structured and transparent information on all the activities (Fig.4 provides a screenshot of maintenance information gathering tool). The information would be stored and aggregated with other information from other machines that follow the same design. The gathered information can then be processed to formulate knowledge. For example for the scheduled maintenance activity would provide the time taken to access the component “x”. While on the unscheduled it would provide how long component “y” in operation before it got replaced.

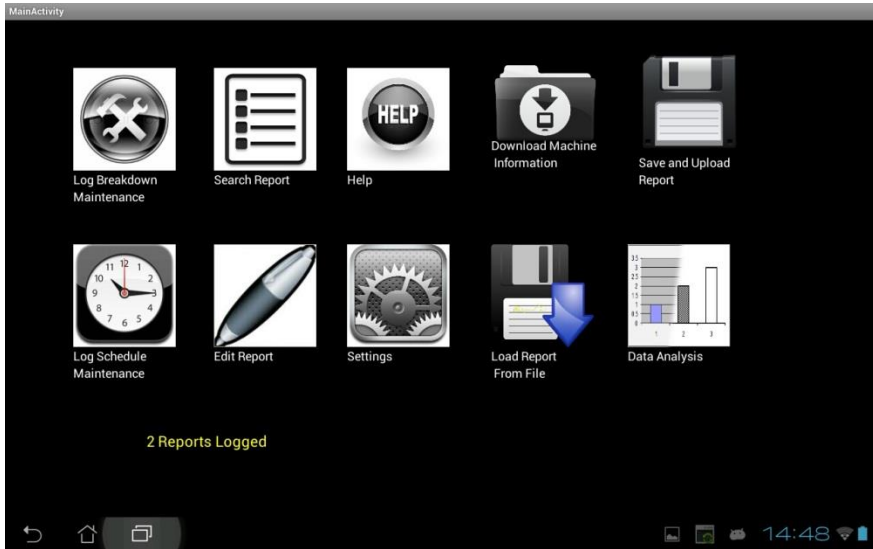


Fig.4. Screenshot of maintenance information gathering tool.

It is clear that one occurrence would not be enough to generate knowledge. Thus, the scenario needs to be extended to consider more machines that follow the same design. With this extra information can establish the mean time to access a component ($MTTR_{Access}$) by making the following calculation:

$$\text{Component } MTTR_{Access} = \frac{\sum \text{relevant timeToAccess}}{\text{count of all relevant Maintenance Activity Reports}} \quad (1)$$

This knowledge can provided to the machine tool designer and if it makes up a greater than expected proportion of the overall time to carry out the activity, then he might opt for an alternative design choice to reduce the component’s time to access $MTTR_{Access}$.

Similarly, for the replacement of component “y” one can establish the mean time between failures (MTBF), which can be obtain by the following calculation:

$$\text{Component MTBF} = \frac{\text{Overall uptime while the component is embedded}}{\text{count of relevant BreakDownMaintenanceTaskReport}} \quad (2)$$

Again, this knowledge could be provide for the machine tool designer making it possible to compare the frequency of failure between the two alternative components and hence allowing the designer make an informed design choice.

6. CONCLUSION

This paper is the first step towards establishing a knowledge framework for life-cycle-long gathering of maintenance information for decision support in machine tool design. An outline of the overall knowledge framework is provided as well as the base structure for its operation. The maintenance activities are analysed and a new maintenance information gathering mechanism is proposed. The paper also presents a preliminary software tool for the capture of information that will be used in future work to establish a formal semantic model for the framework.

Further work will focus on gathering maintenance information and establishing a full model for the knowledge framework for life-cycle-long gathering of maintenance information for decision support in machine tool design.

ACKNOWLEDGEMENTS

The reported work is partially funded by the European Commission as part of the NMP-2009-3.4-2 246273 TRANSPARENCY project. The support is gratefully acknowledged.

REFERENCES

- [1] TRANSPARENCY. (2013). Adaptive Business Collaboration by progressive knowledge sharing and engineering. Available: <http://www.transparency-project.eu/>
- [2] J. L. J.Ni and D. Djurdjanovic, "Watchdog-information technology for proactive product maintenance and its implications to ecological product re-use," in Symposium on Ecological Manufacturing, Berlin, Germany, 2003, pp. 101-110.
- [3] R.-L. Hsiao, S. D.-H. Tsai, and C.-F. Lee, "The Problems of Embeddedness: Knowledge Transfer, Coordination and Reuse in Information Systems," *Organization Studies*, vol. 27, pp. 1289-1317, September 1, 2006 2006.
- [4] A. W. Labib, "World-class maintenance using a computerised maintenance management system," *Research paper*, vol. 4 Iss: 1., pp. 66 - 75, 1998.
- [5] W. Wang, P. W. Tse, J. Lee, and "Remote machine maintenance system through Internet and mobile communication," *The International Journal of Advanced Manufacturing Technology*, vol. 31, pp. 783-789, January 2007 2007.
- [6] R. C. M. Yam, P. W. Tse, L. Li, and P. Tu, "Intelligent Predictive Decision Support System for Condition-Based Maintenance," *The International Journal of Advanced Manufacturing Technology*, vol. 17, pp. 383-391, 2001/02/01 2001.
- [7] P. Y. L. Tu, R. Yam, P. Tse, and A. O. Sun, "An Integrated Maintenance Management System for an Advanced Manufacturing Company," *The International Journal of Advanced Manufacturing Technology*, vol. 17, pp. 692-703, 2001/05/01 2001.
- [8] Z. Yang, D. Djurdjanovic, and J. Ni, "Maintenance scheduling in manufacturing systems based on predicted machine degradation," *Journal of Intelligent Manufacturing*, vol. 19, pp. 87-98, 2008/02/01 2008.
- [9] S. A. Patel and A. K. Kamrani, "Intelligent decision support system for diagnosis and maintenance of automated systems," *Computers & Industrial Engineering*, vol. 30, pp. 297-319, 4// 1996.
- [10] S. Kara, M. Mazhar, H. Kaebernick, and A. Ahmed, "Determining the Reuse Potential of Components Based on Life Cycle Data," *CIRP Annals - Manufacturing Technology*, vol. 54, pp. 1-4, // 2005.
- [11] S. Takata, H. Hiraoka, H. Asama, N. Yamaoka, and D. Saito, "Facility Model for Life-Cycle Maintenance System," *CIRP Annals - Manufacturing Technology*, vol. 44, pp. 117-121, // 1995.
- [12] S. Takata, Y. Inoue, T. Kohda, H. Hiraoka, and H. Asama, "Maintenance Data Management System," *CIRP Annals - Manufacturing Technology*, vol. 48, pp. 389-392, // 1999.

Improved automatic experimental modal analysis of machine tool spindles

Piotr Andrzej Bąk, Krzysztof Jemielniak

Warsaw University of Technology, Poland
piotr.andrzej.bak@zaoios.pw.edu.pl

ABSTRACT

Dynamic compliance of machine tool spindle is crucial to machine resistance to self-excited vibrations (chatter). Systematic determination this compliance allows for detection of its degradation and for planning of preventive service. The dynamic compliance can be calculated from a frequency response function (FRF) of the machine tool spindle, which is usually measured using the modal analysis. Conventional modal analysis requires both knowledge and skill for evaluation of registered signals and selection of the proper hits and selection of the frequency ranges corresponding to the single modes. In developed software all these operations and analysis were automatized, thus they can be done directly on the factory floor without the engagement of highly qualified personnel. Moreover, the correlation between the measured and modelled FRF has been improved by automatic optimization of modal damping. An alternative solution proposed in the paper is the use of the polynomial fitting.

KEYWORDS: experimental modal analysis, dynamic compliance

1. INTRODUCTION

Dynamic compliance of machine tool spindle is an important indicator of machine resistance to self-excited vibration. Systematic determination this compliance allows for detection of machine tool degradation and for planning of preventive service. Therefore it should be done directly on the factory floor without the engagement of highly qualified personnel.

Modal analysis allows computing of modal parameters (frequency, damping, stiffness and mass) of vibrating system. The advantage of the impulse technique is the fact that the energy of the hit is distributed continuously in the frequency domain. A force impulse excites all resonances within its useful frequency range inversely proportional to the duration of the impulse [14]. Replaceable modal hammer tips of different hardness allow for a different excitement range [8]. The dynamic compliance can be calculated from a frequency response function (FRF) of the machine tool spindle. The most often used method of FRF determination is the single input-single output (SISO) modal analysis where vibrations of a tool or specially prepared shank placed in the spindle are induced by the hit of a modal hammer exerted on the

other side of the tool e.g. [6]. Modal parameters for MDS model – mass, damping and stiffness – can be calculated from FRF for each modal mode separately using characteristic features of the real and imaginary part of FRF e.g. [8]. Manual determination of modal parameters is time-consuming and requires experience and knowledge for evaluation of registered signals and selection the proper hits and selection of the frequency ranges corresponding to the single modes. It is difficult even using professional, commercial software (like CutPro), because operator has to have the ability to manually extract single hit and evaluate its correctness, then perform mode selection on Re and Im of FRF [7].

Algorithms for SISO modal analysis which allowed for automation of those manual procedures, thus producing the results less dependent on human errors were presented in [1]. However the complete model of FRF obtained by superposition of all individual modes into one FRF model suffers from the mutual influence of modal damping of neighboring modes one on another. This causes inconsistencies between the modeled and measured FRF. Increase of correlation between experimental and modeled FRF can be achieved by the modal damping optimization performed during calculation of the entire model instead of single modes. Another approach is polynomial modeling [5]. The advantage of this method is a significant increase of the correlation between modeled and experimental FRF. On the other side the major disadvantage of this method is high computational cost (computation time). Both methods were applied in the improved automatic modal analysis described here.

2. FUNDAMENTALS OF SISO MODAL ANALYSIS

Frequency response function $H(f)$ of single-degree-of-freedom (SDOF) system equals to the inverse of the dynamic stiffness of the system in the frequency domain [12]:

$$H(f) = \frac{1}{-m(2\pi f)^2 + jc(2\pi f) + k} \quad (1)$$

where: m – mass [kg], c – damping coefficient [Ns/m], k – stiffness [N/m].

Despite the machine tool spindle cannot be accurately modeled by a SDOF system, it can be represented as the linear superposition of a number of SDOF characteristics, assuming, that the system is linear time-invariant. Mode identification is based on selection of the frequency range of the individual mode in real and imaginary part of the FRF. Synchronized observation of the two plots increases accuracy of such selection. In case of distorted $\text{Re}(H)$ and $\text{Im}(H)$ courses, or modes of close frequencies, proper selection of these frequency ranges manually is difficult even for experienced operators e.g. [2]. When the frequency range corresponding to a particular mode is identified, modal parameters can be determined from characteristic features of real and imaginary parts of the FRF (Fig. 1).

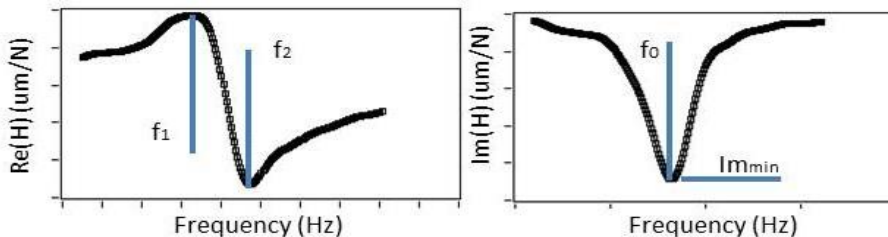


Fig.1. FRF characteristic features of single mode.

The resonance frequency f_0 is the easiest modal parameter to determine. It is identified directly as the peak in the imaginary part of the FRF - $\text{Im}(H)$. Damping ratio can be determined by formula: $d = (f_1 - f_2)/2f_0$ where f_1 and f_2 are nearest maximum and minimum of $\text{Re}(H)$ surrounding f_0 respectively. Stiffness coefficient can be found from a minimum value of $\text{Im}(H)$: $k = -1/(2d \text{Im}_{\min})$ and modal mass is equal to: $m = k/(2\pi f_0)^2$. Finally modal damping can be calculated as: $c = 2d\sqrt{km}$. Example of 2DOF modal parameters is presented in Table 1 in order to calculate the FRF model.

Table 1. Modal parameters

Mode	f_0 [Hz]	m [kg]	c [Ns/m]	k [N/m]
1	897	2.75	891	8.76E+7
2	944	2.01	828	7.12E+7

By substituting these modal parameters into the transfer function equation (1), two single plots, each representing the single mode are obtained, see Fig. 2. The 2DOF characteristic is then obtained by superposition of single modes. Superposition of modes closely located to each other results in overestimation of modal damping and poor correlation of between experimental and estimated characteristics.

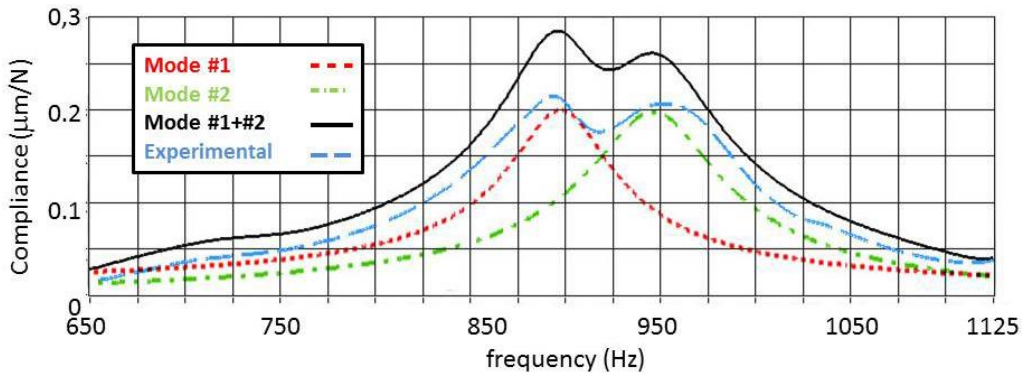


Fig.2. Characteristics of 2DOF system obtained by mode superposition.

3. AUTOMATIC MODAL ANALYSIS

Important and time-consuming stage of modal analysis is a selection of short fragments of measured signals containing the actual exciting force and object acceleration signals. To browse the entire signal, assess of every hit and response and to reject non-proper ones requires lots of time, experience and attention of the operator. An automatic signal fragmentation is based on the detection beginning of a single hit e.g. [1]. It is recognized in the force signal as exceeding of a threshold, which is five times higher than the maximum value of the first 200 samples of the signal, see Fig. 3. Then 2000 samples are extracted, beginning from the fiftieth sample preceding the threshold crossing. For the applied sampling frequency 40 kHz the sampling window is equal to 50 ms, which is bigger than the longest system response on the rubber hammer hit. Longer window would cause overlap of succeeding hits and a proper hit would be assessed as a wrong one.

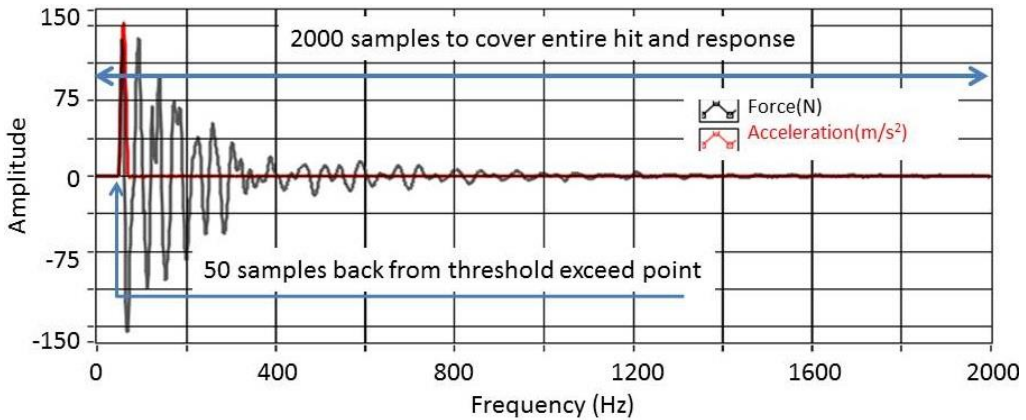


Fig.3. Hits and responses extraction method.

All selected fragments of both signals are then evaluated for their correctness to eliminate those fulfilling the following criteria:

- maximum of the hit force is higher than 10 N
- absence of overload of force and/or acceleration transducers
- absence of double hit – occurrence of the second maximum in the force signal within 2000 samples window
- maximum of the force is higher than a half of the strongest correct hit.

Automatically selected proper hits are taken for further analysis. In the next step complex frequency response functions are computed for every extracted excitation and response signals, and obtained results are averaged. Then the coherence function calculated and used for assessment of distortion, lack of correlation or non-linearity. The function value is 1 for linear system with no distortion of input and output. Values between 0 and 1 it indicates distortion, lack of correlation or nonlinearities.

Automatic modes detection begins with searching of local minima in $\text{Im}(H)$ frequency response function, see point 1 in Fig. 4. Every minimum indicates potential resonance frequency f_0 , however there are usually hundreds of them, mostly accidental, inessential. The following procedure is applied for evaluation the mode relevance and elimination those not relevant. First, the nearest $\text{Im}(H)$ local maximum on the left (point 2 in Fig. 4) and on the right (point 3 in Fig. 4.) from the detected local minimum are detected. The frequencies of detected local maxima indicate the frequency range for a single mode. Then the following criteria are used for selection of relevant modes: coherence function value at modal frequency f_0 is higher than 0.6 and modal frequency f_0 is within the useful range. Example of automatically detected modes and frequency ranges, are shown in Fig. 5. The presented method enables to detect even closely located modes. It could be difficult even for experienced users if manual identification of the modes would be needed.

For the modes considered relevant, within each mode frequency range maximum and minimum values of $\text{Re}(H)$, and corresponding to them frequencies f_1 and f_2 are identified. Thus for every mode values of f_0, f_1, f_2 and Im_{\min} are obtained and used for calculation of modal parameters as was shown above. Modal parameters computed for frequency ranges in the example shown in Fig. 5 are presented in Table 2.

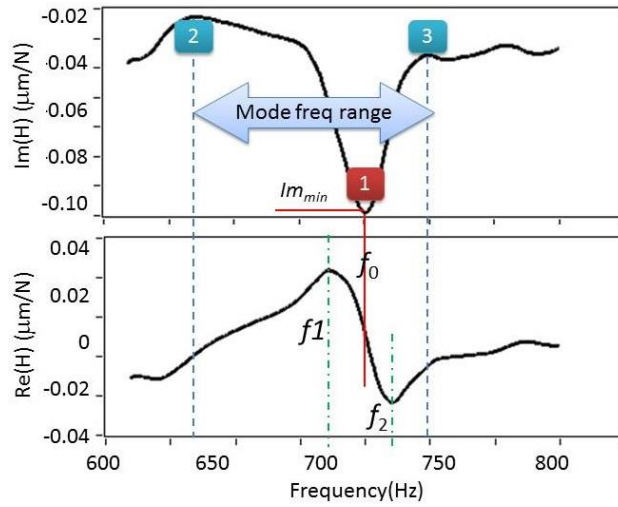


Fig.4. Automatic mode detection method.

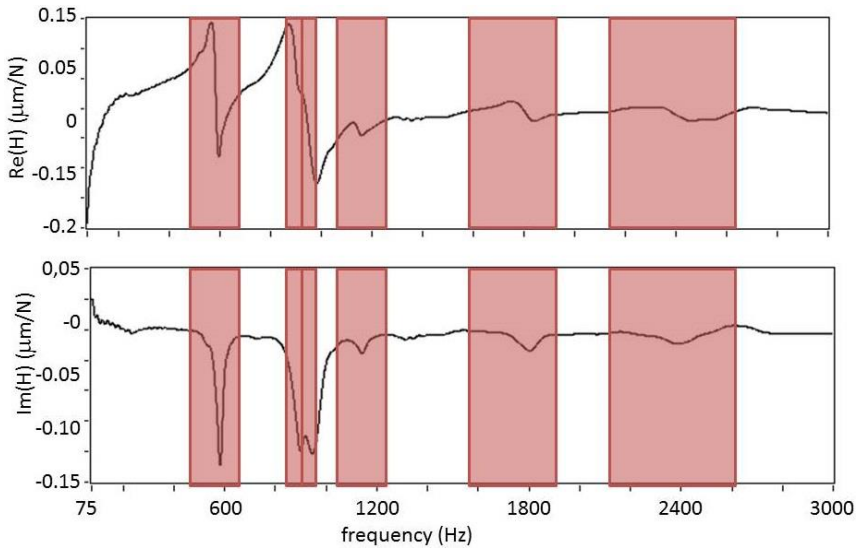


Fig.5. Recognized frequency ranges.

Table 2. Modal parameters

Mode	f_0 [Hz]	m [kg]	c [Ns/m]	k [N/m]
1	582	6.71	1232.97	89782
2	897	2.52	891.43	80453
3	944	2.11	829.29	74682
4	1142	17.58	3570.11	905485
5	1800	4.16	2555.01	533422
6	2383	3.52	2826.67	791037

Modal parameters substituted in equation (1) give a FRF model, shown in Fig. 6. As can be seen here, while system modes are widely separated from each other, FRF model is correct – at mode frequency FRF model amplitude is equal to experimental data (e.g. for 1st, 5th and 6th mode). However if the system modes are located closely (especially 2nd and 3rd mode in Fig. 6) the modes influences each other which results in overestimation of FRF compliance and dramatically reduces the correlation between experimental and estimated FRF.

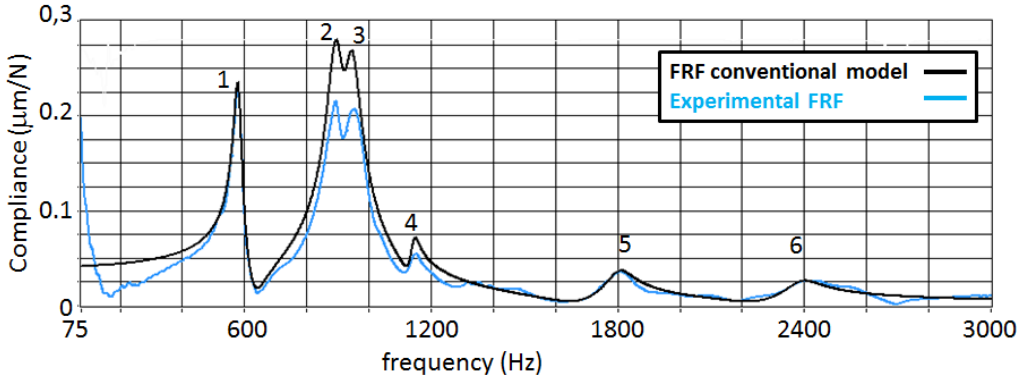


Fig.6. Automatic modal analysis result – modeled vs. experimental FRF.

4. AUTOMATIC OPTIMIZATION OF THE FRF MODEL

In order to increase correlation between experimental and estimated FRF the methodology of modal damping optimization was developed. It is based on change of single mode damping by comparing model amplitude at mode frequency with the experimental FRF.

Automatic optimization of the MDS model is implemented in three successive stages. Each of the stages aims to provide damping adjustments of all single modes separately to minimize the difference between the model and the experimental FRF at modal frequency, see Fig. 7. The amplitude of FRF compliance (A_{model}) at the modal frequency of individual mode is compared with the amplitude of experimental FRF compliance (A_{exp}). If the absolute value of the difference $X = (A_{model} - A_{exp})$ is higher than $0.005 \mu\text{m/N}$, then for too small compliance the damping of the considered mode is increased by 10%, while for too big compliance it is reduced by 10%. Then the entire model is recalculated. When the difference X is lower than $0.005 \mu\text{m/N}$, the allowed difference is reduced to $0.002 \mu\text{m/N}$ and the procedure is repeated. Finally it is repeated for $\text{abs}(X) > 0.001 \mu\text{m/N}$. All the above coefficients have been chosen empirically. Results of application of this procedure are presented in Fig. 8.

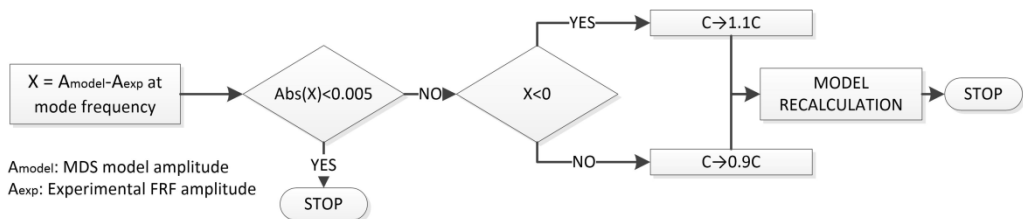


Fig.7. Simplified automatic MDS model optimization algorithm.

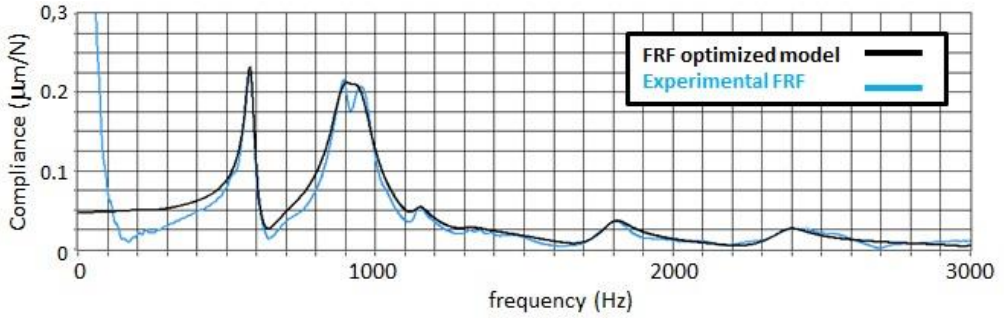


Fig.8. Comparison of original and optimized FRF models with the experimental FRF.

Automatic adjustment of modal damping allows for increasing of the correlation between experimental and estimated FRF's being still simple mathematical method.

5. MODAL PARAMETER ESTIMATION BY POLYNOMIAL FIT

Before Fourier invented his transformation of time domain signals into frequency domain spectra, Gaspard Riche de Prony developed a method which allows for the estimation of modal parameters of a system directly from the time domain signal. It is based on transformation of continuous signal into a series of damped sine waves in time domain. Such decomposed signals allow the calculation of the relevant information such as modal frequency, amplitude, phase and damping. Nowadays the Prony's method is applied for modeling of the FRF by polynomial fit model [5]. However instead of original signals acquired during experiments, here inverse Fourier transform of a complex frequency response function is used to obtain time domain waveform. Using the transformation based on the Euler equation the method for polynomial fitting is obtained:

$$\hat{f}(t) = \sum_{i=1}^N A_i e^{\sigma_i t} \cos(2\pi f_i t + \theta_i) = \sum_{i=1}^N \frac{1}{2} A_i e^{\pm j\theta_i} e^{\lambda_i t} \quad (3)$$

where: $\lambda_i = (\sigma_i \pm j\omega_i)$ system eigenvalues; σ_i damping coefficient (D); φ_i phase coefficient; f_i frequency coefficient (F); A_i amplitude.

Here modal parameters are as follows: frequency coefficient, damping coefficient, residua (there are no stiffness and mass). The first two come from the Prony's method. Residua are computed by solving a linear matrix equation by multiplying the inverted matrix of decomposed polynomial roots by the time waveform. Finally, a system model for single mode is calculated then composite of all modes integrated.

$$X_n = \frac{\{Im[residua] + jRe[residua]\}}{2\pi df_n - \left(\frac{-2\pi F \cdot D}{100}\right) + j\left(\sqrt{2\pi F \cdot \left(\frac{D}{100}\right)^2}\right)} + \frac{\{Im[residua] + jRe[residua]\}}{2\pi df_r - \left(\frac{-2\pi F \cdot D}{100}\right) - j\left(\sqrt{2\pi F \cdot \left(\frac{D}{100}\right)^2}\right)} \quad \text{where } n \in \{0 \dots N/2\} \quad (4)$$

Results of application of polynomial fit for the same data as in previous sections are shown in Fig. 9. As can be seen there polynomial method assures the best correlation, but it is much more mathematically complicated and requires more computational-time to present the results. Another disadvantage is lack of conventional modal parameters (mass and stiffness), which makes the results less intuitively understandable.

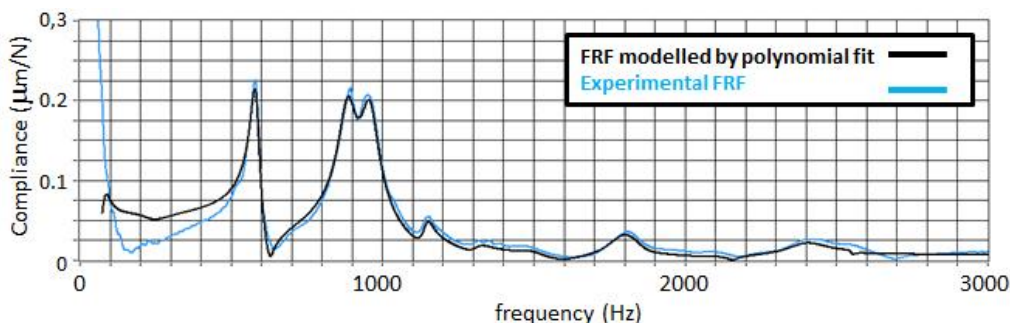


Fig.9. Polynomial fit results

6. INDUSTRY APPLICATION

Described methodology was applied in the aerospace industry facility in the Aviation Valley in Poland [3]. The objective of the test was determination of dynamic condition of twelve identical CNC machining centers (two lines, six machines in each line). Tests were performed while spindle was not moving and accelerometer fixed with a mounting wax at the end of special shank mounted in the spindle. During the measurement (on x and y axes) the machine tool was warmed up to the operational temperature. Modal hammer was equipped with a rubber or plastic tip. Experimental setup for 1D SISO modal analysis is simple and easy to use in factory floor conditions. It consists of modal hammer B&K 8206-03, accelerometer B&K 4514-001, conditioning amplifier B&K NEXUS 2693, DAQ card NI USB-6259 BNC and PC with LabVIEW 2010 environment. The developed software automatically creates reports with obtained results, examples of parts of it are presented in Fig. 10.

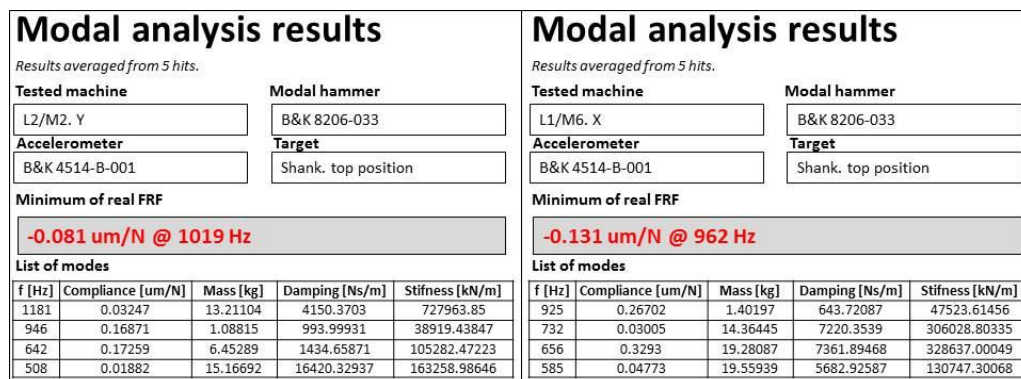


Fig.10. Fragments of automatically generated report on the SISO modal analysis.

The most indicative for the chatter resistance is minimum of real part of FRF. These values for all twelve tested machines are presented in Fig. 11. The average values were marked by a dashed line. Values lower than average minus standard deviation were considered as safe (green field), values higher than average plus standard deviation were considered as indication for maintenance. One machine – the third in the first line appeared to be in the worst condition. Actually it was already withdrawn from production, waiting for maintenance. The best results on both axis were achieved by machine two in the second line.

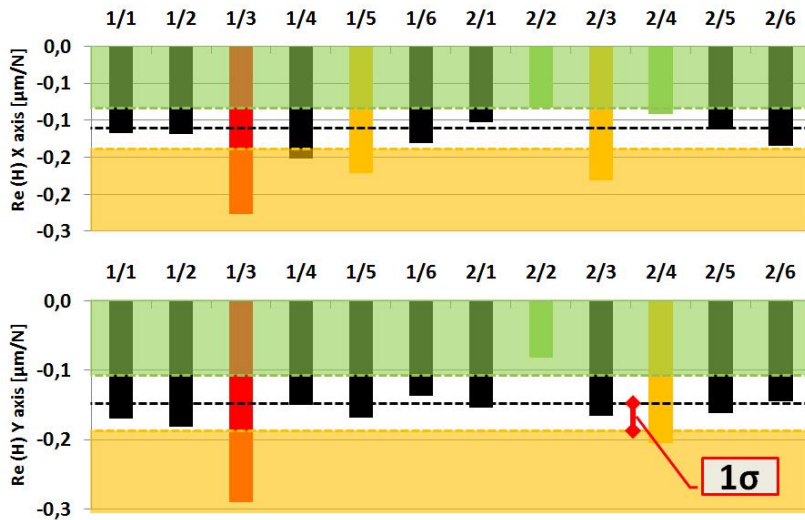


Fig.11. Dynamic compliance of tested high speed spindles.

Simultaneously the speed spindle error motions were tested using Lion Precision hardware, but our own software [4]. Obtained results (example shown in Fig. 12) confirm those presented by the automatic modal analysis. Machine 2/2 has the lowest measured dynamic compliance and total radial error movement 5.6 μm . On the other hand machine 2/4 which on Y axis exceeded warning level (one standard deviation of the average), has total error movement more than twice higher - 12.1 μm .

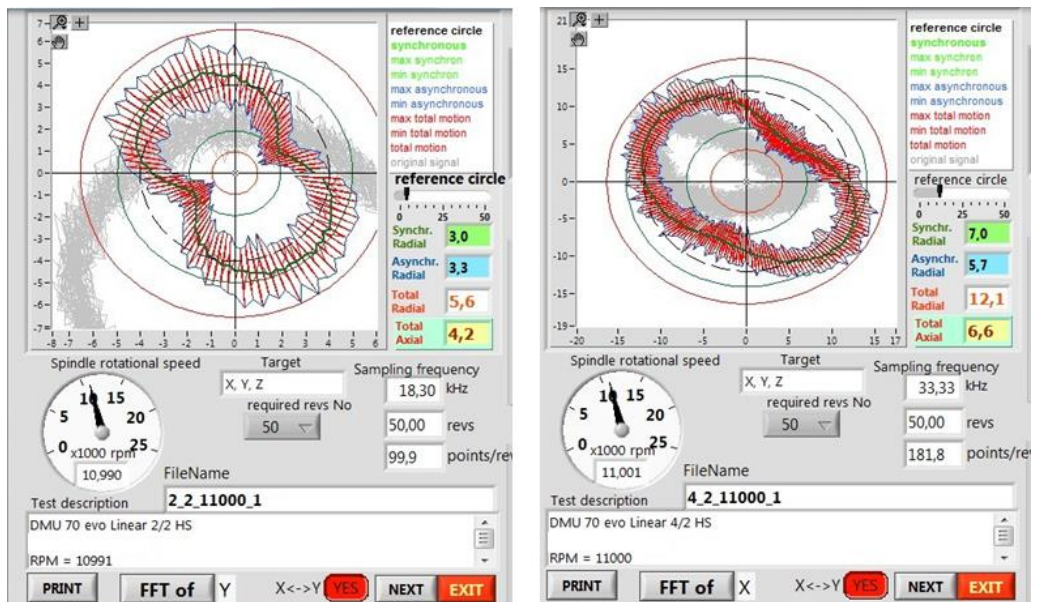


Fig.12. An example of the speed spindle error motions testing.

7. CONCLUSIONS

Conventional modal analysis requires both knowledge and skill for evaluation of registered signals, selection of the proper hits and selection of the frequency ranges corresponding to the single modes. Using the software developed on the base of presented algorithms, all these operations and analysis are automatized, thus they can be done directly on the factory floor without the engagement of highly qualified personnel. The experimental test performed in factory floor conditions confirms the propriety of developed automatic modal analysis methodology and the software.

Automatic adjustment of modal damping allows to increase correlation between experimental and estimated FRF's still maintaining simple mathematical method. The polynomial method represents the best correlation, but it is much more mathematically complicated and requires mode computational-time to present the results.

ACKNOWLEDGEMENTS

Financial support of Structural Funds in the Operational Programme - Innovative Economy (IE OP) financed from the European Regional Development Fund - Project "Modern material technologies in aerospace industry", Nr POIG.01.01.02-00-015/08-00 is gratefully acknowledged

REFERENCES

- [1] Bąk.P.A., Jemielniak K., „Development of methods, algorithm and software for automatic modal analysis”, report from the project “Modern material technology in aerospace industry” – see acknowledgments.
- [2] Bąk P.A., K. Jemielniak, Automatic modal analysis of milling machine tool spindle, Journal of Machine Engineering, Vol 17, No 1, 2012, Page 81-92, ISSN 1426-708X
- [3] Bąk.P.A., Jemielniak K., „Modal characteristics and dynamic compliance test in factory floor conditions”, report from the project “Modern material technology in aerospace industry” – see acknowledgments.
- [4] K. Jemielniak, J. Chrzanowski, „Analysis of high speed spindle error movement”, report from the project “Modern material technology in aerospace industry” – see acknowledgments.
- [5] PEETERS, Bart, et al. The PolyMAX frequency-domain method: a new standard for modal parameter estimation?. Shock and Vibration, 2004, 11.3: 395-409.
- [6] Thusty J, King, R. I., ed., 1985, Chapman and Hall “Machine Dynamics. Handbook of High Speed Machining Technology”, New York, Ch. 3, 48-153.
- [7] CutPro User Manual, Manufacturing Automation Laboratories Inc. (MAL), 2000,
- [8] Y. Altintas, “Machining process Modeling, Machine Tap testing and Chatter Vibration Avoidance” , Manufacturing Automation Laboratory, University of British Columbia, Vancouver, Canada, 2002
- [9] Abele E, Fiedler U, “Creating Stability Lobe Diagrams during Milling”, Annals of the CIRP, 53(1):309–312, 2004
- [10] E. Budak, “Dynamic Analysis and Control”, Faculty of Engineering and natural Sciences, Sabanci University, Tuzla, Istanbul, Turkey, 2009
- [11] Ole Døssing, “Structural Testing. Part 1. Mechanical Mobility Measurements”, Brüel & Kjær, April 1988, p.20
- [12] Patrick Guillaume, “Modal Analysis”, Department of Mechanical Engineering, Vrije Universiteit Brussel, Pleinlaan 2, B-1050 Brussel, Belgium, p.4-6
- [13] N. M. M. Maia and J. M. M. Silva, Phil. Trans, “Modal analysis identification techniques” R. Soc. Lond. A 2001 359, 29-40
- [14] William G. Halvorsen, “Impulse technique for structural frequency response testing”, Anatrol Corporation and David L. Brown, University of Cincinnati, Sound and Vibration, November 1977
- [15] Svend Gade, Henrik Herlufsen and Hans Konstantin-Hansen, “How to Determine the Modal Parameters of Simple Structures”, Brüel&Kjær, Denmark
- [16] Faassen R.P.H., “Prediction of regenerative chatter by modelling and analysis of high-speed milling”, International Journal of Machine Tools & Manufacture 43 (2003) 1437–1446

Experimental analysis of the CNx nano-damping material's effect on the dynamic performance of a milling process

Constantinos Frangoudis, Qilin Fu, Md.Masud-Ur-Rashid, Cornel-Mihai Nicolescu, Amir Rashid

KTH Royal Institute of Technology, Dept. of Production Engineering, Stockholm, Sweden
confra@kth.se

ABSTRACT

Vibration phenomena are a main consideration during the material removal operation, as it has prominent effects on the product quality, cutting tool life, and productivity of that machining operation. Within the context of machining performance, the role of enhanced stiffness and damping on the dynamic behaviour of machining systems such as turning and milling is well established. In this experimental analysis, investigations have been conducted for identifying the natural characteristics and dynamic responses of a milling process with the application of a novel carbon based (CNx) nano-composite damping material. The CNx material has been applied into the joint interface of a work holding device with adaptive dynamic stiffness. Prior investigations of this material, produced by the plasma enhanced chemical vapour (PECVD) process, showed inherent damping capacity via interfacial frictional losses of its micro-columnar structures. For this study, natural characteristics of the work holding system have been characterized by the modal impact testing method. Dynamic responses during the machining process have been measured through the vibration acceleration signals. The ultimate objective of this study is to comprehend the potentiality of CNx coating material for improving machining process performance by analysing the frequency response functions and measured vibration signals of the investigated milling process with varying stiffness and damping levels.

KEYWORDS: carbon based nano-composite material, PECVD, damping, stiffness, milling, vibration

1. INTRODUCTION

Vibration phenomena are a main consideration during the material removal operation, as it has prominent effects on the product quality, cutting tool life, machine health, and productivity of that machining operation etc. [1]. A great deal of work had been dedicated in understanding the nature of vibrations and finding ways to counter their consequences. A

recent review summarizes the research efforts carried out so far to address the problem of self-excited vibrations [2]. Such efforts address the problem from a process perspective, a from machine tools' structural dynamic behavior point of view [3], or through passive [4-6] or active vibration control [7]. This research is reporting the developments of a work holding device with adaptive dynamic behavior, where the joint interface is used as a source of designed-in damping in order to improve dynamic stiffness. The source for damping is a carbon based coating applied on one of the components, acting as an intermediate layer between the two components forming the interface. In previous investigations this material when coated on components showed inherent damping capacity through the interfacial frictional losses of its micro-columnar structures.

2. DESCRIPTION OF THE SYSTEM UNDER STUDY

The system under study consists of an end milling tool (solid carbide, 16 mm diameter, 4 teeth), a steel workpiece (100mm cube) and a work holding device, bolted on the machine table. The workpiece is bolted on an intermediate plate, which is then bolted on the work holding device. The work holding device, made of aluminium alloy, consists of two components, which create an inner interface and is bolted on the machine table.

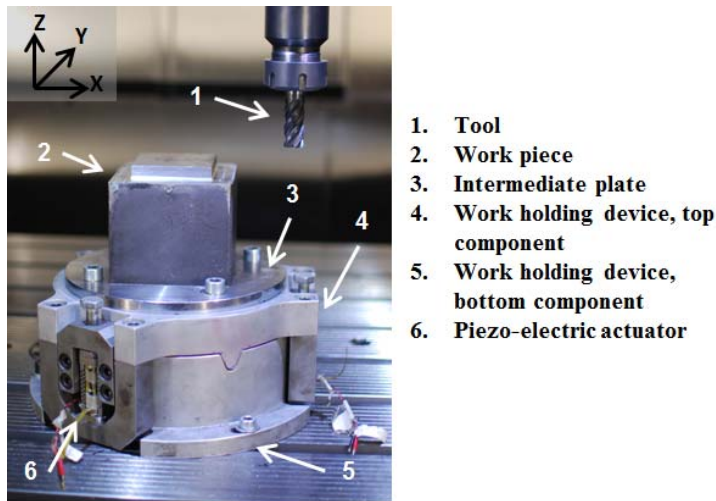


Fig. 1. The system under study

Controlling the supplied voltage on the 3 piezo-actuators that are placed on the side of the device as seen in Fig. 1 allows the alteration of pre-stress between the two parts of the device and therefore the alteration of its stiffness. An increase in the supplied voltage to the actuators will pull the two components of the device towards each other, increasing the pre-stress between them. The system is examined between two configurations of stiffness (min / max) and two configurations of damping (with / without coating). Between the contacting surfaces of the abovementioned two components, the coating is applied to create the second designed-in damping configuration. In all tests, data were collected by an appropriate data acquisition device and analyzed in LMS.Test Lab software platform.

3. DEPOSITION PROCESS OF THE NOVEL CARBON BASED (CN_x) NANO- COMPOSITE MATERIAL

In order to apply the nano-composite CN_x damping material into the joint interface of the work-holding device, the state-of-art plasma enhanced chemical vapour deposition (PECVD) process coupled with magnetron sputtering was used. The 700 µm thick CN_x film layer was deposited onto the 'top component' (substrate for this study) of the work-holding device by the high energetic ion sputtering of a graphite target plate in a reactive atmosphere of gaseous precursors of Argon (Ar), Nitrogen (N₂) and Acetylene (C₂H₂).

The system is equipped with an in-house developed power supply unit which can deliver 2000V and 200A peak current rating, and with a standard planar rectangular magnet (surface area 10x45 cm²) coupled with the graphite target plate (62.5 cm in length, 12.8 cm in width and 0.6 cm in height) mounted in a cylindrical vacuum chamber (200 cm in length and 100 cm in diameter). Prior to the deposition process, the vacuum chamber was pumped down to the required background pressure of about 2.2×10^{-2} Pa to 1×10^{-3} Pa by using a Pfeiffer vacuum system consisting of a rotary vane pump and a turbo molecular pump. After reaching the desired vacuum pressure, the process gas mixture was (Ar, N₂ and C₂H₂) leaked into the reaction chamber with the ratio of approximately 1:1:1.

During the deposition process, a peak current rating of 50 A to 60 A and a peak voltage rating of 800 V to 1000 V with a pulse width of 400 µs and a repetition frequency of 330 Hz were applied across the gas mixture between the cathode (magnetron with target plate) and the anode (chamber wall with substrate). The high power pulses generated from such a power supply ignites the desired plasma discharge by ionizing the free working gas (Ar) atoms and eventually creates reactive species required for energetic bombardment of growing thick film [8]. The CN_x deposition process was carried out for 70 hours at an ambient temperature without external heating treatment to the substrate. The deposition rate was recorded to be 9 to 10 µm per hour.

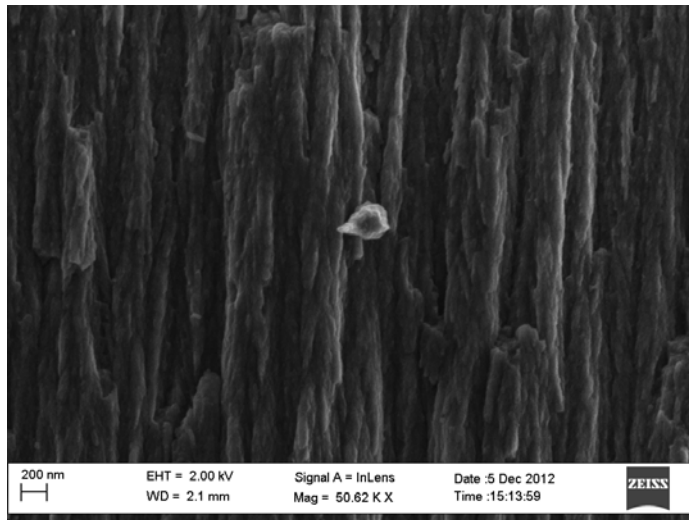


Fig. 2 Cross section of the deposited CN_x Layer

4. MODAL TESTING OF THE SYSTEM UNDER STUDY

Both the work holding device and the tool used for the machining tests were subjected to modal tests in order to identify their natural characteristics and trace how they interact with the process parameters in the resultant response of the system during machining. In the case of the work holding device, they would provide necessary information for the effect of the application of the coating as well as the change in pre-stress. The source of excitation was an impact hammer and the response was measured with 3 accelerometers. Tests were conducted in both X and Y direction but due to space restrictions most of the results for the Y direction are omitted. The structural behavior of the system in the configuration with a metal-to-metal interface has been reported previously by the authors [9].

4.1. Impact testing of the work holding device

Fig.3 shows the receptance FRFs for one measurement point for the X direction. The red continuous curve corresponds to the non-coated configuration, while the blue dashed one corresponds to the coated one. It can be seen in this figure that the application of the coating causes a shift of the natural frequencies of the system to lower levels, an indication that the coated system has reduced static stiffness. Estimates of static stiffness between configurations are given in table 1 and show that the interface with the coating causes a loss of static stiffness as compared to a metal-to-metal interface.

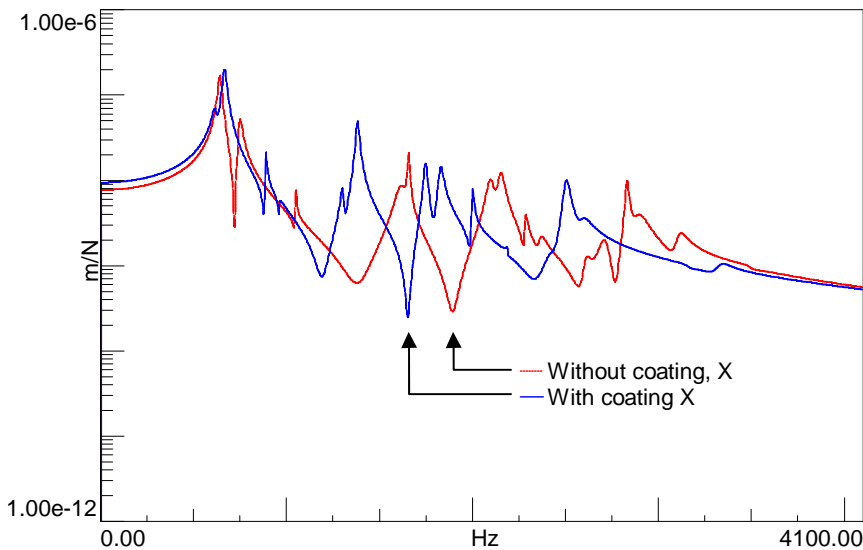


Fig. 3. Receptance FRFs in the high pre-stress configuration

Fig 4 exhibits the effects of altering pre-stress on the system's structural behaviour in the coated configuration. As the green dashed line shows, together with the data in table 1, when pre-stress is released to its minimum, the stiffness of the structure is reduced and consequently the Eigen frequency values are reduced.

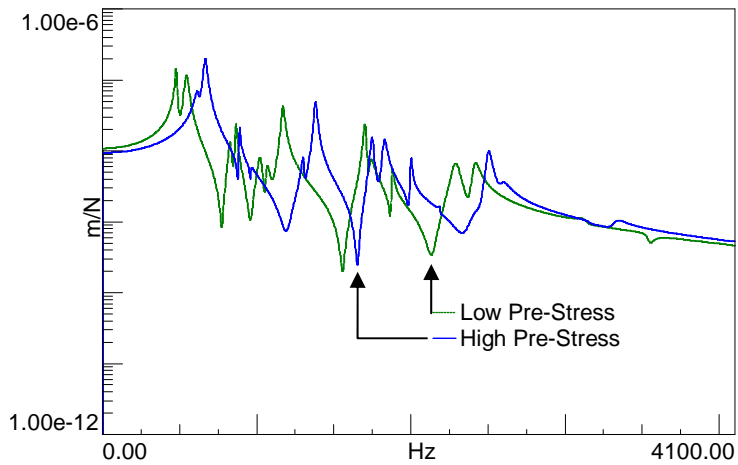


Fig. 4. Receptance FRFs for the coated configuration

In Table 2, the Eigen frequencies and the damping (as a percentage of critical damping) for the first ten modes are presented in the X direction of measurement in order to exhibit the effect of coating and the effect of stiffness change in the coated configuration. An observation of the values in the table columns 2 and 3 reveals that in most cases the coating improves damping. A comparison of the values in columns 1 and 2 shows that an increase in pre-stress, and therefore in stiffness, is detrimental to the system's damping.

Table 1. Static Stiffness estimates between configurations

X direction	Y direction			
	Without Coating	With Coating	Without Coating	With Coating
Low Pre-Stress	104841 N/mm	91743 N/mm	81300 N/mm	59880 N/mm
High Pre-Stress	129534 N/mm	103950 N/mm	131752 N/mm	100502 N/mm

Table 2. Eigen frequencies of the work holding/workpiece system, damping as percentage of critical damping (ζ)

	Low Pre-Stress/Coated	High Pre-Stress/Coated	High Pre-Stress/Uncoated
1	477.827 Hz, 1.33 %	616.852 Hz, 2.20 %	642.228 Hz, 1.56 %
2	543.902 Hz, 2.37 %	666.279 Hz, 1.66 %	748.142 Hz, 1.44 %
3	827.491 Hz, 1.38 %	888.073 Hz, 0.42 %	1049.016 Hz, 0.29 %
4	864.876 Hz, 0.71 %	959.576 Hz, 0.52 %	1615.336 Hz, 2.00 %
5	1023.602 Hz, 1.82 %	1302.353 Hz, 0.63 %	1656.684 Hz, 0.30 %
6	1065.134 Hz, 1.39 %	1381.690 Hz, 0.62 %	2096.948 Hz, 0.99 %
7	1169.641 Hz, 0.86 %	1747.520 Hz, 0.56 %	2151.898 Hz, 0.83 %
8	1701.434 Hz, 0.51 %	1827.006 Hz, 0.77 %	2283.503 Hz, 0.29 %
9	1733.210 Hz, 0.89 %	1999.783 Hz, 0.26 %	2361.229 Hz, 0.84 %
10	1878.792 Hz, 0.32 %	2187.654 Hz, 0.23 %	2001.292 Hz, 0.26 %

4.2. Impact testing of the tool

Six points were tested on the tool to identify its natural characteristics. Fig 5 exhibits the receptance FRFs for the measurement point at the tip of the cutter for both directions, while table 3 presents the data for the first five natural frequencies of the tool.

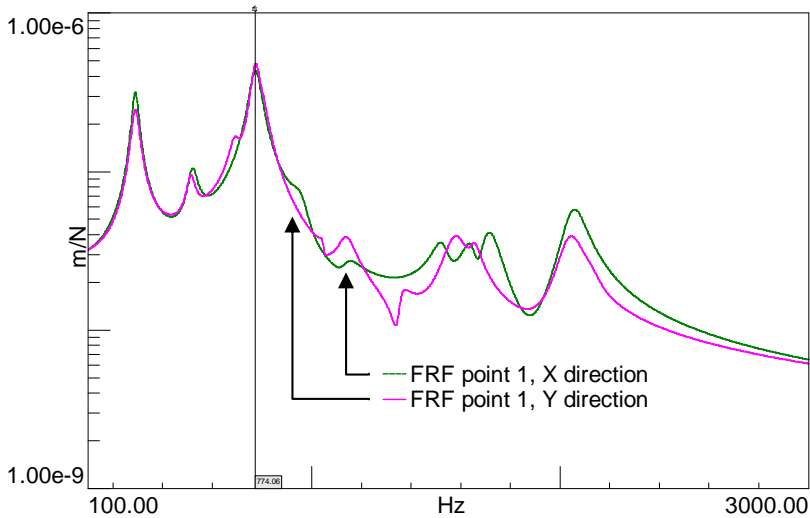


Fig. 5. Receptance FRFs for the tool used.

Table 3. Eigen frequencies of the tool, damping as percentage of critical damping (ζ)

X direction	Y direction
Mode 1 : 289.449 Hz, 4.75 %	Mode 1 : 289.445 Hz, 5.63 %
Mode 2 : 519.547 Hz, 4.00 %	Mode 2 : 512.537 Hz, 3.52 %
Mode 3 : 773.284 Hz, 3.12 %	Mode 3 : 691.964 Hz, 3.03 %
Mode 4 : 962.135 Hz, 3.98 %	Mode 4 : 774.402 Hz, 2.30 %
Mode 5 : 1137.038 Hz, 3.57 %	Mode 5 : 800.523 Hz, 3.31 %

5. MACHINING TESTS

Machining tests were carried out in a Hermle 5-axis milling machine. Acceleration signals were recorded by two tri-axial accelerometers mounted on the spindle bearing and the work piece respectively. A 16 mm solid carbide end mill with 4 teeth was used, with a 3.2 length to diameter ratio. Cutting speeds in a range from 140-190 m/min were tested in order to distinguish stable and unstable process parameters. The cutting speed selected for the following investigations was 150 m/min, at 2984 RPM resulting in a tooth engagement frequency of 199 Hz. Feed was 0.05 mm/tooth. The process was end/down milling with the feed direction along both YZ and XZ planes. Axial depth of cut was 10 mm and radial starting from 1 mm. The aim was to identify the differences in the response of the system to machining as a result of the coating on the interface and examine if the stability limit can be affected. Additionally, the effect of altering the stiffness of the work-holding device in the presence of the coating was examined.

5.1. Examination of the coating effect on the response to machining excitations

This examination is carried out for the high stiffness configurations. From the tests conducted, in the uncoated configuration chatter was manifesting (with the distinctive sound and surface pattern that are associated with an unstable milling process) at an axial depth of cut of 1.5mm. In the case of the configuration with the coating, chatter developed at 2.5 mm

depth of cut, providing an increase of 1 mm in the stability limit. Figures 6 and 7 exhibit the acceleration signals acquired during the tests in the frequency domain for both spindle and work piece sensors. Chatter was present only the case of machining with the tool moving in the YZ plane and given the symmetrical nature of the work holding device, and the tool this highlights the importance of the machine's structure in the dynamic response to machining excitations [10]. The frequency associated with the chatter phenomenon is observed at around 830 Hz (highlighted by a circle), which is close to the third mode of the tool (which shows the highest response amplitude) as revealed by the modal tests.

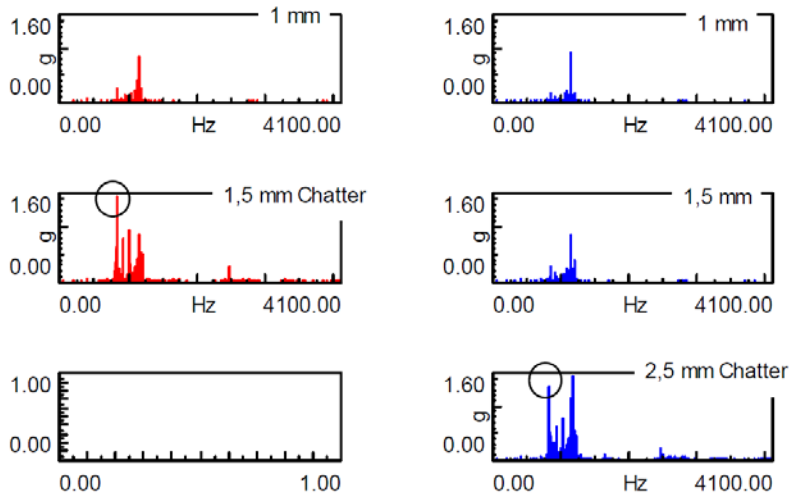


Fig. 6. Spindle acceleration signals, YZ feed plane, red/left: without coating, blue/right: with Coating

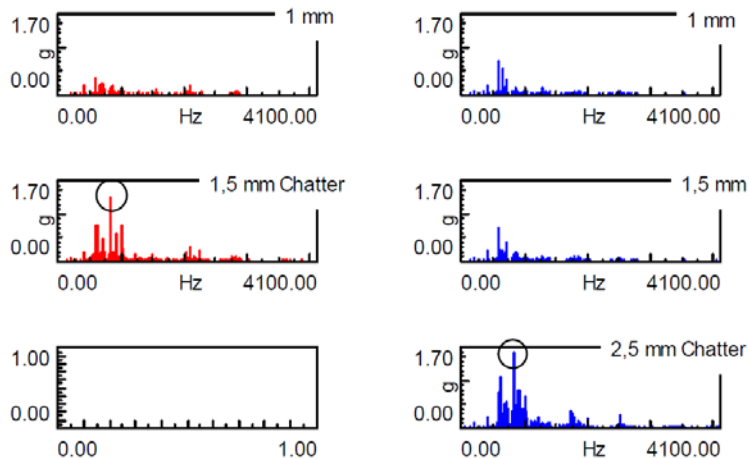


Fig. 7. Work piece acceleration signals, YZ feed direction, on the left/red: without coating, on the right/blue: with coating

5.2. Examination of the stiffness effect on the response, in the presence of the coating

As mentioned earlier, the system was tested in two pre-stress configurations, resulting in two extremes of stiffness. In the case of the high pre-stress -and therefore stiffness- configuration, at the cutting depth of 2.5 mm, the chatter sound was more profound than in the low stiffness configuration. As seen in Fig. 8, vibration amplitudes were lower in the case of the low stiffness configuration in both the spindle and the work piece measurement. As shown in Fig. 9, the amplitude at 830 Hz, which was the chatter frequency, was slightly higher in the high pre-stress configuration. Additionally, the response of the system seems to deteriorate slightly across the whole spectrum, as a result of the lower damping observed in this configuration. No significant change was observed on the frequency where chatter occurred.

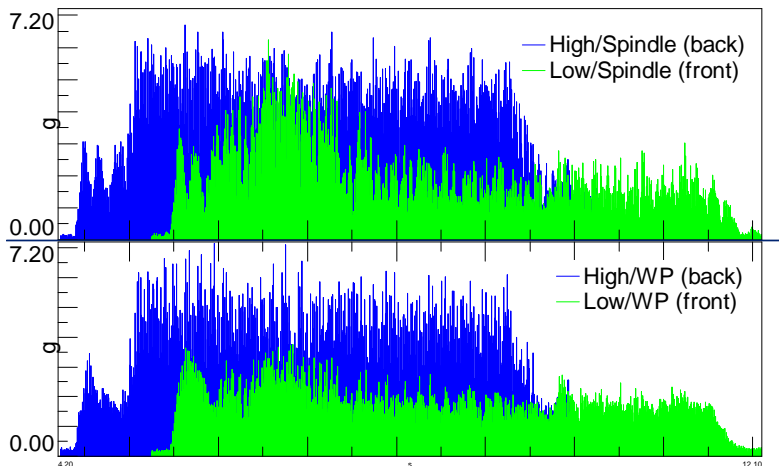


Fig. 8. Acceleration signal from spindle (top) and work piece (bottom), coated configuration, green: low pre-stress, blue: high pre stress, time domain

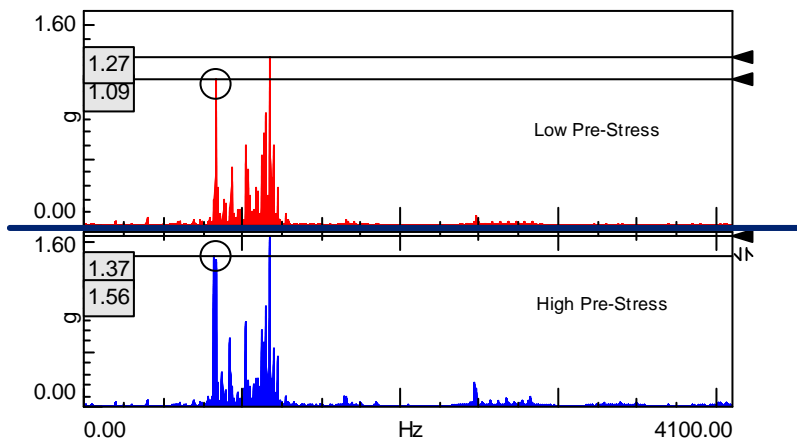


Fig. 9. Acceleration signal from spindle in frequency domain.

5.3. Response of the system in different cutting speeds

As mentioned earlier the system was tested in a range of cutting speeds from 140-190 m/min (2785-3780 RPM). Fig 10 shows how the system (coated, high pre-stress configuration) responded to excitation from different process parameter combinations (depth of cut and cutting speed).

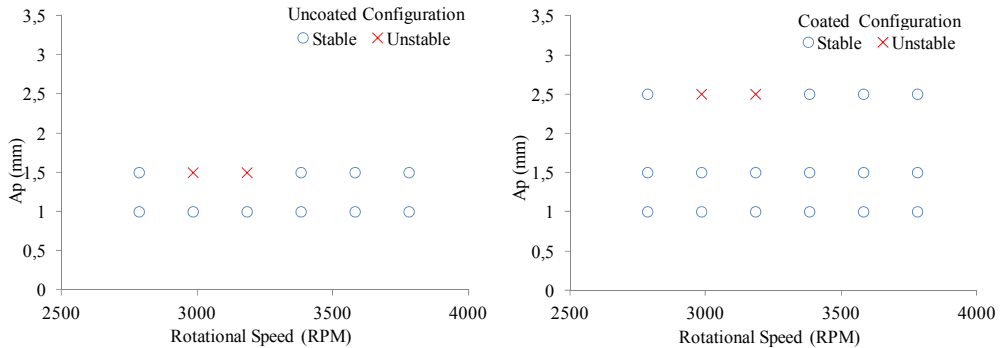


Fig. 10. Experimental testing of the stability limit

6. CONCLUSIONS

A novel carbon based (CNx) nano-composite damping material was applied on the interface of a work holding device with adaptive dynamic stiffness. Investigations over its effects on the structural characteristics of the system showed that the coating on the interface causes a reduction of static stiffness in comparison to the configuration with a metal to metal interface. With respect to the effects on damping, the impact tests revealed an increase in damping. With respect to the effects of changing pre-stress in the presence of the coating, an increase in pre-stress will cause an increase in static stiffness and at the same time a decrease in damping.

When the system was subjected to an end milling process, the configuration with the coating exhibited chatter at 2.5 mm depth of cut while the configuration without the coating exhibited chatter at 1.5 mm depth of cut. With regards to the effects of altering stiffness, the configuration with the coating exhibited lower machining vibration amplitudes in the low pre-stress configuration, as a result of the increased damping observed in the low pre-stress configuration.

This investigation provided promising results about the application of this material as a coating on components that are in close proximity to the cutting process, aiming to reduce self-excited vibrations during machining. According to the stability lobe theory [11], chatter is caused by the relative movement between the tool and the work piece. In this experimental work, the frequency band where chatter was observed remained the same even after the application of the coating and the change in pre-stress. This suggests that what determines if the machining process is stable or not is the dynamic stiffness between the work piece and the tool in this frequency band. Therefore, improving the damping capacity from either tool or work piece side, is expected to improve the critical stability limit. This has been observed in this experimental work.

ACKNOWLEDGEMENTS

The research leading to these results has received funding from the Seventh Framework Programme (FP7/2007-2013) of the European Union, under grant agreement no. 260048 (PoPJIM project). The authors would like to thank the consortium partners CEDRAT, PROFACTOR, PLASMATRIX and Ebner-Tec for their support in carrying out this study as well as the Initiative for Excellence in Production Research (XPRES).

REFERENCES

- [1] D. A. Stephenson and J. S. Agapiou, *Metal Cutting, Theory and Practice*, 2nd Edition, Taylor & Francis, 2006.
- [2] G. Quintana and J. Ciurana, "Chatter in machining processes: A review," *International Journal of Machine Tools and Manufacture*, vol. 51, no. 5, pp. 363-376, 2011.
- [3] Y. Altintas and E. Budak, "Analytical prediction of stability lobes in milling," *CIRP Annals-Manufacturing Technology*, vol. 44.1, pp. 357-362, 1995.
- [4] A. Rashid, *On Passive and Active Control of Machining System Dynamics, Analysis and implementation*, Ph.D. Thesis, 2005.
- [5] K. Liu and K. Rouch, "Optimal passive vibration control of cutting process stability in milling," *Journal of Materials Processing Technology*, vol. 28, no. 1-2, pp. 285-294, 1991.
- [6] L. Daghini, *Improving Machining System Performance through designed-in Damping: Modelling, Analysis and Design Solutions* (Ph.D. Thesis), Stockholm, 2012.
- [7] C. R. Fuller, S. J. Elliott and P. A. Nelson, *Active control of vibration*, Academic Press, 1997.
- [8] M. Ohring, *Material Science of Thin films: Deposition and Structure*, 2nd edition, San Diego, USA: Academic Press, 2002.
- [9] C. Frangoudis, A. Rashid and C.-M. Nicolescu, "Experimental Analysis of a Machining System with Adaptive Dynamic Stiffness," *Journal of Machine Engineering*, vol. 13, no. 1, 2013.
- [10] E. I. Rivin, *Stiffness and Damping in Mechanical Design*, Marcel Dekker, Inc., 1999.
- [11] S. A. Tobias, *Machine Tool Vibration*, J. Wiley, 1965.

Using design of experiments approach to determine the essential designing parameters for an anti-vibration turning tool with finite element analysis

Qilin Fu, Amir Rashid, Cornel-Mihai Nicolescu

KTH Royal Institute of Technology, Sweden

qilin@kth.se

ABSTRACT

Anti-vibration turning tools mainly concerns the cutting tool's capability of resisting oscillating cutting force during the machining process. The design of such a machining tool concerns all aspects that are influencing the dynamic response (receptance) under cyclic loading. Different design concept for optimizing the tool's behaviour has different emphasis on each of the parameters in the design matrix. In this paper, the design of experiment approach together with finite element method is utilized to analyse the essential parameters for anti-vibration tool design with 7 times length to diameter ratio (L/D).

KEYWORDS: Design of experiments, chatter, damping tools, design

1. INTRODUCTION

Chatter [1] during machining process leads to bad surface finish, and short tool life. In order to suppress chatter, damping effect is needed from either the mechanical structure [2] (structure damping) or the friction [3] between the tool and the workpiece (process damping). When designing damped machining tools, there are several factors that affect the tool's performance including the maximum dynamic response, static stiffness, and mode frequency.

Damped machining tools offer a wider operation parameter domain for machining processes concerning the length to diameter ratio (L/D). For an internal turning process, a conventional tool made of steel can usually satisfy the overhang length to diameter ratio (L/D) less than 4 [4]. While longer overhang length is needed for an internal turning process, damped tools are usually needed to sustain a stable machining process.

Damped machining tools are usually divided into two main categories namely active damped tools and passive damped tools. Active damping tools utilize the piezo-electric device to exert a compensating dynamic force on the machining tool and stabilize the machining tool [5]. Passive damped machining tools uses tuned mass dampers [6], or embed high damping materials in the mechanical structure [7].

While a tuned viscoelastic damper is used for improving machining process stability, A. Rashid et al [2] had clearly illustrated that the tuned viscoelastic dampers should be applied closed to the cutting zone to be effective. When a mechanical structure is vibrating at a certain frequency, the anti-node regions have the highest vibration amplitude whereas the node

regions have the highest vibration strain energy [8]. In the passive damping treatment category, a common strategy is to apply high damping materials such as viscoelastic materials in the constrained areas where vibration strain energy concentrates [9]. L.Daghini [10] had discussed in his work about how the constrained damping treatment should be designed towards optimizing its capability of providing the highest dynamic stiffness to the machining tool.

FEM (Finite Element Method) is widely used by design engineers to explore the design matrix and predict the outcome of the designed products. The accuracy of its prediction is mainly influenced by how accurately we model the physical world. Y. Altintas [11] et al used the FEM approach to analyse the effects of bearings placement on the spindle's machining performance. In this work, the bearings placement was optimized to shift the stability lobes over the spindle speed axis and optimize the machining operation. I. Hassab-Allah [12] and so on had used the FEM approach to successfully develop a vibration damping tool with mandrel made of synthetic-granite embedded in the central of the tool.

In this paper, Design of Experiments (DoE) approach is used to analyse the essential parameters in vibration damping tool design. The purpose of this study is to find out which are the main factors that affect a machining tool's performance against regenerative chatter.

The research questions that have been addressed are:

- What are the factors that mostly influence a machining tool's static stiffness when the tool is clamped in a fixture with a fixed overhang length in the node regions?
- What are the factors that mostly influence a machining tool's dynamic stiffness when the tool is clamped in a fixture with a fixed overhang length in the node regions?
- Is there any strategy that can be more effective than the damping treatment in the node regions?
- What are the factors that mostly influence a machining tool's resonance frequency when the tool is clamped in a fixture with a fixed overhang length?

The contribution of this paper for vibration tool design is that it generates a holistic view for the design of damped machining tools with damping treatment in node regions, and point out the essential factors that influence the machining tool's performance.

2. DESIGN SPACE AND DESIGN EXPERIMENTS

The case study refers to an internal turning tool that is clamped in a fixture as shown in Fig. 1. The overhang length (L) of the tool is 175mm and the diameter (D) of the tool is 25mm ($L/D=7$). The tool's clamping end length in the fixture is 50mm according to the recommendation clamping length provided by the fixture manufacturer ETP Transmission AB in Sweden. In the design space, the tool surface is coated with a vibration damping material along the full length of the tool surface shown in Fig. 1.

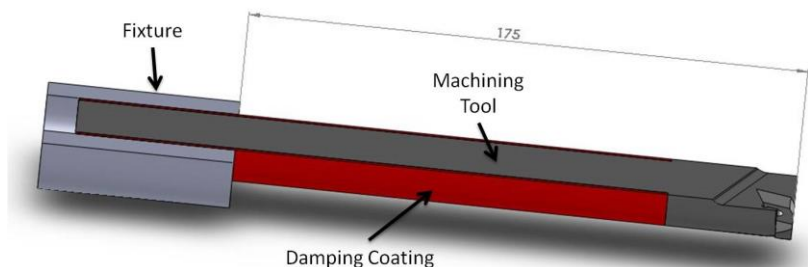


Fig. 1. Assembly of a machining tool coated with a damping coating (red) and clamped in a fixture.

In the simulation, the fixed boundary constraint is the fixture's end (shown in Fig. 2), and the force is applied on the tool in the area where the insert is fixed (shown in Fig. 2). The contact between the coating and the fixture is modelled as a thin elastic layer with both stiffness and damping. They are named as clamping interface stiffness and clamping interface damping in design matrix.

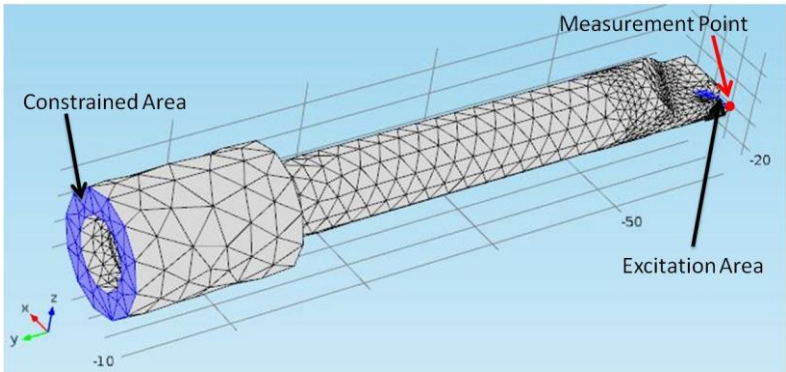


Fig. 2. Physical condition of the simulation.

The parameters that are thought to be important for the design including the Young's modulus of the coating, loss factor of the coating, thickness of the coating, clamping interface stiffness, clamping interface loss factor and the tool material's loss factor. The base values for each of the parameters are decided based on idealized values from assumptions. The experimental values are either plus 50% (+1) or minus 50% (-1) comparing to the base values. The design matrix including the factors and their value setting is summarized in Table 1:

Table 1. Design of experiment parameter matrix.

	<i>A</i>	<i>B</i>	<i>C</i>	<i>D</i>	<i>E</i>	<i>F</i>
	<i>Coating Thickness</i>	<i>Coating loss factor</i>	<i>Coating Young's modulus</i>	<i>Clamping interface stiffness</i>	<i>Clamping interface loss factor</i>	<i>Tool material's loss factor</i>
<i>+1</i>	<i>1.2mm</i>	<i>0.3</i>	<i>30 GPa</i>	<i>12e9 N/m</i>	<i>0.15</i>	<i>0.15</i>
<i>0</i>	<i>0.8mm</i>	<i>0.2</i>	<i>20 GPa</i>	<i>8e9 N/m</i>	<i>0.10</i>	<i>0.1</i>
<i>-1</i>	<i>0.4mm</i>	<i>0.1</i>	<i>10 GPa</i>	<i>4e9 N/m</i>	<i>0.05</i>	<i>0.05</i>

The clamping interface stiffness defines the compression interface stiffness in both X and Z direction as shown in Fig. 2, and the stiffness in Y direction defined as 1/3 of the stiffness in X and Z direction due to the sliding phenomenon can be interpreted as material functioning in shear motion.

Parameters that have not been changed during the simulation study are listed in Table 2 below:

Table 2. Parameters used for simulation.

Parameter	Value
Tool Material's Young's Modulus (GPa)	210
Tool Material's poisson's ratio	0.29
Tool Material's density (kg/m ³)	7850
Fixture material's Young's modulus (GPa)	210
Fixture material's Poisson's ratio	0.29
Coating material's Poisson's ratio	0.29
Coating Material's density (kg/m ³)	2800

As chatter theory stresses the cross transfer function of the tool or the workpieces, the performance of a vibration damping tool is judged by its transfer function in three directions namely cutting speed direction, cutting depth direction, and feed direction. L Andren et al [13] had analysed the vibration condition of a boring bar and pointed out that the bending motion of the first two resonance frequency is to a large extend in the cutting speed direction. In the FEM analysis, the comparison of the tool's performance will be focused on the cutting speed direction. The insert clamping area is excited with 1N force in the cutting speed direction (Z direction in Fig. 2). The receptance on tip of the insert clamping area in cutting speed direction is used to judge the tool's performance. The interested frequency band is 0-1000Hz. The impact factor is calculated as the sum of values obtained at level (+1) minus the sum of values obtained at level (-1).

3. RESUTLS AND DUSCUSSION

A full factorial design of experiments is done with 64 experiments for the 6 parameters. A summary of the simulation results is attached in the appendix of the paper.

3.1. Single factor impact study

The impact factor for each parameter on static displacement is summarized in Table 3:

Table 3. Impact factors of each parameter on static displacement.

A	B	C	D	E	F
Coating Thickness	Coating loss factor	Coating Young's modulus	Interface stiffness	Interface loss factor	Tool material's loss factor
6.98749	-0.02295	-1.01295	-2.17925	-0.02259	-0.25681

It is obviously seen in Table 3 that the thicker the coating is, the higher will be the static displacement. The highest impact factor is coming from parameter A, the coating thickness. Apart from that, increase the coating Young's modulus (factor C) and interface stiffness (factor D) will result in decreased static displacement whereas interface stiffness has a higher impact factor.

The impact factors of each parameter on maximum absolute receptance value are summarized in Table 4:

Table 4. Impact factors of each parameter on maximum absolute receptance value.

A	B	C	D	E	F
Coating Thickness	Coating loss factor	Coating Young's modulus	Interface stiffness	Interface loss factor	Tool material's loss factor
63.1	-29.4	-22.4	-23.1	-42.9	-268.6

The coating thickness has a positive impact factor over the maximum absolute receptance value which means increase coating thickness, the machining tool's performance against regenerative chatter is worse. The highest impact factor (-268.6) is from the tool material's loss factor (factor F) and increasing the tool material's loss factor will enhance the tool's machining performance suppressing regenerative chatter. Increasing the interface loss factor (factor E) value will also lead to decreased maximum absolute receptance value and the interface loss factor (factor E) has a higher impact than coating loss factor (factor B). Increasing coating Young's modulus and interface stiffness will also lead to a decrease of the maximum absolute receptance value whereas improving the machining tool's performance for suppressing regenerative chatter.

The impact factors of each parameter on 1st bending mode frequency are summarized in Table 5:

Table 5. Impact factor of each parameter on 1st bending mode frequency in cutting speed direction.

A	B	C	D	E	F
Coating Thickness	Coating loss factor	Coating Young's modulus	Interface stiffness	Interface loss factor	Tool material's loss factor
-1276	48	228	692	-4	-4

The thicker the coating is, the lower will be the 1st bending mode frequency in cutting speed direction. The 1st bending mode frequency is also influenced by the interface stiffness and coating young's modulus whereas interface stiffness has a higher impact. Coating loss factor, interface loss factor and tool material's loss factor does not have a clear influence on the 1st bending mode frequency in cutting speed direction.

3.2. Multiple factors interaction study

In order to find out some of the interactions between the investigated factors, a full multiple factor interaction study is done. The analysis of static displacement with multi factor interaction shows that none of the interactions is significant compare to the impact factor of parameters A, C and D.

The factors interactions which have significant impact on the maximum absolute receptance value are summarized in Table 6:

Table 6. Impact factor of the parameters' interaction on maximum absolute receptance value.

AB	AC	AF	BF	CF	DE	EF	ABF	ACF
-16.9	-14.0	-19.5	21.1	15.3	9.4	31.0	12.0	9.6

The interactions between interface loss factor (E) and tool material's loss factor (F) shows that it is important to keep the factor F at high level (+1) to avoid the effects from the interface loss factor (E) while low absolute receptance value is desired. The same applies to other parameters that result in a positive impact factor while combined with tool material's loss factor (F)

Table 7. Impact factor of the parameters' interaction on 1st bending mode frequency in cutting speed direction.

AB	AC	AD	BC	BE	BF	CD	DE
-48	124	-20	-48	-48	-48	76	52
DF	ABC	ABE	ABF	ACD	ADE	ADF	BCE
52	48	48	48	-44	-52	-52	48
BCF	BEF	CDE	CDF	DEF	ABCE	ABCF	ABEF
48	48	-52	-52	-44	-48	-48	-48
ACDE	ACDF	ADEF	BCEF	CDEF	ACDEF	ABCEF	
52	52	44	-48	44	-44	48	

The factors interactions which have significant impact on the 1st mode frequency is only AC with impact factor of 124 according to Table 7. This means the coating thickness (A) should be kept at high level (+1) to avoid interactions by the coating Young's modulus (C) while aiming for a low 1st bending frequency. However, the effect can still be negligible depending on designer's judgment.

As chatter phenomenon is always complicate and difficult to understand, improve the performance of a machining tool against vibration cannot solve all the problems. Y.Altintas [3] et al had analysed the process damping factor during an internal turning process. The result

shows that the process damping factor has a much higher influence on a machining process's stability over the structure damping factor.

In the design space, some of the design options are not yet available, and the main concern while choosing the design options are based on what might be available in the future. The study results are limited by the design space which means when some parameters are outside the design space, the study results and conclusion might not be valid anymore. Another type of design such as applying tuned mass dampers or constrained viscoelastic materials to manufacture a vibration damping tool, the results cannot be directly applied to those concepts. However, the same methodology can be utilized to optimize the new type of design.

4. CONCLUSION

While there are usually deviations between results predicted by numerical method and by practical experiment, the finite element method can be applied to study the causal relationship in mechanical design cases virtually.

The paper demonstrated one example of using design of experiments (DoE) method for analysing the design factor's impact on the cutting tool's dynamic performance against vibration during machining.

To answer the research questions:

- The coating thickness (A) has the highest impact on the machining tool's static stiffness.
- In the node region, the coating thickness (A) and interface loss factor (D) have the highest impact on the machining tool's dynamic stiffness.
- The tool material's loss factor (E) has the highest impact factor on the machining tool's dynamic stiffness.
- The coating thickness (A), interface stiffness (D) and coating Young's modulus (C) have the highest impact factor on the tool's 1st mode resonance frequency.

It shows that when low static displacement and low maximum absolute receptance value is desired, it is important to keep the coating thickness at low level (-1), and the other factors at high level (+1). The most significant factor that affects the machining tool's receptance in cutting speed direction is the tool material's loss factor (F). In the design space, when high tool materials loss factor (F) cannot be obtained due to the limited available materials for tool design, designers should focus either on the joint interface loss factor (E) or coating material's loss factor (B). According to the analysis results, there is rarely any interaction between factor coating loss factor (B) and interface loss factor (E) on maximum absolute receptance.

While the cutting tool's 1st bending mode frequency is critical for a specific machining process to avoid force vibration, it is critical to have coating thickness (A), interface stiffness (B), and coating young's modulus (C) under control.

Design of experiments (DoE) method has successfully been applied to point out the important parameters for vibration tooling design, though only limited numbers of parameters are studied.

APPENDIX

Design Factors						Results		
A	B	C	D	E	F	Static response (μm)	Maximum receptance ($\mu\text{m/N}$)	1st Bending Mode Frequency (Hz)
+1	+1	+1	+1	+1	+1	0.92	5.52	433
+1	+1	+1	+1	+1	-1	0.93	11.76	433
+1	+1	+1	+1	-1	+1	0.92	5.81	433
+1	+1	+1	+1	-1	-1	0.93	13.15	433
+1	+1	+1	-1	+1	+1	0.99	5.99	411
+1	+1	+1	-1	+1	-1	1.00	12.40	411
+1	+1	+1	-1	-1	+1	0.99	6.45	411
+1	+1	+1	-1	-1	-1	1.00	14.48	411
+1	+1	-1	+1	+1	+1	0.97	6.00	421
+1	+1	-1	+1	+1	-1	0.98	13.95	421
+1	+1	-1	+1	-1	+1	0.97	6.29	421
+1	+1	-1	+1	-1	-1	0.98	15.62	421
+1	+1	-1	-1	+1	+1	1.04	6.50	401
+1	+1	-1	-1	+1	-1	1.05	14.63	401
+1	+1	-1	-1	-1	+1	1.04	6.98	401
+1	+1	-1	-1	-1	-1	1.05	17.31	401
+1	-1	+1	+1	+1	+1	0.92	6.04	433
+1	-1	+1	+1	+1	-1	0.93	14.40	433
+1	-1	+1	+1	-1	+1	0.92	6.39	433
+1	-1	+1	+1	-1	-1	0.93	16.52	433
+1	-1	+1	-1	+1	+1	0.99	6.52	411
+1	-1	+1	-1	+1	-1	1.00	14.87	411
+1	-1	+1	-1	-1	+1	0.99	7.05	411
+1	-1	+1	-1	-1	-1	1.00	17.96	411
+1	-1	-1	+1	+1	+1	0.97	6.32	421
+1	-1	-1	+1	+1	-1	0.98	15.80	421
+1	-1	-1	+1	-1	+1	0.97	6.44	421
+1	-1	-1	+1	-1	-1	0.98	17.96	421
+1	-1	-1	-1	+1	+1	1.04	6.79	401
+1	-1	-1	-1	+1	-1	1.05	16.16	401
+1	-1	-1	-1	-1	+1	1.04	7.31	401

+1	-1	-1	-1	-1	-1	1.05	19.47	401
-1	+1	+1	+1	+1	+1	0.73	4.55	471
-1	+1	+1	+1	+1	-1	0.73	10.95	471
-1	+1	+1	+1	-1	+1	0.73	4.81	471
-1	+1	+1	+1	-1	-1	0.73	12.64	471
-1	+1	+1	-1	+1	+1	0.79	4.96	445
-1	+1	+1	-1	+1	-1	0.80	11.30	445
-1	+1	+1	-1	-1	+1	0.79	5.41	445
-1	+1	+1	-1	-1	-1	0.80	13.88	445
-1	+1	-1	+1	+1	+1	0.74	4.65	467
-1	+1	-1	+1	+1	-1	0.74	11.48	467
-1	+1	-1	+1	-1	+1	0.74	4.92	467
-1	+1	-1	+1	-1	-1	0.74	13.24	467
-1	+1	-1	-1	+1	+1	0.80	5.07	441
-1	+1	-1	-1	+1	-1	0.81	11.83	443
-1	+1	-1	-1	-1	+1	0.80	5.52	443
-1	+1	-1	-1	-1	-1	0.81	14.57	467
-1	-1	+1	+1	+1	+1	0.73	4.66	471
-1	-1	+1	+1	+1	-1	0.73	11.67	471
-1	-1	+1	+1	-1	+1	0.73	4.95	471
-1	-1	+1	+1	-1	-1	0.73	13.61	471
-1	-1	+1	-1	+1	+1	0.79	5.08	445
-1	-1	+1	-1	+1	-1	0.80	11.93	445
-1	-1	+1	-1	-1	+1	0.79	5.55	445
-1	-1	+1	-1	-1	-1	0.80	14.85	445
-1	-1	-1	+1	+1	+1	0.74	4.73	467
-1	-1	-1	+1	+1	-1	0.74	11.99	467
-1	-1	-1	+1	-1	+1	0.74	5.01	467
-1	-1	-1	+1	-1	-1	0.74	13.92	443
-1	-1	-1	-1	+1	+1	0.80	5.14	441
-1	-1	-1	-1	+1	-1	0.81	12.20	443
-1	-1	-1	-1	-1	+1	0.80	5.60	443
-1	-1	-1	-1	-1	-1	0.81	15.13	443

ACKNOWLEDGEMENTS

The research leading to these results has received funding from the Seventh Framework Programme (FP7/2007-2013) of the European Union, under grant agreement no. 260048 (PoPJIM project). Eurostars NanoComfort project funded by Vinnova, Sweden and the XPRES LAB in Kungliga Tekniska Högskolan (KTH) provided the infrastructure for this research work.

REFERENCES

- [1] S. A. Tobias and W. Fishwick, "Theory of regenerative machine tool chatter," *The engineer*, 1958.
- [2] A. Rashid and C. M. Nicolescu, "Design and implementation of tuned viscoelastic dampers for vibration control in milling," *International Journal of Machine Tools and Manufacture*, vol. 48, pp. 1036-1053, 21st Dec 2007 2007.
- [3] Y. Altintas, M. Eynian, and H. Onozuka, "Identification of dynamic cutting force coefficients and chatter stability with process damping," *CIRP Annals-Manufacturing Technology*, vol. 57, pp. 371-374, 2008.
- [4] S. Coromant, "Application guide: Silent Tools," in *Sandvik Coromant AB*, ed, 2012.
- [5] A. Harms, B. Denkena, and N. Lhermet, "Tool adaptor for active vibration control in turning operations," presented at the 9th International Conference on New Actuators, Bremen, Germany, 2004.
- [6] K. D. Garnjost, C. A. Rauch, and G. J. Rey, "Method and Apparatus for Actively Adjusting and Controlling a Resonant Mass-Spring System," United States Patent, 1995.
- [7] L. Daghini, A. Archenti, and T. Österlind, "Extending stability limits by designed-in damping," *Journal of Machine Engineering*, vol. 13, pp. 45-56, 2013.
- [8] Leo Leroy Beranek and I. L. Vér, *Noise and vibration control engineering: principles and applications*: A Wiley Interscience publication, 1992.
- [9] L. Daghini, A. Andreas, and C. M. Nicolescu, "Design, implementation and Analysis of composite material dampers for turning operations," Tokyo, Japan 2009.
- [10] L. Daghini, "Improving Machining System Performance through designed-in Damping: Modelling, Analysis and Design Solutions," KTH, 2012.
- [11] Y. Altintas and Y. Cao, "Virtual design and optimization of machine tool spindles," *CIRP Annals-Manufacturing Technology*, vol. 54, pp. 379-382, 2005.
- [12] I. Hassab-Allah, W. Shewakh, and A. El-Abd, "Finite element analysis of a new-damped cutting tool for vibration reduction."
- [13] L. Andren, L. Håkansson, A. Brandt, and I. Claesson, "Identification of motion of cutting tool vibration in a continuous boring operation-correlation to structural properties " *Mechanical Systems and Signal Processing*, vol. 18, pp. 903-927, 2004.

Effect of thin viscoelastic material treatments of the clamping region on dynamic stiffness of the cantilever beams

Mahdi Eynian

University West, Sweden

Email: mahdi.eynian@hv.se

ABSTRACT

Cantilever beams and similar structures are found in machining systems. Often a set of cantilever beams attached to each other on spindle-tool holder and tool holder-cutter interfaces position the cutting edge with respect to the workpiece. Small static stiffness leads to deformations and geometrical errors due to the process forces, while small dynamic stiffness initiates chatter vibrations. Dynamic stiffness of structures could be improved by passive or active damping methods. Passive damping methods are suitable design choices considering their low cost and ease of application. In this paper, the constrained layer damping (CLD) method is compared to the application of viscoelastic damper materials on the clamping region and the resulting improvements are compared in terms of enhancement of damping ratio and dynamic stiffness. The maximum enhancement of dynamic stiffness was 487% using a thick layer of viscoelastic material on the clamping region. The effect of the thickness of the viscoelastic material is also studied which shows a linear increase in dynamic stiffness as the thickness of the viscoelastic layer increases.

KEYWORDS: Passive Damping, Viscoelastic, Dynamic stiffness

1. INTRODUCTION

In machine tools and machining, dynamic stiffness of the tool, workpiece and the work holding system at the tool-workpiece engagement region plays an important role in robustness of the cutting process. A low dynamic stiffness leads to self-excited chatter vibrations in turning [1] and milling [2].

Dynamic stiffness of structures built up by connecting multiple parts is affected by the normal pressure, lubrication and surface quality as discussed by Andrew et al [3]. Dynamic stiffness of structures could be improved by active or passive methods. Active methods need an energy source and often a control system to diminish the vibrations and increase the dynamic stiffness [4]. Passive damping methods are suitable in a range of applications due to their simplicity and robustness. Passive methods such as applications of constrained layer

damping (CLD) has been discussed by Daghini [5] while tuned mass dampers (TMD) are discussed by Rashid et. al [6, 7] and Yang et. al [8] for applications in cutting tools. Free layer dampers (FLD) are discussed by Rao [9] and Harris [10] in for applications other than cutting tools.

An important mechanism for energy dissipation is viscoelastic damping in polymers [10]. In this mechanism the energy is dissipated from breakage and re-establishment of van der Waals inter-molecular bonds between long polymer molecules [10]. Viscoelastic materials could be employed as free layer dampers (FLD) as shown in Fig. 1 (a), where they are mainly subjected to the normal strains and stresses [10]. The ratio between the treatment thickness to the beam thickness should be kept large (> 0.1) to achieve noticeable improvement in dynamic stiffness. This is the reason for the widespread use of FLD in shells and plates such as those found in sheet metal panels of automobiles or fuselage skins of airplanes [9]. The need for thick coats may be impractical in cutting tool applications, such as boring bars and milling tools, since it is better to use the limited available space for increasing the static stiffness by increasing the thickness and height of the beams or diameter of the tools.

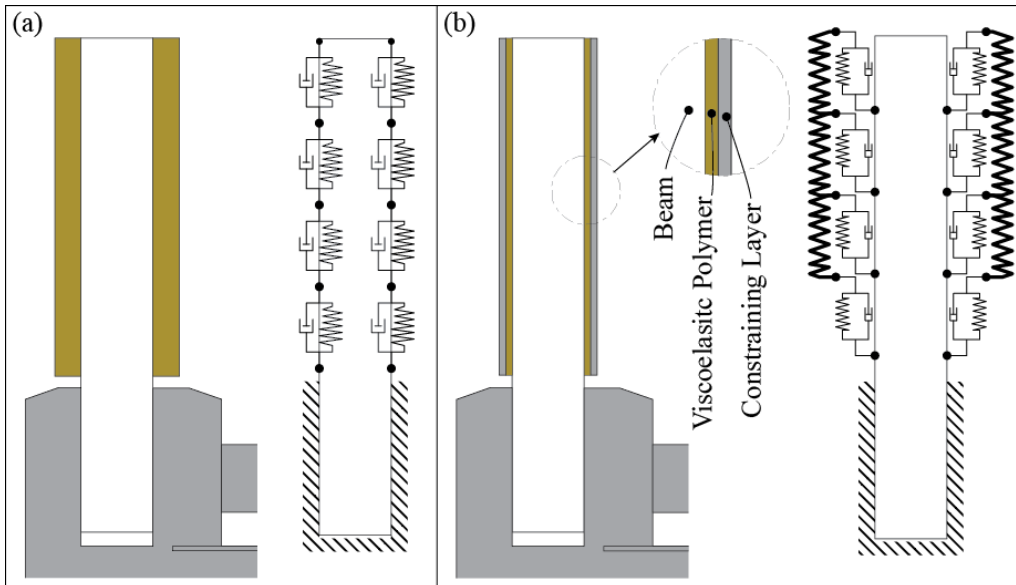


Fig. 1. Free layer damping (a) versus constrained layer damping (b)

The energy dissipation in constrained layer damping (CLD), shown in Fig. 1 (b), is based on the shear of the viscoelastic material between the base material and a constraining layer of higher elastic modulus. Analytical studies show that the constrained layer damping could be effective even with very thin layers of the viscoelastic material [10], therefore these materials are offered in the form of adhesive tapes and rolls, consisting of a thin layer of the viscoelastic material backed by a thicker constraining layer of metals such as aluminum.

Very little has been discussed on application of viscoelastic polymers on clamping interfaces of beams in literature so far. Recently Rashid et al studied incorporation of viscoelastic damping layers between the connecting surfaces of a two-piece workholding system and studied the effects of pre-load (created by piezoelectric actuators) and viscoelastic treatments [11]. The design by Daghini [5] used multiple layers of viscoelastic disks, constrained by metal disks, between the tool holder and the clamping region of the boring bar and achieved an improvement of 152% in dynamic stiffness when a hydrostatic tool holder

was used and an improvement of 26% with a VDI adapter with screw clamp. The setup presented in this paper is simpler as the thin viscoelastic layers are used along the clamped length of the beam as shown in Fig. 2 and no additional parts were needed. The viscoelastic material is subjected to shear and normal deformations, which could be modeled by distributed horizontal and vertical spring-damper arrangements. These shear and normal deformation mechanisms could be translated into torsional, and linear damping and stiffness mechanisms as shown in Fig. 2(c).

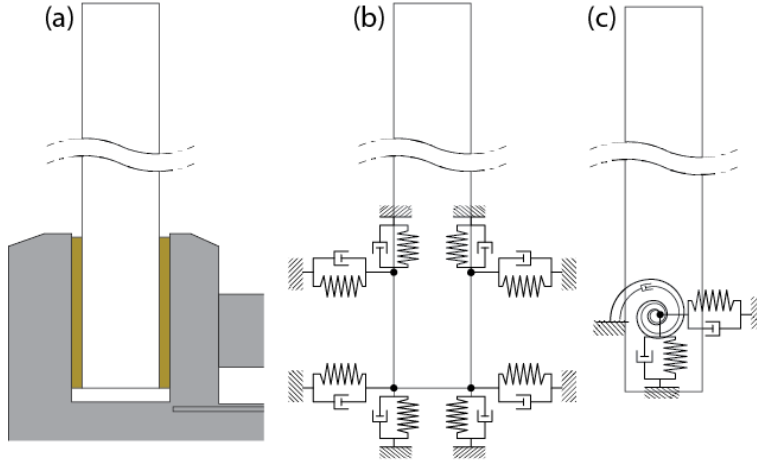


Fig. 2. (a) Beam with viscoelastic damping in the interface, viscoelastic material is represented by horizontal and vertical spring-dampers in (b) and by horizontal, vertical and torsional spring-dampers in (c).

The compliance or the frequency domain displacement response of the beam to the lateral force is shown in this paper by the symbol $\Phi(\omega)$. The compliance in a specific point of measurement of a structure is determined by the modal stiffness and damping ratio of the modes of vibration at that point. The compliance in a system with proportional damping is described as:

$$\Phi(\omega) = \sum_{i=1}^N \frac{1}{K_i \left(1 + 2j\zeta_i \frac{\omega}{\omega_{n_i}} - \left(\frac{\omega}{\omega_{n_i}} \right)^2 \right)} \quad (1)$$

Here, ω_{n_i} , K_i and ζ_i are the natural frequency, modal stiffness and damping ratio for the mode number i and $j = \sqrt{-1}$. While theoretically the number of modes for a continuous structure is unlimited, it is common to consider only a limited number of modes (N), or even a single mode. If one single mode is dominant, it is possible to approximate the system as a single degree of freedom system:

$$\Phi(\omega) = \frac{1}{K \left(1 + 2j\zeta \frac{\omega}{\omega_n} - \left(\frac{\omega}{\omega_n} \right)^2 \right)} \quad (2)$$

Systems with viscoelastic damping are often described with a slightly different frequency response function:

$$\Phi(\omega) = \frac{1}{K \left(1 + j\eta - \left(\frac{\omega}{\omega_n} \right)^2 \right)} \quad (3)$$

The parameter η is referred to as loss factor. For systems with small loss factor (i.e. $\eta < 0.2$ or so), the errors in modeling of the system is small if a viscos damping system model, eq. (2), with a damping ratio of $\zeta = \eta/2$ is used. The parameter $K_d = K\eta \cong 2K\zeta$ is referred to as dynamic stiffness [10]. The maximum damping ratio (ζ) measured in experiments is $\sim 3\%$ ($\zeta = 0.03$) corresponding to $\eta = 0.06$, justifying this approximation.

The threshold stable width of cut is related to the real part of the compliance and the cutting coefficient in the feed direction (K_f) in an orthogonal turning system as [12]:

$$a = \frac{-1}{2K_f \operatorname{Re}(\Phi(\omega))} \quad (4)$$

The absolute minimum depth of cut (see Fig. 3) that can cause chatter is:

$$a_{\lim} = \frac{-1}{2K_f \min[\operatorname{Re}(\Phi(\omega))]} \quad (5)$$

It is also shown that [12]

$$\operatorname{Min}(\operatorname{Re}(\Phi(\omega))) = -\frac{1}{4K\zeta\sqrt{1+\zeta}} \quad (6)$$

For small values of ζ , the above equation could be approximated as

$$\operatorname{Min}(\operatorname{Re}(\Phi(\omega))) \cong -\frac{1}{4K\zeta} \quad (7)$$

Combining Eq. (5) and (7) results in:

$$a_{\lim} \cong \frac{4K\zeta}{2K_f} = \frac{K_d}{K_f} \quad (8)$$

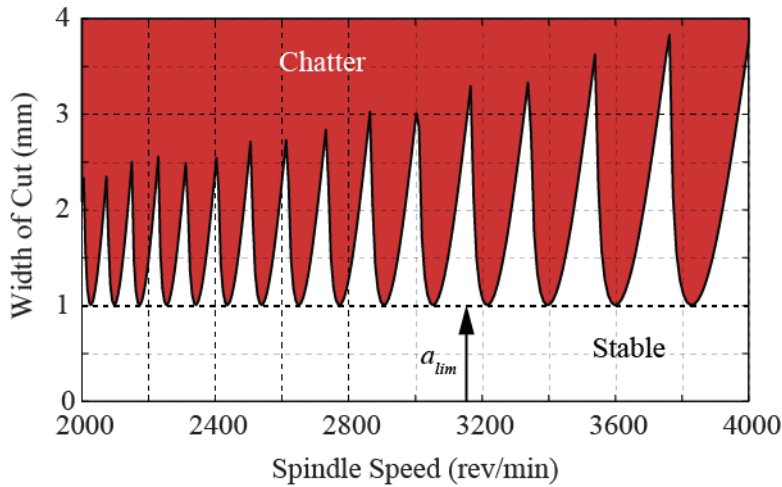


Fig. 3: Stability chart in orthogonal turning, with dynamic stiffness in the feed direction of $K_d = 1000 \text{ kN/m}$ and cutting coefficient in the feed direction of $K_f = 1000 \text{ MPa}$. Natural frequency of the flexible mode $\omega_n = 2\pi \times 1000 \text{ Hz}$

Similar relationships could be obtained between the absolute minimum stability limit in other machining operations. Equation (7) shows the importance of the dynamic stiffness (K_d), since the $a_{lim} = K_d/K_f$ determines the overall vertical location of the stability lobes as shown in Fig. 3. Based on this equation, increasing the dynamic stiffness directly increases the stable metal cutting capacity of the machining system. Based on this, the main objective of the tests described in this paper is to evaluate the capability of different methods to enhance the dynamic stiffness of structures.

2. EXPERIMENTS

The experiments consist of impact tests on a steel beam clamped on a hydraulic vise as shown in Fig. 4 and the critical measurements are given in Fig. 5. The beam's thickness, width and length are 22.2mm, 60.7mm and 300mm respectively. The free length of the beam was 255mm, and 45mm of the beam was under the jaws of the vise. Since the height of the clamp jaws are 30mm, the effective length of clamping was 30mm and 15mm of the beam was free under the clamping region. Hammer impact points and accelerometer attachment points were 20mm below the top edge of the beam. The jaws of the precision hydraulic vise were closed with a clamping force of 19.6kN. This force was measured by placing a short hydraulic cylinder of known diameter between the jaws of the vise and reading out the hydraulic pressure from the attached oil pressure sensor. This clamping force creates a contact pressure on the clamping region equal to 11MPa. In addition to tests on a bare steel beam (S), three different treatments has been applied on both sides of the clamping region (C) or Free region (F) or both regions. The size and location of C and F regions are shown in Fig. 5. The treatments included butyl rubber (R), a commercial constrained layer damping tape with viscoelastic material backed by aluminum layer (tape A), and a viscoelastic polymer (tape B). The details of tests, eight in total are listed in Table 1. Since it was noted that the clamping condition may not be completely repeatable after each clamping, each measurement (which itself consisted of five hammer impacts) is repeated three times and the beam was clamped and unclamped between these measurements. This method is used as a means of tracking the repeatability of the measurements. The reported values are the average of these measurements

and the differences are presented as error bars in the reported diagrams. The hydraulic vise was mounted securely to the heavy table of the 3axis CNC machine tool.



Fig. 4. Beam on the hydraulic vise

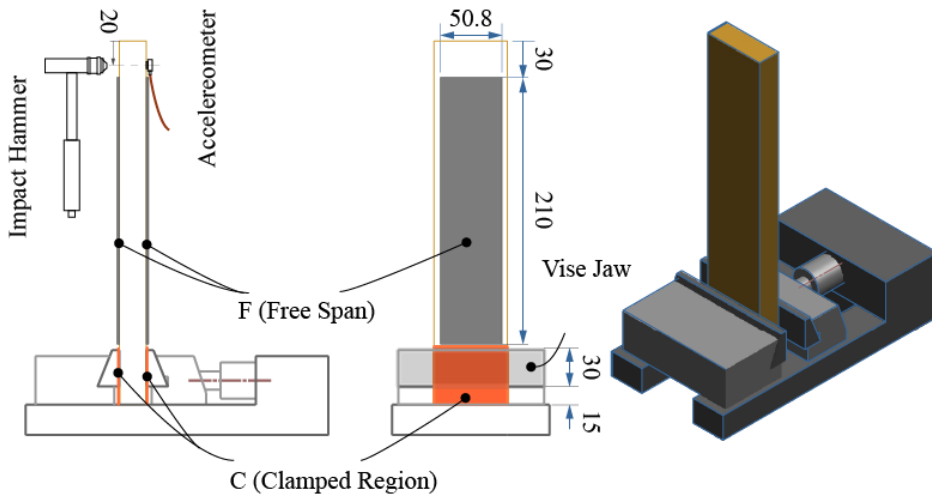


Fig. 5. Experiment setup, impact and acceleration measurement points and positions for application of damping materials in the free span (F) and clamping region (C) are specified

Table 1. Description of experiments

	Title	Material	Application Region	Damping Polymer Thickness/side, t (mm)	Constraining Layer Thickness/side (mm)
1	S	None	-	-	-
2	R1	Rubber	C	0.64	-
3	AF	Tape A	F	0.13	0.25
4	AC	Tape A	C	0.13	0.25
5	ACF	Tape A	C and F	0.13	0.25
6	B1C	Tape B	C	0.15	-
7	B2C	Tape B	C	0.30	-
8	B3C	Tape B	C	0.45	-

3. RESULTS

After each impact test and simultaneous measurement of the impact force and acceleration (Fig. 6), the frequency response function (Fig. 7) is extracted. Using a nonlinear fitting method, a single-degree-of-freedom, mass-spring-damper model is fitted on the measurement in the frequency range of 150-300Hz and stiffness (K), damping ratio (ζ) and natural frequency (F_n) parameters are extracted. The dynamic stiffness (K_d) is calculated from stiffness and damping ratio measurement ($K_d = 2K\zeta$). These results are presented in diagrams in Fig. 8.

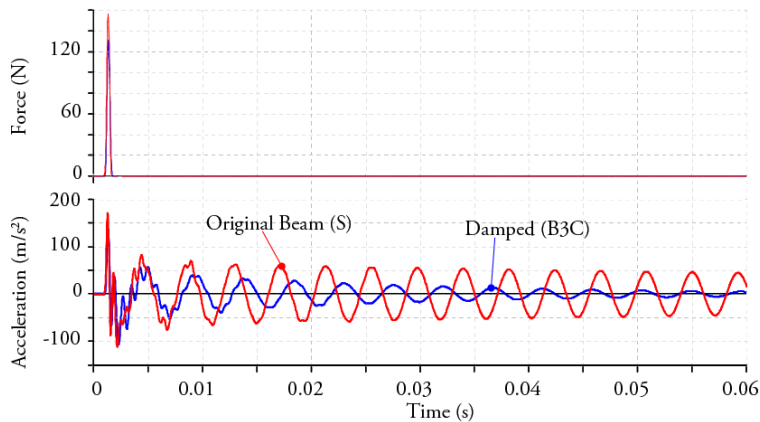


Fig. 6. Impact force and resulted acceleration measurement for original beam (S) and the beam with viscoelastic treatment in the clamping region (B3C)

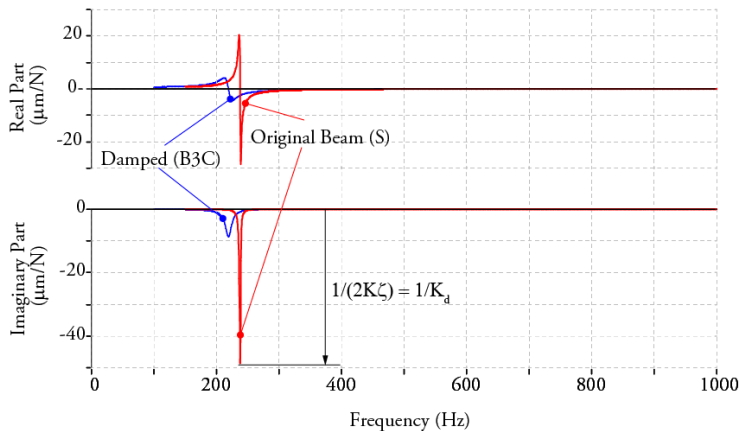


Fig. 7. Real and imaginary parts of the FRF ($\Phi(\omega)$) for the bare beam (S) and the beam with viscoelastic treatment in the clamping region (B3C)

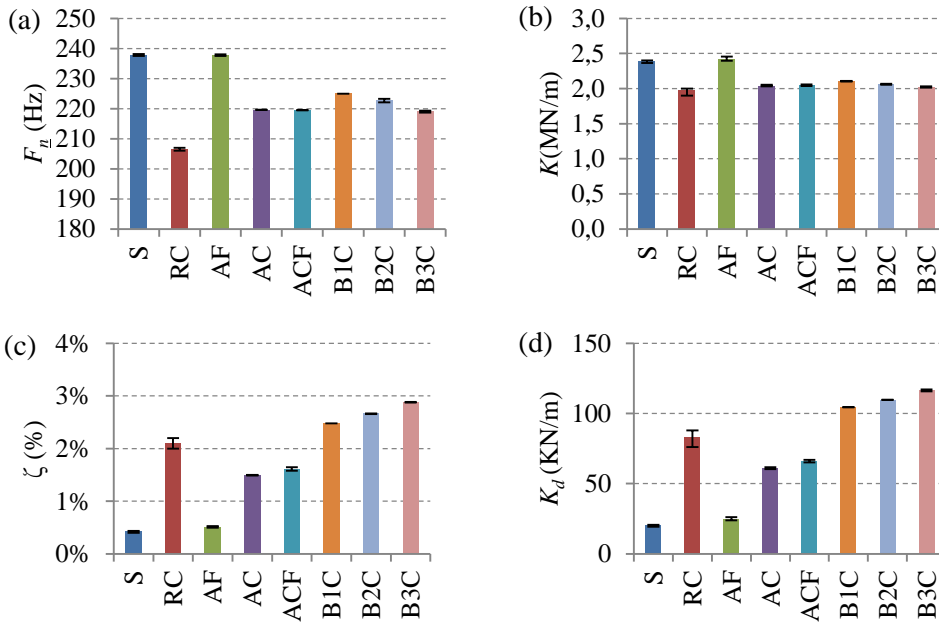


Fig. 8. Summary of experiment results (a): Natural frequency, (b): Modal Stiffness, (c): damping ratio and (d): dynamic stiffness

The ratios of change compared to the untreated beam (S) in the stiffness (K) and dynamic stiffness (K_d) are presented in Fig. 9 (a) and Fig. 9 (b) respectively.

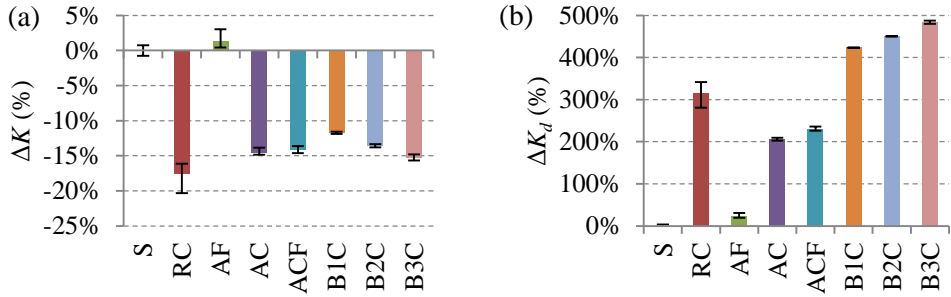


Fig. 9. (a) Changes in modal stiffness (K) and (b) dynamic stiffness (K_d) with respect to the bare beam (S)

4. DISCUSSION

As shown in Fig. 9, an increase of 487% is achieved in dynamic stiffness after the application of 3 layers of tape B in clamping region (the percentages are based on the original beam). This increase is due to a 589% increase in the damping ratio and a 15% decrease in the stiffness. Application of rubber (RC) increases the damping ratio by 402%, but it reduces the stiffness by 18% and increases in the dynamic stiffness 315% in total. The measurements are less repeatable with rubber; which could be due to the changing deformations during clamping and unclamping of the rubber covered beam. Application of tape A (commercial constrained layer damping tape), on the free span of the beam (test AF) increases the stiffness slightly (1%), attributed to the stiffness contribution of the aluminum constraining layer and increases the damping ratio slightly (22%), and increase the dynamic stiffness 24%. This improvement is almost 20 times smaller than the improvement achieved by viscoelastic polymer application on the clamping region (B3C). A higher increase in the dynamic stiffness is achieved (205%) when then this tape is applied on the clamping region (AC), although this would decrease the stiffness by 15%. To study the effect of thickness of the viscoelastic tape, the percentage of changes of stiffness, damping ratio and dynamic stiffness versus viscoelastic layer thickness (t) in experiments B1C, B2C and B3C are presented in Fig. 10. These parameters are all linearly proportional to the thickness of the viscoelastic material, however, the y-intercept is non-zero. If this extrapolation is proven correct, it would mean that even a very thin layer of viscoelastic material can effectively increase the damping ratio and the dynamic stiffness.

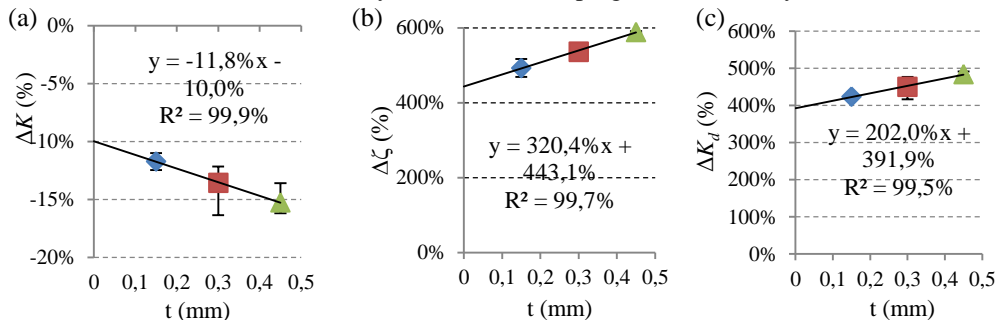


Fig. 10. (a) stiffness, (b) damping ratio and (c) dynamic stiffness as a function of viscoelastic layer thickness (t)

While the high increase in the dynamic stiffness is promising, further studies and machining experiments may be needed for verifying the load carrying capacity and precision

requirements of tooling systems, machine tools and fixturing systems incorporating the presented form of viscoelastic material treatments in clamping and joining surfaces.

ACKNOWLEDGEMENT

The experiments were performed as a supporting part of a “PTC innovation” project, a “European Regional Development Fund” project in Production Technology Center, under the direction of Professor Per Nylen, University West, Sweden.

REFERENCES

- [1] J. Tlustý and M. Poláček, "The stability of machine tool against self excited vibrations in machining," *International research in production engineering, ASME*, , pp. 465-474, 1963.
- [2] Y. Altıntaş and E. Budak, "Analytical prediction of stability lobes in milling," *CIRP Annals-Manufacturing Technology*, vol. 44, pp. 357-362, 1995.
- [3] C. Andrew, J. Cockburn, and A. Waring, "Paper 22: Metal Surfaces in Contact under Normal Forces: Some Dynamic Stiffness and Damping Characteristics," 1967, pp. 92-100.
- [4] T. BAILEY, "Distributed Piezoelectric-Polymer Active Vibration Control of a Cantilever Beam," *Journal of Guidance, Control, and Dynamics*, vol. 8, pp. 605-611, 1985.
- [5] L. Daghini, "Improving Machining System Performance through designed-in Damping: Modelling, Analysis and Design Solutions," PhD, Department of Production Engineering, Machine and Process Technology, KTH, Royal Institute of Technology, Stockholm, Sweden, 2012.
- [6] A. Rashid, "On passive and active control of machining system dynamics: analysis and implementation," KTH, 2005.
- [7] A. Rashid and C. M. Nicolescu, "Design and implementation of tuned viscoelastic dampers for vibration control in milling," *International Journal of Machine Tools and Manufacture*, vol. 48, pp. 1036-1053, 2008.
- [8] Y. Yang, J. Munoa, and Y. Altintas, "Optimization of multiple tuned mass dampers to suppress machine tool chatter," *International Journal of Machine Tools and Manufacture*, vol. 50, pp. 834-842, 2010.
- [9] M. D. Rao, "Recent applications of viscoelastic damping for noise control in automobiles and commercial airplanes," *Journal of Sound and Vibration*, vol. 262, pp. 457-474, 2003.
- [10] C. M. Harris and A. G. Piersol, *Harris' shock and vibration handbook* vol. 5: McGraw-Hill New York, 2002.
- [11] A. Rashid, C. Frangoudis, and C. M. Nicolescu, "Experimental Analysis of a Machining System with Adaptive Dynamic Stiffness," in *Proceedings of the 31st Imac, a Conference on Structural Dynamics*, 2013.
- [12] Y. Altintas, *Manufacturing Automation: Metal Cutting Mechanics, Machine Tool Vibrations, and CNC Design*: Cambridge University Press, 2000.